Universidad Nacional del Nordeste

Facultad de Ingeniería

Carrera:

Doctorado de la Universidad Nacional del Nordeste en el Área de la Ingeniería

Modelado multiescala de medios porosos heterogéneos considerando interacción poro-estructura.

T E S I S

Para obtener el título de:

Doctor de la Universidad Nacional del Nordeste en el Área de la Ingeniería

Presenta:

Reinaldo Adrián Anonis

Director de tesis:

Prof. Dr. Ing. Javier Luis Mroginski

Co-Director de tesis:

Prof. Dr. Ing. Pablo Alejandro Beneyto

Resistencia, Chaco Argentina

2026

Resumen

En esta tesis se desarrollan formulaciones multiescala variacionalmente consistentes aplicadas a problemas hidromecánicos, empleando el concepto de Elemento de Volumen Representativo (RVE: Representative Volume Element) junto con técnicas específicas de homogeneización computacional.

Si bien el empleo de metodologías multiescala se encuentra ampliamente consolidado y ha demostrado gran eficacia en el análisis de materiales complejos y fenómenos multifísicos, existe una dificultad particular cuando se modelan, bajo un esquema de homogeneización de primer orden, problemas gobernados por ecuaciones de balance de una cantidad escalar con término fuente, como es el caso del balance de masas o de determinadas particularizaciones de las ecuaciones de difusión-reacción. En estos casos, la presencia de un término transitorio induce una dependencia de la respuesta macroscópica con respecto al tamaño de la microescala. Debido a las implicaciones que se tienen de homogeneizar dicho término, comúnmente se lo ha denominado ``efecto de segundo orden''. En consecuencia, surge la problemática de que no es posible encontrar un tamaño físicamente admisible de la microestructura a partir del cual la respuesta homogeneizada resulte insensible a dicho tamaño, perdiéndose así la noción básica de existencia de RVE. Esto representa un tópico no tratado aún apropiadamente en la literatura, que plantea desafíos teóricos y numéricos de gran interés ingenieril.

Las ideas fundamentales del presente trabajo de tesis son dos. Primero, obtener un modelo macroscópico que preserve la objetividad de la respuesta homogeneizada al abordar este tipo de fenómenos, con especial énfasis en medios porosos saturados. Posteriormente, extender el tratamiento a microarquitecturas formadas por una matriz de materiales porosos saturados conteniendo inclusiones sólidas impermeables. Este tipo de medios heterogéneos, con microestructura interna conformada por componentes que requieren un número o carácter diferente de campos primarios para describir su comportamiento físico, exige revisiones detalladas y ajustes novedosos en las teorías multiescala basadas en RVE, conformando el segundo punto neurálgico de la presente contribución. En este contexto, se dedica especial atención a las reglas de homogeneización aplicadas al campo de poropresiones y su gradiente, con el fin de construir un Modelo Multiescala Mínimamente Restringido (MCMM: Minimally Constrained Multiscale Model). A partir de esta base, se plantean además modelos alternativos que incorporan restricciones adicionales definidas en particiones adecuadamente establecidas sobre la micro-celda (MC: Micro-Cell) generando una familia de submodelos aplicables a escenarios de mayor complejidad.

Los modelos propuestos se formulan de manera axiomática y variacional mediante el Método de la Potencia Virtual Multiescala (MMVP: Method of Multiscale Virtual Power), y su resolución numérica se aborda mediante el enfoque FE^2 (Finite Element squared). Con este fin, se desarrolló un código computacional general, cuya estructura de datos está específicamente diseñada para un entorno de modelado multiescala. Finalmente, los diversos ejemplos verifican la formulación propuesta, incluyendo comparaciones con metodologías de Simulación Numérica Directa (DNS: Direct Numerical Simulation).

Esta tesis se fundamenta en tres publicaciones realizadas y dos manuscritos actualmente en revisión en revistas científicas internacionales.

Abstract

In this thesis, variationally consistent multiscale formulations are developed and applied to hydro-mechanical problems, employing the concept of Representative Volume Element (RVE) together with specific computational homogenization techniques. Although the use of multiscale methodologies is widely established and has proven highly effective in the analysis of complex materials and multiphysics phenomena, a particular difficulty arises when modeling, within a first-order homogenization framework, problems governed by balance equations for a scalar quantity with a source term, such as the mass balance equation or certain specific forms of diffusion–reaction equations. In such cases, the presence of a transient term induces a dependence of the macroscopic response on the size of the micro-scale. Due to the implications of homogenizing this term, it has commonly been referred to as the ``second-order effect''. Consequently, the problem arises that no physically admissible size of the micro-structure can be identified for which the homogenized response becomes insensitive to that size, thus losing the basic notion of RVE existence. This represents a topic not yet properly addressed in the literature, which poses theoretical and numerical challenges of great engineering interest.

There are two fundamental ideas in this thesis. First, to obtain a macroscopic model that preserves the objectivity of the homogenized response when addressing this type of phenomenon, with special emphasis on saturated porous media. Subsequently, to extend the treatment to micro-architectures formed by a matrix of saturated porous materials containing impermeable solid inclusions. This type of heterogeneous media, with an internal micro-structure consisting of components that require a different number or nature of primary fields to describe their physical behavior, requires detailed revisions and novel adjustments to RVE-based multiscale theories, constituting the second key point of this contribution. In this context, special attention is devoted to the homogenization rules applied to the pore-pressure field and its gradient, with the aim of building a Minimally Constrained Multiscale Model (MCMM). On this basis, alternative models are also proposed that incorporate additional constraints defined over appropriately established partitions on the micro-cell (MC), generating a family of sub-models applicable for more complex scenarios.

The proposed models are formulated axiomatically and variationally using the Method of Multiscale Virtual Power (MMVP), and their numerical solution is addressed through the FE^2 (Finite Element squared) approach. To this end, a general computational code was developed, whose data structure is specifically designed for a multiscale modeling environment. Finally, several examples verify the proposed formulation, including comparisons with Direct Numerical Simulation (DNS) methodologies.

This thesis is based on three published articles and two manuscripts currently under review in international scientific journals.

UNIVERSIDAD
NACIONAL
DEL NORDESTE

DOCTORADO DE LA UNIVERSIDAD NACIONAL DEL NORDESTE EN EL ÁREA DE LA INGENIERÍA

Modelado multiescala de medios porosos heterogéneos considerando interacción poro-estructura.

Reinaldo Adrián Anonis

FI - UNNE

FACULTAD DE INGENIERÍA

UNIVERSIDAD NACIONAL DEL NORDESTE

LAMEC

LABORATORIO DE MECÁNICA COMPUTACIONAL

En el marco de una beca interna doctoral CONICET

Tesis de Doctorado **2026**

Doctorado de la Universidad Nacional del Nordeste en el Área de la Ingeniería

Título de la obra:

Modelado multiescala de medios porosos heterogéneos considerando interacción poro-estructura.

Autor: Reinaldo Adrián Anonis

Lugar: Resistencia, Chaco. Argentina

Palabras Claves:

Mecánica computacional, modelado multiescala,
mecánica de medios porosos, inclusiones sólidas,
problemas de difusión-reacción, objetividad macro-escala,
RVE, efecto tamaño, materiales compuestos,
método de elemento finito cuadrados.

UNIVERSIDAD NACIONAL DEL NORDESTE

Facultad de Ingeniería

Laboratorio de Mecánica Computacional

Modelado multiescala de medios porosos heterogéneos considerando interacción poro-estructura

Reinaldo Adrián Anonis

Tesis remitida al Comité Académico del Doctorado
como requisito parcial para la obtención
del grado de
DOCTOR DE LA UNIVERSIDAD NACIONAL DEL NORDESTE EN EL ÁREA DE LA INGENIERÍA

2026

UNIVERSIDAD NACIONAL DEL NORDESTE

Facultad de Ingeniería

Laboratorio de Mecánica Computacional

Modelado multiescala de medios porosos heterogéneos considerando interacción poro-estructura

Reinaldo Adrián Anonis

Lugar de trabajo:
Laboratorio de Mecánica Computacional (LAMEC)
Facultad de Ingeniería
Universidad Nacional del Nordeste

Director:
Mroginski, Javier Luis LAMEC-IMIT (CONICET-UNNE) / FI - UNNE

Co-director:
Beneyto, Pablo Alejandro LAMEC-IMIT (CONICET-UNNE) / FI - UNNE

Jurado Evaluador:

Dr. Giusti, Sebastián Alejandro	UTN-FRC/CONICET. Córdoba, Argentina.
Dr. Blanco, Pablo Javier	LNCC/MCTI, INCT-MACC. Petrópolis, Brasil.
Dr. Caggiano Antonio	DICCA. Genoa, Italia.

2026

Declaración legal del autor

Esta Tesis ha sido remitida como parte de los requisitos para la obtención del grado de Doctor de la Universidad Nacional del Nordeste en el Área de Ingeniería y ha sido entregada al Decano de la Facultad de Ingeniería en tres ejemplares a ser remitidos a la Biblioteca de la Facultad de Ingeniería, a la Biblioteca de Posgrado de la Facultad de Ingeniería y a la Biblioteca Central de la Universidad Nacional del Nordeste para que esté disponible a sus lectores bajo las condiciones estipuladas por las normas que fijan el reglamento de la carrera.

Reinaldo Adrián Anonis

Agradecimientos

En primer lugar, agradezco a las instituciones que hicieron posible la realización de esta tesis doctoral, en particular al Consejo Nacional de Investigaciones Científicas y Técnicas (CONICET), que financió mi beca de estudios, y a la Facultad de Ingeniería de la Universidad Nacional del Nordeste, que además me brindó la oportunidad de desempeñarme como docente. Asimismo, agradezco al personal del Laboratorio de Mecánica Computacional y del Departamento de Mecánica Aplicada, donde se llevó a cabo el doctorado.

Quiero expresar un agradecimiento especial al Dr. Javier Mroginski, director de esta tesis doctoral, por su constante motivación, apoyo incondicional y gran generosidad a lo largo de todo este proceso.

Extiendo también mi gratitud al Dr. Pablo Sánchez, por haber sido un gran maestro durante el desarrollo de mi doctorado, orientando mi camino y aportando ideas sumamente enriquecedoras. Del mismo modo, agradezco al Dr. Sebastián Toro, cuyas extensas charlas y discusiones, compartidas junto al Dr. Sánchez, resultaron de gran valor formativo y científico.

Además, agradezco a todos aquellos con quienes tuve la oportunidad y el gusto de colaborar y compartir a lo largo de esta experiencia, en particular al Dr. Pablo Beneyto, al Dr. Javier Zambrano y al Dr. Rodrigo Rossi.

Particularmente agradecido a mis padres, por transmitirme la importancia del estudio, acompañarme en todo este camino y con su constante apoyo ser los responsables de quien soy hoy. A mis hermanos por todo lo compartido durante este proceso.

A mi esposa Ori, que con amor, paciencia y muchas charlas me acompaño durante todos estos años.

Por último, a la Trinidad Santa que todo lo envuelve.

Resumen

En esta tesis se desarrollan formulaciones multiescala variacionalmente consistentes aplicadas a problemas hidromecánicos, empleando el concepto de Elemento de Volumen Representativo (RVE: Representative Volume Element) junto con técnicas específicas de homogeneización computacional. Si bien el empleo de metodologías multiescala se encuentra ampliamente consolidado y ha demostrado gran eficacia en el análisis de materiales complejos y fenómenos multifísicos, existe una dificultad particular cuando se modelan, bajo un esquema de homogeneización de primer orden, problemas gobernados por ecuaciones de balance de una cantidad escalar con término fuente, como es el caso del balance de masas o de determinadas particularizaciones de las ecuaciones de difusión-reacción. En estos casos, la presencia de un término transitorio induce una dependencia de la respuesta macroscópica con respecto al tamaño de la microescala. Debido a las implicaciones que se tienen de homogeneizar dicho término, comúnmente se lo ha denominado "efecto de segundo orden". En consecuencia, surge la problemática de que no es posible encontrar un tamaño físicamente admisible de la microestructura a partir del cual la respuesta homogeneizada resulte insensible a dicho tamaño, perdiéndose así la noción básica de existencia de RVE. Esto representa un tópico no tratado aún apropiadamente en la literatura, que plantea desafíos teóricos y numéricos de gran interés ingenieril.

Las ideas fundamentales del presente trabajo de tesis son dos. Primero, obtener un modelo macroscópico que preserve la objetividad de la respuesta homogeneizada al abordar este tipo de fenómenos, con especial énfasis en medios porosos saturados. Posteriormente, extender el tratamiento a microarquitecturas formadas por una matriz de materiales porosos saturados conteniendo inclusiones sólidas impermeables. Este tipo de medios heterogéneos, con microestructura interna conformada por componentes que requieren un número o carácter diferente de campos primarios para describir su comportamiento físico, exige revisiones detalladas y ajustes novedosos en las teorías multiescala basadas en RVE, conformando el segundo punto neurálgico de la presente contribución. En este contexto, se dedica especial atención a las reglas de homogeneización aplicadas al campo de poropresiones y su gradiente, con el fin de construir un Modelo Multiescala Mínimamente Restringido (MCMM: Minimally Constrained Multiscale Model). A partir de esta base, se plantean además modelos alternativos que incorporan restricciones adicionales definidas en particiones adecuadamente establecidas sobre la micro-celda (MC: Micro-Cell) generando una familia de submodelos aplicables a escenarios de mayor complejidad.

Los modelos propuestos se formulan de manera axiomática y variacional mediante el Método de la Potencia Virtual Multiescala (MMVP: Method of Multiscale Virtual Power), y su resolución numérica se aborda mediante el enfoque FE^2 (Finite Element squared). Con este fin, se desarrolló un código computacional general, cuya estructura de datos está específicamente diseñada para un entorno de modelado multiescala. Finalmente, los diversos ejemplos verifican la formulación propuesta, incluyendo comparaciones con metodologías de Simulación Numérica Directa (DNS: Direct Numerical Simulation).

Esta tesis se fundamenta en tres publicaciones realizadas y dos manuscritos actualmente en revisión en revistas científicas internacionales.

Abstract

In this thesis, variationally consistent multiscale formulations are developed and applied to hydro-mechanical problems, employing the concept of Representative Volume Element (RVE) together with specific computational homogenization techniques. Although the use of multiscale methodologies is widely established and has proven highly effective in the analysis of complex materials and multiphysics phenomena, a particular difficulty arises when modeling, within a first-order homogenization framework, problems governed by balance equations for a scalar quantity with a source term, such as the mass balance equation or certain specific forms of diffusion–reaction equations. In such cases, the presence of a transient term induces a dependence of the macroscopic response on the size of the micro-scale. Due to the implications of homogenizing this term, it has commonly been referred to as the "second-order effect". Consequently, the problem arises that no physically admissible size of the micro-structure can be identified for which the homogenized response becomes insensitive to that size, thus losing the basic notion of RVE existence. This represents a topic not yet properly addressed in the literature, which poses theoretical and numerical challenges of great engineering interest.

There are two fundamental ideas in this thesis. First, to obtain a macroscopic model that preserves the objectivity of the homogenized response when addressing this type of phenomenon, with special emphasis on saturated porous media. Subsequently, to extend the treatment to micro-architectures formed by a matrix of saturated porous materials containing impermeable solid inclusions. This type of heterogeneous media, with an internal micro-structure consisting of components that require a different number or nature of primary fields to describe their physical behavior, requires detailed revisions and novel adjustments to RVE-based multiscale theories, constituting the second key point of this contribution. In this context, special attention is devoted to the homogenization rules applied to the pore-pressure field and its gradient, with the aim of building a Minimally Constrained Multiscale Model (MCMM). On this basis, alternative models are also proposed that incorporate additional constraints defined over appropriately established partitions on the micro-cell (MC), generating a family of sub-models applicable for more complex scenarios.

The proposed models are formulated axiomatically and variationally using the Method of Multiscale Virtual Power (MMVP), and their numerical solution is addressed through the FE^2 (Finite Element squared) approach. To this end, a general computational code was developed, whose data structure is specifically designed for a multiscale modeling environment. Finally, several examples verify the proposed formulation, including comparisons with Direct Numerical Simulation (DNS) methodologies.

This thesis is based on three published articles and two manuscripts currently under review in international scientific journals.

Índice general

Índice de figuras

Índice de tablas

Parte I

Introducción

Capítulo 1

Introducción

1.1. Motivación

El uso cada vez más exigente de materiales naturales y diseñados, junto con la necesidad de contar con predicciones numéricas y computacionales confiables en problemas actuales de la industria y la tecnología, ha impulsado un esfuerzo considerable para comprender mejor el comportamiento de los materiales y desarrollar teorías constitutivas más precisas. En este contexto, la respuesta de materiales porosos saturados heterogéneos o de sistemas gobernados por ecuaciones de difusión-reacción, requiere un enfoque multiescala riguroso. Para obtener predicciones macroscópicas realistas, resulta esencial la incorporación explicita de todas las características físicas presentes en la escala microscópica, la cual se modela mediante el Elemento de Volumen Representativo (RVE).

Las metodologías multiescala basadas en el concepto de RVE parten de utilizar un elemento de volumen que intenta reproducir la microestructura compleja del material. A partir de dicho volumen se puede determinar una respuesta homogeneizada que permite construir una descripción del comportamiento en la macroescala. En general, a fin de capturar una respuesta representativa de la heterogeneidad del material para este tipo de aproximación se considera que dicho elemento debe ser lo suficientemente grande. Por otro lado, debe ser de tamaño limitado en dimensiones si es comparado con la longitud característica de la macroestructura. Estas consideraciones se satisfacen en la medida que haya una separación de escalas marcada entre los fenómenos que se describen en la macroescala, con respecto a los fenómenos microscópicos gobernados por la heterogeneidad del material.

Conforme al trabajo pionero de Hill [1], la existencia del RVE está relacionada con la invariancia de la respuesta homogeneizada de la muestra microestructural cuando se aplica una tracción uniforme o un desplazamiento afín sobre su frontera. Expresado en otros términos, se puede definir al RVE como el tamaño mínimo del elemento de volumen de material en estudio a partir del cual, con tamaños mayores, la respuesta homogeneizada macroscópica que se extrae permanece inalterable (Hill [1, 2, 3]). Precisamente, la invariancia de la respuesta efectiva fundamenta el concepto de objetividad (Hill [1]).

Las aproximaciones multiescala que emplean el concepto de RVE pueden clasificarse, según Belytschko et al. [4], en modelos jerárquicos, semiconcurrentes y concurrentes, conforme al grado de acoplamiento involucrado y la forma en que se transfiere la información entre escalas. Todas comparten el hecho de utilizar los conceptos de macroescala y microescala, diferenciándose en el tratamiento que se da a la transferencia de información entre ambas escalas. En la presente tesis se emplea como estrategia global de análisis multiescala al modelo semiconcurrente.

En general, este tipo de análisis se implementa casi exclusivamente mediante técnicas de homogeneización computacional. Estas consisten en la aplicación del método de elementos finitos con la bien conocida metodología FE^2 introducida por Feyel y Chaboche [5] y Feyel [6], y posteriormente extendida por diferentes autores (Michel et al. [7], Miehe et al. [8], Terada y Kikuchi [9], Kouznetsova et al. [10], Miehe y Koch [11], de Souza Neto y Feijóo [12]).

En relación con el estudio de problemas regidos por ecuaciones de balance genéricas con término fuente[1], diversas contribuciones han abordado este tipo de sistemas. Entre ellas se destacan los trabajos de Larsson et al. [13, 14], Runesson et al. [15], Khoei y Hajiabadi [16], Kaessmair y Steinmann [17], Lopez Rivarola et al. [18]. Estos trabajos, junto con otros antecedentes relevantes, serán revisados y profundizados en capítulos posteriores.

El primer propósito fundamental de esta tesis es precisamente desarrollar una formulación multiescala de primer orden completo que sea objetiva para modelar dichos problemas, es decir, que garantice la existencia de un dominio microestructural mínimo a partir del cual la respuesta a macroescala resulte insensible al tamaño. En este contexto, se adopta un enfoque de primer orden en la macroescala. En esta dirección, se propone un modelo multiescala aplicable a problemas gobernados por ecuaciones de balance de un campo escalar con término fuente, con especial énfasis en la difusión-reacción y el balance de masas del fluido[2], prestando particular atención al modelado de materiales porosos saturados. Entre las diversas contribuciones científicas sobre el modelado multiescala, el presente trabajo descansa en una estructura axiomática que recibe el nombre de Método de la Potencia Virtual Multiescala (MMVP), formulada por Blanco et al. [19] y Taroco et al. [20], en cuyo marco teórico se ahondará en los siguientes capítulos.

No obstante, a pesar de los avances alcanzados en la caracterización de materiales heterogéneos mediante paradigmas multiescala basados en el concepto de RVE, persisten diversos aspectos y desafíos relevantes que requieren de un desarrollo continuo. Entre ellos destaca la necesidad de contar con un marco multiescala capaz de tratar microestructuras con componentes que requieren diferentes variables primitivas para su descripción física, lo cual constituye el segundo eje central de esta tesis. En particular, se estudian materiales altamente complejos compuestos por inclusiones sólidas impermeables incrustadas de forma completamente aleatoria en una matriz de tipo medio poroso saturado. De esta manera, el trabajo continúa con la formulación multiescala correspondiente a este tipo de microarquitecturas, desarrollada en dos etapas. En primera instancia, se aborda la discontinuidad que presentan el campo de poropresiones y su gradiente en estas micro-celdas (MCs), aportando una mirada novedosa sobre las restricciones necesarias a imponer en la microescala, aunque limitando el estudio a escenarios resolubles mediante el reconocido modelo Periódico. La segunda etapa extiende este enfoque a situaciones más generales, donde la periodicidad ya no existe y se requieren condiciones de borde más adecuadas, que se establecen a partir de un manejo riguroso del gradiente de poropresiones. En ese contexto, se presenta un esquema alternativo que consiste en incrementar las restricciones del Modelo Multiescala Mínimamente Restringido (MCMM) al imponer condiciones adicionales en particiones apropiadamente definidas sobre la MC, criterio propuesto al abordar microestructuras sólidas con vacíos por Blanco et al. [21].

Finalmente, resulta de especial interés implementar estrategias numéricas que permitan abordar estos modelos mediante la metodología FE^2, con el objetivo de desarrollar una herramienta computacional adecuada.

1.2. Objetivos

1.2.1. Objetivo general

El objetivo principal del presente trabajo es construir un modelo en el marco de una formulación multiescala, desarrollar las estrategias numéricas necesarias para su implementación y evaluarlo computacionalmente mediante un código de elaboración propia. Este propósito se articula en dos ejes centrales: (i) modelar, de manera robusta y precisa, problemas gobernados por ecuaciones de balance genéricas con

[1] Entre sus principales particularizaciones se incluyen las ecuaciones de balance de masas, difusión-reacción y la transferencia transitoria de calor.

[2] En particular, se aborda el modelado multiescala de problemas hidromecánicos que incluyen la ecuación de balance de masas.

término fuente, en concreto, problemas de difusión-reacción y problemas hidromecánicos, con especial interés en el comportamiento de materiales porosos saturados altamente heterogéneos, y (ii) considerar microestructuras con una distribución aleatoria de inclusiones sólidas impermeables en una matriz porosa saturada.

1.2.2. Objetivos específicos

- Proponer una formulación multiescala que preserve el concepto de existencia del elemento de volumen representativo y conduzca a una respuesta objetiva en la macroescala para problemas gobernados por especializaciones de la ecuación de balance de una cantidad escalar con término fuente (problemas hidromecánicos y de difusión–reacción).
- Desarrollar una fomulación multiescala para modelar materiales en el que coexisten componentes caracterizados físicamente por diferentes conjuntos de campos primarios. Aplicar la formulación propuesta a microestructuras conformadas por inclusiones sólidas impermeables embebidas en una matriz porosa saturada.
- Extender el modelo para tratar microarquitecturas con distribuciones aleatorias de inclusiones sólidas irregulares.
- Verificar las estrategias desarrolladas mediante experimentos numéricos, analizando su precisión frente a métodos tradicionales como la simulación numérica directa (DNS).

1.3. Estructura de la tesis

Esta trabajo se presenta en formato de tesis por compilación, cuyo objetivo es integrar de manera coherente los trabajos científicos llevados a cabo durante el doctorado, publicados y en etapa de revisión. En consecuencia, la estructura diseñada pretende proporcionar al lector una visión clara de la evolución del trabajo y los aprendizajes adquiridos, destacando tanto las dificultades encontradas y las decisiones propuestas que guiaron el proceso de investigación. Las publicaciones que contienen los aportes concretos alcanzados se reproducen íntegramente en los Apéndices.

Para evitar redundancias, se ha minimizado la reiteración de información o resultados ya expuestos en los artículos. No obstante, algunos capítulos incluyen contenido inédito destinado a reforzar los conceptos principales. Particularmente, en los capítulos 4 y 5, se presentan dos posibles expansiones del campo de poropresiones que, en las publicaciones, fueron consideradas de forma independiente.

La tesis se organiza en cinco partes:

- Parte I: Introducción. En el Capítulo 1 se contextualiza el tema de investigación y se delinean los objetivos planteados.
- Parte II: Conceptos preliminares involucrados en esta tesis. Se presentan los conceptos básicos que sustentan la teoría, establecidos en la literatura, y que no representan aportes originales de esta tesis. Estos conceptos son expuestos en el Capítulo 2 y reúnen los fundamentos teóricos empleados durante el doctorado. Entre ellos se encuentran: las nociones fundamentales del modelado multiescala basado en el concepto de RVE, la teoría de la poromecánica para el tratamiento del medio poroso, los avances del modelado multiescala aplicado a la poromecánica, los aspectos de implementación numérica en ambas escalas y, finalmente, una breve mención a los problemas gobernados por alguna especialización de la ecuación de balance de una cantidad escalar. Aunque se hace referencia a este material a lo largo de la tesis, los lectores familiarizados con estos temas pueden omitirlo.

- Parte III: Contribuciones al desarrollo de metodologías multiescala aplicado a problemas hidro-mecánicos y de difusión-reacción. Se conforma por tres capítulos que presentan las principales contribuciones de esta tesis. El Capítulo 3 se centra en el análisis de la dependencia con el tamaño de la microescala y la consecuente pérdida de objetividad de la respuesta macroescala. En los Capítulos 4 y 5 se desarrolla la formulación multiescala de microestructuras constituidas por una matriz porosa saturada dotadas de inclusiones sólidas no porosas impermeables, y su extensión al tratamiento de distribución verdaderamente aleatoria de estas últimas.

- Parte IV: Conclusiones. En el Capítulo 6 se sintetiza los aportes fundamentales del presente trabajo.

- Parte V: Apéndices. Contiene en los Apéndices A, B y D los tres trabajos publicados y, en los Apéndices C y E, los dos trabajos remitidos a revisión en revistas internacionales.

Por último, en la Figura 1.1 se propone una secuencia de lectura recomendada, organizada segun el contenido de los capítulos y su relación con las publicaciones

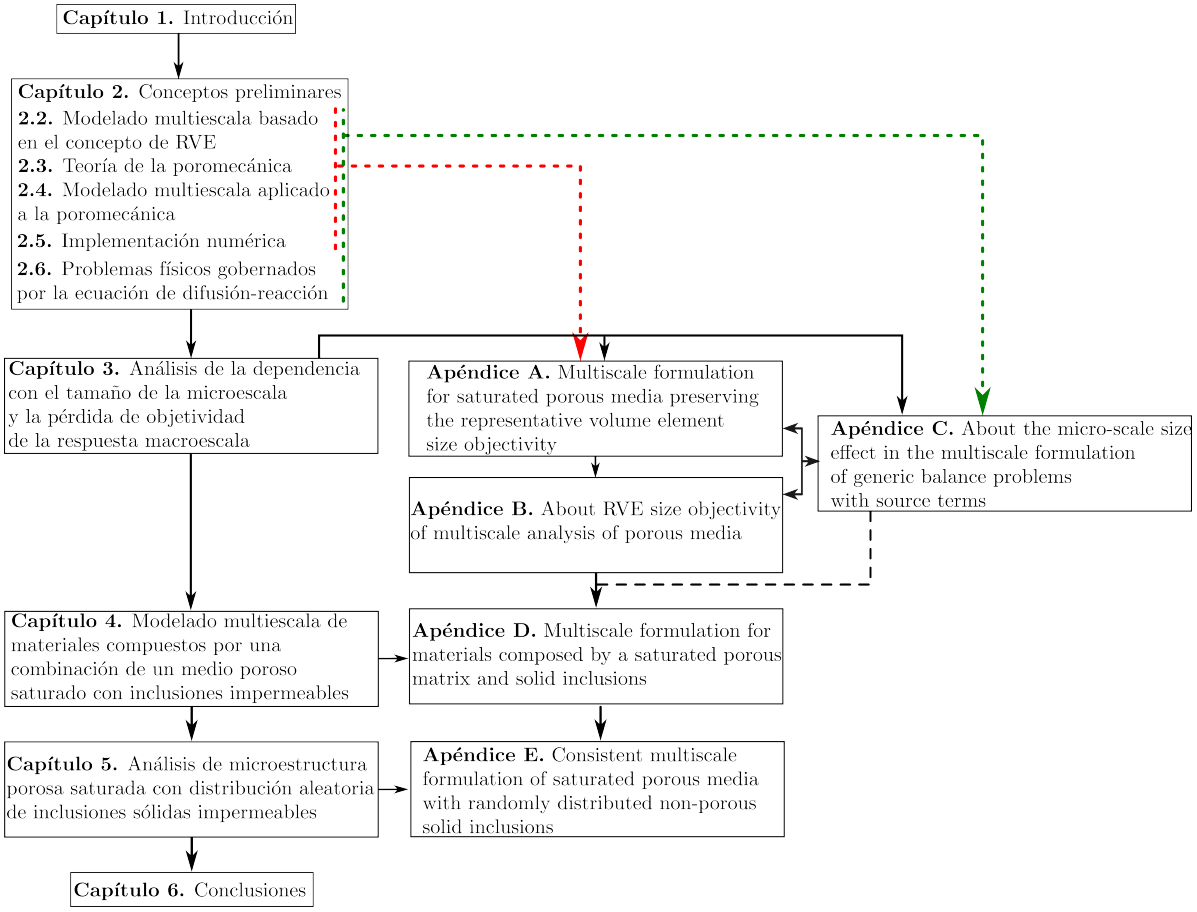

Figura 1.1: Estructura de la tesis.

Parte II

Conceptos preliminares involucrados en esta tesis

Capítulo 2

Conceptos preliminares

2.1. Introducción

En este capítulo se presentan de forma sintética los principales fundamentos teóricos y numéricos empleados en el desarrollo de esta tesis, y que resultan esenciales para la comprensión de los próximos capítulos. La exposición se organiza del siguiente modo: en la sección 2.2 se introducen las nociones referentes al Método de la Potencia Virtual Multiescala (MMVP) para el modelado multiescala variacionalmente consistente utilizando el concepto de RVE. Seguidamente, en la sección 2.3 se describe brevemente la mecánica de medios porosos saturados y su formulación basada principios variacionales. Luego, en la sección 2.4 se repasa la bibliografía existente sobre la metodología multiescala aplicada a medios porosos saturados, proporcionando la formulación teórica correspondiente, en concreto la caracterización de la microescala y el enlace entre ambos niveles en estudio. Posteriormente, en la sección 2.5 se ofrece una descripción resumida de la implementación numérica para las dos escalas. Por último, en la sección 2.6 se introduce una discusión simplificada sobre problemas físicos regidos por una ecuación genérica de balance de un campo escalar.

2.2. Modelado multiescala basado en el concepto de RVE

Tal como se menciono en el Capítulo 1, de las metodologías multiescala basadas en el concepto de RVE, en el presente trabajo se adopta el marco teórico desarrollado por Blanco et al. [19] y Taroco et al. [20], denominado Método de la Potencia Virtual Multiescala (MMVP) el cual simplifica notablemente la formulación y permite desarrollar rigurosamente diversas teorías multiescala. Dicha metodología ha sido empleada para abordar diversos problemas físicos, incluyendo fractura y falla (Sánchez et al. [22], Toro et al. [23], Toro et al. [24], Toro et al. [25]), efectos dinámicos (de Souza Neto et al. [26]), modelos mecánicos de segundo orden (Blanco et al. [27]), mecánica de fluidos (Blanco et al. [28]) y medios con distribuciones altamamente aleatorias de vacíos (Blanco et al. [21]). El MMVP se asienta en tres axiomas o principios fundamentales:

(a) Principio de admisibilidad cinemática: se propone con el fin de garantizar la transferencia adecuada y físicamente coherente de los descriptores primitivos relevantes en el proceso de salto de escala. La admisibilidad se establece mediante dos procedimentos secuenciales: el proceso de inserción de las variables macroscópicas en la microescala y el consiguiente proceso de homogeneización de las variables primarias microscópicas. Estos procedimientos permiten derivar las restricciones microescala apropiadas para que los campos admisibles preserven su magnitud en la transición micro-macro, definiendo además los espacios funcionales dentro de los cuales debe buscarse la solución de los problemas de balance asociados.

(b) Dualidad matemática: asegura una definición consistente de las magnitudes de tipo fuerza y de tipo

tensión (o flujo), las cuales no pueden ser independientes de la cinemática subyacente, sino que son consecuencia de ellas, garantizando su compatibilidad con el modelo adoptado. En efecto, dichas magnitudes emergen de manera inequívoca como los duales matemáticos, es decir, los conjugados de potencia de las variables cinemáticas adoptadas.

(c) Principio de Potencia Virtual Multiescala (PMVP: Principle of Multiscale Virtual Power): constituye una generalización del principio de la macro-homogeneidad de Hill-Mandel (Hill [29] y Mandel [30]), con el fin de abarcar mayor variedad de fenómenos físicos. Establecido el acople físico entre las escalas envueltas en un problema concreto, se derivan de forma natural, mediante argumentos variacionales sencillos, las relaciones de homogeneización para las cantidades de tipo fuerzas y tensiones, y se obtienen las ecuaciones de balance de la microescala.

Conforme a Blanco et al. [19] y Taroco et al. [20], el único grado de arbitrariedad recae en la definición de los descriptores primarios adoptados en las escalas macro y micro, y en la forma en que estos se vinculan con la premisa de que conserven sus magnitudes durante la transferencia entre escalas. A partir de esta definición, el resto de las ecuaciones del modelo se derivan unívocamente como resultado del Principio de Potencia Virtual Multiescala y la dualidad matemática (pares conjugados).

Los lineamientos del MMVP dan lugar a un conjunto mínimo de restricciones para los campos de la microescala, necesarias para garantizar una transferencia adecuada entre escalas. Esto es, dicho procedimiento define el denominado Modelo Multiescala Mínimamente Restringido (MCMM), cuyo espacio funcional puede contener submodelos multiescala bien conocidos, tales como el modelo de Taylor, Lineal o Periódico. Es decir, estos últimos podrían interpretarse como casos particulares del MCMM.

Un aspecto esencial señalado por Blanco et al. [21] es la distinción conceptual entre micro-celda (MC) y RVE. Los autores sostienen que, en la selección de un esquema de homogeneización, deben considerarse dos factores que condicionan su capacidad predictiva: (i) la definición de la morfología que da forma a la MC, y (ii) la definición de las restricciones que se aplicarán al modelo a microescala, las cuales deben permanecer dentro del espacio mínimamente restringido. Asumiendo resuelta la primera cuestión, el segundo factor está directamente asociado al grado de representatividad de la MC. En efecto, las condiciones de contorno influyen directamente en el tamaño requerido para que la MC pueda considerarse un RVE: cuanto más adecuadas sean dichas restricciones, menor será el tamaño necesario. Al contrario, condiciones de contorno menos apropiadas requieren mayor tamaño de la MC para alcanzar representatividad material. De esta manera, establecer las condiciones de borde apropiadas constituye un aspecto crítico del modelado multiescala, especialmente en materiales con microestructuras altamente heterogéneas o no periódicas. A lo largo del presente trabajo se empleará el término micro-celda (MC) para referirse, de manera general, al problema formulado en la microescala, independientemente de si cumple estrictamente con los requisitos de un RVE.

2.3. Teoría de la poromecánica

La mecánica de los medios porosos saturados resulta de gran relevancia en áreas del conocimiento tales como la geomecánica, la biomecánica y la ciencia de los materiales. A partir de las contribuciones fundacionales de Biot [31, 32] se han realizado significativos desarrollos tanto en la formulación teórica (de Boer [33], Carter et al. [34], Coussy et al. [35], Coussy [36, 37]) como en su implementación numérica (Carter et al. [38], Zienkiewicz y Shiomi [39], Zienkiewicz et al. [40] Lewis y Schrefler [41], Mroginski et al. [42], Beneyto et al. [43], Mroginski et al. [44]).

2.3.1. La teoría del medio poroso y el enfoque continuo

En el presente trabajo, se emplea la teoría poromecánica acorde a los desarrollos dados por Coussy [36, 37]. Conforme a las nociones introducidas por este autor y con la finalidad de poder abordar el

análisis del medio poroso, es necesario considerarlo como la superposición de dos continuos: el continuo esquelético (matriz) y el continuo fluido. De este modo, como se ilustra en la Figura 2.1 [36], cualquier volumen infinitesimal puede considerarse como la superposición de dos partículas de material. La primera es la partícula esquelética formada por la matriz y el espacio poroso conectado vaciado de fluido. La segunda es la partícula fluida formada por el fluido que satura el espacio poroso conectado y por el espacio restante sin la matriz. En consecuencia, al considerar un cuerpo $\mathcal{B}$ constituido por un medio poroso saturado como los de la Figura 2.2, se postula que en cada punto material es posible definir un volumen infinitesimal de esta naturaleza, donde resultan aplicables los principios de la mecánica del continuo.

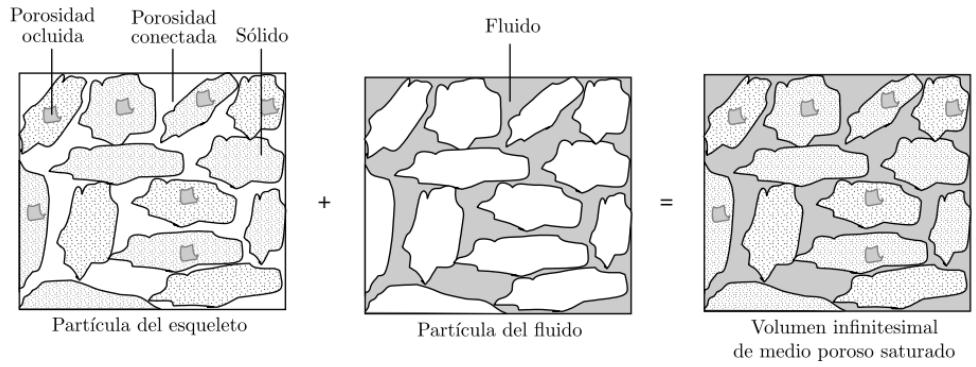

Figura 2.1: Medio poroso como superposición de dos medios continuos.

Como se aprecia en la Figura 2.1, la matriz puede constituirse de una porción sólida con una posible porosidad ocluida, ya sea saturada o no, pero a través de la cual no se produce filtración. El flujo se da concretamente a través del espacio poroso conectado, donde la fase fluida permanece continua. Esto permite definir la porosidad n, que es la relación entre el volumen del espacio de poros conectado y el volumen total. De aquí en adelante, cuando corresponda y sea necesario, las propiedades que refieran al esqueleto sólido y al fluido serán denotados con los superindices s y f.

Resulta importante destacar que las leyes de la física que rigen la evolución de un continuo poroso saturado implican la tasa temporal de las magnitudes físicas asociadas al esqueleto o al fluido, dado que el problema hidromecánico acoplado no es estacionario (debido al fenómeno de infiltración). Esto significa que se incorpora al tiempo t como un parámetro para trazar la evolución de todas las variables.

Para la descripción matemática del modelo se utiliza un dominio acotado $\Omega \in \mathbb{R}^3$, relacionado con el cuerpo $\mathcal{B}$, tal como se observa en la Figura 2.2. Cualquier punto material de $\mathcal{B}$ se denota mediante el

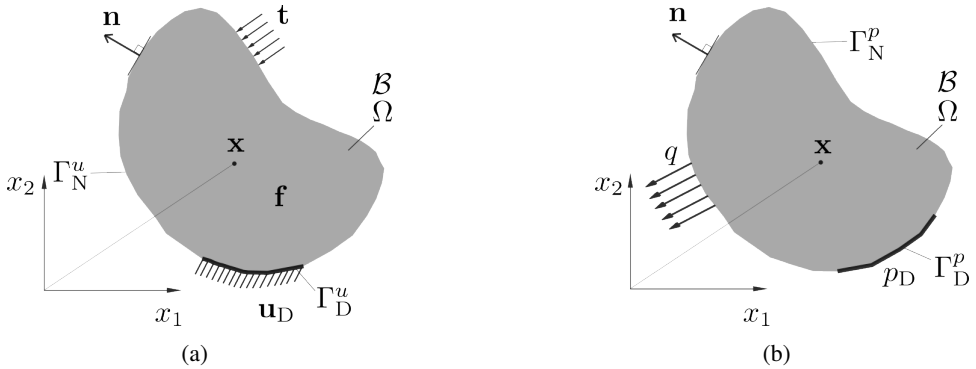

Figura 2.2: Cuerpo para modelado hidromecánico. (a) Problema mecánico. (b) Fenómeno de filtración.

vector $\mathbf{x}$, que se relaciona con un sistema cartesiano. Como de costumbre, Γ representa la frontera suave por partes de Ω, mientras que $\mathbf{n}$ es el vector unitario (hacia fuera) ortogonal a Γ.

2.3.1.1. Descriptores primitivos del esqueleto sólido y la fase fluida

Cuando se somete a agentes externos y a variaciones en la poropresión del fluido que satura, el esqueleto se deforma. Con la finalidad de poder describir la cinemática se introduce el primero de los descriptores primarios: el campo (vectorial) de desplazamiento del esqueleto sólido, $\mathbf{u}(\mathbf{x},t)$. Asumiendo la hipótesis de transformaciones infinitesimales se define el tensor gradiente de los desplazamientos como $\boldsymbol{\nabla}\,\mathbf{u}(\mathbf{x},t) = \boldsymbol{\varepsilon}(\mathbf{x},t) + \boldsymbol{\omega}(\mathbf{x},t)$, el cual se descompone como la suma del tensor de deformaciones infinitesimales del esqueleto sólido (simétrico), $\boldsymbol{\varepsilon}(\mathbf{x},t)$ y del tensor de rotaciones infinitesimales (antisimétrico), $\boldsymbol{\omega}(\mathbf{x},t)$, siendo $\boldsymbol{\nabla}$ el operador gradiente. El primero, que es el de interés en este trabajo se determina como el gradiente simétrico ($\boldsymbol{\nabla}^{sym}$) de los desplazamientos quedando expresado $\boldsymbol{\varepsilon}(\mathbf{x},t) = \boldsymbol{\nabla}^{sym}\,\mathbf{u}(\mathbf{x},t)$. De igual modo, se dispone de la tasa del tensor de deformación infinitesimal $\dot{\boldsymbol{\varepsilon}}(\mathbf{x},t) = \boldsymbol{\nabla}^{sym}\,\dot{\mathbf{u}}(\mathbf{x},t)$

Por otra parte, para una adecuada caracterización del comportamiento de los medios porosos saturados tambien es imprescindible describir le evolución de la fase fluida. Para dicho fin, se incluye el segundo de los descriptores primarios: el campo (escalar) de poropresiones del fluido, aquí denotado con p. Este, como se ha mencionado previamente, a causa de las posibles variaciones que pueda experimentar incide en la cinemática del esqueleto sólido. A partir de esta variable primaria se puede establecer a su vez el gradiente de presión de poros especificado como $\boldsymbol{\varphi} = \boldsymbol{\nabla}\,p$.

Además de las transformaciones infinitesimales, una segunda hipótesis simplificativa que se adopta a lo largo del trabajo es despreciar los términos de inercia para ambas fases, tanto la sólida como la fluida.

2.3.1.2. Vector de flujo relativo de la masa del fluido y vector de filtración

Teniendo en cuenta los acoplamientos entre el esqueleto y el fluido, para la adecuada formulación del problema hidromecánico, se requiere referir el movimiento del fluido respecto de la fase sólida. El flujo relativo de la masa del fluido se representa con el vector $\mathbf{w}(\mathbf{x},t)$ y queda determinado por la expresión $\mathbf{w} = \rho^f\,\boldsymbol{\mathcal{V}} = \rho^f\,n\,\left(\mathbf{V}^f - \mathbf{V}^s\right)$, donde $\boldsymbol{\mathcal{V}}(\mathbf{x},t)$ es el flujo o vector de velocidad de filtración relativo entre la velocidad del fluido $\mathbf{V}^f$ y la del esqueleto sólido $\mathbf{V}^s$ y ρ^f la densidad de masa intrínseca de la fase fluida. En este punto, se establece uno de los agentes externos que contribuye en la evolución del problema hidromecánico el cual consiste en el flujo normal del fluido q (ver Figura 2.2(b)), quedando establecida por la expresión $\frac{q}{\rho^f} = \boldsymbol{\mathcal{V}}\,\cdot\,\mathbf{n}$. El símbolo $(\cdot)$ denota un producto interno de contracción simple.

2.3.1.3. Ecuaciones de balance de masa

Sea ρ^s la densidad de masa intrínseca de la matriz, se dispone de la masa del esqueleto por unidad de volumen de material total diferencial $d\Omega$ como $m^s = \rho^s\,(1-n)$ mientras que el contenido de masa del fluido por unidad de volumen total diferencial del medio continuo poroso, queda determinado como $m^f = \rho^f\,n$. A partir de esto, se enuncia el balance de masa de cada fase de la siguiente forma

$$\dot{m}^s = 0 \quad \forall\,\mathbf{x}\,\in\,\Omega, \quad \forall t,$$

$$\dot{m}^f + \mathrm{Div}\,\mathbf{w} = 0 \quad \forall\,\mathbf{x}\,\in\,\Omega, \quad \forall\,t,$$

siendo Div $(\bullet)$ la divergencia de $(\bullet)$.

Se introduce la variable de la tasa de volumen de poros (por unidad de volumen de poros) con la expresión $\dot{\chi}(\mathbf{x},t) = \frac{\dot{m}^f}{\rho^f}$. Operando matemáticamente sobre el balance de masa del fluido se llega a la

ecuación empleada a lo largo del trabajo

$$\dot{\chi}\left(\mathbf{x},t\right)+\text{Div}\,\boldsymbol{\mathcal{V}}\left(\mathbf{x},t\right)=0\quad\forall\,\mathbf{x}\;\in\;\Omega,\quad\forall\,t. \tag{2.1}$$

2.3.1.4. Ecuación de balance de cantidad de movimiento

Adicional al flujo externo del fluido q presentado anteriormente, en la poromecánica se considera que cualquier dominio material Ω está sometido a dos tipos de agentes externos, tal como en la teoría de medios sólidos. Estas fuerzas externas son las de cuerpo $\mathbf{f}\left(\mathbf{x},t\right)$ y las de superficie $\mathbf{t}$, ver Figura 2.2(a). La primera, para los medios porosos saturados se definen como $\mathbf{f}=\rho\,\mathbf{g}$, donde $\rho=\rho^{s}\;(1-n)+\rho^{f}\,n$ denota la densidad de masa del volumen total de material, incluyendo tanto el esqueleto como el fluido y $\mathbf{g}$ es la aceleración de la gravedad. Por otra parte, la tracción superficial externa se establece como $\mathbf{t}\;=\;\boldsymbol{\sigma}\,\mathbf{n}$. En esta última expresión se ha introducido al tensor de tensiones de Cauchy del esqueleto sólido, $\boldsymbol{\sigma}\left(\mathbf{x},t\right)$, que tiene un papel fundamental en el balance de cantidad movimiento, ecuación que se escribe de la siguiente manera

$$\text{Div}\,\boldsymbol{\sigma}\left(\mathbf{x},t\right)+\mathbf{f}\left(\mathbf{x},t\right)=\mathbf{0},\quad\forall\,\mathbf{x}\;\in\;\Omega,\quad\forall\,t, \tag{2.2}$$

2.3.1.5. Condiciones iniciales y condiciones de contorno

La resolución de las ecuaciones de balance (2.1) y (2.2) permite obtener la respuesta en cada instante de tiempo t de un cuerpo de medio poroso saturado frente a los agentes externos que actuan sobre el mismo. Sin embargo, a fin de poder resolver el problema es necesario establecer las condiciones iniciales y de borde.

Las condiciones iniciales definen completamente el campo de desplazamiento y el campo de poropresiones al inicio del análisis en la forma

$$\begin{aligned}\mathbf{u}&=\mathbf{u}^{0}\quad\forall\,\mathbf{x}\;\in\;\Omega,\;\text{para}\;t=0,\\ p&=p^{0}\quad\forall\,\mathbf{x}\;\in\;\Omega,\;\text{para}\;t=0.\end{aligned} \tag{2.3}$$

Las condiciones de contorno esenciales, o de tipo Dirichlet, pueden imponerse a ambos descriptores primarios especificando funciones prescritas $\mathbf{u}_{\text{D}}$ y p_{D} para los campos de desplazamiento y poropresiones, respectivamente. Estas se expresan como

$$\begin{aligned}\mathbf{u}&=\mathbf{u}_{\text{D}}\quad\forall\mathbf{x}\in\Gamma_{\text{D}}^{u},\quad\forall\,t,\\ p&=p_{\text{D}}\quad\forall\mathbf{x}\in\Gamma_{\text{D}}^{p},\quad\forall\,t,\end{aligned} \tag{2.4}$$

donde Γ_{D}^{u} y Γ_{D}^{p} son las particiones de frontera de Dirichlet correspondientes de Γ relacionadas con las variables de desplazamiento y poropresiones, respectivamente.

Por otro lado, también se pueden aplicar al problema flujos generalizados externos, es decir condiciones de contorno de tipo Neumann, que se definen mediante las expresiones ya establecidas para $\mathbf{t}$ y q reescritas a continuación.

$$\begin{aligned}\boldsymbol{\sigma}\,\mathbf{n}&=\mathbf{t}\quad\forall\,\mathbf{x}\;\in\;\Gamma_{\text{N}}^{u},\quad\forall\,t,\\ \boldsymbol{\mathcal{V}}\,\cdot\,\mathbf{n}&=\frac{q}{\rho^{f}}\quad\forall\mathbf{x}\in\Gamma_{\text{N}}^{p},\quad\forall\,t,\end{aligned} \tag{2.5}$$

siendo que Γ_{N}^{u} y Γ_{N}^{p} representan las particiones de frontera de Neumann correspondientes de Γ para los descriptores de desplazamiento y poropresiones, respectivamente.

Finalmente, teniendo en cuenta las definiciones anteriores se tiene que para el contorno Γ, y tal como puede apreciarse en la Figura 2.2, se han definido subconjuntos que a su vez satisfacen las siguientes condiciones: $\Gamma=\Gamma_{\text{D}}^{u}\cup\Gamma_{\text{N}}^{u}$ ($\Gamma_{\text{D}}^{u}\cap\Gamma_{\text{N}}^{u}=\varnothing$) y además $\Gamma=\Gamma_{\text{D}}^{p}\cup\Gamma_{\text{N}}^{p}$ ($\Gamma_{\text{D}}^{p}\cap\Gamma_{\text{N}}^{p}=\varnothing$).

2.3.1.6. Funcionales de potencia interna y externa

Hasta este punto, se han presentado todos los elementos para la adecuada descripción del medio poroso saturado. No obstante, el concepto de potencia resulta de extrema importancia para los desarrollos posteriores. De este modo, se parte de la expresión de lo que Coussy [36, 37] denomina de tasa de trabajo de deformación total y considerando las hipótesis planteadas al principio de esta sección, se establece el funcional de potencia interna $\mathcal{P}^{int}$, conforme a la notación del presente trabajo

$$\mathcal{P}^{int} = \int_{\Omega} \left[\boldsymbol{\sigma} : \dot{\boldsymbol{\varepsilon}} - \text{Div} \left(\frac{p}{\rho^f} \mathbf{w} \right) \right] d\Omega. \tag{2.6}$$

Trás cierto trabajo matemático sobre el segundo término del integrando del lado derecho de la ecuación y sustituyendo la expresión del balance de masa (2.1), se reescribe la ecuación (2.6) la siguiente forma

$$\mathcal{P}^{int} = \int_{\Omega} \left(\boldsymbol{\sigma} : \dot{\boldsymbol{\varepsilon}} + \dot{\chi}\, p - \boldsymbol{\mathcal{V}} \cdot \boldsymbol{\varphi} \right) d\Omega. \tag{2.7}$$

En el contexto de materiales porosos saturados se observa que la potencia interna no queda completamente descripta por un solo par de variables duales, como sucede con problema de la mecánica de sólidos convencional, donde basta el producto del tensor de tensiones de Cauchy y la tasa del tensor de deformación infinitesimal simétrico $\{\boldsymbol{\sigma}; \dot{\boldsymbol{\varepsilon}}\}$. Aquí, otro fenómeno físico contribuye a definir $\mathcal{P}^{int}$. Así, el segundo término del lado derecho de la ecuación (2.7) representa la tasa de trabajo realizada, en el espacio de vacíos (poroso), por la fase fluida. El tercer producto de dualidad en (2.7) tiene en cuenta el efecto de disipación viscosa debido al movimiento relativo de la fase fluida con respecto al esqueleto sólido. En resumen, es necesario introducir dos pares adicionales de variables de potencia conjugada, $\{\dot{\chi}; p\}$ y $\{\boldsymbol{\mathcal{V}}; \boldsymbol{\varphi}\}$, con respecto al problema mecánico sólido clásico.

Por otra parte, acorde a lo que Coussy [36, 37] denomina la tasa de trabajo de las fuerzas externas de cuerpo y superficie, habiendo efectuado ciertas manipulaciones matemáticas, se define la potencia externa $\mathcal{P}^{ext}$, que es ejercido por el conjunto de agentes externos $\{\mathbf{f}; \mathbf{t}; q\}$ del siguiente modo

$$\mathcal{P}^{ext} = \int_{\Omega} \mathbf{f} \cdot \dot{\mathbf{u}}\, d\Omega + \int_{\Gamma} \left(\mathbf{t} \cdot \dot{\mathbf{u}} - p\, \frac{q}{\rho^f} \right) d\Gamma. \tag{2.8}$$

Finalmente, se arriba a la expresión para la potencia total $\mathcal{P}^{tot}$

$$\mathcal{P}^{tot} = \mathcal{P}^{int} - \mathcal{P}^{ext} = \int_{\Omega} \left(\boldsymbol{\sigma} : \dot{\boldsymbol{\varepsilon}} + \dot{\chi}\, p - \boldsymbol{\mathcal{V}} \cdot \boldsymbol{\varphi} - \mathbf{f} \cdot \dot{\mathbf{u}} \right) d\Omega - \int_{\Gamma} \left(\mathbf{t} \cdot \dot{\mathbf{u}} - p\, \frac{q}{\rho^f} \right) d\Gamma. \tag{2.9}$$

2.3.2. Principios variacionales aplicados a la teoría poromecánica

Los principios variacionales dan lugar a las ecuaciones que rigen los procesos reales, por lo que juegan un papel importante en la mecánica aplicada (Taroco et al. [20], Berdichevsky [45], Reddy [46]). El enfoque variacional, se presenta como una herramienta de carácter universal, tanto para la descripción de fenómenos físicos como para el desarrollo de métodos cualitativos y cuantitativos para estudiar problemas concretos. Entre las muchas implicancias, se destaca su practicidad de reducir en una única expresión integral todos los elementos que intervienen en el problema en análisis, tales como ecuaciones de balance, ecuaciones constitutivas, condiciones de contorno, condiciones iniciales, etcétera. A su vez, la formulación variacional induce de manera natural los métodos de resolución para la obtención de soluciones aproximadas, en muchos casos de sencilla implementación computacional, lo cual resulta de gran importancia desde el punto de vista de las aplicaciones. El objetivo de la presente sección es, precisamente, implementar las nociones del cálculo variacional de una forma simple, sin profundizar en su desarrollo teórico, y aplicarlas en concreto sobre la teoría poromecánica presentada con anterioridad.

En este punto, se introduce el concepto de variaciones de las acciones reales o como se denominarán de aqui en adelante acciones virtuales. En la mecánica clásica, dichas acciones se formulan en relación con el movimiento (desplazamiento), mientras que en el contexto poromecánico se consideran además las poropresiones virtuales, quedando ambas asociadas a las acciones virtuales del problema. De este modo, con el símbolo δ, que precede a cualquier entidad, se denota su variación virtual.

El concepto formal de configuraciones admisibles o admisibilidad que se aplica en el contexto de la mecánica de los medios porosos saturados, y conforme a las condiciones de Dirichtlet que se presentaron previamente en (2.4), se propone mediante los siguientes conjuntos

$$\begin{aligned} \mathcal{U}(\Omega) &\equiv \left\{ \mathbf{u} \in \mathbf{H}^1(\Omega);\ \mathbf{u} = \mathbf{u}_{\mathrm{D}}\ \forall\, \mathbf{x} \in \Gamma^u_{\mathrm{D}} \right\}, \\ \mathcal{P}(\Omega) &\equiv \left\{ p \in \mathrm{H}^1(\Omega);\ p = p_{\mathrm{D}}\ \forall\, \mathbf{x} \in \Gamma^p_{\mathrm{D}} \right\}, \end{aligned} \tag{2.10}$$

para los campos primarios $\mathbf{u}(\mathbf{x},t)$ y $p(\mathbf{x},t)$, respectivamente. En (2.10), $\mathbf{H}^1(\bullet)$ y $\mathrm{H}^1(\bullet)$ denotan los espacios vectorial y escalar de funciones cuya primera derivada es cuadrada-integrable, respectivamente. Por su parte, para las acciones virtuales $\delta\mathbf{u} \in \mathcal{U}^*(\Omega)$ y $\delta p \in \mathcal{P}^*(\Omega)$, los correspondientes espacios vectoriales y escalares lineales resultan

$$\begin{aligned} \mathcal{U}^*(\Omega) &\equiv \left\{ \delta\mathbf{u} \in \mathbf{H}^1(\Omega);\ \delta\mathbf{u} = \mathbf{0}\ \forall\, \mathbf{x} \in \Gamma^u_{\mathrm{D}} \right\}, \\ \mathcal{P}^*(\Omega) &\equiv \left\{ \delta p \in \mathrm{H}^1(\Omega);\ \delta p = 0\ \forall\, \mathbf{x} \in \Gamma^p_{\mathrm{D}} \right\}. \end{aligned} \tag{2.11}$$

Para establecer la potencia virtual total, $\delta\mathcal{P}^{tot}$, se sustituyen las cantidades primitivas $\{\dot{\mathbf{u}}; \dot{\boldsymbol{\varepsilon}}; p; \boldsymbol{\varphi}\}$ por sus correspondientes acciones virtuales admisibles $\{\delta\dot{\mathbf{u}}; \delta\dot{\boldsymbol{\varepsilon}}; \delta p; \delta\boldsymbol{\varphi}\}$ en la expresíon (2.9), con lo cual se obtiene

$$\begin{aligned} \delta\mathcal{P}^{tot} = \delta\mathcal{P}^{int} - \delta\mathcal{P}^{ext} = \int_\Omega \left(\boldsymbol{\sigma} : \delta\dot{\boldsymbol{\varepsilon}} + \dot{\chi}\,\delta p - \boldsymbol{\mathcal{V}} \cdot \delta\boldsymbol{\varphi} - \mathbf{f} \cdot \delta\dot{\mathbf{u}} \right) d\Omega \\ - \int_{\Gamma^u_{\mathrm{N}}} \mathbf{t} \cdot \delta\dot{\mathbf{u}}\, d\Gamma + \int_{\Gamma^p_{\mathrm{N}}} \frac{q}{\rho^f}\,\delta p\, d\Gamma,\ \forall\, t. \end{aligned} \tag{2.12}$$

Las dos últimas integrales solo incluyen las particiones de frontera de Neumann, debido a la admisibilidad de las acciones virtuales $\delta\dot{\mathbf{u}} \in \mathcal{U}^*(\Omega)$ y $\delta p \in \mathcal{P}^*(\Omega)$, definidas en (2.11).

El equilibrio se establece cuando los campos primarios son tales que la potencia total es nula para toda variación admisible. Esto es equivalente al principio de potencia virtual, que asume que la integral (2.12) desaparezca para todas las acciones virtuales $\delta\dot{\mathbf{u}}$ y δp. Como se menciono al principio, con los métodos variacionales se pueden establecer las ecuaciones que gobiernan un determinado problema o fenómeno físico. En este caso, al aplicar los principios variacionales sobre la ecuación (2.12) es posible derivar las ecuaciones de balance en forma débil que describen el comportamiento del medio poroso saturado. Las ecuaciones de balance en forma débil postulan que la potencia virtual externa ejercida por el conjunto de agentes externos debe ser igual a la potencia virtual interna de las variables de tipo tensión, para todas las variaciones admisibles en los descriptores primarios, es decir

$$\begin{aligned} \int_\Omega \left(\boldsymbol{\sigma} : \delta\dot{\varepsilon} + \dot{\chi}\,\delta p - \boldsymbol{\mathcal{V}} \cdot \delta\boldsymbol{\varphi} \right) d\Omega = \int_\Omega \mathbf{f} \cdot \delta\dot{\mathbf{u}}\, d\Omega \\ + \int_{\Gamma^u_{\mathrm{N}}} \mathbf{t} \cdot \delta\dot{\mathbf{u}}\, d\Gamma - \int_{\Gamma^p_{\mathrm{N}}} \frac{q}{\rho^f}\,\delta p\, d\Gamma, \quad \forall\, \delta\dot{\mathbf{u}} \in \mathcal{U}^*(\Omega)\ \mathrm{y}\ \delta p \in \mathcal{P}^*(\Omega),\ \forall\, t. \end{aligned} \tag{2.13}$$

Dado que $\delta\dot{\mathbf{u}}$ y δp son independientes entre sí, la forma débil es finalmente descripta como un sistema de dos ecuaciones escalares acopladas. Estás son la ecuaciones de balance de cantidad de movimiento, G, y el balance de masas, H. Entonces, el problema hidromecánico se puede enunciar de la siguiente manera:

encontrar los campos de desplazamiento $\mathbf{u} \in \mathcal{U}(\Omega)$ y poropresiones $p \in \mathcal{P}(\Omega)$ tales que

$$\begin{aligned} \mathrm{G} &= \int_\Omega \boldsymbol{\sigma} \,:\, \delta\dot{\boldsymbol{\varepsilon}}\, d\Omega - \int_\Omega \mathbf{f} \cdot \delta\dot{\mathbf{u}}\, d\Omega - \int_{\Gamma_{\mathrm{N}}^u} \mathbf{t} \cdot \delta\dot{\mathbf{u}}\, d\Gamma = 0,\ \forall\, \delta\dot{\mathbf{u}} \in \mathcal{U}^*(\Omega),\ \forall\, t, \\ \mathrm{H} &= \int_\Omega \left(\dot{\chi}\, \delta p - \boldsymbol{\mathcal{V}} \cdot \delta\boldsymbol{\varphi}\right) d\Omega + \int_{\Gamma_{\mathrm{N}}^p} \frac{q}{\rho^f}\, \delta p\, d\Gamma = 0,\ \forall\, \delta p \in \mathcal{P}^*(\Omega),\ \forall\, t. \end{aligned} \tag{2.14}$$

Es evidente que, a partir de las ecuaciones de balance de masa y de cantidad de movimiento, siguiendo pasos matemáticos directos, es posible derivar las correspondientes ecuaciones de balance en forma fuerte. En particular, estas se expresan mediante (2.1) y (2.2), junto con las condiciones de Neumman (2.5). No obstante, aunque desde el enfoque variacional hubiese resultado más claro y conveniente derivarlas directamente a partir de los funcionales de potencia interna (2.7) y externa (2.8), se optó en este trabajo por seguir lo más fielmente posible los desarrollos de la teoría poromecánica expuesta por Coussy [36, 37].

Hasta este punto, esta tesis se ha desarrollado sin introducir distinciones entre la macroescala y microescala, con el propósito de presentar los conceptos de forma general. Sin embargo, a partir de ahora resulta conveniente señalar que el sistema de ecuaciones (2.14), en la manera en que aparece escrito, describe el comportamiento de un medio poroso saturado homogeneizado que se asume para la macroescala dentro de un entorno de metodología multiescala.

No obstante, se requieren aún de las funciones constitutivas para el conjunto de magnitudes similares a tensiones $\{\boldsymbol{\sigma}, \dot{\chi}, \boldsymbol{\mathcal{V}}\}$ y las fuerzas de cuerpo $\mathbf{f}$. Dichas funciones no se definen de forma explícita en la escala de longitud mayor, sino que se derivan implícitamente de un marco variacional multiescala consistente, cuyo desarrollo general se presenta en la sección 2.4 y como se observa en la Figura 2.3. En otras palabras, en el marco del modelado multiescala, los funcionales constitutivos macroscópicos se obtienen a partir de la respuesta de la microestructura. Con este objetivo, la expresión (2.12) que ya ha sido empleada para establecer las ecuaciones de forma débil de la macroescala, será retomada más adelante en este manuscrito para establecer el correspondiente acoplamiento entre escalas dentro del enfoque variacional propuesto.

Cabe resaltar que, desde una perspectiva variacional, el modelo macroscópico descrito en esta sección constituye un enfoque de primer orden para el problema hidromecánico acoplado. Esto se debe a que, en la forma débil (2.14), únicamente intervienen los productos duales virtuales asociados a los campos primarios y a sus gradientes de primer orden. No obstante, en esta clase de modelos podrían manifestarse efectos de segundo orden siempre que las leyes constitutivas de $\{\boldsymbol{\sigma}, \dot{\chi}, \boldsymbol{\mathcal{V}}\}$ incluyan, por ejemplo, fenómenos no locales o gradientes de orden superior como argumentos de entrada. Una manera formal de abordar estas características mejoradas es suponer la existencia de una longitud característica, ℓ_{ch}, representando un nuevo parámetro material finito con un significado físico claro, en la que se producen los efectos de segundo orden. Para el presente trabajo, en virtud de que los materiales subyacentes carecen de un parámetro característico con un significado físico evidente que justifique su inclusión, no se incorporan efectos de segundo orden. En consecuencia, se propone como objetivo principal el desarrollo de un modelo multiescala total o estrictamente de primer orden para los fenómenos hidromecánicos, donde el término "total o estrictamente de primer orden" alude a un enfoque en el cual tanto la formulación variacional como las respuestas constitutivas se limitan al primer orden. Sobre estas ideas se profundiza en el Capítulo 3.

2.4. Modelado multiescala aplicado a la poromecánica

Los materiales naturales como el suelo, los tejidos y el hueso, así como materiales artificiales como el hormigón, suelen describirse por medio de la teoría de los medios porosos. La necesidad de caracteri-

zaciones más precisas ha impulsado a recurrir a técnicas de homogeneización, tales como las derivadas de la teoría de la micromecánica (Luc Dormieux [47]). Sin embargo, y conforme a lo presentado en la Sección 2.2, este trabajo se centra en los desarrollos multiescala basados en el concepto de RVE. El objetivo de esta sección es ofrecer un introducción breve al estado del arte, mientras que consideraciones mas profundas se desarrollan en el Capítulo 3. Asimismo, se presentan todas las ecuaciones fundamentales para el modelado multiescala de medios porosos saturados.

Los primeros aportes relevantes corresponden a Larsson et al. [14], quienes propusieron un esquema de homogeneización variacionalmente consistente para consolidación no acoplada, luego extendida al caso acoplado por Su et al. [48]. Posteriormente, Jänicke et al. [49] proponen un modelo poro-viscoelástico que permite que el gradiente de poropresión pueda desarrollarse en la escala macroscópica. Ekre et al. [50] aplican técnicas numéricas de orden reducido con el fin de disminuir el costo computacional en la homogeneización de la consolidación no lineal. Por su parte, Khoei y Hajiabadi [16] mediante homogeneización de primer orden en medios porosos saturados completamente acoplados entre escalas, usando una extensión de la teoría de Hill-Mandel y considerando además efectos microdinámicos presentan un modelo multiescala para el problema de consolidación de un suelo saturado. A partir de este trabajo, Khoei y Saeedmonir [51] ampliaron la herramienta de homogeneización computacional para considerar el flujo multifásico. Diversos fenómenos acoplados también han sido abordados, tales como problemas termo-hidro-mecánicos (Lopez Rivarola et al. [18] y Saeedmonir y Khoei [52]), medios porosos con microfracturas (Khoei et al. [53]) y procesos quimio-hidromecánicos asociados a reacciones químicas en medios porosos (Saeedmonir et al. [54]). A su vez, Ricken et al. [55] y Klahr et al. [56] incorporaron deformaciones finitas para tratar la micromecánica de tejidos biológicos. Finalmente, Thiesen et al. [57, 58] demostraron numéricamente las limitaciones de la homogeneización de primer orden en materiales con cambios volumétricos significativos, proponiendo un marco multiescala que vincula modelos poromecánicos clásicos a microescala con formulaciones de segundo orden a macroescala.

Con lo anterior concluye el breve repaso de la literatura existente relativa a la aplicación de metodologías multiescalas basados en el concepto de RVE en el ámbito de la poromecánica. En lo que sigue, se introducen los conceptos y formulaciones necesarias para la implementación del modelado multiescala hidromecánico. Cabe señalar que, si bien estas expresiones han sido previemente desarrolladas por los autores mencionados, aquí se adaptan y exponen de acuerdo con el enfoque y la notación propias de este estudio. Los desarrollos planteados en esta sección serán utilizados en los capítulos posteriores, ya sea sin modificaciones, como es el caso del Capítulo 3, o bien con las adaptaciones necesarias que serán propiamente incluidas en los Capítulos 4 y 5, según corresponda.

En concreto, en esta parte del manuscrito se establece el acoplamiento físico entre las escalas de longitud macro y micro. Con este propósito, se recurre al MMVP, ya descripto en la Sección 2.2. Esta formulación variacional se aplicará en conjunto con los conceptos de la poromecánica expuestos en la Sección 2.3, proporcionando un marco formal para construir un modelo multiescala hidromecánicamente consistente, a partir del cual derivar todos los elementos necesarios. Se presentan a continuación todas las suposiciones y la notación que serán empleadas para describir la microescala.

2.4.1. Supuestos básicos del modelo a microescala

Al igual que en el problema macroscópico, la escala microscópica se modela como un medio poroso saturado continuo. En consecuencia, se adopta la misma teoría poromecánica y se emplean los mismos descriptores primarios. En otras palabras, las principales hipótesis de modelado en la microescala son idénticas a las expuestas en la Sección 2.3. Para distinguir las entidades correspondientes a la microescala, se emplea el subíndice $(\bullet)_\mu$ en todo objeto asociado con el dominio microscópico, como se ilustra en la Figura 2.3. El cuerpo microestructural analizado se denota con $\mathcal{B}_\mu$. Para identificar cualquier punto material $\mathbf{x}_\mu$ perteneciente a $\mathcal{B}_\mu$, se incorpora un sistema de coordenadas cartesianas a la microescala

(independiente del propuesto para la macroescala). El dominio acotado $\Omega_\mu \in \mathbb{R}^3$ se establece para representar al cuerpo $\mathcal{B}_\mu$, y se conoce además como micro-celda (MC). Cualquier punto macroscópico $\mathbf{x}$ está unívocamente relacionado con una MC. El contorno de Ω_μ, es denotado como Γ_μ, siendo $\mathbf{n}_\mu$ el vector unitario (hacia afuera) normal a Γ_μ.

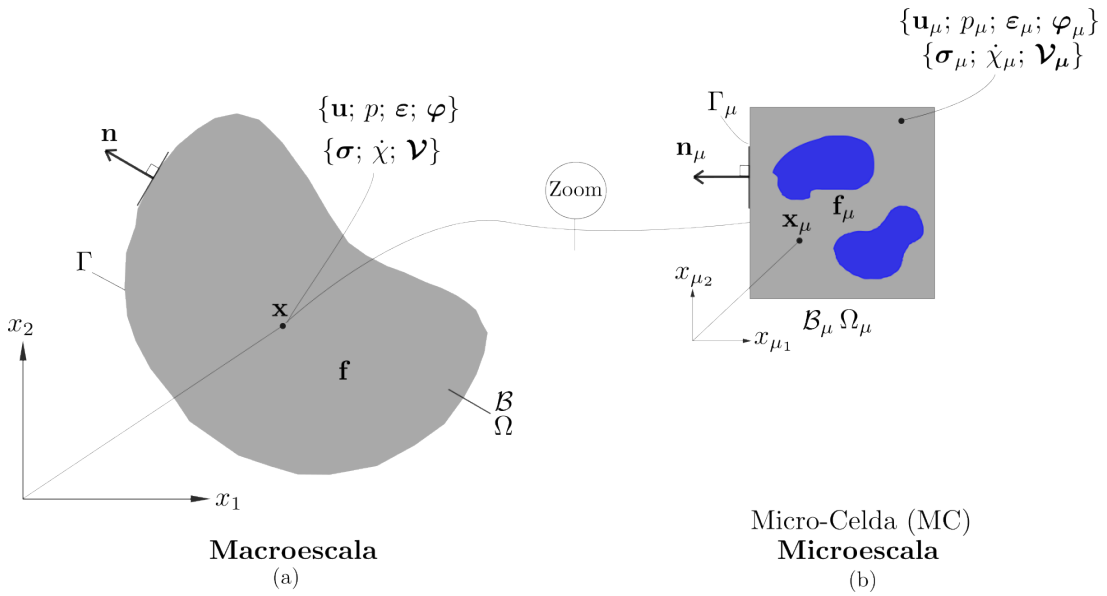

Figura 2.3: Ingredientes básicos de un modelo multiescala basado en el concepto RVE.

Siguiendo con los lineamientos del MMVP es necesario implementar el principio de admisibilidad para una adecuada transferencia de información. Esto permite definir el concepto de admisibilidad que hace compatibles los descriptores primitivos entre las dos escalas implicadas. En el presente desarrollo, estos son los campos de desplazamientos, poropresiones y sus gradientes correspondientes. Seguidamente, se exhibe el principio de admisibilidad con los respectivos procesos de inserción y homogeneización.

2.4.2. Principio de admisibilidad de los descriptores primitivos

2.4.2.1. Inserción en la microescala

Diversos trabajos citados en la primera parte de está sección consideran que, dentro de cada MC, la solución a escala fina se divide en una parte suavizada y otra fluctuante (Larsson et al. [14], Su et al. [48], Jänicke et al. [49] y Ekre et al. [50]). En estos enfoques, el vínculo entre las escalas se establece a partir de la solución suavizada dentro de cada MC, lo cual representa los descriptores primitivos correspondientes a la macroescala. Además, se asume que las propiedades homogeneizadas se definen explícitamente mediante una suposición adecuada sobre la suavidad de dicha solución. En general, se adopta lo que se denomina homogeneización de primer orden, es decir, se supone que la parte suavizada varía linealmente dentro de la MC, incluyendo derivadas hasta el primer orden. Está técnica de homogeneización de primer orden ha sido tambien la empleada por la mayoría de los autores anteriormente mencionados (Khoei y Hajiabadi [16], Khoei y Saeedmonir [51], Khoei et al. [53], Saeedmonir y Khoei [52], Saeedmonir et al. [54], Lopez Rivarola et al. [18], Ricken et al. [55] y Klahr et al. [56]), con excepción de los enfoques de segundo orden propuestos (Thiesen et al. [57, 58]).

Siguiendo los lineamientos del MMVP, los desarrollos posteriores se formulan siguiendo la propuesta de inserción (Sánchez et al. [22], Toro et al. [23], Toro et al. [24], Blanco et al. [27], Taroco et al. [20]), la cual establece como los descriptores primarios de la macroescala son insertados en el dominio de la MC, desempeñando posteriormente un papel fundamental en el problema de balance hidromecánico de

la microescala.

A partir de la inserción de las cantidades evaluadas en puntos $\mathbf{x}$ de la macroescala, $\{\mathbf{u}(t), \boldsymbol{\nabla}\mathbf{u}(t)\}$, se construye el desplazamiento en la microescala, $\mathbf{u}_\mu(\mathbf{x}_\mu, t)$, basado en una regla de expansión de tipo Taylor que permite definir

$$\mathbf{u}_\mu(\mathbf{x}_\mu, t) = \mathbf{u}(t) + \boldsymbol{\nabla}\mathbf{u}(t)\left(\mathbf{x}_\mu - \mathbf{x}_\mu^G\right) + \tilde{\mathbf{u}}_\mu(\mathbf{x}_\mu, t), \quad \forall \mathbf{x}_\mu \in \Omega_\mu, \tag{2.15}$$

donde $\tilde{\mathbf{u}}_\mu(\mathbf{x}_\mu, t)$ es el campo de los desplazamientos fluctuantes en el dominio de la MC y $\mathbf{x}_\mu^G$ es un vector constante que se definirá más adelante. No obstante, para la descripción cinemática de la formulación multiescala se adopta exclusivamente la parte simétrica del gradiente de desplazamientos, en consonancia con las expresiones de potencia total (véase (2.9)) y con el PMVP propuesto más adelante (véase (2.41)). De esta manera se reescribe (2.15) como

$$\mathbf{u}_\mu(\mathbf{x}_\mu, t) = \mathbf{u}(t) + \boldsymbol{\varepsilon}(t)\left(\mathbf{x}_\mu - \mathbf{x}_\mu^G\right) + \tilde{\mathbf{u}}_\mu(\mathbf{x}_\mu, t), \quad \forall \mathbf{x}_\mu \in \Omega_\mu, \tag{2.16}$$

A partir de la expresión (2.16), el tensor de deformación infinitesimal de la microescala, $\boldsymbol{\varepsilon}_\mu(\mathbf{x}_\mu, t)$, se expresa de la siguiente manera

$$\boldsymbol{\varepsilon}_\mu(\mathbf{x}_\mu, t) = \boldsymbol{\nabla}^{sym}_{\mathbf{x}_\mu}\mathbf{u}_\mu(\mathbf{x}_\mu, t) = \boldsymbol{\varepsilon}(t) + \boldsymbol{\nabla}^{sym}_{\mathbf{x}_\mu}\tilde{\mathbf{u}}_\mu(\mathbf{x}_\mu, t) = \boldsymbol{\varepsilon}(t) + \tilde{\boldsymbol{\varepsilon}}_\mu(\mathbf{x}_\mu, t), \quad \forall \mathbf{x}_\mu \in \Omega_\mu, \tag{2.17}$$

donde el operador $\boldsymbol{\nabla}^{sym}_{\mathbf{x}_\mu}(\bullet)$ representa el gradiente simétrico con respecto a la coordenada $\mathbf{x}_\mu$.

El campo de deformación en (2.17) se compone de la suma de la deformación a macroescala, $\boldsymbol{\varepsilon}(t)$, que se supone distribuida uniformemente por todo el dominio Ω_μ, y el componente de fluctuación de la deformación a microescala $\tilde{\boldsymbol{\varepsilon}}_\mu(\mathbf{x}_\mu, t)$, condición ampliamente difundida en la bibliografía (de Souza Neto y Feijóo [12], de Souza Neto et al. [26]).

Por otra parte, resulta evidente que el campo de poropresiones juega en el presente trabajo el rol de variable primaria, conforme a las ecuaciones desarrolladas en la Sección 2.3 que describen el comportamiento poromecánico del medio poroso saturado. En términos generales, la mayoría de los trabajos citados consideran a la poropresión como descriptor primario en ambas escalas, con excepción de Lopez Rivarola et al. [18], quienes adoptaron como variable primaria a la porosidad en la formulación multiescala de materiales termo-poroplásticos. Siguiendo un razonamiento análogo al empleado con los desplazamientos en la microescala, esto es, expandir conforme a una serie de tipo Taylor, el campo microescala de poropresiones puede expandirse en términos de las cantidades valoradas en puntos $\mathbf{x}$ de la macroescala $\{p(t), \boldsymbol{\varphi}(t)\}$ como

$$p_\mu(\mathbf{x}_\mu, t) = p(t) + \boldsymbol{\varphi}(t) \cdot \left(\mathbf{x}_\mu - \mathbf{x}_\mu^G\right) + \tilde{p}_\mu(\mathbf{x}_\mu, t), \quad \forall \mathbf{x}_\mu \in \Omega_\mu, \tag{2.18}$$

siendo $\tilde{p}_\mu(\mathbf{x}_\mu, t)$ el campo de poropresiones fluctuantes en la MC.

Finalmente, de acuerdo a la expresión (2.18), el gradiente de las poropresiones de la microescala $\boldsymbol{\varphi}_\mu(\mathbf{x}_\mu, t)$, se obtiene como resultado de aplicar el operador $\boldsymbol{\nabla}_{\mathbf{x}_\mu}(\bullet)$ sobre el campo fluctuante de poropresiones, $p_\mu(\mathbf{x}_\mu, t)$, para obtener

$$\boldsymbol{\varphi}_\mu(\mathbf{x}_\mu, t) = \boldsymbol{\nabla}_{\mathbf{x}_\mu} p_\mu(\mathbf{x}_\mu, t) = \boldsymbol{\varphi}(t) + \boldsymbol{\nabla}_{\mathbf{x}_\mu}\tilde{p}_\mu(\mathbf{x}_\mu, t) = \boldsymbol{\varphi}(t) + \tilde{\boldsymbol{\varphi}}_\mu(\mathbf{x}_\mu, t), \quad \forall \mathbf{x}_\mu \in \Omega_\mu, \tag{2.19}$$

donde el gradiente $\boldsymbol{\nabla}_{\mathbf{x}_\mu}(\bullet)$ se relaciona con el sistema de coordenadas $\mathbf{x}_\mu$ de la microescala.

Es importante señalar que, conforme al enfoque de primer orden adoptado en la macroescala, los descriptores primarios evaluados en puntos macroscópicos $\{\mathbf{u}(t), \boldsymbol{\varepsilon}(t)\}$ y $\{p(t), \boldsymbol{\varphi}(t)\}$, se transfieren al dominio de la MC mediante distribuciones uniformes y lineales, como se refleja en los dos primeros términos de las expresiones (2.16) y (2.18), respectivamente. Este supuesto corresponde al esquema de homogeneización de primer orden, ampliamente empleado en la literatura. Por otro lado, la tercera

contribución en (2.16) y (2.18) representa la fluctuación de los campos primarios en la microescala, constituyendo un término adicional que solo emerge en la escala fina y cuya finalidad es capturar las heterogeneidades del material en el modelado multiescala.

2.4.2.2. Homogeneización en la microescala

El segundo proceso contemplado en el principio de admisibilidad consiste en postular los operadores de homogeneización de los descriptores primitivos de la microescala, los cuales deben asumirse al diseñar un modelo basado en RVE de acuerdo con la naturaleza física del problema tratado. Estos operadores definen cómo se promedian los campos microscópicos para obtener los valores puntuales de las variables macroescala correspondientes (Sánchez et al. [22], Blanco et al. [27], Taroco et al. [20]). En el actual escenario de los medios porosos saturados se definen cuatro procedimientos de homogeneización. El primer grupo incluye los operadores de homogeneización cinemática $\mathcal{H}_{\mathbf{u}}$ y $\mathcal{H}_{\boldsymbol{\varepsilon}}$, que determinan la correspondencia entre los descriptores microescala de desplazamientos $\mathbf{u}_\mu$ y deformaciones $\boldsymbol{\varepsilon}_\mu$ con los valores puntuales macroscópicos del desplazamiento $\mathbf{u}$ y la deformación $\boldsymbol{\varepsilon}$, respectivamente. El segundo grupo, $\mathcal{H}_p$ y $\mathcal{H}_{\boldsymbol{\varphi}}$, establece un procedimiento análogo para los campos microscópicos de poropresiones p_μ y su gradiente $\boldsymbol{\varphi}_\mu$ vinculándolos con sus contrapartes macroscópicas p y $\boldsymbol{\varphi}$, respectivamente. A continuación, se exponen cada uno de ellos de forma ordenada.

Homogeneización del desplazamiento

El operador de homogeneización del desplazamiento, simbolizado como $\mathcal{H}_{\mathbf{u}}$, establece que el promedio del campo de los desplazamientos de la MC debe ser igual al campo de los desplazamientos evaluados en un punto de la macroescala. Esto se formula como

$$\mathcal{H}_{\mathbf{u}}\left(\mathbf{u}_\mu\right) = \mathbf{u} = \frac{1}{|\Omega_\mu|}\int_{\Omega_\mu} \mathbf{u}_\mu \, d\Omega_\mu. \tag{2.20}$$

Desarrollando la ecuación (2.20) al sustituir la expansíon de los desplazamientos de la escala menor definidos en (2.16), se obtiene

$$\mathbf{u} = \mathbf{u} + \boldsymbol{\varepsilon}\left[\frac{1}{|\Omega_\mu|}\int_{\Omega_\mu}\left(\mathbf{x}_\mu - \mathbf{x}_\mu^G\right)\, d\Omega_\mu\right] + \frac{1}{|\Omega_\mu|}\int_{\Omega_\mu} \tilde{\mathbf{u}}_\mu \, d\Omega_\mu. \tag{2.21}$$

Dado que la igualdad de la expresión (2.21) debe cumplirse incluso para un campo de desplazamiento fluctuante homogéneo de la microescala, es decir, al asumir $\tilde{\mathbf{u}}_\mu = \mathbf{0}\ \forall \mathbf{x}_\mu \in \Omega_\mu$, se llega a la definición del vector constante

$$\mathbf{x}_\mu^G = \frac{1}{|\Omega_\mu|}\int_{\Omega_\mu} \mathbf{x}_\mu \, d\Omega_\mu, \tag{2.22}$$

que identifica la posición del centroide de la MC, de dominio Ω_μ, con respecto al sistema de coordenadas global en la microescala. Al reemplazar en (2.21) el vector $\mathbf{x}_\mu^G$ por su definición de (2.22) se deriva la primera restricción cinemática a ser impuesta en la escala microscópica, la cual es la responsable de impedir las traslaciones de cuerpo rígido, y se expresa como

$$\int_{\Omega_\mu} \tilde{\mathbf{u}}_\mu \, d\Omega_\mu = \mathbf{0}. \tag{2.23}$$

Homogeneización de las deformaciones

La regla de homogeneización para el campo de deformación en la microescala resulta en

$$\mathcal{H}_{\boldsymbol{\varepsilon}}\left(\boldsymbol{\varepsilon}_\mu\right) = \boldsymbol{\varepsilon} = \frac{1}{|\Omega_\mu|}\int_{\Omega_\mu} \boldsymbol{\varepsilon}_\mu \, d\Omega_\mu \tag{2.24}$$

Al sustituir en (2.24) la expansión de las deformaciones infinitesimales de la escala microscópica dada por la expresión (2.17) y aplicando el teorema de Green, se obtiene la segunda condición de restricción cinemática

$$\int_{\Gamma_\mu} \tilde{\mathbf{u}}_\mu \otimes^{sym} \mathbf{n}_\mu \, d\Gamma_\mu = \mathbb{O}, \tag{2.25}$$

donde el operador $\otimes^{sym}$ simboliza el producto diádico externo simétrico, mientras que $\mathbb{O}$ representa el tensor nulo de segundo orden. Obsérvese que, conforme a la expresión (2.25), es posible que los campos cinemáticos a microescala no se controlen adecuadamente. Es decir, dicha restricción limitada al producto diádico simétrico no fija el grado de libertad asociado a la rotación. En tales casos, se requieren restricciones adicionales sobre $\tilde{\mathbf{u}}_\mu$ para garantizar la correcta colocación matemática del problema a microescala. Conforme a Blanco et al. [19], dichas restricciones adicionales deben ser homogéneas y depender de las hipótesis de modelización basadas en consideraciones físicas para el problema a escala microscópica.

En el presente trabajo, con el fin de excluir cualquier posibilidad de movimiento rígido, se adopta la siguiente expresión

$$\int_{\Gamma_\mu} \tilde{\mathbf{u}}_\mu \otimes \mathbf{n}_\mu \, d\Gamma_\mu = \mathbb{O}, \tag{2.26}$$

es decir, considerando el producto diádico externo $\otimes$ no limitado a la parte simétrica, se incorpora la restricción adicional que excluye la rotación y garantiza una formulación adecuada del problema cinemático microescala, preservando el hecho de ser compatible con (2.24)[1].

Homogeneización de las poropresiones

El proceso de homogeneización $\mathcal{H}_p$ que vincula el campo de poropresiones entre las escalas, se obtiene a partir del promedio de las poropresiones microscópicas. Dicho procedimiento se efectúa de la siguiente manera

$$\mathcal{H}_p\left(p_\mu\right) = p = \frac{1}{|\Omega_\mu|} \int_{\Omega_\mu} p_\mu \, d\Omega_\mu. \tag{2.27}$$

Introduciendo la expansión de las poropresiones de la microescala según la expresión (2.18) y luego el vector coordenada baricéntrica de la MC definido en (2.22), se arriba a la primera restricción requerida para el campo de las poropresiones fluctuantes, y que debe ser satisfecha en todo el volumen. Tal condición se especifica conforme a la siguiente ecuación

$$\int_{\Omega_\mu} \tilde{p}_\mu \, d\Omega_\mu = 0. \tag{2.28}$$

Homogeneización del gradiente de poropresiones

Finalmente, la regla de homogeneización para el gradiente de las poropresiones de la microescala se postula como

$$\mathcal{H}_{\boldsymbol{\varphi}}\left(\boldsymbol{\varphi}_\mu\right) = \boldsymbol{\varphi} = \frac{1}{|\Omega_\mu|} \int_{\Omega_\mu} \boldsymbol{\varphi}_\mu \, d\Omega_\mu, \tag{2.29}$$

la cual, al sustituir (2.19) y desenvolver conforme al teorema de Green, conduce a la obtención de una restricción adicional sobre el campo de poropresiones fluctuantes en el dominio de la microescala, formulada como

$$\int_{\Gamma_\mu} \tilde{p}_\mu \, \mathbf{n}_\mu \, d\Gamma_\mu = \mathbf{0}. \tag{2.30}$$

[1] La ecuación (2.26) se deriva de forma natural en el caso de controlar completamente el gradiente de los desplazamientos macroscópico.

2.4.2.3. Espacios de las variables admisibles de la microescala

Anteriormente, partiendo de los postulados propuestos para las reglas de homogeneización se han establecido todas las restricciones que se deben imponer a los campos de desplazamiento y poropresiones fluctuantes, tal como se puede ver en las expresiones (2.23), (2.26), (2.28) y (2.30). Solo los campos $\tilde{\mathbf{u}}_\mu$ y $\tilde{p}_\mu$, que satisfacen todas estas restricciones pueden considerarse admisibles, es decir, compatibles con los procedimientos de homogeneización adoptados en (2.20), (2.24), (2.27) y (2.29).

En este punto, es posible introducir los espacios vectoriales funcionales para los campos fluctuantes $\tilde{\mathbf{u}}_\mu$ y $\tilde{p}_\mu$, que definen el reconocido Modelo Multiescala de Mínimas Restricciones (MCMM) (de Souza Neto y Feijóo [12], Blanco et al. [19, 21]).

$$\widetilde{\mathcal{U}}_\mu\left(\Omega_\mu\right)=\left\{\tilde{\mathbf{u}}_\mu\ \in\ \mathbf{H}^1\left(\Omega_\mu\right);\ \int_{\Omega_\mu}\tilde{\mathbf{u}}_\mu\, d\Omega_\mu=\mathbf{0};\ \int_{\Gamma_\mu}\tilde{\mathbf{u}}_\mu\ \otimes\ \mathbf{n}_\mu\, d\Gamma_\mu=\mathbb{O}\right\},\tag{2.31}$$

$$\widetilde{\mathcal{P}}_\mu\left(\Omega_\mu\right)=\left\{\tilde{p}_\mu\ \in\ \mathrm{H}^1\left(\Omega_\mu\right);\ \int_{\Omega_\mu}\tilde{p}_\mu\, d\Omega_\mu=0;\ \int_{\Gamma_\mu}\tilde{p}_\mu\ \mathbf{n}_\mu\, d\Gamma_\mu=\mathbf{0}\right\}.\tag{2.32}$$

Estos espacios, tal como su nombre lo indica, contienen las mínimas restricciones requeridas en el nivel de la microescala para garantizar admisibilidad. Se podría, por lo general, asumir subespacios contenidos dentro del espacio de mínima restricciones que conduzcan a esquemas de homogeneización alternativos, los cuales se denotan como $\widetilde{\mathcal{U}}_\mu^{\square}\left(\Omega_\mu\right)\subseteq\widetilde{\mathcal{U}}_\mu\left(\Omega_\mu\right)$ y $\widetilde{\mathcal{P}}_\mu^{\square}\left(\Omega_\mu\right)\subseteq\widetilde{\mathcal{P}}_\mu\left(\Omega_\mu\right)$. De este modo, generalmente se trabaja con campos fluctuantes que pertenecen a estos subespacios construidos de manera apropiada, esto es, $\tilde{\mathbf{u}}_\mu\in\widetilde{\mathcal{U}}_\mu^{\square}\left(\Omega_\mu\right)$ y $\tilde{p}_\mu\in\widetilde{\mathcal{P}}_\mu^{\square}\left(\Omega_\mu\right)$. Claramente, estos modelos son más restrictivos para los campos $\tilde{\mathbf{u}}_\mu$ y $\tilde{p}_\mu$ que el MCMM. Entre los submodelos más utilizados y difundidos destacan los de Taylor, el Lineal y el Periódico, pero también es posible proponer cualquier otro submodelo multiescala con condiciones de contorno alternativas y más elaboradas, algunas de las cuales se mencionan en el Capítulo 5.

Partiendo de las expresiones (2.16)-(2.19), se definen las acciones virtuales en el dominio de la MC como

$$\delta\mathbf{u}_\mu=\delta\mathbf{u}+\delta\boldsymbol{\varepsilon}\left(\mathbf{x}_\mu-\mathbf{x}_\mu^G\right)+\delta\tilde{\mathbf{u}}_\mu,\quad\forall\mathbf{x}_\mu\in\Omega_\mu,\tag{2.33}$$

$$\delta\boldsymbol{\varepsilon}_\mu=\delta\boldsymbol{\varepsilon}+\delta\tilde{\boldsymbol{\varepsilon}}_\mu=\delta\boldsymbol{\varepsilon}+\boldsymbol{\nabla}_{\mathbf{x}_\mu}^{sym}\delta\tilde{\mathbf{u}}_\mu,\quad\forall\mathbf{x}_\mu\in\Omega_\mu,\tag{2.34}$$

$$\delta p_\mu=\delta p+\delta\boldsymbol{\varphi}\cdot\left(\mathbf{x}_\mu-\mathbf{x}_\mu^G\right)+\delta\tilde{p}_\mu,\quad\forall\mathbf{x}_\mu\in\Omega_\mu,\tag{2.35}$$

$$\delta\boldsymbol{\varphi}_\mu=\delta\boldsymbol{\varphi}+\delta\tilde{\boldsymbol{\varphi}}_\mu=\delta\boldsymbol{\varphi}+\boldsymbol{\nabla}_{\mathbf{x}_\mu}\delta\tilde{p}_\mu,\quad\forall\mathbf{x}_\mu\in\Omega_\mu.\tag{2.36}$$

Finalmente, se fijan los espacios de variaciones virtuales fluctuantes admisibles

$$\widetilde{\mathcal{U}}_\mu^*\left(\Omega_\mu\right)=\left\{\delta\tilde{\mathbf{u}}_\mu\ \in\ \mathbf{H}^1\left(\Omega_\mu\right);\ \int_{\Omega_\mu}\delta\tilde{\mathbf{u}}_\mu\, d\Omega_\mu=\mathbf{0};\ \int_{\Gamma_\mu}\delta\tilde{\mathbf{u}}_\mu\ \otimes\ \mathbf{n}_\mu\, d\Gamma_\mu=\mathbb{O}\right\},\tag{2.37}$$

$$\widetilde{\mathcal{P}}_\mu^*\left(\Omega_\mu\right)=\left\{\delta\tilde{p}_\mu\ \in\ \mathrm{H}^1\left(\Omega_\mu\right);\ \int_{\Omega_\mu}\delta\tilde{p}_\mu\, d\Omega_\mu=0;\ \int_{\Gamma_\mu}\delta\tilde{p}_\mu\ \mathbf{n}_\mu\, d\Gamma_\mu=\mathbf{0}\right\},\tag{2.38}$$

siendo $\delta\tilde{\mathbf{u}}_\mu\in\widetilde{\mathcal{U}}_\mu^*\left(\Omega_\mu\right)$ y $\delta\tilde{p}_\mu\in\widetilde{\mathcal{P}}_\mu^*\left(\Omega_\mu\right)$. Los espacios $\widetilde{\mathcal{U}}_\mu^*\equiv\widetilde{\mathcal{U}}_\mu$ y $\widetilde{\mathcal{P}}_\mu^*\left(\Omega_\mu\right)\equiv\widetilde{\mathcal{P}}_\mu$ coinciden a causa de que las restricciones de los campos fluctuantes de la microescala son todas homogéneas, como se ve en las expresiones (2.23), (2.26), (2.28) y (2.30).

Todas las definiciones presentadas a lo largo de la Sub-sección (2.4.2), también son válidas en forma de tasas.

Habiendo precisado la admisibilidad entre las escalas para los descriptores primitivos, se presenta a continuación la ecuación que conduce a la admisibilidad energética.

2.4.3. Principio de Potencia Virtual Multiescala (PMVP)

En el ámbito del modelado multiescala de los medios porosos saturados, la condición de Hill-Mandel extendida ha sido ampliamente difundida e implementada (Larsson et al. [14], Khoei y Hajiabadi [16]). Sin embargo, en el presente trabajo se adopta una formulación análoga a tal condición, denominado como Principio de Potencia Virtual Multiescala (PMVP) presentado en la Sección 2.2, el cual se enmarca dentro del enfoque del MMVP (Blanco et al. [19], Taroco et al. [20], de Souza Neto et al. [26]).

Para enunciar el PMVP, es necesario especificar los conceptos de potencias virtuales totales que intervienen durante el proceso de transición entre las escalas. En este punto, se retoma la definición de potencia virtual total por unidad de volumen a nivel macroscópico, de acuerdo a los términos contenidos en la primera integral del lado derecho de la ecuación (2.9). De esta forma, se postula que la potencia virtual total, $\delta\mathcal{P}^{tot}$, ejercida en un punto $\mathbf{x}$ de la macroescala y vinculada al dominio correspondiente de la microescala de tamaño $|\Omega_\mu|$, puede escribirse como

$$\delta\mathcal{P}^{tot}\left(\delta\dot{\mathbf{u}}, \delta\dot{\boldsymbol{\varepsilon}}, \delta p, \delta\boldsymbol{\varphi}\right) = |\Omega_\mu| \left[\boldsymbol{\sigma} \,:\, \delta\dot{\boldsymbol{\varepsilon}} + \dot{\chi}\,\delta p - \boldsymbol{\mathcal{V}} \cdot \delta\dot{\boldsymbol{\varphi}} - \mathbf{f} \cdot \delta\dot{\mathbf{u}}\right]. \tag{2.39}$$

Análogamente, se asume la misma estructura matemática indicada en la primera integral del lado derecho de la expresión (2.9), con el propósito de disponer de la potencia virtual total que corresponde al dominio de la microescala Ω_μ, la cual se expresa como sigue

$$\delta\mathcal{P}^{tot}_\mu\left(\delta\dot{\mathbf{u}}_\mu, \delta\dot{\boldsymbol{\varepsilon}}_\mu, \delta p_\mu, \delta\boldsymbol{\varphi}_\mu\right) = \int_{\Omega_\mu} \left(\boldsymbol{\sigma}_\mu \,:\, \delta\dot{\boldsymbol{\varepsilon}}_\mu + \dot{\chi}_\mu\,\delta p_\mu - \boldsymbol{\mathcal{V}}_\mu \cdot \delta\boldsymbol{\varphi}_\mu - \mathbf{f}_\mu \cdot \delta\dot{\mathbf{u}}_\mu\right) d\Omega_\mu. \tag{2.40}$$

En (2.40), se ha introducido el campo de fuerza de cuerpo de la microescala, definido como $\mathbf{f}_\mu = \rho_\mu\,\mathbf{g}$. De acuerdo con la teoría de la poromecánica expuesta en la Sección 2.3, dicha componente representa el peso por unidad de volumen del medio poroso saturado. Por su parte, la densidad del medio en la microescala se formula como $\rho_\mu = \rho^f_\mu n_\mu + \rho^s_\mu\,(1 - n_\mu)$, donde los parámetros materiales ρ^f_μ, n_μ y ρ^s_μ, previamente definidos, se particularizan al contexto del nivel microscópico.

El PMVP establece que, para todas las acciones virtuales admisibles, la potencia virtual total de la macroescala, en un punto $\mathbf{x}$, debe ser igual a la potencia virtual total de la microescala en la MC correspondiente. Así, relacionando (2.39) y (2.40) e introduciendo las definiciones (2.33)-(2.36), se llega a la siguiente ecuación variacional

$$\begin{aligned}
|\Omega_\mu| \left(\boldsymbol{\sigma} \,:\, \delta\dot{\boldsymbol{\varepsilon}} - \mathbf{f} \cdot \delta\dot{\mathbf{u}} + \dot{\chi}\,\delta p - \boldsymbol{\mathcal{V}} \cdot \delta\boldsymbol{\varphi}\right) = \int_{\Omega_\mu} \Big[& \boldsymbol{\sigma}_\mu \,:\, \left(\delta\dot{\boldsymbol{\varepsilon}} + \boldsymbol{\nabla}^{sym}_{\mathbf{x}_\mu}\,\delta\dot{\tilde{\mathbf{u}}}_\mu\right) \\
& - \mathbf{f}_\mu \cdot \left(\delta\dot{\mathbf{u}} + \delta\dot{\boldsymbol{\varepsilon}}\,\left(\mathbf{x}_\mu - \mathbf{x}^G_\mu\right) + \delta\dot{\tilde{\mathbf{u}}}_\mu\right) \\
& + \dot{\chi}_\mu \left(\delta p + \delta\boldsymbol{\varphi} \cdot \left(\mathbf{x}_\mu - \mathbf{x}^G_\mu\right) + \delta\tilde{p}_\mu\right) - \boldsymbol{\mathcal{V}}_\mu \cdot \left(\delta\boldsymbol{\varphi} + \boldsymbol{\nabla}_{\mathbf{x}_\mu}\,\delta\tilde{p}_\mu\right) \Big]\, d\Omega_\mu, \\
\forall\, \left(\delta\dot{\boldsymbol{\varepsilon}}\,, \delta\dot{\mathbf{u}}\,, \delta\boldsymbol{\varphi}\,, \delta p\right) \in \mathbb{R}^6 \times \mathbb{R}^3 \times \mathbb{R}^3 \times \mathbb{R},\ & \left(\delta\dot{\tilde{\mathbf{u}}}_\mu\,, \delta\tilde{p}_\mu\right) \in \widetilde{\mathcal{U}}^*_\mu\left(\Omega_\mu\right) \times \widetilde{\mathcal{P}}^*_\mu\left(\Omega_\mu\right),\ \forall\, t.
\end{aligned} \tag{2.41}$$

Una vez colocado el marco formal teórico, es posible obtener las implicancias derivadas del modelo, en particular la identificación de las variables matemáticas duales y la formulación de las ecuaciones de balance de la microescala.

2.4.4. Consecuencias de implementar el MMVP

Recurriendo a simples argumentos del calculo variacional sobre la ecuación (2.41), se obtienen de forma natural las consecuencias de la aplicación conjunta del principio de admisibilidad y el PMVP. Tales implicancias son: (i) las fórmulas de homogeneización para las cantidades duales del tipo tensión $\{\boldsymbol{\sigma}; \dot{\chi}; \boldsymbol{\mathcal{V}}\}$ y fuerza de cuerpo macroscópica $\mathbf{f}$, y (ii) las formas variacionales de las ecuaciones de balance

en la escala de longitud menor. A continuación, se presentan en primer lugar las entidades homogeneizadas y posteriormente las ecuaciones de balance correspondientes a la escala microscópica.

2.4.4.1. Variables duales homogeneizadas

Tensor de tensiones homogeneizado:

$$\boldsymbol{\sigma} = \frac{1}{|\Omega_\mu|}\int_{\Omega_\mu}\left[\boldsymbol{\sigma}_\mu - \mathbf{f}_\mu \otimes^{sym} \left(\mathbf{x}_\mu - \mathbf{x}_\mu^G\right)\right] d\Omega_\mu,\ \forall\, t. \tag{2.42}$$

Lo cual se consigue a partir de (2.41), tomando $\delta\dot{\tilde{\mathbf{u}}}_\mu = \mathbf{0},\ \delta p = 0,\ \delta\tilde{p}_\mu = 0,\ \delta\boldsymbol{\varphi} = \mathbf{0}, \delta\dot{\mathbf{u}} = \mathbf{0}$ y permitiendo variaciones arbitrarias de $\delta\dot{\boldsymbol{\varepsilon}}$.

Tasa de volumen de poros homogeneizada (por unidad de volumen de poros):

$$\dot{\chi} = \frac{\dot{m}^f}{\rho^f} = \frac{1}{|\Omega_\mu|}\int_{\Omega_\mu}\dot{\chi}_\mu\, d\Omega_\mu,\ \forall\, t. \tag{2.43}$$

Derivada por admitir, en (2.41), variaciones arbitrarias de δp y adoptar $\delta\dot{\boldsymbol{\varepsilon}} = \mathbf{0},\ \delta\dot{\tilde{\mathbf{u}}}_\mu = \mathbf{0},\ \delta\tilde{p}_\mu = 0,\ \delta\dot{\mathbf{u}} = \mathbf{0}$ y $\delta\boldsymbol{\varphi} = \mathbf{0}$.

Si se supone que la densidad de masa del fluido ρ_μ^f es uniforme en todo el dominio de la MC, la fórmula homogeneizada para la tasa de contenido de masa del fluido, $\dot{m}^f$, se puede recuperar tras unas simples manipulaciones sobre (2.43)

$$\dot{m}^f = \frac{1}{|\Omega_\mu|}\int_{\Omega_\mu}\dot{m}_\mu^f\, d\Omega_\mu,\ \forall\, t. \tag{2.44}$$

Vector de velocidad del flujo homogeneizado:

$$\boldsymbol{\mathcal{V}} = \frac{1}{|\Omega_\mu|}\int_{\Omega_\mu}\left[\boldsymbol{\mathcal{V}}_\mu - \dot{\chi}_\mu\, \left(\mathbf{x}_\mu - \mathbf{x}_\mu^G\right)\right] d\Omega_\mu,\ \forall\, t. \tag{2.45}$$

La cual se deduce a partir de la ecuación (2.41), adoptando $\delta\dot{\boldsymbol{\varepsilon}} = \mathbf{0},\ \delta\dot{\tilde{\mathbf{u}}}_\mu = \mathbf{0},\ \delta p = 0,\ \delta\tilde{p}_\mu = 0,\ \delta\dot{\mathbf{u}} = \mathbf{0}$ con variaciones arbitrarias de $\delta\boldsymbol{\varphi}$.

Campo de fuerza de cuerpo homogeneizado:

$$\mathbf{f} = \frac{1}{|\Omega_\mu|}\int_{\Omega_\mu}\mathbf{f}_\mu\, d\Omega_\mu = \frac{\mathbf{g}}{|\Omega_\mu|}\int_{\Omega_\mu}\rho_\mu\, d\Omega_\mu,\ \forall\, t. \tag{2.46}$$

Se obtiene a partir de la ecuación (2.41), con $\delta\dot{\boldsymbol{\varepsilon}} = \mathbf{0},\ \delta\dot{\tilde{\mathbf{u}}}_\mu = \mathbf{0},\ \delta p = 0,\ \delta\tilde{p}_\mu = 0, \delta\boldsymbol{\varphi} = \mathbf{0}$ y variaciones arbitrarias de $\delta\dot{\mathbf{u}}$.

2.4.4.2. Formas variacionales de balance en la microescala

Forma variacional de la ecuación de balance de cantidad de movimiento en la MC:

$$\mathrm{G}_\mu = \int_{\Omega_\mu}\left(\boldsymbol{\sigma}_\mu : \boldsymbol{\nabla}_{\mathbf{x}_\mu}^{sym}\,\delta\dot{\tilde{\mathbf{u}}}_\mu - \mathbf{f}_\mu \cdot \delta\dot{\tilde{\mathbf{u}}}_\mu\right) d\Omega_\mu = 0,\ \ \forall\,\delta\dot{\tilde{\mathbf{u}}}_\mu \in \widetilde{\mathcal{U}}_\mu^*\left(\Omega_\mu\right),\ \forall\, t. \tag{2.47}$$

La ecuación (2.47) se deriva de las variaciones cinemáticamente admisibles de $\delta\dot{\tilde{\mathbf{u}}}_\mu$ en la ecuación (2.41), donde, a su vez se asume $\delta\dot{\boldsymbol{\varepsilon}} = \mathbf{0},\ \delta p = 0,\ \delta\tilde{p}_\mu = 0,\ \delta\boldsymbol{\varphi} = \mathbf{0}$ y $\delta\dot{\mathbf{u}} = \mathbf{0}$.

Forma variacional de la ecuación de balance de masas en la MC:

$$\mathrm{H}_\mu = \int_{\Omega_\mu} \left(\dot{\chi}_\mu \, \delta\tilde{p}_\mu - \boldsymbol{\mathcal{V}}_\mu \cdot \boldsymbol{\nabla}_{\mathbf{x}_\mu} \delta\tilde{p}_\mu \right) \, d\Omega_\mu = 0, \;\; \forall \, \delta\tilde{p}_\mu \in \; \widetilde{\mathcal{P}}^*_\mu \left(\Omega_\mu \right), \; \forall \, t, \tag{2.48}$$

Se deduce de (2.41) al permitir variaciones admisibles de $\delta\tilde{p}_\mu$ con $\delta\dot{\boldsymbol{\varepsilon}} = \mathbf{0}$, $\delta\dot{\tilde{\mathbf{u}}}_\mu = \mathbf{0}$, $\delta p = 0$, $\delta\dot{\mathbf{u}} = \mathbf{0}$ y $\delta\boldsymbol{\varphi} = \mathbf{0}$.

2.4.5. Ecuaciones constitutivas de la microescala y comentarios finales

En este punto queda por introducir los funcionales que describen las leyes constitutivas del material que se asume para la MC. Cada componente del dominio a microescala es un medio poroso saturado; por lo tanto, se requieren relaciones constitutivas para el vector de velocidad de filtración $\boldsymbol{\mathcal{V}}_\mu$, así como para las magnitudes mecánicas del tipo tensión $\{\boldsymbol{\sigma}_\mu; \dot{\chi}_\mu\}$. A lo largo de este manuscrito se asumen las formas más simples para estas leyes constitutivas.

De esta manera, con respecto al fenómeno de filtración en la microescala, se asume que la siguiente ley generalizada de Darcy caracteriza el vector de velocidad (media) del fluido en el medio poroso saturado.

$$\boldsymbol{\mathcal{V}}_\mu = \hat{\mathcal{V}}_\mu(\boldsymbol{\varphi}_\mu) = \mathbf{k}_\mu \Big[- \boldsymbol{\varphi}_\mu + \rho^f_\mu \, \mathbf{g} \Big], \tag{2.49}$$

donde $\mathbf{k}_\mu$ es el tensor de permeabilidad simétrico de segundo orden y el símbolo del sombrero, $\hat{(\cdot)}$, denota un funcional constitutivo. En el caso de materiales isotrópicos saturados, resulta $\mathbf{k}_\mu = k_\mu \mathbf{I}$; $k_\mu = \frac{\kappa_\mu}{\rho^f_\mu \, |\mathbf{g}|}$ es la permeabilidad hidráulica, que es una función de la conductividad hidráulica κ_μ y del peso específico del fluido $\rho^f_\mu \, |\mathbf{g}|$, donde $|\mathbf{g}|$ es el módulo de la aceleración de la gravedad.

Para describir el comportamiento mecánico (isotérmico) de un medio poroso saturado se propone la misma estructura matemática según Coussy [36] (en el contexto de los modelos fenomenológicos). Por lo tanto, se tiene para $\{\boldsymbol{\sigma}_\mu; \dot{\chi}_\mu\}$

$$\dot{\boldsymbol{\sigma}}_\mu = \hat{\dot{\sigma}}_\mu(\dot{\boldsymbol{\varepsilon}}_\mu, \dot{p}_\mu) = \mathbf{C}_\mu \; : \; \dot{\boldsymbol{\varepsilon}}_\mu - \mathbf{b}_\mu \, \dot{p}_\mu, \tag{2.50}$$

$$\dot{\chi}_\mu = \hat{\dot{\chi}}_\mu(\dot{\boldsymbol{\varepsilon}}_\mu, \dot{p}_\mu) = \mathbf{b}_\mu \; : \; \dot{\boldsymbol{\varepsilon}}_\mu + \frac{1}{M_\mu} \, \dot{p}_\mu. \tag{2.51}$$

La respuesta hidromecánica del medio poroso en la microescala viene definida principalmente por el tensor de rigidez elástica del esqueleto $\mathbf{C}_\mu$, el tensor de Biot $\mathbf{b}_\mu$ y el coeficiente M_μ^{-1}. Para el caso particular de constituyentes isotrópicos, se tiene $\mathbf{b}_\mu = b_\mu \, \mathbf{I}$, donde el coeficiente de Biot $b_\mu = 1 - \frac{K_\mu}{K^s_\mu}$ viene dado por la relación entre el módulo de compresibilidad del esqueleto K_μ y el módulo volumétrico del material granulado K^s_μ. Finalmente, se tiene $\frac{1}{M_\mu} = \frac{b_\mu - n_\mu}{K^s_\mu} + \frac{n_\mu}{K^f_\mu}$, donde K^f_μ es el módulo de compresibilidad del fluido (Biot [31, 32]). Tenga en cuenta que, por conveniencia, las definiciones constitutivas relacionadas con $\dot{\boldsymbol{\sigma}}_\mu$ y $\dot{\chi}_\mu$ se consideran en formato de tasa.

Se remarca en este punto, la extrema importancia que reviste el modo en el que se propongan las expansiones de los descriptores primitivos $\boldsymbol{\varphi}_\mu$, $\dot{\boldsymbol{\varepsilon}}_\mu$ y $\dot{p}_\mu$ en los funcionales constitutivos (2.49), (2.50) y (2.51). La razón de ello es que las intervenciones efectuadas en las ecuaciones constitutivas constituyen la principal novedad respecto de la literatura existente sobre implementación multiescala abordando problemas hidromecánicos, y, por ende revisten particular relevancia en las publicaciones que conforman este manuscrito. Por esta razón, se tratará exclusivamente sobre este asunto en el Capítulo 3, el cual adquiere un carácter central en la presente tesis, con el fin de exponer apropiadamente los inconvenientes reportados en la bibliografía y presentar las propuestas originales desarrolladas en este trabajo.

2.5. Implementación numérica

Luego de presentados los desarrollos teóricos de las secciones 2.3 y 2.4, se procede con la implementación computacional de la formulación multiescala propuesta. Para abordar el problema multiescala en forma numérica desde una perspectiva global, el paradigma computacional básico puede concebirse como dos esquemas de elementos finitos anidados, acoplados en ambas direcciones (macro-micro) y que evolucionan en el tiempo. La conexión entre las escalas se establece en cada punto de Gauss o punto de integración de la macroescala. En la literatura, este enfoque recibe comúnmente el acrónimo de FE^2 (Feyel y Chaboche [5], Feyel [6]).

Para llevar a cabo la resolución numérica, resulta necesario efectuar la discretización tanto temporal como espacial. Cabe señalar que, en la teoría actual, tanto a nivel macroscópico como microscópico se comparte la misma escala temporal. De este modo, se expone a continuación las formulaciones referentes a la discretización del tiempo, t. Para el mismo, se propone una secuencia monótona creciente de intervalos de tiempo $[t^0, t^1, t^2, \ldots, t^n, t^{n+1}, \ldots]$, donde cualquier intervalo genérico se denota como $I_t = [t^n, t^{n+1}]$. Esto a su vez permite definir al incremento del paso de tiempo correspondiente al intervalo I_t como $\Delta t = t^{n+1} - t^n$. Con el fin de tomar en consideración la evolución del problema dentro de cualquier intervalo de tiempo I_t, se emplea la regla generalizada θ o regla trapezoidal generalizada (Lewis y Schrefler [41], Bathe [59], Hughes [60]). En esta metodología se asumen las siguientes aproximaciones para las variables primitivas y sus tasas

$$\begin{aligned} (\bullet)^{n+\theta} &= (1-\theta)\,(\bullet)^n + \theta\,(\bullet)^{n+1}, \\ \dot{(\bullet)}^{n+\theta} &= \frac{(\bullet)^{n+1} - (\bullet)^n}{t^{n+1} - t^n} = \frac{\Delta(\bullet)}{\Delta t}, \end{aligned} \tag{2.52}$$

donde θ es el parámetro de integración temporal el cual varia entre $[0, 1]$.

En lo que sigue se presentan los criterios de discretización espacial y los desarrollos propios de la implementación numérica, tratados en primera instancia para las ecuaciones de la escala macroscópica y, posteriormente, se continua con la microescala. En ambos casos, el propósito es únicamente exponer las estrategias de resolución adoptadas, por lo que, en caso de ser necesario profundizar sobre el tema, se recomienda al lector consultar bibliografía especializada. En particular, se mencionan los trabajos de Toro et al. [23] y Toro [61], donde se discute un procedimiento generalizado para imponer restricciones en un entorno multiescala, capaz de generar diferentes submodelos como también modificar las condiciones de borde durante el cálculo de forma muy simple y flexible, así como también el estudio de Perić et al. [62].

2.5.1. Implementación numérica en la macroescala

Con el fin de representar el dominio físico Ω de la macroescala, se emplea una discretización del espacio a través de una malla de elementos finitos, denotada por Ω_h. A partir de esta discretización, es posible definir matrices de interpolación globales asociadas a los campos de desplazamiento y poropresión, las cuales se construyen de la siguiente manera

$$\begin{aligned} \mathbf{u} &= \mathbf{N}_u\,\bar{\mathbf{u}}, \\ p &= \mathbf{N}_p\,\bar{\mathbf{p}}, \end{aligned} \tag{2.53}$$

donde $\bar{\mathbf{u}}$ y $\bar{\mathbf{p}}$ son los vectores que recogen todos los desplazamientos nodales y los valores de las poropresiones de los nodos, respectivamente.

Al tratar con medios porosos saturados, es posible modelar situaciones próximas al estado límite no drenado, en el cual tanto la matriz de permeabilidad como en muchos casos, la matriz de compresibilidad, se aproximan a cero (Zienkiewicz et al. [40]). En tales condiciones, existen limitaciones que

deben considerase para las funciones de aproximación $\mathbf{N}_u$ y $\mathbf{N}_p$, si se quiere satisfacer los requisitos de convergencia de Babuška-Brezzi (Babuška [63, 64], Brezzi [65]). Esto significa que es necesario adoptar diferentes órdenes de interpolación para cada variable primal (Lewis y Schrefler [41]). De esta manera, se propone para la implementación actual considerar elementos finitos cuadrangulares, isoparamétricos, bicuadráticos y bilineales para los campos de desplazamientos y poropresiones, respectivamente.

Siguiendo el método Galerkin, se adopta la misma aproximación espacial para las acciones virtuales que la utilizada en los campos primales, con lo cual es posible expresar dichas variables en términos de las mismas funciones de interpolación y expresar de la siguiente manera

$$\begin{aligned} \delta\dot{\mathbf{u}} &= \mathbf{N}_u\, \delta\dot{\bar{\mathbf{u}}}, \\ \delta p &= \mathbf{N}_p\, \delta\bar{\mathbf{p}}, \end{aligned} \tag{2.54}$$

siendo $\delta\dot{\bar{\mathbf{u}}}$ y $\delta\bar{\mathbf{p}}$ los vectores de las variaciones virtuales admisibles nodales para desplazamientos y poropresiones, respectivamente.

Sustituyendo ahora las expresiones de discretización temporal (2.52) y espacial (2.54) en las ecuaciones de balance de forma débil que gobiernan la macroescala, dadas por las ecuaciones (2.14), y tras realizar las manipulaciones estándar específicas del método de elementos finitos, se alcanza la versión discreta, tanto temporal como espacial, del balance para el paso de tiempo $t^{n+\theta}$, la que se escribe como

$$\begin{aligned} \dot{\mathbf{G}}_h^{n+\theta} &\equiv \int_{\Omega_h} \mathbf{B}_u^T\, \dot{\boldsymbol{\sigma}}^{n+\theta}\, d\Omega - \int_{\Omega_h} \mathbf{N}_u^T\, \dot{\mathbf{f}}^{n+\theta}\, d\Omega - \int_{\Gamma^u_{\mathrm{N},\,h}} \mathbf{N}_u^T\, \dot{\mathbf{t}}^{n+\theta}\, d\Gamma = \mathbf{0}, \\ \mathbf{H}_h^{n+\theta} &\equiv \int_{\Omega_h} \mathbf{N}_p^T\, \dot{\chi}^{n+\theta}\, d\Omega - \int_{\Omega_h} \mathbf{B}_p^T\, \boldsymbol{\mathcal{V}}^{n+\theta}\, d\Omega + \int_{\Gamma^p_{\mathrm{N},\,h}} \mathbf{N}_p^T\, \frac{q^{n+\theta}}{\rho^f}\, d\Gamma = \mathbf{0}. \end{aligned} \tag{2.55}$$

Siendo que $\mathbf{B}_u = \boldsymbol{\nabla}^{sym}\, \mathbf{N}_u$ es la matriz global de deformación-desplazamiento, $\mathbf{B}_p = \boldsymbol{\nabla}\, \mathbf{N}_p$ es la matriz global que relaciona las poropresiones con sus gradientes, $(\bullet)^T$ representa el operador transpuesto y $\Gamma^{(\bullet)}_{\mathrm{N},\,h}$ la versión discreta del borde de tipo Neumann. Cabe aclarar que, en la primera línea de (2.55), la ecuación de balance de cantidad de movimiento se ha considerado en forma de tasa (Lewis y Schrefler [41]).

A fin de resolver el sistema de ecuaciones (2.55) se utiliza el método estándar de Newton-Raphson, tal como lo han empleado diversos autores en el modelado multiescala de problemas hidromecánicos (Larsson et al. [14], Su et al. [48], Khoei y Hajiabadi [16], Klahr et al. [56]). Así, los valores nodales de los desplazamientos y poropresiones se actualizan en el paso de tiempo t^{n+1} en términos de los incrementos iterativos $\Delta\bar{\mathbf{u}}$ y $\Delta\bar{\mathbf{p}}$, respectivamente. Para una iteración k dada en el intervalo de tiempo I_t del esquema de Newton-Raphson, estos incrementos se evalúan de la siguiente manera

$$\begin{bmatrix} \Delta\bar{\mathbf{u}} \\ \Delta\bar{\mathbf{p}} \end{bmatrix} = -\left(\mathbf{J}_k^{n+\theta}\right)^{-1} \begin{bmatrix} \dot{\mathbf{G}}_k^{n+\theta} \\ \mathbf{H}_k^{n+\theta} \end{bmatrix}, \tag{2.56}$$

donde $\mathbf{J}_k^{n+\theta}$ es el operador lineal jacobiano de la macroescala. Se destaca además que, por simplicidad se ha omitido el subindice h que indica la discretización espacial. El jacobiano se calcula como sigue

$$\mathbf{J}_k^{n+\theta} = \begin{bmatrix} \frac{\partial \dot{\mathbf{G}}_k^{n+\theta}}{\partial \bar{\mathbf{u}}^{n+1}} & \frac{\partial \dot{\mathbf{G}}_k^{n+\theta}}{\partial \bar{\mathbf{p}}^{n+1}} \\ \frac{\partial \mathbf{H}_k^{n+\theta}}{\partial \bar{\mathbf{u}}^{n+1}} & \frac{\partial \mathbf{H}_k^{n+\theta}}{\partial \bar{\mathbf{p}}^{n+1}} \end{bmatrix}. \tag{2.57}$$

Cada una de las componentes de la matriz jacobiana a escala macroscópica debe ser determinada. Sin embargo, con lo desarrollado hasta la presente sección aún no es posible establecer la forma final de

dichos elementos, las cuales ya han sido caracterizados en contribuciones previas, tanto de otros autores como propias. Para obtener una vision más profunda del tema, se remite al lector al trabajo realizado por Khoei y Hajiabadi [16], así como a dos de las contribuciones que integran la tesis, Anonis et al. [66, 67], los cuales se incluyen en los Apéndices A y D, respectivamente.

2.5.2. Implementación numérica en la microescala

El espacio del dominio de la microescala Ω_μ, se discretiza proponiendo la misma tecnología de elementos finitos que se ha empleado en el contexto del modelado de la macroescala. De este modo, se genera una malla que constituye el dominio discreto, denotado por $\Omega_{\mu,\,h}$. Sobre este espacio se describen los descriptores primales $\dot{\tilde{\mathbf{u}}}_\mu$ y $\tilde{p}_\mu$ mediante matrices globales de funciones de forma, correspondientes a los desplazamientos fluctuantes y las poropresiones fluctuantes de la microescala, como sigue

$$\begin{aligned} \tilde{\mathbf{u}}_\mu &= \mathbf{N}_{\tilde{u}_\mu}\,\tilde{\tilde{\mathbf{u}}}_\mu, \quad \text{con}\,\tilde{\tilde{\mathbf{u}}}_\mu \in \widetilde{\mathcal{U}}^{\square}_{\mu,\,h}, \\ \tilde{p}_\mu &= \mathbf{N}_{\tilde{p}_\mu}\,\tilde{\tilde{\mathbf{p}}}_\mu, \quad \text{con}\,\tilde{\tilde{\mathbf{p}}}_\mu \in \widetilde{\mathcal{P}}^{\square}_{\mu,\,h}, \end{aligned} \tag{2.58}$$

donde $\tilde{\tilde{\mathbf{u}}}_\mu$ y $\tilde{\tilde{\mathbf{p}}}_\mu$ denotan los vectores que contienen todos los desplazamientos y poropresiones fluctuantes nodales, respectivamente, mientras que $\widetilde{\mathcal{U}}^{\square}_{\mu,\,h}$ y $\widetilde{\mathcal{P}}^{\square}_{\mu,\,h}$ representan los subespacios de dimensión finita que son contraparte de los subespacios continuos $\widetilde{\mathcal{U}}^{\square}_{\mu}\left(\Omega_\mu\right) \subseteq \widetilde{\mathcal{U}}_\mu\left(\Omega_\mu\right)$ y $\widetilde{\mathcal{P}}^{\square}_{\mu}\left(\Omega_\mu\right) \subseteq \widetilde{\mathcal{P}}_\mu\left(\Omega_\mu\right)$.

Así como lo realizado para el nivel macroscópico, también en la microescala se propone la misma aproximación espacial, en este caso para las variaciones virtuales fluctuantes admisibles

$$\begin{aligned} \delta\tilde{\mathbf{u}}_\mu &= \mathbf{N}_{\tilde{u}_\mu}\,\delta\tilde{\tilde{\mathbf{u}}}_\mu, \quad \text{con}\,\delta\tilde{\tilde{\mathbf{u}}}_\mu \in \widetilde{\mathcal{U}}^{*}_{\mu,\,h} \equiv \widetilde{\mathcal{U}}^{\square}_{\mu,\,h}, \\ \delta\tilde{p}_\mu &= \mathbf{N}_{\tilde{p}_\mu}\,\delta\tilde{\tilde{\mathbf{p}}}_\mu, \quad \text{con}\,\delta\tilde{\tilde{\mathbf{p}}}_\mu \in \widetilde{\mathcal{P}}^{*}_{\mu,\,h} \equiv \widetilde{\mathcal{P}}^{\square}_{\mu,\,h}, \end{aligned} \tag{2.59}$$

siendo $\delta\tilde{\tilde{\mathbf{u}}}_\mu$ y $\delta\tilde{\tilde{\mathbf{p}}}_\mu$ los vectores globales que recogen las variaciones admisibles virtuales de los deplazamientos y poropresiones fluctuantes, repectivamente.

Reemplazando las expresiones (2.52) y (2.59) en las formas variacionales (2.47)-(2.48) y tras efectuar las manipulaciones matemáticas habituales del método de elementos finitos, se arriba a la aproximación espacial y temporal discreta en el tiempo $t^{n+\theta}$ para las ecuaciones de balance en la microescala, las cuales se expresan del siguiente modo

$$\begin{aligned} &\underbrace{\left[\int_{\Omega_{\mu,\,h}} \left(\mathbf{B}^T_{\tilde{u}_\mu}\,\dot{\boldsymbol{\sigma}}^{n+\theta}_\mu - \mathbf{N}^T_{\tilde{u}_\mu}\,\dot{\mathbf{f}}^{n+\theta}_\mu\right) d\Omega_\mu\right]}_{\dot{\mathbf{G}}^{n+\theta}_{\mu,\,h}} \cdot \delta\dot{\tilde{\tilde{\mathbf{u}}}}_\mu = 0,\ \forall\,\delta\dot{\tilde{\tilde{\mathbf{u}}}}_\mu \in \widetilde{\mathcal{U}}^{*}_{\mu,\,h},\ \text{con}\ \dot{\tilde{\tilde{\mathbf{u}}}}_\mu \in \widetilde{\mathcal{U}}^{\square}_{\mu,\,h}\ \text{y}\ \tilde{\tilde{\mathbf{p}}}_\mu \in \widetilde{\mathcal{P}}^{\square}_{\mu,\,h}, \\ &\underbrace{\left[\int_{\Omega_{\mu,\,h}} \left(\mathbf{N}^T_{\tilde{p}_\mu}\,\dot{\chi}^{n+\theta}_\mu - \mathbf{B}^T_{\tilde{p}_\mu}\,\boldsymbol{\mathcal{V}}^{n+\theta}_\mu\right) d\Omega_\mu\right]}_{\mathbf{H}^{n+\theta}_{\mu,\,h}} \cdot \delta\tilde{\tilde{\mathbf{p}}}_\mu = 0,\ \forall\,\delta\tilde{\tilde{\mathbf{p}}}_\mu \in \widetilde{\mathcal{P}}^{*}_{\mu,\,h},\ \text{con}\ \dot{\tilde{\tilde{\mathbf{u}}}}_\mu \in \widetilde{\mathcal{U}}^{\square}_{\mu,\,h}\ \text{y}\ \tilde{\tilde{\mathbf{p}}}_\mu \in \widetilde{\mathcal{P}}^{\square}_{\mu,\,h}, \end{aligned} \tag{2.60}$$

donde $\mathbf{B}_{\tilde{u}_\mu} = \boldsymbol{\nabla}^{sym}_{\mathbf{x}_\mu}\mathbf{N}_{\tilde{u}_\mu}$ y $\mathbf{B}_{\tilde{p}_\mu} = \boldsymbol{\nabla}_{\mathbf{x}_\mu}\mathbf{N}_{\tilde{p}_\mu}$, son las matrices globales a microescala que relacionan las variables primarias con sus gradientes correspondientes. Una vez más, la ecuación de balance de cantidad de movimiento se ha establecido en forma de tasa.

La solución numérica para los valores nodales correspondientes a los desplazamientos y poropresiones fluctuantes en el paso de tiempo actual t^{n+1}, se calculan utilizando un procedimiento convencional de Newton-Raphson aplicado al sistema de ecuaciones (2.60). En consecuencia, la respuesta en el paso actual se obtiene en términos de los incrementos iterativos $\Delta\tilde{\tilde{\mathbf{u}}}_\mu$ y $\Delta\tilde{\tilde{\mathbf{p}}}_\mu$, respectivamente. En este sentido,

para una iteración genérica k y omitiendo por simplicidad el subíndice h, se puede expresar

$$\left\{ \mathbf{J}_{\mu,\,k}^{n+\theta} \begin{bmatrix} \Delta\tilde{\mathbf{u}}_\mu \\ \Delta\tilde{\mathbf{p}}_\mu \end{bmatrix} + \begin{bmatrix} \dot{\mathbf{G}}_{\mu,\,k}^{n+\theta} \\ \mathbf{H}_{\mu,\,k}^{n+\theta} \end{bmatrix} \right\} \cdot \begin{bmatrix} \delta\dot{\tilde{\mathbf{u}}}_\mu \\ \delta\tilde{\mathbf{p}}_\mu \end{bmatrix} = \begin{bmatrix} 0 \\ 0 \end{bmatrix}, \tag{2.61}$$
$$\forall\, \delta\dot{\tilde{\mathbf{u}}}_\mu \in \widetilde{\mathcal{U}}_{\mu,\,h}^{*},\ \forall\, \delta\tilde{\mathbf{p}}_\mu \in \widetilde{\mathcal{P}}_{\mu,\,h}^{*},\ \text{con}\ \Delta\tilde{\mathbf{u}}_\mu \in \widetilde{\mathcal{U}}_{\mu}^{\square},\ \text{y}\ \Delta\tilde{\mathbf{p}}_\mu \in \widetilde{\mathcal{P}}_{\mu}^{\square},$$

En (2.61), se incluye el operador jacobiano de la microescala $\mathbf{J}_{\mu,\,k}^{n+\theta}$, que se define de la siguiente la forma

$$\mathbf{J}_{\mu,\,k}^{n+\theta} = \begin{bmatrix} \dfrac{\partial \dot{\mathbf{G}}_{\mu,\,k}^{n+\theta}}{\partial \tilde{\mathbf{u}}_\mu^{n+1}} & \dfrac{\partial \dot{\mathbf{G}}_{\mu,\,k}^{n+\theta}}{\partial \tilde{\mathbf{p}}_\mu^{n+1}} \\ \dfrac{\partial \mathbf{H}_{\mu,\,k}^{n+\theta}}{\partial \tilde{\mathbf{u}}_\mu^{n+1}} & \dfrac{\partial \mathbf{H}_{\mu,\,k}^{n+\theta}}{\partial \tilde{\mathbf{p}}_\mu^{n+1}} \end{bmatrix}. \tag{2.62}$$

Cada uno de los componentes de la expresión (2.62) puede determinarse a partir de las leyes constitutivas de la microescala definidas en la sección precedente. No obstante, dichos elementos no se presentan a continuación, recomendándose al lector consultar los trabajos incluidos en los Apéndices A y D.

2.6. Problemas físicos gobernados por la ecuación genérica de balance de una cantidad escalar

En la literatura, numerosos problemas descritos mediante alguna forma especializada de la ecuación de balance de una cantidad escalar con término fuente han sido abordados mediante técnicas multiescala basadas en esquemas de homogeneización de primer orden, los cuales son presentados oportunamente en el Capítulo 3. No obstante, se menciona aquí que un hallazgo recurrente en dichos estudios, así como en aquellos dedicados a problemas hidromecánicos, es que la presencia del término transitorio introduce una dependencia de la respuesta macroscópica respecto del tamaño característico de la microescala, lo que motiva el análisis de su origen y significado en el marco de formulaciones estrictamente de primer orden.

En este contexto, se extienden las ideas del modelado multiescala de medios porosos saturados hacia un espectro más amplio de procesos físicos regidos por ecuaciones de balance de una cantidad escalar, incluyendo, como casos particulares, la transferencia de calor transitoria y el transporte de especies. Para ello, se aprovecha la correspondencia formal entre la ecuación de balance de masas (2.1) y la ecuación general de balance de un campo escalar con término fuente, lo que permite establecer un marco unificado para el tratamiento de estos fenómenos.

En consecuencia, los lineamientos propuestos en Anonis et al. [66, 68] se generalizan a los diversos fenómenos físicos que pueden ser descritos mediante ecuaciones de tipo balance de una cantidad escalar, tal como se analiza en un trabajo actualmente en revisión Anonis et al. [69]. Esta correspondencia refleja la secuencia cronológica de las publicaciones, aunque también puede interpretarse a la inversa, considerando el segundo trabajo como el marco general que engloba al primero. En este sentido, y dado el estrecho vínculo entre ambas contribuciones, en el Capítulo 3 se presentan de forma conjunta los principales resultados de estas propuestas, complementados con los antecedentes más relevantes reportados en la literatura.

La formulación teórica y la implementación numérica del modelado multiescala en problemas genéricos regidos por la ecuación de balance de una cantidad escalar no se presentan en detalle en esta sección, sino que se remiten directamente a Anonis et al. [69], y se reproducen en el Apéndice C, donde se abordan casos de mayor generalidad.

Parte III

Contribuciones al desarrollo de metodologías multiescala aplicado a problemas hidromecánicos y de difusión-reacción

Capítulo 3

Análisis de la dependencia con el tamaño de la microescala y la pérdida de objetividad de la respuesta macroescala

3.1. Introducción

Este capítulo tiene como propósito ofrecer una descripción detallada de las contribuciones novedosas que sustentan la formulación multiescala propuesta, así como presentar las diferencias con respecto a las alternativas existentes en la bibliografía actual, particularmente en lo referido al tratamiento de la dependencia con el tamaño de la microescala. Estas ideas son el fundamento y la razón de dos trabajos publicados, Anonis et al. [66] y Anonis et al. [68], y uno sometido a revisión Anonis et al. [69]. En ellos, se pretendía por un lado clarificar las ideas relativas a esta cuestión teórica crítica y, por otro, introducir una nueva alternativa de modelización que preserva tanto la noción de RVE como el principio de separación de escalas. Estos documentos se reproducen en los Apéndices A, B y C, respectivamente.

A su vez, los conceptos aquí presentados también resultan aplicables al modelado de una matriz de tipo medio poroso en la cual se embeben inclusiones sólidas impermeables, lo que representa una extensión natural de las nociones propuestas hacia un caso más general de materiales compuestos. Esta línea de trabajo dio lugar a otras dos contribuciones, una de ellas publicada, Anonis et al. [67], y la otra en revisión, Anonis et al. [70], que se incluyen en los Apéndices D y E.

Por lo expuesto anteriormente, y dado que las ideas aquí desarrolladas constituyen la base fundamental, ya sea de forma directa o indirecta, de cada uno de los trabajos publicados, este capítulo resulta esencial para todos los desarrollos posteriores presentados en esta tesis.

Este capítulo se estructura de la siguiente manera: en la Sección 3.2 se exponen los principales avances que evidencian el notable interés por comprender el efecto del tamaño inherente al modelado multiescala de problemas hidromecánicos acoplados[1], así como problemas gobernados por una ecuación genérica de balance de una cantidad escalar. En la Sección 3.3, se identifica el principal término responsable de introducir los efectos de segundo orden. Luego, en la Sección 3.4 se presenta formalmente la causa que origina la dependencia indeseable con el tamaño de la microescala y la consecuente pérdida de objetividad de la respuesta efectiva. Por su parte, en la Sección 3.5 se proponen las modificaciones mínimamente invasivas, aportando una solución dirigida al núcleo del problema. Posteriormente, en la Sección 3.6 se efectúan algunas conclusiones particulares referidas a los resultados analíticos y numéricos obtenidos en los artículos publicados. Por último, la Sección 3.7 resume las conclusiones generales sobre el modelado multiescala existente y el propuesto.

[1] Incluye la ecuación de balance de masa del fluido.

3.2. Discusión de la aplicación de metodologías multiescala en problemas gobernados por una ecuación de balance de una cantidad escalar (hidromecánicos y de difusión-reacción)

El punto de partida y la idea base de las metodologías multiescala basadas en el concepto de RVE, desde los trabajos pioneros de Hill [1, 2, 3, 29], se sustenta en la existencia de un dominio microestructural mínimo a partir del cual la respuesta a macroescala resulte insensible al tamaño. En la literatura, diversos fenómenos físicos descritos mediante ecuaciones de balance de una cantidad escalar con término fuente han sido estudiados a través de formulaciones multiescala basadas en enfoques de homogeneización de primer orden. En este marco, numerosos autores han destacado la presencia de un término transitorio (también denominado inercial o dinámico) que compromete la objetividad de la respuesta a macroescala, al introducir una dependencia con respecto al tamaño del dominio de la microescala. Este hecho ha motivado el uso extendido de la expresión "segundo orden" para referirse a los efectos asociados a la homogeneización del término transitorio. No obstante, esto representa una situación controvertida cuando el objetivo principal es la formulación de un esquema de homogeneización estrictamente de primer orden a escala macroscópica, ya que conlleva la pérdida del concepto fundamental de elemento de volumen representativo (RVE), aspecto sobre el cual se pretende realizar un análisis exhaustivo.

En lo que sigue, se presentan las principales contribuciones que han abordado problemas hidromecánicos y fenómenos que pueden describirse como casos particulares de la ecuación de balance de una cantidad escalar con término fuente.

En el campo de los problemas referentes a la conducción del calor, uno de los primeros aportes fue el de Özdemir et al. [71], quienes simplificaron el análisis asumiendo un estado estacionario para las temperaturas en la microescala, basándose en la premisa de que el almacenamiento de calor a dicha escala es insignificante debido al pequeño tamaño del dominio. Al omitir el término transitorio en la escala menor, no se registraron efectos de segundo orden. Posteriormente, Larsson et al. [13] y Runesson et al. [15] propusieron un marco variacional para la homogeneización de primer orden, ampliando el enfoque a problemas transitorios dependientes del tiempo en ambas escalas. Estos autores incluyeron explícitamente la tasa de energía interna de la microestructura. Partiendo de la hipótesis de una variación lineal de la parte suavizada de la temperatura microscópica (véase Sub-sección 2.4.2), demostraron que la homogeneización introduce efectivamente un efecto de tamaño. Este se manifiesta con la aparición de un término de segundo orden, al que denominaron momento de contenido térmico, que interpretan físicamente como la inercia de la microescala ante un cambio de temperatura (y su gradiente) desde la perspectiva macroscópica. En otras palabras, se requiere un tiempo finito para redistribuir la energía dentro de un RVE de tamaño limitado. Finalmente, señalaron que estas cantidades de alto orden desaparecen en el límite en que el tamaño del RVE tiende a cero.

Luego, Ramos et al. [72] establecieron la homogeneización de problemas de conducción transitoria de calor, considerando, ademas del carácter transitorio, la generación de calor en ambas escalas. Ellos mostraron con claridad los términos adicionales dependientes del tamaño que surgen en la descripción macroscópica. A dichos términos denominaron de inercia térmica de la microescala, ya sea que se encuentre relacionado con la tasa de la energía interna o con la generación de calor en la microestructura. Además, demostraron la importancia de considerar los efectos microscópicos de la inercia térmica en los problemas de conducción transitoria del calor.

Más recientemente, Waseem et al. [73] construyeron un modelo numérico de orden reducido para tratar problemas térmicos transitorios. Los autores indican que la relación entre los distintos tiempos de difusión característicos y el tiempo de carga determina el grado de separación existente entre la micro- y macroescala, estableciendo tres regímenes: separación completa, inexistente y relajada, concentrándose en estos dos últimos. En dichos casos, destacan que existen efectos transitorios significativos en la mi-

croescala que deben incorporarse explícitamente en el proceso de homogeneización. Caso contrario, de asumir un estado estacionario, los efectos transitorios microscópicos, asociados a la denominada inercia térmica de microescala (término de segundo orden), no quedarían reflejados en la respuesta macroscópica. Por lo tanto, al reconocer dichos efectos, la ecuación de balance energético, con su correspondiente término transitorio, debe resolverse en ambas escalas.

En cuanto a los medios porosos saturados, Larsson et al. [14] propusieron un método de homogeneización variacionalmente consistente para la consolidación transitoria no acoplada, mientras que Su et al. [48] abordaron el problema acoplado. Ambos trabajos muestran que la aproximación lineal multiescala introduce un efecto de tamaño con la microescala asociado a un término de segundo orden. Dicha cantidad, según los autores solo desaparecerá cuando el tamaño del RVE sea infinitamente pequeño. En tal caso, recuperan la hipótesis de respuesta subescala cuasi estacionaria planteada por Özdemir et al. [71].

Posteriormente, Jänicke et al. [74] consideraron una mesoescala fuertemente heterogénea con propiedades poroelásticas que varían espacialmente, sustituida a nivel macroscópico por un material viscoelástico homogéneo equivalente. Consideran a la difusión del fluido en los poros como un fenómeno local, analizando el proceso de redistribución de fluido dentro de la MC. Obviamente, al tratar la macroescala como un medio de Cauchy monofásico, no hay ecuación de balance de masa del fluido y en consecuencia no sería posible observar el efectos de dependencia con el tamaño. Esta línea fue extendida por Jänicke et al. [75, 76] mediante modelos numéricos reducidos y, más tarde, por Jänicke et al. [49] quienes lo aplicaron a la homogeneización computacional de un medio poroelástico en condiciones transitorias. En este contexto, suponen los campos de desplazamiento y poropresión poseen partes en ambas escalas y las ecuaciones de evolución que describen el comportamiento macroescala poro-viscoelástico aparente se derivan de la ecuación de continuidad pertinente a la microescala. Como caso particular, obtienen un modelo macroescala poroelástico cuando las propiedades viscoelásticas quedan inactivas. La hipótesis subyacente es que el problema se describe completamente mediante el problema estacionario, en tanto que las fluctuaciones transitorias se desvanecen, ya sea porque (i) el tamaño de la MC tiende a cero, o (ii) los parámetros materiales del modelo a escala fina se eligen de manera que la parte fluctuante atenúa su contribución en comparación con la respuesta estacionaria.

Por otro lado, Khoei y Hajiabadi [16] proponen modelos de homogeneización para medios porosos saturados, asumiendo la descomposición de la respuesta macroescala en un término estacionario y otro dinámico, incluyendo el efecto del tamaño de la microescala en este ultimo. Señalan que dicho efecto desaparece cuando el dominio de la MC se reduce a un tamaño infinitesimal. A medida que aumentan las dimensiones de la escala fina, estos autores reportan diferencias entre los resultados homogeneizados y los obtenidos mediante DNS. Posteriormente, Khoei y Saeedmonir [51] extendieron el modelado a flujos multifásicos, efectuando un análisis con respecto al tamaño de la MC, concluyendo que las MCs más pequeñas ofrecen mejores aproximaciones del comportamiento macroscópico. Más recientemente, Khoei et al. [53] ampliaron el análisis hidromecánico incorporando el estudio de un medio con microfracturas.

Otros autores, como Ricken et al. [55], Klahr et al. [56], desarrollaron una formulación variacional multiescala basada en RVE aplicada a medios porosos saturados bajo grandes deformaciones. En este escenario, Klahr et al. [56] identificaron una componente que presenta dependencia con el tamaño del dominio microescala, observable a través de la velocidad de flujo homogeneizada. Mediante comparaciones numéricas mostraron que los modelos de primer orden resultan insuficientes para representar con precisión los cambios de volumen, ya que en ellos se obtiene invariablemente un flujo neto nulo en la microescala, limitación relevante en el análisis de grandes deformaciones. Para superar esta deficiencia, Thiesen et al. [57, 58] propusieron un enfoque de segundo orden que permite capturar de manera adecuada el flujo de fluido no uniforme a través del contorno del RVE, logrando así resultados en mejor concordancia con simulaciones numéricas directas. Cabe señalar, sin embargo, que tales desarrollos exceden el alcance del presente trabajo, puesto que aquí se considera un régimen de transformaciones infinitesimales donde no resulta necesario capturar cambios volumétricos significativos. Finalmente, otros investigadores (Ekre et al. [50], Wu et al. [77, 78]) han realizado importantes contribuciones en el ámbi-

to de los métodos multiescala aplicados a medios porosos saturados, aunque sin abordar el efecto del tamaño de la microescala mencionado.

Además de los problemas térmicos transiente e hidromecánicos acoplados, otros autores han abordado el tratamiento computacional de problemas de difusión transitoria utilizando homogeneización de primer orden. Kaessmair y Steinmann [17] al modelar el transporte de especies a través de un cuerpo mediante el balance del contenido de especies, destacan el efecto del tamaño de la microescala en la respuesta transitoria efectiva. Es decir, se tiene un término análogo a la inercia microscópica observada en la conducción de calor. Waseem et al. [79, 80] trataron el problema de difusión de especies en sólidos, incluyendo un continuo enriquecido a macroescala y posteriormente un enfoque de homogeneización de orden reducido basado en datos. Por su parte, René et al. [81] estudiaron la difusión en materiales compuestos de partículas con interfaces de materiales mediante potencial químico dual a macroescala, pero considerando régimen microscópico estacionario. Asimismo, se han desarrollado estudios que acoplan el transporte de especies con otros fenómenos físicos mediante homogeneización computacional de primer orden, tales como el mecánico (Kaessmair y Steinmann [82], Waseem et al. [83], Kaessmair et al. [84], Mao et al. [85]), los cuales incluyen la definición anterior de un flujo macroscópico el cual introduce un efecto de tamaño en la respuesta a macroescala, y el transporte electroquímico de iones (Tu et al. [86]), aunque en este último caso se ha despreciando los efectos transitorios de difusión a microescala.

Finalmente, dentro del ámbito de la homogeneizacion de primer orden, cabe mencionar las contribuciones que abordan el acoplamiento de más de dos procesos físicos. Entre ellas, se destacan el problema termo-hidro-mecánico (Lopez Rivarola et al. [18], Saeedmonir y Khoei [52]) y el quimio-hidro-mecánico [54]. En dichos estudios, el acoplamiento de dos fenómenos físicos, que incluyen la ecuación de balance de masa del fluido y otra particularización de la ecuación de balance de una cantidad escalar (hidro-térmico y quimio-hidráulico), agrega más términos inerciales a todo el tratamiento, los cuales introducen la dependencia con el tamaño de la MC, como se demostrará más adelante. Al desarrollar la formulación de dos escalas para el análisis termo-hidro-mecánico de medios porosos heterogéneos, Saeedmonir y Khoei [52] advierten que, al considerar los términos microdinámicos, el enfoque basado en condiciones de contorno periódicas convencionales, con cuatro nodos de esquina restringidos, conduce a errores sustanciales para problemas altamente transitorios en la fase transitoria de la solución. Por lo tanto, propusieron tres condiciones alternativas acopladas al modelo periódico en lugar de prescribir cuatro nodos de esquina, para obtener una mejor respuesta al considerar los términos microinerciales. Resaltan además, que dos de estas restricciones alternativas parecen las más prometedoras al contrastar con las soluciones DNS, motivo por el cual las adoptaron en trabajos posteriores (Khoei et al. [53], Saeedmonir et al. [54]). No obstante, tal como se demuestra en Anonis et al. [69] la dependencia de la respuesta con respecto al tamaño de la microescala persiste, independientemente de las condiciones de contorno impuestas a nivel microscópico.

Todas las contribuciones mencionadas anteriormente ponen de manifiesto la importancia física del término transitorio que surge del proceso de homogeneización en problemas gobernados por alguna forma especializada de la ecuación de balance de una cantidad escalar, así como en problemas hidromecánicos. Dichos avances reflejan un notable interés por comprender este efecto colateral de segundo orden, cuyo carácter resulta controvertido cuando el objetivo principal es formular un enfoque de homogeneización total o estrictamente de primer orden en la macroescala. De estos estudios pueden extraerse dos ideas fundamentales: (i) la identificación del denominado término transitorio como el responsable de inducir la dependencia con el tamaño de la microescala, afectando así la objetividad de la respuesta macroscópica, y (ii) el reconocimiento de la riqueza que aporta este término en la caracterización del material. Este último aspecto plantea una paradoja, ya que por un lado resulta necesario el término inercial para una descripción más realista en la evaluación de estos fenómenos y por otro lado la dependencia del tamaño de la microescala entra en conflicto con la noción clásica e intuitiva de la existencia de un RVE. En consecuencia, este aspecto permanece como un tema abierto y un desafío de investigación en

el campo del modelado multiescala.

El objetivo principal de este capítulo es examinar en detalle las implicancias del término transitorio. En primer lugar, señalando cómo puede introducir dependencia con el tamaño de la MC. Posteriormente, se plantea una estrategia que elimina exclusivamente los componentes responsables de la falta de objetividad, con el propósito de preservar la mayor parte de los efectos transitorios, y, de este modo, mantener la capacidad predictiva que sustenta los desarrollos previos en la literatura.

Con el fin de dar claridad sobre las ideas relativas a esta cuestión teórica crítica y además introducir una nueva alternativa de modelización multiescala mejorada que preserve tanto la noción de RVE como el principio de separación de escalas se presentan las siguientes secciones.

Cabe aclarar que los desarrollos posteriores se limitan al problema hidromecánico, sin pretender abarcar una formulación genérica para fenómenos gobernados por una ecuación genérica de balance con término fuente. Esta decisión se justifica en tres aspectos fundamentales: (i) aprovechar el marco teórico establecido en el capítulo precedente, especificamente concebido para describir a los medios porosos saturados; (ii) garantizar que los conceptos aqui empleados sean de aplicabilidad directa en los capítulos posteriores 4 y 5, donde se analizan microestructuras compuestas conformados por una matriz de medio poroso saturado y (iii) reconocer que, para un tratamiento general de problemas gobernados por una ecuación genérica de balance en el contexto multiescala, resulta mas claro y conveniente remitir al lector a los desarrollos contenidos en el trabajo sometido a revisión de Anonis et al. [69] incluido en el Apéndice C.

No obstante, se efectuarán comentarios referentes a la formulación general de problemas regidos por una ecuación de balance de una cantidad escalar cuando sea pertinente.

3.3. Identificación del término transitorio

Conforme a los desarrollos de la teoría poromecánica y su implementación en el ámbito multiescala, expuestas en el capítulo precedente, es posible identificar de forma sencilla el denominado término transitorio (o bien, inercial o dinámico) el cual induce el efecto de segundo orden. Este se presenta en la formula de homogeneización del vector de velocidad de flujo (2.45), el cual se reescribe a continuación de la siguiente manera

$$\boldsymbol{\mathcal{V}} = \boldsymbol{\mathcal{V}}_{est} + \boldsymbol{\mathcal{V}}_{tra} = \frac{1}{|\Omega_\mu|}\int_{\Omega_\mu} \boldsymbol{\mathcal{V}}_\mu \, d\Omega_\mu - \frac{1}{|\Omega_\mu|}\int_{\Omega_\mu} \dot{\chi}_\mu \, \mathbf{x}'_\mu \, d\Omega_\mu, \ \forall\, t. \tag{3.1}$$

donde, por conveniencia, se introdujo el vector auxiliar $\mathbf{x}'_\mu$ que representa la traslación de las coordenadas y se define como $\mathbf{x}'_\mu = \mathbf{x}_\mu - \mathbf{x}^G_\mu$. Esta definición se preserva de aquí en adelante. Al primer término del lado derecho de la igualdad, Khoei y Hajiabadi [16] lo denominaron de parte estacionaria. Por su parte, el segundo término del lado derecho constituye precisamente la parte transitoria[2], ampliamente mencionada e identificada en contribuciones previas y es el que será evaluado de forma integral a continuación. Dada la relevancia que $\boldsymbol{\mathcal{V}}_{tra}$ presenta, se extrae de (3.1), reescribiendo

$$\boldsymbol{\mathcal{V}}_{tra} = -\frac{1}{|\Omega_\mu|}\int_{\Omega_\mu} \dot{\chi}_\mu \, \mathbf{x}'_\mu \, d\Omega_\mu. \tag{3.2}$$

[2]Es posible extraer una parte transitoria semejante a la dada en (3.2) de cualquier proceso físico regido por una forma de la ecuación de balance de una cantidad escalar y evaluado en un marco de metodologías multiescala.

Por otra parte, la ecuación constitutiva (2.51) de la cantidad $\dot{\chi}_\mu$ fue establecida en la Sub-sección 2.4.5, la cual se reescribe a continuación por conveniencia

$$\dot{\chi}_\mu = \hat{\dot{\chi}}_\mu\left(\dot{\boldsymbol{\varepsilon}}_\mu, \dot{p}_\mu\right) = \mathbf{b}_\mu \;:\; \dot{\boldsymbol{\varepsilon}}_\mu + \frac{1}{M_\mu}\,\dot{p}_\mu. \tag{3.3}$$

Al presentar este funcional constitutivo junto con los de $\hat{\dot{\sigma}}_\mu\big(\dot{\boldsymbol{\varepsilon}}_\mu, \dot{p}_\mu\big)$ y $\hat{\mathcal{V}}_\mu\big(\boldsymbol{\varphi}_\mu\big)$, se destacó en la Sub-sección 2.4.5 lo significativo que resulta, para los fines del presente trabajo, la forma en que se definen los argumentos constitutivos de entrada empleados para evaluar las correspondientes respuestas del material. En efecto, el nivel de riqueza de una formulación constitutiva depende en gran medida de la cantidad de información incorporada. En este sentido, el modo en que se expanden los descriptores primitivos que determinan dichas respuestas ($\boldsymbol{\varphi}_\mu$, $\dot{\boldsymbol{\varepsilon}}_\mu$ y $\dot{p}_\mu$) adquiere especial importancia en este punto del desarrollo. Una caracterización más completa permite reflejar con mayor fidelidad el comportamiento del material y transferir a la escala macroscópica múltiples efectos propios de la microestructura. Entre estos, puede aparecer la dependencia del tamaño a microescala, fenómeno que como se señaló previamente, compromete la objetividad de la respuesta macroscópica en modelos de homogeneización de primer orden basados en RVE. En particular, resultan de interés aquellos materiales que no presenten efectos de segundo orden a lo largo de longitudes características de la microescala.

Este aspecto justifica el tratamiento detallado de los argumentos constitutivos en las siguientes secciones. Sin embargo, el análisis se restringirá, por razones de simplicidad y extensión, a aquellos efectos que inciden directamente sobre la ecuación constitutiva (3.3), dada que es la única que influye de forma directa en $\boldsymbol{\mathcal{V}}_{tra}$, (véase (3.2)). Cabe remarcar, no obstante, que todas las consideraciones posteriores que se realizan respecto de las expansiones de los descriptores primitivos resultan igualmente válidas y aplicables a los demás funcionales constitutivos $\hat{\dot{\sigma}}_\mu\big(\dot{\boldsymbol{\varepsilon}}_\mu, \dot{p}_\mu\big)$ y $\hat{\mathcal{V}}_\mu\big(\boldsymbol{\varphi}_\mu\big)$ que fueron expuestos en la Sub-sección 2.4.5, así como en un contexto más general de problemas de balance de una cantidad escalar con término fuente Anonis et al. [69].

3.4. Ecuaciones constitutivas en la microescala basados en expansión de orden completo (FOE) de los descriptores primarios

En primera instancia, resulta necesario definir el concepto de expansión de orden completo (FOE: Full-Order Expansion) de los descriptores primarios en el entorno de los funcionales constitutivos de la microescala. Aplicado al caso particular de la ley constitutiva propuesta para $\dot{\chi}_\mu = \hat{\dot{\chi}}_\mu\left(\dot{\boldsymbol{\varepsilon}}_\mu, \dot{p}_\mu\right)$, donde son necesarias solamente las expansiones de la tasa de deformaciones, $\dot{\boldsymbol{\varepsilon}}_\mu$, y la tasa de poropresiones, $\dot{p}_\mu$, en la microescala. En este caso, la versión totalmente expandida de estos descriptores primarios que forman parte de la lista de argumentos de entrada en la ecuación (3.3) se escriben como

$$\dot{\boldsymbol{\varepsilon}}_\mu^{\text{FOE}} = \dot{\boldsymbol{\varepsilon}} + \dot{\tilde{\boldsymbol{\varepsilon}}}_\mu, \tag{3.4}$$

$$\dot{p}_\mu^{\text{FOE}} = \dot{p} + \dot{\boldsymbol{\varphi}} \;\cdot\; \mathbf{x}'_\mu + \dot{\tilde{p}}_\mu, \tag{3.5}$$

donde se ha agregado el superindice $(\bullet)^{\text{FOE}}$ a los descriptores primarios para indicar la expansión completa. Al introducir las definiciones dadas en (3.4)-(3.5) en el funcional constitutivo (3.3), conducen a lo que se denomina en este manuscrito como relación constitutiva de expansión completa, particularmente en este caso de la cantidad $\dot{\chi}_\mu^{\text{FOE}}$, y que se expresa como

$$\dot{\chi}_\mu^{\text{FOE}} = \hat{\dot{\chi}}_\mu^{\text{FOE}}\left(\dot{\boldsymbol{\varepsilon}}_\mu^{\text{FOE}}, \dot{p}_\mu^{\text{FOE}}\right) = \mathbf{b}_\mu \;:\; \left(\dot{\boldsymbol{\varepsilon}} + \dot{\tilde{\boldsymbol{\varepsilon}}}_\mu\right) + \frac{1}{M_\mu}\left[\dot{p} + \dot{\boldsymbol{\varphi}} \;\cdot\; \mathbf{x}'_\mu + \dot{\tilde{p}}_\mu\right]. \tag{3.6}$$

A lo largo de este trabajo, el esquema de homogeneización resultante de esta elección para los descriptores primitivos se identificará como el modelo Multiescala-FOE. Es decir, la técnica de homogeneización que considera una expansión completa a nivel constitutivo conduce a este modelo en particular[3]. Es notorio que la mayoría de los métodos de homogeneización de primer orden disponibles en la bibliografía para problemas de balance de una cantidad escalar e hidromecánicos, siguen el esquema Multiescala-FOE. El motivo es que esta estrategia probablemente representa la opción más natural y directa para describir los comportamientos de los materiales a microescala, pero como se ha comentado previamente, presenta efectos de segundo orden en la macroescala.

Una vez introducida la relación constitutiva (3.6) en la expresión (3.2) se puede analizar el componente transitorio, $\boldsymbol{\mathcal{V}}_{tra}$, del vector de velocidad homogeneizado y la objetividad en la respuesta a macroescala. Por lo tanto, se tiene

$$\begin{aligned}\boldsymbol{\mathcal{V}}_{tra} &= -\frac{1}{|\Omega_\mu|}\int_{\Omega_\mu} \dot{\chi}_\mu^{\text{FOE}}\,\mathbf{x}'_\mu\,d\Omega_\mu = -\frac{1}{|\Omega_\mu|}\int_{\Omega_\mu} \hat{\dot{\chi}}_\mu^{\text{FOE}}\big(\dot{\boldsymbol{\varepsilon}}_\mu^{\text{FOE}}, \dot{p}_\mu^{\text{FOE}}\big)\,\mathbf{x}'_\mu\,d\Omega_\mu \\ &= \underbrace{-\frac{\dot{\boldsymbol{\varepsilon}}}{|\Omega_\mu|} \,:\, \int_{\Omega_\mu}\big(\mathbf{b}_\mu \otimes \mathbf{x}'_\mu\big)\,d\Omega_\mu}_{\mathbf{T}_1} \underbrace{-\frac{\dot{p}}{|\Omega_\mu|}\int_{\Omega_\mu} M_\mu^{-1}\,\mathbf{x}'_\mu\,d\Omega_\mu}_{\mathbf{T}_2} \\ &\underbrace{-\frac{1}{|\Omega_\mu|}\int_{\Omega_\mu}\mathbf{b}_\mu \,:\, \big(\dot{\tilde{\boldsymbol{\varepsilon}}}_\mu \otimes \mathbf{x}'_\mu\big)\,d\Omega_\mu}_{\mathbf{T}_3} \underbrace{-\frac{1}{|\Omega_\mu|}\int_{\Omega_\mu} M_\mu^{-1}\,\dot{\tilde{p}}_\mu\,\mathbf{x}'_\mu\,d\Omega_\mu}_{\mathbf{T}_4} \underbrace{-\frac{1}{|\Omega_\mu|}\int_{\Omega_\mu} M_\mu^{-1}\,(\mathbf{x}'_\mu \otimes \mathbf{x}'_\mu)\,d\Omega_\mu\,\dot{\boldsymbol{\varphi}}}_{\mathbf{T}_5}.\end{aligned} \tag{3.7}$$

En primer lugar, al observar (3.7), siempre que se asuman distribuciones aproximadamente simétricas de las propiedades $\mathbf{b}_\mu$ y M_μ con respecto del centroide de la MC, los términos $\mathbf{T}_1$ y $\mathbf{T}_2$ no generan efectos asociados con el tamaño de la microescala. De hecho, la influencia de estas contribuciones se atenúa progresivamente conforme aumenta el tamaño de la MC, al incorporarse un número suficientemente grande y representativo de heterogeneidades. En consecuencia, estos términos contribuyen a determinar cuándo una MC genérica puede o no considerarse un RVE.

En contraste, el integrando del último término en el lado derecho de (3.7), $\mathbf{T}_5$, presenta una dependencia cuadrática con respecto a la coordenada $\mathbf{x}'_\mu$, constituyendo así una contribución de segundo orden. Claramente, la magnitud de esta contribución aumenta de forma monótona al ampliarse las dimensiones de la MC, con lo que introduce un efecto de tamaño en la respuesta homogeneizada que se denomina de directo o explícito.

No obstante, la expresión (3.7) incluye también fuentes adicionales de efectos de tamaño a microescala que pueden no ser inmediatamente evidentes. Para identificarlas, es necesario tener en cuenta que los campos fluctuantes $\tilde{\mathbf{u}}_\mu$ y $\tilde{p}_\mu$ dependen del proceso de inserción a microescala, al ser obtenidos tras la resolución de las ecuaciones de balance de la microescala (2.47)-(2.48). En particular, puede establecerse en primer lugar que $\tilde{\mathbf{u}}_\mu$ y $\tilde{p}_\mu$ son funciones de la cantidad macroescala insertada $\dot{\boldsymbol{\varphi}}_\mu \cdot \mathbf{x}'_\mu$ (la cual se destaca entre las demás). A partir de ello, al aplicar el gradiente simétrico y las tasas correspondientes, se obtiene

$$\begin{aligned}\dot{\tilde{\boldsymbol{\varepsilon}}}_\mu &= f_{\dot{\tilde{\boldsymbol{\varepsilon}}}_\mu}\big(\ldots, \dot{\boldsymbol{\varphi}}_\mu \cdot \mathbf{x}'_\mu, \ldots\big)\,, \\ \dot{\tilde{p}}_\mu &= f_{\dot{\tilde{p}}_\mu}\big(\ldots, \dot{\boldsymbol{\varphi}}_\mu \cdot \mathbf{x}'_\mu, \ldots\big)\,.\end{aligned}$$

Esta dependencia funcional implícita, combinada con la presencia de productos como $\big(\dot{\tilde{\boldsymbol{\varepsilon}}}_\mu \otimes \mathbf{x}'_\mu\big)$ y $(\dot{\tilde{p}}_\mu\,\mathbf{x}'_\mu)$ en los integrandos de $\mathbf{T}_3$ y $\mathbf{T}_4$, respectivamente, permite concluir que ambos términos homoge-

[3] En el contexto de los medios porosos saturados modelados con el esquema Multiescala-FOE, se requieren además las correspondientes expansiones sobre los funcionales constitutivos (2.49) y (2.50) que se reescriben como $\boldsymbol{\mathcal{V}}_\mu^{\text{FOE}} = \hat{\mathcal{V}}_\mu^{\text{FOE}}\big(\boldsymbol{\varphi}_\mu^{\text{FOE}}\big)$ y $\dot{\boldsymbol{\sigma}}_\mu^{\text{FOE}} = \hat{\dot{\sigma}}_\mu^{\text{FOE}}\big(\dot{\boldsymbol{\varepsilon}}_\mu^{\text{FOE}}, \dot{p}_\mu^{\text{FOE}}\big)$, respectivamente, y siendo $\boldsymbol{\varphi}_\mu^{\text{FOE}} = \boldsymbol{\varphi} + \tilde{\boldsymbol{\varphi}}_\mu$.

neizados producen también una dependencia de segundo orden con la coordenada $\mathbf{x}'_\mu$. En este trabajo, a tales contribuciones se las denomina de efecto de tamaño a microescala indirectos o implícitos.

En este escenario, se plantea a una especie de paradoja de la formulación de primer orden: para materiales altamente heterogéneos se requiere de un proceso de ampliación del dominio de la MC hasta alcanzar la representatividad, es decir obtener el RVE. Sin embargo, de forma controvertida, en la regla de homogeneización (3.7) las contribuciones $\mathbf{T}_3$, $\mathbf{T}_4$ y $\mathbf{T}_5$ nunca alcanzarán a satisfacer dicha condición durante el mismo proceso. Esta inconsistencia se deriva de la aparición, tanto directa como implícita, del producto entre la tasa del gradiente de poropresiones macroescala y las coordenadas $\left(\dot{\boldsymbol{\varphi}}_\mu \cdot \mathbf{x}'_\mu\right)$, proveniente de la expansión de orden completo de la tasa de poropresiones a microescala $\dot{p}_\mu^{\text{FOE}}$ en (3.5) admitida como argumento de entrada en el funcional constitutivo (3.6). Por esta razón, en la sección posterior se propone una expansión alternativa que elimina este efecto.

Cabe mencionar, además, que en caso de que las propiedades de los parámetros materiales presenten dependencia con las variables primitivas, podrían inducirse más términos de segundo orden en cada una de las cantidades duales homogeneizadas del problema en estudio. Esta situación, se analiza para un contexto mas general en Anonis et al. [69].

3.5. Ecuaciones constitutivas en la microescala basados en expansión de orden selectivo (SOE) de los descriptores primarios

Se ha demostrado en la sección precedente que la falta de objetividad en la respuesta efectiva a macroescala se debe al tipo de expansión aceptada para las poropresiones fluctuantes, que se incorpora como argumento de entrada al evaluar la ecuación constitutiva (3.6). Identificada la causa de la dependencia cuadrática con la coordenada $\mathbf{x}'_\mu$, es posible introducir ligeras modificaciones en la formulación.

La propuesta y principal novedad de este trabajo consiste en postular un orden de expansiones diferente para la tasa de poropresiones de la microescala, $\dot{p}_\mu$, siempre que dicho campo se considere como argumento constitutivo de entrada en las leyes constitutivas de $\hat{\dot{\chi}}_\mu$ y $\hat{\dot{\sigma}}_\mu$, a nivel microscópico. Concretamente, al evaluar el funcional $\hat{\dot{\chi}}_\mu\left(\dot{\boldsymbol{\varepsilon}}_\mu, \dot{p}_\mu\right)$, $\dot{p}_\mu$ se expande de forma reducida, despreciando la contribución lineal $\dot{\boldsymbol{\varphi}}_\mu \cdot \mathbf{x}'_\mu$ (ROE: Reduced-Order Expanded) y se identifica con el superindice $(\bullet)^{\text{ROE}}$. Así, tomando las ecuaciones (3.4)-(3.5) se reescribe

$$\dot{\boldsymbol{\varepsilon}}_\mu^{\text{FOE}} = \dot{\boldsymbol{\varepsilon}} + \dot{\tilde{\boldsymbol{\varepsilon}}}_\mu, \tag{3.8}$$

$$\dot{p}_\mu^{\text{ROE}} = \dot{p} + \dot{\tilde{p}}_\mu, \tag{3.9}$$

donde la tasa de deformaciones microescala permanece inalterada, esto es, con la expansión de orden completa.

Al aplicar los descriptores (3.8)-(3.9) a la ecuación (3.3), esta se reescribe como

$$\dot{\chi}_\mu^{\text{SOE}} = \hat{\dot{\chi}}_\mu^{\text{SOE}}\left(\dot{\boldsymbol{\varepsilon}}_\mu^{\text{FOE}}, \dot{p}_\mu^{\text{ROE}}\right) = \mathbf{b}_\mu \,:\, \left(\dot{\boldsymbol{\varepsilon}} + \dot{\tilde{\boldsymbol{\varepsilon}}}_\mu\right) + \frac{1}{M_\mu}\left(\dot{p} + \dot{\tilde{p}}_\mu\right). \tag{3.10}$$

El procedimiento de homogeneización que surge al establecer la redefición de los descriptores empleados como argumentos constitutivos, tal como se hizo en (3.8)-(3.10), se denomina de modelo multiescala de expansión de orden selectivo, o en forma abreviada modelo Multiescala-SOE, el cual se simboliza mediante el superindice $(\bullet)^{\text{SOE}}$ (SOE: Selective-Order Expanded). Este enfoque introduce una expansión de orden selectivo para el conjunto de variables primitivas únicamente en lugares selectivos/específicos de la formulación, a fin de proporcionar un procedimiento de homogeneización que restablezca el concepto fundamental de RVE, tal y como se demuestra a continuación[4].

[4]Para el modelado con el enfoque Multiescala-SOE, los funcionales constitutivos (2.49) y (2.50) se redefinen como $\boldsymbol{\mathcal{V}}_\mu^{\text{SOE}} =$

Sustituyendo la redefinición constitutiva (3.10) dentro de la regla de homogeneización de la parte transitoria de la velocidad de flujo macroescala, $\boldsymbol{\mathcal{V}}_{tra}$, definida por (3.2), se obtiene

$$\begin{aligned}\boldsymbol{\mathcal{V}}_{tra} &= -\frac{1}{|\Omega_\mu|}\int_{\Omega_\mu} \dot{\chi}_\mu^{\text{SOE}}\,\mathbf{x}'_\mu\,d\Omega_\mu = -\frac{1}{|\Omega_\mu|}\int_{\Omega_\mu} \hat{\chi}_\mu^{\text{SOE}}\big(\dot{\boldsymbol{\varepsilon}}_\mu^{\text{FOE}}, \dot{p}_\mu^{\text{ROE}}\big)\,\mathbf{x}'_\mu\,d\Omega_\mu \\ &= \underbrace{-\frac{\dot{\boldsymbol{\varepsilon}}}{|\Omega_\mu|} : \int_{\Omega_\mu}\big(\mathbf{b}_\mu \otimes \mathbf{x}'_\mu\big)\,d\Omega_\mu}_{\mathbf{T}_1} \underbrace{-\frac{\dot{p}}{|\Omega_\mu|}\int_{\Omega_\mu} M_\mu^{-1}\,\mathbf{x}'_\mu\,d\Omega_\mu}_{\mathbf{T}_2} \\ &\quad \underbrace{-\frac{1}{|\Omega_\mu|}\int_{\Omega_\mu}\mathbf{b}_\mu : \big(\dot{\tilde{\boldsymbol{\varepsilon}}}_\mu \otimes \mathbf{x}'_\mu\big)\,d\Omega_\mu}_{\mathbf{T}_3} \underbrace{-\frac{1}{|\Omega_\mu|}\int_{\Omega_\mu} M_\mu^{-1}\,\dot{\tilde{p}}_\mu\,\mathbf{x}'_\mu\,d\Omega_\mu}_{\mathbf{T}_4}. \end{aligned} \tag{3.11}$$

Resulta claro al observar (3.11) que se ha eliminado el término explícito de segundo orden, $\mathbf{T}_5$ al aplicar el enfoque Multiescala-SOE. Además, la dependencia funcional implícita conflictiva de los campos $\tilde{\mathbf{u}}_\mu$ y $\tilde{p}_\mu$ con la componente $\dot{\boldsymbol{\varphi}}_\mu \cdot \mathbf{x}'_\mu$ desaparece, lo que permite escribir

$$\begin{aligned}\dot{\tilde{\boldsymbol{\varepsilon}}}_\mu &= f_{\dot{\tilde{\boldsymbol{\varepsilon}}}_\mu}\left(\ldots, \cancel{\dot{\boldsymbol{\varphi}}_\mu \cdot \mathbf{x}'_\mu}, \ldots\right), \\ \dot{\tilde{p}}_\mu &= f_{\dot{\tilde{p}}_\mu}\left(\ldots, \cancel{\dot{\boldsymbol{\varphi}}_\mu \cdot \mathbf{x}'_\mu}, \ldots\right).\end{aligned}$$

Es decir, los términos $\mathbf{T}_3$ y $\mathbf{T}_4$ dejan de introducir efectos de segundo orden, ya que no existe mas una contribución cuadrática en los productos $\big(\dot{\tilde{\boldsymbol{\varepsilon}}}_\mu \otimes \mathbf{x}'_\mu\big)$ y $(\dot{\tilde{p}}_\mu\,\mathbf{x}'_\mu)$. En consecuencia, se remueve completamente el efecto de tamaño en la parte transitoria de la respuesta.

En definitiva, con la expresión redefinida de $\boldsymbol{\mathcal{V}}_{tra}$ en (3.11), es posible argumentar que la propuesta apunta al núcleo del problema, resultando mínimamente invasiva, ya que solo excluye al término $\mathbf{T}5$, mientras que conserva los restantes términos de $\boldsymbol{\mathcal{V}}_{tra}$ con sus enriquecedoras y necesarias características, con excepción del contraproducente efecto indirecto, cuando el objetivo principal es formular un enfoque de homogeneización estrictamente de primer orden a escala macroscópica. De esta manera, se restaura el proceso clásico de ampliar el tamaño del dominio a microescala hasta alcanzar la representatividad adecuada en la respuesta homogeneizada, lo cual es indispensable para aceptar el concepto de la existencia de RVE en materiales altamente heterogéneos sin renunciar a las capacidades de modelado.

3.6. Conclusiones particulares sobre soluciones analíticas y numéricas

A continuación se presenta un resumen de las principales conclusiones derivadas de las soluciones analíticas y numéricas de los problemas gobernados por ecuaciones de balance de una cantidad escalar con término fuente, como lo son los problemas hidromecánicos y de difusión–reacción, abordados en los artículos publicados, en relación tanto con el modelado Multiescala-FOE como con la propuesta superadora del enfoque Multiescala-SOE. En lo sucesivo, se emplea la denominación de campo primario escalar a microescala en lugar de poropresiones a microescala, con el objetivo de retomar un enfoque general aplicable a problemas de balance de una cantidad escalar, al presentar tanto las conclusiones particulares de esta sección como las generales de la siguiente.

En primer lugar, en Anonis et al. [69] se resolvió un caso unidimensional sencillo correspondiente a un escenario simplificado de la ecuación de difusión–reacción, bajo hipótesis idealizadas entre las que se destaca el uso de un material homogéneo en la microescala. De la solución analítica cerrada obtenida pueden extraerse dos conclusiones de particular relevancia: (i) El campo primario escalar fluctuante de la microescala modelado por el esquema Multiescala-FOE presenta una solución distinta de cero para

$\hat{\mathcal{V}}_\mu^{\text{SOE}}\big(\boldsymbol{\varphi}_\mu^{\text{FOE}}\big)$ y $\dot{\boldsymbol{\sigma}}_\mu^{\text{SOE}} = \hat{\sigma}_\mu^{\text{SOE}}\big(\dot{\boldsymbol{\varepsilon}}_\mu^{\text{FOE}}, \dot{p}_\mu^{\text{ROE}}\big)$, respectivamente.

todo tiempo, aun tratándose de un material homogéneo. En cambio, al adoptar el enfoque Multiescala-SOE, dicho campo resulta nulo en todo instante, tal como era físicamente de esperar. (ii) La variable dual homogeneizada correspondiente permite identificar las componentes que incluyen efectos de segundo orden, resultando esclarecedor para demostrar la inconsistencia de la dependencia con el tamaño de la microescala y como se manifiesta la pérdida de objetividad de la respuesta efectiva con el modelo FOE. Al aplicar el esquema SOE, dicha inconsistencia desaparece, restituyéndose el comportamiento esperado.

En segundo lugar, tanto en Anonis et al. [66, 68] como en Anonis et al. [69], se resolvieron, aplicando las nociones introducidas en la Sección 2.5, los problemas hidromecánico acoplado y de conducción transitoria de calor, respectivamente. Entre las hipótesis simplificativas adoptadas se destacan por su relevancia: (i) el carácter unidimensional de los problemas y (ii) la naturaleza homogénea del material a microescala. En estos casos, se observó que la evolución de la respuesta, tanto para las variables primarias como duales, obtenidas mediante el esquema Multiecala-FOE se aparta progresivamente de la solución de referencia pertinente a medida que aumenta el tamaño de la MC. Por el contrario, al aplicar el modelo Multiescala-SOE, las respuestas numéricas presentan un total acuerdo con las soluciones de referencia, independientemente del tamaño de la microescala.

Por último, en Anonis et al. [66–68, 70] se plantearon escenarios numéricos más complejos, en los cuales se verifica de manera definitiva la capacidad del enfoque Multiescala-SOE para reproducir respuestas coherentes y libres de efectos de tamaño espurios. Para un análisis más detallado, se remite al lector a los Apéndices A, B, D y E.

3.7. Conclusiones

En este capítulo se ha revisado un problema frecuentemente mencionado en la literatura: la dependencia de la respuesta macroscópica con el tamaño de la microescala, y la consecuente falta de objetividad que se manifiesta cuando se aplican formulaciones clásicas de homogeneización de primer orden en problemas hidromecánicos y aquellos regidos por ecuaciones genéricas de balance de una cantidad escalar con término fuente.

Si bien el desarrollo previo se limitó al contexto de la poromecánica, todas las conclusiones obtenidas resultan totalmente válidas para problemas genericos de balance de una cantidad escalar. Por lo que las consideraciones que siguen se presentan de forma general.

De esta manera, mediante el análisis se identificó el término transitorio, que constituye el responsable principal (o el más básico) de introducir el efecto de dependencia con el tamaño de la microescala. Sin embargo, en contextos más generales pueden aparecer otros términos y/o cantidades duales efectivas que exhiban esta inconsitencia de inducir efecto tamaño, como se discute en Anonis et al. [69].

Una vez identificado el término responsable, se efectuó un análisis exhaustivo de la respuesta homogeneizada obtenida con la implementación del esquema Multiescala-FOE, demostrando que contribuciones, y de que manera, son las que introducen la falta de objetividad en la escala de longitud macroscópica. Se esclareció que la causa fundamental radica en la dependencia explícita o implícita respecto de la tasa del gradiente del campo primario escalar de la escala macroscópica, la cual surge al considerar la expansión de orden completo (FOE) del campo escalar primario microscópico como argumento de entrada al evaluar los funcionales constitutivos.

Basándose en los estudios realizados, se propuso una intervención coherente y conceptualmente sencilla: la aplicación de expansiones de orden selectivo (SOE) para los descriptores primitivos escalares a microescala que se incluyen en la lista de argumentos de los funcionales constitutivos a nivel de la microescala. Se introdujo así, el modelo Multiescala-SOE que recupera la existencia del concepto de RVE, tornandose objetiva la respuesta homogeneizada. De esta manera, la propuesta resulta aplicable e imprescindible en los desarrollos posteriores.

Capítulo 4

Modelado multiescala de materiales compuestos por una combinación de un medio poroso saturado con inclusiones impermeables

4.1. Introducción

En este capítulo se presenta una formulación multiescala basada en el concepto de RVE de primer orden para abordar una fenomenología particular que se manifiesta en la escala de longitud menor. En particular, se consideran microestructuras constituidas por una matriz porosa saturada, que requiere el establecimiento adecuado de los campos de desplazamiento y poropresiones, dotadas de inclusiones sólidas no porosas impermeables, descriptos únicamente por el campo de desplazamiento como variable principal. Este tipo de medio no homogéneo, en el que coexisten componentes caracterizados físicamente por diferentes conjuntos de campos primarios, ha motivado la revisión y extensión de las teorías multiescala basadas en RVE. Dichas contribuciones se encuentran desarrolladas en el trabajo publicado de Anonis et al. [67] y el remitido a revisión Anonis et al. [70], que se replican en los Apéndices D y E, respectivamente.

Este nuevo nivel de heterogeneidad, derivada de la coexistencia de distintos conjuntos de descriptores primarios a microescala es característica de numerosos materiales naturales complejos, como geomateriales y tejidos biológicos. En los primeros, pueden mencionarse formaciones geológicas con fragmentos de roca cuasi impermeables dispersos en un estrato de materiales arcillosos o granulares, así como las lutitas, que si bien pueden tratarse como medios porosos homogéneos a macroescala, al ser examinadas más de cerca en la microescala, revelan una composición heterogénea caracterizada por una matriz de arcilla y materia orgánica, intercalada con inclusiones sólidas no porosas (calcita, cuarzo, pirita), Jianting et al. [87], Han et al. [88], Chunxiao et al. [89]. En el ámbito biológico, se han desarrollado modelos multiescala poroelásticos para tejidos biológicos mediante un enfoque de homogeneización asintótica (Laura y Raimondo [90], Miller y Penta [91], Miller [92], Miller et al. [93]). Entre ellos destaca la propuesta destinada a modelar tejidos de microestructura miocárdica (Miller y Penta [94]), constituidos predominantemente por una matriz extracelular en la que se encuentran incrustados vasos sanguíneos y células miocíticas. Un enfoque alternativo, análogo al aquí propuesto, podría abordarse utilizando una técnica basada en RVE, en la que la matriz extracelular junto con los vasos sanguíneos formarían un medio poroelástico que contiene los miocitos como inclusiones sólidas no porosas.

El objetivo de este capítulo es, por tanto, desarrollar un esquema multiescala capaz de describir materiales heterogéneos cuya microestructura involucra componentes con diferentes campos descriptores. La

matriz se describe mediante la teoría de la poromecánica (veáse Sección 2.3), mientras que las inclusiones se incorporan a la teoría convencional de la mecánica de sólidos. A escala macroscópica, se recupera un comportamiento hidromecánico acoplado, siendo que la respuesta constitutiva se obtiene mediante la homogeneización del problema correspondiente a microescala.

El modelo propuesto presenta dos atributos fundamentales: (i) se enmarca en el marco general del Método de Potencia Virtual Multiescala (MMVP), garantizando una metodología variacionalmente consistente; y (ii) la formulación conserva la objetividad con respecto al tamaño del RVE, una característica indispensable pero poco común en los enfoques multiescala basados en RVE para medios porosos saturados, gracias a que se aplica el modelo Multiescala-SOE introducido en el Capítulo 3.

Dado que la capacidad intrínseca de tratar materiales heterogéneos con componentes descriptos por diferentes campos constituye el rasgo distintivo y principal aporte del presente cápitulo, en la Sección 4.2 se ofrece una exposición detallada de este tipo de microestructura, que servirá de base para los desarrollos posteriores.

Finalmente, los aspectos numéricos y de implementación se presentan exclusivamente en el trabajo reproducido en el Apéndice D.

4.2. Suposiciones básicas del modelo en la microescala

El dominio acotado $\Omega_\mu \in \mathbb{R}^3$, que representa al cuerpo $\mathcal{B}_\mu$ de la microestructura, difiere del presentado en la Sub-sección 2.4.1, pues presenta particularidades específicas que deben ser consideradas. Este se asume compuesto por una matriz porosa saturada, la cual constituye un subdominio acotado de Ω_μ, denotado por Ω_μ^p. En dicho subdominio, el comportamiento del material se describe mediante la teoría general de la poromecánica (Coussy [36, 37]), que requiere para su caracterización la evaluación del campo de desplazamiento a microescala, $\mathbf{u}_\mu$, y del campo de poropresiones a microescala, p_μ, tal como se ha desarrollado en los capítulos precedentes. Por su parte, el espacio complementario de Ω_μ, que se define como Ω_μ^s, está ocupado por inclusiones de volumen sólido e impermeable. Estas últimas solo requieren la definición del campo de desplazamiento a microescala, $\mathbf{u}_\mu$, para determinar su respuesta física. En consecuencia, el campo p_μ existe únicamente en el subdominio Ω_μ^p de la MC.

Esta particularidad hace necesario abordar el estudio del dominio de la MC de manera específica. En primer lugar, el contorno de Ω_μ, denotado aquí como Γ_μ, se subdivide en diferentes subdominios superficiales, véase la Figura 4.1, a saber:

- Γ_μ: superficie límite externa del dominio Ω_μ de la MC, que tiene un versor normal orientado hacia afuera representado por $\mathbf{n}_\mu$;
- Γ_μ^p: superficie externa del medio poroso que tiene un vector normal externo $\mathbf{n}_\mu^p$;
- Γ_μ^s: superficie externa del medio sólido que tiene un vector normal dirigido hacia afuera indicado con $\mathbf{n}_\mu^s$;
- Γ_μ^i: superficie de interfaz interna entre la matriz porosa saturada y las inclusiones sólidas impermeables. El vector normal externo que apunta desde el medio poroso hacia la inclusión se define como $\mathbf{n}_\mu^p = \mathbf{n}_\mu^i$; mientras que el vector normal que apunta desde las partículas sólidas hacia la matriz porosa se denota como $\mathbf{n}_\mu^s = -\mathbf{n}_\mu^i$.

Dadas las definiciones anteriores, se tiene: $\Gamma_\mu = \Gamma_\mu^p \bigcup \Gamma_\mu^s$ y $\Gamma_\mu^p \bigcap \Gamma_\mu^s = \varnothing$. Además, es posible escribir para el dominio $\Omega_\mu = \Omega_\mu^s \bigcup \Omega_\mu^p$ y $\Omega_\mu^s \bigcap \Omega_\mu^p = \varnothing$.

El esquema mostrado en la Figura 4.1, pretende respresentar la configuración más general posible, en la cual la distribución de las inclusiones se ocurre de manera totalmente aleatoria, alcanzando la frontera de la MC. Sin embargo, en el presente capítulo, se limita exclusivamente a modelar dos posibles configuraciones de distribuciones de inclusiones impermeables en la MC: (i) cuando se adopta un patrón

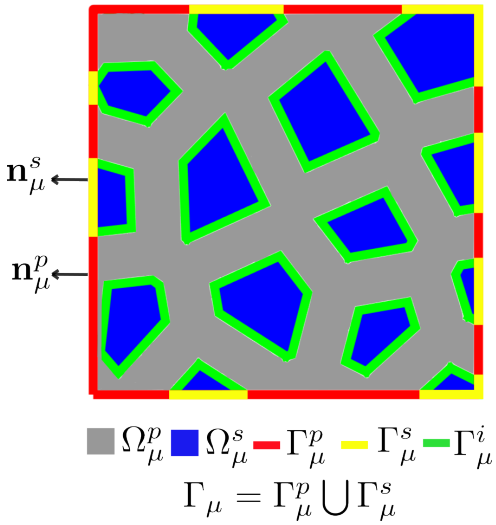

Figura 4.1: MC genérica compuesta por dos materiales diferentes: una matriz porosa saturada (gris) e inclusiones sólidas impermeables (azul).

en el que las partículas sólidas alcanzan el límite del dominio, pero conservan una disposición simétrica, de modo que se cumple la condición de periodicidad en el contorno de la MC, véase la Figura 4.2(a); o (ii) cuando se presupone que todas las inclusiones sólidas son internas, véase la Figura 4.2(b), en cuyo caso $\Gamma_\mu = \Gamma_\mu^p$ y $\Gamma_\mu^s = \varnothing$. Frente a estos escenarios se tienen las siguientes propiedades geométricas

$$\begin{aligned} \int_{\Gamma_\mu^p} \mathbf{n}_\mu^p \, d\Gamma_\mu &= \mathbf{0}, \\ \int_{\Gamma_\mu^s} \mathbf{n}_\mu^s \, d\Gamma_\mu &= \mathbf{0}. \end{aligned} \tag{4.1}$$

Las MC que satisfacen la ecuación (4.1) se denominan $\mathbf{n}_\mu$-equilibradas, mientras que aquellas que no lo hacen se consideran $\mathbf{n}_\mu$-desequilibradas. Esta clasificación, junto con otros conceptos fundamentales, se ha tomado y adaptado de las contribuciones recientes de Blanco et al. [21]. El motivo de esta denominación parte desde una perspectiva puramente geométrica, ya que las ecuaciones (4.1) implican que el vector normal hacia afuera está equilibrado tanto en el medio poroso como en los límites del medio sólido de la MC. Desde un punto de vista conceptual, la hipótesis detrás de las ecuaciones (4.1) garantiza que el modelo multiescala mínimamente restringido se equilibra por sí mismo en términos del vector de velocidad de flujo a microescala a través de toda la frontera Γ_μ^p. Esta propiedad resulta especialmente deseable porque tiene un claro sentido físico, al asegurar un comportamiento intrínsecamente balanceado. Es posible relajar la condición (4.1) y, por lo tanto, considerar una distribución realmente aleatoria de las inclusiones sólidas como el de la Figura 4.1. No obstante, este escenario debe ir acompañado de redefiniciones adecuadas de la regla de homogeneización para el gradiente de poropresiones, con el fin de obtener, de nuevo, velocidades de flujo a microescala autoequilibradas. Este tema es un ingrediente muy específico de la formulación que requiere un desarrollo exhaustivo, lo que podría desviar la atención del núcleo conceptual del presente capítulo, que consiste exclusivamente en desarrollar un marco multiescala capaz de manejar microestructuras heterogéneas con componentes que requieren diferentes variables primitivas para su descripción física. Por esta razón, se posterga abordar dicha generalización hasta el Capítulo 5.

A partir de la hipótesis basada en la geometría que se incluye en la formulación (4.1), se presupone, de manera artificial, una disposición simétrica de las partículas cada vez que alcanzan el contorno de la MC. Por lo tanto, el modelo de homogeneización Periódico puede utilizarse sin objeciones, tal como fue

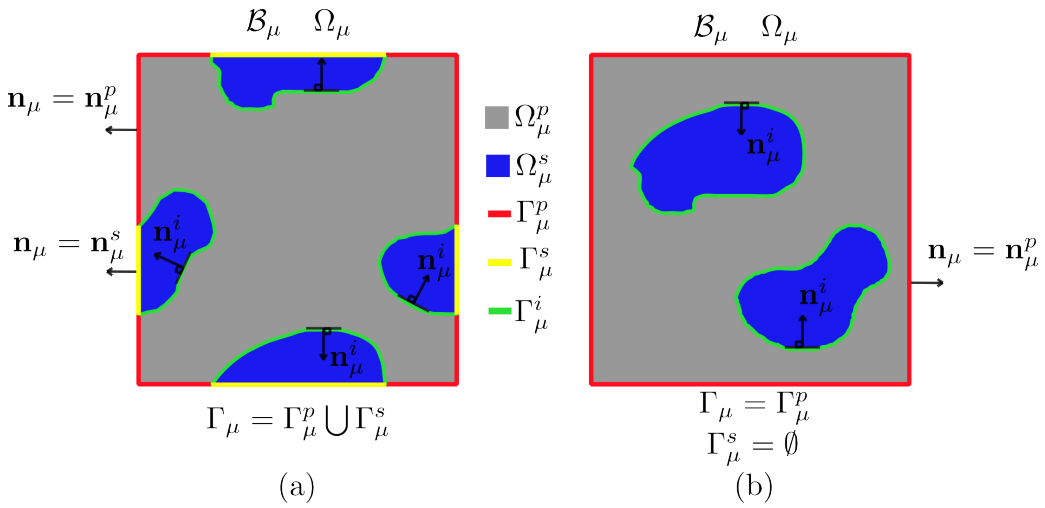

Figura 4.2: MCs compuestas por dos materiales diferentes: una matriz porosa saturada (gris) e inclusiones sólidas (azul). (a) MC con inclusiones sólidas impermeables que alcanzan el límite. (b) MC con inclusiones sólidas impermeables internas únicamente.

realizado en Anonis et al. [67].

Al igual que en la Sub-sección 2.4.2, es necesario definir el concepto de admisibilidad para los descriptores primitivos entre las dos escalas implicadas. Cabe destacar que los campos, $\mathbf{u}(t)$ y $\boldsymbol{\varepsilon}(t)$, se encuentran definidos en todo el dominio $\Omega_\mu = \Omega_\mu^p \cup \Omega_\mu^s$, incluyendo tanto el esqueleto de la matriz porosa saturada como el volumen de inclusión sólida, véanse las Figuras 4.1 y 4.2. Por este motivo, todo lo expuesto previamente en dicha sección en relación a los desplazamientos y deformaciones a microescala permanece inalterado. Sin embargo, a diferencia de lo anteriormente presentado, las nociones vinculadas a las poropresiones en la microescala y a su gradiente se ven afectadas por el hecho de que dichos campos existen únicamente en una parte de la MC. Por esta razón, en lo que sigue se introducen únicamente los cambios pertinentes a este descriptor, al establecer los procedimientos secuenciales de inserción y homogeneización.

El hecho de que el campo de poropresiones de la microescala solo exista en Ω_μ^p, conduce a que puedan asumirse dos posibilidades respecto de su expansión conforme a una serie de tipo Taylor, en función de las cantidades $\{p(t), \boldsymbol{\varphi}(t)\}$ valoradas en puntos $\mathbf{x}$ de la macroescala. En consecuencia, las dos opciones viables para expandir el campo de poropresiones microescala consisten en:

- Expansión alrededor del centro geométrico o centroide $\mathbf{x}_\mu^G$ de toda la MC.
- Expansión a partir del centroide del subdominio Ω_μ^p, que se establece posteriormente en (4.3).

El campo de los desplazamientos del nivel microscópico se expande en ambos casos, como antes, alrededor de $\mathbf{x}_\mu^G$. Este identifica la posición del centroide de Ω_μ, que ya fue introducido en (2.22). Por conveniencia, se reescribe a continuación

$$\mathbf{x}_\mu^G = \frac{1}{|\Omega_\mu|} \int_{\Omega_\mu} \mathbf{x}_\mu \, d\Omega_\mu. \tag{4.2}$$

Por su parte, se identifica la posición del centroide del subdominio correspondiente al medio poroso saturado, Ω_μ^p, con respecto al sistema de coordenadas global en la microescala, de la siguiente manera

$$\mathbf{x}_\mu^{Gp} = \frac{1}{|\Omega_\mu^p|} \int_{\Omega_\mu^p} \mathbf{x}_\mu \, d\Omega_\mu, \tag{4.3}$$

Cabe destacar que las dos propuestas de expansión, deberían converger a un único modelo en presencia de MCs suficientemente representativas, es decir, al alcanzar el RVE. En tal situación la microestructura tiende a la simétria y, bajo dicha condición, el centroide $\mathbf{x}_\mu^{Gp}$ del subdominio Ω_μ^p coincide con el centro geométrico de la MC, $\mathbf{x}_\mu^G$. Ante este escenario, se cumple que el campo de poropresiones fluctuantes p_μ será el mismo, de modo que las expresiones presentadas posteriormente en (4.4) y (4.21) colapsan a una única forma.

A lo largo de las Secciones 4.3 y 4.4, se establece, una vez más, el marco variacional siguiendo las directrices dadas por el MMVP (Blanco et al. [19], Taroco et al. [20], Blanco et al. [21]), del mismo modo que en la Sección 2.4, aunque adaptado ahora a la compleja microestructura cuyo tratamiento se pretende abordar. Dado que existen dos posibles esquemas de expansión del campo de poropresiones a microescala, en la Sección 4.3 se presentan en primer lugar los desarrollos referidos a la expansión en torno a $\mathbf{x}_\mu^G$. Posteriormente, en la Sección 4.4 se describen los pasos de aplicación de la metodología conforme a la segunda forma de expansión propuesta.

Por último, cabe remarcar que, por conveniencia y para evitar sobrecargar la notación, no se introducen símbolos adicionales (como subíndices o superíndices) que indiquen explicitamente el tipo de expansión del campo de poropresiones utilizado, a excepción de cuando se presentan el conjunto (véase 4.3.3) y el espacio admisibles (véase 4.4.3) que permiten establecer los modelos mínimamente restringidos para uno u otro caso. Esta decisión permite preservar la coherencia de la notación conforme a lo establecido en los capítulos precedentes. No obstante, aunque todas las cantidades se denoten y definan de manera análoga, los valores que pueden adoptar cada una de ellas difieren según sea el modelo de expansión considerado en la Sección 4.3 o en la Sección 4.4.

4.3. MMVP con poropresiones microescala expandidas alrededor del centro geométrico del dominio de la MC

4.3.1. Inserción de los descriptores correspondientes al subdominio del medio poroso saturado

En esta sección se establece el modo en que se insertan los descriptores primarios que únicamente existen en el subdominio Ω_μ^p de la MC, contribuyendo en el problema del balance hidromecánico a microescala.

El proceso de inserción debe garantizar la coherencia física derivada del hecho que el medio sólido no admite variables de poropresiones, es decir, este descriptor primario solo existe en el subdominio Ω_μ^p. Al asumir la expansión alrededor del centroide $\mathbf{x}_\mu^G$ de toda la MC, acorde a una serie de tipo Taylor en términos de las cantidades $\{p(t), \boldsymbol{\varphi}(t)\}$ evaluadas en puntos $\mathbf{x}$ de la macroescala, se tiene que

$$p_\mu(\mathbf{x}_\mu, t) = p(t) + \boldsymbol{\varphi}(t) \cdot \left(\mathbf{x}_\mu - \mathbf{x}_\mu^G\right) + \tilde{p}_\mu(\mathbf{x}_\mu, t), \quad \forall \mathbf{x}_\mu \in \Omega_\mu^p, \tag{4.4}$$

donde $\tilde{p}_\mu(\mathbf{x}_\mu, t)$ representa el campo fluctuante de las poropresiones a microescala, definido únicamente en la matriz porosa Ω_μ^p.

De acuerdo con la expresión (4.4), el gradiente de las poropresiones a microescala se obtiene como resultado de aplicar el operador diferencial $\boldsymbol{\nabla}_{\mathbf{x}_\mu}(\bullet)$ de la siguiente manera

$$\boldsymbol{\varphi}_\mu(\mathbf{x}_\mu, t) = \boldsymbol{\nabla}_{\mathbf{x}_\mu} p_\mu(\mathbf{x}_\mu, t) = \boldsymbol{\varphi}(t) + \boldsymbol{\nabla}_{\mathbf{x}_\mu} \tilde{p}_\mu(\mathbf{x}_\mu, t) = \boldsymbol{\varphi}(t) + \tilde{\boldsymbol{\varphi}}_\mu(\mathbf{x}_\mu, t), \quad \forall \mathbf{x}_\mu \in \Omega_\mu^p. \tag{4.5}$$

donde $\tilde{\boldsymbol{\varphi}}_\mu(\mathbf{x}_\mu, t)$ es el vector gradiente de las poropresiones fluctuantes en el subdominio Ω_μ^p de la MC.

4.3.2. Homogeneización de los descriptores correspondientes al subdominio del medio poroso saturado

De los cuatro procedimientos de homogeneización propuestos en la Sub-sección 2.4.2, únicamente el segundo grupo, represantado por $\mathcal{H}_p$ y $\mathcal{H}_{\boldsymbol{\varphi}}$, encargado de establecer la correspondencia entre el campo de poropresiones y los gradientes de poropresiones a microescala con sus respectivos valores puntuales a macroescala, p y $\boldsymbol{\varphi}$, resulta modificado para el tipo de microestructura analizado en este capítulo. Los otros dos procedimientos se expresan de forma análoga a (2.20) y (2.24), respectivamente.

Homogeneización de las poropresiones

Tal como se refleja en la expresión (4.4), las poropresiones de la macroescala y su gradiente se introducen únicamente dentro del subdominio de la matriz a microescala Ω_μ^p, donde poseen significado físico. Por el mismo motivo, se propone el proceso de homogeneización para las poropresiones a microescala expandidas en torno a $\mathbf{x}_\mu^G$, denotado por $\mathcal{H}_p$, que consiste en una regla de promediado restringida al subdominio Ω_μ^p y que se define como

$$\mathcal{H}_p\left(p_\mu\right) = p = \frac{1}{|\Omega_\mu^p|}\int_{\Omega_\mu^p} p_\mu \, d\Omega_\mu. \tag{4.6}$$

Si se sustituye (4.4) en (4.6), se obtiene

$$p = p + \boldsymbol{\varphi} \cdot \left[\frac{1}{|\Omega_\mu^p|}\int_{\Omega_\mu^p}\left(\mathbf{x}_\mu - \mathbf{x}_\mu^G\right)\, d\Omega_\mu\right] + \frac{1}{|\Omega_\mu^p|}\int_{\Omega_\mu^p}\tilde{p}_\mu \, d\Omega_\mu, \tag{4.7}$$

donde, la expresión (4.7) proporciona una restricción no homogénea sobre la integral del campo de poropresiones fluctuantes a microescala, que se escribe de la siguiente manera

$$\int_{\Omega_\mu^p}\tilde{p}_\mu \, d\Omega_\mu = -\boldsymbol{\varphi} \cdot \int_{\Omega_\mu^p}\left(\mathbf{x}_\mu - \mathbf{x}_\mu^G\right)\, d\Omega_\mu = -\boldsymbol{\varphi} \cdot \left(\mathbf{x}_\mu^{Gp}\,|\Omega_\mu^p| - \mathbf{x}_\mu^G\,|\Omega_\mu^p|\right). \tag{4.8}$$

En presencia de un patrón aleatorio de las inclusiones sólidas impermeables dentro del dominio de la MC, el gradiente de las poropresiones a macroescala, $\boldsymbol{\varphi}$, insertado en Ω_μ^p, induce un efecto que debe ser compensado por el valor integral de las poropresiones fluctuantes de la microescala, a fin de garantizar el cumplimiento de (4.6). La condición (4.8) debe, por tanto, imponerse en la formulación multiescala para el campo de poropresiones a microescala dentro del subdominio de la matriz porosa saturada Ω_μ^p. Sin embargo, ante una distribución simétrica, como la que se asume al considerar un elemento representativo, se tiene que $\mathbf{x}_\mu^{Gp} \equiv \mathbf{x}_\mu^G$, y la restricción (4.8) se reduce entonces a una condición homogénea.

Homogeneización del gradiente de poropresiones

Se presenta a continuación la formulación de la regla de homogeneización correspondiente al gradiente del campo de poropresiones, asociado al modelado de MCs $\mathbf{n}_\mu^p$-equilibradas ($\mathbf{n}_\mu^s$-equilibradas), esto es, aquellas que satisfacen las condiciones dadas en (4.1). En el caso de microestructuras más generales, $\mathbf{n}_\mu^p$-desequilibradas ($\mathbf{n}_\mu^s$-desequilibradas), se requieren desarrollos adicionales que se tratan específicamente en el Capítulo 5.

De esta manera, para los casos particulares esquematizados en la Figura 4.2 y de acuerdo con la propuesta de expansión para p_μ, se adopta la regla de homogeneización $\mathcal{H}_{\boldsymbol{\varphi}}$, la cual se define como

$$\mathcal{H}_{\boldsymbol{\varphi}}\left(\boldsymbol{\varphi}_\mu\right) = \boldsymbol{\varphi} = \frac{1}{|\Omega_\mu^p|}\left[\int_{\Omega_\mu^p}\boldsymbol{\varphi}_\mu \, d\Omega_\mu - \int_{\Gamma_\mu^i}\tilde{p}_\mu \, \mathbf{n}_\mu^i \, d\Gamma_\mu\right], \tag{4.9}$$

donde el segundo término que involucra la interfaz interna Γ_μ^i, se incluye con el propósito de obtener una

expresión de homogeneización del gradiente de poropresiones formulada exclusivamente sobre el límite externo de la matriz Γ_μ^p, como es de esperar.

Teniendo en cuenta (4.5) y aplicando el teorema de Green, la expresión (4.9) puede reescribirse como

$$\boldsymbol{\varphi} = \boldsymbol{\varphi} + \frac{1}{|\Omega_\mu^p|}\left[\int_{\Omega_\mu^p} \boldsymbol{\nabla}_{\mathbf{x}_\mu}\tilde{p}_\mu \, d\Omega_\mu - \int_{\Gamma_\mu^i} \tilde{p}_\mu \, \mathbf{n}_\mu^i \, d\Gamma_\mu\right] = \boldsymbol{\varphi} + \frac{1}{|\Omega_\mu^p|}\int_{\Gamma_\mu^p} \tilde{p}_\mu \, \mathbf{n}_\mu^p \, d\Gamma_\mu. \tag{4.10}$$

De (4.10) surge una restricción adicional para el campo de poropresiones fluctuantes a microescala en el contorno Γ_μ^p

$$\int_{\Gamma_\mu^p} \tilde{p}_\mu \, \mathbf{n}_\mu^p \, d\Gamma_\mu = \mathbf{0}. \tag{4.11}$$

4.3.3. Conjunto admisible de los descriptores correspondientes al subdominio del medio poroso saturado

Para el campo de desplazamientos fluctuantes, el espacio que define el modelo multiescala mínimamente restringido permanece con su expresión inalterada, dado que dicho descriptor es continuo en toda la MC. Por lo tanto, la definición (2.31) continúa siendo válida.

Sin embargo, el campo de poropresiones a microescala se ve alterado por el hecho de que solo existe en Ω_μ^p, considerándose admisible solo si satisface las condiciones (4.8) y (4.11), garantizando la compatibilidad con los procedimientos de homogeneización descritos en (4.6) y (4.9). Por esta razón, el espacio que define el MCMM y representa la admisibilidad, definido en (2.32), debe ser modificado a fin de ser adecuado para capturar los cambios introducidos por el modelo microestructural actual. En consecuencia, se define el conjunto funcional admisible

$$\widehat{\widetilde{\mathcal{P}}}_\mu\left(\Omega_\mu^p\right) = \left\{\tilde{p}_\mu \in \mathrm{H}^1\left(\Omega_\mu^p\right); \int_{\Omega_\mu^p}\left[\boldsymbol{\varphi}\cdot\left(\mathbf{x}_\mu - \mathbf{x}_\mu^G\right) + \tilde{p}_\mu\right] d\Omega_\mu = 0; \int_{\Gamma_\mu^p} \tilde{p}_\mu \, \mathbf{n}_\mu^p \, d\Gamma_\mu = \mathbf{0}\right\}. \tag{4.12}$$

El conjunto considerado impone las mínimas restricciones necesarias en la microescala para garantizar la admisibilidad y junto a (2.31) definen el modelo de mínimas restricciones que se denomina $\widehat{\text{MCMM}}$. A partir de él, pueden definirse subconjuntos más restrictivos, $\widehat{\widetilde{\mathcal{P}}}_\mu^{\square}\left(\Omega_\mu^p\right) \subseteq \widehat{\widetilde{\mathcal{P}}}_\mu\left(\Omega_\mu^p\right)$, que dan lugar a esquemas de homogeneización alternativos. En tales casos, los campos de poropresiones fluctuantes se asumen pertenecientes a estos subconjuntos con los que es común trabajar, es decir, $\tilde{p}_\mu \in \widehat{\widetilde{\mathcal{P}}}_\mu^{\square}\left(\Omega_\mu\right)$.

De manera análoga a lo establecido en la Sub-sección 2.4.2, se definen las acciones virtuales, preservando las variaciones de los desplazamientos y deformaciones a microescala conforme a lo presentado en (2.33) y (2.34), respectivamente. En contraste, las variables de poropresiones y sus gradientes a microescala se formulan para el modelo actual teniendo en cuenta (4.4) y (4.5), de la siguiente manera

$$\delta p_\mu = \delta p + \delta\boldsymbol{\varphi}\cdot\left(\mathbf{x}_\mu - \mathbf{x}_\mu^G\right) + \delta\tilde{p}_\mu, \quad \forall \mathbf{x}_\mu \in \Omega_\mu^p, \tag{4.13}$$

$$\delta\boldsymbol{\varphi}_\mu = \delta\boldsymbol{\varphi} + \boldsymbol{\nabla}_{\mathbf{x}_\mu}\delta\tilde{p}_\mu, \quad \forall \mathbf{x}_\mu \in \Omega_\mu^p. \tag{4.14}$$

A partir de estas expresiones se introduce el espacio lineal para las fluctuaciones virtuales admisibles

$$\widetilde{\mathcal{P}}_\mu^*\left(\Omega_\mu^p\right) = \left\{\delta\tilde{p}_\mu \in \mathrm{H}^1\left(\Omega_\mu^p\right); \int_{\Omega_\mu^p}\delta\tilde{p}_\mu \, d\Omega_\mu = 0; \int_{\Gamma_\mu^p}\delta\tilde{p}_\mu \, \mathbf{n}_\mu^p \, d\Gamma_\mu = \mathbf{0}\right\}, \tag{4.15}$$

con $\delta\tilde{p}_\mu \in \widetilde{\mathcal{P}}_\mu^*\left(\Omega_\mu^p\right)$.

A causa de que la restricción (4.8) es de tipo no homogénea, el conjunto $\widehat{\widetilde{\mathcal{P}}}_\mu\left(\Omega_\mu^p\right)$ y el espacio $\widetilde{\mathcal{P}}_\mu^*\left(\Omega_\mu^p\right)$ no coinciden.

4.3.4. Principio de Potencia Virtual Multiescala (PMVP)

La expresión que define la potencia virtual total que se produce en un punto $\mathbf{x}$ de la macorescala, y se vincula con el dominio de la MC, se conserva como fue establecida en la ecuación (2.39) de la Sub-sección 2.4.2. En cambio, la potencia virtual total correspondiente al dominio de la microescala se redefine del siguiente modo

$$\delta\mathcal{P}_{\mu}^{tot}\left(\delta\dot{\mathbf{u}}_{\mu},\delta\dot{\boldsymbol{\varepsilon}}_{\mu},\delta p_{\mu},\delta\boldsymbol{\varphi}_{\mu}\right)=\int_{\Omega_{\mu}}\left(\boldsymbol{\sigma}_{\mu}\,:\,\delta\dot{\boldsymbol{\varepsilon}}_{\mu}\,-\,\mathbf{f}_{\mu}\,\cdot\,\delta\dot{\mathbf{u}}_{\mu}\right)d\Omega_{\mu}+\int_{\Omega_{\mu}^{p}}\left(\dot{\chi}_{\mu}\,\delta p_{\mu}-\boldsymbol{\mathcal{V}}_{\mu}\,\cdot\,\delta\boldsymbol{\varphi}_{\mu}\right)d\Omega_{\mu}. \tag{4.16}$$

Cabe notar que los pares conjugados $\{\dot{\chi}_{\mu},\delta p_{\mu}\}$ y $\{\boldsymbol{\mathcal{V}}_{\mu},\delta\boldsymbol{\varphi}_{\mu}\}$, inherentes a la matriz porosa saturada, solo ejercen potencia virtual sobre el subdominio correspondiente Ω_{μ}^{p}. En esta formulación, el campo de fuerzas de cuerpo a microescala se introduce como $\mathbf{f}_{\mu}=\rho_{\mu}^{(\bullet)}\,\mathbf{g}$, que representa el peso por unidad de volumen del medio. El valor de $\rho_{\mu}^{(\bullet)}$ depende del subdominio al que pertence el punto material. Si pertenece a Ω_{μ}^{p}, se utiliza la densidad saturada $\rho_{\mu}^{p}=\rho^{p,f}n_{\mu}+\rho^{p,s}\left(1-n_{\mu}\right)$, donde $\rho^{p,s}$ denota la densidad de la fase sólida en el medio poroso. En cambio, si pertenece a Ω_{μ}^{s}, se emplea la densidad de la inclusión sólida ρ_{μ}^{s}.

Entonces, por aplicación del PMVP al relacionar las potencias virtuales de ambas escalas conforme a las definiciones (2.39) y (4.16), y considerando todas las acciones virtuales admisibles definidas en (2.33), (2.34), (4.13) y (4.14), se obtiene la siguiente ecuación variacional

$$\begin{aligned}\left|\Omega_{\mu}\right|\left(\boldsymbol{\sigma}\,:\,\delta\dot{\boldsymbol{\varepsilon}}-\mathbf{f}\,\cdot\,\delta\dot{\mathbf{u}}+\dot{\chi}\,\delta p-\boldsymbol{\mathcal{V}}\,\cdot\,\delta\boldsymbol{\varphi}\right)&=\int_{\Omega_{\mu}}\Big[\boldsymbol{\sigma}_{\mu}\,:\,\left(\delta\dot{\boldsymbol{\varepsilon}}+\boldsymbol{\nabla}_{\mathbf{x}_{\mu}}^{sym}\,\delta\dot{\tilde{\mathbf{u}}}_{\mu}\right)\\&\qquad-\,\mathbf{f}_{\mu}\,\cdot\,\left(\delta\dot{\mathbf{u}}+\delta\boldsymbol{\varepsilon}\,\left(\mathbf{x}_{\mu}-\mathbf{x}_{\mu}^{G}\right)+\delta\dot{\tilde{\mathbf{u}}}_{\mu}\right)\Big]\,d\Omega_{\mu}\\&+\int_{\Omega_{\mu}^{p}}\Big[\dot{\chi}_{\mu}\left(\delta p+\delta\boldsymbol{\varphi}\,\cdot\,\left(\mathbf{x}_{\mu}-\mathbf{x}_{\mu}^{G}\right)+\delta\tilde{p}_{\mu}\right)-\boldsymbol{\mathcal{V}}_{\mu}\,\cdot\,\left(\delta\boldsymbol{\varphi}+\boldsymbol{\nabla}_{\mathbf{x}_{\mu}}\,\delta\tilde{p}_{\mu}\right)\Big]\,d\Omega_{\mu},\\\forall\left(\delta\dot{\boldsymbol{\varepsilon}}\,,\delta\dot{\mathbf{u}}\,,\delta\boldsymbol{\varphi}\,,\delta p\right)&\in\mathbb{R}^{6}\times\mathbb{R}^{3}\times\mathbb{R}^{3}\times\mathbb{R},\ \left(\delta\dot{\tilde{\mathbf{u}}}_{\mu}\,,\delta\tilde{p}_{\mu}\right)\in\widetilde{\mathcal{U}}_{\mu}^{*}\left(\Omega_{\mu}\right)\times\widetilde{\mathcal{P}}_{\mu}^{*}\left(\Omega_{\mu}^{p}\right),\,\forall\,t.\end{aligned} \tag{4.17}$$

Donde se observa que todos los términos que caracterizan la potencia virtual total a microescala se normalizan por el volumen total de la microcelda $|\Omega_{\mu}|$, incluidos aquellos definidos únicamente sobre el subdominio Ω_{μ}^{p}.

Finalmente, al operar de forma variacional, se derivan naturalmente las consecuencias del PMVP y de las condiciones admisibilidad. Entre ellas, las expresiones de la tensión a macroescala $\boldsymbol{\sigma}$, la regla de promediado para la fuerza de cuerpo $\mathbf{f}$, y la forma variacional de la ecuación de balance de cantidad de movimiento a escala de longitud menor coinciden con las ecuaciones (2.42), (2.46) y (2.47), respectivamente. En cambio, el modelo de MCs propuesto en este capítulo conduce a diferentes fórmulas de homogeneización para $\dot{\chi}$ y $\boldsymbol{\mathcal{V}}$, así como a una formulación modificada de la ecuación del balance de masa, que se presentan a continuación.

Tasa de volumen de poros homogeneizada (por unidad de volumen de poros):

$$\dot{\chi}=\frac{\dot{m}^{f}}{\rho^{f}}=\frac{1}{|\Omega_{\mu}|}\int_{\Omega_{\mu}^{p}}\dot{\chi}_{\mu}\,d\Omega_{\mu},\ \forall\,t. \tag{4.18}$$

Cabe señalar que en (4.18) el factor de promediado y el dominio de integración son diferentes entre sí.

Vector de velocidad del flujo homogeneizado:

$$\boldsymbol{\mathcal{V}}=\frac{1}{|\Omega_{\mu}|}\int_{\Omega_{\mu}^{p}}\left[\boldsymbol{\mathcal{V}}_{\mu}-\dot{\chi}_{\mu}\,\left(\mathbf{x}-\mathbf{x}_{\mu}^{G}\right)\right]d\Omega_{\mu},\ \forall\,t. \tag{4.19}$$

Una vez más, obsérvese que en (4.19) el dominio de integración difiere de la medida de normalización.

Forma variacional de la ecuación de balance de masas en la MC:

$$\mathrm{H}_\mu = \int_{\Omega_\mu^p} \left(\dot{\chi}_\mu \, \delta\tilde{p}_\mu - \boldsymbol{\mathcal{V}}_\mu \cdot \boldsymbol{\nabla}_{\mathbf{x}_\mu} \delta\tilde{p}_\mu \right) d\Omega_\mu = 0, \;\; \forall \, \delta\tilde{p}_\mu \in \widetilde{\mathcal{P}}_\mu^* \left(\Omega_\mu^p \right), \; \forall \, t, \tag{4.20}$$

donde, como era de esperar, solo interviene el subdominio Ω_μ^p, ya que el medio sólido, Ω_μ^s, no admite el campo de poropresiones a microescala.

4.4. MMVP con poropresiones microescala expandidas alrededor del centro geométrico del subdominio de la matriz

De forma semejante a lo desarrollado en la Sección 4.3, se adoptan los lineamientos del MMVP aplicados a la misma MC compuesta, aunque considerando ahora la expansión propuesta en torno al centroide del subdominio Ω_μ^p. Las definiciones que preserven su estructura no se reescriben aquí, sino que se remite al apartado y/o ecuación correspondiente.

4.4.1. Inserción de los descriptores correspondientes al subdominio del medio poroso saturado

La forma en que se insertan los descriptores primarios debe garantizar que estos existan únicamente dentro del subdominio Ω_μ^p, incluso cuando la expansión se plantea a partir del centro geométrico $\mathbf{x}_\mu^{Gp}$. En este caso, la expresión se escribe como

$$p_\mu \left(\mathbf{x}_\mu, t \right) = p \left(t \right) + \boldsymbol{\varphi} \left(t \right) \cdot \left(\mathbf{x}_\mu - \mathbf{x}_\mu^{Gp} \right) + \tilde{p}_\mu \left(\mathbf{x}_\mu, t \right), \quad \forall \mathbf{x}_\mu \in \Omega_\mu^p. \tag{4.21}$$

Nuevamente, el campo fluctuante de las poropresiones a microescala, $\tilde{p}_\mu \left(\mathbf{x}_\mu, t \right)$, solo existe en Ω_μ^p.

Al aplicar el operador gradiente $\boldsymbol{\nabla}_{\mathbf{x}_\mu} (\bullet)$ sobre p_μ dado por (4.21), se obtiene el correspondiente gradiente de las poropresiones a microescala, cuya forma resulta completamente equivalente a la presentada en (4.5).

4.4.2. Homogeneización de los descriptores correspondientes al subdominio del medio poroso saturado

El proceso de homogeneización $\mathcal{H}_{\boldsymbol{\varphi}}$ resulta totalmente equivalente, en su formulación, al propuesto en la sección precedente mediante la definición (4.9). Esto conduce a una restricción para el campo de poropresiones fluctuantes a microescala acorde a la forma indicada en (4.11). Por lo tanto, a continuación se reformula unicamente el procedimiento de homogeneización $\mathcal{H}_p$, adaptado al criterio de expansión asumido en está sección.

Homogeneización de las poropresiones

El procedimiento correspondiente a $\mathcal{H}_p$, se expresa nuevamente como

$$\mathcal{H}_p \left(p_\mu \right) = p = \frac{1}{|\Omega_\mu^p|} \int_{\Omega_\mu^p} p_\mu \, d\Omega_\mu. \tag{4.22}$$

Sin embargo, al reemplazar (4.21) en (4.22), se obtiene como nueva formulación lo siguiente

$$p = p + \boldsymbol{\varphi} \cdot \left[\frac{1}{|\Omega_\mu^p|} \int_{\Omega_\mu^p} \left(\mathbf{x}_\mu - \mathbf{x}_\mu^{Gp} \right) \, d\Omega_\mu \right] + \frac{1}{|\Omega_\mu^p|} \int_{\Omega_\mu^p} \tilde{p}_\mu \, d\Omega_\mu, \tag{4.23}$$

donde el segundo término se anula, según (4.3), debido a que la expansión de p_μ se realiza alrededor del centro geométrico $\mathbf{x}_\mu^{Gp}$ de la fracción del medio poroso saturado Ω_μ^p de la MC. Como consecuencia, se alcanza una restricción homogénea para el campo de poropresiones a microescala, es decir

$$\int_{\Omega_\mu^p} \tilde{p}_\mu \, d\Omega_\mu = 0. \tag{4.24}$$

De esta manera, el criterio adoptado para expandir el campo de poropresiones en la microescala puede conducir a distintas formas de restricción volumétrica para las poropresiones fluctuantes. No obstante, es probable que en el caso de materiales con una población de inclusiones verdaderamente aleatoria, las expresiones (4.8) y (4.24) tenderán a coincidir, reduciéndose ambas a una única restricción volumétrica de carácter homogéneo.

4.4.3. Espacio admisible de los descriptores correspondientes al subdominio del medio poroso saturado

El espacio que define la admisibilidad de las poropresiones fluctuantes de la microescala, afectado por la suposición de la expansón de p_μ alrededor de $\mathbf{x}_\mu^{Gp}$, será aquel que satisface la condición (4.24) en lugar de (4.8). De esta manera, el espacio funcional particularizado a la propuesta de esta sección, se construye como

$$\overline{\widetilde{\mathcal{P}}}_\mu\left(\Omega_\mu^p\right) = \left\{ \tilde{p}_\mu \ \in \ \mathrm{H}^1\left(\Omega_\mu^p\right); \ \int_{\Omega_\mu^p} \tilde{p}_\mu \, d\Omega_\mu = 0; \ \int_{\Gamma_\mu^p} \tilde{p}_\mu \, \mathbf{n}_\mu^p \, d\Gamma_\mu = \mathbf{0} \right\}, \tag{4.25}$$

que en conjunto con el espacio $\widetilde{\mathcal{U}}_\mu$ definido en (2.31) establece el modelo de mínimas restricciones, denotado por $\overline{\text{MCMM}}$. Asimismo, se pueden construir esquemas de homogeneización alternativos y más restringidos para el campo de poropresiones fluctuantes, tal que se cumpla que $\tilde{p}_\mu \in \overline{\widetilde{\mathcal{P}}}_\mu^{\square}\left(\Omega_\mu^p\right) \subseteq \overline{\widetilde{\mathcal{P}}}_\mu\left(\Omega_\mu^p\right)$.

En este punto cabe remarcar, que entre los espacios mínimamente restringidos que se derivan de considerar la expansión de p_μ alrededor de $\mathbf{x}_\mu^G$ expuesto en (4.12) y en torno a $\mathbf{x}_\mu^{Gp}$ recién presentado en (4.25), difieren únicamente en la restricción volumétrica que se impone como condición al campo de poropresiones fluctuantes en la microescala.

Considerando (4.21), la acción virtual del presente descriptor bajo el esquema de expansión adoptado en el dominio de la MC, puede reescribirse como

$$\delta p_\mu = \delta p + \delta \boldsymbol{\varphi} \cdot \left(\mathbf{x}_\mu - \mathbf{x}_\mu^{Gp}\right) + \delta \tilde{p}_\mu, \quad \forall \mathbf{x}_\mu \in \Omega_\mu^p. \tag{4.26}$$

Por su parte, las variaciones del gradiente a microescala conservan la definición establecida en (4.14), mientras que el espacio lineal de fluctuaciones virtuales admisibles $\widetilde{\mathcal{P}}_\mu^*\left(\Omega_\mu^p\right)$ se formula análogo al presentado en (4.15), con $\delta\tilde{p}_\mu \in \widetilde{\mathcal{P}}_\mu^*\left(\Omega_\mu^p\right)$. No obstante, debido a que la restricción (4.24) es homogénea, se cumple ahora que $\widetilde{\mathcal{P}}_\mu^*\left(\Omega_\mu^p\right) \equiv \overline{\widetilde{\mathcal{P}}}_\mu\left(\Omega_\mu^p\right)$.

4.4.4. Principio de Potencia Virtual Multiescala (PMVP)

La ecuación que define el PMVP se escribe de forma análoga a la establecida en (4.17), incluyendo $\mathbf{x}_\mu^{Gp}$ en lugar de $\mathbf{x}_\mu^G$ donde corresponda, y quedando expresada como

$$\begin{aligned}|\Omega_\mu|\,\left(\boldsymbol{\sigma}\,:\,\delta\dot{\boldsymbol{\varepsilon}}-\mathbf{f}\,\cdot\,\delta\dot{\mathbf{u}}+\dot{\chi}\,\delta p-\boldsymbol{\mathcal{V}}\,\cdot\,\delta\boldsymbol{\varphi}\right)=&\int_{\Omega_\mu}\Big[\boldsymbol{\sigma}_\mu\,:\,\left(\delta\dot{\boldsymbol{\varepsilon}}+\boldsymbol{\nabla}^{sym}_{\mathbf{x}_\mu}\,\delta\dot{\tilde{\mathbf{u}}}_\mu\right)\\&-\,\mathbf{f}_\mu\,\cdot\,\left(\delta\dot{\mathbf{u}}+\delta\boldsymbol{\varepsilon}\,\left(\mathbf{x}_\mu-\mathbf{x}_\mu^G\right)+\delta\dot{\tilde{\mathbf{u}}}_\mu\right)\Big]\,d\Omega_\mu\\&+\int_{\Omega_\mu^p}\Big[\dot{\chi}_\mu\left(\delta p+\delta\boldsymbol{\varphi}\,\cdot\,\left(\mathbf{x}_\mu-\mathbf{x}_\mu^{Gp}\right)+\delta\tilde{p}_\mu\right)-\boldsymbol{\mathcal{V}}_\mu\,\cdot\,\left(\delta\boldsymbol{\varphi}+\boldsymbol{\nabla}_{\mathbf{x}_\mu}\,\delta\tilde{p}_\mu\right)\Big]\,d\Omega_\mu,\\\forall\,\left(\delta\dot{\boldsymbol{\varepsilon}}\,,\delta\dot{\mathbf{u}}\,,\delta\boldsymbol{\varphi}\,,\delta p\right)\,\in\mathbb{R}^6\times\mathbb{R}^3\times\mathbb{R}^3\times\mathbb{R},\;&\left(\delta\dot{\tilde{\mathbf{u}}}_\mu\,,\delta\tilde{p}_\mu\right)\in\widetilde{\mathcal{U}}^*_\mu\left(\Omega_\mu\right)\times\widetilde{\mathcal{P}}^*_\mu\left(\Omega^p_\mu\right),\,\forall\,t.\end{aligned}\tag{4.27}$$

Al manipular variacionalmente, se obtienen de forma natural las implicancias del PMVP. La tasa de volumen de poros homogeneizada se mantiene equivalente a la expresada en (4.18) de la Sección 4.3, por lo que no es necesario reescribirla. De igual modo sucede con la forma variacional del balance de masa, la ecuación (4.20). De esta manera, la única diferencia se dá en la ecuación que define la homogeneización del vector de flujo $\boldsymbol{\mathcal{V}}$ que se reformula a continuación.

Vector de velocidad del flujo homogeneizado:

$$\boldsymbol{\mathcal{V}}=\frac{1}{|\Omega_\mu|}\int_{\Omega_\mu^p}\left[\boldsymbol{\mathcal{V}}_\mu-\dot{\chi}_\mu\,\left(\mathbf{x}-\mathbf{x}_\mu^{Gp}\right)\right]\,d\Omega_\mu,\;\forall\,t.\tag{4.28}$$

4.5. Ecuaciones constitutivas de la microestructura compuesta

A fin de alcanzar una formulación cerrada de los modelos multiescala propuestos en las Secciones 4.3 y 4.4, es necesario especificar el comportamiento constitutivo de cada componente de la microescala.

En el caso de la matriz porosa saturada, Ω_μ^p, deben establecerse las leyes constitutivas correspondientes a las magnitudes mecánicas simil tensión $\{\dot{\boldsymbol{\sigma}}_\mu^p;\dot{\chi}_\mu\}$, así como la relación que permite obtener el vector de velocidad de filtración $\boldsymbol{\mathcal{V}}_\mu$. Cada una de estas ya fue introducida en la Sub-sección 2.4.5.

Asimismo, en el contexto del modelado multiescala de medios porosos saturados, tal como se discutió extensamente en el Capítulo 3, con el propósito de evitar dependencias no deseadas con el tamaño de la microescala, resulta conveniente adoptar distintos órdenes de expansión para las variables que actúan como argumentos de entrada en los funcionales constitutivos. Este enfoque, denominado modelo Multiescala-SOE, fue propuesto en dicho capítulo y presenta ventajas adicionales significativas.

En consecuencia, considerando el modelo Multiescala-SOE y con el fin de distinguir la variable dual correspondiente al subdominio Ω_μ^p, la ecuación constitutiva de la tensión dada en (2.50) se reescribe como

$$\dot{\boldsymbol{\sigma}}_\mu^p=\hat{\dot{\sigma}}_\mu^{p,\,\mathrm{SOE}}\left(\dot{\boldsymbol{\varepsilon}}_\mu^{\mathrm{FOE}},\dot{p}_\mu^{\mathrm{ROE}}\right)=\mathbf{C}_\mu^p\,:\,\dot{\boldsymbol{\varepsilon}}_\mu^{\mathrm{FOE}}-\mathbf{b}_\mu\,\dot{p}_\mu^{\mathrm{ROE}}=\mathbf{C}_\mu^p\,:\,\left(\dot{\boldsymbol{\varepsilon}}+\dot{\tilde{\boldsymbol{\varepsilon}}}_\mu\right)\,-\,\mathbf{b}_\mu\,(\dot{p}+\dot{\tilde{p}}_\mu),\tag{4.29}$$

donde las expansiones constitutivas $\dot{\boldsymbol{\varepsilon}}_\mu^{\mathrm{FOE}}$ y $\dot{p}_\mu^{\mathrm{ROE}}$ son las presentadas en (3.8)-(3.9)

Por su parte, en el subdominio Ω_μ^s, ocupado por las inclusiones sólidas impermeables, solo se necesita especificar la respuesta micromecánica para $\dot{\boldsymbol{\sigma}}_\mu^s$. Es decir, basta con proporcionar las relación constitutiva para el estado de tensión, la cual esta completamente definida por el tensor consititutivo elástico de las partículas sólidas $\mathbf{C}_\mu^s$. De este modo, la ley constitutiva se expresa como

$$\dot{\boldsymbol{\sigma}}_\mu^s=\hat{\dot{\sigma}}_\mu^{s,\,\mathrm{SOE}}\left(\dot{\boldsymbol{\varepsilon}}_\mu^{\mathrm{FOE}}\right)=\mathbf{C}_\mu^s\,:\,\dot{\boldsymbol{\varepsilon}}_\mu^{\mathrm{FOE}}=\mathbf{C}_\mu^s\,:\,\left(\dot{\boldsymbol{\varepsilon}}+\dot{\tilde{\boldsymbol{\varepsilon}}}_\mu\right),\tag{4.30}$$

donde el superíndice $(\bullet)^{\text{SOE}}$ se incluye únicamente para enfatizar el tipo de modelo multiescala adoptado. No obstante, en la forma funcional se cumple que $\hat{\hat{\sigma}}_{\mu}^{s,\,\text{SOE}}\big(\dot{\boldsymbol{\varepsilon}}_{\mu}^{\text{FOE}}\big) = \hat{\hat{\sigma}}_{\mu}^{s,\,\text{FOE}}\big(\dot{\boldsymbol{\varepsilon}}_{\mu}^{\text{FOE}}\big)$

Los superíndices $(\bullet)^{s}$ y $(\bullet)^{p}$ se utilizan para distinguir los estados de tensión correspondientes a los subdominios Ω_{μ}^{s} o Ω_{μ}^{p}, respectivamente.

4.6. Conclusiones

La idea subyacente al presente capítulo y la publicación Anonis et al. [67], reproducida en el Apéndice D, pretende establecer un primer avance para el desarrollo de modelos multiescala novedosos y/o alternativos, capaces de abordar microestructuras altamente heterogéneas compuestas por inclusiones sólidas impermeables incrustadas en una matriz de tipo medio poroso saturado.

Tras una especial atención a las características de la microescala, cobrando relevancia el tratamiento dado al campo de poropresiones en la microescala. Dentro del marco del MMVP, se evaluaron los procedimientos de inserción y homogeneización que permiten construir espacios admisibles óptimos. Con respecto al primer proceso, se consideraron dos posibles expansiones en la inserción del descriptor primitivo de poropresiones a microescala (i) expandir alrededor del centroide de la MC completa, (ii) o bien, expandir en torno del centro geométrico del subdominio Ω_{μ}^{p}. Se asume que ambas deberían converger a un único modelo en presencia de microceldas representativas (RVE). Sobre esta variable, al aplicar las reglas de homogeneización se derivan restricciones volumétricas para las poropresiones fluctuantes a nivél microscópico no homogeneas y homogeneas respectivamente. Para promediar el gradiente de poropresiones fue necesario incorporar un término adicional que capture la influencia de las poropresiones a microescala en la interfaz entre los dos medios y conduzca a una formulación admisible.

Teniendo en cuenta todos estos ajustes, los modelos multiescala mínimamente restringido expuestos en las Secciones 4.3 y 4.4 presentan características específicas que impactan, a su vez, en los submodelos más restringidos derivados de ellos (tales como el Períodico), los cuales deben tratarse cuidadosamente para su formulación teórica y numérica.

El modelo multiescala con condiciones períodicas formulado como submodelo del $\widehat{\text{MCMM}}$, esto es, con el descriptor p_{μ} expandido en torno a $\mathbf{x}_{\mu}^{G}$, mostró un excelente desempeño, ajustándose a las soluciones obtenidas a partir de la estrategia DNS, como se evidencia en la publicación Anonis et al. [67].

Como siguiente paso, en el Capítulo 5 se extiende el análisis a escenarios donde la aleatoriedad de las inclusiones alcanza también el contorno de la MC, aplicando el enfoque desarrollado en este capítulo.

Capítulo 5

Análisis de microestructura porosa saturada con distribución aleatoria de inclusiones sólidas impermeables

5.1. Introducción

Claramente, para medios a microescala con una estructura periódica, el denominado modelo periódico ofrece la solución más precisa. Sin embargo, las condiciones de contorno periódicas requieren la continuidad en las propiedades de los materiales a través de presentar el mismo tipo de material en los contornos opuestos para garantizar la periodicidad de la microestructura, lo cual rara vez se observa en materiales heterogéneos reales. Más aún, a está falta de periodicidad material, en entornos generales se le agrega que tampoco existe periodicidad en la geometría. Esto es, se pueden presentar vacíos que conducen a la ausencia del campo de desplazamiento, el cual puede no existir en el contorno de la MC. Es precisamente un escenario similar al asociado a la presencia de vacíos el que se presenta en el tipo de microestructura que se pretende modelar en este capítulo, debido a la heterogeneidad que induce la ausencia del campo de poropresiones en la microescala. En estos casos, la selección de las condiciones de borde apropiadas resulta fundamental. No obstante, debido a que no se ha encontrado en la bibliografía que se haya abordado este tipo de MCs, y dada la semejanza con el análisis de materiales con vacíos, se recurre a los estudios de modelos alternativos propuestos en esta línea de investigación.

En particular, Rocha [95] y Blanco et al. [21] al abordar el tratamiento de MC con distribuciones verdaderamente aleatorias de vacíos, propusieron un nuevo modelo multiescala mínimamente restringido e incorporaron alternativas más restringidas como subespacios del mismo, con el fin de obtener una amplia familia de submodelos multiescala. Feijóo et al. [96] por su parte propusieron nuevos modelos que mejoran el MCMM prescribiendo desplazamientos o tracciones en el contorno de la MC, considerando las interacciones mecánicas entre MCs vecinas de forma iterativa a través de condiciones de límite alternas y seleccionadas adecuadamente.

En busqueda de desarrollar un modelo multiescala que de continuidad y completitud al tratamiento de microestructuras conformadas por materiales que requieren de diferentes campos descriptores se consideraron los avances propuestos por Rocha [95] y Blanco et al. [21]. En concreto, se pretende retomar el estudio de aquellas MCs constituidas por una matriz que contiene inclusiones sólidas no porosas e impermeables, con la principal novedad de evaluar ahora escenarios en los que la distribución de las inclusiones alcanzan la frontera de la MC de forma completamente aleatoria, tópico que se había postergado en el capítulo anterior. Los desarrollos de tal caso fueron presentados por Anonis et al. [70] en un trabajo aún en revisión, el cual se replica en el Apéndice E.

El capítulo se estructura de la siguiente manera. En la Sección 5.2, se retoma la MC genérica del

Capítulo 4 y se destacan los cambios esenciales a ser abordados. Luego, en la Sección 5.3 se introduce el procedimiento de homogenización del gradiente de poropresiones, que constituye la principal modificación y novedad respecto del capítulo previo. Luego en la Sección 5.4 se presentan el conjunto y el espacio apropiado para el campo de poropresiones fluctuantes que permiten definir el modelo multiescala mínimamente restringido conforme a la nueva regla de homogeneización asumida y el tipo de expansión de las poropresiones microescala. Posteriomente, en la Sección 5.5 se proponen las restricciones adicionales que permiten construir submodelos mas restringidos que el MCMM. Luego, se presentan resultados novedosos que contrastan los dos MCMM derivados de las dos supocisiones respecto a la variable de poropresiones microescala. Finalmente, en la Sección 5.7 se presentan algunas conclusiones.

5.2. Suposiciones básicas del modelo en la microescala

En relación con los medios sólidos con distribuciones aleatorias de vacíos, Blanco et al. [21] introdujeron el concepto de MCs $\mathbf{n}_\mu$-equilibradas, que, según la notación anterior, satisfacen una ecuación del siguiente tipo

$$\int_{\Gamma_\mu} \mathbf{n}_\mu \, d\Gamma_\mu = \mathbf{0} \tag{5.1}$$

Dado que las microestructuras abordadas en este capítulo tienen continuidad material (sin vacíos), cumplen con la expresión geométrica (5.1). Por lo tanto, se obtienen MC $\mathbf{n}_\mu$-equilibradas a lo largo de todo su contorno. Sin embargo, es evidente que una distribución aleatoria de inclusiones sólidas, tal como el esquema de la Figura 4.1, induce un desequilibrio geométrico si se considera por separado cada subdominio superficial del contorno Γ_μ. Es decir, las MC resultan $\mathbf{n}^p_\mu$-desequilibradas en Γ^p_μ y $\mathbf{n}^s_\mu$-desequilibradas en Γ^s_μ. Esto se expresa mediante

$$\begin{aligned} \int_{\Gamma^p_\mu} \mathbf{n}^p_\mu \, d\Gamma_\mu &\neq \mathbf{0}, \\ \int_{\Gamma^s_\mu} \mathbf{n}^s_\mu \, d\Gamma_\mu &\neq \mathbf{0}. \end{aligned} \tag{5.2}$$

Este segundo atributo de las microestructuras abordadas en este manuscrito no supone un inconveniente importante si los campos de variables que describen el comportamiento de sus componentes son continuos en todo el dominio. Tal es el caso del campo de desplazamientos a microescala. Sin embargo, no ocurre lo mismo con el campo de poropresiones a microescala. Por lo tanto, para abordar la ausencia del campo p_μ en parte de la MC y el hecho de que esta resulte $\mathbf{n}\mu^p$-desequilibrada sobre $\Gamma\mu^p$, se propone una homogeneización adecuada del gradiente de poropresiones, basada en las ideas de Blanco et al. [21], como se muestra en la sección 5.3. Esto permite modelar las MCs descritas anteriormente y garantiza un patrón de autoequilibrio de las velocidades de flujo a microescala en todo el límite poroso Γ^p_μ.

5.3. Homogeneización del gradiente de poropresiones en la MC

En este punto reside la principal y novedosa contribución del presente capítulo. Se propone como regla de homogeneización para el gradiente del campo de poropresiones la siguiente expresión

$$\begin{aligned} \mathcal{H}^{(\overline{\mathbf{n}}^p_\mu)}_{\boldsymbol{\varphi}}(\boldsymbol{\varphi}_\mu) = \boldsymbol{\varphi} &= \frac{1}{|\Omega^p_\mu|}\left[\int_{\Omega^p_\mu} \boldsymbol{\varphi}_\mu \, d\Omega_\mu - \int_{\Gamma^i_\mu} \tilde{p}_\mu \, \mathbf{n}^i_\mu \, d\Gamma_\mu - \int_{\Gamma^p_\mu} \tilde{p}_\mu \, \overline{\mathbf{n}}^p_\mu \, d\Gamma_\mu\right] \\ &= \frac{1}{|\Omega^p_\mu|}\left[\int_{\Omega^p_\mu} \boldsymbol{\nabla}_{\mathbf{x}_\mu} p_\mu \, d\Omega_\mu - \int_{\Gamma^i_\mu} \tilde{p}_\mu \, \mathbf{n}^i_\mu \, d\Gamma_\mu - \int_{\Gamma^p_\mu} \tilde{p}_\mu \, \overline{\mathbf{n}}^p_\mu \, d\Gamma_\mu\right], \end{aligned} \tag{5.3}$$

donde se incluye el segundo término que involucra la interfaz interna Γ_μ^i con el fin de obtener una fórmula de homogeneización del gradiente de poropresiones expresada únicamente sobre el límite externo de la matriz porosa Γ_μ^p, tal como lo presentado en el Capítulo 4. El tercer término es responsable de mantener la consistencia del modelo al garantizar que la homogeneización del gradiente de poropresiones a microescala reproduzca correctamente la variable correspondiente a macroescala, esto es, el gradiente macroscópico $\boldsymbol{\varphi}$. Dicho término depende de un campo vectorial $\overline{\mathbf{n}}_\mu^p$[1], el cual se define como

$$\overline{\mathbf{n}}_\mu^p = \frac{1}{|\Gamma_\mu^p|}\int_{\Gamma_\mu^p} \mathbf{n}_\mu^p \, d\Gamma_\mu, \tag{5.4}$$

Este término adicional asegura que la fórmula de homogeneización funcione de manera consistente incluso en el caso más general, cuando las inclusiones impermeables alcanzan de forma aleatoria el contorno de la MC. Además, garantiza que las velocidades de flujo a microescala se equilibren por sí mismas, tal como se demuestra en Appendix C.2 del Apéndice E.

Considerando (4.5) y aplicando el teorema de Green, la expresión (5.3) puede expandirse para dar

$$\begin{aligned}\boldsymbol{\varphi} = \boldsymbol{\varphi} + \frac{1}{|\Omega_\mu^p|}\left[\int_{\Omega_\mu^p} \boldsymbol{\nabla}_{\mathbf{x}_\mu}\, \tilde{p}_\mu \, d\Omega_\mu - \int_{\Gamma_\mu^i} \tilde{p}_\mu \, \mathbf{n}_\mu^i \, d\Gamma_\mu - \int_{\Gamma_\mu^p} \tilde{p}_\mu \, \overline{\mathbf{n}}_\mu^p \, d\Gamma_\mu\right] \\ = \boldsymbol{\varphi} + \frac{1}{|\Omega_\mu^p|}\left[\int_{\Gamma_\mu^p} \tilde{p}_\mu \, \left(\mathbf{n}_\mu^p - \overline{\mathbf{n}}_\mu^p\right) \, d\Gamma_\mu\right].\end{aligned} \tag{5.5}$$

De (5.5) se deriva la restricción para el campo de poropresiones fluctuantes a escala microscópica en el límite Γ_μ^p, que se define como

$$\int_{\Gamma_\mu^p} \tilde{p}_\mu \, \left(\mathbf{n}_\mu^p - \overline{\mathbf{n}}_\mu^p\right) \, d\Gamma_\mu = \mathbf{0}. \tag{5.6}$$

La restricción (5.6) es consecuencia de imponer el concepto de admisibilidad a los gradientes de poropresiones a macro- y microescala relacionados a través del operador de homogeneización (5.3), tal y como estipula el MMVP[2].

Esta particular elección para el vector $\overline{\mathbf{n}}_\mu^p$, es el que posibilita la definición dada en la Seccíon 5.2. Así, en caso de que la media de normales en el contorno Γ_μ^p resulte nulo, esto es $\overline{\mathbf{n}}_\mu^p = \mathbf{0}$, la MC sea denominada de $\mathbf{n}_\mu^p$-equilibrada (y por ende $\mathbf{n}_\mu^s$-equilibrada). Es decir, geométricamente la distribución de las inclusiones en el contorno de la MC esta balanceado. Caso contrario, se recupera la definición (5.2) siendo precisamente la situación que se pretende abordar.

5.4. Conjunto y espacio admisibles de la variable fluctuante de poropresiones de la microescala

La ecuación (5.6), de la restricción en el contorno del campo de poropresiones fluctuantes se expresa de forma identica sin importar con respecto a que coordenada se efectue la expansión del campo de poropresiones microescala. Sin embargo, la restricción volumétrica si difiere, siendo que para el caso

[1] Una formulación mas general parte de introducir un campo vectorial $\mathbf{m}_\mu^p$ que debe satisfacer la propiedad

$$\int_{\Gamma_\mu^p} \mathbf{m}_\mu^p \, d\Gamma_\mu = \int_{\Gamma_\mu^p} \mathbf{n}_\mu^p \, d\Gamma_\mu, \quad \mathbf{m}_\mu^p \neq \mathbf{n}_\mu^p,$$

cuya forma más sencilla viene dada por asumir $\mathbf{m}_\mu^p$ como un campo vectorial constante en la parte del contorno Γ_μ^p, lo cual conduce a (5.4). Para un análisis más detallado, se remite al lector a la bibliografía especializada (Blanco et al. [19]).

[2] En caso de considerar la expansión alrededor del centro geométrico de la MC, $\mathbf{x}_\mu^G$, se arriba a una restricción en el contorno que se expresa tal como en (5.6), difiriendo únicamente en los valores que pueden alcanzar el campo $\tilde{p}_\mu$.

de la expansión alrededor de $\mathbf{x}_\mu^G$ se considera la ecuación (4.8) mientras que de asumir la expansión en torno a $\mathbf{x}_\mu^{Gp}$ se debe emplear la ecuación (4.24). De esta manera, se define para la primera condición el conjunto dado por la siguiente expresión

$$\widetilde{\widehat{\mathcal{P}}}_\mu^{\left(\overline{\mathbf{n}}_\mu^p\right)}\left(\Omega_\mu^p\right) \equiv \left\{\tilde{p}_\mu \in \mathrm{H}^1\left(\Omega_\mu^p\right); \int_{\Omega_\mu^p}\left[\boldsymbol{\varphi}\cdot\left(\mathbf{x}_\mu-\mathbf{x}_\mu^G\right)+\tilde{p}_\mu\right]d\Omega_\mu=0; \int_{\Gamma_\mu^p}\tilde{p}_\mu\left(\mathbf{n}_\mu^p-\overline{\mathbf{n}}_\mu^p\right)d\Gamma_\mu=\mathbf{0}\right\}. \quad (5.7)$$

En cuyo caso, el campo fluctuante a microescala $\tilde{p}_\mu$ es compatible con el procedimiento de homogeneización adoptado en (4.6) y (5.3), en caso de que pertenezca a este conjunto.

Por su parte, para el segundo caso se define el espacio dado por

$$\widetilde{\overline{\mathcal{P}}}_\mu^{\left(\overline{\mathbf{n}}_\mu^p\right)}\left(\Omega_\mu^p\right) \equiv \left\{\tilde{p}_\mu \in \mathrm{H}^1\left(\Omega_\mu^p\right); \int_{\Omega_\mu^p}\tilde{p}_\mu\, d\Omega_\mu = 0; \int_{\Gamma_\mu^p}\tilde{p}_\mu\left(\mathbf{n}_\mu^p-\overline{\mathbf{n}}_\mu^p\right)d\Gamma_\mu=\mathbf{0}\right\}, \quad (5.8)$$

siendo $\tilde{p}_\mu$ admisible en caso de que pertenezca al espacio, resultando compatible con el procedimiento de homogeneización adoptado en (4.22) y (5.3).

En base a cualquiera de las dos, en conjunto con el espacio de la variable fluctuante de desplazamientos de la microescala (2.31), es posible introducir un modelo multiescala con restricciones mínimas. Para distinguir uno de otro y siguiendo la notación introducida en el Capítulo 4, estos se denominan $\widehat{\mathrm{MCMM}}\left(\overline{\mathbf{n}}_\mu^p\right)$ o bien $\overline{\mathrm{MCMM}}\left(\overline{\mathbf{n}}_\mu^p\right)$, según se adopte (5.7) o bien (5.8), respectivamente.

Tanto el $\widehat{\mathrm{MCMM}}\left(\overline{\mathbf{n}}_\mu^p\right)$ como el $\overline{\mathrm{MCMM}}\left(\overline{\mathbf{n}}_\mu^p\right)$, se corresponden con el denominado modelo de tracción y flujo uniforme, ya que el sistema resultante de tracciones y flujos sobre todos los bordes de las MCs con normal constante son uniformes, aunque no necesariamente igual entre límites con vectores normales diferentes. Esto, en general, no refleja el verdadero estado del material a nivel microscópico. Así, con el propósito de obtener configuraciones más restringidas para los campos $\tilde{\mathbf{u}}_\mu$ y $\tilde{p}_\mu$, que conduzcan a mejores soluciones en la respuesta efectiva se pretende construir modelos alternativos. En este contexto, cualquier subespacio $\widetilde{\mathcal{U}}_\mu^\square \subseteq \widetilde{\mathcal{U}}_\mu$ en combinación con cualquier subconjunto $\widetilde{\widehat{\mathcal{P}}}_\mu^{\square\left(\overline{\mathbf{n}}_\mu^p\right)} \subseteq \widetilde{\widehat{\mathcal{P}}}_\mu^{\left(\overline{\mathbf{n}}_\mu^p\right)}$ o bien, subespacio $\widetilde{\overline{\mathcal{P}}}_\mu^{\square\left(\overline{\mathbf{n}}_\mu^p\right)} \subseteq \widetilde{\overline{\mathcal{P}}}_\mu^{\left(\overline{\mathbf{n}}_\mu^p\right)}$, son opciones viables para desarrollar estos esquemas de homogeneización alternativos. En particular, mas adelante en la Sección 5.5 se proponen restricciones adicionales a $\widehat{\mathrm{MCMM}}\left(\overline{\mathbf{n}}_\mu^p\right)$ y $\overline{\mathrm{MCMM}}\left(\overline{\mathbf{n}}_\mu^p\right)$ con el fin de lograr estrategias de homogeneización óptimas para microestructuras que consisten en una matriz con inclusiones embebidas de forma completamente aleatorias.

Dado que el PMVP, para cada una de las expansiones posibles del campo de poropresiones a microescala, se formula de manera análoga a lo desarrollado en el Capítulo 4, no se reproduce aquí su deducción ni las consecuencias que de el se derivan.

5.5. Modelo multiescala alternativo: MCMM con particiones

En esta sección se propone un submodelo a cualquiera de los modelos presentados en la sección anterior, sea el $\widehat{\mathrm{MCMM}}\left(\overline{\mathbf{n}}_\mu^p\right)$ o bien el $\overline{\mathrm{MCMM}}\left(\overline{\mathbf{n}}_\mu^p\right)$. En el primer caso, se logra introduciendo restricciones adicionales al par espacio-conjunto $\widetilde{\mathcal{U}}_\mu$ y $\widetilde{\widehat{\mathcal{P}}}_\mu^{\left(\overline{\mathbf{n}}_\mu^p\right)}$ dados en (2.31) y (5.7), respectivamente. Para el segundo caso es necesario considerar agregar restricciones al par de espacios $\widetilde{\mathcal{U}}_\mu$ y $\widetilde{\overline{\mathcal{P}}}_\mu^{\left(\overline{\mathbf{n}}_\mu^p\right)}$ dados en (2.31) y (5.8), respectivamente. Por simplicidad y dado que la metodología es idéntica en ambos casos, a lo largo de

esta sección se escribe unicamente MCMM($\overline{\mathbf{n}}_\mu^p$) y $\widetilde{\mathcal{P}}_\mu^{(\overline{\mathbf{n}}_\mu^p)}$.

Sin perder la generalidad de la teoría desarrollada anteriormente, por simplicidad se limita el siguiente análisis a problemas bidimensionales y a casos en los que la MC es un cuadrilátero alineado con los ejes cartesianos. En este contexto, se considera que todo el contorno de la MC, Γ_μ, y el contorno del subdominio del medio poroso, Γ_μ^p, pueden ser "particionados" en $R_u \geq 2$ y $R_p \geq 2$ partes disjuntas, respectivamente, de la siguiente manera

$$\begin{aligned} \Gamma_\mu &= \bigcup_{j=1}^{R_u} \Gamma_\mu^j, \\ \Gamma_\mu^p &= \bigcup_{k=1}^{R_p} \Gamma_\mu^{p,k}, \end{aligned} \tag{5.9}$$

donde

$$\begin{aligned} \Gamma_\mu^j &= \Gamma_\mu^{j,+} \cup \Gamma_\mu^{j,-}, \quad j = 1, \ldots, R_u \\ \Gamma_\mu^{p,k} &= \Gamma_\mu^{k,+} \cup \Gamma_\mu^{k,-}, \quad k = 1, \ldots, R_p \end{aligned} \tag{5.10}$$

es decir, cada partición $\Gamma_\mu^j \subset \Gamma_\mu$ y $\Gamma_\mu^{p,k} \subset \Gamma_\mu^p$ consiste en la unión de dos subdominios opuestos, $\left\{\Gamma_\mu^{j,+};\ \Gamma_\mu^{j,-}\right\}$ y $\left\{\Gamma_\mu^{k,+};\ \Gamma_\mu^{k,-}\right\}$, respectivamente. Además, se pueden tomar particiones o divisiones que describan subdominios opuestos que no necesariamente sean iguales, esto es, $\Gamma_\mu^{j,+} \neq \Gamma_\mu^{j,-}$ y $\Gamma_\mu^{k,+} \neq \Gamma_\mu^{k,-}$. La razón para diferenciar las particiones de Γ_μ y Γ_μ^p, aunque la segunda pertenece a la primera, se debe a la forma en que se impondrán las restricciones adicionales. La partición de Γ_μ es adecuada para el campo de desplazamientos fluctuantes de la microescala, que es un campo continuo. Por su parte, la partición de Γ_μ^p es apropiada para el campo de poropresiones fluctuantes, ya que es la única porción del contorno donde este descriptor existe.

En este punto, se introducen diferentes listas de índices j e índices k, que son útiles para identificar en notación compacta conjuntos de particiones de los contornos, Γ_μ^j y $\Gamma_\mu^{p,k}$, según corresponda. La lista que incluye los índices j para todos los subdominios se denota $\mathcal{R}_u = \{1, \ldots, R_u\}$ y para los índices k es $\mathcal{R}_p = \{1, \ldots, R_p\}$. También se considera un subconjunto de $\mathcal{R}_u$ y otro para $\mathcal{R}_p$, denotados como $\mathcal{C}_u \subseteq \mathcal{R}_u$ y $\mathcal{C}_p \subseteq \mathcal{R}_p$, respectivamente. Por lo tanto, los complementos correspondientes son $\mathcal{W}_u = \mathcal{R}_u \setminus \mathcal{C}_u$ y $\mathcal{W}_p = \mathcal{R}_p \setminus \mathcal{C}_p$, respectivamente. Los números de elementos para las listas $\mathcal{R}_{(\bullet)}$, $\mathcal{C}_{(\bullet)}$ y $\mathcal{W}_{(\bullet)}$ son $R_{(\bullet)} = \text{card}\left(\mathcal{R}_{(\bullet)}\right)$, $C_{(\bullet)} = \text{card}\left(\mathcal{C}_{(\bullet)}\right)$ y $W_{(\bullet)} = \text{card}\left(\mathcal{W}_{(\bullet)}\right)$, respectivamente, donde card $(\bullet)$ representa la cardinalidad del conjunto $(\bullet)$. Pueden darse dos situaciones típicas: (i) $\mathcal{C}_{(\bullet)} = \mathcal{R}_{(\bullet)}$, entonces $C_{(\bullet)} = R_{(\bullet)}$, $\mathcal{W}_{(\bullet)} = \varnothing$ y $W_{(\bullet)} = 0$; (ii) $\mathcal{C}_{(\bullet)} \subset \mathcal{R}_{(\bullet)}$, entonces $C_{(\bullet)} < R_{(\bullet)}$, $\mathcal{W}_{(\bullet)} \neq \varnothing$ y $W_{(\bullet)} > 0$.

A su vez, análogo a la definición de vector normal medio en el contorno Γ_μ^p establecido en (5.4) se propone un vector normal promediado en cada partición que se proponga sobre Γ_μ^p. Esto se expresa de la siguiente manera

$$\overline{\mathbf{n}}_\mu^{p,k} = \frac{1}{|\Gamma_\mu^{p,k}|} \int_{\Gamma_\mu^{p,k}} \mathbf{n}_\mu^p \, d\Gamma_\mu, \quad k = 1, \ldots, R_p. \tag{5.11}$$

Asimismo, para las particiones que se asuman sobre Γ_μ, es posible establecer vectores normales medios, que se definen como

$$\overline{\mathbf{n}}_\mu^j = \frac{1}{|\Gamma_\mu^j|} \int_{\Gamma_\mu^j} \mathbf{n}_\mu \, d\Gamma_\mu. \tag{5.12}$$

Con todos los elementos introducidos en las definiciones anteriores, se propone la siguiente familia

de subespacios que restringen los espacios definidos por (2.31) y (5.8)

$$\begin{aligned}\widetilde{\mathcal{U}}_{\mu}^{C_u}\left(\Omega_{\mu}\right) &\equiv \left\{\tilde{\mathbf{u}}_{\mu} \in \widetilde{\mathcal{U}}_{\mu}\left(\Omega_{\mu}\right); \int_{\Gamma_{\mu}^{j}} \tilde{\mathbf{u}}_{\mu} \otimes \left(\mathbf{n}_{\mu}-\overline{\mathbf{n}}_{\mu}^{j}\right) d\Gamma_{\mu}=\mathbb{O}, \ \forall j \in \mathcal{C}_u\right\}, \\ \widetilde{\mathcal{P}}_{\mu}^{\left(\overline{\mathbf{n}}_{\mu}^{p}\right),C_p}\left(\Omega_{\mu}^{p}\right) &\equiv \left\{\tilde{p}_{\mu} \in \widetilde{\mathcal{P}}_{\mu}^{\left(\overline{\mathbf{n}}_{\mu}^{p}\right)}\left(\Omega_{\mu}^{p}\right); \int_{\Gamma_{\mu}^{p,k}} \tilde{p}_{\mu}\left(\mathbf{n}_{\mu}^{p}-\overline{\mathbf{n}}_{\mu}^{p,k}\right) d\Gamma_{\mu}=\mathbf{0}, \ \forall k \in \mathcal{C}_p\right\}.\end{aligned} \tag{5.13}$$

Claramente, tenemos $\widetilde{\mathcal{U}}_{\mu}^{C_u} \subset \widetilde{\mathcal{U}}_{\mu}$ y $\widetilde{\mathcal{P}}_{\mu}^{\left(\overline{\mathbf{n}}_{\mu}^{p}\right),C_p} \subset \widetilde{\mathcal{P}}_{\mu}^{\left(\overline{\mathbf{n}}_{\mu}^{p}\right)}$, dado que estos espacios contienen C_u y C_p restricciones adicionales sobre partes no superpuestas, Γ_{μ}^{j}, con $j \in \mathcal{C}_u$ y $\Gamma_{\mu}^{p,k}$, con $k \in \mathcal{C}_p$. Obsérvese que, de acuerdo con (5.13), y dado que $C_u \leq R_u$ y $C_p \leq R_p$, se pueden utilizar todas las particiones R_u y/o R_p para imponer restricciones adicionales, pero también es posible dejar alguna(s) parte(s) sin ninguna restricción adicional. En este último caso, las particiones del contorno Γ_{μ}^{j}, con $j \in \mathcal{W}_u$ y $\Gamma_{\mu}^{p,k}$, con $k \in \mathcal{W}_p$, solo tienen la restricción que define el MCMM primitivo, ya que afecta a todo el borde de la MC y a toda la superficie del medio poroso saturado, respectivamente, véase (2.31)-(5.8).

5.6. Resultados

En el trabajo en revisión Anonis et al. [70] se presentan dos ejemplos numéricos que evidencian el buen desempeño del modelo alternativo al considerar particiones que incluyen restricciones adicionales sobre el Modelo Multiescala de Mínimas Restricciones, tanto en su comparación con otros esquemas de homogeneización, tales como el Lineal y el $\overline{\text{MCMM}}\left(\overline{\mathbf{n}}_{\mu}^{p}\right)$[3], como frente a la solución en única escala mediante Simulación Numérica Directa (DNS). Puesto que dichos resultados se incluyen en el Apéndice E, no se vuelven a reproducir aquí.

Sin embargo, se agrega a continuación un análisis adicional, que no ha sido considerado en la publicación previemante citada, la cual compara las dos posibles expansiones del campo de poropresiones en la microescala, tal como se presentó en el Capítulo 4 y se continuó en el presente. Para ello, se retoma el ejemplo presentado en la sección E.6.2 de dicho trabajo. Las Figuras E.5 y E.6 presentan el esquema del problema analizado, mientras que las propiedades materiales se pueden ver en la Tabla E.1. De este ejemplo, se emplean las soluciones obtenidas mediante la técnica DNS y mediante el submodelo multiescala denominado $\overline{\text{MCMM}}\left(\overline{\mathbf{n}}_{\mu}^{p}\right)_4^4$, definido por los espacios de las ecuaciones (E.52)-(E.53), que surgen siguiendo el esquema de particiones presentado en las Figuras E.7-E.8.

El objetivo es reconstruir dicho submodelo, pero ahora considerando la expansión alrededor del centroide de la MC, $\mathbf{x}_{\mu}^{G}$, es decir, empleando la ecuación (4.12), que conduce al espacio dado en (5.7). Este nuevo submodelo se denomina de $\widehat{\text{MCMM}}\left(\overline{\mathbf{n}}_{\mu}^{p}\right)_4^4$ para distinguirlo del implementando en la publicación original.

Por otra parte, aún cuando el modelo lineal constituye una opción viable para describir un patrón aleatorio de inclusiones, siempre que el tamaño de la microescala (MC) sea lo suficientemente grande, se descarta su empleo debido al deficiente desempeño observado en los resultados presentados en Anonis et al. [70]. Este hecho parece indicar que sería necesario considerar microestructuras de dimensiones mayores que las propuestas.

Para realizar las comparaciones pertinentes se evalúan las siguientes variables en su evolución temporal:

- En la Figura 5.1(a) se representa el desplazamiento vertical macroscopico u_2 en el nodo ubicado bajo el centro de la zapata (véase la Figura E.5), cuyas coordenadas son $x_1 = 0m$ y $x_2 = 4,5m$ (vértice superior izquierdo en las Figuras E.6a y E.6c.1).

[3] En dicha publicación se omite la linea superior y se escribe solamente $\text{MCMM}\left(\overline{\mathbf{n}}_{\mu}^{p}\right)$, dado que no se presento el modelo $\widehat{\text{MCMM}}\left(\overline{\mathbf{n}}_{\mu}^{p}\right)$

- En la Figura 5.1(b) se grafica la evolución temporal del caudal a través de la única superficie de salida, correspondiente al borde en rojo de la Figura E.5. Dicho borde posee una longitud de $0,75m$ entre el extremo de la zapata y el límite derecho del dominio. Para cada modelo, el caudal total se obtiene sumando los caudales de descarga a lo largo de esta longitud.

- Las componentes σ'_{11}, σ'_{12} y σ'_{22} del tensor de tensiones efectivas $\boldsymbol{\sigma}'$ se observan en las Figuras 5.1(c), 5.1(d) y 5.1(e), respectivamente. La respuesta homogeneizada se evalúa en cada punto de Gauss de la macroescala (véase E.6-(c.1)), seleccionado en el presente caso el de coordenadas $x_1 = 0.338m$ y $x_2 = 2.682m$. Para el caso DNS, la tensión efectiva se promedia en un entorno de radio $r = 0,5\ l_\mu$, obteniendo $\boldsymbol{\sigma}'_{Av}$ sobre el área $\Omega_r = \pi\, r^2$, según la expresión (E.54).

- Finalmente, las Figuras 5.1(f) y 5.1(g) corresponden a las componentes $\mathcal{V}_1$ y $\mathcal{V}_2$ del vector de velocidad del flujo $\boldsymbol{\mathcal{V}}$. Al igual que en el caso de las tensiones, se evalúan en el mismo punto de Gauss y se calcula el promedio DNS mediante (E.54), sustituyendo $\boldsymbol{\mathcal{V}}$ en lugar de $\boldsymbol{\sigma}'$, para obtener el vector de velocidad promediado $\boldsymbol{\mathcal{V}}_{Av}$.

En cada una de las figuras se aprecia el buen acuerdo que existe entre ambas soluciones multiescala y, a su vez, entre estas con la respuesta de referencia de única escala obtenida mediante el procedimiento DNS. No obstante, es importante destacar que las respuestas proporcionadas por los modelos homogeneizados no son plenamente coincidentes, existiendo una ligera discrepancia entre ellas. Esto sugiere que aún no se esta estrictamente en presencia de un RVE, en cuyo caso ambas respuestas deberían colapsar en un única solución. No obstante, resta realizar mayor número de experimentos numéricos y análisis mas exhaustivo en lo que refiere a la comparación entre ambos modelos propuestos.

Aún así, este comportamiento pone de relieve la importancia de los modelos alternativos propuestos en este capítulo, ya que permite obtener resultados altamente satisfactorios para un problema complejo en el que se desconoce a priori el tamaño mínimo de la MC a partir del cual la respuesta homogeneizada se vuelve insensible al tamaño (es decir, el RVE) y no se dispone de soluciones de referencia rigurosas.

5.7. Conclusiones

En este capítulo se desarrolló un marco multiescala capaz de modelar de forma confiable materiales conformados por una matriz porosa saturada con una distribución aleatoria de inclusiones sólidas irregulares, configuraciones que se pueden encontrar en los tejidos biológicos o los geomateriales. Estas microestructuras presentan la no existencia del campo de poropresiones en la microescala y carecen de periodicidad, lo que imposibilita el uso del esquema de homogeneización periódica y plantea desafíos adicionales, como la inexistencia de soluciones de referencia rigurosas, la falta de límites inferiores bien establecidos, ya sea de forma analítica o numérica, y la imposibilidad de conocer a priori el tamaño mínimo de la MC que determine el RVE. Por último, la intersección irregular de las inclusiones con los bordes de la MC genera diseños $\mathbf{n}^p_\mu$-desequilibrados ($\mathbf{n}^s_\mu$-desequilibrados).

Para abordar estas particularidades se estableció un Modelo Multiescala de Mínimas Restricciones, MCMM($\overline{\mathbf{n}}^p_\mu$), generalizado mediante la incorporación de una entidad geométrica adicional representada por el campo vectorial $\overline{\mathbf{n}}^p_\mu$, introducido en la regla de homogeneización para el gradiente de poropresiones, lo que permite evitar la aparición de gradientes de poropresión macroscópico espurios. Según el tipo de expansión adoptado para el campo de poropresiones, se obtuvieron dos formulaciones del modelo de mínimas restricciones ($\widehat{\text{MCMM}}\,(\overline{\mathbf{n}}^p_\mu)$ y $\overline{\text{MCMM}}\,(\overline{\mathbf{n}}^p_\mu)$). A su vez, para mejorar la capacidad predictiva de estos modelos basados en el campo $\overline{\mathbf{n}}^p_\mu$, se propuso un procedimiento que permite construir familias de submodelos multiescala mediante la incorporación progresiva de restricciones adicionales en la MC. Tal como se evidencia en la Sección 5.6, estos submodelos logran reproducir con gran precisión las soluciones de referencia obtenidas mediante la estrategia DNS, al particionar tanto $\widehat{\text{MCMM}}\,(\overline{\mathbf{n}}^p_\mu)$ como $\overline{\text{MCMM}}\,(\overline{\mathbf{n}}^p_\mu)$, confirmando el potencial del enfoque propuesto.

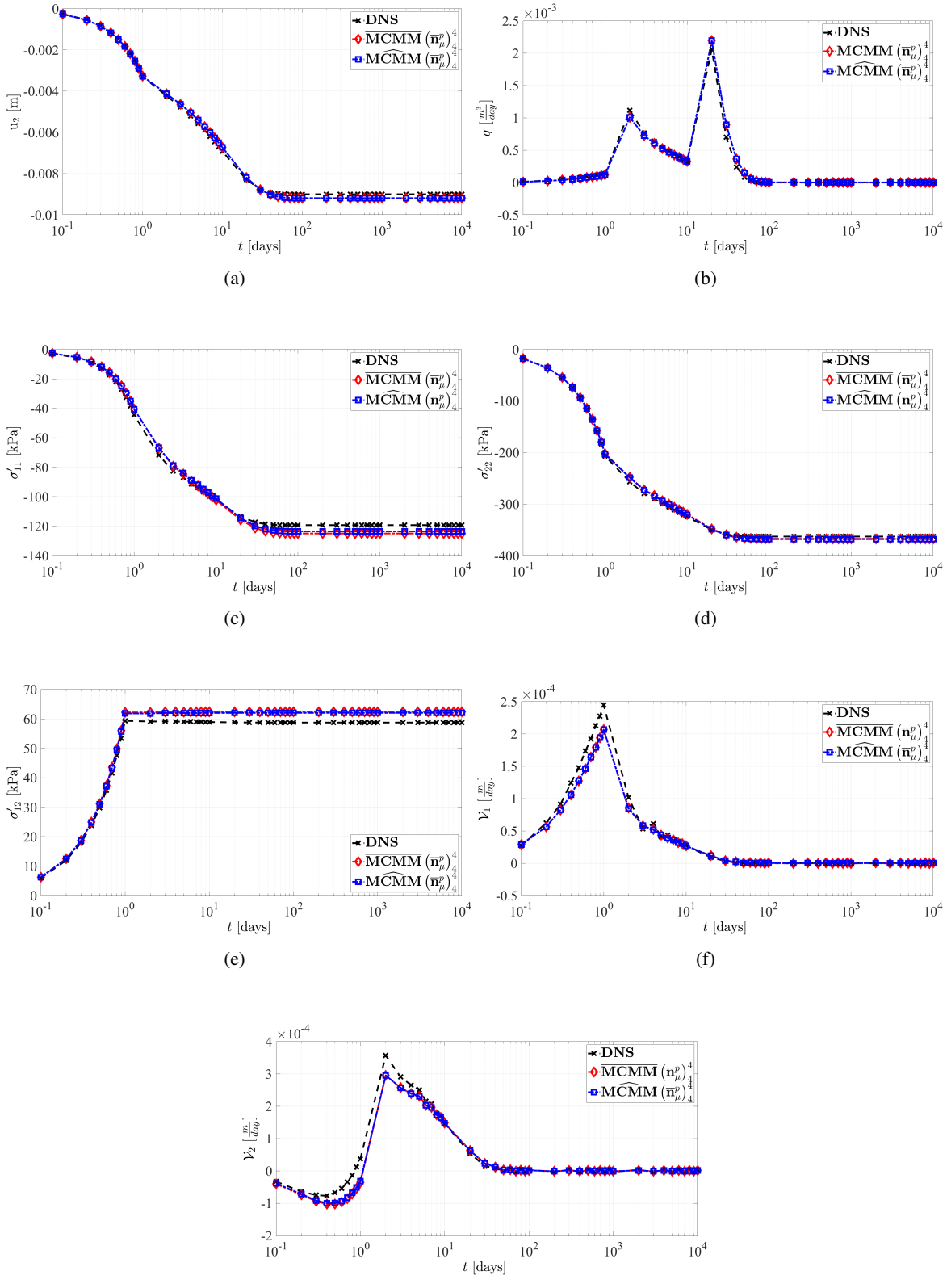

Figura 5.1: Evolución temporal de diferentes variables macroescala.

Parte IV

Conclusiones

Capítulo 6

Conclusiones

En este capítulo se resumen los principales aportes al modelado multiescala logrados mediante el desarrollo de la tesis, junto con las publicaciones realizadas. Además, se incluye un listado de los artículos publicados en revistas indexadas y de los trabajos presentados en congresos. Por último se listan algunas posibles líneas de trabajo a futuro.

6.1. Contribuciones

Las principales contribuciones del trabajo pueden presentarse a partir de los dos ejes definidos como objetivos. Estos son: (i) la propuesta de un modelo multiescala que garantice la objetividad en la macroescala, aplicable a problemas regidos por la ecuación genérica de balance de una cantidad escalar, con especial énfasis en materiales porosos saturados sometidos a problemas hidromecánicos, y (ii) el desarrollo de una formulación multiescala para microarquitecturas formadas por inclusiones sólidas impermeables distribuidas aleatoriamente en una matriz correspondiente a un medio poroso saturado. Los aportes asociadas al primer eje se presentan en la Sub-sección 6.1.1 mientras que las correspondientes al segundo en la Sub-sección 6.1.2. Ambos aportes fueron implementados numéricamente y se integraron en una herramienta computacional.

6.1.1. Contribuciones al análisis de la dependencia con el tamaño de la microescala y la pérdida de objetividad de la respuesta macroescala

Se estableció una formulación que elimina la dependencia de la respuesta macroscópica respecto del tamaño de la microescala en problemas gobernados por la ecuación genérica de balance de una cantidad escalar con término fuente (problemas hidromecánicos y de difusión-reacción), permitiendo así obtener una respuesta homogeneizada objetiva de primer orden.

La propuesta introduce lo que se denomino de modelo Multiescala-SOE, basado en proponer expansiones de orden selectivo (SOE) para los descriptores primitivos microescala empleados como argumentos de los funcionales constitutivos. Se pueden listar las siguientes características relevantes del modelo propuesto:

- **Recuperación del concepto de RVE.** Se ha propuesto una formulación multiescala alternativa en la que se recupera la existencia del elemento de volumen representativo (RVE). En consecuencia, el dominio de la microescala puede aumentar según sea necesario, con un límite dado por el principio de separación de escalas, hasta alcanzar la representatividad en distribuciones de materiales heterogéneos.

- **Respuesta homogeneizada objetiva en la macroescala.** El enfoque Multiescala-SOE elimina el efecto de tamaño de la microescala sin necesidad de que la dimensión de la MC tienda necesaria-

mente a cero, lo que resulta especialmente valioso para estudiar el comportamiento homogeneizado de materiales con elevado grado de heterogeneidad.

- **Mínima intervención en el marco multiescala.** El esquema preserva el mayor número de componentes, aunque de una manera ligeramente redefinida. Solo son removidos de forma coherente aquellos términos que introducen un efecto de tamaño directo o explícito en la respuesta homogeneizada, mientras que las denominadas contribuciones indirectas o implícitas resultan independientes de la tasa de gradiente del campo escalar primario y, por lo tanto, insensibles al tamaño de la MC. Esto permite afirmar que la propuesta es mínimamente invasiva, ya que evita los efectos espurios de tamaño microescala, pero conserva el resto del marco multiescala casi intacto. Además, la retención del mayor número de términos es importante dentro de un modelo multiescala porque, en aplicaciones realistas, contribuyen a mejorar la respuesta homogeneizada y a cuantificar cuándo el tamaño de una MC con una distribución aleatoria de fases está más cerca, o no, de ser lo suficientemente representativo.

- **Independencia respecto de las propiedades materiales.** El modelo es insensible al tamaño de la microescala, independientemente de los parámetros materiales involucrados. Dado que en problemas genéricos de balance de una cantidad escalar con término fuente, el rango de variabilidad de las propiedades de los materiales puede ser significativamente amplio, es esencial contar con una formulación multiescala que elimine el efecto del tamaño, independientemente de la constantes de los materiales involucrados. Esta característica asegura la robustez del enfoque Multiescala-SOE.

- **Interpretación constitutiva.** La idea central de la propuesta puede considerarse formalmente una hipótesis simplificada de tipo constitutivo, ya que la expansión de orden selectivo (SOE) solo ejerce un efecto a nivel local cuando deben evaluarse las leyes materiales a microescala. Fuera de estos entornos específicos, se mantiene la expansión de orden completo para las variables primarias a microescala. Tal como ocurre para todo el marco variacional que caracteriza la solución del problema de balance a microescala y las reglas de homogeneización, que se han construido basándose en el concepto de expansión de orden completo.

- **Coherencia energética.** Dado que el equilibrio a microescala y todas las reglas de homogeneización se dedujeron como consecuencia directa del cumplimiento del principio variacional de Hill-Mandel, el procedimiento Multiescala-SOE es energéticamente coherente. Cualquier manipulación ad hoc de las fórmulas de promediado, como eliminar o descuidar términos, dará lugar, en general, a una formulación que viola dicho principio.

En síntesis, se considera que la presente propuesta constituye una contribución fundamental para la comprensión y la aplicación rigurosa de los métodos de homogeneización en el estudio de fenómenos gobernados por alguna especialización de la ecuación de balance de una cantidad escalar con término fuente (problemas hidromecánicos y de difusión-reacción).

6.1.2. Contribuciones al modelado multiescala de materiales compuestos por una combinación de un medio poroso saturado con inclusiones impermeables distribuidos aleatoriamente

En lo que refiere al formulación multiescala de microestructuras con componentes que requieren diferentes variables primitivas para su descripción física, los avances se dieron en dos etapas. En primer lugar, se estableció una formulación multiescala capaz de incorporar inclusiones sólidas impermeables embebidas en una matriz de porosa saturada, restringiendo inicialemente el estudio a escenarios compatibles con el reconocido modelo periódico. En una segunda etapa, se avanzó en el tratamiento de distribuciones verdaderamente aleatorias de las inclusiones a través de submodelos multiescala novedosos obtenidos al imponer restricciones adicionales sobre el MCMM.

Siguiendo los lineamientos del MMVP, se propuso una fomulación multiescala específica para modelar este tipo de microestructuras. En este contexto, las principales modificaciones se concentraron en los procedimientos que involucran al campo de poropresiones. La existencia exclusiva de este campo en el subdominio Ω_μ^p de la MC se trató mediante una meticulosa forma de efectuar el proceso de inserción. En particular, se plantearon dos variantes de expansiones de dicho descriptor primitivo a microescala que consisten en

- Expansión alrededor del centro geométrico $\mathbf{x}_\mu^G$ de la MC completa.
- Expansión en torno del centroide $\mathbf{x}_\mu^{Gp}$ del subdominio Ω_μ^p.

Cada elección conlleva particularidades relevantes.

- En el primer caso, un análisis detallado reveló que la ecuación de restricción volumétrica para las poropresiones fluctuantes a nivél microscópico no equivalía a cero, esto es, no resulta homogénea, sino que incluía un término adicional que representa la influencia de la distribución espacial de las inclusiones sólidas dentro de la matriz porosa. Este término tiende a anularse a medida que el patrón de partículas adquiere simetría.
- En la segunda propuesta, correspondiente a la expansión en torno al centroide $\mathbf{x}_\mu^{Gp}$, se recupera la condición homogénea en la ecuación de restricción volumétrica para las poropresiones fluctuantes a microescala.

Cabe destacar, que aunque las dos propuestas de expansión conducen a restricciones volumétricas diferentes, ambas deberían converger a un único modelo en presencia de MCs representativas (RVE).

Por su parte, en la regla de promediado del gradiente de poropresiones se incorporan dos términos adicionales con el fin de satisfacer la admisibilidad multiescala y no inducir magnitudes espurias similar al gradiente de poro-presiones macroscópico. El primero de ellos captura la influencia de las poropresiones a microescala en la interfaz entre los dos medios, mientras que el segundo refleja las caracteristicas geométricas de la microestructura a través de un campo vectorial propiciamente formulado.

A partir de todas estas adaptaciones se construyeron formas generalizadas del MCMM, los cuales contienen como submodelos a los modelos ampliamente conocidos como el Períodico, Lineal y Taylor. En un primer avance, con base en hipótesis basadas en la geometría que se incluyo en la formulación se admitió, de manera artificial, una disposición simétrica de las partículas cada vez que alcanzan el contorno de la MC. Por lo tanto, el modelo de homogeneización periódica pudo ser utilizado sin objeciones en la resolución de experimentos numéricos que confirmaron la factibilidad de las propuestas al ser contrastados con soluciones en única escala mediante técnica DNS.

Posteriormente, para modelar materiales con una distribución no periódica de inclusiones sólidas, se propusieron familias de submodelos multiescala que se generan al asumir nuevas restricciones implementadas en particiones adecuadamente establecidas en el contorno de la MC. Estas se denominaron de MCMM alternativos o MCMM con particiones, que conducen a mejoras significativas en la capacidad predictiva del modelado multiescala siendo posible tratar de forma confiable escenarios en los que la distribución aleatoria de inclusiones sólidas alcancen el borde de la MC.

6.2. Publicaciones científicas

6.2.1. Artículos publicados en revistas

- **R. A. Anonis**, J. L. Mroginski, P. J. Sánchez, L. E. Kosteski, About RVE size objectivity of multiscale analysis of porous media, Latin American Journal of Solids and Structures, Vol. 23 No. 1 (2026): Thematic Section: MecSol 2024: e8781-e8781, 2025. https://doi.org/10.1590/1679-7825/e8781

- **R. A. Anonis**, J. L. Mroginski, P. J. Sánchez, Multiscale formulation for materials composed by a saturated porous matrix and solid inclusions, Computer Methods in Applied Mechanics and Engineering, Volume 429, 2024, 117162, ISSN 0045-7825, https://doi.org/10.1016/.cma.2024.117162.
- **R. A. Anonis**, J. L. Mroginski, P. J. Sánchez. Multiscale formulation for saturated porous media preserving the representative volume element size objectivity. Int. Journal for Numerical Methods in Engineering. 2024;125(3):e7381. doi: 10.1002/nme.7381. https://doi.org/10.1002/nme.7381.

6.2.2. Artículos en revisión

- **R. A. Anonis**, J. L. Mroginski, S. Toro, P. J. Sánchez, Consistent multiscale formulation of saturated porous media with randomly distributed non-porous solid inclusions. Under review.
- **R. A. Anonis**, J. L. Mroginski, S. Toro, R, Rossi, P. J. Sánchez, About the micro-scale size effect in the multiscale formulation of generic balance problems with source terms. Under review.

6.2.3. Publicaciones y presentaciones en congresos

- Rossi, R. de Souza Kichel, L., dos Santos, T., **Anonis, R. A.**, Mroginski, J. L. (2025). Multiscale assessment of damage during hydration of large structures. XVLI CILAMCE - XVLI Ibero-Latin American Congress on Computational Methods in Engineering. Vitória, Espírito Santo, Brazil.
- **Anonis, R. A.**, Mroginski, J. L., Sánchez, P. J., Toro, S. and Rossi, R. (2025). On the objectivity of the multiscale response in transient thermal conduction problems. MECOM 2025 - XLI Congreso Argentino de Mecánica Computacional. Sesion: Modelado Multiescala de Materiales . Buenos Aires, Argentina.
- **Anonis, R. A.**, Mroginski, J. L., Sánchez, P. J. and Kosteski E. L. (2024). About RVE size objectivity of multiscale analysis of porous media. MECSOL 2024 - 9th International Symposium on Solid Mechanics. Florianópolis, Brazil.
- **Anonis, R. A.**, Mroginski, J. L., Sánchez, P. J. and Toro, S. (2024). Mechanically consistent multiscale formulation for saturated porous media with randomly distributed solid (non-porous) inclusions. MECOM 2024 - XL Congreso Argentino de Mecánica Computacional. Sesion: Modelado Multiescala de Materiales. Rosario, Argentina.
- **Anonis, R. A.**, Mroginski, J. L. and Sánchez, P. J. (2023). Method of multiscale virtual power applied to an RVE composed of a saturated porous medium matrix and solid inclusions. MECOM 2023 - XXXIX Congreso Argentino de Mecánica Computacional - I Congreso Argentino Uruguayo de Mecánica Computacional. Sesión: Modelado Multiescala de Materiales . Concordia, Argentina - Salto, Uruguay.
- **Anonis, R. A.**, Mroginski, J. L., Sánchez, P. J. and Beneyto, P. A. (2022). Principle of Multiscale Virtual Power Applied to Multiphase Porous Mediums. MECOM 2022- XXXVIII Congreso Argentino de Mecánica Computacional. Sesión: Modelado Multiescala de Materiales . Bahía Blanca, Argentina.
- **Anonis, R. A.**, Mroginski, J. L., and Beneyto, P. A. (2021). Formulacion matematica consistente entre porosidad y poropresiones para modelado multiescala de medios porosos saturados. MECOM 2021- XXXVII Congreso Argentino de Mecánica Computacional. Sesión: Modelado Multiescala de Materiales . Resistencia, Argentina.

Así mismo, las referencias listadas a continuación representan aportes preliminares, los cuales poseen una relación tangencial respecto al tema específico de la tesis:

- J. L. Mroginski, J. M. López, N. Araujo, J. M. Podestá, **R. A. Anonis** (2022). Numerical Modelling of the Internal Erosion Process in Granular Soils Using the Material Point Method. MECOM 2022- XXXVIII Congreso Argentino de Mecánica Computacional. Sesión: Geomecánica Computacional. Bahía Blanca, Argentina.

- Mroginski, J.L., Castro, H.G., Podestá, J.M., Beneyto, P. A. **Anonis, R. A**. A fully coupled particle method for dynamic analysis of saturated soil. Computational Particle Mechanics. 8, 845–857 (2021). https://doi.org/10.1007/s40571-020-00373-y

6.3. Líneas de investigación a futuro

A continuación se presentan algunas direcciones viables a corto y mediano plazo en el ámbito del modelado multiescala de problemas hidromecánicos y de difusión–reacción:

- Implementar técnicas de reducción de modelos, tales como High-Performance Reduced-Order Model, para la solución eficiente de problemas de homogeneización computacional de dos escalas, que de otro modo resultarían prohibitivamente costosos.

- Extender el análisis hacia medios porosos con saturación parcial, junto con el desarrollo de una herramienta numérica que permita predecir el comportamiento de materiales heterogéneos bajo estas condiciones.

- Incorporar modelos constitutivos elastoplásticos para la fase sólida, con el fin de abordar materiales más realistas, como suelos y hormigones.

- Abordar problemas termomecánicos transitorios empleando la formulación objetiva Multiescala-SOE.

- En el contexto termomecánico, estudiar microestructuras con vacíos y distintas modalidades de transmisión de calor.

Parte V

Apéndices

Apéndice A

Multiscale formulation for saturated porous media preserving the representative volume element size objectivity

Reinaldo. A. Anonis, Javier. L. Mroginski, Pablo. J. Sánchez. Multiscale formulation for saturated porous media preserving the representative volume element size objectivity. Int J Numer Methods Eng. 2024; 125(3):e7381.

Multiscale formulation for saturated porous media preserving the representative volume element size objectivity

Anonis, Reinaldo A.[1], **Mroginski, Javier L.**[1,1], **Sánchez, Pablo J.**[2,3]

[1]LAMEC-IMIT-CONICET Laboratorio de Mecánica Computacional, Universidad Nacional del Nordeste, Las Heras 727, CP 3500 Chaco, Argentina
[2]CIMEC-UNL-CONICET, Ruta Nac. 168, Km 0, Paraje el Pozo, CP 3000 Santa Fe, Argentina
[3]GIMNI-UTN-FRSF, Lavaise 610, CP 3000 Santa Fe, Argentina

Keywords: multiscale model, saturated porous medium, RVE, objectivity, size effect.

Abstract. A multiscale model for saturated porous media is proposed, based on the concept of Representative Volume Element (RVE). The physics between macro and micro-scales is linked in terms of virtual power measures given by the general theory of poromechanics. Then, applying the so-called Principle of Multiscale Virtual Power, together with suitable admissible constraints on micro-scale displacement and pore pressure fields, a well-established variational framework is obtained. This setting allows deriving the weak form of micro-scale balance equations as well as the homogenization rules for the macro-scale stress-like variables and body forces.

Whenever the micro-scale mechanical constitutive functionals admit, as input arguments, the full-order expansion of the micro-scale pore pressure field, a size effect is inherited on the macro-scale material response. The current literature attributes this issue to the so-called "dynamical" or "second-order" term of the homogenized flux velocity. It has been commonly suggested that the influence of this term is negligible by assuming infinitely small micro-scale dimensions. However, such an idea compromises the fundamental notion of the existence of RVE for highly heterogeneous media.

In this work, we show that the micro-scale size dependence can be consistently eliminated by a simple constitutive-like assumption. Accordingly, slight and selective redefinitions in the input arguments of micro-scale material laws are proposed, leading to a constitutive formulation that allows the combination of micro-scale variables with different orders of expansion. Just at this specific (constitutive) level, a reduced-order expansion is selectively adopted for the micro-scale pore pressure field. Thus, the RVE notion is restored while still retaining the major effects of the "dynamical" component of the homogenized flux velocity.

The proposed formulation is implemented within a finite element squared (FE^2) environment. Some numerical experiments are presented showing the viability of the methodology, including comparisons against analytical, mono-scale and DNS solutions.

A.1. Introduction

Mechanics of porous saturated materials [97] is a discipline of great relevance in several areas of knowledge such as geomechanics, biomechanics, and materials science, among others, which has undergone significant development since the pioneering work of Biot, M [31, 32]. The proper definition of constitutive relations at the macro-scale level is essential to capture intricate interactions between material constituents and phases. From a modelling viewpoint, these equations can be: (i) explicitly assumed by phenomenological considerations, or (ii) implicitly derived through consistent homogenization techniques [47]. The latter paradigm has demonstrated enormous potential to predict complex material behaviors; therefore it is adopted throughout this work. Such a methodology retrieves the homogenized constitutive response by means of averaged quantities of fine-scale fields. The existence of a minimum micro-structural domain from which the macro-scale response turns out size-insensitive, i.e. the so-called

[1]Corresponding author. E-mail address: javierm@ing.unne.edu.ar (Mroginski, Javier L.).

Representative Volume Element (or simply RVE), is a fundamental cornerstone for this kind of homogenization techniques [1–3, 29].

A great number of RVE-based multiscale strategies depart from the fulfillment of the Hill-Mandel lemma [1–3, 12, 29, 30], where an equivalence in terms of internal strain powers (between macro and micro-scales) is enforced. Some extensions to this approach were analyzed in the past with the aim of modelling complex problems, for example, material failure [22–24, 98–103], inertial and body force effects [26, 104], and high-order multiscale models [27, 105–108], among many other coupled applications. Recently, a unified/generalized theory was developed by Blanco P. and co-authors [19]. In this work, they proposed a variational formulation where the Principle of multiscale Virtual Power (PMVP) was established, which provides a clear and well-axiomatic framework able to develop novel and alternative families of multiscale models based on the RVE concept. Along with all the acquired progress at a conceptual level, there have also been substantial advances in the computational homogenization counterpart for such theoretical models based, mainly, on the multilevel finite element strategy (FE^2) [5].

Regarding saturated porous media, the subject of interest of this manuscript, Larsson et al. have proposed a variationally consistent homogenization method for the analysis of transient uncoupled [14] and coupled [48] consolidation phenomena. A fundamental observation was reported in these works. They show that the linear multiscale approximation introduces a micro-scale size effect due to the appearance of a "second-order" term affecting the objectivity of macro-scale response. This fact suggests that conventional homogenization models cannot be straightforwardly extended to saturated porous media without careful revision. To overcome this problem, Larsson et al. [14, 48], show that the second-order effect will disappear as the size of the RVE becomes infinitely small. In such a case they recover the idea proposed by Özdemir et al. [71] (in the context of heat conduction), which was based on the assumption of a "quasi-stationary" subscale response.

Subsequently, Jänicke et al. [49, 74] introduce a multiscale approach with numerical model reduction applied to a macro-scale poro-viscoelastic model. From it, as a special case, a poroelastic macro-scale model is derived whose underlying assumption is that the problem is completely described by the stationary counterpart of the problem when transient fluctuations disappear. It is achieved if the size of the RVE tends to zero or if the material parameters of the sub-scale are chosen so that the fluctuating contribution is negligible compared to the stationary response.

On the other hand, Khoei et al. [16, 51] propose computational homogenization models of saturated and multiphase porous media assuming the decomposition of the macro-scale response in two terms, one stationary and the other dynamic, enclosing the size effect in the second one. It vanishes in the case of an infinitely small micro-scale domain. As the dimensions of the fine-scale increase, these authors report differences in the homogenized results when compared with a Direct Numerical Simulation analysis (DNS).

Saeedmonir and Khoei [52] developed a two-scale formulation for the thermo-hydro-mechanical analysis of heterogeneous porous media. For this phenomenon, they warn that when considering the micro-dynamic terms, the approach based on conventional periodic boundary conditions, with four corner nodes restricted, leads to substantial errors for highly transient problems in the transient phase of the solution. Thus, they proposed to couple several additional constraints in order to take into account micro-inertial terms. Based on this approach, Khoei et al. [53] extended the hydro-mechanical analysis to include micro-fractures.

Klahr et al. [56] established a variational RVE-based multiscale formulation applied to a saturated porous medium under large strains. In this scenario, they found that there is also a dependence on the size of the Micro-Cell domain which can be observed through the homogenized flow velocity.

In addition, some authors have recently provided significant contributions in the field of multiscale methods applied to saturated porous media but without addressing the aforementioned size effect subject [18, 50, 55, 77, 78].

All the advancements cited in the last paragraphs exhibit a notable interest to gain insight into the

size effect issue inherent to the multiscale modelling of saturated porous media, being, currently, a challenging topic and an open line of research. The idea of preserving transient effects with the purpose of not limiting predictive capabilities underlies all those previous contributions. The micro-scale size dependence seems to be contrary to the intuitive concept of RVE existence and, therefore, compromises one of the basic pillars on which the whole homogenization theory was founded [1–3, 29]. The main motivation of this work is to contribute to clarifying ideas concerning this critical theoretical issue and also to introduce a new modelling alternative. Any improved multiscale constitutive formulation should preserve both the RVE notion and the principle of separation of scales as well. To achieve these goals, we depart from the general framework posited by the above-mentioned Principle of Multiscale Virtual Power (PMVP)[19].

In summary, this manuscript presents a consistent PMVP-based homogenization model along with its corresponding numerical implementation, which is devised to deal with the consolidation phenomenon in saturated soils [42, 43]. For the mechanical description of the porous medium, the general theory of poromechanics due to Coussy [36] is used. To define the internal power functionals, at macro and micro-scale levels, two additional pairs of power-conjugate variables (to be discussed later) are required if compared with the classical case of a non-porous medium.

The present work points to the core of the RVE existence issue. Indeed, our proposal guarantees (by construction) the well-accepted notion of RVE along with all their physical implications. To this end, the mechanical constitutive equations at the micro-scale level describing the behavior of the porous medium are slightly redefined. Generally, these material laws take as input arguments the fully expanded micro-scale strains and micro-scale pore pressures variables. In contrast, a selective reduced-order expansion is assumed here for the micro-scale pore pressures in the input arguments of some constitutive functionals. Such a strategy allows the elimination of the RVE size effect. Under these circumstances we obtain a procedure with three important peculiarities: (i) the transient or dynamical terms are not neglected at all, ensuring the contribution that they provide to the homogenized response (only one component is naturally eliminated), (ii) the micro-scale domain can increase as required (with a limit given by the scale separation principle) in order to reach representativeness in heterogeneous material distributions, and (iii) the micro-scale size insensitivity of the model is attained irrespective of the material parameters involved. The last property is of great importance for our purposes, since it enables to extend the current formulation to more general situations (not only to the context of fully saturated porous media). This paragraph summarizes all the novel contributions behind our multiscale formulation and the differences with existing alternatives in the current literature.

The computational implementation of the model is carried out within the context of the Finite Element squared method (FE^2) and follows several previous developments [23, 41–43, 109].

The article is organized as follows. In Section (A.2), the strong and weak forms of macro-scale governing equations for saturated porous media are described. In the first part of Section (A.3), we discuss the minimally constrained setting to be considered at the micro-scale domain in order to guarantee admissibility requirements between macro and micro-scale primal descriptors. Then, the Principle of Multiscale Virtual Power (PMVP) is invoked, which encompasses all the necessary ingredients to bridge the physical length scales involved. The homogenization rules and the micro-scale variational forms of balance are deduced next. Section (A.4) provides specifications concerning the constitutive laws for the sub-scale problem. According to the treatment given to the input arguments in constitutive functionals, two approaches are introduced, named FOE (Full Order Expansion) and SOE (Selective Order Expansion) models. Such terminology will be systematically employed throughout the rest of the manuscript. Section (A.5) describes the so-called periodic homogenization scheme which fully defines the set of constraints considered at the smaller length scale. Details related to the spatial and time discretization methods, used to approach the variational forms of balance at the macro and micro-scale level, are given in Sections (A.6) and (A.7), respectively. In addition, Sections (A.6) and (A.7) feature flowcharts that elucidate the computational implementation steps involved in FE^2-based environments. Some academic examples of

one-dimensional consolidation problems are described in Section (A.8.1) to evaluate the performance of the FOE and SOE multiscale models. The assessment considers homogeneous as well as heterogeneous materials. Results provided in that Section clearly put in evidence the benefits introduced by the SOE-strategy, in contrast to the FOE-method, concerning the elimination of the micro-scale size effect. In Section A.8.2 we demonstrate the practical application of the SOE-approach to a real-world geotechnical engineering problem and its numerical validation through a comparison with the DNS (reference) solution. Finally, some conclusions are elaborated in Section (A.9). The paper ends with two appendices that show derivations related to tangent operators of the present multiscale formulation.

A.2. Governing equations of the macro-scale

In this section, fundamental equations for modelling the macro-scale problem are presented. At this level, the material is considered as a continuum porous medium, geometrically identified through a finite total volume domain Ω and having a smooth boundary Γ (at least piece-wise), see Figure (A.1). Material points are denoted by vector $\mathbf{x}$, which implies that a Cartesian coordinate system is introduced at this scale. The main hypotheses to be adopted here are the followings: (i) the porous volume is fully saturated with a pressurized fluid, thus only two phases constitute the continuum medium (the solid and the fluid phases), (ii) infinitesimal transformations, (iii) linear elasticity and (iv) the inertial terms can be neglected for both, solid as well as fluid, phases.

A.2.1. Strong form of the macro-scale balance equations

For an appropriate description of the mechanical behavior of saturated porous media, it is important to consider the fluid flow and the deformation of the solid skeleton. With this aim, two primal descriptors are introduced: the displacement (vector) field for the solid phase, $\mathbf{u}$, and the (scalar) pore pressure field of the fluid, here called p. The coupled hydro-mechanical problem is not stationary due to the seepage phenomenon, thus a monotonically increasing parameter, t, denoting the time, is incorporated to trace the evolution of all variables.

In the fully saturated case, the pore fraction is fulfilled by a single fluid referred with superscript f. The total porosity of the system, n, is defined so that the infinitesimal volume occupied by the fluid is $d\Omega^f = n\, d\Omega$, where $d\Omega$ is the differential total volume of the porous continuum. Let ρ^f and m^f be the intrinsic mass density and mass content of the fluid phase, respectively, the relationship between them is written as

$$m^f = \rho^f\, n. \tag{A.1}$$

The mass balance equations or continuity equation, under the hypothesis of infinitesimal transformations, results in

$$\dot{m}^f + \boldsymbol{\nabla} \cdot \mathbf{w} = 0 \quad \forall \mathbf{x} \in \Omega, \quad \forall t, \tag{A.2}$$

where $\boldsymbol{\nabla} \cdot (\bullet)$ defines the divergence of $(\bullet)$ and $\mathbf{w}$ represents the relative mass flow vector of the fluid and is expressed by

$$\mathbf{w} = \rho^f\, \boldsymbol{\mathcal{V}} = \rho^f\, n\, \left(\mathbf{V}^f - \mathbf{V}^s \right), \tag{A.3}$$

$\boldsymbol{\mathcal{V}}$ being the flux or the relative seepage velocity vector between the velocity vector of the fluid $\mathbf{V}^f$ and the solid skeleton $\mathbf{V}^s$.

On the other hand, neglecting the inertia forces, the momentum balance equation is stated in terms of the divergence of the total Cauchy stress tensor $\boldsymbol{\sigma}$ and the external body force field $\mathbf{f}$ as

$$\boldsymbol{\nabla} \cdot \boldsymbol{\sigma} + \mathbf{f} = \mathbf{0}, \quad \forall \mathbf{x} \in \Omega, \quad \forall t, \tag{A.4}$$

where $\mathbf{f}$ is related with the porous saturated medium (typically the saturated weight per unit volume of

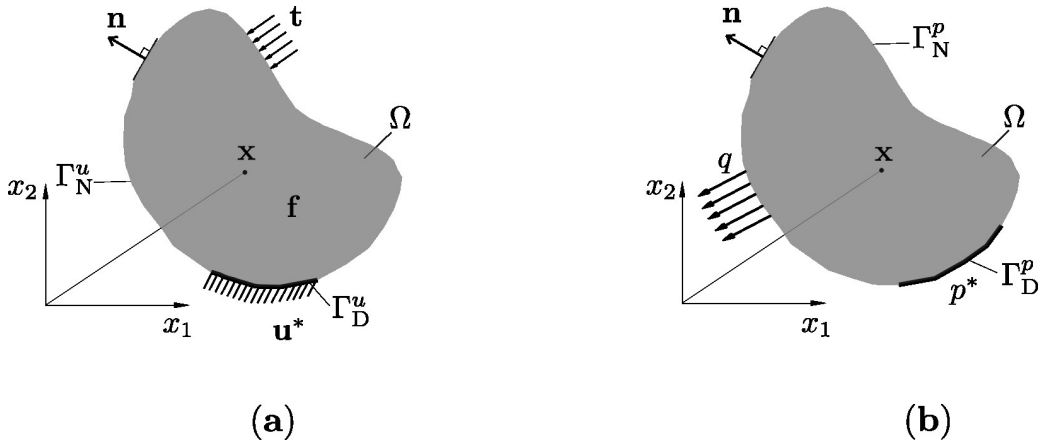

Figura A.1: Macro-scale model layout and nomenclature. (a) Mechanical problem. (b) Seepage phenomenon.

solid and fluid phases).

A.2.2. Initial and boundary conditions

The initial conditions completely define the displacement field ($\mathbf{u}^0$) and pore pressure field (p^0) at the beginning of the analysis [41, 109] in the form

$$\mathbf{u} = \mathbf{u}^0 \qquad \forall\, \mathbf{x} \in \Omega, \text{for } t = 0, \tag{A.5}$$

$$p = p^0 \qquad \forall\, \mathbf{x} \in \Omega, \text{for } t = 0. \tag{A.6}$$

Essential, or Dirichlet-type, boundary conditions can be imposed on both primary descriptors specifying prescribed functions $\mathbf{u}^*$ and p^* for displacement and pore pressure fields, respectively. They are expressed as

$$\mathbf{u} = \mathbf{u}^* \quad \forall \mathbf{x} \in \Gamma^u_{\mathrm{D}}, \quad \forall t, \tag{A.7}$$

$$p = p^* \quad \forall \mathbf{x} \in \Gamma^p_{\mathrm{D}}, \quad \forall t, \tag{A.8}$$

Γ^u_{D} and Γ^p_{D} being the corresponding Dirichlet boundary partitions of Γ related to displacement and pore pressure variables, respectively (see Figure A.1).

On the other hand, external generalized fluxes (or Neumann-type boundary conditions) can also be applied to the problem, which are defined by means of

$$\boldsymbol{\sigma} \cdot \mathbf{n} = \mathbf{t} \quad \forall \mathbf{x} \in \Gamma^u_{\mathrm{N}}, \quad \forall t, \tag{A.9}$$

$$\boldsymbol{\mathcal{V}} \cdot \mathbf{n} = \frac{q}{\rho^f} \quad \forall \mathbf{x} \in \Gamma^p_{\mathrm{N}}, \quad \forall t, \tag{A.10}$$

where $\mathbf{t}$ and q represent the systems of total external traction and normal fluid flux, respectively, $\mathbf{n}$ is the (outward) unit vector orthogonal to Γ, whereas Γ^u_{N} and Γ^p_{N} stand for the corresponding Neumann boundary partitions of Γ for displacement and pore pressure descriptors, respectively (see Figure A.1). In view of (A.7)-(A.10) we have $\Gamma = \Gamma^u_{\mathrm{D}} \cup \Gamma^u_{\mathrm{N}}$ ($\Gamma^u_{\mathrm{D}} \cap \Gamma^u_{\mathrm{N}} = \varnothing$) and also $\Gamma = \Gamma^p_{\mathrm{D}} \cup \Gamma^p_{\mathrm{N}}$ ($\Gamma^p_{\mathrm{D}} \cap \Gamma^p_{\mathrm{N}} = \varnothing$). The symbol $(\cdot)$ denotes a single contraction inner product.

A.2.3. Internal and External power functionals

The concepts of internal and external powers, $\mathcal{P}^{int}$ and $\mathcal{P}^{ext}$, respectively, turn out key ingredients for the purposes of the present multiscale formulation, as shown in the following.

For the fully saturated case and under the hypothesis of infinitesimal transformations, the internal power $\mathcal{P}^{int}$ was defined by Coussy [36] as

$$\mathcal{P}^{int} = \int_{\Omega} \left[\boldsymbol{\sigma} : \dot{\boldsymbol{\varepsilon}} - \boldsymbol{\nabla} \cdot \left(\frac{p}{\rho^f} \mathbf{w} \right) + \mathbf{g} \cdot \mathbf{w} \right] d\Omega, \tag{A.11}$$

where $\dot{\boldsymbol{\varepsilon}} = \boldsymbol{\nabla}^{sym} \dot{\mathbf{u}}$ is the rate of infinitesimal strain tensor of the solid skeleton, $\boldsymbol{\nabla}^{sym}(\bullet)$ denotes the macro-scale symmetric gradient of $(\bullet)$ and $\dot{\mathbf{u}}$ is the rate of macro-displacement field. The symbol $(:)$ designates a double contraction inner product.

After some mathematical manipulation and taking into account Eqs. (A.2-A.3), expression (A.11) can be rewritten as

$$\mathcal{P}^{int} = \int_{\Omega} \left[\boldsymbol{\sigma} : \dot{\boldsymbol{\varepsilon}} + \dot{\chi}\, p - \boldsymbol{\mathcal{V}} \cdot \left(\boldsymbol{\varphi} - \mathbf{f}^f \right) \right] d\Omega, \tag{A.12}$$

where, for ease of notation, the following nomenclature is accepted hereafter: $\dot{\chi} = \frac{\dot{m}^f}{\rho^f}$, $\boldsymbol{\varphi} = \boldsymbol{\nabla} p$ and $\mathbf{f}^f = \rho^f \mathbf{g}$ ($\mathbf{f}^f$ being the weight per unit volume of fluid phase).

For non-porous media, the internal power is fully described by the product of a single pair of dual variables, namely the Cauchy stress tensor and the rate of the symmetric strain tensor $\{\boldsymbol{\sigma}; \dot{\boldsymbol{\varepsilon}}\}$. In the present context of porous saturated materials, another physical phenomena contribute to define $\mathcal{P}^{int}$. Thus, the second term in the r.h.s. of (A.12) represents the work rate done, in the pore space, by the fluid phase. The third duality product in (A.12) takes into account the viscous dissipation effect due to the relative motion of the fluid phase concerning the solid skeleton. In summary, two additional pairs of power-conjugate variables, $\{\dot{\chi}; p\}$ and $\{\boldsymbol{\mathcal{V}}; (\boldsymbol{\varphi} - \mathbf{f}^f)\}$, are necessary to introduce with respect to the classical solid mechanical problem.

The external power, $\mathcal{P}^{ext}$, exerted by the set of external agencies $\{\mathbf{f}; \mathbf{f}^f; \mathbf{t}; q\}$ has also been established by Coussy [36]. The following expression is a straightforward manipulation from the Coussy proposal

$$\mathcal{P}^{ext} = \int_{\Omega} \left(\mathbf{f} \cdot \dot{\mathbf{u}} + \boldsymbol{\mathcal{V}} \cdot \mathbf{f}^f \right) d\Omega + \int_{\Gamma} \left[\mathbf{t} \cdot \dot{\mathbf{u}} - p \frac{q}{\rho^f} \right] d\Gamma. \tag{A.13}$$

The related concepts of internal and external virtual powers, here denoted as $\delta\mathcal{P}^{int}$ and $\delta\mathcal{P}^{ext}$ respectively, can be easily established from (A.12) and (A.13) if we replace the realizable primal quantities $\{\dot{\mathbf{u}}; \dot{\boldsymbol{\varepsilon}}; p; \boldsymbol{\varphi}\}$ by their corresponding admissible virtual actions $\{\delta\dot{\mathbf{u}}; \delta\dot{\boldsymbol{\varepsilon}}; \delta p; \delta\boldsymbol{\varphi}\}$[2]. Then, the total virtual power, $\delta\mathcal{P}^{tot}$, can be expressed as

$$\delta\mathcal{P}^{tot} = \delta\mathcal{P}^{int} - \delta\mathcal{P}^{ext} = \int_{\Omega} \left(\boldsymbol{\sigma} : \delta\dot{\boldsymbol{\varepsilon}} + \dot{\chi}\, \delta p - \boldsymbol{\mathcal{V}} \cdot \delta\boldsymbol{\varphi} - \mathbf{f} \cdot \delta\dot{\mathbf{u}} \right) d\Omega - \int_{\Gamma_{\mathrm{N}}^u} \mathbf{t} \cdot \delta\dot{\mathbf{u}}\, d\Gamma + \int_{\Gamma_{\mathrm{N}}^p} \frac{q}{\rho^f}\, \delta p\, d\Gamma. \tag{A.14}$$

Analogous definition to Eq. (A.14) will be subsequently considered to describe the total virtual power in the micro-scale domain as well as to establish the physical connection between the macro and micro scales.

[2]Throughout the manuscript, the symbol δ preceding any mechanical entity is used to denote its spatial virtual variation.

A.2.4. Weak form of the macro-scale balance equations

The balance equations in a weak form postulate that the external virtual power exerted by the set of external agencies must be equal to the internal virtual power of the stress-like variables, for all admissible variations in primal descriptors. In view of (A.14), we can write

$$\int_{\Omega} \left(\boldsymbol{\sigma} : \delta\dot{\boldsymbol{\varepsilon}} + \dot{\chi}\, \delta p - \boldsymbol{\mathcal{V}} \cdot \delta\boldsymbol{\varphi} \right) d\Omega = \int_{\Omega} \mathbf{f} \cdot \delta\dot{\mathbf{u}}\, d\Omega + \int_{\Gamma^u_{\mathrm{N}}} \mathbf{t} \cdot \delta\dot{\mathbf{u}}\, d\Gamma - \int_{\Gamma^p_{\mathrm{N}}} \frac{q}{\rho^f}\, \delta p\, d\Gamma, \ \forall\, \delta\dot{\mathbf{u}} \text{ and } \delta p \text{ admissible.} \tag{A.15}$$

The underlying admissibility requirements invoked in (A.15), for virtual variations $\delta\dot{\mathbf{u}}$ and δp, take into account proper regularity demands such that all the integral terms can be formally evaluated as well as homogeneous prescribed values for both continuous fields on Γ^u_{N} and Γ^p_{N} (i.e. where Dirichlet boundary conditions are specified for $\mathbf{u}$ and p, see (A.7) and (A.8)), respectively.

Since $\delta\dot{\mathbf{u}}$ and δp are independent from each other, the variational form of equilibrium is finally described as a system of two coupled scalar equations [36, 41, 109]

$$\begin{aligned} G &\equiv \int_{\Omega} \boldsymbol{\sigma} : \delta\dot{\boldsymbol{\varepsilon}}\, d\Omega - \int_{\Omega} \mathbf{f} \cdot \delta\dot{\mathbf{u}}\, d\Omega - \int_{\Gamma^u_{\mathrm{N}}} \mathbf{t} \cdot \delta\dot{\mathbf{u}}\, d\Gamma = 0, \quad \forall\, \delta\dot{\mathbf{u}} \text{ admissible,} \\ H &\equiv \int_{\Omega} \left(\dot{\chi}\, \delta p - \boldsymbol{\mathcal{V}} \cdot \delta\boldsymbol{\varphi} \right) d\Omega + \int_{\Gamma^p_{\mathrm{N}}} \frac{q}{\rho^f}\, \delta p\, d\Gamma = 0, \quad \forall\, \delta p \text{ admissible,} \end{aligned} \tag{A.16}$$

which is valid $\forall\, t$.

A.2.5. Constitutive equations of the macro-scale

In order to close the macro-scale governing equations, constitutive functionals for the set of stress-like quantities $\{\boldsymbol{\sigma}, \dot{\chi}, \boldsymbol{\mathcal{V}}\}$ are required. Such material laws are not explicitly defined at the macro-scale level. Instead, they are implicitly obtained from a variationally consistent multiscale formulation which is detailed below (see in particular homogenization formulae (A.37), (A.38), and (A.40), respectively, in Section A.3.4.1).

A.3. Principle of multiscale Virtual Power

In this part of the manuscript, the physical coupling between macro and micro length scales is established by appealing to the so-called Principle of Multiscale Virtual Power [19] (PMVP). This variational statement offers a formal framework to derive all basic ingredients of the multiscale formulation, as we show in sections A.3.3 and A.3.4.

Before discussing the PMVP, it is necessary to postulate an adequate mechanism for transferring information and define the concept of admissibility that makes compatible the primitive descriptors (displacements, pore pressures and their corresponding gradients) between the two involved scales (see sections A.3.1 and A.3.2).

Henceforth, any object related to the micro-scale will be endowed with the subscript μ, preserving the same physical meaning. The micro-scale domain is denoted Ω_μ (also called Micro-Cell or simply MC), with boundary Γ_μ, $\mathbf{n}_\mu$ being the unit (outward) vector normal to Γ_μ. In addition, the vector $\mathbf{y}$ is used to describe material points in a Cartesian system at the sub-scale, see Figure (A.2). Without loss of generality, the origin of coordinates is located at the geometric center of Ω_μ, implying that

$$\int_{\Omega_\mu} \mathbf{y}\, d\Omega_\mu = \mathbf{0}. \tag{A.17}$$

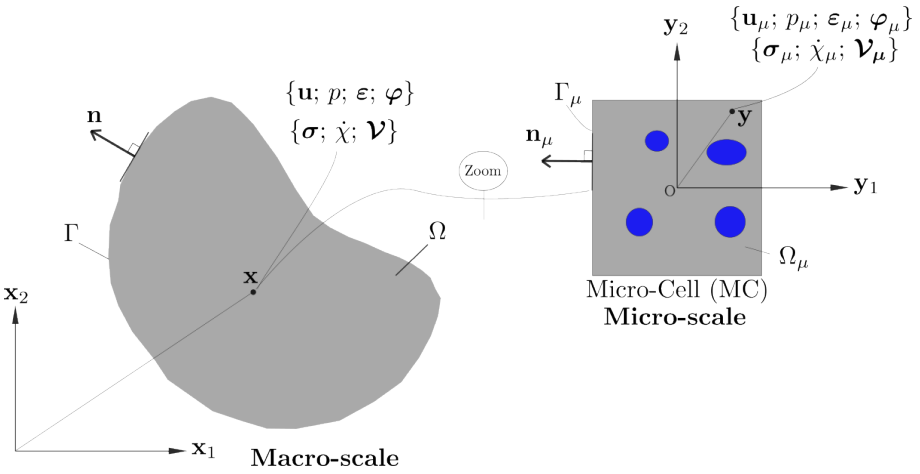

Figura A.2: Basic ingredients of a multiscale model.

A.3.1. Primal descriptors at the micro-scale level

As in the macro-scale problem, the Micro-Cell is constituted by a continuum saturated porous medium. Thus, the same theory of poromechanics, described by means of the same primal descriptors, is adopted.

A fundamental assumption in the present modelling context is that the micro-scale displacement, $\mathbf{u}_\mu$, can be expanded in terms of macro-scale quantities ($\mathbf{u}$ and $\boldsymbol{\varepsilon}$) as follows [12, 22, 26]

$$\mathbf{u}_\mu\left(\mathbf{y},t\right)=\mathbf{u}\left(\mathbf{x},t\right)+\boldsymbol{\varepsilon}\left(\mathbf{x},t\right)\cdot\mathbf{y}+\tilde{\mathbf{u}}_\mu\left(\mathbf{y},t\right), \tag{A.18}$$

$\tilde{\mathbf{u}}_\mu\left(\mathbf{y},t\right)$ being the *displacement fluctuation field* of the MC. Based on Eq. (A.18), the micro-scale infinitesimal strain tensor yields

$$\boldsymbol{\varepsilon}_\mu\left(\mathbf{y},t\right)=\boldsymbol{\nabla}_y^{sym}\mathbf{u}_\mu\left(\mathbf{y},t\right)=\boldsymbol{\varepsilon}\left(\mathbf{x},t\right)+\boldsymbol{\nabla}_y^{sym}\tilde{\mathbf{u}}_\mu\left(\mathbf{y},t\right)=\boldsymbol{\varepsilon}\left(\mathbf{x},t\right)+\tilde{\boldsymbol{\varepsilon}}_\mu\left(\mathbf{y},t\right), \tag{A.19}$$

where operator $\boldsymbol{\nabla}_y^{sym}\left(\bullet\right)$ represents the symmetric gradient concerning $\mathbf{y}$-coordinates. The strain field in (A.19) is composed as the addition of the macro-scale strain, $\boldsymbol{\varepsilon}(\mathbf{x},t)$, which is assumed to be uniformly distributed over the entire domain Ω_μ, and the micro-scale strain fluctuation $\tilde{\boldsymbol{\varepsilon}}_\mu(\mathbf{y},t)$. On the other hand, the micro-pore pressure, and its spatial gradient, can also be decomposed in an additive manner analogous to the displacement [16, 18, 51]

$$p_\mu\left(\mathbf{y},t\right)=p\left(\mathbf{x},t\right)+\boldsymbol{\varphi}\left(\mathbf{x},t\right)\cdot\mathbf{y}+\tilde{p}_\mu\left(\mathbf{y},t\right), \tag{A.20}$$

$$\boldsymbol{\varphi}_\mu\left(\mathbf{y},t\right)=\boldsymbol{\nabla}_y\, p_\mu\left(\mathbf{y},t\right)=\boldsymbol{\varphi}\left(\mathbf{x},t\right)+\boldsymbol{\nabla}_y\,\tilde{p}_\mu\left(\mathbf{y},t\right)=\boldsymbol{\varphi}\left(\mathbf{x},t\right)+\tilde{\boldsymbol{\varphi}}_\mu\left(\mathbf{y},t\right), \tag{A.21}$$

$\tilde{p}_\mu\left(\mathbf{y},t\right)$ being the *pore pressure fluctuation field* on the MC and $\tilde{\boldsymbol{\varphi}}_\mu$ its corresponding vector gradient which is obtained from the $\boldsymbol{\nabla}_y\left(\bullet\right)$ operator, related to the micro-scale coordinate system.

All previous definitions (A.18)-(A.21) are also valid in rate forms. With the aim to simplify notation, the arguments denoting spatial and time dependencies are removed in the subsequent developments.

A.3.2. Admissibility requirements in the primal descriptors

In order to relate the primitive descriptors between the two scales under study, the following simple and averaged-based homogenization relationships are assumed

$$\mathbf{u} = \frac{1}{|\Omega_\mu|}\int_{\Omega_\mu} \mathbf{u}_\mu \, d\Omega_\mu, \tag{A.22}$$

$$\boldsymbol{\varepsilon} = \frac{1}{|\Omega_\mu|}\int_{\Omega_\mu} \boldsymbol{\varepsilon}_\mu \, d\Omega_\mu, \tag{A.23}$$

$$p = \frac{1}{|\Omega_\mu|}\int_{\Omega_\mu} p_\mu \, d\Omega_\mu, \tag{A.24}$$

$$\boldsymbol{\varphi} = \frac{1}{|\Omega_\mu|}\int_{\Omega_\mu} \boldsymbol{\varphi}_\mu \, d\Omega_\mu. \tag{A.25}$$

The postulates provided by Eqs. (A.22-A.25), after some simple mathematical manipulation, are equivalent to imposing specific constraints on the fluctuation counterparts, $\tilde{\mathbf{u}}_\mu$ and $\tilde{p}_\mu$, of primary variables. Thus, substituting Eq. (A.18) in Eq. (A.22) and considering Eq. (A.17), it is possible to derive the first kinematical restriction to be imposed on the fine-scale

$$\int_{\Omega_\mu} \tilde{\mathbf{u}}_\mu \, d\Omega_\mu = \mathbf{0}, \tag{A.26}$$

which is responsible for precluding rigid translations of the MC.

Then, replacing Eq. (A.19) in (A.23), and applying Green's theorem, we arrive at the following condition

$$\int_{\Gamma_\mu} \tilde{\mathbf{u}}_\mu \otimes \mathbf{n}_\mu \, d\Gamma_\mu = \mathbf{0}, \tag{A.27}$$

$\otimes$ being the external dyadic product. Also, considering the definitions (A.17), (A.20) and (A.24), on Eqs. (A.21-A.25) as well as Green's theorem, two additional restrictions emerge

$$\int_{\Omega_\mu} \tilde{p}_\mu \, d\Omega_\mu = 0, \tag{A.28}$$

$$\int_{\Gamma_\mu} \tilde{p}_\mu \, \mathbf{n}_\mu \, d\Gamma_\mu = \mathbf{0}. \tag{A.29}$$

Only micro-scale displacement and pore pressure fluctuation fields that satisfy the constraints (A.26)-(A.29) can be considered admissible, i.e. compatible with the homogenization rules (A.22)-(A.25).

At this point, it is possible to introduce the functional vector spaces, for $\tilde{\mathbf{u}}_\mu$ and $\tilde{p}_\mu$, that define the so-called Minimally Constrained multiscale model

$$\tilde{\mathcal{U}}_\mu^{\text{MConst}} \equiv \left\{ \mathbf{v} \text{ regular enough}; \int_{\Omega_\mu} \mathbf{v} \, d\Omega_\mu = \mathbf{0}; \int_{\Gamma_\mu} \mathbf{v} \otimes \mathbf{n}_\mu \, d\Gamma_\mu = \mathbf{0} \right\}, \tag{A.30}$$

$$\tilde{\mathcal{P}}_\mu^{\text{MConst}} \equiv \left\{ v \text{ regular enough}; \int_{\Omega_\mu} v \, d\Omega_\mu = 0; \int_{\Gamma_\mu} v \, \mathbf{n}_\mu \, d\Gamma_\mu = \mathbf{0} \right\}. \tag{A.31}$$

Any pair of sub-spaces, generically denoted as $\tilde{\mathcal{U}}_\mu$ and $\tilde{\mathcal{P}}_\mu$, such that $\tilde{\mathcal{U}}_\mu \subseteq \tilde{\mathcal{U}}_\mu^{\text{MConst}}$ and $\tilde{\mathcal{P}}_\mu \subseteq \tilde{\mathcal{P}}_\mu^{\text{MConst}}$ (i.e. more constrained settings for $\tilde{\mathbf{u}}_\mu$ and $\tilde{p}_\mu$), is an a priori viable option to build alternative homogenization strategies. Typical examples are: the Taylor sub-model ($\tilde{\mathbf{u}}_\mu \equiv \mathbf{0}$ and $\tilde{p}_\mu \equiv 0, \forall \, \mathbf{y} \in \Omega_\mu$),

the Linear sub-model ($\tilde{\mathbf{u}}_\mu \equiv \mathbf{0}$ and $\tilde{p}_\mu \equiv 0, \forall\, \mathbf{y} \in \Gamma_\mu$), the Periodic sub-model (to be described later) or any other more elaborated scheme). Thus, in general we have: $\tilde{\mathbf{u}}_\mu \in \tilde{\mathcal{U}}_\mu$ and $\tilde{p}_\mu \in \tilde{\mathcal{P}}_\mu$.

Taking into account (A.18)-(A.21), virtual actions in the MC domain are defined as follows

$$\delta\mathbf{u}_\mu = \delta\mathbf{u} + \delta\boldsymbol{\varepsilon}\cdot\mathbf{y} + \delta\tilde{\mathbf{u}}_\mu, \tag{A.32}$$

$$\delta\boldsymbol{\varepsilon}_\mu = \delta\boldsymbol{\varepsilon} + \delta\tilde{\boldsymbol{\varepsilon}}_\mu = \delta\boldsymbol{\varepsilon} + \boldsymbol{\nabla}_y^{sym}\delta\tilde{\mathbf{u}}_\mu, \tag{A.33}$$

$$\delta p_\mu = \delta p + \delta\boldsymbol{\varphi}\cdot\mathbf{y} + \delta\tilde{p}_\mu, \tag{A.34}$$

$$\delta\boldsymbol{\varphi}_\mu = \delta\boldsymbol{\varphi} + \delta\tilde{\boldsymbol{\varphi}}_\mu = \delta\boldsymbol{\varphi} + \boldsymbol{\nabla}_y\,\delta\tilde{p}_\mu, \tag{A.35}$$

with $\delta\tilde{\mathbf{u}}_\mu \in \tilde{\mathcal{U}}_\mu$ and $\delta\tilde{p}_\mu \in \tilde{\mathcal{P}}_\mu$, due to all constraints (A.26)-(A.29) are homogeneous.

A.3.3. Principle of Multiscale Virtual Power

The Principle of Multiscale Virtual Power, see Blanco et al. [19], states that the total virtual power per unit volume, at a point $\mathbf{x}$ of the macro-scale, must be equal to the volumetric average of the total micro-scale virtual power (per unit volume) at the corresponding MC, for all admissible virtual actions.

Thus, recalling the definition of macro-scale total virtual power per unit volume (given by the first integrand term of the r.h.s. in Eq. (A.14)) and assuming the same mathematical structure for its micro-scale counterpart, the PMVP gives us the following variational sentence

$$\begin{aligned}\boldsymbol{\sigma}{:}\delta\dot{\boldsymbol{\varepsilon}} + \dot{\chi}\,\delta p - \boldsymbol{\mathcal{V}}\cdot\delta\boldsymbol{\varphi} \;-\; \mathbf{f}\cdot\delta\dot{\mathbf{u}} = \frac{1}{|\Omega_\mu|}\int_{\Omega_\mu}\left(\sigma_\mu{:}\delta\dot{\boldsymbol{\varepsilon}}_\mu + \dot{\chi}_\mu\,\delta p_\mu - \boldsymbol{\mathcal{V}}_\mu\cdot\delta\boldsymbol{\varphi}_\mu \;-\; \mathbf{f}_\mu\cdot\delta\dot{\mathbf{u}}_\mu\right) d\Omega_\mu,\\ \forall\,\delta\dot{\boldsymbol{\varepsilon}}\in\mathbb{R}^6,\ \forall\,\delta\dot{\mathbf{u}}\in\mathbb{R}^3,\ \forall\,\delta\boldsymbol{\varphi}\in\mathbb{R}^3,\ \forall\,\delta p\in\mathbb{R}^1,\ \forall\,\delta\dot{\mathbf{u}}_\mu\in\tilde{\mathcal{U}}_\mu,\ \forall\delta p_\mu\in\tilde{\mathcal{P}}_\mu,\ \forall\, t,\end{aligned} \tag{A.36}$$

where the compact notation $\dot{\chi}_\mu = \frac{\dot{m}_\mu^f}{\rho_\mu^f}$ and $\mathbf{f}_\mu = \rho_\mu\,\mathbf{g}$ has been considered; $\mathbf{f}_\mu$ being the saturated weight per unit volume of the porous medium which can be obtained from the saturated density $\rho_\mu = \rho^f n_\mu + \rho^s\,(1-n_\mu)$, with ρ^s denoting the density on the solid phase. Besides $\mathbb{R}^6$, $\mathbb{R}^3$, and $\mathbb{R}^1$ identify spaces of second-order symmetric tensors, three-dimensional and one-dimensional Euclidean space, respectively. Expression (A.36) can be viewed as a particular instance of the PMVP for the case of saturated porous media, at both scales of analysis.

A.3.4. Homogenized variables and variational forms of balance at the micro-scale

The variational identity (A.36) contains all the ingredients to deduce [19, 26]

(I) the homogenization formulae for the macro-scale stress-like entities $\{\boldsymbol{\sigma};\dot{\chi};\boldsymbol{\mathcal{V}}\}$ and body force $\mathbf{f}$,

(II) the variational equilibrium problem at micro-scale.

To attain this goal, definitions (A.32)-(A.35) must be replaced in expression (A.36) and then, by resorting to simple variational manipulations, the consequences (I)-(II) mentioned above can be easily derived, as we show next.

A.3.4.1. Homogenized variables

(I-a) Homogenized stress tensor:

$$\boldsymbol{\sigma} = \frac{1}{|\Omega_\mu|}\int_{\Omega_\mu}\Big(\boldsymbol{\sigma}_\mu - \mathbf{f}_\mu\,\otimes\,\mathbf{y}\Big)\,d\Omega_\mu,\ \forall\, t. \tag{A.37}$$

Which is obtained from (A.36), taking $\delta\dot{\tilde{\mathbf{u}}}_\mu = \mathbf{0},\ \delta p = 0,\ \delta\tilde{p}_\mu = 0,\ \delta\boldsymbol{\varphi} = \mathbf{0}, \delta\dot{\mathbf{u}} = \mathbf{0}$ and allowing arbitrary variations of $\delta\dot{\boldsymbol{\varepsilon}}$.

(I-b) Homogenized mass content rate of fluid (per unit fluid density):

$$\dot{\chi} = \frac{\dot{m}^f}{\rho^f} = \frac{1}{|\Omega_\mu|}\int_{\Omega_\mu} \dot{\chi}_\mu \, d\Omega_\mu,\ \forall\, t. \tag{A.38}$$

Deduced by admitting, in (A.36), arbitrary variations of δp and adopting $\delta\dot{\boldsymbol{\varepsilon}} = \mathbf{0},\ \delta\dot{\tilde{\mathbf{u}}}_\mu = \mathbf{0},\ \delta\tilde{p}_\mu = 0,\ \delta\dot{\mathbf{u}} = \mathbf{0}$ and $\delta\boldsymbol{\varphi} = \mathbf{0}$. If the fluid mass density ρ^f is assumed to be uniform throughout the MC domain, the homogenized formula for the mass content rate, $\dot{m}^f$, can be retrieved after simple manipulations on (A.38)

$$\dot{m}^f = \frac{1}{|\Omega_\mu|}\int_{\Omega_\mu} \dot{m}^f_\mu \, d\Omega_\mu,\ \forall\, t. \tag{A.39}$$

(I-c) Homogenized flux velocity vector:

$$\boldsymbol{\mathcal{V}} = \frac{1}{|\Omega_\mu|}\int_{\Omega_\mu} \left(\boldsymbol{\mathcal{V}}_\mu - \dot{\chi}_\mu\, \mathbf{y}\right) d\Omega_\mu,\ \forall\, t. \tag{A.40}$$

It is achieved from Eq. (A.36), adopting $\delta\dot{\boldsymbol{\varepsilon}} = \mathbf{0},\ \delta\dot{\tilde{\mathbf{u}}}_\mu = \mathbf{0},\ \delta p = 0,\ \delta\tilde{p}_\mu = 0, \delta\dot{\mathbf{u}} = \mathbf{0}$ with arbitrary variations of $\delta\boldsymbol{\varphi}$.

In view of (A.40), it is possible to decompose the homogenized flux velocity vector into a stationary part ($\boldsymbol{\mathcal{V}}_{sta}$) and a dynamic or transient part ($\boldsymbol{\mathcal{V}}_{tra}$) as [16, 49, 51, 52]:

$$\boldsymbol{\mathcal{V}} = \boldsymbol{\mathcal{V}}_{sta} + \boldsymbol{\mathcal{V}}_{tra} = \frac{1}{|\Omega_\mu|}\int_{\Omega_\mu} \boldsymbol{\mathcal{V}}_\mu \, d\Omega_\mu - \frac{1}{|\Omega_\mu|}\int_{\Omega_\mu} \dot{\chi}_\mu\, \mathbf{y}\, d\Omega_\mu,\ \forall\, t. \tag{A.41}$$

Decomposition (A.41) is used latter (see section A.4.1.1) to discuss the MC size effect problem.

(I-d) Homogenized body force field:

$$\mathbf{f} = \frac{1}{|\Omega_\mu|}\int_{\Omega_\mu} \mathbf{f}_\mu \, d\Omega_\mu = \frac{\mathbf{g}}{|\Omega_\mu|}\int_{\Omega_\mu} \rho_\mu \, d\Omega_\mu,\ \forall\, t. \tag{A.42}$$

It is obtained from Eq. (A.36), with $\delta\dot{\boldsymbol{\varepsilon}} = \mathbf{0},\ \delta\dot{\tilde{\mathbf{u}}}_\mu = \mathbf{0},\ \delta p = 0,\ \delta\tilde{p}_\mu = 0, \delta\boldsymbol{\varphi} = \mathbf{0}$ and arbitrary variations of $\delta\dot{\mathbf{u}}$.

A.3.4.2. Variational forms of balance in the MC

(II-a) Integral equation of momentum balance:

$$\int_{\Omega_\mu} \left(\boldsymbol{\sigma}_\mu{:}\delta\dot{\tilde{\boldsymbol{\varepsilon}}}_\mu \,-\, \mathbf{f}_\mu\cdot\delta\dot{\tilde{\mathbf{u}}}_\mu\right) d\Omega_\mu = \int_{\Omega_\mu} \left(\boldsymbol{\sigma}_\mu{:}\boldsymbol{\nabla}_y^{sym}\,\delta\dot{\tilde{\mathbf{u}}}_\mu \,-\, \mathbf{f}_\mu\cdot\delta\dot{\tilde{\mathbf{u}}}_\mu\right) d\Omega_\mu = 0,\ \ \forall\,\delta\dot{\tilde{\mathbf{u}}}_\mu \in\, \tilde{\mathcal{U}}_\mu,\ \forall\, t. \tag{A.43}$$

Eq. (A.43) derives from kinematically permissible variations of $\delta\dot{\tilde{\mathbf{u}}}_\mu$ in Eq. (A.36) where, in turn, $\delta\dot{\boldsymbol{\varepsilon}} = \mathbf{0},\ \delta p = 0,\ \delta\tilde{p}_\mu = 0,\ \delta\boldsymbol{\varphi} = \mathbf{0}$ and $\delta\dot{\mathbf{u}} = \mathbf{0}$.

(II-b) Integral mass balance equation:

$$\int_{\Omega_\mu} (\,\dot{\chi}_\mu\,\delta\tilde{p}_\mu - \boldsymbol{\mathcal{V}}_\mu\cdot\delta\tilde{\boldsymbol{\varphi}}_\mu\,)\ d\Omega_\mu = \int_{\Omega_\mu} (\,\dot{\chi}_\mu\,\delta\tilde{p}_\mu - \boldsymbol{\mathcal{V}}_\mu\cdot\boldsymbol{\nabla}_y\,\delta\tilde{p}_\mu\,)\ d\Omega_\mu = 0,\ \ \forall\,\delta\tilde{p}_\mu \in\, \tilde{\mathcal{P}}_\mu,\ \forall\, t. \tag{A.44}$$

It follows from (A.36) by allowing for admissible variations of $\delta\tilde{p}_\mu$ with $\delta\dot{\boldsymbol{\varepsilon}} = \mathbf{0},\ \delta\dot{\tilde{\mathbf{u}}}_\mu = \mathbf{0},\ \delta p = 0,\ \delta\dot{\mathbf{u}} = \mathbf{0}$ and $\delta\boldsymbol{\varphi} = \mathbf{0}$.

A.4. Constitutive equations in the micro-scale

The only remaining ingredient in the proposed multiscale formulation is the specification of the material behavior in the smaller length scale. Each constituent of the micro-scale domain is a two-phase saturated porous medium; therefore constitutive relations for the seepage velocity vector $\boldsymbol{\mathcal{V}}_\mu$, as well as for the mechanical stress-like quantities $\{\boldsymbol{\sigma}_\mu; \dot{\chi}_\mu\}$, are required. The form in which constitutive input arguments are considered to evaluate such material responses plays an important role for the purposes of this work. The more information is incorporated, the better characterization of the material is generally obtained or, in other words, a major number of micro hydro-mechanical effects can be inherited at the larger length scale. The above-mentioned micro-scale size dependence could be one of them, which is objectionable in the realm of RVE-based homogenization models because induces a lack of objectivity in the macro-scale response. This topic justifies the detailed treatment of the constitutive arguments presented in the following sections.

A.4.1. Constitutive laws based on Full Order Expansions (FOE) for primal descriptors

This strategy probably represents the most natural and straightforward choice to describe the micro-scale material behaviors. Indeed, it has been adopted in some previous contributions [14, 16, 48, 49, 51, 52, 77]. In this approach, the fully expanded version of primal descriptors, see definitions (A.19)-(A.21), are part of the list of arguments in the constitutive functionals. For future reference, the multiscale model derived from this assumption is denoted as FOE, meaning Full Order Expanded constitutive arguments. Also, the superscript $(\cdot)^{\text{FOE}}$ will be added to some entities, in subsequent expressions, in order to emphasize that concept.

Therefore, with respect to the seepage phenomenon at the micro-scale level, the following generalized Darcy's law is assumed to characterize the (mean) fluid velocity vector in the porous saturated medium [36, 41, 42]

$$\boldsymbol{\mathcal{V}}_\mu = \hat{\mathcal{V}}_\mu^{\text{FOE}}\big(\boldsymbol{\varphi}_\mu^{\text{FOE}}\big) = \mathbf{k}_\mu \cdot \Big[-\big(\overbrace{\boldsymbol{\varphi} + \tilde{\boldsymbol{\varphi}}_\mu}^{\boldsymbol{\varphi}_\mu^{\text{FOE}}}\big) + \rho_\mu^f\, \mathbf{g}\Big] = \hat{\mathcal{V}}_\mu^{\text{FOE}}\big(\boldsymbol{\varphi}, \tilde{\boldsymbol{\varphi}}_\mu\big), \tag{A.45}$$

where $\mathbf{k}_\mu$ is the symmetric second order permeability tensor and the hat-symbol, $(\hat{\cdot})$, denotes a generic constitutive functional. In case of isotropic saturated materials it is $\mathbf{k}_\mu = k_\mu \mathbf{I}$; $k_\mu = \frac{\kappa_\mu}{\rho_\mu^f |\mathbf{g}|}$ being the hydraulic permeability which is a function of the hydraulic conductivity κ_μ and the specific weight of the fluid $\rho_\mu^f |\mathbf{g}|$, $|\mathbf{g}|$ is the modulus of the acceleration of gravity and $\mathbf{I}$ denotes the second order identity tensor.

The same mathematical structure that describes the (isothermal) mechanical behavior of saturated porous medium due to Coussy O. [36] (in the context of phenomenological models), is assumed valid for each constituent of the micro-scale domain. Thus, we have for $\{\dot{\boldsymbol{\sigma}}_\mu; \dot{\chi}_\mu\}$ (rate format is used)

$$\dot{\boldsymbol{\sigma}}_\mu = \hat{\dot{\sigma}}_\mu^{\text{FOE}}\big(\dot{\boldsymbol{\varepsilon}}_\mu^{\text{FOE}}, \dot{p}_\mu^{\text{FOE}}\big) = \mathbf{C}_\mu : \overbrace{\big(\dot{\boldsymbol{\varepsilon}} + \dot{\tilde{\boldsymbol{\varepsilon}}}_\mu\big)}^{\dot{\boldsymbol{\varepsilon}}_\mu^{\text{FOE}}} - \mathbf{b}_\mu \overbrace{\big(\dot{p} + \dot{\boldsymbol{\varphi}} \cdot \mathbf{y} + \dot{\tilde{p}}_\mu\big)}^{\dot{p}_\mu^{\text{FOE}}} = \hat{\dot{\sigma}}_\mu^{\text{FOE}}\big(\dot{\boldsymbol{\varepsilon}}, \dot{\tilde{\boldsymbol{\varepsilon}}}_\mu, \dot{p}, \dot{\boldsymbol{\varphi}}, \dot{\tilde{p}}_\mu\big), \tag{A.46}$$

$$\dot{\chi}_\mu = \hat{\dot{\chi}}_\mu^{\text{FOE}}\big(\dot{\boldsymbol{\varepsilon}}_\mu^{\text{FOE}}, \dot{p}_\mu^{\text{FOE}}\big) = \mathbf{b}_\mu : \underbrace{\big(\dot{\boldsymbol{\varepsilon}} + \dot{\tilde{\boldsymbol{\varepsilon}}}_\mu\big)}_{\dot{\boldsymbol{\varepsilon}}_\mu^{\text{FOE}}} + \frac{1}{M_\mu} \underbrace{\big(\dot{p} + \dot{\boldsymbol{\varphi}} \cdot \mathbf{y} + \dot{\tilde{p}}_\mu\big)}_{\dot{p}_\mu^{\text{FOE}}} = \hat{\dot{\chi}}_\mu^{\text{FOE}}\big(\dot{\boldsymbol{\varepsilon}}, \dot{\tilde{\boldsymbol{\varepsilon}}}_\mu, \dot{p}, \dot{\boldsymbol{\varphi}}, \dot{\tilde{p}}_\mu\big). \tag{A.47}$$

The micro-hydromechanical response of the porous medium is mainly defined by the elastic stiffness tensor of the skeleton $\mathbf{C}_\mu$, the Biot tensor $\mathbf{b}_\mu$ and the coefficient M_μ^{-1}. For the particular case of isotropic constituents it is $\mathbf{b}_\mu = b_\mu\,\mathbf{I}$, where the Biot coefficient $b_\mu = 1 - \frac{K_\mu}{K_\mu^s}$ is given by the relationship between the bulk modulus of the skeleton K_μ and the volumetric modulus of the grain material K_μ^s. Finally, we have $\frac{1}{M_\mu} = \frac{b_\mu - n_\mu}{K_\mu^s} + \frac{n_\mu}{K_\mu^f}$, where K_μ^f is the bulk modulus of fluid [31, 32, 41].

In saturated porous media significant mechanical changes undergone by the soil skeleton are attributed to the concept of the *effective* stress field, here denoted as $\boldsymbol{\sigma}'_\mu$. According to the poromechanics theory, $\boldsymbol{\sigma}'_\mu$ depends on the strain tensor of the soil grains ($\boldsymbol{\varepsilon}_\mu$), then in agreement with the previous constitutive law (A.46), it can be expressed as

$$\dot{\boldsymbol{\sigma}}'_\mu = \hat{\dot{\sigma}}'^{\text{FOE}}_\mu\big(\dot{\varepsilon}^{\text{FOE}}_\mu\big) = \mathbf{C}_\mu : \overbrace{\big(\dot{\boldsymbol{\varepsilon}} + \dot{\tilde{\boldsymbol{\varepsilon}}}_\mu\big)}^{\dot{\varepsilon}^{\text{FOE}}_\mu} = \hat{\dot{\sigma}}'^{\text{FOE}}_\mu\big(\dot{\boldsymbol{\varepsilon}}, \dot{\tilde{\boldsymbol{\varepsilon}}}_\mu\big). \tag{A.48}$$

A.4.1.1. About the micro-scale size dependence on the macro-scale response

Once introduced the constitutive relations (A.45)-(A.47), the multiscale model is closed and the objectivity in the macro-scale response can be analyzed.

The dynamic/transient component, $\boldsymbol{\mathcal{V}}_{tra}$, of the homogenized velocity vector (see second integral in the r.h.s. of (A.41)), has already been identified as responsible for introducing a size effect in the multiscale modelling of porous saturated solids [14, 16, 48, 49, 52]. It was also referred to as a "second-order" term. Some possible solutions have been proposed in the current literature. One is to extend the applied proposal in the context of heat flow [13, 71] and simply ignore the transient effect of the sub-scale by neglecting the $\boldsymbol{\mathcal{V}}_{tra}$-contribution so that the micro-scale problem can be considered as "quasi-stationary" at all times. Another one is to adopt an infinitely small micro-scale domain size, which allows the dynamic term to be negligible and thus avoids the problem of fine-scale size dependence [14, 16, 48, 49]. The possibility of choosing specific material parameters at the MC level in order to make the dynamic fluctuating response negligible compared with the stationary one was also mentioned [49]. Finally, another proposed solution was to over-restrict the micro-scale fields by adding additional independent constraints to the periodic homogenization model [52, 53]. In view of the previous background and the importance assigned to the transient component of the multiscale formulation, this term is now examined meticulously.

If the constitutive law (A.47) is replaced within the expression for $\boldsymbol{\mathcal{V}}_{tra}$, and reordering conveniently, it yields

$$\begin{aligned}
\boldsymbol{\mathcal{V}}_{tra} &= -\frac{1}{|\Omega_\mu|}\int_{\Omega_\mu} \dot{\chi}_\mu\,\mathbf{y}\,d\Omega_\mu = -\frac{1}{|\Omega_\mu|}\int_{\Omega_\mu} \hat{\dot{\chi}}^{\text{FOE}}_\mu\big(\dot{\boldsymbol{\varepsilon}}^{\text{FOE}}_\mu, \dot{p}^{\text{FOE}}_\mu\big)\,\mathbf{y}\,d\Omega_\mu \\
&= \overbrace{-\frac{1}{|\Omega_\mu|}\int_{\Omega_\mu}\big(\mathbf{b}_\mu : \dot{\boldsymbol{\varepsilon}}\big)\,\mathbf{y}\,d\Omega_\mu}^{\mathbf{T}_1} \overbrace{-\frac{1}{|\Omega_\mu|}\int_{\Omega_\mu}\frac{\dot{p}}{M_\mu}\,\mathbf{y}\,d\Omega_\mu}^{\mathbf{T}_2} \\
&\quad \underbrace{-\frac{1}{|\Omega_\mu|}\int_{\Omega_\mu}\big[\mathbf{b}_\mu : \dot{\tilde{\boldsymbol{\varepsilon}}}_\mu(\ldots,\dot{\boldsymbol{\varphi}},\ldots)\big]\,\mathbf{y}\,d\Omega_\mu}_{\mathbf{T}_3\to\mathcal{O}(\mathbf{y}^2)} \underbrace{-\frac{1}{|\Omega_\mu|}\int_{\Omega_\mu}\frac{\dot{\tilde{p}}_\mu(\ldots,\dot{\boldsymbol{\varphi}},\ldots)}{M_\mu}\,\mathbf{y}\,d\Omega_\mu}_{\mathbf{T}_4\to\mathcal{O}(\mathbf{y}^2)} \\
&\quad \underbrace{-\frac{1}{|\Omega_\mu|}\int_{\Omega_\mu}\frac{\dot{\boldsymbol{\varphi}}}{M_\mu}\cdot(\mathbf{y}\otimes\mathbf{y})\,d\Omega_\mu}_{\mathbf{T}_5\to\mathcal{O}(\mathbf{y}^2)}.
\end{aligned} \tag{A.49}$$

By arguing nearly symmetric distributions for $\mathbf{b}_\mu$ and M_μ properties with respect to the micro-cell

barycenter, the first two terms in the r.h.s. of (A.49), i.e. $\mathbf{T}_1$ and $\mathbf{T}_2$, do not introduce micro-scale size dependence problems. The effect of these contributions tends to decrease as the micro-cell size enlarges including a major (and representative) number of heterogeneities. So, these terms contribute to qualify when a generic micro-cell is (or not) an RVE.

The last $\mathbf{T}_5$-term in the r.h.s. of (A.49) has a quadratic dependence on the $\mathbf{y}$-coordinate. In fact, it can be expressed as

$$\mathbf{T}_5 = \frac{1}{|\Omega_\mu|}\int_{\Omega_\mu}\frac{1}{M_\mu}\,\dot{\boldsymbol{\varphi}}\cdot(\mathbf{y}\otimes\mathbf{y})\,d\Omega_\mu = \frac{1}{|\Omega_\mu|}\int_{\Omega_\mu^*}\dot{\boldsymbol{\varphi}}\cdot(\mathbf{y}\otimes\mathbf{y})\,d\Omega_\mu^* = \frac{\dot{\boldsymbol{\varphi}}}{|\Omega_\mu|}\cdot\mathbf{I}_{\Omega_\mu^*}, \tag{A.50}$$

$\mathbf{I}_{\Omega_\mu^*}$ being the inertia tensor of Ω_μ^*, where the fictitious differential volume $d\Omega_\mu^*$ is obtained from scaling $d\Omega_\mu$ with the point-wise $M_\mu^{-1}(\mathbf{y})$-distribution. Clearly, such a term introduces a size effect in the homogenized response because it increases monotonically for enlarging micro-cell dimensions and seriously compromises the concept of RVE existence. The gradient rate of pore pressures ($\dot{\boldsymbol{\varphi}}$) in the neighborhood of macro-scale external loads can take large values, especially if short-term analysis for low permeability and cohesive soils is considered. In this way, it can amplify the effect produced by the second-order contribution given in (A.50).

Although it is not so straightforward to see, $\mathbf{T}_3$ and $\mathbf{T}_4$ terms also incorporate size effect issues whenever the FOE-multiscale formulation is employed. This is because the solution of the fluctuating components $\dot{\tilde{\boldsymbol{\varepsilon}}}_\mu$ and $\dot{\tilde{p}}_\mu$ (present in $\mathbf{T}_3$ and $\mathbf{T}_4$, respectively) depend on the inserted macro-scale quantity $\dot{\boldsymbol{\varphi}}$ (see this detail in expression A.49), and such kind of implicit functionality gives rise to a second-order dependence on $\mathbf{y}$-coordinate for $\mathbf{T}_3$ and $\mathbf{T}_4$. The previous sentence can be proved in some simple multiscale modelling scenarios by solving analytically the coupled system of differential equations, for $\dot{\tilde{\mathbf{u}}}_\mu$ and $\dot{\tilde{p}}_\mu$ at the micro-scale, and then performing the homogenization process. Such a demonstration requires further and more detailed developments, thus it is left for a future contribution. However, in the present manuscript, numerical evidence concerning the size effect induced by $\mathbf{T}_3$ and $\mathbf{T}_4$ is reported, see Section (A.8.1.2.1).

The homogenization rule (A.49) brings out a sort of paradox in the current multiscale formulation since, for highly heterogeneous materials, the presence of terms $\mathbf{T}_1$ and $\mathbf{T}_2$ requires a process of enlarging micro-cell domains until to reach representativeness but, controversially, the $\mathcal{O}(\mathbf{y}^2)$-contributions ($\mathbf{T}_3$, $\mathbf{T}_4$ and $\mathbf{T}_5$) will never reach such a property during the same process.

Notice that the (direct and implicit) presence of the macro-scale pore pressure gradient rate $\dot{\boldsymbol{\varphi}}$ in (A.50), and thus the source of the size effect on $\mathbf{T}_3$, $\mathbf{T}_4$ and $\mathbf{T}_5$ terms, emerges from the kind of expansion considered for the micro-scale pore-pressure, $\dot{p}_\mu^{\text{FOE}}$, as input argument in the constitutive functional $\hat{\dot{\sigma}}_\mu^{\text{FOE}}$ and $\hat{\dot{\chi}}_\mu^{\text{FOE}}$. In particular, the first-order contribution, $\dot{\boldsymbol{\varphi}}\cdot\mathbf{y}$, is the conflicting term in that expansion (see again (A.20)). The issue cannot be removed by using alternative homogenization procedures (for example Taylor, Linear, Periodic, or the Minimally Constrained model), i.e. by modifying the restrictions to be considered on fields $\dot{\tilde{\mathbf{u}}}_\mu$ and $\dot{\tilde{p}}_\mu$, which define the spaces $\tilde{\mathcal{U}}_\mu \subseteq \tilde{\mathcal{U}}_\mu^{\text{MConst}}$ and $\tilde{\mathcal{P}}_\mu \subseteq \tilde{\mathcal{P}}_\mu^{\text{MConst}}$ where the micro-scale equilibrium is sought. Even in the simplest case of a fully homogeneous material (in all their physical properties), the terms responsible for the size effect remain present in the FOE-multiscale formulation. This last aspect can be readily appreciated in Section A.8.1.2 of numerical results.

A.4.2. Constitutive laws based on Selective Order Expansions (SOE) for primal descriptors

It has been shown that the lack of objectivity in the macro-scale response stems from the type of expansion accepted to evaluate input arguments in constitutive laws. This analysis allows us to introduce minimally invasive modifications, pointing to the core of the problem, whereas all the remainder features and ingredients of the proposed (variationally consistent) multiscale formulation are preserved, in order to not disclaim modelling capabilities.

With this purpose in mind, slight variations are now incorporated in the definition of the stress-like functionals $\hat{\dot{\boldsymbol{\sigma}}}_\mu$ and $\hat{\dot{\chi}}_\mu$. The idea aims to postulate dissimilar order of expansions for the micro-scale strain rate, $\dot{\boldsymbol{\varepsilon}}_\mu$, and for the micro-scale pore-pressure rate, $\dot{p}_\mu$, whenever both fields are considered as input constitutive arguments for $\hat{\dot{\boldsymbol{\sigma}}}_\mu$ and $\hat{\dot{\chi}}_\mu$. In other words, a Selective Order of Expansions (in short SOE) is assumed to be valid. To enforce this concept, the superscript $(\cdot)^{\text{SOE}}$ will be added to some material laws in our subsequent developments and in the multiscale model derived from. Taking into account the outcomes reported in the previous Section, the following selective expansion choices are proposed:

- A Full Order Expansion for the micro-scale strain rate descriptor, denoted as $\dot{\boldsymbol{\varepsilon}}_\mu^{\text{FOE}}$, identical to expression (A.19).
- A Reduced Order Expansion (ROE) for the micro-scale pore-pressures rate, defined as $\dot{p}_\mu^{\text{ROE}} = \dot{p}+\dot{\tilde{p}}_\mu$. It means that just the first-order term $(\dot{\boldsymbol{\varphi}}\cdot\mathbf{y})$, considered in (A.20) to expand $\dot{p}_\mu$, is neglected. Hereafter, the super-script $(\cdot)^{\text{ROE}}$, appended to a variable, implies that it has been Reduced Order Expanded.

Then, the material functionals (A.46)-(A.47) can be rewritten as[3]

$$\dot{\boldsymbol{\sigma}}_\mu = \hat{\dot{\sigma}}_\mu^{\text{SOE}}\big(\dot{\boldsymbol{\varepsilon}}_\mu^{\text{FOE}}, \dot{p}_\mu^{\text{ROE}}\big) = \mathbf{C}_\mu : \overbrace{\big(\dot{\boldsymbol{\varepsilon}}+\dot{\tilde{\boldsymbol{\varepsilon}}}_\mu\big)}^{\dot{\boldsymbol{\varepsilon}}_\mu^{\text{FOE}}} - \mathbf{b}_\mu \overbrace{\big(\dot{p}+\dot{\tilde{p}}_\mu\big)}^{\dot{p}_\mu^{\text{ROE}}} = \hat{\dot{\sigma}}_\mu^{\text{SOE}}\big(\dot{\boldsymbol{\varepsilon}}, \dot{\tilde{\boldsymbol{\varepsilon}}}_\mu, \dot{p}, \dot{\tilde{p}}_\mu\big), \tag{A.51}$$

$$\dot{\chi}_\mu = \hat{\dot{\chi}}_\mu^{\text{SOE}}\big(\dot{\boldsymbol{\varepsilon}}_\mu^{\text{FOE}}, \dot{p}_\mu^{\text{ROE}}\big) = \mathbf{b}_\mu : \underbrace{\big(\dot{\boldsymbol{\varepsilon}}+\dot{\tilde{\boldsymbol{\varepsilon}}}_\mu\big)}_{\dot{\boldsymbol{\varepsilon}}_\mu^{\text{FOE}}} + \frac{1}{M_\mu}\underbrace{\big(\dot{p}+\dot{\tilde{p}}_\mu\big)}_{\dot{p}_\mu^{\text{ROE}}} = \hat{\dot{\chi}}_\mu^{\text{SOE}}\big(\dot{\boldsymbol{\varepsilon}}, \dot{\tilde{\boldsymbol{\varepsilon}}}_\mu, \dot{p}, \dot{\tilde{p}}_\mu\big). \tag{A.52}$$

It is worth mentioning at this point that the Reduced Order Expansion for $\dot{p}_\mu$ ($\dot{p}_\mu^{\text{ROE}}$) has a very limited local effect in the multiscale formulation, since it has only meaningful within the constitutive functions characterizing $\dot{\boldsymbol{\sigma}}_\mu$ and $\dot{\chi}_\mu$. On the contrary, out of those specific environments, the micro-scale pore-pressure field is still Full Order Expanded. In summary, our proposal can be formally cataloged as a simplifying constitutive-like hypothesis for $\dot{\boldsymbol{\sigma}}_\mu$ and $\dot{\chi}_\mu$.

The generalized Darcy's law remains unchanged as defined in (A.45), thus the complete field $\dot{p}_\mu^{\text{FOE}}$ is required at this instance. The presence of pore-pressure fluctuation terms in the three material laws validates all the previous treatment given to boundary as well as domain constraints for $\dot{\tilde{p}}_\mu$[4].

The constitutive equation for the micro-scale effective stress, $\dot{\boldsymbol{\sigma}}'_\mu$, in the SOE procedure, also remains invariable if compared with the Full Order Expanded multiscale scheme. Therefore it is given by an expression similar to (A.48).

Although the same list of constitutive arguments and identical mathematical structures have been assumed for the material functionals $\hat{\dot{\sigma}}'_\mu(\dot{\boldsymbol{\varepsilon}}, \dot{\tilde{\boldsymbol{\varepsilon}}}_\mu)$ and $\hat{\mathcal{V}}_\mu(\dot{\boldsymbol{\varphi}}_\mu, \dot{\tilde{\boldsymbol{\varphi}}}_\mu)$, in the FOE and SOE approaches, the final values obtained for the effective stress and seepage velocity fields are dissimilar in each multiscale context. This is because the micro-scale fluctuating variables $\dot{\tilde{\boldsymbol{\varepsilon}}}_\mu$ and $\dot{\tilde{p}}_\mu$ are different between the two analyzed models. This aspect will become clearer later, in Section A.8.1.3 of numerical experiments (in particular through the results reported in Figure A.26).

[3] An even simpler alternative is to consider a Zero Order Expansion (ZOE) for the micro-scale pore-pressures rate, defined as $\dot{p}_\mu^{\text{ZOE}} = \dot{p}$, when evaluating the constitutive functionals $\hat{\dot{\sigma}}_\mu^{\text{SOE}}$ and $\hat{\dot{\chi}}_\mu^{\text{SOE}}$ according with (A.51) and (A.52), respectively.

[4] Even if a Zero Order of Expansion (ZOE) is considered ($\dot{p}_\mu^{\text{ZOE}}$) to evaluate the constitutive functionals $\hat{\dot{\sigma}}_\mu^{\text{SOE}}$ and $\hat{\dot{\chi}}_\mu^{\text{SOE}}$, the micro-scale pore-pressure fluctuation rate, $\dot{\tilde{p}}_\mu$, plays a role within the SOE formulation due to Darcy's Law.

A.4.2.1. Recovering the objectivity of the macro-scale response

Substituting the constitutive redefinition (A.52) within the homogenization rule for the transient counterpart of the macro-scale velocity, $\mathcal{V}_{tra}$, see second integral in the r.h.s. of (A.41), it yields

$$\begin{aligned}\boldsymbol{\mathcal{V}}_{tra} &= -\frac{1}{|\Omega_\mu|}\int_{\Omega_\mu}\dot{\chi}_\mu\,\mathbf{y}\,d\Omega_\mu = -\frac{1}{|\Omega_\mu|}\int_{\Omega_\mu}\hat{\dot{\chi}}_\mu^{\text{SOE}}\big(\dot{\boldsymbol{\varepsilon}}_\mu^{\text{FOE}},\dot{p}_\mu^{\text{ROE}}\big)\,\mathbf{y}\,d\Omega_\mu \\ &= \underbrace{-\frac{1}{|\Omega_\mu|}\int_{\Omega_\mu}\big(\mathbf{b}_\mu:\dot{\boldsymbol{\varepsilon}}\big)\,\mathbf{y}\,d\Omega_\mu}_{\mathbf{T}_1} \underbrace{-\frac{1}{|\Omega_\mu|}\int_{\Omega_\mu}\frac{\dot{p}}{M_\mu}\,\mathbf{y}\,d\Omega_\mu}_{\mathbf{T}_2} \underbrace{-\frac{1}{|\Omega_\mu|}\int_{\Omega_\mu}\big[\mathbf{b}_\mu:\dot{\tilde{\boldsymbol{\varepsilon}}}_\mu(\ldots,\dot{\boldsymbol{\not\varphi}},\ldots)\big]\,\mathbf{y}\,d\Omega_\mu}_{\mathbf{T}_3} \\ &\quad \underbrace{-\frac{1}{|\Omega_\mu|}\int_{\Omega_\mu}\frac{\dot{\tilde{p}}_\mu(\ldots,\dot{\boldsymbol{\not\varphi}},\ldots)}{M_\mu}\,\mathbf{y}\,d\Omega_\mu}_{\mathbf{T}_4}. \end{aligned} \tag{A.53}$$

Clearly, by using the Selective Order Expansion procedure, the second-order term $\mathbf{T}_5$ has been naturally removed. Besides, $\mathbf{T}_3$ and $\mathbf{T}_4$ contributions do not introduce further size effects because the *conflictive* implicit dependency of fields $\dot{\tilde{\boldsymbol{\varepsilon}}}_\mu$ and $\dot{\tilde{p}}_\mu$ with the macro-scale pore pressure gradient $\dot{\boldsymbol{\varphi}}$ disappears in the SOE-scheme. The size effect is eliminated and it is no longer required to adopt an infinitely small micro-scale domain to attain objectivity. Moreover, it is not necessary to disregard the whole contribution of $\boldsymbol{\mathcal{V}}_{tra}$ since only one component is not taken into account[5]. The typical process of enlarging the micro-scale domain size until to reach proper representativeness in the homogenized response is restored, which is indispensable to accept the concept of RVE existence in highly heterogeneous materials.

A.4.3. Unified micro-scale constitutive description

In order to simplify the forthcoming developments, from now on a unified format to describe the micro-scale constitutive laws is considered, namely

$$\dot{\boldsymbol{\sigma}}_\mu = \hat{\dot{\sigma}}_\mu\big(\dot{\boldsymbol{\varepsilon}},\dot{\tilde{\boldsymbol{\varepsilon}}}_\mu,\dot{p},\alpha\,\dot{\boldsymbol{\varphi}},\beta\,\dot{\tilde{p}}_\mu\big) = \mathbf{C}_\mu:\big(\dot{\boldsymbol{\varepsilon}}+\dot{\tilde{\boldsymbol{\varepsilon}}}_\mu\big) - \mathbf{b}_\mu\,(\dot{p}+\alpha\,\dot{\boldsymbol{\varphi}}\cdot\mathbf{y}+\beta\,\dot{\tilde{p}}_\mu), \tag{A.54}$$

$$\dot{\chi}_\mu = \hat{\dot{\chi}}_\mu\big(\dot{\boldsymbol{\varepsilon}},\dot{\tilde{\boldsymbol{\varepsilon}}}_\mu,\dot{p},\alpha\,\dot{\boldsymbol{\varphi}},\beta\,\dot{\tilde{p}}_\mu\big) = \mathbf{b}_\mu:\big(\dot{\boldsymbol{\varepsilon}}+\dot{\tilde{\boldsymbol{\varepsilon}}}_\mu\big) + \frac{1}{M_\mu}\big(\dot{p}+\alpha\,\dot{\boldsymbol{\varphi}}\cdot\mathbf{y}+\beta\,\dot{\tilde{p}}_\mu\big), \tag{A.55}$$

$$\boldsymbol{\mathcal{V}}_\mu = \hat{\mathcal{V}}_\mu\big(\boldsymbol{\varphi},\tilde{\boldsymbol{\varphi}}_\mu\big) = \mathbf{k}_\mu\cdot\Big[-\big(\boldsymbol{\varphi}+\tilde{\boldsymbol{\varphi}}_\mu\big)+\rho_\mu^f\,\mathbf{g}\Big], \tag{A.56}$$

where, with certain abuse in notation, the binary parameters α and β enable or disable the functional dependency of certain arguments in the constitutive laws according to the type of expansion adopted, such that the set $\{\alpha=1,\,\beta=1\}$ characterizes the Full Order Expansion model whereas $\{\alpha=0,\,\beta=1\}$ defines the Selective Order Expansion approach[6].

A.5. The choice of admissible constraints in the Micro-Cell

To complete the characterization of the micro-scale equilibrium problem (A.43)-(A.44), proper definitions for the linear vector spaces $\tilde{\mathcal{U}}_\mu \subseteq \tilde{\mathcal{U}}_\mu^{\text{MConst}}$ and $\tilde{\mathcal{P}}_\mu \subseteq \tilde{\mathcal{P}}_\mu^{\text{MConst}}$ must be specified. In general, different choices lead to different macroscopic constitutive responses [26, 62]. A comparative study evaluating the different alternatives is beyond the scope of the present manuscript. In this work, one of

[5] If a Zero Order Expansion $\dot{p}_\mu^{\text{ZOE}} = \dot{p}$ is adopted to evaluate (A.51) and (A.52), the $\mathbf{T}_4$ will not be present in expression (A.53).

[6] If a Zero Order Expansion $\dot{p}_\mu^{\text{ZOE}} = \dot{p}$ is adopted to evaluate (A.51) and (A.52), we have $\{\alpha=0,\,\beta=0\}$.

the most widely spread homogenization schemes is adopted, the so-called periodic multiscale model [12, 26, 62]. It is briefly described in the following sub-section.

A.5.1. Periodic boundary fluctuation model

The micro-scale material distribution must satisfy certain geometrical properties to be compatible with the assumption of periodic media. Let us consider for simplicity two-dimensional problems and rectangular micro-cells. Under such conditions, opposite MC-edges are identified in pairs. Each pair "i" of edges consists of equally sized subsets $\Gamma^{+}_{\mu i}$ and $\Gamma^{-}_{\mu i}$ of Γ_μ, with unit normals $\mathbf{n}^{+}_{i}$ and $\mathbf{n}^{-}_{i}$, respectively. So we have $\Gamma_{\mu i} = \Gamma^{+}_{\mu i} \cup \Gamma^{-}_{\mu i}$ for $i = 1, 2$. In particular, for rectangular domains at the smaller length scale the following definitions apply: $\Gamma^{+}_{\mu 1} = \Gamma^{\text{right}}_{\mu}$, $\Gamma^{-}_{\mu 1} = \Gamma^{\text{left}}_{\mu}$, $\Gamma^{+}_{\mu 2} = \Gamma^{\text{top}}_{\mu}$, $\Gamma^{-}_{\mu 1} = \Gamma^{\text{bottom}}_{\mu}$, then $\Gamma_{\mu 1} = \Gamma^{\text{right}}_{\mu} \cup \Gamma^{\text{left}}_{\mu}$ and $\Gamma_{\mu 2} = \Gamma^{\text{top}}_{\mu} \cup \Gamma^{\text{bottom}}_{\mu}$. A one-to-one correspondence exists between points of $\Gamma^{+}_{\mu i}$ and $\Gamma^{-}_{\mu i}$. That is, each point $\mathbf{y}^{+}_{i} \in \Gamma^{+}_{\mu i}$ has its corresponding point $\mathbf{y}^{-}_{i} \in \Gamma^{-}_{\mu i}$. Obviously, this geometrical correspondence must reflects the material periodicity property. The main feature of periodic model is recovered by the following constraints on primal descriptors

$$\tilde{\mathbf{u}}_\mu\left(\mathbf{y}^{+}_{i}, t\right) = \tilde{\mathbf{u}}_\mu\left(\mathbf{y}^{-}_{i}, t\right), \ \forall \text{ pair } \{\mathbf{y}^{+}_{i}, \mathbf{y}^{-}_{i}\} \text{ and } \forall i, \tag{A.57}$$

$$\tilde{p}_\mu\left(\mathbf{y}^{+}_{i}, t\right) = \tilde{p}_\mu\left(\mathbf{y}^{-}_{i}, t\right), \ \forall \text{ pair } \{\mathbf{y}^{+}_{i}, \mathbf{y}^{-}_{i}\} \text{ and } \forall i. \tag{A.58}$$

i.e. it imposes identical displacements and pore pressures fluctuations on opposite boundary points, in the sense explained above.

In summary, the specific vector spaces $\tilde{\mathcal{U}}_\mu$ and $\tilde{\mathcal{P}}_\mu$ adopted throughout this contribution to solve the micro-scale equilibrium problem coincide with the vector spaces $\tilde{\mathcal{U}}^{\text{Per}}_{\mu}$ and $\tilde{\mathcal{P}}^{\text{Per}}_{\mu}$ provided by the Periodic model, respectively ($\tilde{\mathcal{U}}_\mu \equiv \tilde{\mathcal{U}}^{\text{Per}}_{\mu}$ and $\tilde{\mathcal{P}}_\mu \equiv \tilde{\mathcal{P}}^{\text{Per}}_{\mu}$). The formal definitions for $\tilde{\mathcal{U}}^{\text{Per}}_{\mu}$ and $\tilde{\mathcal{P}}^{\text{Per}}_{\mu}$ are the followings

$$\tilde{\mathcal{U}}^{\text{Per}}_{\mu} = \Bigg\{ \mathbf{v} \text{ regular enough, } \mathbf{v}\left(\mathbf{y}^{+}_{i}, t\right) = \mathbf{v}\left(\mathbf{y}^{-}_{i}, t\right) \ \forall \text{ pair } \{\mathbf{y}^{+}_{i}, \mathbf{y}^{-}_{i}\} \\ \text{and } \forall i, \ \mathbf{v} = \frac{1}{|\Omega_\mu|} \int_{\Omega_\mu} \mathbf{v}_\mu \, d\Omega_\mu = \mathbf{0} \Bigg\} \subset \tilde{\mathcal{U}}^{\text{MConst}}_{\mu}, \tag{A.59}$$

$$\tilde{\mathcal{P}}^{\text{Per}}_{\mu} = \Bigg\{ v \text{ regular enough, } v\left(\mathbf{y}^{+}_{i}, t\right) = v\left(\mathbf{y}^{-}_{i}, t\right) \ \forall \text{ pair } \{\mathbf{y}^{+}_{i}, \mathbf{y}^{-}_{i}\} \\ \text{and } \forall i, \ v = \frac{1}{|\Omega_\mu|} \int_{\Omega_\mu} v_\mu \, d\Omega_\mu = 0 \Bigg\} \subset \tilde{\mathcal{P}}^{\text{MConst}}_{\mu}. \tag{A.60}$$

A.6. Solution of the variational equations at the macro-scale

The global numerical paradigm consists of two nested, time-evolving, finite element schemes where the connection between them is established at each macro-scale Gauss point. In the literature, such an approach is referred to as FE^2 [5] strategy. This section briefly describes the numerical implementation in the macro-scale, whereas the next Section A.7 explains the numerical details for the micro-scale.

The time variable, t, is discretized through a monotonically increasing sequence of time steps $[t^0, t^1, t^2, \ldots, t^n, t^{n+1}, \ldots]$. Any generic time interval is denoted as $I_t = [t^n, t^{n+1}]$, where $\Delta t = (t^{n+1} - t^n)$ represents the corresponding time step increment. The θ-generalized rule [41, 59] is used to account for the problem evolution within any time interval I_t. It is based on the following approximations for the

primitive and rates variables

$$(\cdot)^{n+\theta} = (1-\theta)\,(\cdot)^{n} + \theta\,(\cdot)^{n+1}, \tag{A.61}$$

$$\dot{(\cdot)}^{n+\theta} = \frac{(\cdot)^{n+1} - (\cdot)^{n}}{t^{n+1} - t^{n}} = \frac{\Delta(\cdot)}{\Delta t}, \tag{A.62}$$

$\theta \in [0,1]$ being the time integration parameter ($\theta = 0.5$ was adopted in this work).

Next, let's describe the spatial discretization issue. To model the physical domain Ω, we use a finite element mesh Ω_h. Then it is possible to build global interpolation matrices for the displacement, $\mathbf{N}_u$, and pore pressure, $\mathbf{N}_p$, fields as follows

$$\begin{aligned} \mathbf{u} &= \mathbf{N}_u\,\bar{\mathbf{u}}, \\ p &= \mathbf{N}_p\,\bar{\mathbf{p}}, \end{aligned} \tag{A.63}$$

where $\bar{\mathbf{u}}$ and $\bar{\mathbf{p}}$ are the vectors that collect all nodal displacements and pore pressures values, respectively. In order to satisfy the Babuska-Brezzi convergence requirements [41], it is necessary to adopt different orders of interpolation for each primal variable. Our current implementation considers quadrilateral, iso-parametric, bi-quadratic and bi-linear finite elements for displacements and pore pressures, respectively. Following the Galerkin method, the same spatial approximation is used for virtual actions

$$\begin{aligned} \delta\dot{\mathbf{u}} &= \mathbf{N}_u\,\delta\dot{\bar{\mathbf{u}}}, \\ \delta p &= \mathbf{N}_p\,\delta\bar{\mathbf{p}}, \end{aligned} \tag{A.64}$$

$\delta\dot{\bar{\mathbf{u}}}$ and $\delta\bar{\mathbf{p}}$ being the vectors of nodal admissible virtual variations for displacements and pore pressures, respectively.

Replacing (A.61)-(A.64) into the weak forms (A.16), and after performing standard manipulations specific to the finite element method, the discrete (time and spatial) version of balance, at time step $t^{n+\theta}$, can be written (Dirichlet degrees of freedom are omitted)

$$\begin{aligned} \dot{\mathbf{G}}_h^{n+\theta} &\equiv \int_{\Omega_h} \mathbf{B}_u^T\,\dot{\boldsymbol{\sigma}}^{n+\theta}\,d\Omega - \int_{\Omega_h} \mathbf{N}_u^T\,\dot{\mathbf{f}}^{n+\theta}\,d\Omega - \int_{\Gamma^u_{\mathrm{N},h}} \mathbf{N}_u^T\,\dot{\mathbf{t}}^{n+\theta}\,d\Gamma = \mathbf{0}, \\ \mathbf{H}_h^{n+\theta} &\equiv \int_{\Omega_h} \mathbf{N}_p^T\,\dot{\chi}^{n+\theta}\,d\Omega - \int_{\Omega_h} \mathbf{B}_p^T\,\boldsymbol{\mathcal{V}}^{n+\theta}\,d\Omega + \int_{\Gamma^p_{\mathrm{N},h}} \mathbf{N}_p^T\,\frac{q^{n+\theta}}{\rho^f}\,d\Gamma = \mathbf{0}, \end{aligned} \tag{A.65}$$

$\Gamma^{(\bullet)}_{\mathrm{N},h}$ being the discrete version of Neumann-type boundaries, $\mathbf{B}_u = \boldsymbol{\nabla}^{sym}\,\mathbf{N}_u$ is the global deformation-displacement matrix, $\mathbf{B}_p = \boldsymbol{\nabla}\,\mathbf{N}_p$ is the global matrix that relates pore pressures to their gradients and $(\cdot)^T$ stands for the transpose operator. Note that, in the first line of (A.65), the momentum balance equation has been considered in rate form.

The system of equations (A.65) is solved by using a standard Newton-Raphson algorithm. Thus, the current displacement and pore pressure nodal values are updated (at time step t^{n+1}) in terms of the iterative increments $\Delta\bar{\mathbf{u}}$ and $\Delta\bar{\mathbf{p}}$, respectively. For a given "k"-iteration in the time interval I_t of the Newton-Raphson scheme, these increments are evaluated as follows [16, 51, 52] (subscript h is omitted hereafter)

$$\begin{bmatrix} \Delta\bar{\mathbf{u}} \\ \Delta\bar{\mathbf{p}} \end{bmatrix} = -\left(\mathbf{J}_k^{n+\theta}\right)^{-1} \begin{bmatrix} \dot{\mathbf{G}}_k^{n+\theta} \\ \mathbf{H}_k^{n+\theta} \end{bmatrix}, \tag{A.66}$$

where $\mathbf{J}_k^{n+\theta}$ is the macro-scale Jacobian linear operator obtained as (subscript *"k"* is removed to simplify the notation)

$$\mathbf{J}^{n+\theta} = \begin{bmatrix} \frac{\partial\dot{\mathbf{G}}^{n+\theta}}{\partial\bar{\mathbf{u}}^{n+1}} & \frac{\partial\dot{\mathbf{G}}^{n+\theta}}{\partial\bar{\mathbf{p}}^{n+1}} \\ \frac{\partial\mathbf{H}^{n+\theta}}{\partial\bar{\mathbf{u}}^{n+1}} & \frac{\partial\mathbf{H}^{n+\theta}}{\partial\bar{\mathbf{p}}^{n+1}} \end{bmatrix}. \tag{A.67}$$

Each component of the macro-scale Jacobian matrix is defined in Appendix A. They depend on the homogenized constitutive operators of the multiscale model [12, 22, 24, 26, 27, 110], which are also specified in Appendix A.

Figure A.3 shows a simplified flowchart of the macro-scale finite element model. It includes only the core building blocks to emphasize the stage where a transition to the smaller length scale is required. i.e. the coupling point between the two scales involved. The basic input data, driving the micro-scale problem, are indicated by blue-coloured markers. We also highlight with red-coloured insets the fundamental variables, obtained from the micro-scale, that play an important role in the macro-scale hydro-mechanical equilibrium.

A.7. Solution of the variational equations at the Micro-Scale

Macro and micro spatial domains share the same temporal scale. Thus, all definitions and numerical ingredients concerning the time discretization scheme, described in Section A.6, are still valid at the micro-scale level.

The same finite element technology used in the context of the macro-scale problem is employed to conform a mesh, $\Omega_{\mu,h}$, for the micro-scale domain Ω_μ. Then, the primal descriptors $\dot{\tilde{\mathbf{u}}}_\mu$ and $\tilde{p}_\mu$ (and their corresponding admissible virtual variations $\delta\dot{\tilde{\mathbf{u}}}_\mu$ and $\delta\tilde{p}_\mu$) can be approached through global shape function matrices for micro-displacement fluctuations, $\mathbf{N}_{\tilde{u}_\mu}$, and micro-pore pressure fluctuations, $\mathbf{N}_{\tilde{p}_\mu}$, as

$$\begin{aligned} \tilde{\mathbf{u}}_\mu &= \mathbf{N}_{\tilde{u}_\mu}\,\tilde{\tilde{\mathbf{u}}}_\mu, \quad \delta\tilde{\mathbf{u}}_\mu = \mathbf{N}_{\tilde{u}_\mu}\,\delta\tilde{\tilde{\mathbf{u}}}_\mu, \quad \text{with } \tilde{\tilde{\mathbf{u}}}_\mu \text{ and } \delta\tilde{\tilde{\mathbf{u}}}_\mu \in \tilde{\mathcal{U}}^{\text{Per}}_{\mu,h}, \\ \tilde{p}_\mu &= \mathbf{N}_{\tilde{p}_\mu}\,\tilde{\tilde{\mathbf{p}}}_\mu, \quad \delta\tilde{p}_\mu = \mathbf{N}_{\tilde{p}_\mu}\,\delta\tilde{\tilde{\mathbf{p}}}_\mu, \quad \text{with } \tilde{\tilde{\mathbf{p}}}_\mu \text{ and } \delta\tilde{\tilde{\mathbf{p}}}_\mu \in \tilde{\mathcal{P}}^{\text{Per}}_{\mu,h}, \end{aligned} \tag{A.68}$$

where $\tilde{\tilde{\mathbf{u}}}_\mu$ and $\tilde{\tilde{\mathbf{p}}}_\mu$ denote the vectors containing all nodal micro-displacement fluctuations and pore pressure fluctuations, respectively ($\delta\tilde{\tilde{\mathbf{u}}}_\mu$ and $\delta\tilde{\tilde{\mathbf{p}}}_\mu$ are the global vectors collecting their corresponding virtual admissible variations), while $\tilde{\mathcal{U}}^{\text{Per}}_{\mu,h}$ and $\tilde{\mathcal{P}}^{\text{Per}}_{\mu,h}$ represent the finite-dimensional counterparts of sub-spaces $\tilde{\mathcal{U}}^{\text{Per}}_{\mu}$ $\left(\subset \tilde{\mathcal{U}}^{\text{MC}const}_{\mu}\right)$ and $\tilde{\mathcal{P}}^{\text{Per}}_{\mu}$ $\left(\subset \tilde{\mathcal{P}}^{\text{MConst}}_{\mu}\right)$ related to the Periodic multiscale model, see (A.59)-(A.60), respectively.

After some standard mathematical treatment, the substitution of (A.68) into the variational forms (A.43)-(A.44) leads to the spatial and time discrete approximation (at time $t^{n+\theta}$) for the balance equations in the micro-scale

$$\overbrace{\left[\int_{\Omega_{\mu,h}} \left(\mathbf{B}^T_{\tilde{u}_\mu}\,\dot{\boldsymbol{\sigma}}^{n+\theta}_\mu - \mathbf{N}^T_{\tilde{u}_\mu}\,\dot{\mathbf{f}}^{n+\theta}_\mu\right) d\Omega_\mu\right]}^{\dot{\mathbf{G}}^{n+\theta}_{\mu,h}} \cdot\, \delta\dot{\tilde{\tilde{\mathbf{u}}}}_\mu = 0, \quad \forall\, \delta\dot{\tilde{\tilde{\mathbf{u}}}}_\mu \in \tilde{\mathcal{U}}^{\text{Per}}_{\mu,h}, \text{ with } \dot{\tilde{\tilde{\mathbf{u}}}}_\mu \in \tilde{\mathcal{U}}^{\text{Per}}_{\mu,h} \text{ and } \tilde{\tilde{\mathbf{p}}}_\mu \in \tilde{\mathcal{P}}^{\text{Per}}_{\mu,h}, \tag{A.69}$$

$$\underbrace{\left[\int_{\Omega_{\mu,h}} \left(\mathbf{N}^T_{\tilde{p}_\mu}\,\dot{\chi}^{n+\theta}_\mu - \mathbf{B}^T_{\tilde{p}_\mu}\,\boldsymbol{\mathcal{V}}^{n+\theta}_\mu\right) d\Omega_\mu\right]}_{\mathbf{H}^{n+\theta}_{\mu,h}} \cdot\, \delta\dot{\tilde{\tilde{\mathbf{p}}}}_\mu = 0, \quad \forall\, \delta\dot{\tilde{\tilde{\mathbf{p}}}}_\mu \in \tilde{\mathcal{P}}^{\text{Per}}_{\mu,h}, \text{ with } \dot{\tilde{\tilde{\mathbf{u}}}}_\mu \in \tilde{\mathcal{U}}^{\text{Per}}_{\mu,h} \text{ and } \tilde{\tilde{\mathbf{p}}}_\mu \in \tilde{\mathcal{P}}^{\text{Per}}_{\mu,h}, \tag{A.70}$$

where $\mathbf{B}_{\tilde{u}_\mu} = \boldsymbol{\nabla}^{sym}_y\,\mathbf{N}_{\tilde{u}_\mu}$ and $\mathbf{B}_{\tilde{p}_\mu} = \boldsymbol{\nabla}_y\,\mathbf{N}_{\tilde{p}_\mu}$, are the micro-scale global matrices relating the primal variables with their corresponding gradients. Once again, in (A.69), the momentum balance equation has been considered in rate form.

The numerical solution for nodal values of displacements, $\tilde{\tilde{\mathbf{u}}}^{t_{n+1}}_\mu$, and pore pressure fluctuations,

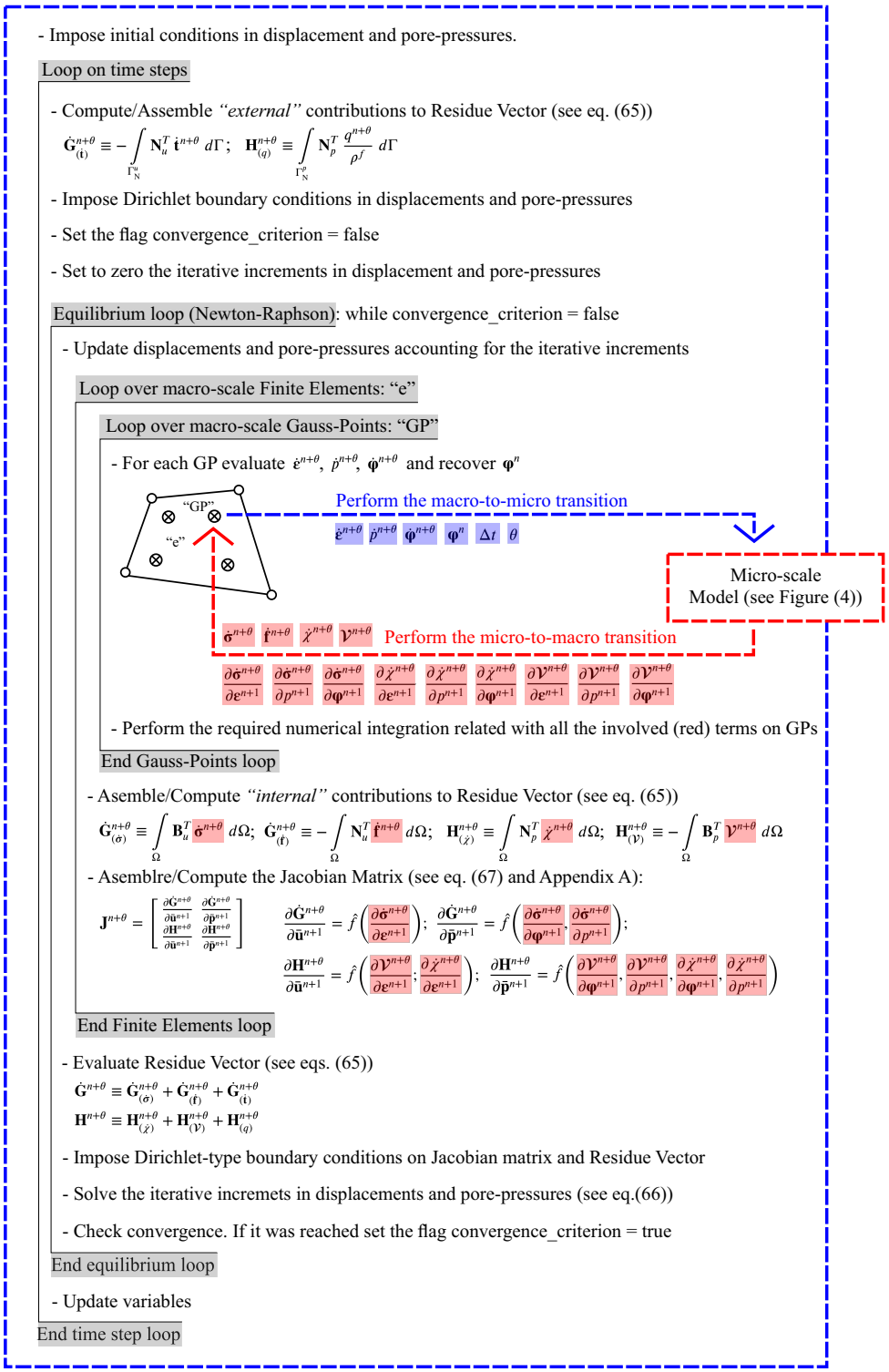

Figura A.3: Schematic flowchart for the macro-scale finite element model.

$\tilde{\tilde{\mathbf{p}}}_\mu^{t_{n+1}}$, at current time step t^{n+1}, is obtained in terms of the iterative increments $\Delta\tilde{\tilde{\mathbf{u}}}_\mu$ and $\Delta\tilde{\tilde{\mathbf{p}}}_\mu$, respectively. They are computed by using a standard Newton-Raphson procedure applied to the system of equations (A.69)-(A.70). In this sense, for a generic "*k*"-iteration it can be expressed (subscript *h* is omitted hereafter)

$$\left\{ \mathbf{J}_{\mu,\,k}^{n+\theta} \begin{bmatrix} \Delta\tilde{\tilde{\mathbf{u}}}_\mu \\ \Delta\tilde{\tilde{\mathbf{p}}}_\mu \end{bmatrix} + \begin{bmatrix} \dot{\mathbf{G}}_{\mu,\,k}^{n+\theta} \\ \mathbf{H}_{\mu,\,k}^{n+\theta} \end{bmatrix} \right\} \cdot \begin{bmatrix} \delta\dot{\tilde{\tilde{\mathbf{u}}}}_\mu \\ \delta\tilde{\tilde{\mathbf{p}}}_\mu \end{bmatrix} = \begin{bmatrix} 0 \\ 0 \end{bmatrix}, \quad \forall\ \delta\dot{\tilde{\tilde{\mathbf{u}}}}_\mu \in \tilde{\mathcal{U}}_\mu^{\text{Per}},\ \forall\ \delta\tilde{\tilde{\mathbf{p}}}_\mu \in \tilde{\mathcal{P}}_\mu^{\text{Per}},\ \text{with } \Delta\tilde{\tilde{\mathbf{u}}}_\mu \in \tilde{\mathcal{U}}_\mu^{\text{Per}},\ \text{and } \Delta\tilde{\tilde{\mathbf{p}}}_\mu \in \tilde{\mathcal{P}}_\mu^{\text{Per}}, \tag{A.71}$$

$\mathbf{J}_{\mu,\,k}^{n+\theta}$ being the Jacobian operator in the micro-scale, which has the form (subscript *"k"* is removed to simplify the notation)

$$\mathbf{J}_\mu^{n+\theta} = \begin{bmatrix} \frac{\partial \dot{\mathbf{G}}_\mu^{n+\theta}}{\partial \tilde{\tilde{\mathbf{u}}}_\mu^{n+1}} & \frac{\partial \dot{\mathbf{G}}_\mu^{n+\theta}}{\partial \tilde{\tilde{\mathbf{p}}}_\mu^{n+1}} \\ \frac{\partial \mathbf{H}_\mu^{n+\theta}}{\partial \tilde{\tilde{\mathbf{u}}}_\mu^{n+1}} & \frac{\partial \mathbf{H}_\mu^{n+\theta}}{\partial \tilde{\tilde{\mathbf{p}}}_\mu^{n+1}} \end{bmatrix} = \begin{bmatrix} \frac{1}{\Delta t}\,\mathbf{K}_\mu & -\frac{\beta}{\Delta t}\,\mathbf{Q}_\mu \\ \frac{1}{\Delta t}\,(\mathbf{Q}_\mu)^T & \left(\frac{\beta}{\Delta t}\,\mathbf{S}_\mu + \theta\,\boldsymbol{\mathcal{K}}_\mu\right) \end{bmatrix}. \tag{A.72}$$

The matrices $\mathbf{K}_\mu$, $\mathbf{Q}_\mu$, $\mathbf{S}_\mu$ and $\boldsymbol{\mathcal{K}}_\mu$, that conform the Jacobian in (A.72), are defined in Appendix B. If a Zero Order Expansion for $\dot{p}_\mu$ is adopted ($\dot{p}_\mu = \dot{p}$), i.e. the binary parameters are such that $\{\alpha = 0,\, \beta = 0\}$, the micro-scale Jacobian results in a non-symmetric operator. In contrast, the SOE-model defined from $\{\alpha = 0,\, \beta = 1\}$, preserves the symmetry property of $\mathbf{J}_\mu$. It is attained simply by scaling the second line of (A.72) (and also (A.71)) by a factor of -1.

Boundary conditions on the discrete fields $\tilde{\mathbf{u}}_\mu$ and $\tilde{p}_\mu$ were implemented via a static condensation procedure, similar to that described in Peric et. al [62] and Toro et. al [23] . However, such a technique results computational inefficient to impose the two restrictions related to the null mean values for $\tilde{\mathbf{u}}_\mu$ and $\tilde{p}_\mu$, over the entire domain Ω_μ, because the condensed Jacobian matrix loses, drastically, the band-like structure. Instead, the Lagrange Multiplier method was used for these restrictions.

Figure A.4 depicts a schematic flowchart of the micro-scale finite element model. As before, this kind of diagram illustrates only essential steps to understand the information transfer mechanism between macro and micro-scales; many details have been deliberately omitted. In this diagram, we stress the influence of macro-scale variables, on the micro-scale discrete equilibrium problem, by means of blue-coloured markers (insertion process). The precise locations where the binary parameters $\{\alpha, \beta\}$ acquire significant relevance have also been pointed out in the flowchart with magenta indicators. It is almost effortless to switch between the FOE or SOE (ROE/ZOE) multiscale formulations. Finally, we utilize red insets to identify all the homogenized variables demanded at the macro-scale Gauss-Point level. They constitute the output data of the micro-scale model.

A.8. Numerical results

The numerical results Section is subdivided into two distinct parts. The first one encompasses a series of simple academic problems related to the one-dimensional consolidation phenomenon (see Section A.8.1). It is devoted to critically analyze the performances of the two multiscale formulations discussed in the paper (i.e. FOE and SOE approaches), in terms of the micro-scale size effect issue. This study comprises rigorous comparisons of the multiscale simulations against reference and analytical (closed-form) solutions. The second part of the numerical experiments Section showcases the potential of the proposed SOE-multiscale framework (the novelty of this work) to its fullest. In this context, the SOE-strategy is applied to a practical geotechnical situation consisting of a two-dimensional consolidation problem of a strip shallow footing on a highly heterogeneous soil stratum (see Section A.8.2).

Giving priority to the main subject of the manuscript, some simplified hypotheses are accounted for in what follows, namely:

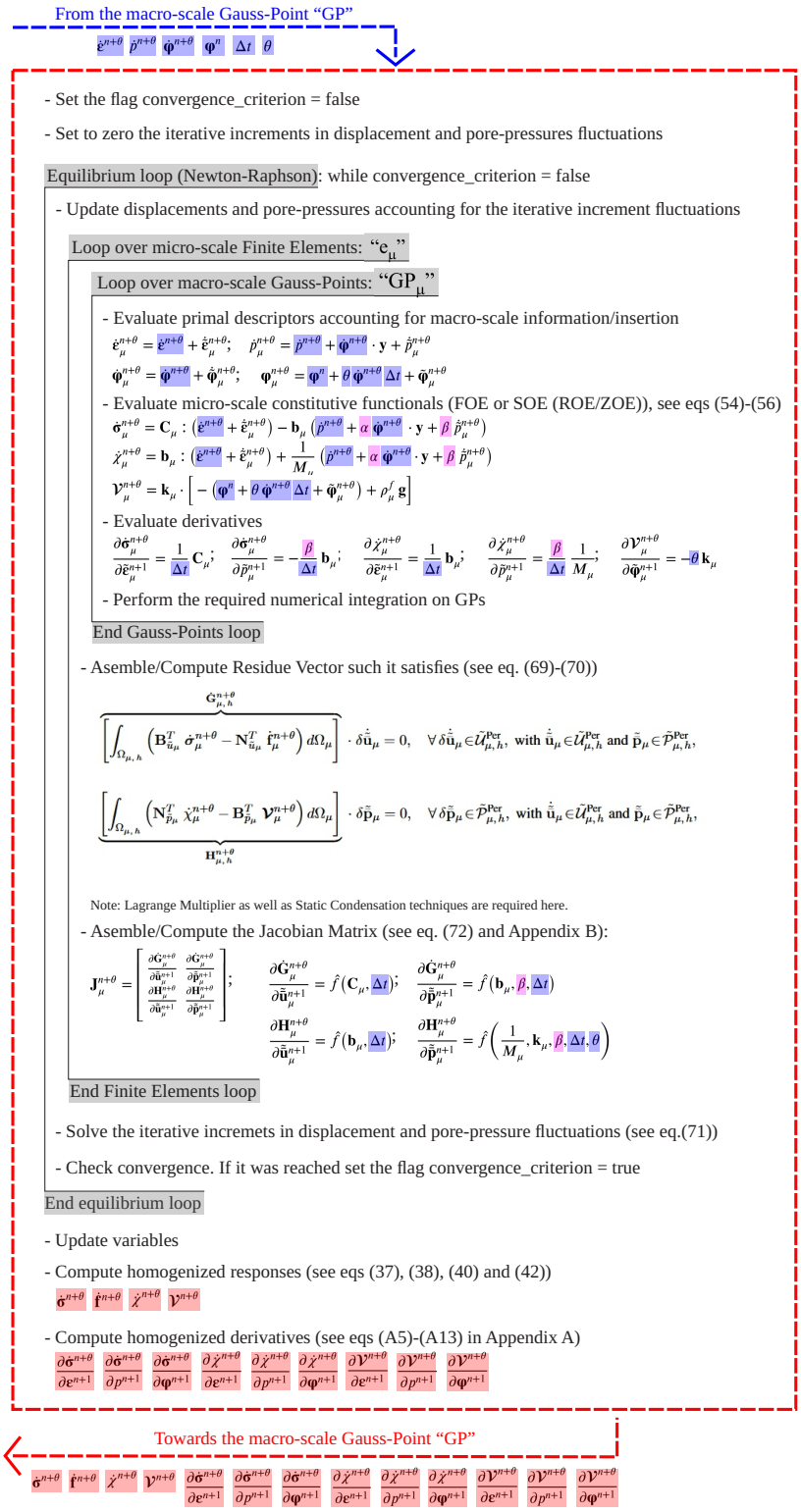

Figura A.4: Schematic flowchart for the micro-scale finite element model.

- Body forces are neglected: $\mathbf{f} \equiv \mathbf{f}_\mu \equiv \mathbf{0}$. Thus a weightless soil is simulated.
- Hydrostatic pore pressure due to the water table position is not accounted for. Under this circumstance, the variable "p" (as well as "p_μ" and "$\tilde{p}_\mu$") must be interpreted as the "*excess of pore-pressure*" generated, exclusively, by the external load ($\mathbf{t}$) during the consolidation process.
- To be consistent with the previous definition, the term containing the gravity effect in the micro-scale Darcy constitutive model must be neglected (recall (A.45)).
- Both the soil grain and the fluid are nearly incompressible.
- Plane strain conditions are assumed.

Besides, throughout this Section, we adopt the more generic Selective Order Expansion multiscale procedure defined by $\{\alpha = 0,\ \beta = 1\}$. This setting implies that solely the macro-scale pore pressure gradient rate, $\dot{\boldsymbol{\varphi}}$, has been neglected when evaluating the constitutive functionals $\dot{\hat{\sigma}}_\mu()$ and $\dot{\hat{\chi}}_\mu()$, see expressions (A.54) and (A.55).

A.8.1. One-dimensional consolidation examples

This Section presents numerical results after applying the proposed multiscale framework to the well-known one-dimensional[7] consolidation problem [36, 41, 111, 112] for fully saturated soils. Here, the assessment focuses on the above-mentioned size effect issue inherent to the FOE-homogenization scheme. We also show that, in contrast, by using the SOE-multiscale model such an objectionable effect can be removed and the conventional notion of RVE is recovered. With this goal in mind, two simple situations are considered, namely:

- a 1D-Homogeneous soil material case, see Section A.8.1.2.
- a 1D-Heterogeneous soil material case, see Section A.8.1.3.

A.8.1.1. Preliminaries

Both, homogeneous and heterogeneous cases, share some basic features and common settings; many of them can be appreciated in the general multiscale model layout, sketched in Figure A.5. The macro-scale domain consists of a narrow soil column of $\mathrm{H} = 10m$ high and $\mathrm{W} = 1m$ width. At this length scale, the material is considered as a homogenized medium. Along left and right vertical boundaries the horizontal displacements are prescribed to zero, while at the bottom boundary, the vertical component of displacement is zero. Lateral and bottom limits act as impermeable boundaries with respect to the seepage process, implying that the flux velocity, $\boldsymbol{\mathcal{V}}$, can only develop in vertical (upward) direction. For all time steps the pore pressure is fixed to zero at the upper limit, conforming the unique boundary with drainage capacity. At the ground soil surface, a purely compressive external traction $\mathbf{t} = [0;\ \mathrm{t}_2]^T$ is imposed, which evolves, linearly and monotonically, from $0kPa$ to $-1kPa$ during the first day of analysis and then it remains constant, around its minimum value ($\mathrm{t}_2 = -1kPa$), see schematic diagram in Figure A.5-(a). The macro-scale spatial discretization is composed of 8 finite elements. The mesh is refined near the ground surface where the external load $\mathbf{t}$ is applied because the largest pore pressure gradients are expected in that region, see Figure A.5-(a).

The time discretization (common for both length scales) varies during the entire analysis. It follows a logarithmic-like sequence: $t = [0.1, 0.2, 0.3, \ldots, 0.8, 0.9, 1, 2, 3, \ldots, 8, 9, 10, 20, 30, \ldots, 80, 90, 100, 200, 300, \ldots]$ (in days).

The restrictions imposed on the micro-scale displacement and pore pressure fluctuations are the same, irrespective of the case. As discussed in Section A.5.1 the so-called periodic multiscale model has been

[7] With the term *one-dimensional* (or simply 1D) we refer to the physical dimensionality of the problem at the macro-scale level.

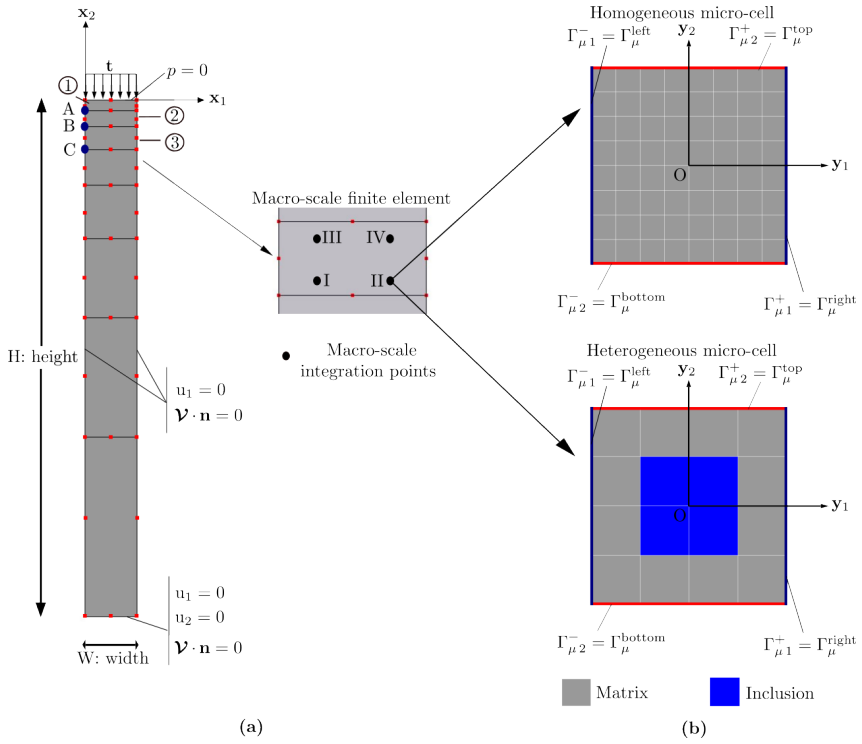

Figura A.5: Multiscale procedure applied to the 1D-consolidation phenomenon of a fully saturated soil. General model layout: (a) Macro-scale; (b) Micro-scale.

adopted in this work, which is characterized by the vector spaces $\tilde{\mathcal{U}}_{\mu}^{\text{Per}}$ and $\tilde{\mathcal{P}}_{\mu}^{\text{Per}}$ (in fact by their discrete counterparts $\tilde{\mathcal{U}}_{\mu,h}^{\text{Per}}$ and $\tilde{\mathcal{P}}_{\mu,h}^{\text{Per}}$), specified in (A.59) and (A.60), respectively. Figure A.5-(b) displays the corresponding boundary partitions $\Gamma_{\mu,1}^{-}$, $\Gamma_{\mu,1}^{+}$, $\Gamma_{\mu,2}^{-}$, and $\Gamma_{\mu,2}^{+}$ which take part in definitions (A.59) and (A.60) to build the periodic model. The vertex nodes strictly preserve the periodicity condition, which is defined as: $\tilde{\mathbf{u}}_{\mu}^{\text{top-left}} = \tilde{\mathbf{u}}_{\mu}^{\text{top-right}} = \tilde{\mathbf{u}}_{\mu}^{\text{bottom-right}} = \tilde{\mathbf{u}}_{\mu}^{\text{bottom-left}}$ and $\tilde{p}_{\mu}^{\text{top-left}} = \tilde{p}_{\mu}^{\text{top-right}} = \tilde{p}_{\mu}^{\text{bottom-right}} = \tilde{p}_{\mu}^{\text{bottom-left}}$; $\tilde{\mathbf{u}}_{\mu}^{\text{top-left}}$ and $\tilde{p}_{\mu}^{\text{top-left}}$ being the displacement fluctuation and pore pressure fluctuation for the node located at the top-left vertex of the Micro-Cell (analogous terminology applies to other vertices). No additional constraint needs to be imposed on them.

Details concerning the characterization of micro-scale domain differ for each case (homogeneous and heterogeneous), thus they are described later, in Sections A.8.1.2 and A.8.1.3. The material parameters do not necessarily are compatible with the physical properties of real soils; artificial values were adopted with the unique purpose to show the size effect issue on the macro-scale response. In this part of the paper, our focus lies not on quantitative numerical assessments, but rather on evaluating the quality of the solution, in terms of whether it retrieves, or not, an objective homogenized response.

A.8.1.2. 1D-Homogeneous fully saturated soil case

The one-dimensional consolidation problem of a homogeneous fully saturated soil material represents, clearly, a situation for which the evaluation of the mechanical response does not require the use of any homogenization strategy. However, even in this simple scenario, a size effect issue will be obtained at the macro-scale if a careless RVE-based multiscale model is employed. Hence, this example serves as a paradigmatic case for our purposes.

The homogeneous material at the micro-scale level, i.e. the matrix constituent in Figure A.5-(b) on top, is characterized by the following properties: Young's modulus $E_{\mu}^{0} = 100kPa$, Poisson's ratio $\nu_{\mu} = 0.3$, isotropic hydraulic conductivity $\kappa_{\mu,1} = \kappa_{\mu,2} = 8.64 \times 10^{-4} m/day$ and initial void ratio

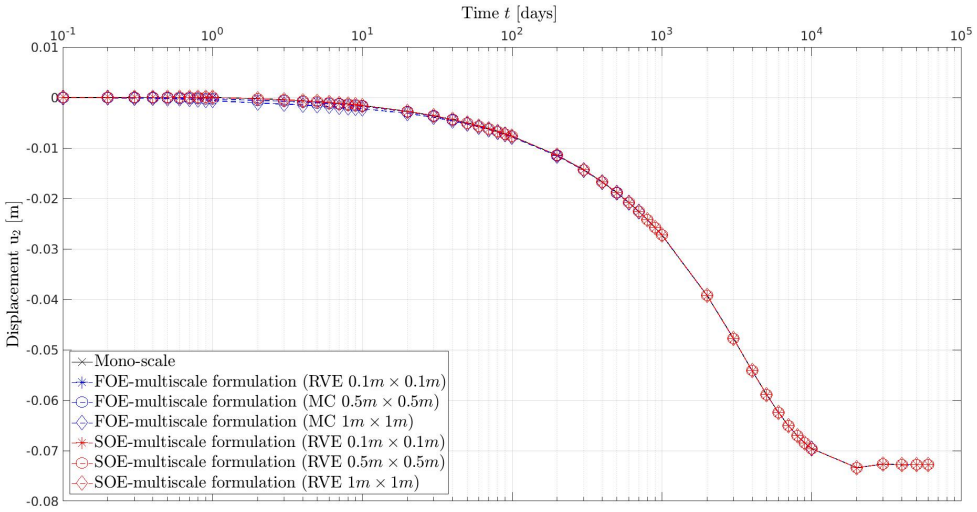

Figura A.6: 1D-Homogeneous fully saturated soil case. Vertical displacement evolution for point A of Figure A.5-(a) (depth: $x_2 = -0.2030\,m$).

$e^0_\mu = 0.6$.

In order to assess the concept of RVE-existence, recall discussions of Section (A.4), different Micro-Cells (MCs) of increasing sizes are used to obtain homogenized responses, via FOE and SOE formulations. In particular, squared MCs of $0.1m \times 0.1m$, $0.5m \times 0.5m$ and $1m \times 1m$ sizes have been adopted. Each MC is discretized through a uniform/structured mesh of 8×8 finite elements, see Figure A.5-(b) on top. Intuitively, one would expect any of these Micro-Cells to result in an RVE for the present test of homogeneous material. However, this is not the case for the FOE-multiscale strategy.

As mentioned in the first paragraph of this Section, the homogeneous problem can be solved, numerically, at a single-length scale appealing to phenomenological constitutive laws. Such a conventional mono-cale procedure is based on the two-field $\mathbf{u}$–p formulation[41, 112] and takes into account the same material properties described previously. Solutions obtained following this approach constitute our reference solutions. Therefore, they serve as a means to test the performance of the present (FOE and SOE) multiscale formulations, as we show next.

The evolution of vertical displacements for the nodes labeled as A, B and C of the macro-scale, see Figure A.5-(a), can be appreciated in Figures A.6, A.7 and A.8, respectively. These plots recover the typical shapes of the consolidation curves commonly observed in soil mechanics problems. Comparing the homogenized (FOE and SOE) values against the results provided by the mono-scale strategy, we conclude that the size effect issue is not significant when examining the macro-scale displacement variable. All curves are almost coincident. It is worth mentioning, however, that as the MC size enlarges, slightly greater settlements have been obtained when using the FOE-multiscale procedure. Figures A.9, A.10 and A.11 depict the pore pressure time-evolution curves for the same nodes A, B and C of the macro-scale mesh, respectively (see again Figure A.5-(a)). All results given by the SOE-multiscale model are in perfect agreement with the mono-scale reference solution, regardless of the dimensions adopted for the micro-structural domain. In contrast, the FOE strategy shows a good fit compared with the single-scale model response only for the smallest Micro-Cell (although it is possible to appreciate a slight difference). Indeed, concerning the FOE-scheme, we can only assign the attribute of being an RVE to the $0.1m \times 0.1m$ Micro-Cell size (see this detail in the legends of all Figures A.6-A.18). As the Micro-Cell size increases, the discrepancies become more evident, leading to curves that exhibit lower values for the p-variable, i.e. a more rapid dissipation of the excess of pore pressures induced by the external load $\mathbf{t}$. Note also that the differences between the FOE-results and the other solutions increase for those points nearest the ground surface, in correspondence with the zone where higher pore pressure gradient rates,

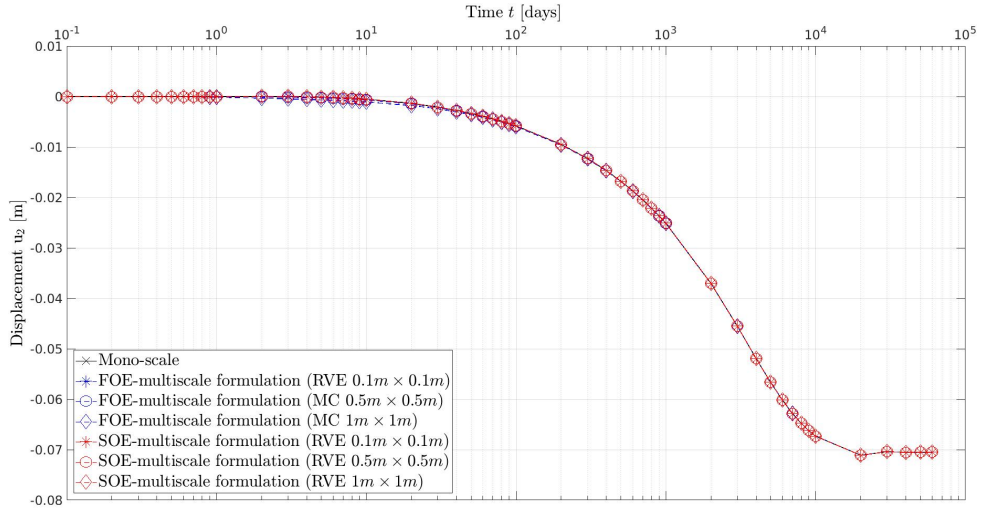

Figura A.7: 1D-Homogeneous fully saturated soil case. Vertical displacement evolution for point B of Figure A.5-(a) (depth: $x_2 = -0.5080\, m$).

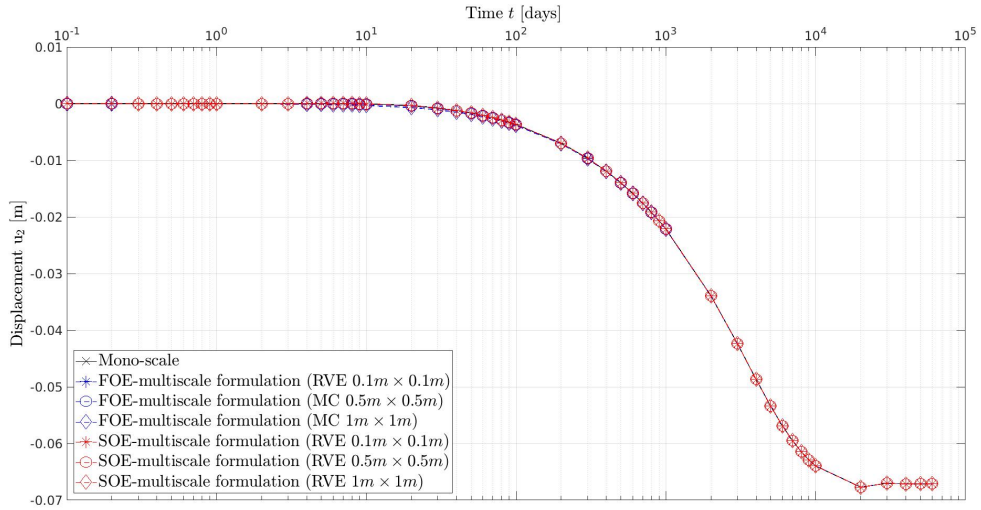

Figura A.8: 1D-Homogeneous fully saturated soil case. Vertical displacement evolution for point C of Figure A.5-(a) (depth: $x_2 = -0.964\, m$).

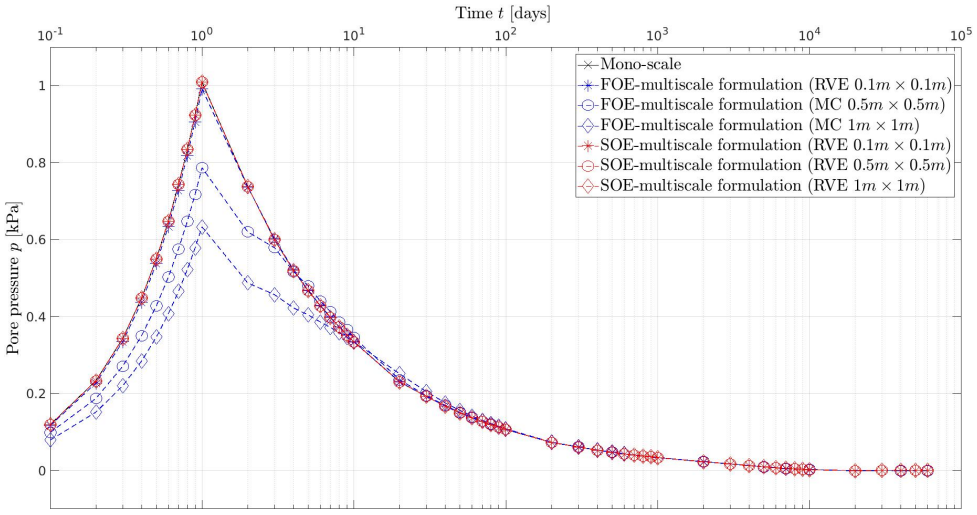

Figura A.9: 1D-Homogeneous fully saturated soil case. Pore pressure evolution for point A of Figure A.5-(a) (depth: $x_2 = -0.2030\,m$).

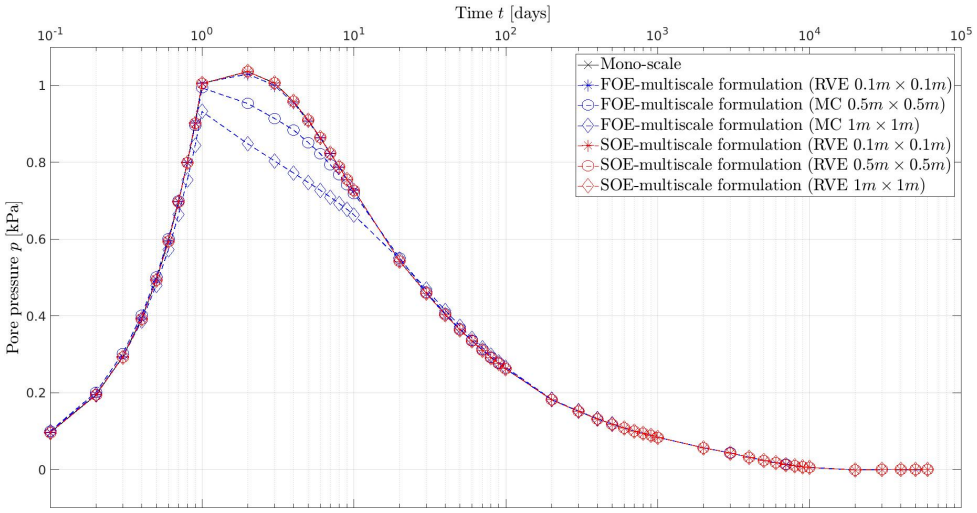

Figura A.10: 1D-Homogeneous fully saturated soil case. Pore pressure evolution for point B of Figure A.5-(a) (depth: $x_2 = -0.5080\,m$).

$\dot{\boldsymbol{\varphi}}$, are generated. Figures A.12, A.13 and A.14 show time-evolution curves for the vertical component of the effective stress tensor, σ'_{22}, in correspondence with the macro-scale finite elements 1, 2 and 3, integration point I in Figure A.5-(a), respectively. The micro-scale size sensitivity also manifests in this homogenized variable whenever the FOE-multiscale procedure is analyzed. The results obtained with this model disagree with respect to the mono-scale ones, giving lower effective stress values, very noticeable for the two largest Micro-Cells. On the contrary, the SOE-based curves for σ'_{22} match perfectly well with the reference solution irrespective of the Micro-Cell size.

The previous analysis considers that the homogenized effective stress tensor, $\boldsymbol{\sigma}'$, is obtained from the expression

$$\boldsymbol{\sigma}' = \frac{1}{|\Omega_\mu|}\int_{\Omega_\mu} \boldsymbol{\sigma}'_\mu \, d\Omega_\mu, \ \forall\, t, \tag{A.73}$$

$\boldsymbol{\sigma}'_\mu$ being the micro-scale effective stress field, see definition (A.48). For the present homogeneous example, (A.73) reduces to $\boldsymbol{\sigma}' = \mathbf{C}_\mu{:}\boldsymbol{\varepsilon}$, implying that the discrepancies between FOE and the other alternatives are given by the macro-scale strain distribution ($\boldsymbol{\varepsilon}(\mathbf{x}, t)$), obtained in each case.

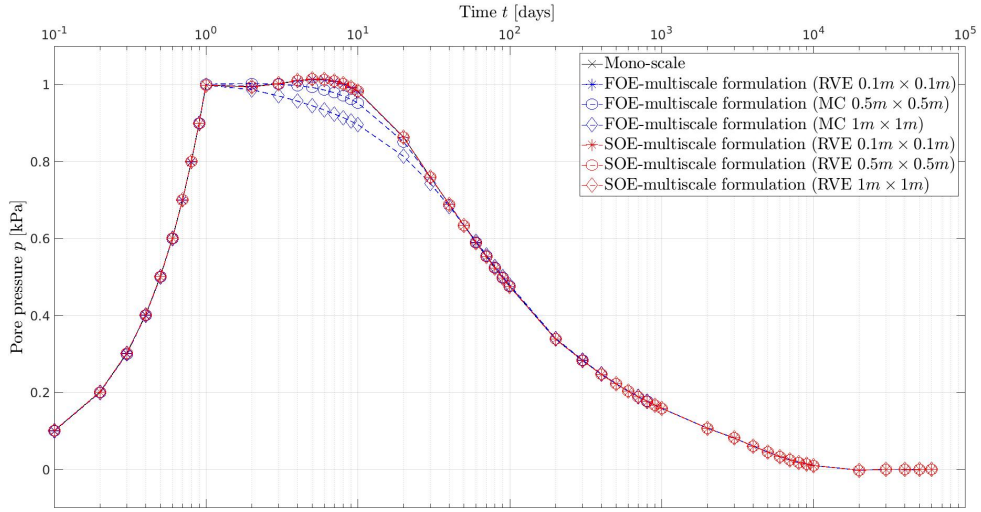

Figura A.11: 1D-Homogeneous fully saturated soil case. Pore pressure evolution for point C of Figure A.5-(a) (depth: $x_2 = -0.9640\,m$).

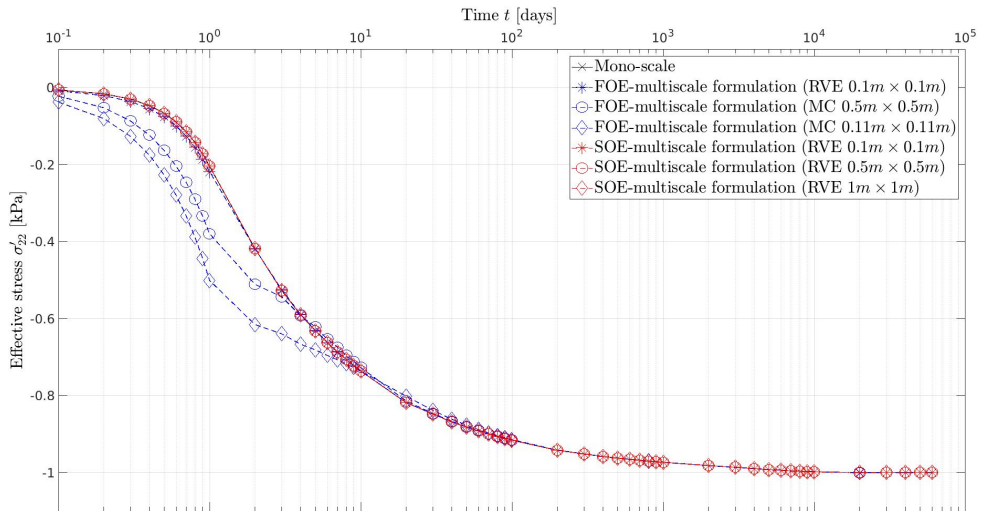

Figura A.12: 1D-Homogeneous fully saturated soil case. Vertical component of the effective stress tensor for macro-scale Finite Element 1, integration point I (see Figure A.5-(a)).

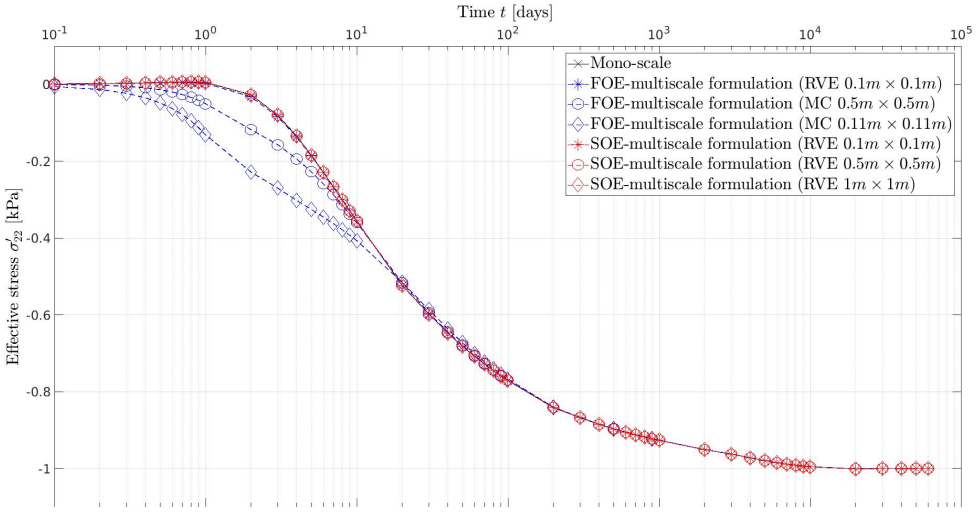

Figura A.13: 1D-Homogeneous fully saturated soil case. Vertical component of the effective stress tensor for macro-scale Finite Element 2, integration point I (see Figure A.5-(a)).

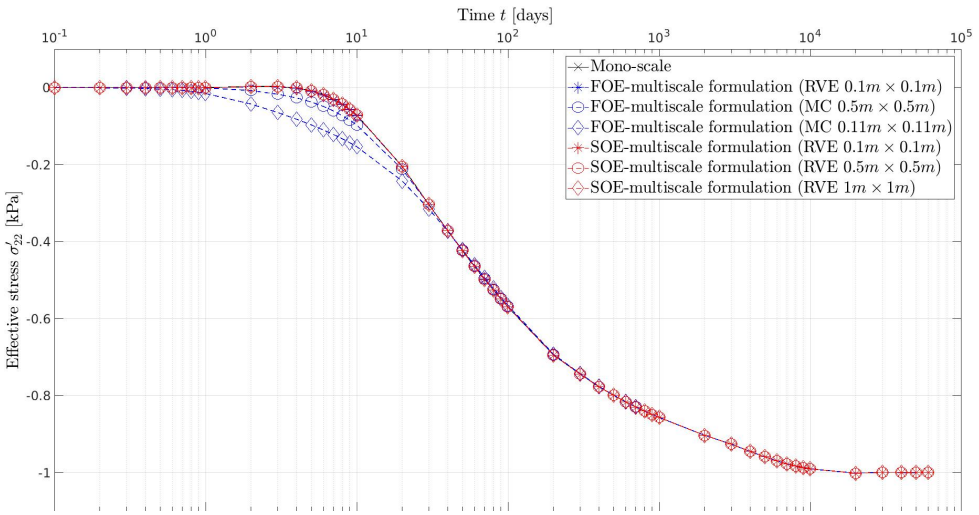

Figura A.14: 1D-Homogeneous fully saturated soil case. Vertical component of the effective stress tensor for macro-scale Finite Element 3, integration point I (see Figure A.5-(a)).

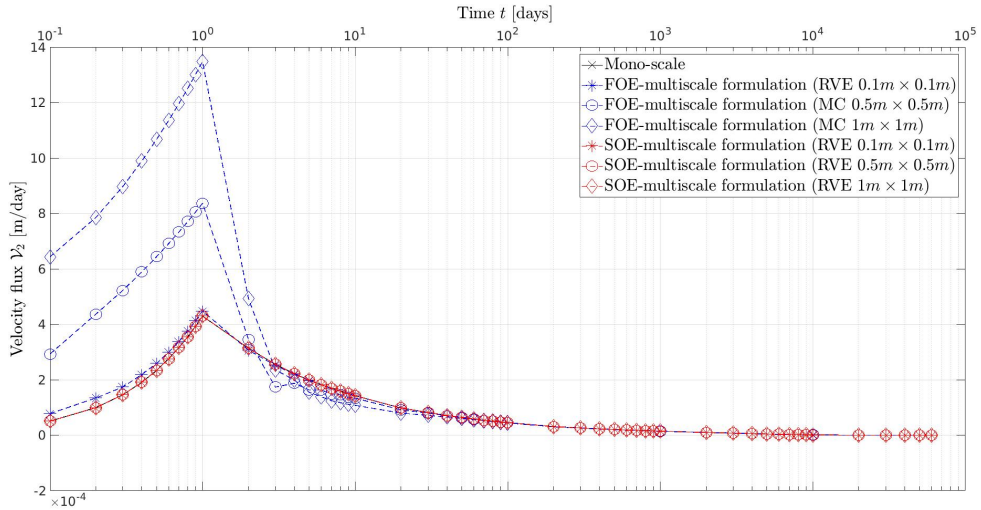

Figura A.15: 1D-Homogeneous fully saturated soil case. Vertical component of flux velocity vector for the macro-scale Finite Element 1, integration point I (see Figure A.5-(a)).

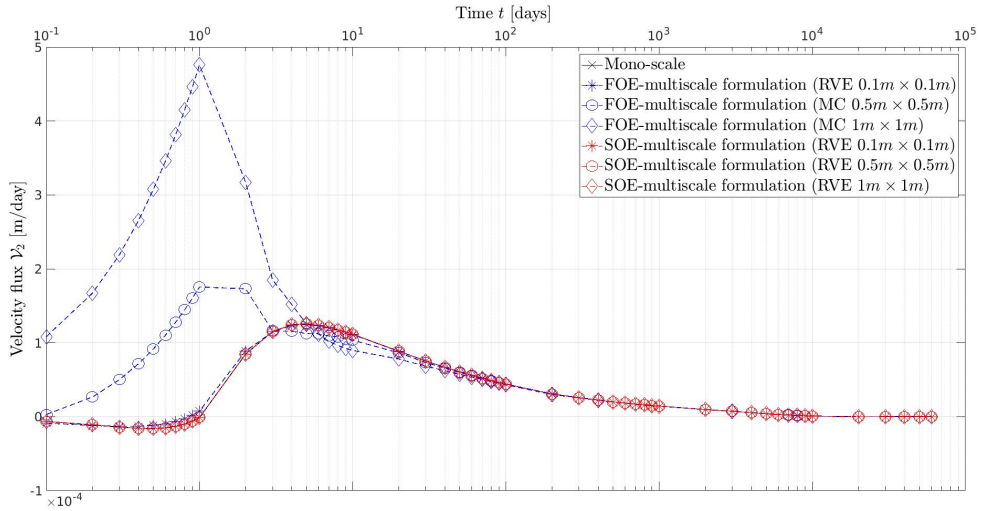

Figura A.16: 1D-Homogeneous fully saturated soil case. Vertical component of flux velocity vector for the macro-scale Finite Element 2, integration point I (see Figure A.5-(a)).

The size effect related to the Full Order Expansion procedure turns out more pronounced yet for the homogenized seepage velocity variable $\boldsymbol{\mathcal{V}}$. This fact can be appreciated for instance through Figures A.15, A.16 and A.17 where the $\mathcal{V}_2$-evolution curves are compared between all the analyzed models, for the macro-scale finite elements 1, 2 and 3, respectively (integration point I in Figure A.5-(a)). As expected, for the two largest MCs the FOE-scheme retrieves results that clearly differ from the mono-scale reference solution. According to the behaviour reported for the pore-pressure variable (recall Figures A.9-A.11), in general the FOE-based simulations predict that the fluid phase drains faster as the size of the micro-cells enlarges (higher permeability). The differences are very noticeable not only in terms of absolute values but also in the tendencies showed by these evolution curves, especially for points B and C during the initial time steps. In general, the discrepancies between the FOE-strategy and the other solutions begin from the first time steps of analysis and extend up to a characteristic time of approximately 1-2 days in the current simulations. After that, all curves tend to coincide. However, in real applications, this time-parameter will depend on the problem geometry, macro-scale boundary conditions and material properties. It is also true that in geotechnical engineering problems, external tractions are not applied in a

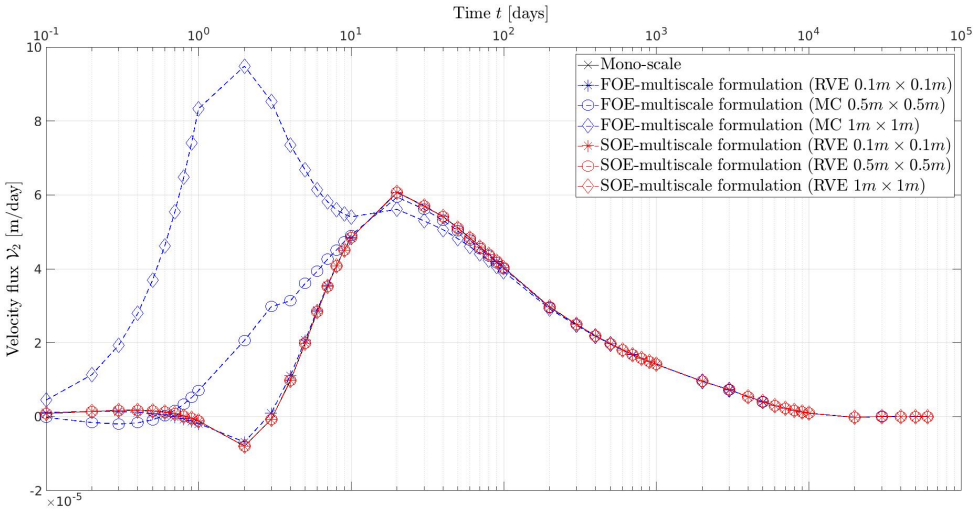

Figura A.17: 1D-Homogeneous fully saturated soil case. Vertical component of flux velocity vector for the macro-scale Finite Element 3, integration point I (see Figure A.5-(a)).

single stage, but rather throughout different construction periods according to the project's progress. For each of these load stages, additional pore pressure gradients are generated at the macro-scale, resulting in new discrepancies that should be expected in the FOE-model.

A.8.1.2.1. Numerical assessment of transient velocity term: $\boldsymbol{\mathcal{V}}_{tra}$

Let us focus just on the FOE-multiscale approach and specifically on the macro-scale transient velocity vector $\boldsymbol{\mathcal{V}}_{tra}$. As shown in Section A.4.1.1, $\boldsymbol{\mathcal{V}}_{tra}$ can be split into five components, denoted $\mathbf{T}_1$-$\mathbf{T}_5$ (see definition (A.49)). While $\mathbf{T}_1$ and $\mathbf{T}_2$ contributions are trivially null for the homogeneous problem under analysis (take into account (A.17)), the remainder terms $\mathbf{T}_3$-$\mathbf{T}_5$ introduce a lack of objectivity into that multiscale formulation. This point is supported next by means of numerical experimentation.

Based on expression (A.50), the term $\mathbf{T}_5$ emerges as the most evident outcome of the size effect problem. Recall that $\mathbf{T}_5$ is entirely independent of the micro-scale equilibrium problem and micro-scale restrictions on primal descriptors $\tilde{\mathbf{u}}_\mu$ and $\tilde{p}_\mu$. This means that it remains unaffected regardless of whether the Taylor, Linear, Periodic or Minimally Constrained model is used. Instead, $\mathbf{T}_5$ depends on the inserted macro-scale pressure gradient rate, $\dot{\boldsymbol{\varphi}}$, the modulus M_μ^{-1} and geometrical properties of the micro-scale domain (area and inertia). Figure A.18 illustrates the time evolution curves for the vertical component of $\mathbf{T}_5$. As the size of the Micro-Cell increases, the magnitude of the $\mathbf{T}_5$-term amplifies, compromising the objectivity of the macro-scale response.

Figures A.19 and A.20 report the values obtained for $\mathbf{T}_3$ and $\mathbf{T}_4$ terms (vertical components), respectively, as a function of time, and spanning different dimensions of MCs. Once again, a clear size effect issue is observed in these plots. Notice that the vertical component of $\mathbf{T}_4$ exhibits the opposite sign compared to $\mathbf{T}_3$ and $\mathbf{T}_5$, i.e. the flux velocity induced by this term is predominantly downward, something difficult to explain for the present problem. Even in the most basic scenario featuring a uniform distribution of material, results showed in Figures A.19 and A.20 indirectly prove that the hydro-mechanical equilibrium requires the development of micro-scale displacement (and so strains) as well as pore pressure fluctuation fields (see the specific definitions given for $\mathbf{T}_3$ and $\mathbf{T}_4$ in (A.49)). This fact cannot be justified by physical arguments, but just through mathematical ones. Fluctuations in the MCs arise because the resulting system of coupled differential equations are no longer of homogeneous character as a consequence of the Full Order Expansion adopted for micro-scale pore pressure variable A.20. In particular, the macro-scale pore pressure gradient rate, $\dot{\boldsymbol{\varphi}}$, induces additional terms in the strong forms of micro-scale momentum and mass balance, which can be interpreted as point-wise distributed external

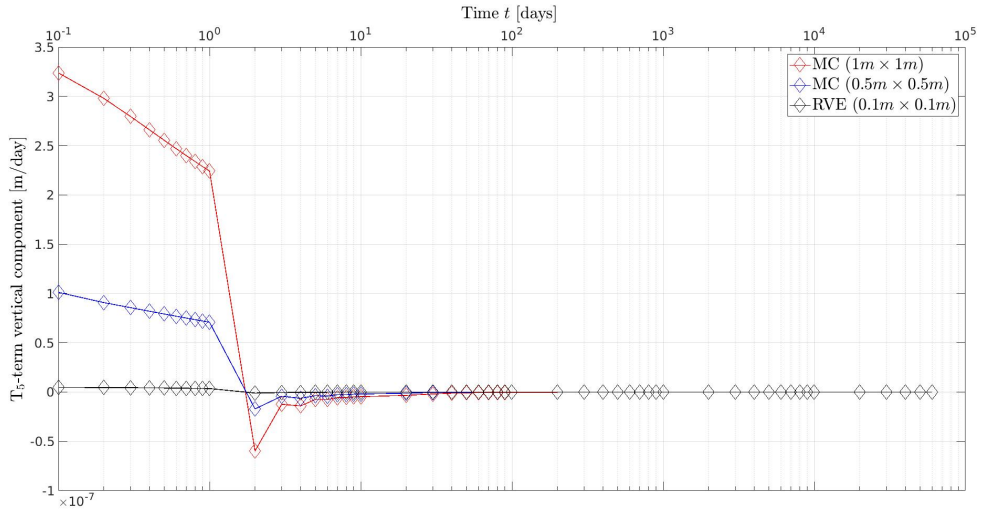

Figura A.18: 1D-Homogeneous fully saturated soil case. FOE-multiscale formulation. Time evolution curves for $\mathbf{T}_5$ (vertical component). Macro-scale Finite Element 1, integration point I (see Figure A.5-(a)).

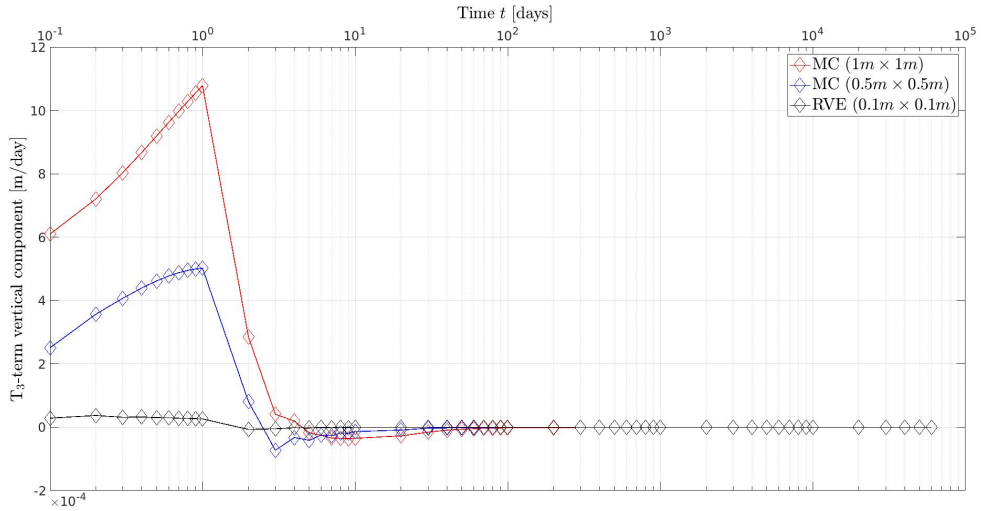

Figura A.19: 1D-Homogeneous fully saturated soil case. FOE-multiscale formulation. Time evolution curves for $\mathbf{T}_3$ (vertical component). Macro-scale Finite Element 1, integration point I (see Figure A.5-(a)).

actions per unit volume. Under these circumstances, the expected homogeneous responses for a homogeneous material, $\tilde{\mathbf{u}}_\mu \equiv \mathbf{0}$ and $\tilde{p}_\mu \equiv 0$ are no longer feasible solutions. Of course, $\mathbf{T}_3$ and $\mathbf{T}_4$ terms depend on the applied restrictions on $\tilde{\mathbf{u}}_\mu$ and $\tilde{p}_\mu$ fields (i.e. on the spaces $\tilde{\mathcal{U}}_\mu$ and $\tilde{\mathcal{P}}_\mu$, respectively). In fact, both of them are null if the most constrained (Taylor) homogenization model is employed. It is well known that the Taylor approach (also called rule-of-mixture) is a very limited multiscale procedure to retrieve reliable homogenized parameters, therefore it is not, in general, a viable option for minimizing the size effect problem in the FOE-scheme.

Concerning quantitative numerical results, the term $\mathbf{T}_3$ has been the dominant contribution in the context of current simulations. Take into account that changes in material properties will lead to different preponderances between the components of $\boldsymbol{\mathcal{V}}_{tra}$ ($\mathbf{T}_3$, $\mathbf{T}_4$ and $\mathbf{T}_5$). It is also possible to obtain negligible values for $\mathbf{T}_3$-$\mathbf{T}_5$ by proper selections of the material constants. However, in our opinion, this last proposal is neither a rigorous nor a generic strategy to deal with the size effect problem in porous media.

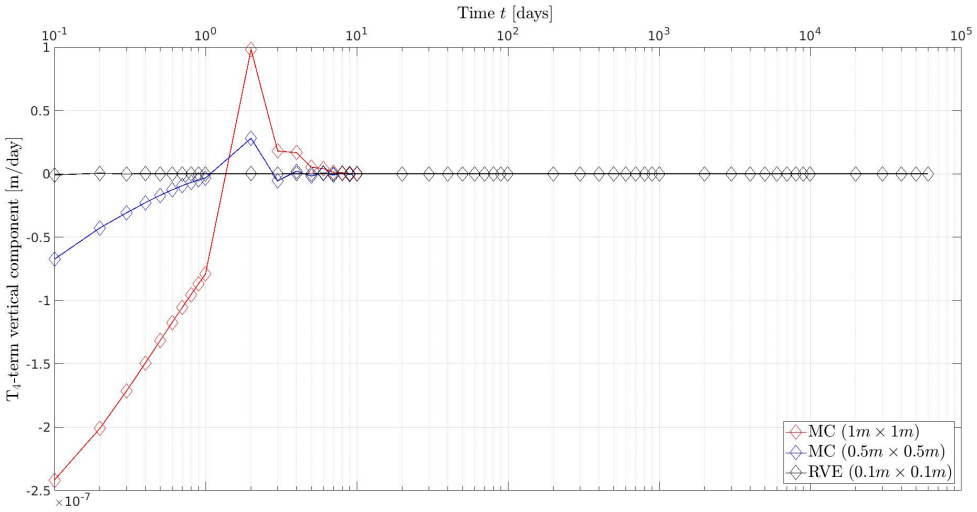

Figura A.20: 1D-Homogeneous fully saturated soil case. FOE-multiscale formulation. Time evolution curves for $\mathbf{T}_3$ (vertical component). Macro-scale Finite Element 1, integration point I (see Figure A.5-(a)).

A.8.1.2.2. Comparison with analytical results: Under simplified conditions, the one-dimensional consolidation problem can be described analytically through Terzaghi's theory, namely: (i) isotropic, homogeneous and fully saturated porous medium, (ii) seepage velocity ruled by Darcy's law, (iii) constant permeability, (iv) the soil grain as well as fluid are incompressible and (v) the external vertical load, t_2, is instantaneously applied to induce a uniform initial distribution of excess of pore pressure $p^0 = p(x_2, t=0) = -\mathrm{t}_2$. According to Terzaghi's idealized model, the closed-form expression for pore pressures (at any depth and time) is given by the infinite series [36, 111, 112]

$$p_{\text{Terzaghi}}(x_2, t) = \sum_{m=0}^{m=\infty} \left[\frac{2\, p^0}{M}\, sin\left(-\frac{M\, x_2}{H_d} \right) \right] e^{-M^2 T_v} \tag{A.74}$$

where $M = \frac{\pi}{2}\ (2\,m+1)$, m denotes an integer taking values $m = 0, 1, 2, 3, \ldots, \infty$, $T_v = \frac{c_v\, t}{H_d^2}$ represents a dimensionless time factor and H_d ($= \mathrm{H} = 10m$ in this case) stands for the average longest drain path. The consolidation parameter $c_v = \frac{k}{m_v\, \rho^f |\mathbf{g}|}$ is determined from the volume compressibility coefficient, m_v, the permeability, k, and the specific weight of the fluid, $\rho^f |\mathbf{g}|$. Besides, $m_v = \left[\frac{E\,(1-\nu)}{1-\nu-2\nu^2} \right]^{-1}$ depend on Young's modulus E and Poisson's ratio ν. The aforementioned definitions are widely accepted within the geotechnical engineering community.

Except for the requirement concerning the load application in Terzaghi's approach, all the remaining hypotheses are shared with the homogeneous example discussed so far. Hence we now introduce a slight change in our simulations to represent a sudden vertical load, from the beginning of the analysis (i.e. for $t \approx 0$), making comparable the numerical and the analytical solution. This is achieved by adopting a much more refined logarithmic-like time discretization, as follows: $t = [0.01, 0.02, 0.03, \ldots, 0.08, 0.09, 0.1, 0.2, 0.3, \ldots, 0.8, 0.9, 1, 2, 3, \ldots, 8, 9, 10, 20, 30, \ldots]$ (in days). The traction component $\mathrm{t}_2 = -1kPa$ is applied in the first time step, i.e. for $t = 0.01$ day, and thereafter it maintains a constant value. A mesh refinement has also been considered in the first-meter depth, near the ground surface, to attain better accuracy in our numerical models.

Figure A.21 compares the macro-scale spatial profiles of water pore pressures given by the theoretical closed-form A.74 with respect to the multiscale solutions (FOE and SOE), at the time $t = 2\,days$, or equivalently for a dimensionless time factor $T_v = 2.37 \times 10^{-4}$. The numerical values reported in this graphic correspond to the largest ($1m \times 1m$) Micro-Cell size. The SOE-based pore pressure profile is

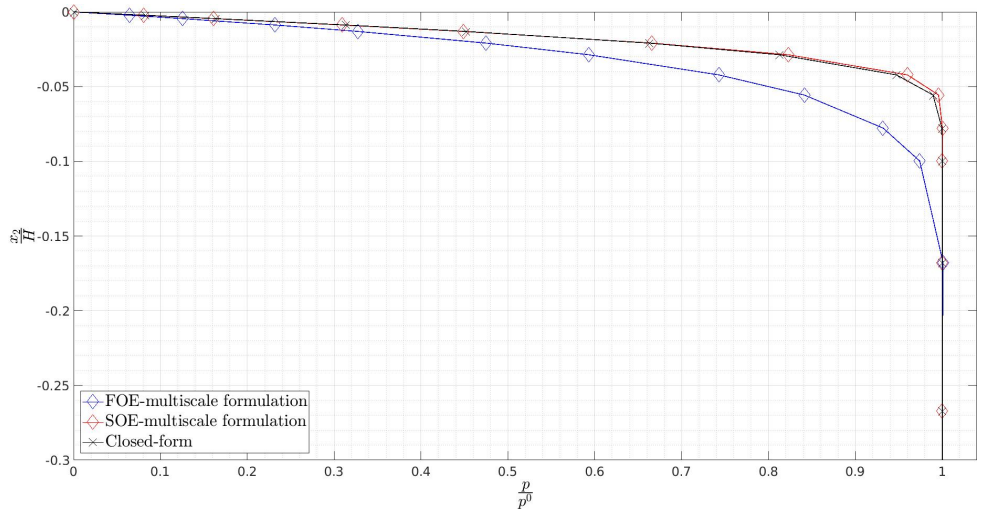

Figura A.21: 1D-Homogeneous fully saturated soil case. Comparison of pore pressures spatial profiles at $t = 2\,days$ ($T_v = 2.37 \times 10^{-4}$). Micro-Cell size $1m \times 1m$.

almost coincident with the analytical response; the minor disparities observed between these curves can be attributed to the typical inaccuracies resulting from the discrete approximation. In contrast, it is noticeable that in the vicinity of the ground surface, the pore pressure profile provided by the FOE-multiscale formulation deviates from the theoretical curve. Such discrepancy can not be ascribed to numerical issues since the same (spatial and temporal) discretizations have been used for the SOE and FOE procedures. Taking advantage we have available a rigorous reference solution, a measure ξ is computed to quantify the relative errors introduced by both FE^2-based multiscale procedures (SOE and FOE)

$$\xi = \frac{\left| p^{\text{Nodal}}_{\text{Terzaghi}} - p^{\text{Nodal}}_{\text{Multiscale}} \right|}{p^{\text{Nodal}}_{\text{Terzaghi}}} \cdot 100 \tag{A.75}$$

where $p^{\text{Nodal}}_{\text{Multiscale}}$ denotes, indistinctly, the nodal values for macro-scale water pore pressures obtained by using the SOE or FOE homogenization method and $p^{\text{Nodal}}_{\text{Terzaghi}}$ the corresponding analytical solution at the same nodal depth. Figure A.22 depicts the distribution of percentage relative error ξ, at $t = 2\,days$, from the ground surface up to the dimensionless depth $\frac{x_2}{\text{H}} = -0.3$ and for the largest ($1m \times 1m$) MC. The proposed Selective Order Expansion method achieves errors lesser than $2\,\%$ throughout the entire pore pressure profile. These values tend to decrease more with mesh and time refinements. On the other hand, as the same Figure A.22 shows, the relative error distribution undergoes a significant amplification reaching a peak of around $25\,\%$ when the FOE-multiscale scheme is employed. It is expected even greater ξ-values for early stages ($t < 2\,days$) in the consolidation process. The convergence of the FOE model towards the closed-form analytical solution is not guaranteed, being an aspect highly dependent on the MC-size used in the simulations.

A.8.1.3. 1D-Heterogeneous fully saturated soil case

The same one-dimensional consolidation problem described in Section A.8.1.2 is now addressed by considering a heterogeneous material at the micro-scale level. It involves an artificial arrangement of square-shaped inclusions, periodically distributed, within a base soil matrix. Each micro-scale constituent (the matrix and the set of inclusions) is idealized as a fully saturated porous medium with dissimilar hydro-mechanical properties. Figure A.5-(b) depicts a schematic unit-cell of the material under analysis, containing a single inclusion centered at the origin which occupies $25\,\%$ of the total area.

The properties of the matrix are the same as those presented for the homogeneous case of Section

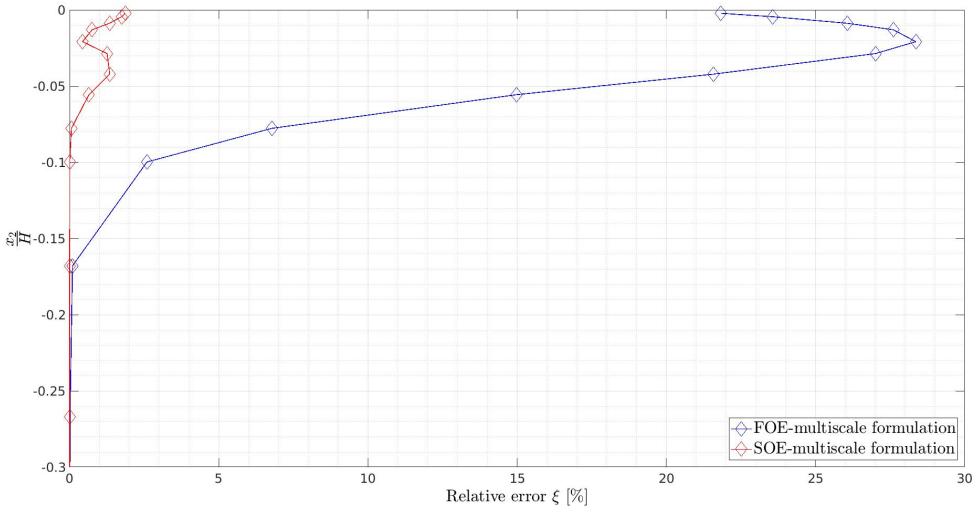

Figura A.22: 1D-Homogeneous fully saturated soil case. Percentage relative error, ξ, between analytical and multiscale numerical solutions (FOE and SOE), for $t = 2\,days$ ($T_v = 2.37 \times 10^{-4}$). Micro-Cell size $1m \times 1m$.

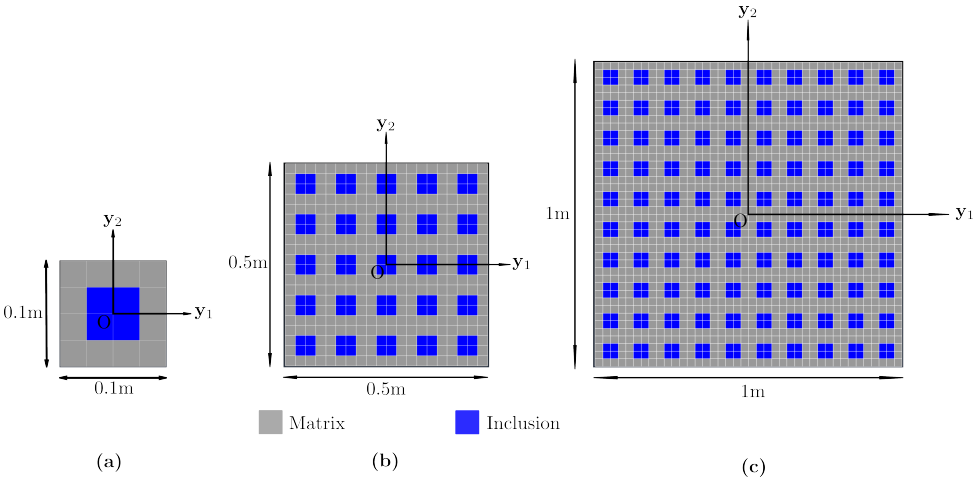

Figura A.23: 1D-Heterogeneous fully saturated soil case. Sequence of MC domains, with their corresponding finite element meshes, used during the homogenization process (drawing not to scale). (a) Micro-Cell of $0.1m \times 0.1m$ size; (b) Micro-Cell of $0.5m \times 0.5m$ size; (a) Micro-Cell of $1m \times 1m$ size.

(A.8.1.2). The inclusion is characterized by: Young's modulus $E^0_\mu = 1500kPa$, Poisson's ratio $\nu_\mu = 0.3$, isotropic hydraulic conductivity $k_{\mu,1} = k_{\mu,2} = 1.296 \times 10^{-2} m/day$, and initial void ratio $e^0_\mu = 2$. From the reported values, the inclusions can be cataloged as an initially more porous, rigid and permeable constituent in comparison with the soil matrix.

Unlike the previous homogeneous problem, the presence of heterogeneities at the smaller length scale introduces a new ingredient from which the appearance of non-zero fluctuation fields ($\tilde{\dot{p}}_\mu$ and $\tilde{\dot{u}}_\mu$) is naturally expected. The purpose of the current simulations is to evaluate the performance of the FOE and SOE multiscale formulations under such modelling scenario, related to the objectivity property in the macro-scale response.

Three MCs of increasing sizes, $0.1m \times 0.1m$, $0.5m \times 0.5m$ and $1m \times 1m$, were considered for the subsequent analysis, see Figures A.23-(a)-(b)-(c) respectively. The smallest MC is discretized through a uniform/structured mesh of 4×4 finite elements. The other two MCs are simple repetitions (along both coordinate directions) of this elementary micro-structural pattern, see again Figure A.23. Since we are dealing with a heterogeneous but strictly periodic material at the smallest length scale, it is reasonable

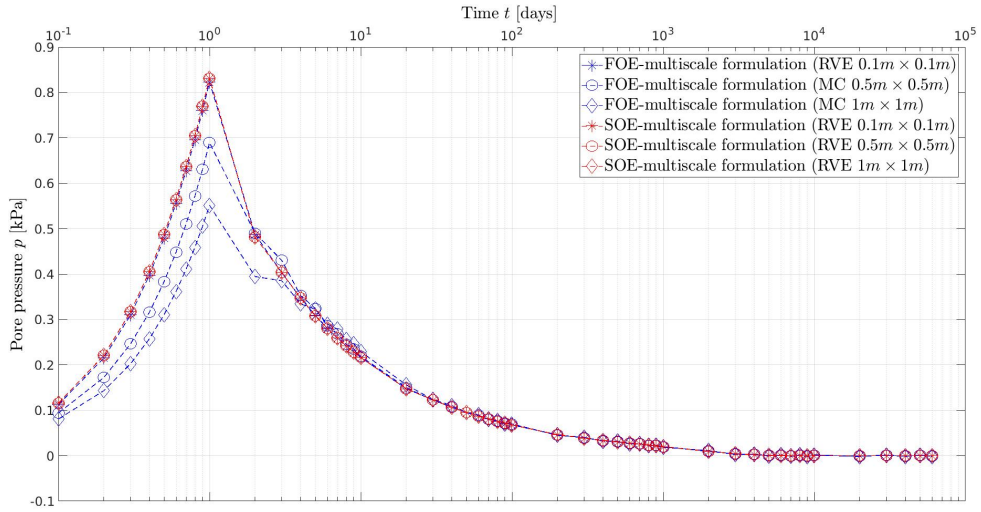

Figura A.24: 1D-Heterogeneous fully saturated soil case. Pore pressures evolution for point A of Figure A.5-(a) (depth: $x_2 = -0.2030\,m$).

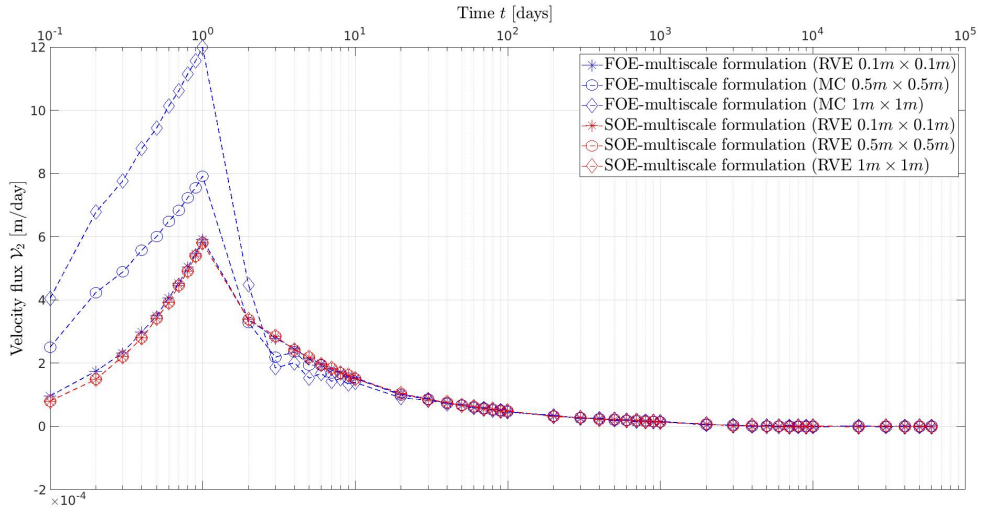

Figura A.25: 1D-Heterogeneous fully saturated soil case. Vertical component of flux velocity vector for macro-scale Finite Element 1, integration point I (see Figure A.5-(a)).

to expect that any of the aforementioned MCs, subjected to periodic boundary conditions (as adopted in this contribution), should provide the correct/true homogenized response of the porous medium, for any variable and irrespective of the micro-cell size. To assess this property, the outcomes given in Figures A.24 and A.25 are examined next.

Figure A.24 depicts time evolution curves related to the pore pressure variable of the macro-scale node A, see Figure A.5-(a), near the ground surface. Regardless of the size of the micro-structural domain, the Selective Order Expansion based model consistently retrieves identical solutions, enabling us to affirm that this approach reinstates the conventional notion of RVE existence. By using the FOE-multiscale procedure, instead, noticeable discrepancies are observed between pore pressure evolution curves as the size of MC enlarges. Only the smallest MC (that of size $0.1m \times 0.1m$) attains results comparable with the size-insensitive SOE-strategy. The same trend as already seen in the case of homogeneous material is here recovered, i.e. the excess of pore pressure dissipates faster with increasing MC sizes, whenever the FOE-scheme is employed. Figure A.25 shows the results for the homogenized vertical component of the flux velocity vector, $\mathcal{V}_2$, for the macro-scale finite element 1 (integration point I), see Figure A.5-

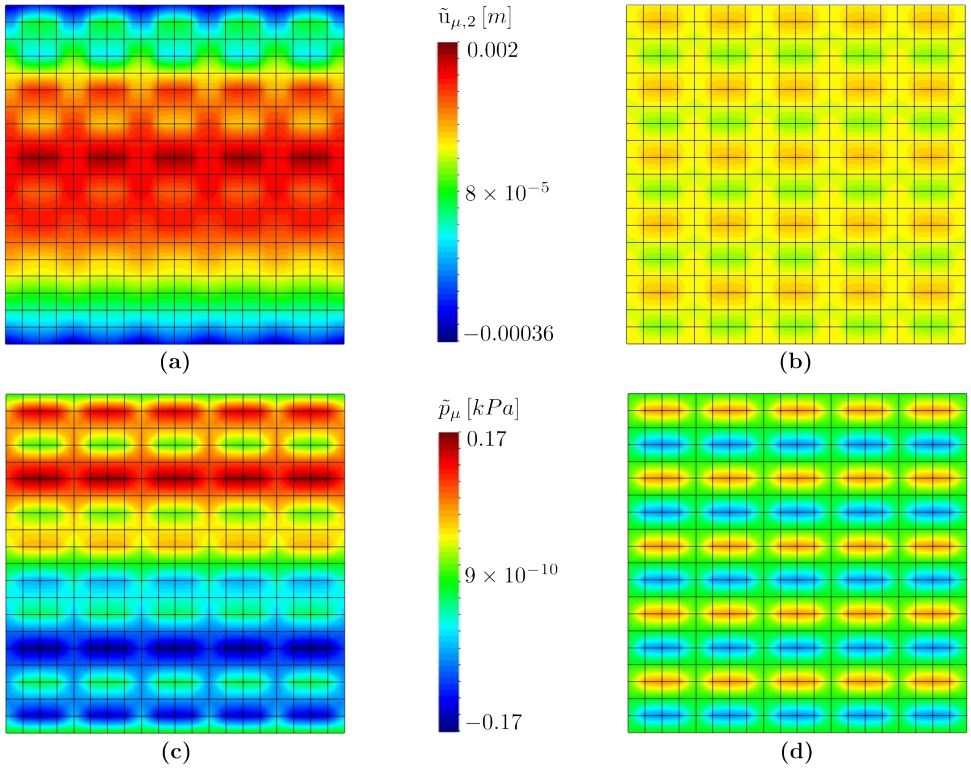

Figura A.26: 1D-Heterogeneous fully saturated soil case. Contour fill maps for micro-scale fluctuations variables $\tilde{u}_{\mu,2}$ and $\tilde{p}_{\mu}$. MC of size $0.5m \times 0.5m$. Elapsed time $t = 1\,day$. (a) Micro-scale displacement fluctuations (FOE-formulation). (b) Micro-scale displacement fluctuations (SOE-formulation). (c) Micro-scale pore pressure fluctuations (FOE-formulation). (d) Micro-scale pore pressure fluctuations (SOE-formulation)

(a). Once again, the lack of objectivity in the FOE-model response has a predominant impact on this homogenized variable. With the enlargement of MC sizes, higher drainage velocities are predicted, resulting in an increase in the macroscopic permeability parameter. In contrast, the SOE-scheme provides the same seepage velocity evolution curves for any MC dimension. All these results provide compelling evidence supporting that the SOE-multiscale proposal preserves the macro-scale objectivity, even within the current modelling scenario that considers a heterogeneous material.

Finally, Figure A.26 displays contour fill maps of micro-scale displacement fluctuations (vertical component), $\tilde{u}_{\mu,2}$, and pore pressure fluctuations, $\tilde{p}_{\mu}$, obtained by using the FOE and SOE multiscale models. These results correspond to the $0.5m \times 0.5m$ sized MC, the macro-scale finite element 1 (integration point I in Figure A.5-(a)), and for an elapsed time of $t = 1\,day$ once the consolidation process initiates. Figure A.26 illustrates that the disparities between the FOE and SOE approaches stem from the micro-scale fields and are not only limited to quantitative numerical values but also encompass very distinct qualitative spatial distributions. In the Selective Order Expansion model, the source of micro-scale fluctuations ($\tilde{u}_{\mu,2}$ and $\tilde{p}_{\mu}$) is exclusively attributed to the presence of material heterogeneities; so they preserve a well-established periodic pattern. Nevertheless, in the FOE-scheme, there is an additional mechanism that plays a decisive role to induce fluctuations in the MC domain. We refer to the term $\dot{\varphi}$ which finally alters the character of the micro-scale balance equations when compared to the SOE-strategy. Of course, all micro-scale fields will manifest discrepancies between FOE and SOE-based models.

A.8.2. Two-dimensional consolidation example

To conclude the numerical results Section, the potentiality of the proposed SOE multiscale formulation is addressed by considering a real-world geotechnical engineering problem. The SOE-strategy is

Material properties	Matrix	Inclusions
Young's modulus E^0 $[kPa]$	40000	1×10^7
Poisson's ratio ν	0.4	0.35
Hydraulic conductivity κ_i $[m/day]$	8.64×10^{-6}	8.64×10^{-4}
Initial void ratio e^0	1.4	0.6
Soil grain bulk modulus K^s $[kPa]$	21×10^6	30×10^6
Fluid bulk modulus K^f $[kPa]$	22.5×10^5	22.5×10^5
Solid density ρ^s $[kg/m^3]$	1800	2700
Fluid density ρ^f $[kg/m^3]$	1000	1000

Tabla A.1: 2D-consolidation example. Material properties for the fully saturated heterogeneous soil stratum.

applied now to the two-dimensional (2D) consolidation phenomenon induced by a strip shallow footing which transfers a uniform traction on a highly heterogeneous soil material. The mesostructure of the stratum to be analyzed comprises two fully saturated constituents, see some details in Figures A.27-(b) and A.28, namely: (i) a soil matrix consisting of high plasticity clays and (ii) isolated nodules of calcium carbonate. According to, we have a highly compressible cohesive, low permeability, continuum medium percolated with stiffer and more permeable carbonate concretions. The volume fraction of the nodular population is $25\,\%$.

The material properties characterizing the soil matrix and inclusions are summarized in Table A.1 (subscript $(\cdot)_\mu$ was omitted for simplicity). Taking advantage of symmetry conditions, the macro-scale domain size for the problem under study can be established in terms of the total height of the stratum H$=2.5m$ and a sufficiently large width-dimension of W$=5m$ (5 times the characteristic size of the footing). The boundary conditions are given by the prescription of zero horizontal displacements along the left and right vertical boundaries, while the vertical component of the displacement is zero at the lower boundary. The lateral and lower boundaries act as impermeable limits regarding the infiltration process. In turn, for all time steps, the pore-pressure is set to zero at the upper portion of the boundary that extends from the end of the footing to the right vertical edge, forming the unique boundary with drainage capacity (see the red lines in Figures A.27-(a) and A.28). In the left part of the ground surface, under the footing of F$=1m$ width, a purely compressive external traction $\mathbf{t} = [0;\, \mathrm{t}_2]^T$ is imposed, which evolves, linearly and monotonically, from $\mathrm{t}_2 = 0kPa$ to $-300kPa$ during the first day of analysis and then remains constant, around its minimum value ($\mathrm{t}_2 = -300kPa$), see schematic diagram in Figures A.27-(a) and A.28.

For the SOE-based multiscale simulations two MCs of increasing sizes, $0.25m \times 0.25m$ and $0.5m \times 0.5m$, have been considered, see Figures A.27-(b)-left and A.27-(b)-right, respectively. The smallest and largest MCs were discretized using meshes containing 352 and 1239 finite elements, respectively. Both MCs are subjected to periodic boundary conditions in displacement and pore-pressure fluctuations, see this detail in Figure A.27-(b). The macro-scale domain, in turn, is discretized using 50 finite elements. Note that a mesh refinement has been considered near the footing where the external traction $\mathbf{t}$ is applied, because the largest excess of pore pressure gradients are expected in that region, see Figure (A.27-(a)). With the aim of assessing the results provided by the SOE-multiscale approach, an alternative methodology (taken as a rigorous reference solution) has been adopted here to address the same problem. This procedure is commonly known in the scientific community as the Direct Numerical Simulation (DNS) method, a brute-force calculation-based algorithm. The DNS technique accounts for all the heterogeneities within a single physical length scale (the macro-scale), see Figure A.28. The spatial pattern to model the calcium carbonate population in the DNS approach was obtained by repetition of similar micro-scale designs as those shown in Figure A.27-(b), after elementary rotation/reflection/relocation of inclusions, in order to improve the material representative-

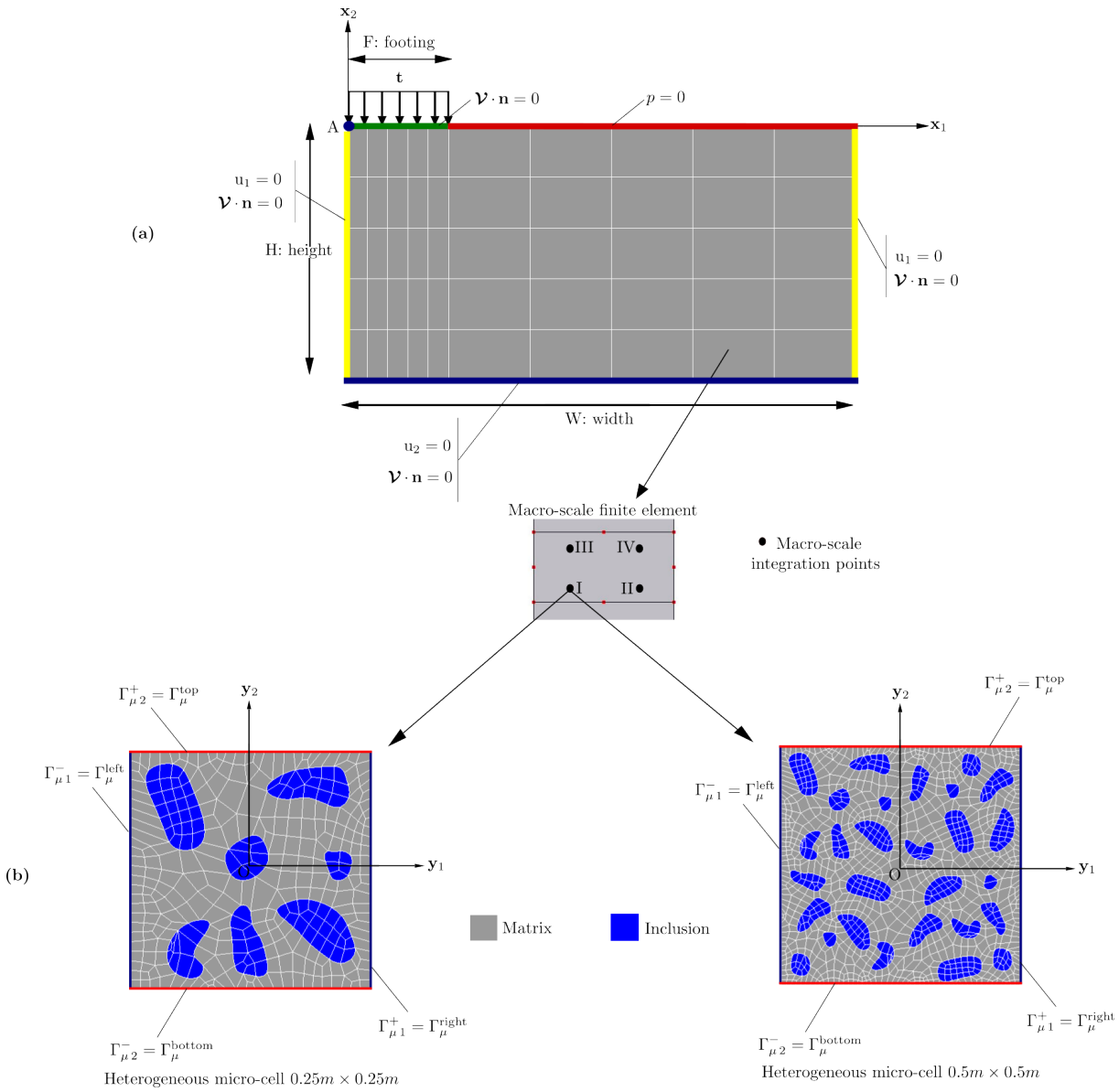

Figura A.27: 2D-consolidation example. SOE multiscale model layout. (a) Macro-scale. (b) Micro-scale. Sequence of MCs with their corresponding finite element meshes (drawing not to scale). Left: MC of $0.25m \times 0.25m$ size. Right: MC of $0.5m \times 0.5m$ size

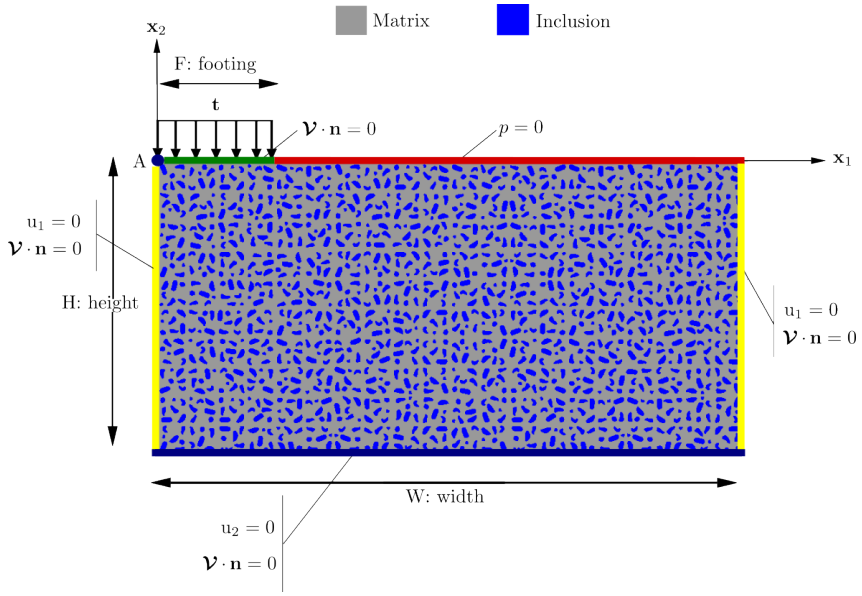

Figura A.28: 2D-consolidation example. DNS model layout.

ness. Following such a procedure the nodular volume fraction of $25\,\%$ is strictly preserved. The high level of detail required by the DNS formulation, to represent the entire macro-scale domain, demanded a mesh of about 71100 finite elements. Either the SOE-multiscale procedure as well as the DNS strategy share the same time discretization setting. It follows a logarithmic-like sequence, defined as: $t = [0.1, 0.2, 0.3, \ldots, 0.8, 0.9, 1, 2, 3, \ldots, 8, 9, 10, 20, 30, \ldots, 80, 90, 100, 200, 300, 400, 500]$ (in days).

Figure (A.29) depicts settlement time-evolution curves for the macro-scale node A shown in Figures A.28 and A.27-(a). The agreement between the solutions obtained from the SOE homogenization scheme (both MCs) and the results given by the DNS strategy is more than evident; the three evolution curves are almost coincident. In the current modelling context, we drew two important conclusions: (i) either of the two MCs can be cataloged as an RVE within the SOE-multiscale formulation and (ii) there are no micro-scale size effect issues since the macro-scale response preserves the objectivity with respect to the RVE-size. Finally, Figures A.30 and A.31 display contour fill maps for displacement (vertical component), u_2, and excess of pore-pressures, p, respectively, at the larger length scale. Such coloured diagrams were obtained by using the SOE-multiscale model (both MCs) and the (reference) DNS approach. Results for the vertical displacement field (Figure A.30) correspond to the end of the consolidation process, at time of $t = 500\,days$, while the pore-pressure distributions (Figure A.31) are compared at the beginning of the process, at time $t = 1\,day$. Both Figures clearly depict the consistency of the SOE predictions with respect to the very refined DNS solution. All contour fill maps show a very good agreement either in terms of qualitative pattern distributions as well as in quantitative values, for both macro-scale primary descriptors.

A.9. Conclusions

The use of standard homogenization techniques to modelling saturated porous media often leads to the emergence of micro-scale size effect problems. The issue has been usually circumvented arguing that this spurious phenomenon mitigates whenever the micro-scale dimension tends to zero. Such an assumption poses a major challenge to the elementary notion about the Representative Volume Element (RVE) existence in highly heterogeneous materials with an aleatory distribution of components. In this class of materials, the micro-scale domain size cannot approach zero since it must be large enough for

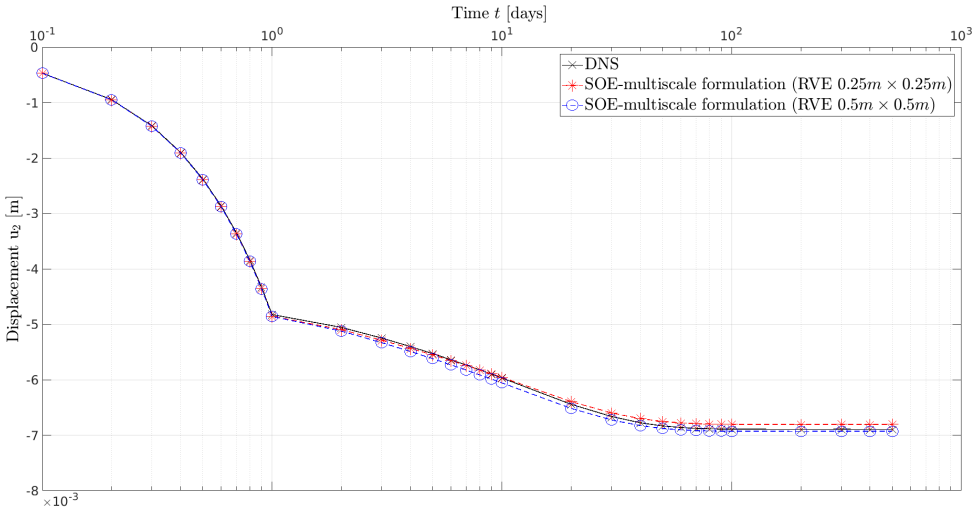

Figura A.29: 2D-consolidation example. Vertical displacement evolution curves for point A of Figures A.27-(a) and A.28. Comparison between SOE multiscale model and DNS approach.

including a great number of heterogeneities (with a limit established by the scale separation principle). In this paper, an alternative multiscale formulation has been proposed where the RVE existence is recovered. In consequence, the size of Micro-Cells can enlarge until attaining both, statistical representativeness and objective hydro-mechanical behaviour on the macro-scale.

Our theoretical background is based on the so-called Principle of Multiscale Virtual Power (PMVP), where some specializations have been done to deal with it in the context of saturated poromechanics. This method provides an axiomatic guideline from which the weak forms of micro-scale balance equations, as well as the homogenization rules for the stress-like variables, are naturally obtained by following straightforward variational steps. Two families of models were deduced within the PMVP-framework, namely the FOE and SOE multiscale models.

The FOE-scheme takes into account Full Order Expanded micro-scale primal variables $\dot{\boldsymbol{\varepsilon}}_\mu$ and $\dot{p}_\mu$, for evaluating all the constitutive laws defined in the smaller length scale. It embraces a series of conventional approaches followed by many authors in the past. As a consequence of the aforementioned assumption, micro-scale size effects are inherited in the resulting models. In our manuscript, this topic has been examined through a detailed analysis of the transient component of the homogenized seepage velocity vector ($\boldsymbol{\mathcal{V}}_{tra}$). It was shown that three contributions of $\boldsymbol{\mathcal{V}}_{tra}$ introduce lack of objectivity at the macroscopic length scale, here denoted as the terms $\mathbf{T}_3$, $\mathbf{T}_4$ and $\mathbf{T}_5$. All of them depend, explicitly or implicitly, on the macro-scale pore pressure gradient rate, $\dot{\boldsymbol{\varphi}}$, used to expand the pore pressure rate field, $\dot{p}_\mu$, at the micro-scale domain. In particular, the presence of $\dot{\boldsymbol{\varphi}}$ is critical when the constitutive responses $\hat{\boldsymbol{\sigma}}_\mu()$ and $\hat{\dot{\chi}}_\mu()$ are required. The size-effect issue persists even in the simplest scenario involving a homogeneous material. Neither it can be removed by restricting, at the maximum extent possible, the fluctuation fields in the micro-scale domain, for example using the so-called Taylor multiscale model, since $\mathbf{T}_5$-term does not depend on micro-scale equilibrium. Unless the MC characteristic length tends to zero, the FOE-procedure does not recover classical mono-scale (phenomenological) predictions nor Terzaghi's closed-form analytical solution for the well-known 1D consolidation problem. The numerical results presented in Section A.8 confirm all the previous conclusions.

The idea behind our alternative SOE (Selective Order Expansion) multiscale procedure, the main novelty of this work, is very simple. We postulate different orders of expansion for the primitive descriptors $\dot{\boldsymbol{\varepsilon}}_\mu$ and $\dot{p}_\mu$ whenever they conform the argument list in *some* constitutive laws, at the micro-scale level. Specifically, we preserve the Full Order of Expansion for the micro-scale strain tensor of the soil-skeleton but remove the linear term $(\dot{\boldsymbol{\varphi}} \cdot \mathbf{y})$ to expand the micro-scale pore pressure rate field, $\dot{p}_\mu$, at the instances

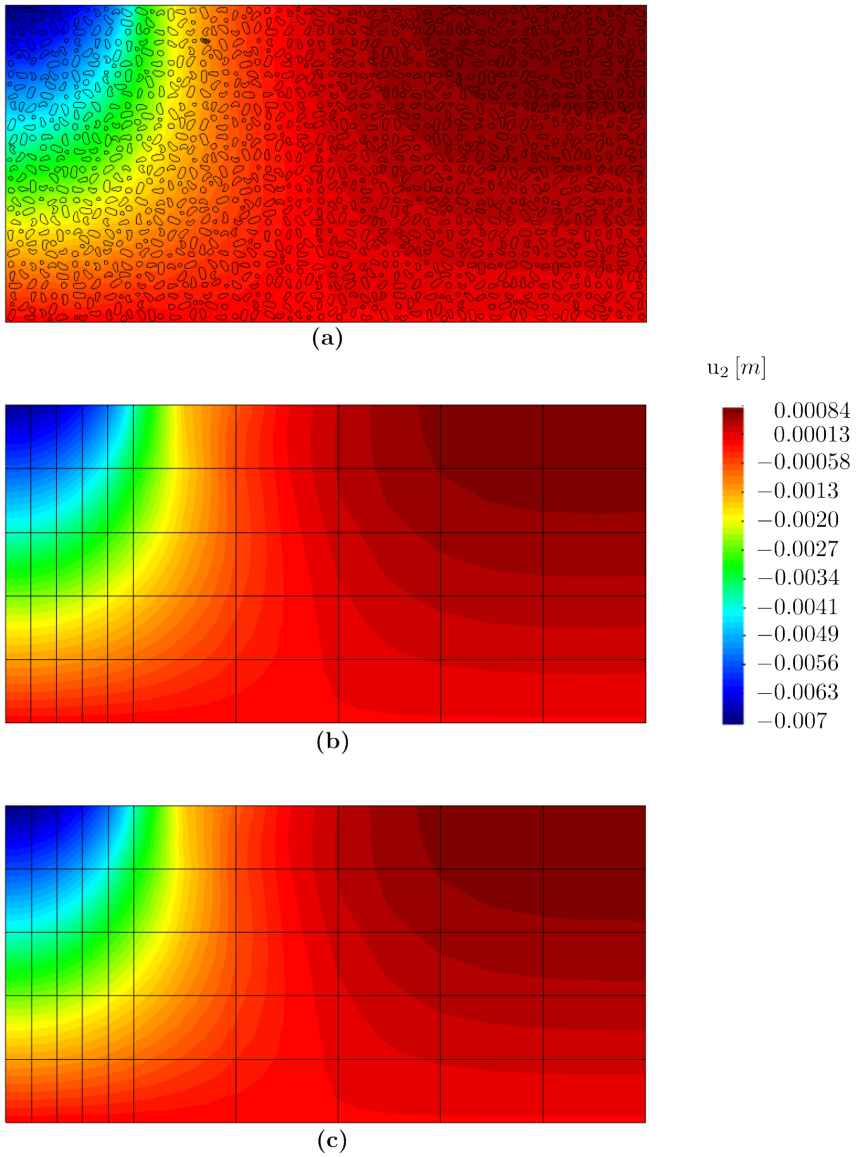

Figura A.30: 2D-consolidation example. Contour fill maps for macro-scale vertical displacements, u_2. Elapsed time $t = 500\,days$. (a) DNS approach. (b) SOE-multiscale model for an RVE size of $0.25m \times 0.25m$. (c) SOE-multiscale model for an RVE size of $0.5m \times 0.5m$

.

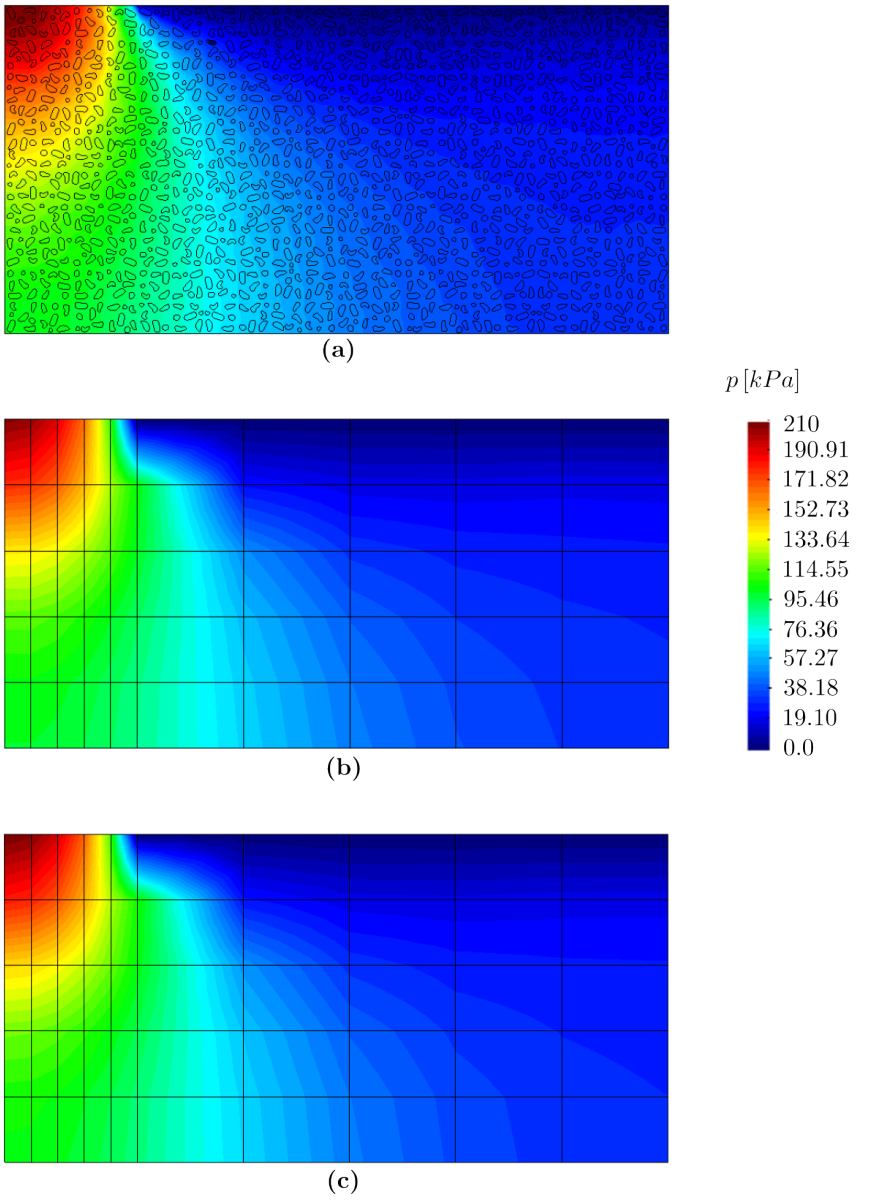

Figura A.31: 2D-consolidation example. Contour fill maps for macro-scale pore-pressures, p. Elapsed time $t = 1\,day$. (a) DNS approach. (b) SOE-multiscale model for an RVE size of $0.25m \times 0.25m$. (c) SOE-multiscale model for an RVE size of $0.5m \times 0.5m$.

of evaluating the material laws $\hat{\hat{\sigma}}_\mu()$ and $\hat{\hat{\chi}}_\mu()$. Just at these specific places, the micro-scale pore pressure rate is expanded in a *Reduced* form (without the first-order contribution); in the rest of the model, the variable $\dot{p}_\mu$ is full-order expanded. For example, the Darcy law is formulated accounting full-order expansion for $\dot{p}_\mu$-field. Importantly, the micro-scale virtual admissible actions regarding pore pressures, denoted as δp_μ in the manuscript, are also full-order expanded. This fact implies that comparing the FOE with respect to the SOE procedure, the same vector spaces play a role to find the micro-scale equilibrium and exactly the same mathematical structure for the homogenization formulae are obtained in each case. In other words, a unified variational framework can be used to describe the FOE and SOE procedures. The only difference lies encapsulated within the constitutive context. However, such a subtle discrepancy is of utmost importance for our purposes. The numerical analysis performed in Section A.8 shows that the SOE scheme effectively eliminates the size effect issue in the multiscale simulation of porous saturated media, either in homogeneous or heterogeneous materials. Besides, under simple modelling scenarios, it can recover conventional mono-scale approaches as well as analytical closed-form solutions.

By way of summary and final message of the manuscript, we enumerate some features inherent to the proposed Selective Order Expansion multiscale formulation. They highlight all the original contributions reported in this article and, at the same time, delineate clear differences from the methodologies currently available.

- Our strategy can retrieve an objective macro-scale response (micro-scale size effect is eliminated) without requiring that the RVE dimension necessarily tends to zero. This aspect is of great value for studying the homogenized behavior of highly heterogeneous materials.

- It has also been demonstrated to be independent of the MC-size regardless of the values of material parameters employed during the simulations. This topic is of utmost relevance to use and even generalize the present SOE-multiscale approach considering more sophisticated modelling environments, for instance: multiphase porous materials, unsaturated or partially saturated cases, other geomechanical and/or biomechanical applications, etc. In each of these situations, the range of variability in material properties can be significantly broader. Therefore, it is essential to have a multiscale formulation that eliminates the size effect irrespective of the material constant involved.

- We claim that our proposal is minimally invasive since it prevents micro-scale size effects but preserves the rest of the multiscale framework almost intact. Importantly, the transient component of the homogenized seepage velocity, $\boldsymbol{\mathcal{V}}_{tra}$, is still accounted for in the SOE-scheme, although in a slightly redefined manner. Just the $\mathbf{T}_5$-term is consistently eliminated from the homogenization formula for $\boldsymbol{\mathcal{V}}_{tra}$, while $\mathbf{T}_3$ and $\mathbf{T}_4$ contributions turn out independent of macro-scale pore pressure gradient rate $\dot{\boldsymbol{\varphi}}$ and, thus, insensitive to the MC-size. The presence of all terms is important within a multiscale model because, in realistic applications, they contribute to improving the homogenized response and to quantifying when a Micro-Cell size (with a random distribution of phases) is closer, or not, to be representative enough.

- Since the micro-scale equilibrium and all the homogenization rules were deduced as a direct consequence of the fulfillment of the Hill-Mandel variational principle, the SOE-procedure is energetically consistent. Note that any ad-hoc manipulation on those averaging formulae, such as removing simply or neglecting terms, will lead, in general, to a formulation that violates the Hill-Mandel lemma.

- The SOE-method assumes simplified hypotheses on the type of expansion considered to define input arguments in constitutive functionals, but not on the mathematical structure of such constitutive laws. Thus, it can be applied to more realistic material models, including any kind of non-linearities (viscosity, plasticity, damage, etc).

- The numerical implementation of the SOE proposal is almost direct. In fact, any existent multiscale program addressed to saturated porous media can be trivially adapted according to the SOE procedure. It is only necessary to introduce a pair of binary parameters in specific places within the finite element code, namely: (i) at the micro-scale constitutive level and (ii) at the instances of evaluating the micro and macro-scale Jacobian operators (see in particular the developments given in the appendices). For 3D and large-strain numerical codes the implementation effort is equally simple.

As a possible numerical disadvantage, we mention that in the SOE-strategy based on a Zero Order Expansion for the micro-scale pore pressure rate (parameter $\beta = 0$), the Jacobian operator at the smaller length scale is not-symmetric. In contrast, if the binary coefficient $\beta = 1$, pore pressure fluctuations are allowed in the previous expansion and the symmetry is restored.

Finally, we would like to emphasize that the proposed method, based on the Selective Order Expansions, embodies a generic concept that can be useful in other physically relevant homogenization problems, ruled by similar coupled governing equations, such as the thermomechanical multiscale constitutive modelling.

Appendix A. Components of the macro-scale Jacobian matrix

The following expressions expand the definitions given in (A.67), concerning the macro-scale Jacobian matrix

$$\frac{\partial \dot{\mathbf{G}}^{n+\theta}}{\partial \bar{\mathbf{u}}^{n+1}} = \int_\Omega \mathbf{B}_u^T \, \frac{\partial \dot{\boldsymbol{\sigma}}^{n+\theta}}{\partial \boldsymbol{\varepsilon}^{n+1}} \, \mathbf{B}_u \, d\Omega, \tag{A.76}$$

$$\frac{\partial \dot{\mathbf{G}}^{n+\theta}}{\partial \bar{\mathbf{p}}^{n+1}} = \int_\Omega \mathbf{B}_u^T \, \frac{\partial \dot{\boldsymbol{\sigma}}^{n+\theta}}{\partial \boldsymbol{\varphi}^{n+1}} \, \mathbf{B}_p \, d\Omega + \int_\Omega \mathbf{B}_u^T \, \frac{\partial \dot{\boldsymbol{\sigma}}^{n+\theta}}{\partial p^{n+1}} \, \mathbf{N}_p \, d\Omega, \tag{A.77}$$

$$\frac{\partial \mathbf{H}^{n+\theta}}{\partial \bar{\mathbf{u}}^{n+1}} = -\int_\Omega \mathbf{B}_p^T \, \frac{\partial \boldsymbol{\mathcal{V}}^{n+\theta}}{\partial \boldsymbol{\varepsilon}^{n+1}} \, \mathbf{B}_u \, d\Omega + \int_\Omega \mathbf{N}_p^T \, \frac{\partial \dot{\chi}^{n+\theta}}{\partial \boldsymbol{\varepsilon}^{n+1}} \, \mathbf{B}_u \, d\Omega, \tag{A.78}$$

$$\begin{aligned} \frac{\partial \mathbf{H}^{n+\theta}}{\partial \bar{\mathbf{p}}^{n+1}} = &-\int_\Omega \mathbf{B}_p^T \, \frac{\partial \boldsymbol{\mathcal{V}}^{n+\theta}}{\partial \boldsymbol{\varphi}^{n+1}} \, \mathbf{B}_p \, d\Omega - \int_\Omega \mathbf{B}_p^T \, \frac{\partial \boldsymbol{\mathcal{V}}^{n+\theta}}{\partial p^{n+1}} \, \mathbf{N}_p \, d\Omega + \int_\Omega \mathbf{N}_p^T \, \frac{\partial \dot{\chi}^{n+\theta}}{\partial \boldsymbol{\varphi}^{n+1}} \, \mathbf{B}_p \, d\Omega \\ &+ \int_\Omega \mathbf{N}_p^T \, \frac{\partial \dot{\chi}^{n+\theta}}{\partial p^{n+1}} \, \mathbf{N}_p \, d\Omega. \end{aligned} \tag{A.79}$$

The derivatives remaining in (A.76)-(A.79) constitute the so-called homogenized tangent operators of the multiscale model. To obtain such terms we need to account: (i) the homogenization rules of macro-scale dual variables as defined in (A.37), (A.38) and (A.40), (ii) the unified format of micro-scale constitutive laws specified in (A.54)-(A.56), and finally (iii) the time integration procedure given by expressions (A.61)-(A.62). In what follows, we include some useful details about this topic in order to complete the presentation:

(I) derivatives of the homogenized stress rate tensor $\dot{\boldsymbol{\sigma}}^{n+\theta}$ with respect to the primal macro-scale variables:

$$\begin{aligned} \frac{\partial \dot{\boldsymbol{\sigma}}^{n+\theta}}{\partial \boldsymbol{\varepsilon}^{n+1}} &= \frac{\partial}{\partial \boldsymbol{\varepsilon}^{n+1}} \left\{ \frac{1}{|\Omega_\mu|} \int_{\Omega_\mu} \left[\hat{\sigma}_\mu^{n+\theta} \left(\dot{\boldsymbol{\varepsilon}}^{n+\theta}, \dot{\tilde{\boldsymbol{\varepsilon}}}_\mu^{n+\theta}, \dot{p}^{n+\theta}, \alpha \, \dot{\boldsymbol{\varphi}}^{n+\theta}, \beta \, \dot{\tilde{p}}_\mu^{n+\theta} \right) - \dot{\mathbf{f}}_\mu^{n+\theta} \otimes \mathbf{y} \right] d\Omega_\mu \right\} \\ &= \frac{1}{|\Omega_\mu|} \int_{\Omega_\mu} \left[\frac{1}{\Delta t} \, \mathbf{C}_\mu : \left(\mathbb{I} + \frac{\partial \tilde{\boldsymbol{\varepsilon}}_\mu^{n+1}}{\partial \boldsymbol{\varepsilon}^{n+1}} \right) - \frac{\beta}{\Delta t} \, \mathbf{b}_\mu \otimes \frac{\partial \tilde{p}_\mu^{n+1}}{\partial \boldsymbol{\varepsilon}^{n+1}} \right] d\Omega_\mu, \end{aligned} \tag{A.80}$$

$$\frac{\partial \dot{\boldsymbol{\sigma}}^{n+\theta}}{\partial \boldsymbol{\varphi}^{n+1}} = \frac{\partial}{\partial \boldsymbol{\varphi}^{n+1}} \left\{ \frac{1}{|\Omega_\mu|} \int_{\Omega_\mu} \left[\hat{\dot{\sigma}}_\mu^{n+\theta} \big(\dot{\boldsymbol{\varepsilon}}^{n+\theta}, \dot{\tilde{\boldsymbol{\varepsilon}}}_\mu^{n+\theta}, \dot{p}^{n+\theta}, \alpha\, \dot{\boldsymbol{\varphi}}^{n+\theta}, \beta\, \dot{\tilde{p}}_\mu^{n+\theta} \big) - \dot{\mathbf{f}}_\mu^{n+\theta} \otimes \mathbf{y} \right] d\Omega_\mu \right\}$$
$$= \frac{1}{|\Omega_\mu|} \int_{\Omega_\mu} \left[\frac{1}{\Delta t}\, \mathbf{C}_\mu : \frac{\partial \tilde{\boldsymbol{\varepsilon}}_\mu^{n+1}}{\partial \boldsymbol{\varphi}^{n+1}} - \frac{1}{\Delta t}\, \mathbf{b}_\mu \otimes \left(\alpha\, \mathbf{y} + \beta\, \frac{\partial \tilde{p}_\mu^{n+1}}{\partial \boldsymbol{\varphi}^{n+1}} \right) \right] d\Omega_\mu, \tag{A.81}$$

$$\frac{\partial \dot{\boldsymbol{\sigma}}^{n+\theta}}{\partial p^{n+1}} = \frac{\partial}{\partial p^{n+1}} \left\{ \frac{1}{|\Omega_\mu|} \int_{\Omega_\mu} \left[\hat{\dot{\sigma}}_\mu^{n+\theta} \big(\dot{\boldsymbol{\varepsilon}}^{n+\theta}, \dot{\tilde{\boldsymbol{\varepsilon}}}_\mu^{n+\theta}, \dot{p}^{n+\theta}, \alpha\, \dot{\boldsymbol{\varphi}}^{n+\theta}, \beta\, \dot{\tilde{p}}_\mu^{n+\theta} \big) - \dot{\mathbf{f}}_\mu^{n+\theta} \otimes \mathbf{y} \right] d\Omega_\mu \right\}$$
$$= \frac{1}{|\Omega_\mu|} \int_{\Omega_\mu} \left[\frac{1}{\Delta t}\, \mathbf{C}_\mu : \frac{\partial \tilde{\boldsymbol{\varepsilon}}_\mu^{n+1}}{\partial p^{n+1}} - \frac{1}{\Delta t}\, \mathbf{b}_\mu \left(1 + \beta\, \frac{\partial \tilde{p}_\mu^{n+1}}{\partial p^{n+1}} \right) \right] d\Omega_\mu, \tag{A.82}$$

(II) derivatives of the homogenized mass content rate of fluid $\dot{\chi}^{n+\theta}$ with respect to the primal macro-scale variables:

$$\frac{\partial \dot{\chi}^{n+\theta}}{\partial \boldsymbol{\varepsilon}^{n+1}} = \frac{\partial}{\partial \boldsymbol{\varepsilon}^{n+1}} \left\{ \frac{1}{|\Omega_\mu|} \int_{\Omega_\mu} \left[\hat{\dot{\chi}}_\mu^{n+\theta} \big(\dot{\boldsymbol{\varepsilon}}^{n+\theta}, \dot{\tilde{\boldsymbol{\varepsilon}}}_\mu^{n+\theta}, \dot{p}^{n+\theta}, \alpha\, \dot{\boldsymbol{\varphi}}^{n+\theta}, \beta\, \dot{\tilde{p}}_\mu^{n+\theta} \big) \right] d\Omega_\mu \right\}$$
$$= \frac{1}{|\Omega_\mu|} \int_{\Omega_\mu} \left[\frac{1}{\Delta t}\, \mathbf{b}_\mu : \left(\mathbb{I} + \frac{\partial \tilde{\boldsymbol{\varepsilon}}_\mu^{n+1}}{\partial \boldsymbol{\varepsilon}^{n+1}} \right) + \frac{\beta}{\Delta t}\, \frac{1}{M_\mu}\, \frac{\partial \tilde{p}_\mu^{n+1}}{\partial \boldsymbol{\varepsilon}^{n+1}} \right] d\Omega_\mu, \tag{A.83}$$

$$\frac{\partial \dot{\chi}^{n+\theta}}{\partial \boldsymbol{\varphi}^{n+1}} = \frac{\partial}{\partial \boldsymbol{\varphi}^{n+1}} \left\{ \frac{1}{|\Omega_\mu|} \int_{\Omega_\mu} \left[\hat{\dot{\chi}}_\mu^{n+\theta} \big(\dot{\boldsymbol{\varepsilon}}^{n+\theta}, \dot{\tilde{\boldsymbol{\varepsilon}}}_\mu^{n+\theta}, \dot{p}^{n+\theta}, \alpha\, \dot{\boldsymbol{\varphi}}^{n+\theta}, \beta\, \dot{\tilde{p}}_\mu^{n+\theta} \big) \right] d\Omega_\mu \right\}$$
$$= \frac{1}{|\Omega_\mu|} \int_{\Omega_\mu} \left[\frac{1}{\Delta t}\, \mathbf{b}_\mu : \frac{\partial \tilde{\boldsymbol{\varepsilon}}_\mu^{n+1}}{\partial \boldsymbol{\varphi}^{n+1}} + \frac{1}{\Delta t}\, \frac{1}{M_\mu} \left(\alpha\, \mathbf{y} + \beta\, \frac{\partial \tilde{p}_\mu^{n+1}}{\partial \boldsymbol{\varphi}^{n+1}} \right) \right] d\Omega_\mu, \tag{A.84}$$

$$\frac{\partial \dot{\chi}^{n+\theta}}{\partial p^{n+1}} = \frac{\partial}{\partial p^{n+1}} \left\{ \frac{1}{|\Omega_\mu|} \int_{\Omega_\mu} \left[\hat{\dot{\chi}}_\mu^{n+\theta} \big(\dot{\boldsymbol{\varepsilon}}^{n+\theta}, \dot{\tilde{\boldsymbol{\varepsilon}}}_\mu^{n+\theta}, \dot{p}^{n+\theta}, \alpha\, \dot{\boldsymbol{\varphi}}^{n+\theta}, \beta\, \dot{\tilde{p}}_\mu^{n+\theta} \big) \right] d\Omega_\mu \right\}$$
$$= \frac{1}{|\Omega_\mu|} \int_{\Omega_\mu} \left[\frac{1}{\Delta t}\, \mathbf{b}_\mu : \frac{\partial \tilde{\boldsymbol{\varepsilon}}_\mu^{n+1}}{\partial p^{n+1}} + \frac{1}{\Delta t}\, \frac{1}{M_\mu} \left(1 + \beta\, \frac{\partial \tilde{p}_\mu^{n+1}}{\partial p^{n+1}} \right) \right] d\Omega_\mu, \tag{A.85}$$

(III) derivatives of the homogenized flux velocity vector $\boldsymbol{\mathcal{V}}^{n+\theta}$ with respect to the primal macro-scale variables:

$$\frac{\partial \boldsymbol{\mathcal{V}}^{n+\theta}}{\partial \boldsymbol{\varepsilon}^{n+1}} = \frac{\partial}{\partial \boldsymbol{\varepsilon}^{n+1}} \left\{ \frac{1}{|\Omega_\mu|} \int_{\Omega_\mu} \left[\hat{\mathcal{V}}_\mu^{n+\theta} \big(\boldsymbol{\varphi}^{n+\theta}, \tilde{\boldsymbol{\varphi}}_\mu^{n+\theta} \big) \right.\right.$$
$$\left.\left. - \hat{\dot{\chi}}_\mu^{n+\theta} \big(\dot{\boldsymbol{\varepsilon}}^{n+\theta}, \dot{\tilde{\boldsymbol{\varepsilon}}}_\mu^{n+\theta}, \dot{p}^{n+\theta}, \alpha\, \dot{\boldsymbol{\varphi}}^{n+\theta}, \beta\, \dot{\tilde{p}}_\mu^{n+\theta} \big)\, \mathbf{y} \right] d\Omega_\mu \right\}$$
$$= \frac{1}{|\Omega_\mu|} \int_{\Omega_\mu} \left[-\theta\, \mathbf{k}_\mu \cdot \frac{\partial \tilde{\boldsymbol{\varphi}}_\mu^{n+1}}{\partial \boldsymbol{\varepsilon}^{n+1}} - \frac{1}{\Delta t}\, \mathbf{y} \otimes \mathbf{b}_\mu : \left(\mathbb{I} + \frac{\partial \tilde{\boldsymbol{\varepsilon}}_\mu^{n+1}}{\partial \boldsymbol{\varepsilon}^{n+1}} \right) \right.$$
$$\left. - \frac{\beta}{\Delta t}\, \mathbf{y} \otimes \frac{1}{M_\mu}\, \frac{\partial \tilde{p}_\mu^{n+1}}{\partial \boldsymbol{\varepsilon}^{n+1}} \right] d\Omega_\mu, \tag{A.86}$$

$$\frac{\partial \boldsymbol{\mathcal{V}}^{n+\theta}}{\partial \boldsymbol{\varphi}^{n+1}} = \frac{\partial}{\partial \boldsymbol{\varphi}^{n+1}} \Bigg\{ \frac{1}{|\Omega_\mu|} \int_{\Omega_\mu} \Big[\hat{\mathcal{V}}_\mu^{n+\theta} \big(\boldsymbol{\varphi}^{n+\theta}, \tilde{\boldsymbol{\varphi}}_\mu^{n+\theta} \big) - \hat{\chi}_\mu^{n+\theta} \big(\dot{\boldsymbol{\varepsilon}}^{n+\theta}, \dot{\tilde{\boldsymbol{\varepsilon}}}_\mu^{n+\theta}, \dot{p}^{n+\theta}, \alpha\, \dot{\boldsymbol{\varphi}}^{n+\theta}, \beta\, \dot{\tilde{p}}_\mu^{n+\theta} \big)\, \mathbf{y} \Big]\, d\Omega_\mu \Bigg\}$$
$$= \frac{1}{|\Omega_\mu|} \int_{\Omega_\mu} \Bigg[-\theta\, \mathbf{k}_\mu \cdot \left(\mathbf{I} + \frac{\partial \tilde{\boldsymbol{\varphi}}_\mu^{n+1}}{\partial \boldsymbol{\varphi}^{n+1}} \right) - \frac{1}{\Delta t} \mathbf{y} \otimes \left(\mathbf{b}_\mu : \frac{\partial \tilde{\boldsymbol{\varepsilon}}_\mu^{n+1}}{\partial \boldsymbol{\varphi}^{n+1}} \right) - \frac{1}{\Delta t}\, \mathbf{y} \otimes \frac{1}{M_\mu} \left(\alpha\, \mathbf{y} + \beta\, \frac{\partial \tilde{p}_\mu^{n+1}}{\partial\, \boldsymbol{\varphi}^{n+1}} \right) \Bigg] d\Omega_\mu, \tag{A.87}$$

$$\frac{\partial \boldsymbol{\mathcal{V}}^{n+\theta}}{\partial p^{n+1}} = \frac{\partial}{\partial p^{n+1}} \Bigg\{ \frac{1}{|\Omega_\mu|} \int_{\Omega_\mu} \Big[\hat{\mathcal{V}}_\mu^{n+\theta} \big(\boldsymbol{\varphi}^{n+\theta}, \tilde{\boldsymbol{\varphi}}_\mu^{n+\theta} \big) - \hat{\chi}_\mu^{n+\theta} \big(\dot{\boldsymbol{\varepsilon}}^{n+\theta}, \dot{\tilde{\boldsymbol{\varepsilon}}}_\mu^{n+\theta}, \dot{p}^{n+\theta}, \alpha\, \dot{\boldsymbol{\varphi}}^{n+\theta}, \beta\, \dot{\tilde{p}}_\mu^{n+\theta} \big)\, \mathbf{y} \Big]\, d\Omega_\mu \Bigg\}$$
$$= \frac{1}{|\Omega_\mu|} \int_{\Omega_\mu} \Bigg[-\theta\, \mathbf{k}_\mu \cdot \frac{\partial \tilde{\boldsymbol{\varphi}}_\mu^{n+1}}{\partial p^{n+1}} - \frac{1}{\Delta t} \left(\mathbf{b}_\mu : \frac{\partial \tilde{\boldsymbol{\varepsilon}}_\mu^{n+1}}{\partial p^{n+1}} \right) \mathbf{y} - \frac{1}{\Delta t} \frac{1}{M_\mu} \left(1 + \beta\, \frac{\partial \tilde{p}_\mu^{n+1}}{\partial p^{n+1}} \right) \mathbf{y} \Bigg] d\Omega_\mu, \tag{A.88}$$

where $\mathbb{I}$ and $\mathbf{I}$ denote the fourth and second-order identity tensors, respectively.

The terms involving the derivatives of the micro-scale fluctuation fields with respect to the macro-scale variables are still required in (A.80)-(A.88) in order to finish defining the homogenized tangent operators. This is a rather standard issue in the realm of RVE-based multiscale modelling. For more details about this topic, the interested reader can refer to previous contributions, for example, those due to de Souza Neto and Feijóo R [12] and/or Perić et al. [62].

Appendix B. Micro-scale Jacobian sub-matrices

In what follows, the components given in (A.72), concerning the Jacobian at the micro-scale level, are further defined:

(I) Micro-scale stiffness matrix $\mathbf{K}_\mu$

$$\frac{\partial \dot{\mathbf{G}}_\mu^{n+\theta}}{\partial \tilde{\bar{\mathbf{u}}}_\mu^{n+1}} = \int_{\Omega_\mu} \mathbf{B}_{\tilde{u}_\mu}^T \frac{\partial \dot{\boldsymbol{\sigma}}_\mu^{n+\theta}}{\partial \tilde{\boldsymbol{\varepsilon}}_\mu^{n+1}} \mathbf{B}_{\tilde{u}_\mu}\, d\Omega_\mu = \frac{1}{\Delta t} \int_{\Omega_\mu} \mathbf{B}_{\tilde{u}_\mu}^T\, \mathbf{C}_\mu\, \mathbf{B}_{\tilde{u}_\mu}\, d\Omega_\mu = \frac{1}{\Delta t}\, \mathbf{K}_\mu. \tag{A.89}$$

(II) Micro-scale coupling matrix between the solid and fluid phases $\mathbf{Q}_\mu$

$$\frac{\partial \dot{\mathbf{G}}_\mu^{n+\theta}}{\partial \tilde{\bar{\mathbf{p}}}_\mu^{n+1}} = \int_{\Omega_\mu} \mathbf{B}_{\tilde{u}_\mu}^T \frac{\partial \dot{\boldsymbol{\sigma}}_\mu^{n+\theta}}{\partial \tilde{p}_\mu^{n+1}} \mathbf{N}_{\tilde{p}_\mu}\, d\Omega_\mu = -\frac{\beta}{\Delta t} \int_{\Omega_\mu} \mathbf{B}_{\tilde{u}_\mu}^T\, \mathbf{b}_\mu\, \mathbf{N}_{\tilde{p}_\mu}\, d\Omega_\mu = -\frac{\beta}{\Delta t}\, \mathbf{Q}_\mu. \tag{A.90}$$

(III) Micro-scale transpose coupling matrix between the solid and fluid phases $(\mathbf{Q}_\mu)^T$

$$\frac{\partial \mathbf{H}_\mu^{n+\theta}}{\partial \tilde{\bar{\mathbf{u}}}_\mu^{n+1}} = \int_{\Omega_\mu} \mathbf{N}_{\tilde{p}_\mu}^T \frac{\partial \dot{\chi}_\mu^{n+\theta}}{\partial \tilde{\boldsymbol{\varepsilon}}_\mu^{n+1}} \mathbf{B}_{\tilde{u}_\mu}\, d\Omega_\mu = \frac{1}{\Delta t} \int_{\Omega_\mu} \mathbf{N}_{\tilde{p}_\mu}^T\, \mathbf{b}_\mu\, \mathbf{B}_{\tilde{u}_\mu}\, d\Omega_\mu = \frac{1}{\Delta t}\, (\mathbf{Q}_\mu)^T. \tag{A.91}$$

(IV) Micro-cale compressibility matrix $\mathbf{S}_\mu$ and permeability matrix $\boldsymbol{\mathcal{K}}_\mu$

$$\begin{aligned}\frac{\partial \mathbf{H}_\mu^{n+\theta}}{\partial \tilde{\bar{\mathbf{p}}}_\mu^{n+1}} &= \int_{\Omega_\mu} \left(\mathbf{N}_{\tilde{p}_\mu}^T \, \frac{\partial \dot{\chi}_\mu^{n+\theta}}{\partial \tilde{p}_\mu^{n+1}} \, \mathbf{N}_{\tilde{p}_\mu} - \mathbf{B}_{\tilde{p}_\mu}^T \, \frac{\partial \boldsymbol{\mathcal{V}}_\mu^{n+\theta}}{\partial \tilde{\boldsymbol{\varphi}}_\mu^{n+1}} \, \mathbf{B}_{\tilde{p}_\mu} \right) d\Omega_\mu \\ &= \frac{\beta}{\Delta t} \int_{\Omega_\mu} \mathbf{N}_{\tilde{p}_\mu}^T \, \frac{1}{M_\mu} \, \mathbf{N}_{\tilde{p}_\mu} \, d\Omega_\mu + \theta \int_{\Omega_\mu} \mathbf{B}_{\tilde{p}_\mu}^T \, \mathbf{k}_\mu \, \mathbf{B}_{\tilde{p}_\mu} \, d\Omega_\mu = \frac{\beta}{\Delta t} \, \mathbf{S}_\mu + \theta \, \boldsymbol{\mathcal{K}}_\mu .\end{aligned} \tag{A.92}$$

Acknowledgments

This work was partially supported by the Consejo Nacional de Investigaciones Cientficas y Tecnicas (CONICET, Argentina, grant PIP 2022-2024-GI-11220210100455CO) as well as Secretaria de General de Ciencia y Tecnica de la Universidad Nacional del Nordeste (UNNE), Argentina (Grants PI 21D003). Also, the authors would like to acknowledge the financial support from the Agencia Nacional de Promoción Científica y Tecnológica (ANPCyT, Argentina, grants PICTO-UNNE-2019-00014 and PICT-2020-SERIEA-02793).

Apéndice B

About RVE size objectivity of multiscale analysis of porous media

Reinaldo A. Anonis, Javier L. Mroginski, Pablo J. Sánchez, Luis E. Kosteski (2026). About RVE size objectivity of multiscale analysis of porous media. Latin American Journal of Solids and Structures, Vol. 23(1): Thematic Section: MecSol 2024: e8781-e8781

About RVE size objectivity of multiscale analysis of porous media

Anonis, Reinaldo A.[1], **Mroginski, Javier L.**[1,1], **Sánchez, Pablo J.**[2,3], **Kosteski, Luis E.**[4]

[1]LAMEC-IMIT-CONICET Laboratorio de Mecánica Computacional, Universidad Nacional del Nordeste, Las Heras 727, CP 3500 Chaco, Argentina. Email: ranonis@ing.unne.edu.ar, javierm@ing.unne.edu.ar

[2]CIMEC-UNL-CONICET, Ruta Nac. 168, Km 0, Paraje el Pozo, CP 3000 Santa Fe, Argentina. Email: sanchez.pablo.javier@gmail.com

[3]GIMNI-UTN-FRSF, Lavaise 610, CP 3000 Santa Fe, Argentina

[4]Department of Civil Engineering and MAEC Group, Universidade Federal do Pampa (UNIPAMPA), Av. Tiaraju, 810, Alegrete, 97546-550, RS, Brazil. Email: luiskosteski@unipampa.edu.br

Keywords: Multiscale model, porous media, RVE

Abstract. This study proposes a multi-scale model formulation for saturated porous media, centered on the concept of the Representative Volume Element (RVE). The linkage between scales is established by enforcing the equivalence of the total virtual power per unit volume at the larger scale with its corresponding volume-averaged counterpart at the smaller length scale. By employing the Principle of Multiscale Virtual Power (PMVP) along with appropriate constraints on micro-scale displacements and pore pressures, a robust variational theory is established. The formulation can be implemented using the finite element squared (FE^2) strategy through spatial discretization. The theoretical evidence presented in this work reveal a pathological inconsistency in the objectivity of the macro scale response with respect to the RVE size. The primary contribution of this work is to offer an alternative solution to the aforementioned issue, aiming to restore the fundamental concept of RVE. To achieve this, a conveniently fine-scale constitutive approach is proposed, introducing useful adjustments in the micro-scale pore pressure field expansion.

B.1. Introduction

The mechanics of porous materials is a highly relevant discipline in various fields of knowledge, such as geomechanics, biomechanics, and materials science, among others. This area has undergone significant development since the pioneering work of Biot [31, 32]. Defining constitutive relations at the macro-scale level is crucial for accurately capturing the complex interactions between material constituents and phases. From a modeling perspective, these equations can be: (i) explicitly assumed based on phenomenological considerations, or (ii) implicitly derived using consistent homogenization techniques Luc Dormieux [47]. The latter approach has proven to be highly effective in predicting complex material behaviors. This methodology derives the homogenized constitutive response by averaging quantities from fine-scale fields. The existence of a minimum micro-structural domain, known as the Representative Volume Element (RVE), from which the macro-scale response becomes size-insensitive, is a fundamental cornerstone for these homogenization techniques Hill [1].

Many RVE-based multiscale strategies are founded on the Hill-Mandel lemma, which ensures equivalence in terms of internal strain energy between the macro and micro scales, Hill [1, 2, 3]. Alongside the conceptual improvements, there have also been significant developments in the computational homogenization of these theoretical models, primarily based on the multilevel finite element strategy (FE^2) Feyel y Chaboche [5].

Concerning saturated porous media, Larsson et al. [14] introduced a variational homogenization method for analyzing transient uncoupled whereas Su et al. [48] studying the coupled consolidation phenomena. They demonstrate that the linear multiscale approximation introduces a micro-scale size effect,

[1]Corresponding author. E-mail address: javierm@ing.unne.edu.ar (Mroginski, Javier L.).

manifested by the emergence of a second-order term that impacts the objectivity of the macro-scale response, implying that conventional homogenization models cannot be straightforwardly applied to saturated porous media without careful reconsideration. To address this issue, those authors indicated that the second-order effect diminishes as the size of the Representative Volume Element (RVE) approaches infinitesimally small dimensions.

In contrast, Khoei y Hajiabadi [16], Khoei y Saeedmonir [51] put forward computational homogenization models for saturated and multiphase porous media, where the macro-scale response is decomposed into two terms: one stationary and the other dynamic, with the size effect encapsulated in the latter. This effect diminishes as the micro-scale domain approaches infinitesimal dimensions. However, as the fine-scale dimensions increase, these authors observe disparities in the homogenized results when compared to Direct Numerical Simulation (DNS) results.

Klahr et al. [56] developed a variational RVE-based multiscale formulation for analyzing a saturated porous medium under large strains. In this context, they discovered a dependence on the size of the micro-cell domain, which manifests in the homogenized flow velocity.

All the advancements mentioned in the preceding paragraphs demonstrate a significant interest in understanding the size effect inherent in multiscale modeling of saturated porous media. Currently, this remains a challenging topic and an open line of research. The concept of preserving transient effects, aimed at avoiding limitations on predictive capabilities, underlies all of these previous contributions. The micro-scale size dependence appears to contradict the intuitive concept of Representative Volume Element (RVE) existence, which is a fundamental pillars upon which the entire homogenization theory was established Hill [1]. The primary motivation of this work is to contribute to clarifying ideas concerning this critical theoretical issue and to introduce a new modeling alternative.

In summary, the present work proposes a consistent homogenization model based on the Principle of Multiscale Virtual Power (PMVP) Blanco et al. [19], along with its corresponding numerical implementation, designed to address the consolidation phenomenon in saturated soils (see Lewis y Schrefler [41], Mroginski et al. [42], Beneyto et al. [43]). For the mechanical description of the porous medium, we employ the general theory of poromechanics developed in Coussy [36]. To define the internal power functionals at both macro and micro-scale levels, two additional pairs of power-conjugate variables are required compared to the classical case of a non-porous medium.

B.2. Principle of multiscale Virtual Power

In this section, the coupling of the physical behavior between macro and micro length scales is established by appealing to the so-called Principle of Multiscale Virtual Power (PMVP) proposed by Blanco et al. [19]. This variational statement offers a formal framework to derive all basic ingredients of the multiscale formulation, but firstly some fundamental concepts should be introduced.

B.2.1. Internal and External power functionals

For the fully saturated case and under the hypothesis of infinitesimal transformations, the internal power $\mathcal{P}^{int}$ was written by Coussy [36] as follows

$$\mathcal{P}^{int} = \int_{\Omega} \left[\boldsymbol{\sigma} : \dot{\boldsymbol{\varepsilon}} - \nabla \cdot \left(\frac{p}{\rho^f} \mathbf{w} \right) \right] d\Omega \,, \tag{B.1}$$

where $\dot{\boldsymbol{\varepsilon}} = \nabla^{sym} \dot{\mathbf{u}}$ is the rate of infinitesimal strain tensor of the solid skeleton, $\dot{\mathbf{u}}$ is the rate of macro-displacement field, p the (scalar) pore pressure field of the fluid, ρ^f intrinsic mass density of the fluid, $\mathbf{w} = \rho^f \boldsymbol{\mathcal{V}}$ is the relative mass flow vector of the fluid, $\boldsymbol{\mathcal{V}}$ is the flux or the relative seepage velocity vector between the fluid and solid velocity vectors. Finally, Ω denotes the porous media macro-scale domain.

After some algebraical manipulation and taking into account the mass balance equations $\dot{m}^f +$

$\nabla \cdot \mathbf{w} = 0$, being m^f the mass content of the fluid phase, assuming of infinitesimal transformations, the (B.1) can be rewritten as

$$\mathcal{P}^{int} = \int_\Omega \left[\boldsymbol{\sigma} : \dot{\boldsymbol{\varepsilon}} + \dot{\chi}\, p - \boldsymbol{\mathcal{V}} \cdot \boldsymbol{\varphi} \right] d\Omega \,, \tag{B.2}$$

where the following nomenclature is adopted hereafter: $\dot{\chi} = \frac{\dot{m}^f}{\rho^f}$ and $\boldsymbol{\varphi} = \nabla p$.

It can be seen that the second term in the r.h.s. of (B.2) represents the work rate done, in the pore space, by the fluid phase. The third duality product in (B.2) takes into account the viscous dissipation effect due to the relative motion of the fluid phase concerning the solid skeleton. Therefore, two additional pairs of power-conjugate variables, $\{\dot{\chi}; p\}$ and $\{\boldsymbol{\mathcal{V}}; \boldsymbol{\varphi}\}$, are necessary to introduce with respect to the classical solid mechanical problem.

The external power, $\mathcal{P}^{ext}$, exerted by the set of external agencies $\{\mathbf{f}; \mathbf{t}; q\}$ has also been presented by Coussy [36]

$$\mathcal{P}^{ext} = \int_\Omega \mathbf{f} \cdot \dot{\mathbf{u}}\, d\Omega + \int_\Gamma \left[\mathbf{t} \cdot \dot{\mathbf{u}} \, - \, p\, \frac{q}{\rho^f} \right] d\Gamma \,, \tag{B.3}$$

where $\mathbf{f}$ is the body force of the porous media, while $\mathbf{t}$ and q represent the systems of total external traction and normal fluid flux, respectively.

The well known concepts of internal and external virtual powers can be easily established from the above expressions, considering the corresponding admissible virtual actions of their primal quantities, i.e., $\{\delta\dot{\mathbf{u}}; \delta\dot{\boldsymbol{\varepsilon}}; \delta p; \delta\boldsymbol{\varphi}\}$. Then, the total virtual power, $\delta\mathcal{P}^{tot}$, can be expressed as

$$\delta\mathcal{P}^{tot} = \delta\mathcal{P}^{int} - \delta\mathcal{P}^{ext} = \int_\Omega \left(\boldsymbol{\sigma} : \delta\dot{\boldsymbol{\varepsilon}} + \dot{\chi}\, \delta p - \boldsymbol{\mathcal{V}} \cdot \delta\boldsymbol{\varphi} - \mathbf{f} \cdot \delta\dot{\mathbf{u}} \right) d\Omega - \int_{\Gamma_{\mathrm{N}}^u} \mathbf{t} \cdot \delta\dot{\mathbf{u}}\, d\Gamma + \int_{\Gamma_{\mathrm{N}}^p} \frac{q}{\rho^f}\, \delta p\, d\Gamma \,. \tag{B.4}$$

B.2.2. Weak form of the macro-scale balance equations

The balance equations in a weak form postulate that the external virtual power must be equal to the internal virtual power, for all admissible variations of primal descriptors. Thus, (B.4) can be rewritten as

$$\int_\Omega \left(\boldsymbol{\sigma} : \delta\dot{\boldsymbol{\varepsilon}} + \dot{\chi}\, \delta p - \boldsymbol{\mathcal{V}} \cdot \delta\boldsymbol{\varphi} \right) d\Omega = \int_\Omega \mathbf{f} \cdot \delta\dot{\mathbf{u}}\, d\Omega + \int_{\Gamma_{\mathrm{N}}^u} \mathbf{t} \cdot \delta\dot{\mathbf{u}}\, d\Gamma - \int_{\Gamma_{\mathrm{N}}^p} \frac{q}{\rho^f}\, \delta p\, d\Gamma, \;\; \forall\, \delta\dot{\mathbf{u}} \text{ and } \delta p \text{ admissible.} \tag{B.5}$$

The underlying admissibility requirements invoked in (B.5), for virtual variations $\delta\dot{\mathbf{u}}$ and δp, take into account proper regularity demands such that all the integral terms can be formally evaluated as well as homogeneous prescribed values for both continuous fields on Γ_{N}^u and Γ_{N}^p (i.e. where Dirichlet boundary conditions should be specified for $\mathbf{u}$ and p), respectively. Since $\delta\dot{\mathbf{u}}$ and δp are independent from each other, the variational form of equilibrium is finally described as a system of two coupled scalar equations, Coussy [36], Lewis y Schrefler [41], Di Rado et al. [113].

$$\begin{aligned} G &\equiv \int_\Omega \boldsymbol{\sigma} : \delta\dot{\boldsymbol{\varepsilon}}\, d\Omega - \int_\Omega \mathbf{f} \cdot \delta\dot{\mathbf{u}}\, d\Omega - \int_{\Gamma_{\mathrm{N}}^u} \mathbf{t} \cdot \delta\dot{\mathbf{u}}\, d\Gamma = 0 \,, \quad \forall\, \delta\dot{\mathbf{u}} \text{ admissible,} \\ H &\equiv \int_\Omega \left(\dot{\chi}\, \delta p \, - \boldsymbol{\mathcal{V}} \cdot \delta\boldsymbol{\varphi} \right) d\Omega \, + \int_{\Gamma_{\mathrm{N}}^p} \frac{q}{\rho^f}\, \delta p\, d\Gamma = 0 \,. \quad \forall\, \delta p \text{ admissible,} \end{aligned} \tag{B.6}$$

B.2.3. Postulates of the Principle of multiscale Virtual Power

Before discussing the PMVP, it is required to postulate an adequate mechanism for transferring information and define the concept of admissibility that makes compatible the primitive descriptors (displacements, pore pressures and their corresponding gradients) between the two involved scales.

Henceforth, any object related to the micro-scale will be endowed with the subscript μ, preserving the same physical meaning. The micro-scale domain is denoted Ω_μ (also called Micro-Cell or simply MC), with boundary Γ_μ, $\mathbf{n}_\mu$ being the unit (outward) vector normal to Γ_μ. In addition, the vector $\mathbf{y}$ is used to describe material points in a Cartesian system at the sub-scale.Without loss of generality, the origin of coordinates is located at the geometric center of Ω_μ, implying that

$$\int_{\Omega_\mu} \mathbf{y}\, d\Omega_\mu = \mathbf{0}\ . \tag{B.7}$$

B.2.4. Primal descriptors at the micro-scale level

As in the macro-scale problem, the Micro-Cell is constituted by a continuum saturated porous medium. Thus, the same primal descriptors of the poromechanics theory of the macro-scale are adopted. A fundamental assumption in the present modelling context is that the micro-scale displacement, $\mathbf{u}_\mu$, can be expanded in terms of macro-scale quantities ($\mathbf{u}$ and $\boldsymbol{\varepsilon}$) as follows (de Souza Neto y Feijóo [12], Sánchez et al. [22], de Souza Neto et al. [26])

$$\mathbf{u}_\mu\left(\mathbf{y},t\right) = \mathbf{u}\left(\mathbf{x},t\right) + \boldsymbol{\varepsilon}\left(\mathbf{x},t\right)\cdot\mathbf{y} + \tilde{\mathbf{u}}_\mu\left(\mathbf{y},t\right)\ , \tag{B.8}$$

being $\tilde{\mathbf{u}}_\mu\left(\mathbf{y},t\right)$ the fluctuation displacement field of the MC, Therefore, the micro-scale infinitesimal strain tensor yields

$$\boldsymbol{\varepsilon}_\mu\left(\mathbf{y},t\right) = \nabla_y^{sym}\mathbf{u}_\mu\left(\mathbf{y},t\right) = \boldsymbol{\varepsilon}\left(\mathbf{x},t\right) + \nabla_y^{sym}\tilde{\mathbf{u}}_\mu\left(\mathbf{y},t\right) = \boldsymbol{\varepsilon}\left(\mathbf{x},t\right) + \tilde{\boldsymbol{\varepsilon}}_\mu\left(\mathbf{y},t\right)\ , \tag{B.9}$$

where operator $\nabla_y^{sym}\left(\bullet\right)$ represents the symmetric gradient concerning $\mathbf{y}$ - coordinates. The strain field in (B.9) is composed as the addition of the macro-scale strain, $\boldsymbol{\varepsilon}(\mathbf{x},t)$, which is assumed to be uniformly distributed over the entire domain Ω_μ, and the micro-scale strain fluctuation $\tilde{\boldsymbol{\varepsilon}}_\mu(\mathbf{y},t)$.

On the other hand, the micro-pore pressure, and its spatial gradient, can also be decomposed in an additive manner analogous to the displacement (see Lopez Rivarola et al. [18], Khoei y Saeedmonir [51], Reinaldo A. et al. [66])

$$p_\mu\left(\mathbf{y},t\right) = p\left(\mathbf{x},t\right) + \boldsymbol{\varphi}\left(\mathbf{x},t\right)\cdot\mathbf{y} + \tilde{p}_\mu\left(\mathbf{y},t\right)\ , \tag{B.10}$$

$$\boldsymbol{\varphi}_\mu\left(\mathbf{y},t\right) = \nabla_y\, p_\mu\left(\mathbf{y},t\right) = \boldsymbol{\varphi}\left(\mathbf{x},t\right) + \nabla_y\,\tilde{p}_\mu\left(\mathbf{y},t\right) = \boldsymbol{\varphi}\left(\mathbf{x},t\right) + \tilde{\boldsymbol{\varphi}}_\mu\left(\mathbf{y},t\right)\ , \tag{B.11}$$

being $\tilde{p}_\mu\left(\mathbf{y},t\right)$ the pore pressure fluctuation field on the MC and $\tilde{\boldsymbol{\varphi}}_\mu$ its corresponding gradient vector which is obtained from the $\nabla_y\left(\bullet\right)$ operator, related to the micro-scale coordinate system.

B.2.5. Formulation of the PMVP

The Principle of multiscale virtual power states that the total virtual power per unit volume, at a point $\mathbf{x}$ *of the macro-scale, must be equal to the volumetric average of the total micro-scale virtual power (per unit volume) at the corresponding MC, for all admissible virtual actions* (Blanco et al. [19]).

Thus, recalling the definition of macro-scale total virtual power per unit volume (given by the first integrand term of the r.h.s. in (B.4)) and assuming the same mathematical structure for its micro-scale counterpart, the PMVP gives us the following variational sentence

$$\boldsymbol{\sigma}\!:\!\delta\dot{\boldsymbol{\varepsilon}} + \dot{\chi}\,\delta p - \boldsymbol{\mathcal{V}}\cdot\delta\boldsymbol{\varphi}\ -\ \mathbf{f}\cdot\delta\dot{\mathbf{u}} = \frac{1}{|\Omega_\mu|}\int_{\Omega_\mu}\left(\sigma_\mu\!:\!\delta\dot{\boldsymbol{\varepsilon}}_\mu + \dot{\chi}_\mu\,\delta p_\mu - \boldsymbol{\mathcal{V}}_\mu\cdot\delta\boldsymbol{\varphi}_\mu\ -\ \mathbf{f}_\mu\cdot\delta\dot{\mathbf{u}}_\mu\right)\,d\Omega_\mu,$$
$$\forall\ \left(\delta\dot{\boldsymbol{\varepsilon}},\delta\dot{\mathbf{u}},\delta\boldsymbol{\varphi},\delta p,\delta\dot{\mathbf{u}}_\mu,\delta p_\mu\right)\text{admissible},\ \forall\, t, \tag{B.12}$$

Expression (B.12) can be viewed as a particular instance of the PMVP for the case of saturated porous media, at both scales of analysis.

B.2.6. Homogenized variables and variational forms of balance at the micro-scale

The variational identity of (B.12) provides all the natural way to obtain the homogenization formulae for the macro-scale stress-like entities $\{\boldsymbol{\sigma}; \dot{\chi}; \boldsymbol{\mathcal{V}}\}$ and body force $\mathbf{f}$, as well as the variational equilibrium equation at micro-scale. To attain this goal, descriptors in Eqs. (B.8-B.11) must be replaced in expression (B.12) for virtual actions in the MC domain, and then, the consequences are shown below.

a) Homogenized stress tensor:

$$\boldsymbol{\sigma} = \frac{1}{|\Omega_\mu|} \int_{\Omega_\mu} \Big(\boldsymbol{\sigma}_\mu - \mathbf{f}_\mu \otimes \mathbf{y} \Big)\, d\Omega_\mu, \ \forall\, t\,. \tag{B.13}$$

Obtained from (B.12), taking $\delta\dot{\tilde{\mathbf{u}}}_\mu = \mathbf{0}$, $\delta p = 0$, $\delta\tilde{p}_\mu = 0$, $\delta\boldsymbol{\varphi} = \mathbf{0}$, $\delta\dot{\mathbf{u}} = \mathbf{0}$ and allowing arbitrary variations of $\delta\dot{\boldsymbol{\varepsilon}}$.

b) Homogenized mass content rate of fluid (per unit fluid density):

$$\dot{\chi} = \frac{\dot{m}^f}{\rho^f} = \frac{1}{|\Omega_\mu|} \int_{\Omega_\mu} \dot{\chi}_\mu\, d\Omega_\mu, \ \forall\, t\,. \tag{B.14}$$

Obtained from (B.12), taking $\delta\dot{\boldsymbol{\varepsilon}} = \mathbf{0}$, $\delta\dot{\tilde{\mathbf{u}}}_\mu = \mathbf{0}$, $\delta\tilde{p}_\mu = 0$, $\delta\dot{\mathbf{u}} = \mathbf{0}$, $\delta\boldsymbol{\varphi} = \mathbf{0}$ and allowing arbitrary variations of δp.

c) Homogenized flux velocity vector:

$$\boldsymbol{\mathcal{V}} = \frac{1}{|\Omega_\mu|} \int_{\Omega_\mu} \Big(\boldsymbol{\mathcal{V}}_\mu - \dot{\chi}_\mu\, \mathbf{y} \Big)\, d\Omega_\mu, \ \forall\, t\,. \tag{B.15}$$

It is achieved from (B.12), adopting $\delta\dot{\boldsymbol{\varepsilon}} = \mathbf{0}$, $\delta\dot{\tilde{\mathbf{u}}}_\mu = \mathbf{0}$, $\delta p = 0$, $\delta\tilde{p}_\mu = 0$, $\delta\dot{\mathbf{u}} = \mathbf{0}$ with arbitrary variations of $\delta\boldsymbol{\varphi}$.

From (B.15) it is possible to decompose the homogenized flux velocity vector into a stationary part ($\boldsymbol{\mathcal{V}}_{sta}$) and a dynamic or transient part ($\boldsymbol{\mathcal{V}}_{tra}$) as Khoei y Hajiabadi [16], Jänicke et al. [49], Khoei y Saeedmonir [51], Saeedmonir y Khoei [52] (This decomposition is useful to discuss the MC size effect problem):

$$\boldsymbol{\mathcal{V}} = \boldsymbol{\mathcal{V}}_{sta} + \boldsymbol{\mathcal{V}}_{tra} = \frac{1}{|\Omega_\mu|} \int_{\Omega_\mu} \boldsymbol{\mathcal{V}}_\mu\, d\Omega_\mu - \frac{1}{|\Omega_\mu|} \int_{\Omega_\mu} \dot{\chi}_\mu\, \mathbf{y}\, d\Omega_\mu, \ \forall\, t\,. \tag{B.16}$$

d) Homogenized body force field:

$$\mathbf{f} = \frac{1}{|\Omega_\mu|} \int_{\Omega_\mu} \mathbf{f}_\mu\, d\Omega_\mu = \frac{\mathbf{g}}{|\Omega_\mu|} \int_{\Omega_\mu} \rho_\mu\, d\Omega_\mu, \ \forall\, t\,. \tag{B.17}$$

Obtained from (B.12), taking $\delta\dot{\boldsymbol{\varepsilon}} = \mathbf{0}$, $\delta\dot{\tilde{\mathbf{u}}}_\mu = \mathbf{0}$, $\delta p = 0$, $\delta\tilde{p}_\mu = 0, \delta\boldsymbol{\varphi} = \mathbf{0}$ and arbitrary variations of $\delta\dot{\mathbf{u}}$.

e) Variational forms of balance in the MC: Integral equation of momentum balance

$$\int_{\Omega_\mu} \left(\boldsymbol{\sigma}_\mu : \delta\dot{\tilde{\boldsymbol{\varepsilon}}}_\mu \; - \; \mathbf{f}_\mu \cdot \delta\dot{\tilde{\mathbf{u}}}_\mu \right) d\Omega_\mu = \int_{\Omega_\mu} \left(\boldsymbol{\sigma}_\mu : \nabla_y^{sym}\, \delta\dot{\tilde{\mathbf{u}}}_\mu \; - \; \mathbf{f}_\mu \cdot \delta\dot{\tilde{\mathbf{u}}}_\mu \right) d\Omega_\mu = 0, \; \forall\, \delta\dot{\tilde{\mathbf{u}}}_\mu \in \; \tilde{\mathcal{U}}_\mu, \; \forall\, t \; . \tag{B.18}$$

From (B.12) by allowing for admissible variations of $\delta\dot{\tilde{\mathbf{u}}}_\mu$ with $\delta\dot{\boldsymbol{\varepsilon}} = \mathbf{0}, \; \delta p = 0, \; \delta\tilde{p}_\mu = 0, \; \delta\boldsymbol{\varphi} = \mathbf{0}$ and $\delta\dot{\mathbf{u}} = \mathbf{0}$.

f) Variational forms of balance in the MC: Integral mass balance equation:

$$\int_{\Omega_\mu} \left(\dot{\chi}_\mu \, \delta\tilde{p}_\mu - \boldsymbol{\mathcal{V}}_\mu \cdot \delta\tilde{\boldsymbol{\varphi}}_\mu \right) \, d\Omega_\mu = \int_{\Omega_\mu} \left(\dot{\chi}_\mu \, \delta\tilde{p}_\mu - \boldsymbol{\mathcal{V}}_\mu \cdot \nabla_y \, \delta\tilde{p}_\mu \right) \, d\Omega_\mu = 0, \; \forall \, \delta\tilde{p}_\mu \in \; \tilde{\mathcal{P}}_\mu, \; \forall \, t \; . \tag{B.19}$$

From (B.12) by allowing for admissible variations of $\delta\tilde{p}_\mu$ with $\delta\dot{\boldsymbol{\varepsilon}} = \mathbf{0}, \; \delta\dot{\tilde{\mathbf{u}}}_\mu = \mathbf{0}, \; \delta p = 0, \; \delta\dot{\mathbf{u}} = \mathbf{0}$ and $\delta\boldsymbol{\varphi} = \mathbf{0}$.

B.3. Constitutive equations in the micro-scale

The only remaining ingredient in the proposed multiscale formulation is the specification of the material behavior in the smaller length scale. Each constituent of the micro-scale domain is a two-phase saturated porous medium; Therefore constitutive relations for the seepage velocity vector $\boldsymbol{\mathcal{V}}_\mu$, as well as for the mechanical stress-like quantities $\{\boldsymbol{\sigma}_\mu; \dot{\chi}_\mu\}$, are required. The way in which constitutive input arguments are considered to evaluate such material responses plays an important role for the purposes of this work. The above-mentioned micro-scale size dependence could be one of them, which is objectionable in the realm of RVE-based homogenization models because induces a lack of objectivity in the macro-scale response. This topic justifies the detailed treatment of the constitutive arguments presented in the following sections.

B.3.1. Constitutive laws based on Full Order Expansions (FOE) for primal descriptors

This strategy probably represents the most natural and straightforward choice to describe the micro-scale material behaviors. Indeed, it has been adopted in some previous contributions Larsson et al. [14], Khoei y Hajiabadi [16], Su et al. [48], Jänicke et al. [49], Khoei y Saeedmonir [51], Saeedmonir y Khoei [52], Wu et al. [77]. In this approach, the Full Order Expanded (FOE) version of primal descriptors, see definitions (B.8)-(B.11), are part of the list of arguments in the constitutive functionals.

With respect to the seepage phenomenon at the micro-scale level, the generalized Darcy's law is assumed to characterize the mean fluid velocity in the saturated porous medium Lewis y Schrefler [41], Mroginski et al. [42].

$$\boldsymbol{\mathcal{V}}_\mu = \hat{\mathcal{V}}_\mu^{\text{FOE}}\big(\boldsymbol{\varphi}_\mu^{\text{FOE}}\big) = \mathbf{k}_\mu \cdot \Big[- \big(\boldsymbol{\varphi} + \tilde{\boldsymbol{\varphi}}_\mu\big) + \rho_\mu^f \, \mathbf{g} \Big] = \hat{\mathcal{V}}_\mu^{\text{FOE}}\big(\boldsymbol{\varphi}, \tilde{\boldsymbol{\varphi}}_\mu\big) \; , \tag{B.20}$$

where $\mathbf{k}_\mu$ is the symmetric second order permeability tensor and the hat-symbol, $(\hat{\cdot})$, denotes a generic constitutive functional. In case of isotropic saturated materials it is $\mathbf{k}_\mu = k_\mu \mathbf{I}$; $k_\mu = \kappa_\mu / (\rho_\mu^f \, |\mathbf{g}|)$ being the hydraulic permeability which is a function of the hydraulic conductivity κ_μ and the specific weight of the fluid $\rho_\mu^f \, |\mathbf{g}|$, $|\mathbf{g}|$ is the modulus of the acceleration of gravity and $\mathbf{I}$ denotes the second order identity tensor.

The same mathematical structure that describes the mechanical behavior of saturated porous medium due to Coussy [36] is assumed valid for each constituent of the micro-scale domain. Thus, we have for

$\{\dot{\boldsymbol{\sigma}}_\mu; \dot{\chi}_\mu\}$ (rate format is used)

$$\dot{\boldsymbol{\sigma}}_\mu = \mathbf{C}_\mu : \left(\dot{\boldsymbol{\varepsilon}} + \dot{\tilde{\boldsymbol{\varepsilon}}}_\mu\right) \; - \; \mathbf{b}_\mu \left(\dot{p} + \dot{\boldsymbol{\varphi}} \cdot \mathbf{y} + \dot{\tilde{p}}_\mu\right) = \hat{\dot{\sigma}}_\mu^{\text{FOE}}\left(\dot{\boldsymbol{\varepsilon}}, \dot{\tilde{\boldsymbol{\varepsilon}}}_\mu, \dot{p}, \dot{\boldsymbol{\varphi}}, \dot{\tilde{p}}_\mu\right) , \tag{B.21}$$

$$\dot{\chi}_\mu = \mathbf{b}_\mu : \left(\dot{\boldsymbol{\varepsilon}} + \dot{\tilde{\boldsymbol{\varepsilon}}}_\mu\right) \; + \; \frac{1}{M_\mu} \left(\dot{p} + \dot{\boldsymbol{\varphi}} \cdot \mathbf{y} + \dot{\tilde{p}}_\mu\right) = \hat{\dot{\chi}}_\mu^{\text{FOE}}\left(\dot{\boldsymbol{\varepsilon}}, \dot{\tilde{\boldsymbol{\varepsilon}}}_\mu, \dot{p}, \dot{\boldsymbol{\varphi}}, \dot{\tilde{p}}_\mu\right) . \tag{B.22}$$

The micro-hydromechanical response of the porous medium is mainly defined by the elastic stiffness tensor of the skeleton $\mathbf{C}_\mu$, the Biot tensor $\mathbf{b}_\mu$ and the coefficient M_μ^{-1}. For the particular case of isotropic constituents it is $\mathbf{b}_\mu = b_\mu \mathbf{I}$, where the Biot coefficient $b_\mu = 1 - K_\mu / K_\mu^s$ is given by the relationship between the bulk modulus of the skeleton K_μ and the volumetric modulus of the grain material K_μ^s. Finally, we have $M_\mu^{-1} = K_\mu^s/(b_\mu - n_\mu) + K_\mu^f / n_\mu$, where K_μ^f is the bulk modulus of fluid Biot [31, 32], Lewis y Schrefler [41].

In saturated porous media significant mechanical changes undergone by the soil skeleton are attributed to the concept of the effective stress field, here denoted as $\boldsymbol{\sigma}'_\mu$. According to the poromechanics theory, $\boldsymbol{\sigma}'_\mu$ depends on the strain tensor of the soil grains ($\boldsymbol{\varepsilon}_\mu$), then in agreement with the previous constitutive law (B.21), it can be expressed as

$$\dot{\boldsymbol{\sigma}}'_\mu = \mathbf{C}_\mu : \left(\dot{\boldsymbol{\varepsilon}} + \dot{\tilde{\boldsymbol{\varepsilon}}}_\mu\right) = \hat{\dot{\sigma}}'^{\text{FOE}}_\mu\left(\dot{\boldsymbol{\varepsilon}}, \dot{\tilde{\boldsymbol{\varepsilon}}}_\mu\right) . \tag{B.23}$$

B.3.2. About the micro-scale size dependence on the macro-scale response

The transient component, $\boldsymbol{\mathcal{V}}_{tra}$, of the homogenized velocity vector (see second integral in the r.h.s. of (B.16)), has already been identified as responsible for introducing a size effect in the multiscale modelling of porous saturated solids (Larsson et al. [13], Khoei y Hajiabadi [16], Su et al. [48], Jänicke et al. [49], Saeedmonir y Khoei [52], Reinaldo A. et al. [66]).

Some possible solutions have been proposed in the current literature. One is to extend the applied proposal in the context of heat flow (Larsson et al. [14], Özdemir et al. [71]) and simply ignore the transient effect of the sub-scale by neglecting the $\boldsymbol{\mathcal{V}}_{tra}$-contribution so that the micro-scale problem can be considered as "quasi-stationary" at all times. Another one is to adopt an infinitely small micro-scale domain size, which allows the dynamic term to be negligible and thus avoids the problem of fine-scale size dependence (Larsson et al. [14], Khoei y Hajiabadi [16], Su et al. [48], Jänicke et al. [49]). The possibility of choosing specific material parameters at the MC level in order to make the dynamic fluctuating response negligible compared with the stationary one was also mentioned Jänicke et al. [49]. In view of the previous background and the importance assigned to the transient component of the multiscale formulation, this term is now examined meticulously.

If the constitutive law (B.22) is replaced within the expression for $\boldsymbol{\mathcal{V}}_{tra}$, and reordering conveniently, it yields

$$
\begin{aligned}
\boldsymbol{\mathcal{V}}_{tra} &= -\frac{1}{|\Omega_\mu|}\int_{\Omega_\mu}\dot{\chi}_\mu\,\mathbf{y}\,d\Omega_\mu = -\frac{1}{|\Omega_\mu|}\int_{\Omega_\mu}\hat{\dot{\chi}}_\mu^{\text{FOE}}\big(\dot{\boldsymbol{\varepsilon}}_\mu^{\text{FOE}},\dot{p}_\mu^{\text{FOE}}\big)\,\mathbf{y}\,d\Omega_\mu \\
&= \underbrace{-\frac{1}{|\Omega_\mu|}\int_{\Omega_\mu}\big(\mathbf{b}_\mu:\dot{\boldsymbol{\varepsilon}}\big)\,\mathbf{y}\,d\Omega_\mu}_{\mathbf{T}_1} \underbrace{-\frac{1}{|\Omega_\mu|}\int_{\Omega_\mu}\frac{\dot{p}}{M_\mu}\,\mathbf{y}\,d\Omega_\mu}_{\mathbf{T}_2} \\
&\quad \underbrace{-\frac{1}{|\Omega_\mu|}\int_{\Omega_\mu}\big[\mathbf{b}_\mu:\dot{\tilde{\boldsymbol{\varepsilon}}}_\mu(\ldots,\dot{\boldsymbol{\varphi}},\ldots)\big]\,\mathbf{y}\,d\Omega_\mu}_{\mathbf{T}_3\to\mathcal{O}(\mathbf{y}^2)} \underbrace{-\frac{1}{|\Omega_\mu|}\int_{\Omega_\mu}\frac{\dot{\tilde{p}}_\mu(\ldots,\dot{\boldsymbol{\varphi}},\ldots)}{M_\mu}\,\mathbf{y}\,d\Omega_\mu}_{\mathbf{T}_4\to\mathcal{O}(\mathbf{y}^2)} \\
&\quad \underbrace{-\frac{1}{|\Omega_\mu|}\int_{\Omega_\mu}\frac{\dot{\boldsymbol{\varphi}}}{M_\mu}\cdot(\mathbf{y}\otimes\mathbf{y})\,d\Omega_\mu}_{\mathbf{T}_5\to\mathcal{O}(\mathbf{y}^2)}\ .
\end{aligned}
\tag{B.24}
$$

Assuming nearly symmetric distributions for $\mathbf{b}_\mu$ and M_μ properties with respect to the micro-cell barycenter, the terms $\mathbf{T}_1$ and $\mathbf{T}_2$ in (B.24) do not introduce micro-scale size dependence problems. The effect of these contributions tends to decrease as the micro-cell size enlarges including a major (and representative) number of heterogeneities. So, these terms contribute to qualify when a generic micro-cell is (or not) an RVE.

The last $\mathbf{T}_5$-term of (B.24) has a quadratic dependence on the $\mathbf{y}$-coordinate. Clearly, such a term introduces a size effect in the homogenized response because it increases monotonically for enlarging micro-cell dimensions and seriously compromises the concept of RVE existence. The gradient rate of pore pressures ($\dot{\boldsymbol{\varphi}}$) in the neighborhood of macro-scale external loads can take large values, especially if short-term analysis for low permeability and cohesive soils is considered.

Although it is not straightforward to see the influence of $\mathbf{T}_3$ and $\mathbf{T}_4$ terms, it can be seen that they also introduce size effect issues whenever the FOE-multiscale formulation is employed. This is because the solution of the fluctuating components $\dot{\tilde{\boldsymbol{\varepsilon}}}_\mu$ and $\dot{\tilde{p}}_\mu$ (present in $\mathbf{T}_3$ and $\mathbf{T}_4$, respectively) depend on the inserted macro-scale quantity $\dot{\boldsymbol{\varphi}}$, and such kind of implicit functionality gives rise to a second-order dependence on $\mathbf{y}$-coordinate for $\mathbf{T}_3$ and $\mathbf{T}_4$. The previous sentence can be proved in some academic multiscale scenarios by solving analytically the coupled system of differential equations.

B.3.3. Constitutive laws based on reduced order expansions for primal descriptors

It has been shown that the lack of objectivity in the macro-scale response stems from the type of expansion accepted to evaluate input arguments in constitutive laws. This analysis allows us to introduce minimally invasive modifications, pointing to the core of the problem, whereas all the remainder features and ingredients of the proposed (variationally consistent) multiscale formulation are preserved, in order to not disclaim modelling capabilities.

For this aim, slight variations are now introduced in the definition of the stress-like functionals $\hat{\boldsymbol{\sigma}}_\mu$ and $\hat{\dot{\chi}}_\mu$. Thus, different expansions order for the micro-scale strain rate $\dot{\boldsymbol{\varepsilon}}_\mu$ and pore-pressure rate $\dot{p}_\mu$ are proposed, in case both fields are arguments of $\hat{\boldsymbol{\sigma}}_\mu$ and $\hat{\dot{\chi}}_\mu$, leading to a Reduced Order of Expansions (ROE) multiscale model derived in this work. In this way, the following selective expansion choices are proposed: **a)** A Full Order Expansion (FOE) for the micro-scale strain rate descriptor, denoted as $\dot{\boldsymbol{\varepsilon}}_\mu^{\text{FOE}}$, identical to expression (B.9); **b)** A Reduced Order Expansion (ROE) for the micro-scale pore-pressures rate as a results of neglecting the first-order term ($\dot{\boldsymbol{\varphi}}\cdot\mathbf{y}$) in (B.10), thus, $\dot{p}_\mu^{\text{ROE}} = \dot{p} + \dot{\tilde{p}}_\mu$.

It is worth mentioning at this point that the ROE for $\dot{p}_\mu$ ($\dot{p}_\mu^{\text{ROE}}$) has a very limited local effect in the multiscale formulation, since it has only meaningful within the constitutive functions characterizing $\dot{\boldsymbol{\sigma}}_\mu$ and $\dot{\chi}_\mu$ and the micro-scale pore-pressure field is still FOE. Therefore, our proposal can be formally

viewed as a simplifying constitutive-like hypothesis for $\dot{\boldsymbol{\sigma}}_\mu$ and $\dot{\chi}_\mu$. Moreover, the generalized Darcy's law remains unchanged as defined in (B.20), thus the complete field $\dot{p}_\mu^{\text{FOE}}$ is required at this instance, and the constitutive equation for the micro-scale effective stress, $\dot{\boldsymbol{\sigma}}'_\mu$, also remains invariable if compared with the FOE multiscale scheme.

B.4. Solution of the variational equations at the macro-scale

The global numerical paradigm consists of two nested, time-evolving, finite element schemes where the connection between them is established at each macro-scale Gauss point. In the literature, such an approach is referred to as FE^2 strategy, Feyel y Chaboche [5].

The time variable, t, is discretized through a monotonically increasing sequence of time steps $\left[t^0, t^1, t^2, \ldots, t^n, t^{n+1}, \ldots\right]$. The θ-generalized rule (Lewis y Schrefler [41]) is used to account for the problem evolution within any time interval.

To describe the physical domain Ω a finite element mesh Ω_h is used. Then it is possible to build global interpolation matrices for the displacement, $\mathbf{N}_u$, and pore pressure, $\mathbf{N}_p$, fields as follows

$$\mathbf{u} = \mathbf{N}_u\, \bar{\mathbf{u}} \quad ; \quad p = \mathbf{N}_p\, \bar{\mathbf{p}}\,, \tag{B.25}$$

where $\bar{\mathbf{u}}$ and $\bar{\mathbf{p}}$ are the vectors that collect all nodal displacements and pore pressures values, respectively. In order to satisfy the Babuska-Brezzi convergence requirements (Lewis y Schrefler [41]), it is necessary to adopt different orders of interpolation for each primal variable. Following the Galerkin method, the same spatial approximation is used for virtual actions. Replacing (B.25) into the weak forms (B.6), and after performing standard manipulations specific to the finite element method, the discrete (time and spatial) version of balance, at time step $t^{n+\theta}$, can be written (Dirichlet degrees of freedom are omitted)

$$\begin{aligned}
\dot{\mathbf{G}}_h^{n+\theta} &\equiv \int_{\Omega_h} \mathbf{B}_u^T\, \dot{\boldsymbol{\sigma}}^{\,n+\theta}\, d\Omega - \int_{\Omega_h} \mathbf{N}_u^T\, \dot{\mathbf{f}}^{\,n+\theta}\, d\Omega - \int_{\Gamma^u_{\text{N},\,h}} \mathbf{N}_u^T\, \dot{\mathbf{t}}^{\,n+\theta}\, d\Gamma = \mathbf{0}\,, \\
\mathbf{H}_h^{n+\theta} &\equiv \int_{\Omega_h} \mathbf{N}_p^T\, \dot{\chi}^{\,n+\theta}\, d\Omega - \int_{\Omega_h} \mathbf{B}_p^T\, \boldsymbol{\mathcal{V}}^{\,n+\theta}\, d\Omega + \int_{\Gamma^p_{\text{N},\,h}} \mathbf{N}_p^T\, \frac{q^{\,n+\theta}}{\rho^f}\, d\Gamma = \mathbf{0}\,,
\end{aligned} \tag{B.26}$$

being $\mathbf{B}_u = \nabla^{sym}\, \mathbf{N}_u$ the deformation-displacement matrix and $\mathbf{B}_p = \nabla\, \mathbf{N}_p$ is the matrix that relates pore pressures to their gradients. The system of equations (B.26) is solved by using a standard Newton-Raphson algorithm. Thus, the current displacement and pore pressure nodal values are updated (at time step $t^{\,n+1}$) in terms of the iterative increments $\Delta\bar{\mathbf{u}}$ and $\Delta\bar{\mathbf{p}}$, respectively. For a given "k"-iteration in the time interval of the Newton-Raphson scheme, these increments are evaluated as (subscript h is omitted hereafter)

$$\begin{bmatrix} \Delta\bar{\mathbf{u}} \\ \Delta\bar{\mathbf{p}} \end{bmatrix} = -\left(\mathbf{J}_k^{n+\theta}\right)^{-1} \begin{bmatrix} \dot{\mathbf{G}}_k^{n+\theta} \\ \mathbf{H}_k^{n+\theta} \end{bmatrix} \quad \text{with } \mathbf{J}^{n+\theta} = \begin{bmatrix} \frac{\partial \dot{\mathbf{G}}^{n+\theta}}{\partial \bar{\mathbf{u}}^{n+1}} & \frac{\partial \dot{\mathbf{G}}^{n+\theta}}{\partial \bar{\mathbf{p}}^{n+1}} \\ \frac{\partial \mathbf{H}^{n+\theta}}{\partial \bar{\mathbf{u}}^{n+1}} & \frac{\partial \mathbf{H}^{n+\theta}}{\partial \bar{\mathbf{p}}^{n+1}} \end{bmatrix}. \tag{B.27}$$

Each component of the Jacobian matrix $\mathbf{J}_k^{n+\theta}$ can be found in Khoei y Hajiabadi [16], Reinaldo A. et al. [66].

B.5. Solution of the variational equations at the Micro-Scale

Macro and micro spatial domains share the same temporal scale. Thus, all definitions concerning to the time discretization scheme, described in the section before are still valid at the micro-scale level.

The same finite element technology used in the context of the macro-scale problem is used to conform a mesh, $\Omega_{\mu,\,h}$, for the micro-scale domain Ω_μ. Then, the primal descriptors $\dot{\tilde{\mathbf{u}}}_\mu$ and $\dot{\tilde{p}}_\mu$ (and their

corresponding admissible virtual variations $\delta\dot{\tilde{\mathbf{u}}}_\mu$ and $\delta\tilde{p}_\mu$) can be approached through global shape function matrices for micro-displacement fluctuations, $\mathbf{N}_{\tilde{u}_\mu}$, and micro-pore pressure fluctuations, $\mathbf{N}_{\tilde{p}_\mu}$, as

$$\begin{aligned} \tilde{\mathbf{u}}_\mu &= \mathbf{N}_{\tilde{u}_\mu}\,\tilde{\tilde{\mathbf{u}}}_\mu, \quad \delta\tilde{\mathbf{u}}_\mu = \mathbf{N}_{\tilde{u}_\mu}\,\delta\tilde{\tilde{\mathbf{u}}}_\mu, \quad \text{with } \tilde{\tilde{\mathbf{u}}}_\mu \text{ and } \delta\tilde{\tilde{\mathbf{u}}}_\mu \in \tilde{\mathcal{U}}^{\text{Per}}_{\mu,\,h}\,, \\ \tilde{p}_\mu &= \mathbf{N}_{\tilde{p}_\mu}\,\tilde{\tilde{\mathbf{p}}}_\mu, \quad \delta\tilde{p}_\mu = \mathbf{N}_{\tilde{p}_\mu}\,\delta\tilde{\tilde{\mathbf{p}}}_\mu, \quad \text{with } \tilde{\tilde{\mathbf{p}}}_\mu \text{ and } \delta\tilde{\tilde{\mathbf{p}}}_\mu \in \tilde{\mathcal{P}}^{\text{Per}}_{\mu,\,h}\,, \end{aligned} \tag{B.28}$$

where $\tilde{\tilde{\mathbf{u}}}_\mu$ and $\tilde{\tilde{\mathbf{p}}}_\mu$ denote the vectors containing all nodal micro-displacement fluctuations and pore pressure fluctuations, respectively, while $\tilde{\mathcal{U}}^{\text{Per}}_{\mu,\,h}$ and $\tilde{\mathcal{P}}^{\text{Per}}_{\mu,\,h}$ represent the finite-dimensional counterparts of subspaces $\tilde{\mathcal{U}}^{\text{Per}}_{\mu}$ and $\tilde{\mathcal{P}}^{\text{Per}}_{\mu}$ related to the Periodic multiscale model (see, namely de Souza Neto y Feijóo [12], Sánchez et al. [22], de Souza Neto et al. [26], Perić et al. [62]).

After some standard mathematical treatment, the substitution of (B.28) into the variational forms Eqs. (B.18)-(B.19) leads to the spatial and time discrete approximation (at time $t^{n+\theta}$) for the balance equations in the micro-scale

$$\underbrace{\left[\int_{\Omega_{\mu,\,h}} \left(\mathbf{B}^T_{\tilde{u}_\mu}\,\dot{\boldsymbol{\sigma}}_\mu^{\,n+\theta} - \mathbf{N}^T_{\tilde{u}_\mu}\,\dot{\mathbf{f}}_\mu^{\,n+\theta}\right) d\Omega_\mu\right]}_{\dot{\mathbf{G}}^{n+\theta}_{\mu,\,h}} \cdot \delta\dot{\tilde{\tilde{\mathbf{u}}}}_\mu = 0, \;\; \forall\,\delta\dot{\tilde{\tilde{\mathbf{u}}}}_\mu \in \tilde{\mathcal{U}}^{\text{Per}}_{\mu,\,h},\; \text{with } \dot{\tilde{\tilde{\mathbf{u}}}}_\mu \in \tilde{\mathcal{U}}^{\text{Per}}_{\mu,\,h} \text{ and } \tilde{\tilde{\mathbf{p}}}_\mu \in \tilde{\mathcal{P}}^{\text{Per}}_{\mu,\,h}\,, \tag{B.29}$$

$$\underbrace{\left[\int_{\Omega_{\mu,\,h}} \left(\mathbf{N}^T_{\tilde{p}_\mu}\,\dot{\chi}_\mu^{n+\theta} - \mathbf{B}^T_{\tilde{p}_\mu}\,\boldsymbol{\mathcal{V}}_\mu^{\,n+\theta}\right) d\Omega_\mu\right]}_{\mathbf{H}^{n+\theta}_{\mu,\,h}} \cdot \delta\dot{\tilde{\tilde{\mathbf{p}}}}_\mu = 0, \;\; \forall\,\delta\dot{\tilde{\tilde{\mathbf{p}}}}_\mu \in \tilde{\mathcal{P}}^{\text{Per}}_{\mu,\,h},\; \text{with } \dot{\tilde{\tilde{\mathbf{u}}}}_\mu \in \tilde{\mathcal{U}}^{\text{Per}}_{\mu,\,h} \text{ and } \tilde{\tilde{\mathbf{p}}}_\mu \in \tilde{\mathcal{P}}^{\text{Per}}_{\mu,\,h}\,, \tag{B.30}$$

where $\mathbf{B}_{\tilde{u}_\mu} = \nabla^{sym}_y\,\mathbf{N}_{\tilde{u}_\mu}$ and $\mathbf{B}_{\tilde{p}_\mu} = \nabla_y\,\mathbf{N}_{\tilde{p}_\mu}$, are the micro-scale global matrices relating the primal variables with their corresponding gradients.

The numerical solution for nodal values of displacements, $\tilde{\tilde{\mathbf{u}}}_\mu^{t_{n+1}}$, and pore pressure fluctuations, $\tilde{\tilde{\mathbf{p}}}_\mu^{t_{n+1}}$, at current time step t^{n+1}, is obtained in terms of the iterative increments $\Delta\tilde{\tilde{\mathbf{u}}}_\mu$ and $\Delta\tilde{\tilde{\mathbf{p}}}_\mu$, respectively. They are computed by using a standard Newton-Raphson procedure applied to the system of Eqs. (B.29)-(B.30). In this sense, for a generic "k"-iteration it can be expressed (subscript h is omitted hereafter)

$$\begin{aligned} &\left\{\mathbf{J}^{n+\theta}_{\mu,\,k}\,\begin{bmatrix}\Delta\tilde{\tilde{\mathbf{u}}}_\mu\\ \Delta\tilde{\tilde{\mathbf{p}}}_\mu\end{bmatrix} + \begin{bmatrix}\dot{\mathbf{G}}^{n+\theta}_{\mu,\,k}\\ \mathbf{H}^{n+\theta}_{\mu,\,k}\end{bmatrix}\right\} \cdot \begin{bmatrix}\delta\dot{\tilde{\tilde{\mathbf{u}}}}_\mu\\ \delta\tilde{\tilde{\mathbf{p}}}_\mu\end{bmatrix} = \begin{bmatrix}0\\0\end{bmatrix}, \\ &\forall\;\delta\dot{\tilde{\tilde{\mathbf{u}}}}_\mu \in \tilde{\mathcal{U}}^{\text{Per}}_{\mu},\; \forall\;\delta\tilde{\tilde{\mathbf{p}}}_\mu \in \tilde{\mathcal{P}}^{\text{Per}}_{\mu},\; \text{with } \Delta\tilde{\tilde{\mathbf{u}}}_\mu \in \tilde{\mathcal{U}}^{\text{Per}}_{\mu},\; \text{and } \Delta\tilde{\tilde{\mathbf{p}}}_\mu \in \tilde{\mathcal{P}}^{\text{Per}}_{\mu}, \end{aligned} \tag{B.31}$$

$\mathbf{J}^{n+\theta}_{\mu,\,k}$ being the Jacobian operator in the micro-scale, which has the form (subscript *"k"* is removed to simplify the notation)

$$\mathbf{J}^{n+\theta}_{\mu} = \begin{bmatrix}\frac{\partial\dot{\mathbf{G}}^{n+\theta}_{\mu}}{\partial\tilde{\tilde{\mathbf{u}}}^{n+1}_{\mu}} & \frac{\partial\dot{\mathbf{G}}^{n+\theta}_{\mu}}{\partial\tilde{\tilde{\mathbf{p}}}^{n+1}_{\mu}}\\ \frac{\partial\mathbf{H}^{n+\theta}_{\mu}}{\partial\tilde{\tilde{\mathbf{u}}}^{n+1}_{\mu}} & \frac{\partial\mathbf{H}^{n+\theta}_{\mu}}{\partial\tilde{\tilde{\mathbf{p}}}^{n+1}_{\mu}}\end{bmatrix} = \begin{bmatrix}\frac{1}{\Delta t}\,\mathbf{K}_\mu & -\frac{\beta}{\Delta t}\,\mathbf{Q}_\mu\\ \frac{1}{\Delta t}\,(\mathbf{Q}_\mu)^T & \left(\frac{\beta}{\Delta t}\,\mathbf{S}_\mu + \theta\,\boldsymbol{\mathcal{K}}_\mu\right)\end{bmatrix}. \tag{B.32}$$

The matrices $\mathbf{K}_\mu$, $\mathbf{Q}_\mu$, $\mathbf{S}_\mu$ and $\boldsymbol{\mathcal{K}}_\mu$, that conform the Jacobian in (B.32), can be found in Reinaldo A. et al. [66], Anonis et al. [67].

B.6. Scope of constitutive formulations based on ROE

We present below a brief discussion on the possible scope of our formulation when applied to multiscale modeling based on the RVE concept of different physical phenomena such as transient heat conduction (Larsson et al. [13], Özdemir et al. [71], Ramos et al. [72], Waseem et al. [73]) or mass conservation of ion species (coupled to other phenomena) (Saeedmonir et al. [54], Kaessmair et al. [84]), among others. Although the present work deals with multiscale modeling of porous media, the resemblance between the mass balance equation presented here and the balance of other physical quantities allows us to advance in this analysis.

Thus, in the author's opinion, whenever one attempts to model by means of multiscale methodology based on RVE physical phenomena that satisfy the conditions mentioned below, there will be a dependence on the RVE size and the loss of objectivity in the macro-scale response. The conditions are:

(i) that both the macro- and micro-scale are described by strong-form governing equations of the type

$$\begin{aligned} \dot{\chi} + \nabla \cdot \mathbf{w} = 0 \,, \\ \dot{\chi}_\mu \left(\dot{p}_\mu\right) + \nabla_\mu \cdot \mathbf{w}_\mu = 0 \,, \end{aligned} \tag{B.33}$$

(ii) and in addition there is a constitutive functional dependence of the type $\dot{\chi}_\mu \left(\dot{p}_\mu^{\text{FOE}}\right) = \dot{\chi}_\mu \left(\dot{p} + \dot{\varphi} \cdot \mathbf{y} + \dot{\tilde{p}}_\mu\right)$ (only the functional dependence of χ_μ is expressed because it is the relevant for the purpose of this discussion).

The reason, is that under these conditions expressions like those given in (B.15) are reached, which in the presence of a full order expansion of $\dot{p}_\mu^{\text{FOE}}$ will lead to the defect explained at length in the preceding sections. On the other hand, if one assumes the constitutive ROE functional $\dot{\chi}_\mu \left(\dot{p}_\mu^{\text{ROE}}\right) = \dot{\chi}_\mu \left(\dot{p} + \dot{\tilde{p}}_\mu\right)$, one recovers the objectivity of the response, as will be demonstrated to the case of saturated porous media in the present work.

However, equations of the type (B.33) can be employed in the analysis of so many other physical phenomena individually or coupled as we mentioned at the beginning, for example the cases of transient heat conduction with $\mathbf{w}$ being the heat flux field and $\dot{\chi}$ the specific internal energy rate dependent on the temperature field or $\mathbf{w}$ the molar flux of species and $\dot{\chi}$ the ion concentration rate.

Therefore, we argue that the ROE constitutive formula is applicable to all these cases and its scope goes beyond the one proposed here.

B.7. Consolidation examples

The macro-scale domain consists of a soil column with a height of $H = 1$ m and a width of $W = 0.1m$. At this scale, the material is treated as a homogenized medium. The boundary conditions are illustrated in Figure B.1. At the ground surface, a compressive external traction is applied, increasing from $0kPa$ to $-100kPa$ during the first day of analysis, and thereafter remaining constant. The macro-scale domain is discretized into 13 finite elements, as shown in Figure B.1-(b). The time discretization employed throughout the analysis follows the sequence: $t = [0.001, 0.002, \ \ldots, 0.009, 0.01, 0.02, \ldots, 0.09, 0.1, 0.2, \ldots, \ 0.9, 1, 2, \ldots, 9, 10, 20, \ldots, 70, 80]$ (in days). At the micro-scale, the periodic multiscale model is adopted. The heterogeneous material properties are defined as follows. For the matrix: Young's modulus $E = 100kPa$, Poisson's ratio $\nu = 0.3$, isotropic hydraulic conductivity $k = 8.64 \times 10^{-4} \frac{m}{day}$, and initial void ratio $e_0 = 0.6$. For the inclusion: Young's modulus $E = 1500kPa$, Poisson's ratio $\nu = 0.3$ isotropic hydraulic conductivity $k = 1.296 \times 10^{-4} \frac{m}{day}$, and initial void ratio $e_0 = 2.0$. Different micro-cells (MCs) of increasing size are considered to obtain homogenized responses using both FOE and ROE formulations. Specifically, square MCs of sizes $0.1m \times 0.1m$, $0.5m \times 0.5m$,

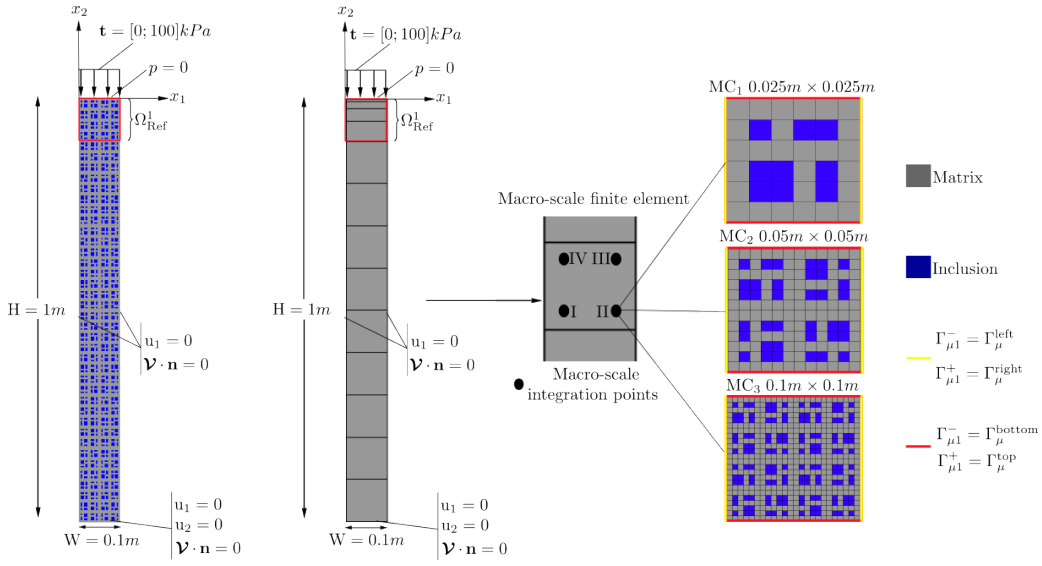

Figura B.1: : Schematic representation of the problem to be solved

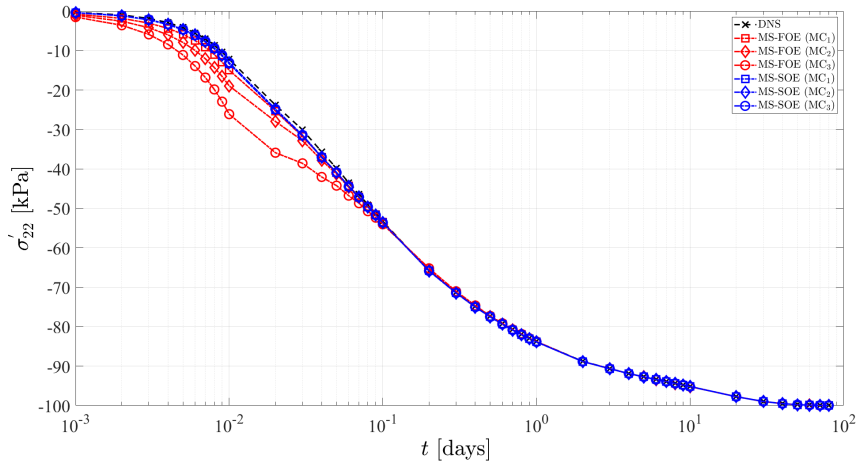

Figura B.2: Time-evolution curves of the vertical component of the effective stress tensor at the reference area Ω^1_{Ref}.

and $1m \times 1m$ are analyzed. Each MC is discretized with 36, 144, and 576 finite elements, respectively. For the Direct Numerical Simulation (DNS), see Figure B.1(a), the spatial discretization required a mesh of approximately 5760 finite elements (mesh not drawing). Figure B.2 presents the time-evolution curves of the vertical component of the effective stress tensor at the reference area Ω^1_{Ref}. The results reveal that micro-scale size sensitivity manifests in the homogenized stress response when the FOE-based multiscale procedure is employed. The FOE model systematically underestimates the effective stress compared to DNS, with discrepancies becoming significant for the two largest micro-cells. In contrast, the SOE-based homogenization yields effective stress curves that are in good agreement with the DNS results, independently of the micro-cell size. The size effect associated with the FOE procedure is even more pronounced for the homogenized seepage velocity. This is illustrated in Figure B.3, where the temporal evolution of seepage velocity is compared among the different models at Ω^1_{Ref}. As expected, for the two largest micro-cells the FOE scheme produces results that markedly deviate from the DNS reference solution, while the SOE formulation provides consistent predictions.

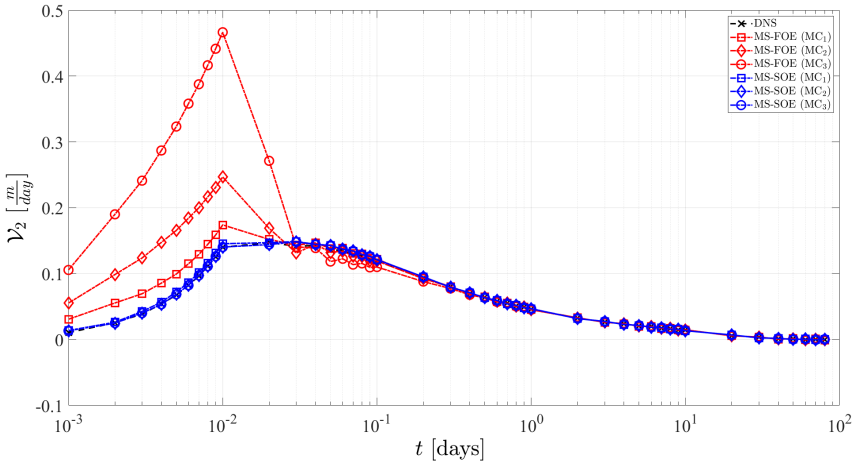

Figura B.3: Time-evolution curves of the vertical component of the seepage velocity at the reference area Ω^1_{Ref}.

B.8. Conclusions

A multiscale model of saturated porous media based on RVE has been presented. In the literature, multiscale models applied to saturated porous media have revealed some inconsistency with respect to the dependence of the micro-scale size. This drawback has been attributed to a second-order term. More specifically, to the seepage or flux velocity. The consistent PMVP-based homogenization model adopted in this work has allowed us to identify that the size effect of the RVE is caused only by one component of the flux velocity term. This component comes from the use of a full expansion of the micro-scale pore pressure at the constitutive level on the fine scale. Thus, a redefinition of the constitutive equations at the micro-scale has been proposed. This is based on a reduced-order expansion of the micro-scale pore pressure field to overcome the problem of dependence on the size of the RVE. But in addition, it is possible to maintain the dynamical term that arises during the homogenization process, and finally, it also preserves the principle of scale separation.

Acknowledgments

This work was partially supported by the Consejo Nacional de Investigaciones Cientficas y Tecnicas (CONICET, Argentina, grant PIP 2023-2025-GI-11220220100332CO) as well as Secretaria de General de Ciencia y Tecnica de la Universidad Nacional del Nordeste (UNNE), Argentina (Grants PI 21D003). Also, the authors would like to acknowledge the financial support from the Agencia Nacional de Promoción Científica y Tecnológica (ANPCyT, Argentina, grants PICTO-UNNE-2019-00014 and PICT 2021-GRF-TI-00488).

Apéndice C

About the micro-scale size effect in the multiscale formulation of generic balance problems with source terms

Reinaldo A. Anonis, Javier L. Mroginski, Sebastián Toro, Rodrigo Rossi, Pablo J. Sánchez, (2026). About the micro-scale size effect in the multiscale formulation of generic balance problems with source terms. Under review.

About the micro-scale size effect in the multiscale formulation of generic balance problems with source terms

Anonis, Reinaldo A.[1,1], **Mroginski, Javier L.**[1], **Toro, Sebastián**[2], **Rossi, Rodrigo**[3] **Sánchez, Pablo J.**[2,4]

[1]LAMEC-IMIT-CONICET Laboratorio de Mecánica Computacional, Universidad Nacional del Nordeste, Las Heras 727, CP 3500 Chaco, Argentina
[2]CIMEC-UNL-CONICET, Ruta Nac. 168, Km 0, Paraje el Pozo, CP 3000 Santa Fe, Argentina
[3]Departamento de Engenharia Mecânica, Universidade Federal do Rio Grande do Sul, Rua Sarmento Leite, 425, Porto Alegre, 90046-902, RS, Brazil
[4]GIMNI-UTN-FRSF, Lavaise 610, CP 3000 Santa Fe, Argentina

Keywords: multiscale formulations, balance problems, source term, First-Order homogenization, micro-scale size effect, macroscopic objectivity.

Abstract. In the literature, various physical phenomena described by balance equations of a scalar quantity with source terms have been addressed using multiscale formulations based on First-Order homogenization approaches. In such problems, the presence of the transient term induces a dependence of the macroscopic response with respect to the micro-scale domain size. This has led to the widespread use of the expression "second-order effect"to refer to the implications of homogenizing the transient term. The aim of this work is to clarify the origin and nature of this issue. First, we highlight a consequence that raises questions regarding the classical interpretation of the Representative Volume Element (RVE) concept. Subsequently, the homogenization of the transient term is meticulously deconstructed into components. According to this analysis, an alternative formulation based on a constitutive intervention is proposed to ensure objectivity of the macro-scale response. This proposition preserves the modeling richness of the First-Order homogenization by appealing to the concept of expansions of different orders solely at the micro-scale constitutive level. The ideas presented in this contribution are corroborated analytically and verified numerically through simple multiscale modeling scenarios.

C.1. Introduction

To gain deeper insight into advanced engineering problems, numerous scientific disciplines investigate the behavior of complex materials and multiphysics phenomena using multiscale methodologies. According to Hill's original proposal [1], the existence of a minimum micro-structural domain, beyond which the macroscopic response becomes insensitive to its size, constitutes one of the fundamental principles underlying First-Order homogenization techniques. Such a specific micro-scale domain is commonly referred to as the Representative Volume Element (RVE).

In particular, the study of homogenization for various specialized cases of balance problems of a scalar quantity has undergone significant development over the last decade.

For instance, the heat conduction problem was addressed by Özdemir et al. [71], who simplified the analysis by assuming a stationary state for the micro-scale temperature field, based on the premise that heat storage at the micro-scale is negligible due to the small size of this domain. Subsequently, Larsson et al. [13] proposed a variational framework for First-Order homogenization of this problem, and Runesson and Larsson [15] extended the approach to time-dependent situations, explicitly including the effect of the internal energy rate at the micro-scale. They demonstrated that the homogenization of micro-scale transient contribution becomes size-dependent, modifying the effective response whenever the micro-scale is not negligibly small. In other words, the upscale averaging process generates second-order effects.

[1]Corresponding author. E-mail address: ranonis@ing.unne.edu.ar (Anonis, Reinaldo A.).

Later, Ramos et al. [72] developed a homogenization model that includes heat generation at both macro- and micro-scales. They also recognize size-dependent results that arise in the macroscopic description, and were the first to coin the expression "thermal inertia"to denote the term from which the size effect arises in transient thermal models. More recently, Waseem et al. [73] constructed a reduced-order model, emphasizing that the scale separation or coupling depends on the relationship between characteristic diffusion times and the loading time. This analysis showed that in regimes lacking clear scale separation, significant micro-scale transient effects emerge and must be considered during homogenization. Both papers underscore the importance and necessity of accounting for the microscopic thermal inertia consequences in transient heat conduction problems. In addition, Zhi et. al. [114] addressed the multiscale modeling of thermal problems using the Direct FE^2 method, noting that in certain cases the temperature is affected by the size of the micro-scale. They further indicated that, depending on the problem, a transient RVE formulation may be necessary to capture the effects of micro-scale thermal inertia.

Additionally, other authors have addressed balance problems in heterogeneous media through First-Order homogenization. Kaessmair and Steinmann [17] investigated species transport, identifying micro-scale inertia effects similar to those found in thermal problems. Waseem et al. [79] studied species diffusion cases in solids and, subsequently in [80], proposed a data-driven reduced-order homogenization approach aimed at capturing diffusional phenomena. In turn, Rollin et al. [81] addressed diffusion in composite materials, although assuming a stationary micro-structure.

In addition, phenomena governed by balance equations for scalar quantities with source terms coupled with other physical processes, such as chemo-mechanics [82–85] and electrochemical ion transport [86], have also been treated using computational homogenization techniques, although in the latter case, transient micro-scale diffusion effects were neglected.

Moreover, within the framework of First-Order computational homogenization of coupled phenomena, extensive research has been conducted on hydro-mechanical problems [14, 16, 48–51, 53, 66, 67, 75–78, 82, 84], thermo-hydro-mechanical cases [52] and chemo-hydro-mechanical examples [54], where the presence of transient terms, once again, introduces a dependence on the micro-scale size.

All the aforementioned contributions highlight the physical importance of the transient term derived from the homogenization process applied to generic balance problems of a scalar quantity. The present work aims to provide clarity on the consequences of this term, pointing out how it can introduce dependence on the micro-scale size, thereby affecting the objectivity of the macro-scale response. Such an induced second-order effect may be regarded as a non-trivial feature when the primary objective is the formulation of a fully First-Order homogenization approach at the macro-scale. As a distinctive contribution of this work, we provide rigorous evidence on this topic through analytical solutions derived from very simplified multiscale settings. These theoretical developments enable us to identify and characterize the origin and underlying nature of the problem. Furthermore, an approach that eliminates the components responsible for the micro-scale size dependence is proposed, while preserving the relevant contributions of the transient flux.

To emphasize the scope of the present work, a generic scalar balance problem with source terms is considered, grounded in concepts introduced in the authors' recent contributions [66, 67]. Hence, the conclusions drawn herein are applicable to multiple areas of physical relevance.

The present multiscale model is formulated following the framework posited by the Method of Multiscale Virtual Power (MMVP) [19, 20], a unified methodology that has proven effective for treating various physical phenomena [21–24, 26]. The MMVP provides a solid theoretical basis and a systematic procedure to construct consistent RVE-based multiscale methodologies. Finally, the FE^2 finite element approach [5] is adopted to develop the computational model.

The organization of the work is outlined below. In Section C.2, the macro-scale governing equations are presented. Next, in Section C.3, the Method of Multiscale Virtual Power (MMVP) is followed, introducing concepts that ensure the admissibility of the scales and the link between them by means of an

extension to the Hill-Mandel principle applied to balance problems. In Section C.4, the corresponding specifications of the constitutive laws for the fine-scale problem are provided. Two approaches, called Full-Order Expansion (FOE) and Selective-Order Expansion (SOE) models, are introduced, based on the treatment given to the input arguments in the constitutive functionals. In C.5, a detailed theoretical analysis is performed to examine the dependence of the macroscopic response on the size of the micro-scale. Some simple scenarios with analytical solutions are proposed in Section C.6 to demonstrate the lack of objectivity in the macro-scale response. Then, in Section C.7, the spatial and temporal discretization methods used to approximate the variational forms of balance at both scales are addressed. Simple numerical examples, which verify and demonstrate the developments presented in the paper, are given in Section C.8. Finally, some conclusions are presented in Section C.9. The article concludes with six appendices that provide complementary mathematical developments for the present multiscale formulation.

C.2. Governing equations of the macro-scale

C.2.1. Basic assumptions of the macro-scale model

An open/bounded domain $\Omega \in \mathbb{R}^{nd}$ is used to describe a general balance problem of a scalar quantity with source terms, at macro-scale, nd being the considered spatial dimension. Each point of Ω is identified through its position vector $\mathbf{x}$, referenced to a Cartesian coordinate system. The smooth boundary of Ω is Γ while $\mathbf{n}$ denotes the corresponding outward normal versor, see Figure C.1. Given the inherently time-dependent nature of physical phenomena, a monotonically increasing parameter t is introduced to characterize the ordered progression of events.

The state of the medium is described through the primary scalar field $\phi(\mathbf{x},t)$, with $\mathbf{g}(\mathbf{x},t) = \boldsymbol{\nabla}\phi(\mathbf{x},t)$ being its associated gradient vector. Besides, a scalar function $S(\phi,t)$ is included to model the source mechanism [2] in Ω. To complete the physics of the balance problem, two additional fields are considered, namely: the scalar rate field $\dot{\xi}(\mathbf{x},t)$ and the flux vector field $\mathbf{Q}(\mathbf{x},t)$, see Figure C.1. They are the corresponding constitutive material responses and power-conjugate quantities with respect to primal variables $\phi(\mathbf{x},t)$ and $\mathbf{g}(\mathbf{x},t)$, respectively. Until the end of this section, the functional dependencies are omitted for simplicity.

To incorporate external environmental interactions at the boundary Γ, it is partitioned into subsets where Dirichlet- and Neumann-type boundary conditions are imposed. Specifically, a prescribed function $\phi = \phi_{\mathrm{D}}$ is enforced over the Dirichlet boundary $\Gamma_{\mathrm{D}}, \forall t$. Conversely, an external generalized flux, defined as $q = \mathbf{Q}\cdot\mathbf{n}$, may be applied on the Neumann boundary subset $\Gamma_{\mathrm{N}}, \forall t$, see Figure C.1. The subdomains Γ_{D} and Γ_{N} complete the entire boundary Γ, and they are mutually exclusive ($\Gamma = \Gamma_{\mathrm{D}}\cup\Gamma_{\mathrm{N}}, \Gamma_{\mathrm{D}}\cap\Gamma_{\mathrm{N}} = \varnothing$).

In addition to boundary interactions, initial conditions for the primary scalar field $\phi = \phi^0$ must be completely defined at the beginning of the analysis, that is, at $t = 0, \forall \mathbf{x} \in \Omega$.

C.2.2. Strong form of the macro-scale balance equations

The differential form of the generic balance equation for a scalar quantity with source terms can be written as

$$\begin{cases} \mathrm{Div}\,\mathbf{Q} + \dot{\xi} - S = 0, \quad \forall \mathbf{x} \in \Omega, \quad \forall t, \\ \mathbf{Q}\cdot\mathbf{n} = q, \quad \forall \mathbf{x} \in \Gamma_{\mathrm{N}}, \quad \forall t. \end{cases} \tag{C.1}$$

Equation (C.1)-(a) governs the balance of the primary scalar field ϕ, while (C.1)-(b) stands for the Neumann-type boundary conditions, as defined above. The system of equations (C.1), together with Dirichlet constraints and initial conditions constitutes the strong form of the problem, at the upper scale.

[2] The function S may represent internal generation and/or externally imposed source terms per unit volume.

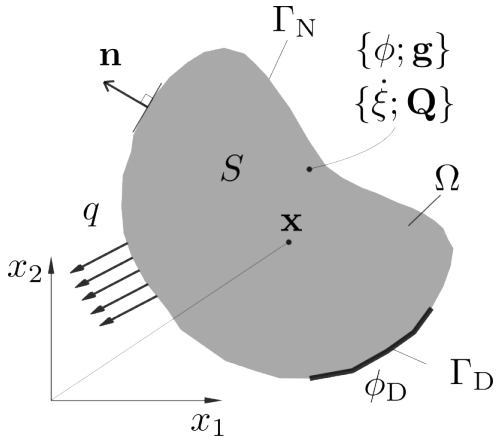

Figura C.1: Macro-scale model layout and nomenclature for a First-Order generic balance problem of a scalar quantity with source terms.

C.2.3. Admissibility in a weak sense

The concept of weak admissibility for the primary field $\phi \in \mathcal{T}(\Omega)$, at the macro-scale level, is defined through the set $\mathcal{T}(\Omega) \equiv \{\phi \in \mathrm{H}^1(\Omega),\ \phi = \phi_{\mathrm{D}}\ \forall \mathbf{x} \in \Gamma_{\mathrm{D}}\}$, where $\mathrm{H}^1(\Omega)$ represents the space of all functions with first derivative squared-integrable. The corresponding linear space for the virtual actions $\delta\phi \in \mathcal{T}^*(\Omega)$ is: $\mathcal{T}^*(\Omega) \equiv \{\delta\phi \in \mathrm{H}^1(\Omega),\ \delta\phi = 0\ \forall \mathbf{x} \in \Gamma_{\mathrm{D}}\}$[3].

C.2.4. Weak form of the macro-scale balance equations

Starting from the differential format given in equation (C.1), and considering the virtual admissible actions $\delta\phi$ and their gradients $\delta\mathbf{g}$, the variational statement of the balance equation at the upper length scale can be enunciated as: find the field $\phi \in \mathcal{T}(\Omega)$ such that:

$$\mathrm{E} = \int_{\Omega} \left[(\dot{\xi} - S)\ \delta\phi - \mathbf{Q} \cdot \delta\mathbf{g} \right] d\Omega + \int_{\Gamma_{\mathrm{N}}} q\ \delta\phi\, d\Gamma = 0,\ \forall\, \delta\phi \in \mathcal{T}^*(\Omega),\ \forall\, t. \tag{C.2}$$

C.2.5. Constitutive equations of the macro-scale

Constitutive relations for quantities $\{\mathbf{Q}, \dot{\xi}, S\}$ are required to close the macro-scale governing equations. In the present contribution such material laws emerge from a homogenization procedure, as detailed later.

From the variational view point, the macro-scale model described in this section constitutes a First-Order approach to the balance problem, in the sense that only virtual dual products involving the primary field and its first-order gradient take part in the weak form (C.2). Even so, in this class of models, second-order effects could arise whenever the constitutive laws for $\{\mathbf{Q}, \dot{\xi}, S\}$ incorporate, for instance, nonlocal phenomena or higher-order gradients as input arguments. A formal way to deal with these enhanced features is by assuming the existence of a characteristic length, ℓ_{ch}, at which the second-order effects occur in the medium; that is, ℓ_{ch} represents a new, finite, material parameter with a clear physical meaning. The term Fully First-Order approach is used to denote a First-Order model (in the variational sense) in which the constitutive responses do not incorporate second-order effects, as the underlying materials lack a characteristic parameter with an evident physical significance. The main objective of this work is to develop a Fully First-Order multiscale scheme for generic problems ruled by balance equations of scalar quantities with source terms.

[3]The symbol δ preceding any entity is used throughout the manuscript to denote its spatial virtual variation.

C.3. Multiscale model for generic balance problems

Following the variational framework of the Method of Multiscale Virtual Power (MMVP) [19–21], an RVE-based homogenization model for a general balance problem is developed in this section.

C.3.1. Basic assumptions of the micro-scale model

To identify micro-scale objects, the same nomenclature is used and the same physical meaning described for the macro-scale is retained, with the only difference consisting of the addition of the subscript $(\bullet)_\mu$. Thus, an open/bounded set $\Omega_\mu \in \mathbb{R}^{nd}$ is defined, representing a relatively small, finite portion of the material microstructure, hereafter referred to as the Micro-Cell (MC). A Cartesian coordinate system is also considered in the lower length scale; hence each point of Ω_μ can be identified through its corresponding position vector $\mathbf{x}_\mu$. The boundary of Ω_μ is Γ_μ, with outward versor $\mathbf{n}_\mu$, see Figure C.2. Additionally, the primary scalar field $\phi_\mu(\mathbf{x}_\mu, t)$ is introduced to describe the state of Ω_μ.

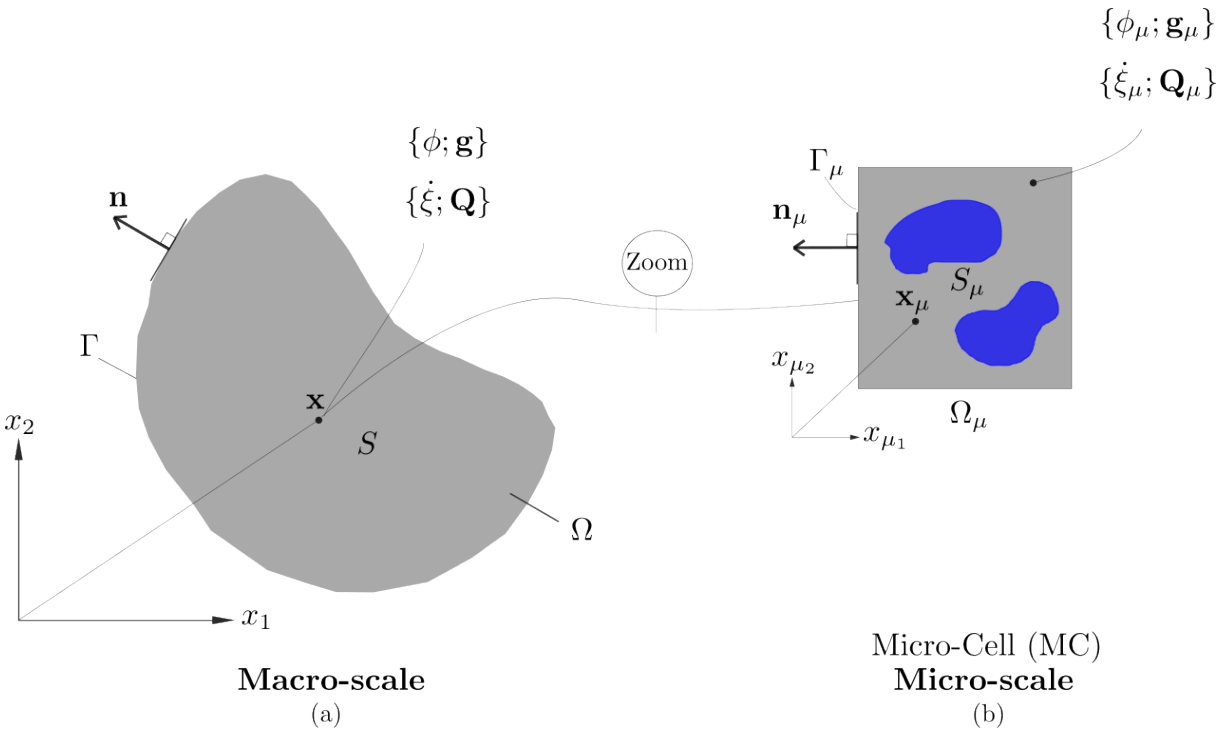

Figura C.2: Basic ingredients of a First-Order multiscale model based on the RVE concept.

One of the basic ideas inherent to homogenization models is the physical connection between each point $\mathbf{x}$, in the macro-scale, with a corresponding Micro-Cell Ω_μ. Before introducing the complete set of scale-bridging equations, it is important to discuss the concept of admissibility for the primitive descriptors (that is, the scalar primary field and its gradient) across the two scales involved. Admissibility is established through two sequential steps: (i) the insertion process [24] presented in Section (C.3.2) and (ii) the homogenization procedure [22] described in Section (C.3.3).

C.3.2. Insertion at the Micro-Cell

This section establishes how the macro-scale primal descriptors play a role in the micro-scale balance problem. Departing from the macroscopic point-valued quantities at any time t, here denoted for simplicity as $\{\phi(t), \mathbf{g}(t)\}$, the micro-scale scalar primary field $\phi_\mu(\mathbf{x}_\mu, t)$ in each MC is constructed based on a

Taylor-like expansion rule as

$$\phi_\mu(\mathbf{x}_\mu, t) = \phi\,(t) + \mathbf{g}\,(t)\ \cdot\ \mathbf{x}'_\mu + \tilde{\phi}_\mu\,(\mathbf{x}_\mu, t)\,, \quad \forall \mathbf{x}_\mu\ \in\ \Omega_\mu, \quad \forall t. \tag{C.3}$$

Note that, in accordance with the First-Order approach assumed at the upper scale, the two macro-scale (point-valued) primary descriptors $\{\phi(t), \mathbf{g}(t)\}$ are transferred to the MC domain; in particular through a uniform and a linear distribution, see the first and second terms in expression (C.3), respectively. Such an assumption is commonly referred to in the literature as a First-Order Homogenization scheme. On the other hand, $\tilde{\phi}_\mu$ (see the third contribution in equation (C.3)) represents the fluctuation of the scalar primary field in the MC, an additional term observable only at the smaller length scale, introduced to account for material heterogeneities in the multiscale model. The vector $\mathbf{x}'_\mu = \mathbf{x}_\mu - \mathbf{x}^G_\mu$ is a convenient auxiliary coordinate translation, $\mathbf{x}^G_\mu$ being a constant that will be defined later (see expression (C.9)).

From (C.3), the micro-scale gradient vector, $\mathbf{g}_\mu\,(\mathbf{x}_\mu, t)$, can be expressed as follows

$$\begin{aligned}\boldsymbol{\nabla}_{\mathbf{x}_\mu}\phi_\mu\,(\mathbf{x}_\mu, t) = \mathbf{g}_\mu\,(\mathbf{x}_\mu, t) &= \mathbf{g}\,(t) + \boldsymbol{\nabla}_{\mathbf{x}_\mu}\tilde{\phi}_\mu\,(\mathbf{x}_\mu, t) \\ &= \mathbf{g}\,(t) + \tilde{\mathbf{g}}_\mu\,(\mathbf{x}_\mu, t)\,, \quad \forall \mathbf{x}_\mu\ \in\ \Omega_\mu, \quad \forall t,\end{aligned} \tag{C.4}$$

where the operator $\boldsymbol{\nabla}_{\mathbf{x}_\mu}(\bullet)$ represents the gradient concerning $\mathbf{x}_\mu$-coordinates.

In order to simplify the notation, the arguments denoting spatial and time dependencies are suppressed in the subsequent developments.

For convenience, we express (C.3)-(C.4) in an equivalent compact form by introducing the generic array $\boldsymbol{\Phi} = [\phi,\, \mathbf{g}]^T$, which collects the point-valued macro-scale primary descriptors, together with the corresponding linear insertion operators $\mathcal{I}_\phi$ and $\mathcal{I}_\mathbf{g}$ used to define the micro-scale primary field and its gradient, respectively. Thus, (C.3)-(C.4) can be rewritten as

$$\phi_\mu = \mathcal{I}_\phi\ \boldsymbol{\Phi} + \tilde{\phi}_\mu, \quad \text{with} \quad \mathcal{I}_\phi = [1,\, \mathbf{x}'_\mu] \tag{C.5}$$

$$\mathbf{g}_\mu = \mathcal{I}_\mathbf{g}\ \boldsymbol{\Phi} + \tilde{\mathbf{g}}_\mu, \quad \text{with} \quad \mathcal{I}_\mathbf{g} = [0,\, 1] \tag{C.6}$$

The above definitions (C.3)-(C.6) can also be established in rate forms.

C.3.3. Homogenization at the Micro-Cell.

Two homogenization procedures are defined, through operators $\mathcal{H}_\phi$ and $\mathcal{H}_\mathbf{g}$, which map the micro-scale scalar primary field ϕ_μ and its gradient $\mathbf{g}_\mu$ into the corresponding point-valued macro-scale quantities ϕ and $\mathbf{g}$, respectively.

C.3.3.1. Primary scalar field homogenization

The scalar field homogenization rule, denoted as $\mathcal{H}_\phi$, states that the average of the micro-scale primal field over the entire MC domain, Ω_μ, must be equal to the macro-scale primal field

$$\mathcal{H}_\phi\,(\phi_\mu) = \phi = \frac{1}{|\Omega_\mu|}\int_{\Omega_\mu} \phi_\mu\, d\Omega_\mu. \tag{C.7}$$

Substituting (C.3) in (C.7) it is obtained

$$\phi = \phi + \mathbf{g}\ \cdot\ \left[\frac{1}{|\Omega_\mu|}\int_{\Omega_\mu} \mathbf{x}'_\mu\, d\Omega_\mu\right] + \frac{1}{|\Omega_\mu|}\int_{\Omega_\mu} \tilde{\phi}_\mu\, d\Omega_\mu. \tag{C.8}$$

Since (C.8) must hold even for a homogeneous micro-scale fluctuation field (that is, $\tilde{\phi}_\mu = 0\ \forall \mathbf{x}_\mu\ \in$

Ω_μ), this leads to

$$\mathbf{x}_\mu^G = \frac{1}{|\Omega_\mu|}\int_{\Omega_\mu} \mathbf{x}_\mu \, d\Omega_\mu, \tag{C.9}$$

where $\mathbf{x}_\mu^G$ identifies the position of the MC barycenter with respect to the global coordinate system at the smaller length scale. Introducing (C.9) into (C.8), a first restriction to be imposed on $\tilde{\phi}_\mu$ is derived

$$\int_{\Omega_\mu} \tilde{\phi}_\mu \, d\Omega_\mu = 0. \tag{C.10}$$

C.3.3.2. Vector gradient field homogenization

The homogenization rule for the micro-scale vector gradient field, $\mathcal{H}_{\mathbf{g}}$, results in

$$\mathcal{H}_{\mathbf{g}}\left(\mathbf{g}_\mu\right) = \mathbf{g} = \frac{1}{|\Omega_\mu|}\int_{\Omega_\mu} \mathbf{g}_\mu \, d\Omega_\mu = \frac{1}{|\Omega_\mu|}\int_{\Omega_\mu} \boldsymbol{\nabla}_{\mathbf{x}_\mu}\phi_\mu \, d\Omega_\mu. \tag{C.11}$$

Then, by replacing (C.4) in (C.11) and applying Green's theorem, another constraint for $\tilde{\phi}_\mu$-field is deduced

$$\int_{\Gamma_\mu} \tilde{\phi}_\mu \, \mathbf{n}_\mu \, d\Gamma_\mu = \mathbf{0}. \tag{C.12}$$

C.3.3.3. Admissibility concept for the primary fluctuation field in the micro-scale

Previously, the two integral constraints to be imposed on the primary scalar fluctuation field have been established, see (C.10) and (C.12). A field $\tilde{\phi}_\mu$ is considered admissible only if it satisfies these conditions, being compatible with the homogenization procedures outlined in (C.7) and (C.11). This leads to the definition of the admissible space $\widetilde{\mathcal{T}}_\mu(\Omega_\mu)$, for $\tilde{\phi}_\mu$, which characterizes the so-called Minimally Constrained Multiscale Model (MCMM) [12, 19, 27]

$$\widetilde{\mathcal{T}}_\mu\left(\Omega_\mu\right) = \left\{\tilde{\phi}_\mu \ \in \ \mathrm{H}^1\left(\Omega_\mu\right); \int_{\Omega_\mu} \tilde{\phi}_\mu \, d\Omega_\mu = 0; \int_{\Gamma_\mu} \tilde{\phi}_\mu \, \mathbf{n}_\mu \, d\Gamma_\mu = \mathbf{0}\right\}. \tag{C.13}$$

Alternative and more constrained homogenization schemes for $\tilde{\phi}_\mu$ can be built from any sub-space $\widetilde{\mathcal{T}}_\mu^{\square}\left(\Omega_\mu\right)$ of $\widetilde{\mathcal{T}}_\mu\left(\Omega_\mu\right)$ as for example the well-known Taylor, Linear and Periodic sub-models. These approaches were extensively documented in the literature; thus, in order to improve readability, the specific sub-spaces that define them are summarized in Appendix A. On this basis, in a generic multiscale formulation the fluctuation field must satisfy the condition $\tilde{\phi}_\mu \in \widetilde{\mathcal{T}}_\mu^{\square}\left(\Omega_\mu\right) \subseteq \widetilde{\mathcal{T}}_\mu\left(\Omega_\mu\right)$.

Virtual actions at the Micro-Cell domain can be defined taking into account (C.3) and (C.4), as follows

$$\delta\phi_\mu = \delta\phi + \delta\mathbf{g} \cdot \mathbf{x}'_\mu + \delta\tilde{\phi}_\mu, \quad \forall \mathbf{x}_\mu \in \Omega_\mu, \quad \forall t, \tag{C.14}$$

$$\delta\mathbf{g}_\mu = \delta\mathbf{g} + \delta\tilde{\mathbf{g}}_\mu = \delta\mathbf{g} + \boldsymbol{\nabla}_{\mathbf{x}_\mu}\delta\tilde{\phi}_\mu, \quad \forall \mathbf{x}_\mu \in \Omega_\mu, \quad \forall t, \tag{C.15}$$

from which it is possible to introduce the linear space $\widetilde{\mathcal{T}}_\mu^{*}\left(\Omega_\mu\right)$ for admissible virtual fluctuations $\delta\tilde{\phi}_\mu \in \widetilde{\mathcal{T}}_\mu^{*}\left(\Omega_\mu\right)$. The spaces $\widetilde{\mathcal{T}}_\mu^{*}\left(\Omega_\mu\right)$ and $\widetilde{\mathcal{T}}_\mu^{\square}\left(\Omega_\mu\right)$ coincide since constraints (C.10) and (C.12) are both homogeneous.

C.3.4. Hill-Mandel principle for balance problems of a scalar quantity

In this section, the last ingredient in the context of the MMVP is introduced [19, 20]. In balance problems, the physical coupling between the involved scales is provided through a specialized version

of the Hill–Mandel principle, see a schematic diagram in Figure C.2, which can be expressed in the following variational form

$$|\Omega_\mu|\left[(\dot{\xi}-S)\,\delta\phi-\mathbf{Q}\cdot\delta\mathbf{g}\right]=\int_{\Omega_\mu}\Big[\left(\dot{\xi}_\mu-S_\mu\right)\overbrace{\left(\delta\phi+\delta\mathbf{g}\cdot\mathbf{x}'_\mu+\delta\tilde{\phi}_\mu\right)}^{\delta\phi_\mu}$$
$$-\mathbf{Q}_\mu\cdot\underbrace{\left(\delta\mathbf{g}+\boldsymbol{\nabla}_{\mathbf{x}_\mu}\delta\tilde{\phi}_\mu\right)}_{\delta\mathbf{g}_\mu}\Big]\,d\Omega_\mu,\quad\forall\left(\delta\phi\,,\delta\mathbf{g}\,,\delta\tilde{\phi}_\mu\right)\in\mathbb{R}\times\mathbb{R}^{nd}\times\widetilde{\mathcal{T}}^{*}_{\mu}\left(\Omega_\mu\right),\forall\,t.\quad\text{(C.16)}$$

From (C.16) it is evident that a First-Order approach has been adopted to model the balance problem at the smaller length scale, since two virtual duality products, involving the primary variable $\delta\phi_\mu$ and its first gradient $\delta\mathbf{g}_\mu$, contribute to the right-hand side of the Hill–Mandel statement.

An alternative version of the Hill–Mandel postulate, in which all the constraints included in $\widetilde{\mathcal{T}}^{*}_{\mu}\left(\Omega_\mu\right)\equiv\widetilde{\mathcal{T}}^{\square}_{\mu}\left(\Omega_\mu\right)$ were relaxed through the introduction of the corresponding Lagrange Multipliers, is presented in Appendix B.

C.3.4.1. Consequences of the Hill–Mandel principle

Applying standard variational procedures in (C.16), the corollaries of the Hill–Mandel statement are obtained, namely: (i) the homogenization formulae for the macro-scale entities $\{\mathbf{Q},\dot{\xi},S\}$ and (ii) the weak form of balance equation at the smaller length scale. These results are enunciated in the following.

Homogenized flux vector:

$$\mathbf{Q}=\frac{1}{|\Omega_\mu|}\int_{\Omega_\mu}\mathbf{Q}_\mu\,d\Omega_\mu-\frac{1}{|\Omega_\mu|}\int_{\Omega_\mu}\left(\dot{\xi}_\mu-S_\mu\right)\mathbf{x}'_\mu\,d\Omega_\mu,\;\forall\,t.\quad\text{(C.17)}$$

The first integrand on the right-hand side of equation (C.17) is commonly referred to in the literature as the stationary contribution. In turn, the second term, extensively analyzed in the aforementioned works, is identified as the transient counterpart and is the main contributor to second-order effects at the macro-scale. Accordingly, the homogenized flux vector can be decomposed as

$$\mathbf{Q}_{sta}=\frac{1}{|\Omega_\mu|}\int_{\Omega_\mu}\mathbf{Q}_\mu\,d\Omega_\mu,\quad\mathbf{Q}_{tra}=-\frac{1}{|\Omega_\mu|}\int_{\Omega_\mu}\left(\dot{\xi}_\mu-S_\mu\right)\mathbf{x}'_\mu\,d\Omega_\mu.\quad\text{(C.18)}$$

The homogenization rule (C.18)-right will be examined in detail in Section C.5, where the influence of the micro-scale size on the effective response is addressed. Furthermore, within highly simplified multiscale modeling scenarios, rigorous evidence of the micro-scale size dependence is provided through analytical deductions in Section C.6.

Homogenized source and time dependent contribution:

$$\dot{\xi}-S=\frac{1}{|\Omega_\mu|}\int_{\Omega_\mu}\left(\dot{\xi}_\mu-S_\mu\right)\,d\Omega_\mu,\;\forall\,t.\quad\text{(C.19)}$$

Variational statement for the balance equation in the MC: find $\tilde{\phi}_\mu\in\widetilde{\mathcal{T}}^{\square}_{\mu}\left(\Omega_\mu\right)$ such that

$$\mathrm{E}_\mu=\int_{\Omega_\mu}\left(\dot{\xi}_\mu-S_\mu\right)\delta\tilde{\phi}_\mu\,d\Omega_\mu-\int_{\Omega_\mu}\mathbf{Q}_\mu\cdot\boldsymbol{\nabla}_{\mathbf{x}_\mu}\delta\tilde{\phi}_\mu\,d\Omega_\mu=0,$$
$$\forall\,\delta\tilde{\phi}_\mu\in\widetilde{\mathcal{T}}^{*}_{\mu}\left(\Omega_\mu\right),\;\forall\,t.\quad\text{(C.20)}$$

The variational formulation presented so far constitutes a well-accepted framework for developing multiscale models of problems governed by balance equations for a scalar quantity with source terms.

C.4. Constitutive equations in the micro-scale

C.4.1. General context

This section describes the general framework adopted in the present multiscale model to address the set of micro-scale constitutive relations $\{\mathbf{Q}_\mu, \dot{\xi}_\mu, S_\mu\}$. In particular, we are interested in materials that do not exhibit second-order effects along characteristic lengths at the micro-scale. Such constitutive laws for $\{\mathbf{Q}_\mu, \dot{\xi}_\mu, S_\mu\}$ may be linear or non-linear; no limitations are imposed on their underlying mathematical structure. A key element of our proposal concerns the way in which the input arguments are evaluated within the constitutive settings. This topic motivates the developments that follow.

First, the commonly accepted functional dependencies for $\{\mathbf{Q}_\mu, \dot{\xi}_\mu, S_\mu\}$ are established, namely

$$\mathbf{Q}_\mu = \hat{\mathcal{F}}_Q(\phi_\mu, \mathbf{g}_\mu), \tag{C.21}$$

$$\dot{\xi}_\mu = \hat{\mathcal{F}}_\xi(\phi_\mu, \dot{\phi}_\mu), \tag{C.22}$$

$$S_\mu = \hat{\mathcal{F}}_S(\phi_\mu), \tag{C.23}$$

where $\hat{\mathcal{F}}_{(\bullet)}$ denotes a generic constitutive law. Of course, additional dependencies could be incorporated in relations (C.21)-(C.23) to account for more sophisticated and coupled effects; nevertheless, we decide to keep the presentation sufficiently general yet simple. In any case, more elaborate dependencies can be addressed in the same manner as discussed below.

At this point, a slight redefinition of the insertion operator $\mathcal{I}_\phi$ is proposed, specifying how the realizable macro-scale primal descriptors $\mathbf{\Phi} = [\phi, \mathbf{g}]^T$ are transferred to the micro-scale domain to construct the ϕ_μ and $\dot{\phi}_\mu$ fields. It will henceforth be referred to as $\mathcal{I}^\alpha_\phi$, whose definition is given by

$$\mathcal{I}^\alpha_\phi = [1,\ \alpha\ \mathbf{x}'_\mu], \tag{C.24}$$

α being a binary parameter. If $\alpha = 1$, the original version is restored (see expression (C.5)-right); then the primary field ϕ_μ (as well as its rate $\dot{\phi}_\mu$) is Full-Order Expanded (FOE) at the micro-scale constitutive level, see expression (C.3). For future reference, the homogenization scheme resulting from this choice ($\alpha = 1$) will be identified as the FOE-Multiscale model. Otherwise, if $\alpha = 0$, the function ϕ_μ (and $\dot{\phi}_\mu$) is Expanded in a Reduced manner within the constitutive functionals, i.e. the linear contribution $(\mathbf{g} \cdot \mathbf{x}'_\mu)$ is neglected. The homogenization procedure that emerges from setting $\alpha = 0$ in (C.24) is hereafter termed the SOE-Multiscale model, denoting a Selective-Order Expansion (SOE) for ϕ_μ (and also $\dot{\phi}_\mu$) at selective/specific places of the formulation.

From previous comments, each time we require to evaluate the realizable fields ϕ_μ and $\mathbf{g}_\mu$ (and their rates $\dot{\phi}_\mu$ and $\dot{\mathbf{g}}_\mu$) as input arguments in any material law, the following expressions are used

$$\phi^\alpha_\mu = \mathcal{I}^\alpha_\phi\ \mathbf{\Phi} + \tilde{\phi}_\mu, \tag{C.25}$$

$$\mathbf{g}_\mu = \mathcal{I}_\mathbf{g}\ \mathbf{\Phi} + \tilde{\mathbf{g}}_\mu, \tag{C.26}$$

where operator $\mathcal{I}_\mathbf{g}$ is the same as defined earlier, see (C.6)-right. Thus, the functional dependencies in constitutive relations (C.21)-(C.23), taking into account (C.25)-(C.26), can be further elaborated as

follows

$$\mathbf{Q}_\mu = \hat{\mathcal{F}}_Q\big(\phi_\mu^\alpha, \mathbf{g}_\mu\big) = \hat{\mathcal{F}}_Q\big(\phi, \alpha\,\mathbf{g}\cdot\mathbf{x}'_\mu, \tilde{\phi}_\mu, \mathbf{g}, \tilde{\mathbf{g}}_\mu\big), \tag{C.27}$$

$$\dot{\xi}_\mu = \hat{\mathcal{F}}_\xi\big(\phi_\mu^\alpha, \dot{\phi}_\mu^\alpha\big) = \hat{\mathcal{F}}_\xi\big(\phi, \alpha\,\mathbf{g}\cdot\mathbf{x}'_\mu, \tilde{\phi}_\mu, \dot{\phi}, \alpha\,\dot{\mathbf{g}}\cdot\mathbf{x}'_\mu, \dot{\tilde{\phi}}_\mu\big), \tag{C.28}$$

$$S_\mu = \hat{\mathcal{F}}_S\big(\phi_\mu^\alpha\big) = \hat{\mathcal{F}}_S\big(\phi, \alpha\,\mathbf{g}\cdot\mathbf{x}'_\mu, \tilde{\phi}_\mu\big), \tag{C.29}$$

where the dependencies on macro-scale variables and micro-scale fluctuations become evident.

The set of expressions (C.24)–(C.29) constitutes the core of the present contribution, specifically regarding what we have termed the SOE-Multiscale model ($\alpha = 0$). This approach aims to provide a homogenization procedure restoring the classical concept of RVE. Most First-Order homogenization methods available in the literature for problems governed by a scalar balance equation with source terms follow the FOE-Multiscale scheme ($\alpha = 1$), which, as discussed in the introduction, exhibits macro-scale second-order effects due to a dependence on the size adopted for the micro-scale domain. A more detailed analysis of this key topic is provided in Sections C.5 and C.6.

Remark. The central idea behind our proposal can be formally deemed a simplified "constitutive-like" hypothesis, since the Selective-Order Expansion exerts a local effect only when the micro-scale material laws must be evaluated. Outside these specific environments, the Full-Order Expansion for micro-scale primary variables is adopted. For instance, the entire variational framework described above, which in turn characterizes the solution of the micro-scale balance problem and the homogenization rules, has been built based on the concept of Full-Order Expansion.

C.4.2. Constitutive specializations

In order to proceed with the forthcoming developments and clearly illustrate the micro-scale size effect issues, this Sub-section proposes a specialization of the general constitutive structure previously outlined. In particular, we adopt a simplified (but extensively used) version of (C.27)-(C.29), which is defined as follows

$$\mathbf{Q}_\mu = \hat{\mathcal{F}}_Q\big(\phi_\mu^\alpha, \mathbf{g}_\mu\big) := -\mathbf{k}_\mu(\phi_\mu^\alpha)\;\mathbf{g}_\mu = -\mathbf{k}_\mu(\phi_\mu^\alpha)\;\big[\mathbf{g} + \tilde{\mathbf{g}}_\mu\big], \tag{C.30}$$

$$\dot{\xi}_\mu = \hat{\mathcal{F}}_\xi\big(\phi_\mu^\alpha, \dot{\phi}_\mu^\alpha\big) := c_\mu(\phi_\mu^\alpha)\;\dot{\phi}_\mu^\alpha = c_\mu(\phi_\mu^\alpha)\;\Big[\dot{\phi} + \alpha\,\dot{\mathbf{g}}\cdot\mathbf{x}'_\mu + \dot{\tilde{\phi}}_\mu\Big], \tag{C.31}$$

$$\begin{aligned} S_\mu = \hat{\mathcal{F}}_S\big(\phi_\mu^\alpha\big) &:= S_\mu^0 - s_\mu(\phi_\mu^\alpha)\;\big[\phi_\mu^\alpha - \phi_\mu^{\text{ref}}\big] \\ &:= S_\mu^0 - s_\mu(\phi_\mu^\alpha)\;\big[\phi + \alpha\,\mathbf{g}\cdot\mathbf{x}'_\mu + \tilde{\phi}_\mu - \phi_\mu^{\text{ref}}\big], \end{aligned} \tag{C.32}$$

where $\mathbf{k}_\mu(\phi_\mu^\alpha)$, $c_\mu(\phi_\mu^\alpha)$, and $s_\mu(\phi_\mu^\alpha)$ denote the corresponding material properties for each equation—a second-order tensor and two scalar functions, respectively—all of which may depend on the primary field at the micro-scale. Furthermore, S_μ^0 and ϕ_μ^{ref} represent additional parameters assumed to be piecewise uniform within each micro-scale constituent.

Remark. Appendix C lists specific cases of the general balance problem discussed above, for which the conclusions of this work may be particularly useful. It also provides the corresponding physical meaning of each symbol introduced in the previous developments.

C.5. About the micro-scale size dependence on the macro-scale response

Once the micro-scale constitutive relations (C.30)-(C.32) have been specified, the multiscale model is closed and the objectivity in the macro-scale response can be addressed. Previous contributions have identified the homogenized transient term $\mathbf{Q}_{tra}$ as the responsible for introducing second-order effects in the coarse scale. Therefore, this term is analyzed in detail in what follows.

By replacing (C.31) and (C.32) into the definition given for $\mathbf{Q}_{tra}$, see equation (C.18), and rearranging conveniently, we obtain

$$\begin{aligned}
\mathbf{Q}_{tra} = -\frac{1}{|\Omega_\mu|}\int_{\Omega_\mu} \Big\{ & c_\mu(\phi_\mu^\alpha)\ \Big[\dot{\phi} + \alpha\, \dot{\mathbf{g}}\ \cdot\ \mathbf{x}'_\mu + \dot{\tilde{\phi}}_\mu\Big] - S_\mu^0 \\
& + s_\mu(\phi_\mu^\alpha)\ \Big[\phi + \alpha\, \mathbf{g}\ \cdot\ \mathbf{x}'_\mu + \tilde{\phi}_\mu - \phi_\mu^{\text{ref}}\Big]\Big\}\ \mathbf{x}'_\mu\, d\Omega_\mu \\
= & \underbrace{-\frac{\dot{\phi}}{|\Omega_\mu|}\int_{\Omega_\mu} c_\mu(\phi_\mu^\alpha)\ \mathbf{x}'_\mu\, d\Omega_\mu}_{\mathbf{T}_1}\ \underbrace{-\frac{\phi}{|\Omega_\mu|}\int_{\Omega_\mu} s_\mu(\phi_\mu^\alpha)\ \mathbf{x}'_\mu\, d\Omega_\mu}_{\mathbf{T}_2} \\
& \underbrace{-\frac{1}{|\Omega_\mu|}\int_{\Omega_\mu} c_\mu(\phi_\mu^\alpha)\ \dot{\tilde{\phi}}_\mu\, \mathbf{x}'_\mu\, d\Omega_\mu}_{\mathbf{T}_3}\ \underbrace{-\frac{1}{|\Omega_\mu|}\int_{\Omega_\mu} s_\mu(\phi_\mu^\alpha)\ \tilde{\phi}_\mu\, \mathbf{x}'_\mu\, d\Omega_\mu}_{\mathbf{T}_4} \\
& \underbrace{-\frac{\alpha}{|\Omega_\mu|}\int_{\Omega_\mu} c_\mu(\phi_\mu^\alpha)\ \big[\mathbf{x}'_\mu \otimes \mathbf{x}'_\mu\big]\, d\Omega_\mu\, \dot{\mathbf{g}}}_{\mathbf{T}_5}\ \underbrace{-\frac{\alpha}{|\Omega_\mu|}\int_{\Omega_\mu} s_\mu(\phi_\mu^\alpha)\ \big[\mathbf{x}'_\mu \otimes \mathbf{x}'_\mu\big]\, d\Omega_\mu\, \mathbf{g}}_{\mathbf{T}_6} \\
& + \underbrace{\frac{1}{|\Omega_\mu|}\int_{\Omega_\mu} S_\mu^0\, \mathbf{x}'_\mu\, d\Omega_\mu}_{\mathbf{T}_7} + \underbrace{\frac{1}{|\Omega_\mu|}\int_{\Omega_\mu} s_\mu(\phi_\mu^\alpha)\, \phi_\mu^{\text{ref}}\, \mathbf{x}'_\mu\, d\Omega_\mu}_{\mathbf{T}_8}
\end{aligned} \tag{C.33}$$

Expression (C.33) displays all terms resulting from a straightforward decomposition of $\mathbf{Q}_{tra}$. In practice, these contributions neither become active nor vanish simultaneously. The net effect of each $\mathbf{T}_i$-term on the homogenized response depends on the modeling assumptions and hypotheses adopted for a given problem. Therefore, the discussion in this section should be understood in a generic sense.

C.5.1. FOE-Multiscale prediction ($\alpha = 1$)

The integrands of $\mathbf{T}_5$ and $\mathbf{T}_6$ terms in (C.33) exhibit, at least, a quadratic dependence on the $\mathbf{x}'_\mu$-coordinate. Indeed, if the material properties are piecewise uniform for each constituent, they could be expressed as

$$\mathbf{T}_5 = -\frac{\alpha}{|\Omega_\mu|}\int_{\Omega_\mu^\triangle} \big[\mathbf{x}'_\mu \otimes \mathbf{x}'_\mu\big]\, d\Omega_\mu^\triangle\, \dot{\mathbf{g}} = -\frac{\alpha}{|\Omega_\mu|}\, \mathbf{I}_{\Omega_\mu^\triangle}\, \dot{\mathbf{g}}, \tag{C.34}$$

$$\mathbf{T}_6 = -\frac{\alpha}{|\Omega_\mu|}\int_{\Omega_\mu^\square} \big[\mathbf{x}'_\mu \otimes \mathbf{x}'_\mu\big]\, d\Omega_\mu^\circ\, \mathbf{g} = -\frac{\alpha}{|\Omega_\mu|}\, \mathbf{I}_{\Omega_\mu^\circ}\, \mathbf{g}, \tag{C.35}$$

where $\mathbf{I}_{\Omega_\mu^\triangle}$ and $\mathbf{I}_{\Omega_\mu^\circ}$ are the inertia tensors of $\Omega_\mu^\triangle$ and Ω_μ°, respectively, with respect to barycenter cartesian axis. In (C.34)-(C.35), the fictitious differential volumes $d\Omega_\mu^\triangle$ and $d\Omega_\mu^\circ$ are obtained from scaling $d\Omega_\mu$ with the C_μ and s_μ distributions, respectively. Thus $\mathbf{T}_5$-$\mathbf{T}_6$ terms introduce a direct or explicit size effect in the homogenized response, as they increase monotonically with the enlargement of the Micro-Cell dimensions. This issue could be further amplified if the material properties exhibit dependence on the primary micro-scale field, as assumed in (C.33).

Expression (C.33) contains additional sources of micro-scale size effects that may not be readily apparent. Note that the $\tilde{\phi}_\mu$-field, obtained after solving the micro-scale balance equation (C.20), also depends on the macro-scale insertion process; thus we can express $\tilde{\phi}_\mu = f_\mu^{\tilde{\phi}}(\phi, \alpha\, \mathbf{g}\cdot\mathbf{x}'_\mu, \ldots)$ and then $\dot{\tilde{\phi}}_\mu = f_\mu^{\dot{\tilde{\phi}}}(\dot{\phi}, \alpha\ \dot{\mathbf{g}}\cdot\mathbf{x}'_\mu, \ldots)$. Such implicit dependencies, in combination with the presence of products like $(\tilde{\phi}_\mu\, \mathbf{x}'_\mu)$ and $(\dot{\tilde{\phi}}_\mu\, \mathbf{x}'_\mu)$ in the integrands of $\mathbf{T}_3$ and $\mathbf{T}_4$, strongly suggest that both homogenized terms

yield at least a quadratic dependence on $\mathbf{x}'_\mu$-coordinates (it could be higher if the material properties depend on the primary micro-scale field), here referred to as indirect or implicit micro-scale size effect.

If the material properties are piecewise uniform within each constituent of the microstructure, the $\mathbf{T}_1$ and $\mathbf{T}_2$ terms, on the right-hand side of (C.33), do not introduce micro-scale size dependencies, provided that the material distribution is quasi-symmetric with respect to the barycenter of the Micro-Cell. Indeed, the influence of these contributions progressively vanishes as the Micro-Cell size increases, owing to the inclusion of a sufficiently large and statistically representative set of heterogeneities. However, if the material parameters depend on the primary micro-scale field, the following functional relations arise: $c_\mu(\phi, \alpha\, \mathbf{g}\cdot\mathbf{x}'_\mu, \tilde{\phi}_\mu)$ and $s_\mu(\phi, \alpha\, \mathbf{g}\cdot\mathbf{x}'_\mu, \tilde{\phi}_\mu)$. Thus, the previous assertion does not necessarily hold, as the occurrence of products such as $(c_\mu\, \mathbf{x}'_\mu)$ and $(s_\mu\, \mathbf{x}'_\mu)$, in the integrands of $\mathbf{T}_1$ and $\mathbf{T}_2$ terms, may give rise to second-order effects.

Finally, the $\mathbf{T}_7$-contribution does not induce micro-scale size dependence, provided the constituent distribution is representative, whereas the $\mathbf{T}_8$-term behaves similarly to $\mathbf{T}_1$ and $\mathbf{T}_2$.

Each of the aforementioned sources of micro-scale size dependence stems from the presence of the linear terms $(\alpha\ \mathbf{g}\cdot\mathbf{x}'_\mu)$ and $(\alpha\ \dot{\mathbf{g}}\cdot\mathbf{x}'_\mu)$, in the fields ϕ_μ and $\dot{\phi}_\mu$, respectively, whenever these fields are required as constitutive arguments in (C.30)-(C.32) or, more generally, in (C.27)-(C.29). Thus, all possible sources of second-order effects are inherited in the FOE-approach $(\alpha = 1)$.

In general, multiscale modeling of highly heterogeneous materials requires a progressive enlargement of the Micro-Cell domain to ensure statistical representativeness, that is, to identify the Representative Volume Element (RVE). The aforementioned idea applies particularly to the homogenization rules (C.18)-left and (C.19). However, such representativeness cannot be attained through the same procedure for the transient contribution of the homogenized flux $\mathbf{Q}_{tra}$ (see (C.18)-right and, in detail, (C.33)), thereby revealing a kind of paradox in the FOE-multiscale strategy.

C.5.2. SOE-Multiscale prediction ($\alpha = 0$)

If the Selective-Order Expansion procedure is adopted (binary parameter $\alpha = 0$) the size effect is removed from the entire multiscale formulation.

First, note that the contributions $\mathbf{T}_5$ and $\mathbf{T}_6$ are inherently excluded from the homogenization rule (C.33). Moreover, the fields $\tilde{\phi}_\mu$ and $\dot{\tilde{\phi}}_\mu$, obtained from the solution of the micro-scale balance equation (C.20), no longer exhibit implicit dependencies on $(\mathbf{g}\cdot\mathbf{x}'_\mu)$ nor $(\dot{\mathbf{g}}\cdot\mathbf{x}'_\mu)$, respectively. In the case of ϕ_μ-dependent material properties (C_μ and/or s_μ), they also become insensitive to the term $(\mathbf{g}\cdot\mathbf{x}'_\mu)$. As a final result, the components $\mathbf{T}_1$–$\mathbf{T}_4$ and $\mathbf{T}_8$, of $\mathbf{Q}_{tra}$, cease to introduce any second-order effects within the SOE-multiscale formulation, see (C.36) for clarity

$$
\begin{aligned}
\mathbf{Q}_{tra}^{\text{SOE}} &= -\frac{1}{|\Omega_\mu|}\int_{\Omega_\mu}\left\{c_\mu(\phi,\tilde{\phi}_\mu)\,\left[\dot{\phi}+\dot{\tilde{\phi}}_\mu\right]+s_\mu(\phi,\tilde{\phi}_\mu)\,\left[\phi+\tilde{\phi}_\mu\right]\right\}\,\mathbf{x}'_\mu\,d\Omega_\mu \\
&= \underbrace{-\frac{\dot{\phi}}{|\Omega_\mu|}\int_{\Omega_\mu}c_\mu(\phi,\tilde{\phi}_\mu)\,\mathbf{x}'_\mu\,d\Omega_\mu}_{\mathbf{T}_1}\ \underbrace{-\frac{\phi}{|\Omega_\mu|}\int_{\Omega_\mu}s_\mu(\phi,\tilde{\phi}_\mu)\,\mathbf{x}'_\mu\,d\Omega_\mu}_{\mathbf{T}_2} \\
&\quad \underbrace{-\frac{1}{|\Omega_\mu|}\int_{\Omega_\mu}c_\mu(\phi,\tilde{\phi}_\mu)\,\dot{\tilde{\phi}}_\mu\,\mathbf{x}'_\mu\,d\Omega_\mu}_{\mathbf{T}_3}\ \underbrace{-\frac{1}{|\Omega_\mu|}\int_{\Omega_\mu}s_\mu(\phi,\tilde{\phi}_\mu)\,\tilde{\phi}_\mu\,\mathbf{x}'_\mu\,d\Omega_\mu}_{\mathbf{T}_4} \\
&\quad \underbrace{+\frac{1}{|\Omega_\mu|}\int_{\Omega_\mu}S^0_\mu\,\mathbf{x}'_\mu\,d\Omega_\mu}_{\mathbf{T}_7}+\underbrace{\frac{1}{|\Omega_\mu|}\int_{\Omega_\mu}s_\mu(\phi,\tilde{\phi}_\mu)\,\phi^{\text{ref}}_\mu\,\mathbf{x}'_\mu\,d\Omega_\mu}_{\mathbf{T}_8}, \\
&\quad \text{with } \tilde{\phi}_\mu = f^{\tilde{\phi}}_\mu(\phi,\cancel{\alpha\,\mathbf{g}\,\mathbf{x}'_\mu},\ldots) \text{ and } \dot{\tilde{\phi}}_\mu = f^{\dot{\tilde{\phi}}}_\mu(\phi,\cancel{\alpha\,\dot{\mathbf{g}}\,\mathbf{x}'_\mu},\ldots).
\end{aligned}
\tag{C.36}
$$

The standard procedure of progressively enlarging the Micro-Cell domain until achieving a representative homogenized response is therefore recovered, which is an essential condition to validate the concept of RVE in highly heterogeneous media. It should be emphasized that the SOE-approach does not entirely eliminate the contribution of the term $\mathbf{Q}_{tra}$, but rather introduces a convenient redefinition of it.

C.6. An analytical approach to the up-scaling problem

In this section, we derive analytical expressions for the homogenized flux $\mathbf{Q}$, with the aim of providing a well-founded basis for the preceding discussion of Section C.5. The methodology comprises four main steps, namely: (i) determination of the primary fluctuation field $\tilde{\phi}_\mu(\mathbf{x}_\mu,t)$, which satisfies the strong form of the micro-scale balance, together with the insertion and homogenization procedures (see sections C.3.2 and C.3.3, respectively); (ii) analytical determination of the required derivatives of $\tilde{\phi}_\mu(\mathbf{x}_\mu,t)$; (iii) analytical evaluation of the constitutive responses $\{\mathbf{Q}_\mu(\mathbf{x}_\mu,t),\dot{\xi}_\mu(\mathbf{x}_\mu,t),S_\mu(\mathbf{x}_\mu,t)\}$; and (iv) application of the spatial averaging operator to these fields, see (C.17), in order to obtain a formula for the effective flux $\mathbf{Q}$, at any given time.

C.6.1. Problem setting

Analytical solutions for the up-scaling transition process are attainable only under highly idealized assumptions. Nevertheless, the conclusions derived therein provide rigorous and indisputable foundations regarding the emergence of micro-scale size effects as well as their underlying nature. With this idea in mind, we now state the set of simplified hypothesis that characterize the multiscale problem under study:

(i) The material is homogeneous.

(ii) The Micro-Cell geometry is a square of side length "ℓ_{MC}" in the x_1-x_2-plane, with thickness denoted as "d" in the x_3-direction. Accordingly, the Micro-Cell volume is given by $|\Omega_\mu| = (d\,\ell^2_{\text{MC}})$.

(iii) The macro-scale imposes prescribed (known) values $\{\phi,\mathbf{g},\dot{\mathbf{g}}\}$ on the Micro-Cell domain, where the latter two quantities have nonzero components only in the x_1-direction.

(iv) The constitutive responses for $\mathbf{Q}_\mu$, $\dot{\xi}_\mu$ and S_μ are described by equations (C.30)-(C.32), respectively.

(v) Two homogenization schemes (denoted as Scenarios A and B), distinguished by the restrictions imposed on the micro-scale problem, are considered. In Scenario A, the Minimally Constrained Multiscale Model is employed, for which $\widetilde{\mathcal{T}}_\mu^{\square}(\Omega_\mu) \equiv \widetilde{\mathcal{T}}_\mu^{*}(\Omega_\mu) \equiv \widetilde{\mathcal{T}}_\mu(\Omega_\mu)$ (see definition (C.13)). In Scenario B, the Taylor (or rule-of-mixtures) Multiscale procedure is adopted, in which $\tilde{\phi}(x_\mu, t) \equiv 0$ is prescribed $\forall x_\mu \in \Omega_\mu$ and $\forall t$.

(vi) Our theoretical approach is based on the following premise. The Micro-Cell state is assumed to be fully known at a given time instant, denoted by t^n. A time interval $I_t = [t^n, t^{n+1}]$, with time increment $\Delta t = t^{n+1} - t^n$, is then considered, during which the macro-scale imposes updated (known) quantities $\{\phi^{n+1}, \mathbf{g}^{n+1}, \dot{\mathbf{g}}^{n+1}\}$ onto the micro-scale domain. This triplet of macro-scale data remains constant over the time interval I_t, thereby enabling the derivation of an analytical expression for the flux $\mathbf{Q}^{n+1}$. Hereafter, the superscripts $(\cdot)^n$ and $(\cdot)^{n+1}$ denote the evaluation of any variable at the time instants t^n and t^{n+1}, respectively.

Items (i)-(iii) of the previous list reduce the multiscale problem to a purely one-dimensional setting, characterized by a single physically relevant coordinate. Thus, for the sake of readability, we denote this coordinate by "x_μ" throughout this section, and all variables are treated as scalar quantities.

Item (v) does not constitute a simplifying assumption *per se*. On the contrary, we argue that contrasting the two proposed homogenization schemes (MCMM and Taylor) provides valuable insight into the net effect of each $\mathbf{T}_i$-term (see (C.33)) on the homogenized response, particularly in view of the markedly different levels of restriction imposed by these models on the primary fluctuation field $\tilde{\phi}_\mu$ (minimal for MCMM and maximal for Taylor). For the one-dimensional problem under consideration, the MCMM and the Periodic models yield identical solutions.

C.6.2. Analytical derivation for the up-scaling mechanism

Appendix B and Appendix D collect useful developments that are systematically invoked in this section, adapted to the one-dimensional problem under consideration and to the simplifying hypotheses outlined above.

C.6.2.1. Scenario A: solution based on the MCMM-scheme

The strong form of the micro-scale balance equation for this case (see (C.68)-(a)) reads

$$\frac{d}{dx_\mu} Q_\mu + \dot{\xi}_\mu - S_\mu + \Theta = 0, \quad \forall x_\mu \in \Omega_\mu, \forall t, \tag{C.37}$$

where Θ denotes the *"spatially uniform"* Lagrange multiplier that enforces the zero-mean-value constraint on the virtual fluctuation field $\delta\tilde{\phi}_\mu$ in Ω_μ.

By introducing the constitutive relations (C.30)-(C.32), and expanding ϕ_μ^α (as well as its rate $\dot{\phi}_\mu^\alpha$) and g_μ according to (C.25) and (C.26), respectively, the previous equation becomes

$$\begin{aligned} -k_\mu \frac{d^2\tilde{\phi}_\mu}{dx_\mu^2} + c_\mu \left(\dot{\phi} + \alpha\, \dot{g}\, x_\mu + \dot{\tilde{\phi}}_\mu\right) \\ - S_\mu^0 + s_\mu \left(\phi + \alpha\, g\, x_\mu + \tilde{\phi}_\mu - \phi_\mu^{\text{ref}}\right) + \Theta = 0, \ \forall x_\mu \in \Omega_\mu, \forall t. \end{aligned} \tag{C.38}$$

From (C.70), it follows that $\Theta = -c_\mu\, \dot{\phi} + S_\mu^0 - s_\mu\, (\phi - \phi_\mu^{\text{ref}})$; hence (C.38) yields

$$\overbrace{k_\mu \frac{d^2\tilde{\phi}_\mu}{dx_\mu^2} = c_\mu\, \dot{\tilde{\phi}}_\mu + s_\mu\, \tilde{\phi}_\mu}^{\text{Homogeneous part}} + \overbrace{\epsilon\, \alpha\, x_\mu}^{\text{Source-like term}}, \quad \forall x_\mu \in \Omega_\mu, \forall t, \tag{C.39}$$

with $\epsilon = c_\mu\,\dot{g} + s_\mu\,g$.

In the present case, the Lagrange multiplier Θ removes from the differential equation (C.38) the effect that the macro-scale exerts on the micro-scale in terms of quantities ϕ and $\dot{\phi}$. Furthermore, since both terms S^0_μ and $(s_\mu\,\phi^{\text{ref}}_\mu)$ are assumed fully uniform in this example, their contributions are likewise canceled by the definition of Θ. Nevertheless, the influences of g and $\dot{g}$ (through the parameter ϵ) are not eliminated; rather, they act as two *"driving excitations"* transmitted from the macro- to the micro-scale level.

Remark. For the FOE-multiscale approach ($\alpha = 1$), (C.39) defines a non-homogeneous parabolic equation whose source-like term is a known function that varies only in space (linearly with respect to x_μ-coordinate). Despite the material homogeneity, the FOE-scheme predicts a non-homogeneous solution for $\tilde{\phi}_\mu(x_\mu, t)$, a result that lacks a clear physical interpretation. As shown below, this source-like term is responsible for the micro-scale size effects inherent to the FOE-procedure. On the contrary, in the SOE-strategy ($\alpha = 0$), (C.39) reduces to a homogeneous parabolic equation, for which $\tilde{\phi}_\mu(x_\mu, t) \equiv 0$ is an admissible solution $\forall x_\mu \in \Omega_\mu$ and $\forall t$. The SOE-multiscale model predicts that the problem at the smaller length scale provides no additional information, thereby making the scale-bridging step superfluous, an expected outcome for the present case of a fully homogeneous material.

Without loss of generality, the general solution $\tilde{\phi}^{n+1}_\mu(x_\mu)$ of (C.39) can be decomposed as

$$\begin{aligned}\tilde{\phi}^{n+1}_\mu(x_\mu) &= \tilde{\phi}^{\text{H n+1}}_\mu(x_\mu) + \tilde{\phi}^{\text{SS}}_\mu(x_\mu)\\ &= \tilde{\phi}^{\text{H n+1}}_\mu(x_\mu) + \tilde{\phi}^{\text{SS-H}}_\mu(x_\mu) + \tilde{\phi}^{\text{SS-NH}}_\mu(x_\mu)\end{aligned} \tag{C.40}$$

where $\tilde{\phi}^{\text{H n+1}}_\mu(x_\mu)$ denotes the solution of the homogeneous part of (C.39), and $\tilde{\phi}^{\text{SS}}_\mu(x_\mu)$ stands for the solution of the corresponding steady state problem. The latter can be further partitioned into a homogeneous contribution $\tilde{\phi}^{\text{SS-H}}_\mu(x_\mu)$ and a non-homogeneous term $\tilde{\phi}^{\text{SS-NH}}_\mu(x_\mu)$. For a generic time interval I_t, with time increment Δt, the analytical solution for $\tilde{\phi}^{n+1}(x_\mu)$ reads[4]

$$\begin{aligned}\tilde{\phi}^{n+1}_\mu(x_\mu) =& \frac{\epsilon^{n+1}\,\alpha\,\ell_{\text{MC}}}{2\,s_\mu\,\sinh\left(\frac{\beta\,\ell_{\text{MC}}}{2}\right)}\,\sinh(\beta\,x_\mu) - \frac{\epsilon^{n+1}\,\alpha}{s_\mu}\,x_\mu\\ &+ \sum_{j=1}^{\infty} b^n_j\,\sin(\omega_j\,x_\mu)\,e^{-\frac{s_\mu + k_\mu\,\omega_j^2}{c_\mu}\,\Delta t}\\ &\text{with } \beta = \sqrt{\frac{s_\mu}{k_\mu}},\ \omega_j = \frac{2\,j\,\pi}{\ell_{\text{MC}}},\ b^n_j = \frac{2\,\epsilon^n\,\alpha\,\beta^2\,(-1)^j}{s_\mu\,\omega_j\,\left(\beta^2 + \omega_j^2\right)},\end{aligned} \tag{C.41}$$

where the Fourier coefficients b^n_j ($j = 1, \ldots, \infty$) are computed from the Micro-Cell state at the previous time instant t^n, i.e. taking into account the initial condition $\tilde{\phi}^n_\mu(x_\mu)$ for the time interval I_t (see Appendix D).

Then, the corresponding spatial and time derivatives of the primary fluctuating field $\tilde{\phi}^{n+1}(x_\mu)$ can

[4]This solution already satisfies the volumetric and boundary constraints defined in (C.10) and (C.12), respectively, as can be readily demonstrated.

be expressed, respectively, as follows

$$\tilde{g}_\mu^{n+1}(x_\mu) = \frac{\beta\,\epsilon^{n+1}\,\alpha\,\ell_{\text{MC}}}{2\,s_\mu\,\sinh\left(\frac{\beta\,\ell_{\text{MC}}}{2}\right)}\,\cosh(\beta\,x_\mu) - \frac{\epsilon^{n+1}\,\alpha}{s_\mu} + \sum_{j=1}^{\infty}\omega_j\,b_j^n\,\cos(\omega_j\,x_\mu)\,e^{-\frac{s_\mu+k_\mu\,\omega_j^2}{c_\mu}\,\Delta t}, \tag{C.42}$$

$$\dot{\tilde{\phi}}_\mu^{n+1}(x_\mu) = -\sum_{j=1}^{\infty}\left(\frac{s_\mu+k_\mu\,\omega_j^2}{c_\mu}\right)b_j^n\,\sin(\omega_j\,x_\mu)\,e^{-\frac{s_\mu+k_\mu\,\omega_j^2}{c_\mu}\,\Delta t}. \tag{C.43}$$

We are now in a position to evaluate the homogenized flux at a given instant t^{n+1}. To this end, the averaging operator (C.17) is employed together with the constitutive relations (C.30)-(C.32) and the analytical expressions previously derived in (C.42)-(C.43). After discarding all identically zero terms, we obtain

$$\begin{aligned}
Q^{n+1} = {} & \overbrace{-k_\mu\,g^{n+1}}^{Q_{sta}} \overbrace{-\frac{1}{|\Omega_\mu|}\int_{\Omega_\mu} c_\mu\,\alpha\,\dot{g}^{n+1}\,x_\mu^2\,d\Omega_\mu}^{\text{T}_5} \\
& + \overbrace{\frac{1}{|\Omega_\mu|}\int_{\Omega_\mu}\sum_{j=1}^{\infty} s_\mu\,b_j^n\,\sin(\omega_j\,x_\mu)\,e^{-\frac{s_\mu+k_\mu\,\omega_j^2}{c_\mu}\,\Delta t}\,x_\mu\,d\Omega_\mu}^{\text{T}_{3a}} \\
& + \overbrace{\frac{1}{|\Omega_\mu|}\int_{\Omega_\mu}\sum_{j=1}^{\infty} k_\mu\,\omega_j^2\,b_j^n\,\sin(\omega_j\,x_\mu)\,e^{-\frac{s_\mu+k_\mu\,\omega_j^2}{c_\mu}\,\Delta t}\,x_\mu\,d\Omega_\mu}^{\text{T}_{3b}} \\
& \overbrace{-\frac{1}{|\Omega_\mu|}\int_{\Omega_\mu} s_\mu\,\alpha\,g^{n+1}\,x_\mu^2\,d\Omega_\mu}^{\text{T}_6} \\
& \overbrace{-\frac{1}{|\Omega_\mu|}\int_{\Omega_\mu}\left[\frac{\epsilon^{n+1}\,\alpha\,\ell_{\text{MC}}\,x_\mu}{2\,\sinh\left(\frac{\beta\,\ell_{\text{MC}}}{2}\right)}\,\sinh(\beta\,x_\mu)\right]d\Omega_\mu}^{\text{T}_{4a}} \\
& + \overbrace{\frac{1}{|\Omega_\mu|}\int_{\Omega_\mu} c_\mu\,\alpha\,\dot{g}^{n+1}\,x_\mu^2\,d\Omega_\mu}^{\text{T}_{4b}} + \overbrace{\frac{1}{|\Omega_\mu|}\int_{\Omega_\mu} s_\mu\,\alpha\,g^{n+1}\,x_\mu^2\,d\Omega_\mu}^{\text{T}_{4c}} \\
& \overbrace{-\frac{1}{|\Omega_\mu|}\int_{\Omega_\mu}\sum_{j=1}^{\infty} s_\mu\,b_j^n\,\sin(\omega_j\,x_\mu)\,e^{-\frac{s_\mu+k_\mu\,\omega_j^2}{c_\mu}\,\Delta t}\,x_\mu\,d\Omega_\mu}^{\text{T}_{4d}}
\end{aligned} \tag{C.44}$$

In this particular example, several contributions cancel exactly (T_{4b} with T_5, T_{4d} with T_{3a} and T_{4c} with T_6), whereas the terms T_{3b} and T_{4a} remain active. After some algebra, the final expression for the effective flux yields

$$Q^{n+1} = \overbrace{-\,k_\mu\, g^{n+1}}^{Q_{\text{sta}}} \overbrace{-\,2\,\epsilon^n\,\alpha\,\zeta\,\ell_{\text{MC}}^2}^{\text{T}_{3b}} \overbrace{-\,\epsilon^{n+1}\,\alpha\left[\frac{1}{2\,\beta}\coth\left(\frac{\beta\,\ell_{\text{MC}}}{2}\right)-\frac{1}{\beta^2\,\ell_{\text{MC}}}\right]\ell_{\text{MC}}}^{\text{T}_{4a}}$$
$$\text{with } \zeta = \sum_{j=1}^{j=\infty} \frac{1}{\ell_{\text{MC}}^2\,(\beta^2+\omega_j^2)}\, e^{-\frac{s_\mu + k_\mu\,\omega_j^2}{c_\mu}\Delta t}, \tag{C.45}$$

where ζ is a constant factor for a given time increment Δt, which can be accurately evaluated by retaining only a few terms of the series (due to its rapid convergence rate). It can be proved that $\zeta \to \zeta^{max}$ if $\Delta t \to 0$ (ζ^{max} being a finite and positive number[5]), while $\zeta \to 0$ if $\Delta t \to \infty$.

From (C.45), it is evident that the T_{3b}-term introduces a size effect associated with the initial conditions of the Micro-Cell that scales as ℓ_{MC}^2; whereas the T_{4a}-contribution incorporates a size-dependence driven by the current macro-scale excitation (ϵ^{n+1}) and scales linearly with ℓ_{MC}.

The simplification achieved in going from (C.44) to (C.45) cannot be regarded as a general result. As shown below, there exist modeling scenarios (among many others not explored here) in which previously canceled terms become active, and vice versa.

Special case: *Problems with uniform source term $S_\mu = S_\mu^0$ ($s_\mu \to 0$)*

This particular instance can be addressed by applying the limiting process to the previously derived complete steady state solution $\tilde{\phi}_\mu^{\text{SS}}(x_\mu)$ (see (C.40)-(C.41)). Thus, we have

$$\lim_{s_\mu \to 0}\left\{\frac{\epsilon^{n+1}\,\alpha\,\ell_{\text{MC}}\,\sinh(\beta\,x_\mu)}{2\,s_\mu\,\sinh\left(\frac{\beta\,\ell_{\text{MC}}}{2}\right)} - \frac{\epsilon^{n+1}\,\alpha}{s_\mu}\,x_\mu\right\} = \frac{c_\mu\,\dot{g}^{n+1}\,\alpha}{6\,k_\mu}\left(x_\mu^3 - \frac{\ell_{\text{MC}}^2\,x_\mu}{4}\right) \tag{C.46}$$

where the original expression—comprising a hyperbolic sine term combined with a linear function—degenerates into a cubic polynomial in space. In view of (C.46) the entire solution for the fluctuating primary field reads

$$\tilde{\phi}_\mu^{n+1}(x_\mu) = \sum_{j=1}^{j=\infty} b_j^n\,\sin(\omega_j\,x_\mu)\,e^{-\frac{k_\mu\,\omega_j^2}{c_\mu}\Delta t} + \frac{c_\mu\,\alpha\,\dot{g}^{n+1}}{6\,k_\mu}\left(x_\mu^3 - \frac{\ell_{\text{MC}}^2\,x_\mu}{4}\right),$$
$$\text{with } b_j^n = \frac{2\,\dot{g}^n\,\alpha\,c_\mu\,(-1)^j}{k_\mu\,\omega_j^3} \tag{C.47}$$

After some additional computations, the homogenized flux, consistent with (C.47), can be expressed as

$$Q^{n+1} = \overbrace{-\,k_\mu\,g^{n+1}}^{Q_{\text{sta}}} \overbrace{-\,\frac{c_\mu\,\dot{g}^n\,\alpha\,\zeta}{2\,\pi^2}\,\ell_{\text{MC}}^2}^{\text{T}_3} \overbrace{-\,\frac{c_\mu\,\dot{g}^{n+1}\,\alpha}{12}\,\ell_{\text{MC}}^2}^{\text{T}_5}$$
$$\text{with } \zeta = \sum_{j=1}^{j=\infty}\frac{1}{j^2}\,e^{-\frac{k_\mu\,\omega_j^2}{c_\mu}\Delta t},\ \zeta \in (\pi^2/6, 0) \tag{C.48}$$

[5] $\zeta^{max} = \frac{1}{4\,\beta\,\ell_{\text{MC}}}\left[\coth\left(\frac{\beta\,\ell_{\text{MC}}}{2}\right) - \frac{2}{\beta\,\ell_{\text{MC}}}\right]$

In this context, T_3 and T_5 remain active. The former is associated with the initial condition of the Micro-Cell, whereas the latter is driven by the current macro-scale insertion $\dot{g}^{n+1}$. Both exhibit a size effect that grows proportionally to ℓ^2_{MC}.

Special case: *Steady state problems ($c_\mu \to 0$)*

Under the steady state assumption, expressions (C.41) and (C.45) reduce straightforwardly to

$$\tilde{\phi}^{n+1}_\mu(x_\mu) = \frac{g^{n+1}\,\alpha\,\ell_{\mathrm{MC}}}{2\,\sinh\left(\frac{\beta\,\ell_{\mathrm{MC}}}{2}\right)}\,\sinh(\beta\,x_\mu) - g^{n+1}\,\alpha\,x_\mu, \tag{C.49}$$

$$Q^{n+1} = \overbrace{-\,k_\mu\,g^{n+1}}^{Q_{\mathrm{sta}}} \overbrace{-\,s_\mu\,g^{n+1}\,\alpha\left[\frac{1}{2\,\beta}\coth\left(\frac{\beta\,\ell_{\mathrm{MC}}}{2}\right) - \frac{1}{\beta^2\,\ell_{\mathrm{MC}}}\right]\ell_{\mathrm{MC}}}^{\mathrm{T}_{4a}}. \tag{C.50}$$

where the superscript referring to the current time step $(\bullet)^{n+1}$, in this setting, serves merely as an indicator to track variations in the macro-scale insertion process, without any additional physical significance.

A size-dependence arises from the T_{4a}-term which scales linearly with the Micro-Cell size ℓ_{MC}.

C.6.2.2. Scenario B: solution based on the Taylor-scheme

This scenario is trivial to analyze, as no explicit solution needs to be determined ($\tilde{\phi}_\mu \equiv 0,\ \forall x_\mu,\ \forall t$). The micro-scale balance equation for this homogenization model

$$\begin{aligned} -k_\mu \cancel{\frac{d^2\tilde{\phi}_\mu}{dx^2_\mu}} + c_\mu\left(\dot{\phi} + \alpha\,\dot{g}\,x_\mu + \cancel{\dot{\tilde{\phi}}_\mu}\right) - S^0_\mu \\ + s_\mu\left(\phi + \alpha\,g\,x_\mu + \cancel{\tilde{\phi}_\mu} - \phi^{\mathrm{ref}}_\mu\right) + \Theta(x_\mu) = 0,\ \forall x_\mu \in \Omega_\mu, \forall t, \end{aligned} \tag{C.51}$$

is automatically satisfied due to the presence of the linear field $\Theta(x_\mu)$, the corresponding Lagrange multiplier which enforces the constraint $\delta\tilde{\phi}_\mu \equiv 0,\ \forall x_\mu,\ \forall t$, on the virtual primary fluctuation field. From (C.33), the effective flux can be readily obtained

$$Q^{n+1} = \overbrace{-\,k_\mu\,g^{n+1}}^{Q_{\mathrm{sta}}} \overbrace{-\frac{c_\mu\,\dot{g}^{n+1}\,\alpha}{12}\,\ell^2_{\mathrm{MC}}}^{\mathrm{T}_5} \overbrace{-\frac{s_\mu\,g^{n+1}\,\alpha}{12}\,\ell^2_{\mathrm{MC}}}^{\mathrm{T}_6} \tag{C.52}$$

In the present case, the T_5 and T_6 terms contribute to the size effect issue. Both depend on the current macro-scale inputs ($\dot{g}^{n+1}$ and g^{n+1}) and exhibit a quadratic scaling with respect to ℓ_{MC}. The specialized forms corresponding to the limits $s_\mu \to 0$ (uniform source term) and $c_\mu \to 0$ (steady state conditions) follow directly from (C.52).

C.6.3. Discusion

Throughout this section, a set of analytical solutions for the homogenized flux has been derived, under idealized settings. Nonetheless, the resulting conclusions are rigorous. Some of them are enunciated next.

All second-order effects originate from the incorporation of the macro-scale gradients $\{\alpha\,g, \alpha\,\dot{g}\}$ into the expansion of the primary fields $\{\phi^\alpha_\mu, \dot{\phi}^\alpha_\mu\}$, respectively, whenever these quantities are required at the constitutive level. It was shown that the inputs $\{\alpha\,g, \alpha\,\dot{g}\}$ generate a, spatially linear, source-like term $(\alpha\,\epsilon\,x_\mu)$ in the micro-scale balance equation, see equations (C.39) and/or (C.51). The presence of

such a source-like term prevents homogeneous solutions from being naturally admissible, even in the case of material homogeneity. Its influence propagates into the definition of Q_{tra} through several T_i-contributions, which neither become active nor vanish simultaneously. The net effect of each T_i depends on the modeling assumptions adopted for the problem at hand. Some T_i-terms scale with ℓ^2_{MC}, while others scale proportionally to ℓ_{MC}. Some of these contributions are inherited from MC initial conditions, whereas others manifest under the current macro-scale excitations.

Higher values of g and/or $\dot{g}$ clearly intensify the size effect issue. In very short-term analyses ($\Delta t \to 0$), the ζ-factor (see (C.45) or (C.48)) attains its maximum value, thereby amplifying the micro-scale size-dependence phenomenon.

There is no general, unified treatment of restrictions on the $\tilde{\phi}_\mu$-field that fully eliminates the second-order effects. Thus, the issue cannot be circumvented through the definition of the sub-space $\widetilde{\mathcal{T}}^{\square}_{\mu}(\Omega_\mu) \subseteq \widetilde{\mathcal{T}}_{\mu}(\Omega_\mu)$, where the micro-scale balance is sought. The more restrictive Taylor model suppresses the size effects introduced by the fluctuating solution $\tilde{\phi}_\mu$, but simultaneously activates the so-called T_5 and T_6 terms. In contrast, within the less restrictive MCMM framework, some of the size dependencies induced by $\tilde{\phi}_\mu$ remain present.

The SOE multiscale formulation introduces a constitutive-like hypothesis at the core of the problem by setting the binary parameter $\alpha = 0$ in the definition of $\mathcal{I}^{\alpha}_{\phi}$ (see (C.24)). The spatially linear source-like term in the micro-scale balance equation is no longer present. As expected, for a homogeneous material, the SOE method predicts a naturally homogeneous $\tilde{\phi}_\mu$-solution, and all T_i-terms therefore vanish. However, in more general scenarios, some T_i-contributions remain active until representativeness is reached, with the advantage of preserving the objectivity of the effective response.

C.7. Numerical solution of the multiscale problem at both lengths scales

To address the multiscale problem numerically, the FE^2 strategy is employed [5]. This approach involves two nested finite element schemes that evolve in time, where the connection between them is established at each macro-scale Gauss point. Since both spatial scales share a common temporal scale, the time discretization is the same. As assumed previously, the time step increment is defined as $\Delta t = (t^{n+1} - t^n)$, corresponding to a generic time Interval $I_t = [t^n, t^{n+1}]$. The implicit Euler backward method is proposed to deal with the evolution of the problem within any time Interval I_t. Two independent finite element meshes, Ω_h and $\Omega_{\mu,h}$, are considered to approximate the macro-scale physical domain Ω and the Micro-Cell Ω_μ, respectively. Our current numerical implementation employs bilinear, isoparametric, quadrilateral finite elements, independently of the scale.

C.7.1. Solution of the variational equations at the macro-scale

Based on the finite element mesh, Ω_h, the primal descriptor ϕ and its corresponding admissible virtual variation $\delta\phi$ are approximated through global interpolation matrix $\mathbf{N}$, as follows

$$\phi = \mathbf{N}\,\bar{\boldsymbol{\phi}}, \quad \delta\phi = \mathbf{N}\,\delta\bar{\boldsymbol{\phi}} \quad \text{with} \quad \bar{\boldsymbol{\phi}} \in \mathcal{T}_h(\Omega_h) \quad \text{and} \quad \delta\bar{\boldsymbol{\phi}} \in \mathcal{T}^*_h(\Omega_h), \tag{C.53}$$

where $\bar{\boldsymbol{\phi}}$ denotes the array collecting all primary scalar nodal values, and the vector $\delta\bar{\boldsymbol{\phi}}$ gathers the nodal admissible virtual variations. The finite-dimensional set $\mathcal{T}_h(\Omega_h)$ and sub-space $\mathcal{T}^*_h(\Omega_h)$, both defined in terms of nodal parameters, are constructed such that they represent the discrete counterparts of $\mathcal{T}(\Omega)$ and $\mathcal{T}^*(\Omega)$, respectively. In accordance with the Galerkin approach, the same spatial approximation is used for both, realizable and virtual actions. After discretizing the macro-scale equation (C.2) in space and time, the corresponding FEM formulation of the balance equation, at time step t^{n+1}, is obtained

(Dirichlet degrees of freedom are omitted)

$$\mathbf{E}_h^{n+1} \equiv \int_{\Omega_h} \left[\mathbf{N}^T \left(\dot{\xi}^{n+1} - S^{n+1} \right) - \mathbf{B}^T \, \mathbf{Q}^{n+1} \right] d\Omega + \int_{\Gamma_{\mathrm{N},\,h}} \mathbf{N}^T \, q^{n+1} \, d\Gamma = \mathbf{0}, \tag{C.54}$$

where $\mathbf{B} = \boldsymbol{\nabla} \mathbf{N}$ is the global matrix relating the primary variable to its gradient, $(\bullet)^T$ stands for the transpose operator and $\Gamma_{\mathrm{N},\,h}$ is the discrete Neumann-type boundary.

The Newton-Raphson scheme is used to solve equation (C.54), whereby the current nodal values of the primary scalar field at time step t^{n+1} are updated in terms of the iterative increments $\Delta\bar{\boldsymbol{\phi}}$. During the k-th iteration within a given time interval I_t, these increments are evaluated as follows (the subscript h is omitted in (C.55))

$$\Delta\bar{\boldsymbol{\phi}} = -\frac{\partial \mathbf{E}_k^{n+1}}{\partial \bar{\boldsymbol{\phi}}^{n+1}} \, \mathbf{E}_k^{n+1} = -\left(\mathbf{J}_k^{n+1}\right)^{-1} \mathbf{E}_k^{n+1}, \tag{C.55}$$

$\mathbf{J}_k^{n+1}$ being the macro-scale Jacobian linear operator, defined in Appendix E. The components of $\mathbf{J}_k^{n+1}$, in turn, depend on the homogenized constitutive tensors of the multiscale model, as detailed in [12, 22], and are also specified in Appendix E.

C.7.2. Solution of the variational equations at the micro-scale

The finite element approximations for the micro-scale fields $\tilde{\phi}_\mu$ and $\delta\tilde{\phi}_\mu$ are expressed as follows

$$\tilde{\phi}_\mu = \mathbf{N}_\mu \, \tilde{\bar{\boldsymbol{\phi}}}_\mu, \;\; \delta\tilde{\phi}_\mu = \mathbf{N}_\mu \, \delta\tilde{\bar{\boldsymbol{\phi}}}_\mu, \;\; \text{with } \tilde{\bar{\boldsymbol{\phi}}}_\mu \in \widetilde{\mathcal{T}}^{\square}_{\mu,\,h}(\Omega_{\mu,h}) \text{ and } \delta\tilde{\bar{\boldsymbol{\phi}}}_\mu \in \widetilde{\mathcal{T}}^{*}_{\mu,\,h}(\Omega_{\mu,h}), \tag{C.56}$$

where $\tilde{\bar{\boldsymbol{\phi}}}_\mu$ denotes the array collecting all primary scalar nodal values, $\delta\tilde{\bar{\boldsymbol{\phi}}}_\mu$ gathers the admissible nodal virtual variations, and $\mathbf{N}_\mu$ is the global interpolation matrix at the smaller length scale. The two finite-dimensional sub-spaces $\widetilde{\mathcal{T}}^{\square}_{\mu,h}(\Omega_{\mu,h})$ and $\widetilde{\mathcal{T}}^{*}_{\mu,h}(\Omega_{\mu,h})$, both associated with nodal parameters, coincide. They are constructed so as to represent the discrete counterparts of $\tilde{\mathcal{T}}^{\square}_{\mu}(\Omega_\mu)$ and $\tilde{\mathcal{T}}^{*}_{\mu}(\Omega_\mu)$, respectively. Recall that such sub-spaces characterize a generic homogenization model, in particular any of those described in Appendix A.

By substituting (C.56) into (C.20), accounting for the time discretization procedure, and performing standard mathematical manipulations, the discrete version of the micro-scale balance equation is obtained at time step t^{n+1}

$$\overbrace{\left[\int_{\Omega_{\mu,\,h}} \left(\mathbf{N}_\mu^T \left(\dot{\xi}_\mu^{n+1} - S_\mu^{n+1} \right) - \mathbf{B}_\mu^T \, \mathbf{Q}_\mu^{n+1} \right) d\Omega_\mu \right]}^{\mathbf{E}_{\mu,\,h}^{n+1}} \cdot \delta\tilde{\bar{\boldsymbol{\phi}}}_\mu = 0,$$
$$\forall \, \delta\tilde{\bar{\boldsymbol{\phi}}}_\mu \in \widetilde{\mathcal{T}}^{*}_{\mu,\,h}(\Omega_{\mu,h}), \text{ with } \tilde{\bar{\boldsymbol{\phi}}}_\mu \in \widetilde{\mathcal{T}}^{\square}_{\mu,\,h}(\Omega_{\mu,h}), \tag{C.57}$$

where $\mathbf{B}_\mu = \boldsymbol{\nabla}_{\mathbf{x}_\mu} \mathbf{N}_\mu$ is the global matrix relating the primal variable to its corresponding gradient at the smaller scale. The subscript h is omitted hereafter.

A standard Newton-Raphson scheme is also employed at the micro-scale. Accordingly, at a generic k-th iteration, the linearized form of equation (C.57) reads

$$\left\{ \frac{\partial \mathbf{E}_{\mu,\,k}^{n+1}}{\partial \tilde{\bar{\boldsymbol{\phi}}}_\mu^{n+1}} \, \Delta\tilde{\bar{\boldsymbol{\phi}}}_\mu + \mathbf{E}_{\mu,\,k}^{n+1} \right\} \cdot \delta\tilde{\bar{\boldsymbol{\phi}}}_\mu = \left\{ \mathbf{J}_{\mu,\,k}^{n+1} \, \Delta\tilde{\bar{\boldsymbol{\phi}}}_\mu + \mathbf{E}_{\mu,\,k}^{n+1} \right\} \cdot \delta\tilde{\bar{\boldsymbol{\phi}}}_\mu = 0,$$
$$\forall \, \delta\tilde{\bar{\boldsymbol{\phi}}}_\mu \in \widetilde{\mathcal{T}}^{*}_{\mu}(\Omega_{\mu,h}), \text{ with } \Delta\tilde{\bar{\boldsymbol{\phi}}}_\mu \in \widetilde{\mathcal{T}}^{\square}_{\mu}(\Omega_{\mu,h}), \tag{C.58}$$

where $\mathbf{J}_{\mu,k}^{n+1}$ is the Jacobian operator in the micro-scale, defined in Appendix F.

Finally, the numerical solution for the nodal values of the primary scalar fluctuation field, $\tilde{\tilde{\phi}}_{\mu}^{n+1}$ at time step t^{n+1}, is obtained from the iterative increments $\Delta\tilde{\tilde{\phi}}_{\mu}$ computed via (C.58).

C.8. Numerical results

This section aims to illustrate, through two simple numerical examples, the concepts presented in the preceding sections. Both examples are based on the premise that, when modeling a homogeneous material using a multiscale approach, the size of the micro-scale should not influence the response at the macroscopic level. In other words, for a homogeneous material, the Representative Volume Element (RVE) is reached with an infinitesimal domain (that is, practically a *"point"*). Therefore, varying the Micro-Cell size by considering progressively larger material windows should not lead to variations in the macroscopic response. Furthermore, this satisfies the foundational criterion which states that the macroscopic response becomes size-insensitive, once a minimum micro-structural domain has been reached [1].

Accordingly, only homogeneous Micro-Cells are considered in both examples. Nevertheless, these cases highlight the limitations and potential inconsistencies derived from the use of a FOE-Multiscale model. The first example consists of a model defined only at the micro-scale level, from which the macroscopic response is obtained. The second analyzes a full multiscale case for which an analytical solution is known.

For simplicity, a transient heat transfer problem in a rigid material is assumed. In this context, all variables and parameters are defined according to Table (C.1), where $\mathbf{Q}_{\mu}$ denotes the heat flux vector at the micro-scale, S_{μ} the heat source, and $\dot{\xi}_{\mu}$ the microscopic internal energy rate. The volumetric heat capacity $c_{\mu} = \rho_{\mu}\, c_{p_{\mu}}$, corresponds to the product of density and specific heat capacity. In both examples, the material under consideration is silver, with thermal properties defined as $c_{p_{\mu}} = 236\ \frac{J}{kg\,K}$, $\rho_{\mu} = 10500 \frac{kg}{m^3}$, $\kappa_{\mu} = 427\ \frac{W}{m\,K}$. The conductivity tensor is proposed to be isotropic and is therefore expressed as $\mathbf{k}_{\mu} = \kappa_{\mu}\ \mathbf{I}$, where $\mathbf{I}$ denotes the identity matrix. Additionally, there is no heat source ($S_{\mu} = 0$). Finally, it is useful to determine the diffusivity, which is calculated as $\mathcal{D}_{\mu} = \frac{\kappa_{\mu}}{c_{\mu}} = \frac{\kappa_{\mu}}{\rho_{\mu}\, c_{p_{\mu}}} = 1.72 \times 10^{-4}\ \frac{m^2}{s}$.

In turn, in both examples, three square-shaped Micro-Cells of increasing size are considered. The first one, $\text{MC}_1 = 0.01\ m \times 0.01\ m$, is shown in Figure C.3-(b). Subsequently, larger windows of homogeneous material are selected, yielding $\text{MC}_2 = 0.03\ m \times 0.03\ m$ and $\text{MC}_3 = 0.05\ m \times 0.05\ m$ (not shown in the figure). Each MC_i is discretized using bilinear quadrilateral elements of uniform size $0.0025\ m \times 0.0025\ m$.

C.8.1. Macroscopic analysis from a single Micro-Cell

In this example, the three homogeneous Micro-Cells described above are excited through prescribed macroscopic variables. The macro-scale fields are arbitrarily prescribed, adopting a macro-scale temperature rate $\dot{\phi}^{n+1} = \frac{1}{\Delta t}\sin(\omega\ t)\ \ [^{\circ}C]$ a macro-scale temperature gradient $\mathbf{g}^{n+1} = [1,\ 0]^T \sin(\omega\ t)$ $\left[\frac{^{\circ}C}{m}\right]$ and the rate of the macro-scale gradient, determined as $\dot{\mathbf{g}}^{n+1} = \frac{\mathbf{g}^{n+1} - \mathbf{g}^{n}}{\Delta t}\ \left[\frac{^{\circ}C}{m\ s}\right]$. Let $\omega = \frac{\pi}{4}$ and constant time steps of $\Delta t = 0.1s$ be adopted for the time discretization. Based on this information, the time evolution of the heat flux vector and the internal energy rate at the macro-scale material point is computed directly using the expressions

$$\mathbf{Q}_{\text{BS}}^{n+1} = -\kappa\ \mathbf{I} \cdot \mathbf{g}^{n+1},$$
$$\dot{\xi}_{\text{BS}}^{n+1} = \rho\ c_p\ \dot{\phi}^{n+1},$$

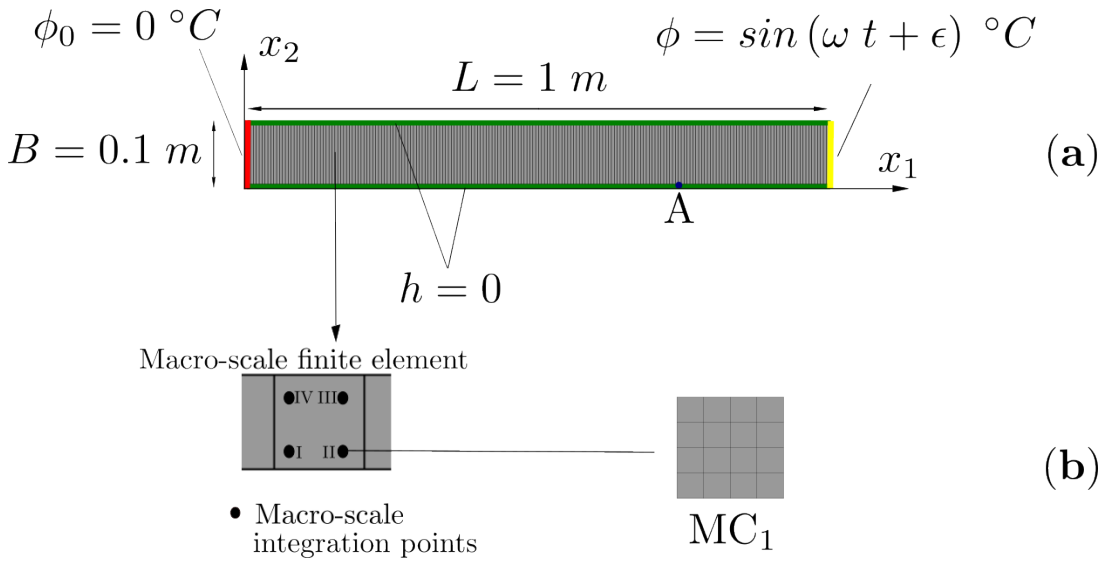

Figura C.3: Multiscale procedure applied to the 1D transient heat transfer problem. (a) Macro-scale. (b) Micro-scale. (Not to scale drawing)

where the macroscopic constitutive properties are assumed to be identical to those adopted at the micro-scale, that is, $\kappa = \kappa_\mu$ and $\rho\ c_p = \rho_\mu\ c_{p_\mu}$. The obtained results serve as the benchmark solution (BS) for comparison.

Regarding the numerical solution, the boundary conditions imposed at the micro-scale correspond to those discussed in Sections C.3.3.3 and in Appendix A, namely: the MCMM (C.13) and the periodic model (C.65), which coincide for this type of example; the Taylor model (C.62); and the linear model (C.63). In addition, the two proposed multiscale schemes are applied: the FOE scheme with $\alpha = 1$ and the SOE approach with $\alpha = 0$.

First, the results obtained by imposing the MCMM boundary condition on the three proposed Micro-Cells are examined. Specifically, the time evolution of the x_1 component of the homogenized heat flux vector $\mathbf{Q}^{n+1}$ is presented in Figure (C.4). In this figure, several relevant aspects are highlighted. It is observed that the smallest Micro-Cell (MC_1) exhibits a slight difference compared to the benchmark solution. This behavior is expected, as demonstrated by analytical results in the expressions (C.45), (C.48), (C.50) and (C.52), where it can be seen that the terms depending on the MC size are negligible when the MC size is sufficiently small. This observation is in agreement with certain proposals in the literature which, in contrast to the traditional notion of RVE, suggest that the micro-scale tends to infinitesimal dimensions. However, it is clearly observed that, as larger windows of the homogeneous material are considered, the heat flux obtained employing the FOE-formulation deviates significantly from the expected result. On the other hand, regardless of the MC size, the SOE scheme successfully recovers the heat flux values of the reference solution, showing complete agreement throughout the entire time interval analyzed.

A clarification is necessary regarding this example, in which only a single point of the macro-scale is analyzed. Since the macroscopic primary variables are arbitrarily prescribed over time, the homogenized internal energy rate, computed according to (C.19), does not include any terms that introduce a size effect. Consequently, both numerical solutions coincide with the benchmark solution at every instant of time, which explains why there is no figure corresponding to this variable. Nevertheless, in a full multiscale context, different temperature values could be obtained at each time step, depending on whether the FOE or SOE formulation is used. This difference arises because the values of the flux vector, which influence the solution of the system of equations, see (C.54), exhibit a dependence on the size of the MC when the FOE scheme is applied.

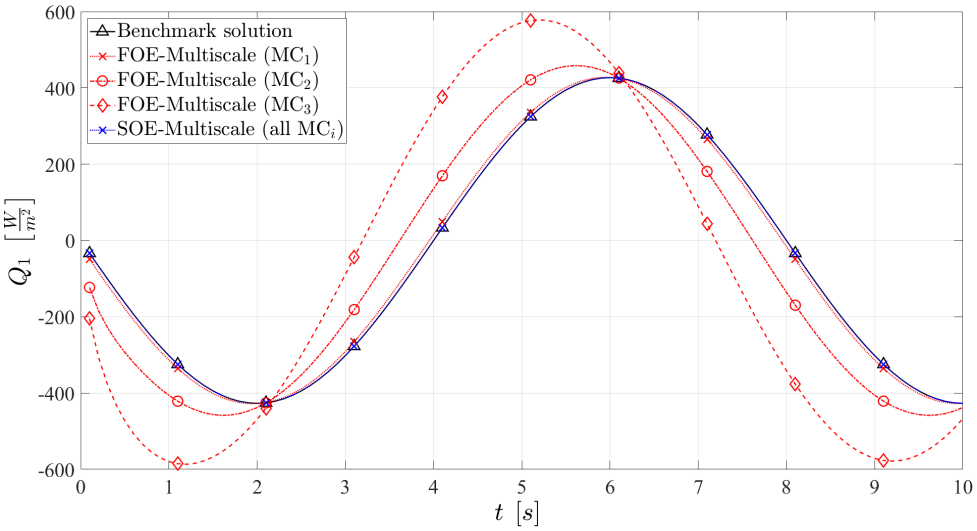

Figura C.4: Time evolution of the x_1-component of the homogenized heat flux vector $\mathbf{Q}^{n+1}$ for different MC sizes, under MCMM boundary conditions.

A common proposition found in some works addressing transient phenomena is that adopting different boundary conditions at the micro-scale can mitigate the size effect inherent to this class of problems. However, as previously demonstrated through analytical solutions (see C.6), it is not merely the choice of alternative fine-scale boundary conditions that allows for overcoming the size-induced inconsistency. Furthermore, a fluctuating micro-scale field will still exist when attempting to homogenize a homogeneous material. To numerically validate these conclusions, the solutions obtained using the different boundary conditions (Taylor, Linear and MCMM/Periodic) for the largest Micro-Cell (MC_3) are considered. Once again, the time evolution of the x_1 component of the homogenized heat flux vector $\mathbf{Q}^{n+1}$ is analyzed. Figure C.5 illustrates that, under the FOE scheme, all imposed boundary conditions lead to a temporal distribution of heat flux similar to that obtained with the MCMM solution and diverge from the benchmark response. In contrast, when the SOE approach is applied, the homogeneous benchmark solution is again recovered regardless of the micro-scale boundary condition.

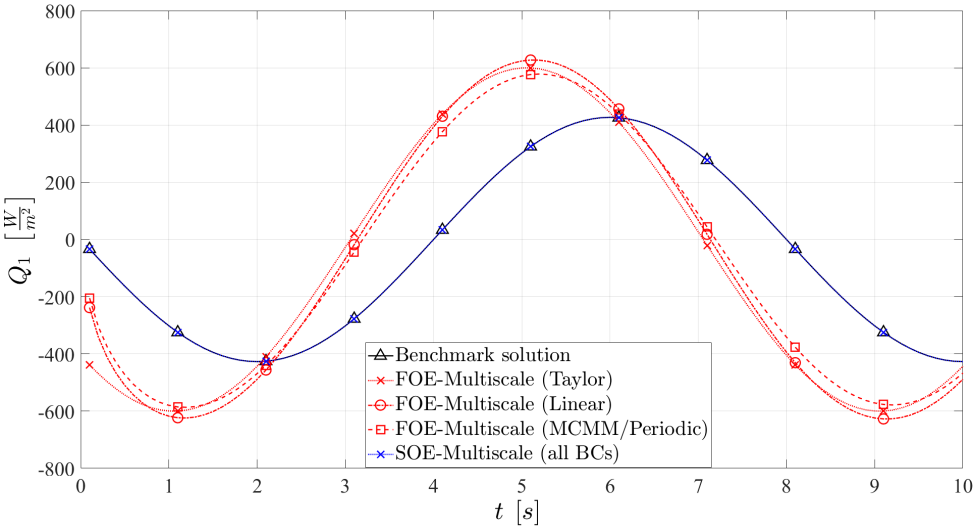

Figura C.5: Time evolution of the x_1-component of the homogenized heat flux vector $\mathbf{Q}^{n+1}$, under different boundary conditions imposed on MC_3.

Finally, to further clarify the role of the boundary conditions imposed at the micro-scale, color maps of the fluctuating scalar field $\tilde{\phi}_\mu$ at time $t = 0.1\ s$ are presented for the largest Micro-Cell (MC_3). These results correspond to the Linear model (Figure C.6) and the MCMM/Periodic model (Figure C.7). In each figure, the left panel depicts the FOE solution, where it is evident that a non-zero $\tilde{\phi}_\mu$ field develops at the fine scale. This field satisfies the imposed boundary conditions but remains non-vanishing despite modeling a homogeneous material. Conversely, the right panel displays a null field (within machine precision) for $\tilde{\phi}_\mu$, as expected when dealing with a homogeneous medium.

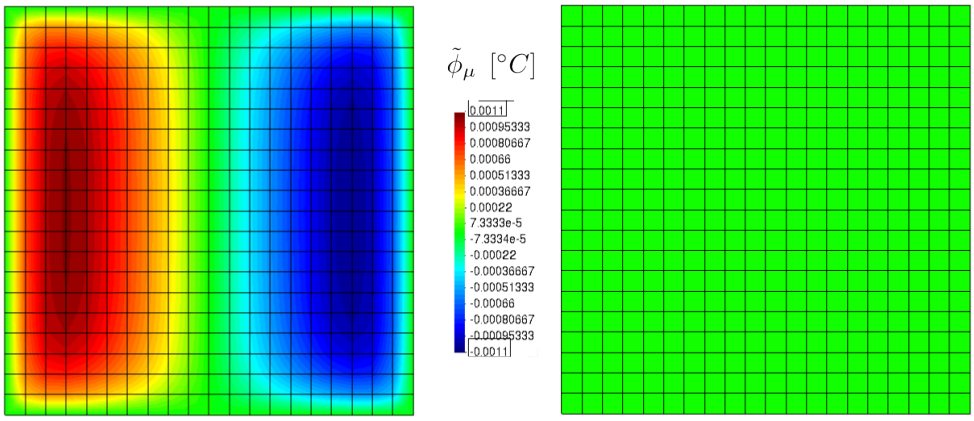

Figura C.6: Scalar field fluctuation at time $t = 0.1\ s$ for MC_3 using the Linear model. Left: FOE scheme. Right: SOE scheme.

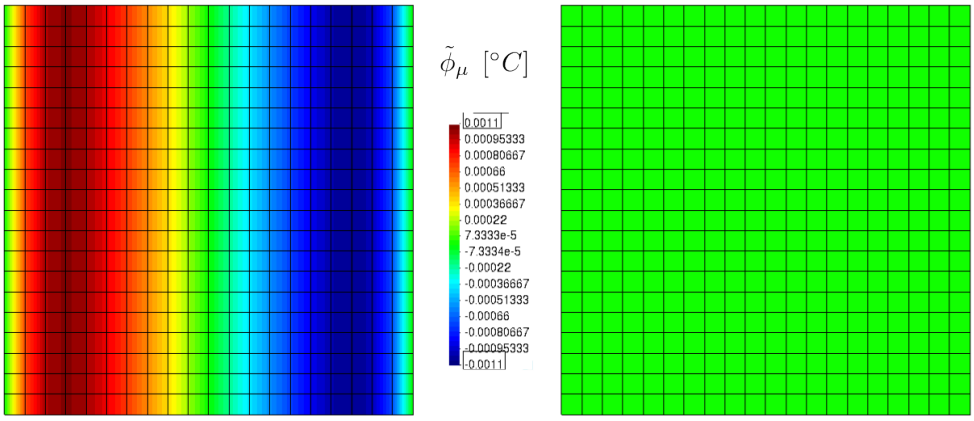

Figura C.7: Scalar field fluctuation at time $t = 0.1\ s$ for MC_3 using the MCMM/Periodic. Left: FOE scheme. Right: SOE scheme.

C.8.2. Fully multiscale example

In this section, a simple numerical scenario involving a transient thermal problem with a time-varying boundary condition is proposed. Specifically, it is a representative problem with a known analytical solution available in the literature [115]. This solution is used as a reference to evaluate the accuracy of numerical modeling approaches. The problem consists of a one-dimensional slab in the domain $0 < x_1 < L$ with zero initial temperature, $\phi\,(x_1, t = 0) = 0\ ^\circ C$, and with the boundary conditions $\phi\,(x_1 = 0, t > 0) = \phi_0 = 0\ ^\circ C$ and $\phi\,(x_1 = L, t > 0) = \phi_L = \sin(\omega\ t + \epsilon)\ ^\circ C$. The analytical expression for the spatial and temporal distribution of the temperature field, $\phi\,(x_1, t)$, can be rewritten

according to the notation of the present work, as follows

$$\phi\left(x_1,t\right)=A\ \sin(\omega\ t+\epsilon+\iota) + 2\ \pi\ \mathcal{D}\ \sum_{n=1}^{\infty}\frac{n\ (-1)^n\ \left(\mathcal{D}\ n^2\ \pi^2\ \sin\ \epsilon-\omega\ L^2\ \cos\ \epsilon\right)}{\mathcal{D}^2\ n^4\ \pi^4+\omega^2\ L^4}\sin\frac{n\pi\ x_1}{L}\ e^{-\frac{\mathcal{D}\ n^2\ \pi^2\ t}{L^2}}, \quad \text{(C.59)}$$

where

$$A=\left\{\frac{\cosh\ 2\mathcal{K}\ x_1-\cos\ 2\mathcal{K}\ x_1}{\cosh\ 2\mathcal{K}\ L-\cos\ 2\mathcal{K}\ L}\right\}^{\frac{1}{2}}, \quad \text{(C.60)}$$

$$\iota=arg\left\{\frac{\sinh\ \mathcal{K}\ x_1\left(1+i\right)}{\sinh\ \mathcal{K}\ L\left(1+i\right)}\right\}, \quad \text{(C.61)}$$

$\mathcal{K}$ is defined as $\mathcal{K}=\left(\frac{\omega}{2\mathcal{D}}\right)^{\frac{1}{2}}$ and $\mathcal{D}$ denotes the thermal diffusivity, as computed previously. The first term of (C.59) represents the periodic steady state solution and the second term the transient. The quantities A and ι denote the amplitude and phase of steady temperature oscillation at the position x_1, respectively, and can be calculated according to formulas (C.60) and (C.61). In particular, a bar of length $L=1\ m$, of the homogeneous material presented above, is modeled. For the sinusoidal variation of the temperature at the right end of the bar, the parameters $\omega=\pi/4$ and $\epsilon=0$ are adopted. Finally, to evaluate the analytical solution, the infinite summation in equation (C.59) was truncated and its upper limit was set to $n=1000$.

For the numerical multiscale modeling approach, the macro-scale domain is defined as a two-dimensional bar. However, due to the problem's symmetry and boundary conditions, the response remains effectively one-dimensional. Thus, at the macro-scale, a bar of length $L=1\ m$ but with a height $B=0.1\ m$ is modeled, as illustrated in Figure C.3-(a). Neumann boundary conditions $q=0$ are applied on the top and bottom surfaces, while the Dirichlet boundary condition previously introduced $\phi\left(t>0,x_1=0\right)=\phi_0=0\ ^\circ C$ and $\phi\left(t>0,x_1=L\right)=\phi_L=\sin(\omega\ t+\epsilon)\ ^\circ C$, are imposed on the left and right end, respectively. The macro-scale bar is discretized using 200 bilinear quadrilateral elements of dimensions $0.005\ m\times 0.1\ m$, resulting in an element length of $h_{\text{FEM}}=0.005\ m$ in the x_1 direction. In order to avoid spurious oscillations in the responses, the time step size must satisfy the minimum stability criterion, given in this particular case for a four-node quadrilateral element and the backward Euler method [116, 117]. It is determined by the formula $\Delta t_{\text{min}}\geq\frac{h_{\text{FEM}}^2}{2\mathcal{D}}=0.0725\ s$. Hence, constant time steps of $\Delta t=0.1\ s$ are assumed for the time discretization.

In line with the multiscale numerical modeling, a Micro-Cell (MC) is associated with each integration point of the macroscopic domain. The three Micro-Cells defined earlier in this section are considered. The previously specified material properties are assigned at the micro-scale. The same time step discretization is adopted. As for the boundary conditions imposed at the micro-scale, only the MCMM is employed in this example. Finally, the two proposed multiscale schemes (FOE and SOE) are implemented.

In particular, the analysis is focused on the values of the primary scalar field ϕ (temperature) at the nodes of coordinates $x_1=0.96m$ and $x_1=0.84m$ (and $x_2=0.0m$). The temporal evolution of the temperature field for $x_1=0.96m$ can be observed in Figure C.8. It can be seen that there is almost perfect agreement between the analytical benchmark solution and the proposed SOE multiscale approach. On the other hand, a slight discrepancy is observed in the red curve corresponding to the smallest Micro-Cell (MC_1) modeled by the FOE scheme. This difference reaches quite pronounced values as the size of the Micro-Cell increases (MC_3), showing a behavior completely different from the expected reference response.

It could be argued that in the vicinity of the right end of the bar, the spatial temperature gradients are steep, potentially limiting the applicability of multiscale modeling. However, in Figure C.9, which corresponds to the temporal evolution of the temperature of a location further away from the end ($x_1=$

$0.84m$), a similar behavior to that described for Figure C.8 is observed. That is, a situation where the FOE scheme exhibits poor performance at increasing Micro-Cell sizes, while the SOE multiscale model consistently yields results that closely match the analytical benchmark solution.

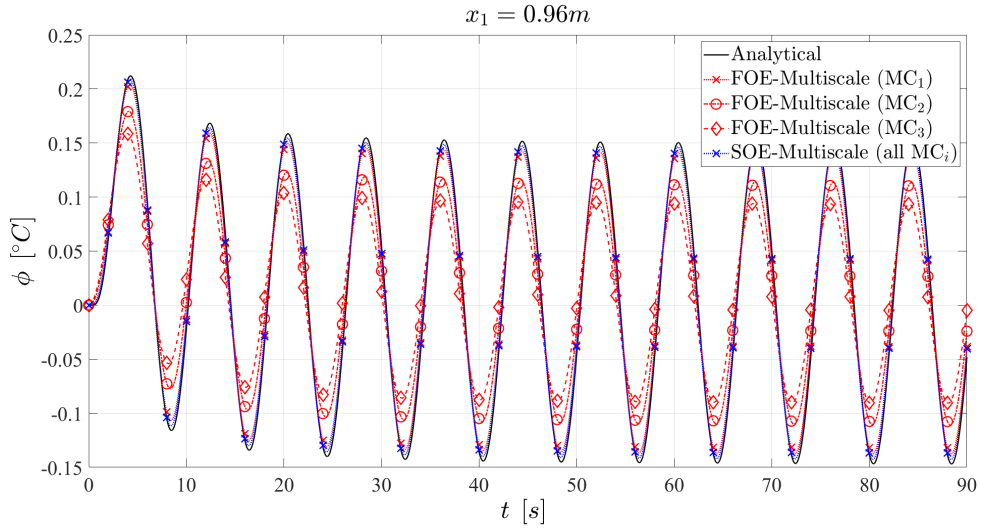

Figura C.8: Evolution of the temperature for point at the nodes of coordinates $x_1 = 0.96m$. MCMM boundary conditions imposed on MCs of different sizes.

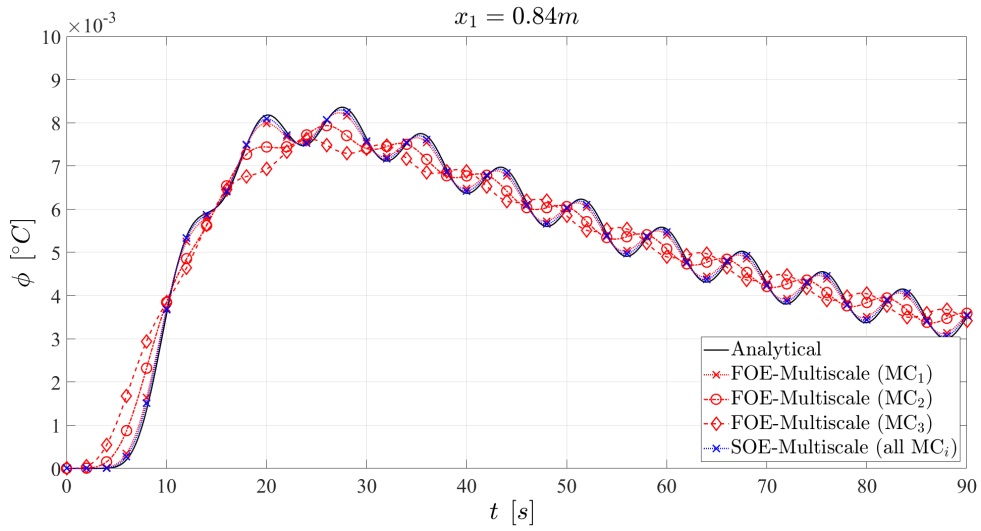

Figura C.9: Evolution of the temperature for point at the nodes of coordinates $x_1 = 0.84m$. MCMM boundary conditions imposed on MCs of different sizes.

The results obtained throughout this section have demonstrated the shortcomings of using Full-Order Expansion in the multiscale modeling of balance problems of a scalar quantity, and secondly, how the Selective-Order Expansion scheme allows the expected responses to be recovered.

C.9. Conclusions

This article offers a comprehensive assessment of the micro-scale size effects in First-Order RVE-based multiscale formulations for generic scalar balance problems with source terms.

The Method of Multiscale Virtual Power (MMVP), in conjunction with a Lagrange multiplier technique, has allowed direct access to the strong form of the micro-scale governing equations, which are not standard due to the constraints inherent to multiscale modeling. Based on this differential description, we derive analytical homogenized solutions from simplified, yet conceptually meaningful, multiscale scenarios. Such an approach enables the isolation and rigorous characterization of the fundamental mechanisms underlying the second-order effects. To the best of the authors' knowledge, this represents one of the first fully transparent and mathematically tractable demonstrations of the size-dependence of the effective response, thereby reducing the ambiguities often associated with purely numerical evidence.

A detailed decomposition of the homogenized transient flux reveals a set of distinct components capable of inducing size-dependent behavior, herein referred to as $\mathbf{T}_i$-terms. The proposed theoretical analysis shows that, within the FOE-based multiscale model, these $\mathbf{T}_i$-terms are not concurrently active, yet they do not vanish simultaneously. Thus, macroscopic size effects are inherently embedded in the FOE-procedure. The loss of macro-scale objectivity is not an intrinsic (non-local) physical feature of the problem under study, but rather a modeling consequence associated with the Full-Order Expansion at the constitutive level. In particular, the incorporation of macro-scale gradients into material law evaluations induces both explicit contributions and implicit effects (the latter arising from the fluctuation field solution), thereby generating size-dependent terms that challenge the classical notion of the existence of a Representative Volume Element.

Additional findings of this study are as follows. The net macro-scale size effect depends on the modeling assumptions, including the material behavior, the imposed loading conditions, and the adopted homogenization scheme. Certain $\mathbf{T}_i$-components scale with ℓ^2_{MC}, whereas others exhibit linear growth with the characteristic length of the Micro-Cell. Both the micro-scale source term and the non-stationary contribution induce second-order phenomena. Short-term regimes (i.e. $\Delta t \to 0$) further amplify the size effect. The loss of macro-scale objectivity arises from both the initial state of the Micro-Cell and the current excitations. Finally, the issue cannot be resolved simply by manipulating the constraints imposed on the primitive fluctuation field.

The so-called Selective Order Expansion (SOE) methodology, previously introduced by the authors in the context of poromechanics, has been extended and adapted to generic multiscale balance problems with source terms. This approach incorporates a minimal yet fundamental modification at the constitutive level and preserves the structure of the underlying multiscale variational framework. As a result, the SOE-formulation eliminates all sources of micro-scale size-dependence, thereby restoring the objectivity of the macroscopic response and re-establishing the classical notion of RVE through standard scale enlargement arguments. A key distinction with respect to our previous works lies in the generalized macro-scale insertion procedure proposed here, which allows material properties to depend on the primitive field, while maintaining objectivity.

Simple numerical examples, based on an FE^2 implementation, are provided to support and confirm all the above conclusions.

The general format in which the multiscale model has been described in this work renders the results broadly applicable across a range of fields of physics, including heat transfer, species diffusion, generic reaction–diffusion systems, flow and seepage in porous media, among many other coupled phenomena. In fact, the main message of the paper can be extended to balance laws for tensor-valued quantities. The proposed SOE-strategy should be understood not as a problem-specific adjustment, but as a systematic paradigm for constructing fully First-Order multiscale models.

Acknowledgments

This study was financed in part by the Coordenação de Aperfeiçoamento de Pessoal de Nível Superior - Brasil (CAPES) - Finance Code 001.

Data availability statement

All data can be reproduced with the provided information.

Financial disclosure

None reported.

Conflict of interest

The authors declare no potential conflict of interests.

Declaration of generative AI and AI-assisted technologies in the writing process

During the preparation of this work the author(s) used ChatGPT/OpenAI in order to improve readability and language of the work. After using this tool/service, the author(s) reviewed and edited the content as needed and take(s) full responsibility for the content of the publication.

Appendix A. Classical homogenization models according to the admissible constraints imposed on the Micro-Cell

This topic is well established in the context of RVE-based multiscale modeling and is included here for the sake of completeness.

The full characterization of the variational problem (C.20) requires an appropriate specification for the linear space $\widetilde{\mathcal{T}}_\mu^{\square}(\Omega_\mu) \subseteq \widetilde{\mathcal{T}}_\mu(\Omega_\mu)$. In general, different macro-scale constitutive responses may be obtained depending on the choice adopted. In this contribution, four classical methods are considered to address both analytical and numerical problems. These are: (i) the Taylor model, (ii) the Linear model, (iii) the Periodic model, and the MCMM, which has already been presented in the body of the paper, see (C.13). The methodologies indicated in items (i)-(iii) are briefly introduced below; for further details, the reader is referred to [21, 66, 67].

(i) Taylor model. This approach assumes that the fluctuating primary scalar field is zero throughout the entire Micro-Cell domain. Thus, the sub-space $\widetilde{\mathcal{T}}_\mu^{\text{Tay}}(\Omega_\mu) \subset \widetilde{\mathcal{T}}_\mu(\Omega_\mu)$ is written as follows

$$\widetilde{\mathcal{T}}_\mu^{\text{Tay}}(\Omega_\mu) = \left\{ \tilde{\phi}_\mu = 0 \; \forall \, \mathbf{x}_\mu \in \Omega_\mu \right\} \equiv \tilde{\mathcal{T}}_\mu^{*\text{Tay}}(\Omega_\mu). \tag{C.62}$$

(ii) Linear model. The restriction on the macro- and micro-scale gradient is guaranteed by imposing $\tilde{\phi}_\mu = 0$ over the entire MC boundary Γ_μ. The formal definition of the sub-space $\widetilde{\mathcal{T}}_\mu^{\text{Lin}}(\Omega_\mu) \subset \widetilde{\mathcal{T}}_\mu(\Omega_\mu)$ is given as

$$\widetilde{\mathcal{T}}_\mu^{\text{Lin}}(\Omega_\mu) = \left\{ \tilde{\phi}_\mu \in \mathrm{H}^1(\Omega_\mu) \, ; \int_{\Omega_\mu} \tilde{\phi}_\mu \, d\Omega_\mu = 0 \right. \\ \left. \text{and } \tilde{\phi}_\mu = 0 \; \forall \, \mathbf{x}_\mu \in \Gamma_\mu \right\} \equiv \tilde{\mathcal{T}}_\mu^{*\text{Lin}}(\Omega_\mu). \tag{C.63}$$

(iii) Periodic model. Certain geometrical properties must be satisfied by the micro-scale material distribution to be consistent with the assumption of periodic media. For simplicity, the description is

restricted to two-dimensional problems and rectangular Micro-Cells. Under such conditions, opposite MC-edges are identified in pairs. There are two pairs of edges. Each pair "i" consists of opposite and equally sized subsets $\Gamma^+_{\mu\, i}$ and $\Gamma^-_{\mu\, i}$ of Γ_μ, with unit normals $\mathbf{n}^+_i$ and $\mathbf{n}^-_i$, respectively. A one-to-one correspondence exists between points of $\Gamma^+_{\mu\, i}$ and $\Gamma^-_{\mu\, i}$. That is, each point $\mathbf{x}^+_{\mu_i} \in \Gamma^+_{\mu\, i}$ has its corresponding point $\mathbf{x}^-_{\mu_i} \in \Gamma^-_{\mu\, i}$. The main feature of the periodic model lies in imposing identical values for the primary scalar field at opposite boundary points, as described below

$$\tilde{\phi}_\mu\left(\mathbf{x}^+_{\mu_i}, t\right) = \tilde{\phi}_\mu\left(\mathbf{x}^-_{\mu_i}, t\right), \ \forall \text{ pair } \{\mathbf{x}^+_{\mu_i}, \mathbf{x}^-_{\mu_i}\}, \ i = 1, 2. \tag{C.64}$$

Accordingly, the sub-space $\widetilde{\mathcal{T}}^{\text{Per}}_\mu(\Omega_\mu) \subset \widetilde{\mathcal{T}}_\mu(\Omega_\mu)$ is defined as

$$\widetilde{\mathcal{T}}^{\text{Per}}_\mu(\Omega_\mu) = \Bigg\{ \tilde{\phi}_\mu \in \mathrm{H}^1(\Omega_\mu) ; \int_{\Omega_\mu} \tilde{\phi}_\mu \, d\Omega_\mu = \mathbf{0} \\ \text{and } \tilde{\phi}_\mu\left(\mathbf{x}^+_{\mu_i}\right) = \tilde{\phi}_\mu\left(\mathbf{x}^-_{\mu_i}\right) \ \forall \text{ pair } \{\mathbf{x}^+_{\mu_i}, \mathbf{x}^-_{\mu_i}\}, \ i = 1, 2 \Bigg\} \equiv \tilde{\mathcal{T}}^{*\text{Per}}_\mu(\Omega_\mu). \tag{C.65}$$

Appendix B. Hill–Mandel principle with Lagrange multipliers for MCMM

The objective of this section is to obtain a deeper insight into the scalar and vector reactions that induce the constraints specified by the minimally constrained multiscale model, and to understand the fundamental link between them and the homogenized quantities appearing at the macro-scale [21, 27].

To build the alternative form of the Hill–Mandel principle (C.16) the constraints (C.10) and (C.12) are enforced by means of appropriate conjugate Lagrange multipliers, denoted as Θ and $\mathbf{\Lambda}$, respectively. Since each of these constraints involves null mean integrals (volumetric or surface averages), the associated Lagrange multipliers are spatially uniform fields, thus we have $\Theta \in \mathbb{R}$ and $\mathbf{\Lambda} \in \mathbb{R}^{nd}$. Consequently, the variational expression (C.16) is rewritten as

$$|\Omega_\mu| \left[\left(\dot{\xi} - S\right) \delta\phi - \mathbf{Q} \cdot \delta\mathbf{g} \right] = \int_{\Omega_\mu} \Big[\left(\dot{\xi}_\mu - S_\mu\right) \left(\delta\phi + \delta\mathbf{g} \cdot \mathbf{x}'_\mu + \delta\tilde{\phi}_\mu\right) \\ - \mathbf{Q}_\mu \cdot \left(\delta\mathbf{g} + \boldsymbol{\nabla}_{\mathbf{x}_\mu} \delta\tilde{\phi}_\mu\right) \Big] d\Omega_\mu + \Theta \int_{\Omega_\mu} \delta\tilde{\phi}_\mu \, d\Omega_\mu + \delta\Theta \int_{\Omega_\mu} \tilde{\phi}_\mu \, d\Omega_\mu \\ + \mathbf{\Lambda} \cdot \int_{\Gamma_\mu} \delta\tilde{\phi}_\mu \, \mathbf{n}_\mu \, d\Gamma_\mu + \delta\mathbf{\Lambda} \cdot \int_{\Gamma_\mu} \tilde{\phi}_\mu \, \mathbf{n}_\mu \, d\Gamma_\mu, \\ \forall \left(\delta\phi, \delta\mathbf{g}, \delta\tilde{\phi}_\mu, \delta\Theta, \delta\mathbf{\Lambda}\right) \in \mathbb{R} \times \mathbb{R}^{nd} \times \mathrm{H}^1(\Omega_\mu) \times \mathbb{R} \times \mathbb{R}^{nd}, \ \forall t. \tag{C.66}$$

Assuming that all the macro-scale virtual actions vanish, the variational form of the micro-scale balance equation with Lagrange multipliers is obtained

$$\int_{\Omega_\mu} \left[\left(\dot{\xi}_\mu - S_\mu\right) \delta\tilde{\phi}_\mu - \mathbf{Q}_\mu \cdot \boldsymbol{\nabla}_{\mathbf{x}_\mu} \delta\tilde{\phi}_\mu \right] d\Omega_\mu + \Theta \int_{\Omega_\mu} \delta\tilde{\phi}_\mu \, d\Omega_\mu \\ + \delta\Theta \int_{\Omega_\mu} \tilde{\phi}_\mu \, d\Omega_\mu + \mathbf{\Lambda} \cdot \int_{\Gamma_\mu} \delta\tilde{\phi}_\mu \, \mathbf{n}_\mu \, d\Gamma_\mu + \delta\mathbf{\Lambda} \cdot \int_{\Gamma_\mu} \tilde{\phi}_\mu \, \mathbf{n}_\mu \, d\Gamma_\mu = 0, \\ \forall \left(\delta\tilde{\phi}_\mu, \, \delta\Theta, \, \delta\mathbf{\Lambda}\right) \in \mathrm{H}^1(\Omega_\mu) \times \mathbb{R} \times \mathbb{R}^{nd}, \ \forall t. \tag{C.67}$$

Following straightforward mathematical manipulations on the weak form (C.67), including integration by parts of some terms and classical variational arguments, the strong form of the balance equation is

reached

$$\begin{cases} \text{Div}_{\mathbf{x}_\mu}\, \mathbf{Q}_\mu + \dot{\xi}_\mu - S_\mu + \Theta = 0, \quad \forall\, \mathbf{x}_\mu \in \Omega_\mu,\ \forall\, t, \\ \mathbf{Q}_\mu \cdot \mathbf{n}_\mu = \mathbf{\Lambda} \cdot \mathbf{n}_\mu, \quad \forall\, \mathbf{x}_\mu \in \Gamma_\mu,\ \forall\, t, \\ \int_{\Omega_\mu} \tilde{\phi}_\mu \, d\Omega_\mu = 0, \\ \int_{\Gamma_\mu} \tilde{\phi}_\mu \, \mathbf{n}_\mu \, d\Gamma_\mu = \mathbf{0}, \end{cases} \tag{C.68}$$

where $\mathbf{Q}_\mu \cdot \mathbf{n}_\mu = \mathbf{\Lambda} \cdot \mathbf{n}_\mu = q_\mu$ is the reactive flux per unit area over the MC boundary Γ_μ.

In the following, additional physical meanings for the Lagrange multipliers $(\Theta, \mathbf{\Lambda})$ are obtained in the particular context of the minimally constrained multiscale model. First, by choosing $\delta\tilde{\phi}_\mu = c \in \mathbb{R}$ as an arbitrary uniform scalar field, with $\delta\Theta = 0$ and $\delta\mathbf{\Lambda} = \mathbf{0}$ in (C.67), it yields

$$\left[\int_{\Omega_\mu} \left(\dot{\xi}_\mu - S_\mu\right) d\Omega_\mu\right] c + |\Omega_\mu|\, \Theta\, c + \mathbf{\Lambda} \cdot \left(c \underbrace{\int_{\Gamma_\mu} \mathbf{n}_\mu \, d\Gamma_\mu}_{\mathbf{0}}\right) = 0,$$

$$\forall\, c \in \mathbb{R},\ \forall\, t, \tag{C.69}$$

which results in

$$\Theta = -\frac{1}{|\Omega_\mu|} \int_{\Omega_\mu} \left(\dot{\xi}_\mu - S_\mu\right) d\Omega_\mu = -\left(\dot{\xi} - S\right). \tag{C.70}$$

The latter equality is achieved by homogenization, see expression (C.19).

Finally, by adopting in (C.67) $\delta\Theta = 0$, $\delta\mathbf{\Lambda} = \mathbf{0}$ and $\delta\tilde{\phi}_\mu = \mathbf{A} \cdot \mathbf{x}'_\mu$, where $\mathbf{A} \in \mathbb{R}^{nd}$ is and arbitrary vector, it follows that

$$\mathbf{A} \cdot \left[\int_{\Omega_\mu} \left(\dot{\xi}_\mu - S_\mu\right) \mathbf{x}'_\mu - \mathbf{Q}_\mu \, d\Omega_\mu\right] + \Theta\, \mathbf{A} \cdot \overbrace{\int_{\Omega_\mu} \mathbf{x}'_\mu \, d\Omega_\mu}^{\mathbf{0}} + \mathbf{A} \cdot \left[\int_{\Gamma_\mu} \mathbf{x}'_\mu \otimes \mathbf{n}_\mu \, d\Gamma_\mu\right] \mathbf{\Lambda} = 0, \quad \forall\, \mathbf{A} \in \mathbb{R}^{nd},\ \forall\, t, \tag{C.71}$$

where the second term is equal to zero according to (C.9). Using the homogenization formula (C.17) and the geometric property $\int_{\Gamma_\mu} \mathbf{n}_\mu \, d\Gamma_\mu = \mathbf{0}$, the variational equation (C.71) characterizes the Lagrange multiplier $\mathbf{\Lambda}$

$$\mathbf{\Lambda} = |\Omega_\mu| \left[\int_{\Gamma_\mu} \mathbf{x}_\mu \otimes \mathbf{n}_\mu \, d\Gamma_\mu\right]^{-1} \mathbf{Q} = \mathbf{Q}. \tag{C.72}$$

Appendix C. Some physical problems encompassed by the proposed general multiscale framework

Generic balance equations for scalar quantities underlie the physics of many phenomena. Table (C.1) summarizes some representative cases and identifies the main variables using the notation introduced in this manuscript.

Coupled problems involving the examples of Table C.1 can also be considered, such as transient thermo-mechanical, chemo-mechanical, and hydro-mechanical phenomena.

Tabla C.1: Variable identification across different physical problems

Problem	Symbol	Interpretation
Transient heat conduction	$\mathbf{Q}$	Heat flux vector
	$\dot{\xi}$	Rate of change of internal thermal energy
	S	Heat source or sink
	q	Prescribed heat flux
	ϕ	Temperature
	$\mathbf{g}$	Temperature gradient
	c	Volumetric heat capacity
	$\mathbf{k}$	Thermal conductivity tensor
Species diffusion	$\mathbf{Q}$	Diffusive mass flux
	$\dot{\xi}$	Rate of mass accumulation of the species
	S	Mass source or sink due to reactions
	q	Prescribed mass flux
	ϕ	Species concentration
	$\mathbf{g}$	Concentration gradient
	c	Storage coefficient
	$\mathbf{k}$	Diffusive mobility
Porous media flow	$\mathbf{Q}$	lux vector
	$\dot{\xi}$	Rate of fluid mass (or volume) storage
	S	Fluid injection or extraction term
	q	Prescribed fluid flux
	ϕ	Pore pressure
	c	Storage coefficient
	$\mathbf{g}$	Pore pressure gradient
	$\mathbf{k}$	Hydraulic conductivity

Appendix D. Calculation of the Fourier coefficient

The Fourier coefficients b_j^n are obtained as a function of the previous condition of the fluctuation field, $\tilde{\phi}_\mu^n(x_\mu)$, as follows

$$b_j^n = \frac{2}{\ell_{\text{MC}}} \int_{x_\mu=-\frac{\ell_{\text{MC}}}{2}}^{x_\mu=\frac{\ell_{\text{MC}}}{2}} \tilde{\phi}_\mu^n(x_\mu)\, \sin\left(\frac{2\,j\,\pi}{\ell_{\text{MC}}} x_\mu\right) dx_\mu, \quad j = 1, \ldots, \infty. \tag{C.73}$$

Assuming a null initial condition $\tilde{\phi}_\mu^0(x_\mu) = 0$, at $t^0 = 0$, all the coefficients b_j^0 are zero. Thus, the first evaluation of $\tilde{\phi}_\mu^1(x_\mu)$, at $t^1 = \Delta t$, from (C.41) yields

$$\tilde{\phi}_\mu^1(x_\mu) = \tilde{\phi}_\mu^{\text{SS}\,1}(x_\mu) = \frac{\epsilon^1\,\alpha\,\ell_{\text{MC}}\,\sinh(\beta\,x_\mu)}{2\,s_\mu\,\sinh\left(\frac{\beta\,\ell_{\text{MC}}}{2}\right)} - \frac{\epsilon^1\,\alpha}{s_\mu}\,x_\mu, \tag{C.74}$$

while the corresponding b_j^1-coefficients are evaluated as follows

$$\begin{aligned} b_j^1 &= \frac{2}{\ell_{\text{MC}}} \int_{x_\mu=-\frac{\ell_{\text{MC}}}{2}}^{x_\mu=\frac{\ell_{\text{MC}}}{2}} \tilde{\phi}_\mu^1\left(x_\mu\right)\, \sin\left(\frac{2\,j\,\pi}{\ell_{\text{MC}}} x_\mu\right) dx_\mu \\ &= \frac{2\,\epsilon^1\,\alpha}{s_\mu\,\ell_{\text{MC}}} \int_{x_\mu=-\frac{\ell_{\text{MC}}}{2}}^{x_\mu=\frac{\ell_{\text{MC}}}{2}} \left[\frac{\ell_{\text{MC}}\,\sinh(\beta\,x_\mu)}{2\,\sinh\left(\frac{\beta\,\ell_{\text{MC}}}{2}\right)} - x_\mu\right]\, \sin\left(\frac{2\,j\,\pi}{\ell_{\text{MC}}} x_\mu\right) dx_\mu,\ j=1,\ldots,\infty. \end{aligned} \tag{C.75}$$

After some straightforward algebraic manipulation, the Fourier coefficients b_j^1 acquire the form

$$b_j^1 = \frac{2\,\epsilon^1\,\alpha\,\beta^2\,(-1)^j}{s_\mu\,\omega_j\,\left(\beta^2+\omega_j^2\right)}, \quad j=1,\ldots,\infty. \tag{C.76}$$

From the second time step ($t^2 = t^1 + \Delta t$) onward, the full mathematical structure of the solution is already established; hence, it follows that $b_j^n = b_j^1$, as given in (C.76).

Appendix E. Components of the macro-scale Jacobian matrix

The macro-scale Jacobian matrix presented in (C.55) is computed as follows (subscript k is omitted here to simplify the notation)

$$\begin{aligned} \frac{\partial \mathbf{E}^{n+1}}{\partial \bar{\boldsymbol{\phi}}^{n+1}} = &\int_\Omega \mathbf{N}^T\, \frac{\partial\left(\dot{\xi}^{n+1}-S^{n+1}\right)}{\partial \phi^{n+1}}\, \mathbf{N}\, d\Omega + \int_\Omega \mathbf{N}^T\, \frac{\partial\left(\dot{\xi}^{n+1}-S^{n+1}\right)}{\partial \mathbf{g}^{n+1}}\, \mathbf{B}\, d\Omega \\ &- \int_\Omega \mathbf{B}^T\, \frac{\partial \mathbf{Q}^{n+1}}{\partial \phi^{n+1}}\, \mathbf{N}\, d\Omega - \int_\Omega \mathbf{B}^T\, \frac{\partial \mathbf{Q}^{n+1}}{\partial \mathbf{g}^{n+1}}\, \mathbf{B}\, d\Omega. \end{aligned} \tag{C.77}$$

The derivatives remaining in (C.77) constitute the so-called homogenized tangent operators of the multiscale model. To derive these terms, the following elements are considered: (i) the homogenization rules of macro-scale dual variables (C.17) and (C.19), (ii) the micro-scale constitutive laws (C.30)-(C.32) and (iii) the time integration procedure based on the implicit backward Euler method. Some additional details are provided below to complete the presentation.

(I) Derivatives of the homogenized source and time dependent contribution $\left(\dot{\xi}^{n+1}-S^{n+1}\right)$ with respect to the primal scalar and vector macro-scale variables

$$\begin{aligned} \frac{\partial\left(\dot{\xi}^{n+1}-S^{n+1}\right)}{\partial \phi^{n+1}} = \frac{1}{|\Omega_\mu|}\Bigg\{ \int_{\Omega_\mu} \Bigg[&\frac{1}{\Delta t}\left(c_\mu\left(\phi_\mu^{\alpha,n+1}\right) + \frac{dc_\mu\left(\phi_\mu^{\alpha,n+1}\right)}{d\phi_\mu^{\alpha,n+1}}\,\Delta\phi_\mu^\alpha\right) \\ &+ s_\mu\left(\phi_\mu^{\alpha,n+1}\right) + \frac{ds_\mu\left(\phi_\mu^{\alpha,n+1}\right)}{d\phi_\mu^{\alpha,n+1}}\left(\phi_\mu^{\alpha,n+1}-\phi_\mu^{\text{ref}}\right)\Bigg]\left(1+\frac{\partial\tilde{\phi}_\mu^{n+1}}{\partial\phi^{n+1}}\right) d\Omega_\mu \Bigg\}, \end{aligned} \tag{C.78}$$

$$\frac{\partial\left(\dot{\xi}^{n+1}-S^{n+1}\right)}{\partial\mathbf{g}^{n+1}}=\frac{1}{|\Omega_\mu|}\Bigg\{\int_{\Omega_\mu}\Bigg[\frac{1}{\Delta t}\left(c_\mu\left(\phi_\mu^{\alpha,n+1}\right)+\frac{dc_\mu\left(\phi_\mu^{\alpha,n+1}\right)}{d\phi_\mu^{\alpha,n+1}}\,\Delta\phi_\mu^{\alpha}\right)+s_\mu\big(\phi_\mu^{\alpha,n+1}\big)+\frac{ds_\mu\big(\phi_\mu^{\alpha,n+1}\big)}{d\phi_\mu^{\alpha,n+1}}\left(\phi_\mu^{\alpha,n+1}-\phi_\mu^{\text{ref}}\right)\Bigg]\left(\alpha\,\mathbf{x}'_\mu+\frac{\partial\tilde{\phi}_\mu^{n+1}}{\partial\mathbf{g}^{n+1}}\right)d\Omega_\mu\Bigg\},\quad\text{(C.79)}$$

(II) Derivatives of the homogenized flux vector $\mathbf{Q}^{n+1}$ with respect to the primal scalar and vector macro-scale variables

$$\begin{aligned}\frac{\partial\mathbf{Q}^{n+1}}{\partial\phi^{n+1}}=\frac{1}{|\Omega_\mu|}\Bigg\{&\int_{\Omega_\mu}\Bigg[-\mathbf{k}_\mu\left(\phi_\mu^{\alpha,n+1}\right)\frac{\partial\tilde{\mathbf{g}}_\mu^{n+1}}{\partial\phi^{n+1}}-\frac{d\mathbf{k}_\mu\left(\phi_\mu^{\alpha,n+1}\right)}{d\phi^{\alpha,n+1}}\left(1+\frac{\partial\tilde{\phi}_\mu^{n+1}}{\partial\phi^{n+1}}\right)\mathbf{g}_\mu^{n+1}\Bigg]d\Omega_\mu\\&-\int_{\Omega_\mu}\mathbf{x}'_\mu\Bigg[\frac{1}{\Delta t}\left(c_\mu\left(\phi_\mu^{\alpha,n+1}\right)+\frac{dc_\mu\left(\phi_\mu^{\alpha,n+1}\right)}{d\phi_\mu^{\alpha,n+1}}\,\Delta\phi_\mu^{\alpha}\right)+s_\mu\big(\phi_\mu^{\alpha,n+1}\big)+\frac{ds_\mu\big(\phi_\mu^{\alpha,n+1}\big)}{d\phi_\mu^{\alpha,n+1}}\left(\phi_\mu^{\alpha,n+1}-\phi_\mu^{\text{ref}}\right)\Bigg]\left(1+\frac{\partial\tilde{\phi}_\mu^{n+1}}{\partial\phi^{n+1}}\right)d\Omega_\mu\Bigg\},\end{aligned}\quad\text{(C.80)}$$

$$\begin{aligned}\frac{\partial\mathbf{Q}^{n+1}}{\partial\mathbf{g}^{n+1}}=\frac{1}{|\Omega_\mu|}\Bigg\{&\int_{\Omega_\mu}\Bigg[-\mathbf{k}_\mu\left(\phi_\mu^{\alpha,n+1}\right)\left(\mathbf{I}+\frac{\partial\tilde{\mathbf{g}}_\mu^{n+1}}{\partial\mathbf{g}^{n+1}}\right)-\frac{d\mathbf{k}_\mu\left(\phi_\mu^{\alpha,n+1}\right)}{d\phi^{\alpha,n+1}}\left(\alpha\,\mathbf{x}'_\mu+\frac{\partial\tilde{\phi}_\mu^{n+1}}{\partial\mathbf{g}^{n+1}}\right)\otimes\mathbf{g}_\mu^{n+1}\Bigg]d\Omega_\mu\\&-\int_{\Omega_\mu}\mathbf{x}'_\mu\otimes\Bigg[\frac{1}{\Delta t}\left(c_\mu\left(\phi_\mu^{\alpha,n+1}\right)+\frac{dc_\mu\left(\phi_\mu^{\alpha,n+1}\right)}{d\phi_\mu^{\alpha,n+1}}\,\Delta\phi_\mu^{\alpha}\right)+s_\mu\big(\phi_\mu^{\alpha,n+1}\big)+\frac{ds_\mu\big(\phi_\mu^{\alpha,n+1}\big)}{d\phi_\mu^{\alpha,n+1}}\left(\phi_\mu^{\alpha,n+1}-\phi_\mu^{\text{ref}}\right)\Bigg]\left(\alpha\,\mathbf{x}'_\mu+\frac{\partial\tilde{\phi}_\mu^{n+1}}{\partial\mathbf{g}^{n+1}}\right)d\Omega_\mu\Bigg\}.\end{aligned}\quad\text{(C.81)}$$

A final challenge, commonly encountered in RVE-based multiscale modeling, involves computing the derivatives of the micro-scale fluctuation fields with respect to the macro-scale variables appearing in equations (C.78)–(C.81), which are required to evaluate the homogenized tangent operators. Procedures for performing this derivation can be found in previous contributions [12, 62].

Appendix F. Micro-scale Jacobian matrix

In what follows, the derivative given in (C.58), concerning the Jacobian at the micro-scale level, is further defined by considering the micro-scale constitutive laws (C.30)-(C.32) and the time integration procedure based on the implicit backward Euler method (subscript k is omitted to simplify the notation)

$$\frac{\partial \mathbf{E}_{\mu}^{n+1}}{\partial \tilde{\tilde{\boldsymbol{\phi}}}_{\mu}^{n+1}} = \frac{1}{\Delta t}\int_{\Omega_\mu} \mathbf{N}_{\mu}^{T}\left[c_\mu\left(\phi_\mu^{\alpha,n+1}\right) + \frac{dc_\mu\left(\phi_\mu^{\alpha,n+1}\right)}{d\phi_\mu^{\alpha}}\,\Delta\phi_\mu^{\alpha}\right]\mathbf{N}_\mu\, d\Omega_\mu$$
$$+\int_{\Omega_\mu} \mathbf{N}_{\mu}^{T}\left[s_\mu\left(\phi_\mu^{\alpha,n+1}\right) + \frac{ds_\mu\left(\phi_\mu^{\alpha,n+1}\right)}{d\phi_\mu^{\alpha}}\,\left(\phi_\mu^{\alpha,n+1} - \phi_\mu^{\text{ref}}\right)\right]\mathbf{N}_\mu\, d\Omega_\mu$$
$$+\int_{\Omega_\mu} \mathbf{B}_{\mu}^{T}\,\mathbf{k}_\mu\left(\phi_\mu^{\alpha,n+1}\right)\,\mathbf{B}_\mu\, d\Omega_\mu + \int_{\Omega_\mu} \mathbf{B}_{\mu}^{T}\,\frac{d\mathbf{k}_\mu\left(\phi_\mu^{\alpha,n+1}\right)}{d\phi_\mu^{\alpha}}\,\mathbf{g}_\mu^{n+1}\,\mathbf{N}_\mu\, d\Omega_\mu. \quad \text{(C.82)}$$

Acknowledgments

This study was financed in part by the Coordenação de Aperfeiçoamento de Pessoal de Nível Superior - Brasil (CAPES) - Finance Code 001.

Apéndice D

Multiscale formulation for materials composed by a saturated porous matrix and solid inclusions

Reinaldo A. Anonis, Javier L. Mroginski, Pablo J. Sánchez, (2024). Multiscale formulation for materials composed by a saturated porous matrix and solid inclusions. Comput. Methods Appl. Mech. Engrg. 429 (2024) 117-162.

Multiscale formulation for materials composed by a saturated porous matrix and solid inclusions

Anonis, Reinaldo A.[1,1], **Mroginski, Javier L.**[1], **Sánchez, Pablo J.**[2,3]

[1]LAMEC-IMIT-CONICET Laboratorio de Mecánica Computacional, Universidad Nacional del Nordeste, Las Heras 727, CP 3500 Chaco, Argentina
[2]CIMEC-UNL-CONICET, Ruta Nac. 168, Km 0, Paraje el Pozo, CP 3000 Santa Fe, Argentina
[3]GIMNI-UTN-FRSF, Lavaise 610, CP 3000 Santa Fe, Argentina

Keywords: multiscale formulations, heterogeneous materials, RVE, saturated porous media, solid inclusions.

Abstract. Despite all the progress achieved in the characterization of heterogeneous materials by using multiscale paradigms based on the Representative Volume Element concept (RVE), there are still many aspects that demand ongoing development. We mention, for instance, in-homogeneous media with internal micro-structure comprising a mixture of components that require a dissimilar number/character of primary fields to describe their physical behavior. Micro-structures constituted by a saturated porous matrix (described through the pair displacement/pore pressure fields) endowed with impermeable non-porous solid inclusions (described only by the displacement field) are a typical example among many other practical applications. This new level of heterogeneity, between the set of primal descriptors for each micro-scale constituent, claims detailed revisions and novel adjustments in multiscale RVE-based theories.

In this work, we present a first-order RVE-based formulation to address with the aforementioned phenomenology at a smaller length scale. At the macro-scale, the well-known poromechanics theory is preserved, where the constitutive response is provided by homogenization of the corresponding micro-scale problem. Two important attributes feature the model: (i) it is encompassed within the general framework posited by the "Method of Multiscale Virtual Power (MMVP)", this leads to a variationally consistent methodology; (ii) our formulation preserves the objectivity with respect to the RVE-size (an indispensable but uncommon characteristic in RVE-based multiscale approaches for saturated porous media), due to it is based in a recent contribution of the authors (the so-called Selective Order Expansion technique "SOE").

The formulation is implemented following the squared Finite Element (FE^2) numerical scheme. The potentialities of the model are demonstrated through a detailed series of numerical examples, including rigorous comparisons against the Direct Numerical Simulation (DNS) procedure.

D.1. Introduction

Many fields of science study the behaviour of complex materials and multi-physical phenomena by applying multiscale methodologies in pursuit of a better understanding of engineering problems. Among several available techniques, multiscale models based on the concept of Representative Volume Element (the RVE) are particularly relevant. The cornerstone of such homogenization techniques is the existence of a minimum micro-structural domain (RVE) beyond which the macro-scale response is insensitive to size, a notion given in Hill's pioneering work [1].

In the particular context of porous media, the main area of interest in the present work, multiscale models have been proposed to deal with the decoupled [14] and coupled [48] consolidation phenomena. In addition, in order to reduce the computational cost, reduced-order numerical models [49, 50] have been applied in this field. Furthermore, homogenization methods for heterogeneous porous media have been implemented in the framework of the Numerical Manifold Method [77, 78]. It is worth mentioning,

[1]Corresponding author. E-mail address: ranonis@ing.unne.edu.ar (Anonis, Reinaldo A.).

moreover, that other authors have included microdynamic effects [16], multiphase flow [51] and the hydro-mechanical problem coupled with other phenomena [18, 52–54]. In turn, the scope of the research has been extended to the analysis of saturated porous media subjected to large deformations [55, 56]. A common issue in the literature concerning the multiscale formulation of porous media is the presence of a pathological effect related with a micro-scale size dependence, which contradicts the fundamental concept of the RVE existence [1], leading to a lack of objectivity in the response at the macro-scale. Recently, in [66] a comprehensive analysis of the causes of the size effect was performed and an optimal and simple solution was proposed which guarantees the well-accepted notion of RVE and ensures objectivity in the homogenized response. This was achieved by a selective expansion of the primitive variables that are accepted as input arguments in the constitutive laws describing the micro-scale behaviour.

Despite all the advances in multiscale techniques based on RVE-model, there are still complex materials in nature that have not been covered. Such is the case of some geomaterials and biological tissues that, on a small length scale, can be considered to be composed of a saturated porous medium matrix containing impermeable non-porous solid inclusions. To mention a few instances, large geological conformations with quasi-impermeable rock fragments dispersed in a stratum of clayey or granular materials could be considered, analyzed and better understood if they were treated as a composite mesoscale, as described above. According to certain authors, another scenario involves shales, which can be treated as homogeneous porous media at the macro-scale. However, upon closer examination at the micro-scale, they reveal a composition characterized by a matrix of clay and organic matter interspersed with non-porous solid inclusions (for example, calcite, quartz and pyrite) [87–89]. In addition, Miller and Penta [94] propose an asymptotic homogenization approach to model a myocardium micro-structure tissue that is predominantly constituted of an extracellular matrix with blood vessels and embedded myocyte cells. Alternatively, this situation could be modeled using the RVE-based technique where the extracellular matrix together with the blood vessels would form a poroelastic medium embracing the myocytes as non-porous inclusions.

To the authors' knowledge, no multiscale scheme has been proposed in which the micro-structure is composed of materials characterized by different descriptor fields. Therefore, this paper aims to elaborate on the treatment of the matrix-inclusion based materials. The matrix is described by the theory of poromechanics requiring the displacement and pore pressure fields to be properly established [31, 32, 36]. The inclusions are embodied in the conventional solid mechanics theory using only the displacement field as the primary descriptive variable. At the macroscopic scale, a coupled hydro-mechanical behaviour is recovered, so that the poro-mechanics theory is suitable for its study.

In this work a unified multiscale framework called the Method of Multiscale Virtual Power (MMVP) [19, 20] is employed. This framework offers a clear and straightforward platform for addressing a range of physical phenomena. We highlight the models involving inertia and body forces [26] and the recent formulation to deal with randomly distributed voids [21], due to their influence on the present contribution. The versatility of the MMVP lies in its solid theoretical background that provides basic principles and well-established steps to construct mechanically coherent multiscale models. This paper takes advantage of the capabilities of such procedure to establish a consistent multiscale hydro-mechanical model.

The computational implementation is placed in the context of the finite element square method (FE^2) [5], as developed in previous communications [66].

The organization of the work is outlined below. In section D.2, the governing equations at the macro-scale are presented. Next, in section D.3, the complete treatment of the Method of Multiscale Virtual Power (MMVP) follows, departing from the basic assumptions that must be taken into account at the micro-scale with the particularities of the micro-structures that are addressed. In section D.4, the constitutive relations of the micro-scale are specified. Here the Selective Order Expansion method (SOE) becomes relevant to guaranty the objectivity of the macro-scale response. The so-called periodic homogenization approach is described in section D.5. Next, section D.6 deals with the space and time discretization issue for both, macro and micro scales. To validate and demonstrate the potentiality of

the present model, numerical results for one- and two-dimensional consolidation problems are given in section D.7 and compared with very high fidelity solutions provided by the Direct Numerical Simulation (DNS) procedure. Finally, some conclusions and possible further developments are drawn in section D.8. The article concludes with two appendices detailing the derivation of tangent operators of the present multiscale formulation.

D.2. Governing equations of the macro-scale

At the larger length scale, we consider an homogeneous saturated porous medium. In this section, the balance equations governing the behaviour at the macro-scale, are exposed. The distinctive feature and novelty reside in determining the effective macro-scale response from a heterogeneous micro-structure that require different descriptor fields for each component. The detailed analysis of the micro-scale is discussed later.

D.2.1. Basic assumptions of the macro-scale model

The continuous medium is identified by $\mathcal{B}$. Any material point of $\mathcal{B}$ is denoted by vector $\mathbf{x}$, see Figure D.1, which is related to a macro-scale Cartesian system. The non-stationary coupled hydro-mechanical problem, induced by the seepage phenomenon, requires the incorporation of time t as a monotonically increasing parameter.

The main hypotheses to be adopted here are the following

(i) The body $\mathcal{B}$ is fully saturated with a pressurized fluid. Hence, the continuous medium comprises only two phases, the solid phase and the fluid phase.

(ii) Infinitesimal transformations for the kinematical description.

(iii) The inertial terms are neglected for both phases.

A bounded domain $\Omega \in \mathbb{R}^3$, related to the body $\mathcal{B}$, is used for the mathematical description of the macro hydro-mechanical model. As usual, Γ denotes the piece-wise smooth boundary of Ω, whereas $\mathbf{n}$ is the (outward) unit vector orthogonal to Γ, see Figure (D.1).

In order to characterize the behaviour of a saturated porous medium, two primal descriptors are introduced: the displacement (vector) field for the solid phase, $\mathbf{u}(\mathbf{x}, t)$ and the (scalar) pore pressure field of the fluid, here called $p(\mathbf{x}, t)$. The domain Ω is subjected to different external agencies, namely: an external body force field $\mathbf{f}(\mathbf{x}, t)$ (typically the saturated weight per unit volume of solid and fluid phases), a total external traction $\mathbf{t}(\mathbf{x}, t)$ and a normal fluid flux $q(\mathbf{x}, t)$.

The boundary domain Γ splits into subsets on which Dirichlet-type and Neumann-type boundary conditions can be imposed. Therefore, prescribed functions $\mathbf{u} = \mathbf{u}_{\mathrm{D}}$ and $p = p_{\mathrm{D}}$ are specified for all $\mathbf{x}$ on the Dirichlet boundary partitions of Γ, namely Γ^u_{D} and Γ^p_{D}, respectively, and for all time t (see Figure D.1). On the other hand, external generalized fluxes $\mathbf{t} = \boldsymbol{\sigma}\,\mathbf{n}$ and $\frac{q}{\rho^f} = \boldsymbol{\mathcal{V}} \cdot \mathbf{n}$ can also be applied on the respective Neumann boundary partitions Γ^u_{N} and Γ^p_{N}, of Γ, respectively (see Figure D.1). Previously, we have introduced the variable $\boldsymbol{\sigma}(\mathbf{x}, t)$ which represents the Cauchy stress tensor of the solid skeleton, $\boldsymbol{\mathcal{V}}(\mathbf{x}, t)$ is the flux or the relative seepage velocity vector, ρ^f is the intrinsic mass density of the fluid phase; finally the symbol $(\cdot)$ designates a simple contraction inner product. In view of previous definitions, we have $\Gamma = \Gamma^u_{\mathrm{D}} \cup \Gamma^u_{\mathrm{N}}$ ($\Gamma^u_{\mathrm{D}} \cap \Gamma^u_{\mathrm{N}} = \varnothing$) and also $\Gamma = \Gamma^p_{\mathrm{D}} \cup \Gamma^p_{\mathrm{N}}$ ($\Gamma^p_{\mathrm{D}} \cap \Gamma^p_{\mathrm{N}} = \varnothing$).

In addition to boundary conditions, initial conditions for the displacement field $\mathbf{u} = \mathbf{u}^0$ and the pore pressure field $p = p^0$ are also required for all $\mathbf{x}$. They are completely defined at the beginning of the analysis at $t = 0$ [41, 109].

To close the description of the hydro-mechanical state of a saturated porous medium [36], see Figure D.2-(a), additional definitions are required, as for example: the infinitesimal strain tensor of the solid

Figura D.1: Macro-scale model layout and nomenclature. (a) Mechanical problem. (b) Seepage phenomenon.

skeleton $\boldsymbol{\varepsilon}(\mathbf{x},t) = \boldsymbol{\nabla}^{sym}\,\mathbf{u}(\mathbf{x},t)$, the pore pressure gradient $\boldsymbol{\varphi}(\mathbf{x},t) = \boldsymbol{\nabla} p(\mathbf{x},t)$ and the pore volume rate (per unit pore volume) $\dot{\chi}(\mathbf{x},t) = \frac{\dot{m}^f}{\rho^f}$, $\dot{m}^f$ and ρ^f being the rate of fluid mass content and the mass density of the fluid phase, respectively (another essential relation for m^f is $m^f = \rho^f\, n$). Alternatively, the flux of the relative seepage velocity vector can be interpreted as $\boldsymbol{\mathcal{V}}(\mathbf{x},t) = n\,\left(\mathbf{V}^f - \mathbf{V}^s\right)$, where $\mathbf{V}^f$ is the velocity vector of the fluid, $\mathbf{V}^s$ represents the velocity vector of the solid skeleton and n is the total porosity index of the system.

D.2.2. Admissibility

Next, we introduce the formal concept of admissibility at the macro-scale level through the sets $\mathcal{U}(\Omega) \equiv \left\{\mathbf{v} \in \mathbf{H}^1(\Omega)\,;\ \mathbf{v} = \mathbf{u}_{\mathrm{D}}\ \forall \mathbf{x} \in \Gamma^u_{\mathrm{D}}\right\}$ and $\mathcal{P}(\Omega) \equiv \left\{v \in \mathrm{H}^1(\Omega)\,;\ v = p_{\mathrm{D}}\ \forall \mathbf{x} \in \Gamma^p_{\mathrm{D}}\right\}$, for the primary fields $\mathbf{u}(\mathbf{x},t)$ and $p(\mathbf{x},t)$, respectively. $\mathbf{H}^1(\bullet)$ and $\mathrm{H}^1(\bullet)$ denote the vector and scalar spaces of functions whose first derivative is square-integrable, respectively. The corresponding linear vector spaces for virtual actions $\delta\mathbf{u}(\mathbf{x},t)$ and $\delta p(\mathbf{x},t)$ are: $\mathcal{U}^*(\Omega) \equiv \left\{\mathbf{v} \in \mathbf{H}^1(\Omega)\,;\ \mathbf{v} = \mathbf{0}\ \forall \mathbf{x} \in \Gamma^u_{\mathrm{D}}\right\}$ and $\mathcal{P}^*(\Omega) \equiv \left\{p \in \mathrm{H}^1(\Omega)\,;\ p = 0\ \forall \mathbf{x} \in \Gamma^p_{\mathrm{D}}\right\}$[2]. With the aim of simplify terminology, the spatial and time dependencies are omitted until the end of this section.

D.2.3. Internal and external power functionals

In the present context of porous saturated materials, the internal power, $\mathcal{P}^{int}$, can be described as the sum of three terms: (i) the classical power contribution exerted between purely mechanical conjugated variables $\{\boldsymbol{\sigma}; \dot{\boldsymbol{\varepsilon}}\}$, (ii) the work rate performed in the pore space by the fluid phase, defined through the pair $\{\dot{\chi}; p\}$ and finally (iii) the viscous dissipation effect due to the relative motion of the fluid phase concerning the solid skeleton, accounted for through the dual product between $\{\boldsymbol{\mathcal{V}}; \boldsymbol{\varphi}\}$. Thus, we can write

$$\mathcal{P}^{int} = \int_\Omega \left[\boldsymbol{\sigma} \,:\, \dot{\boldsymbol{\varepsilon}} + \dot{\chi}\, p - \boldsymbol{\mathcal{V}} \cdot \boldsymbol{\varphi}\right] d\Omega, \tag{D.1}$$

where symbol $(:)$ designates a double contraction inner product.
The external power, $\mathcal{P}^{ext}$, exerted by the set of external agencies $\{\mathbf{f}; \mathbf{t}; q\}$ can be written as follows

$$\mathcal{P}^{ext} = \int_\Omega \mathbf{f} \cdot \dot{\mathbf{u}}\, d\Omega + \int_\Gamma \left[\mathbf{t} \cdot \dot{\mathbf{u}} - p\,\frac{q}{\rho^f}\right] d\Gamma. \tag{D.2}$$

[2]The symbol δ preceding any entity is used throughout the manuscript to denote its spatial virtual variation.

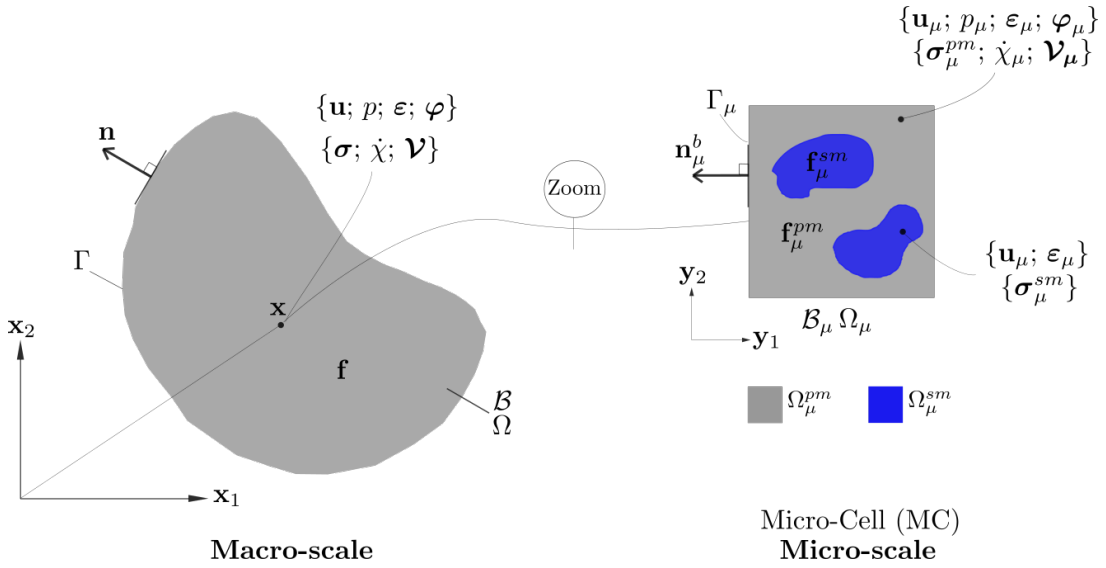

Figura D.2: Basic ingredients of a multiscale model based on the RVE concept.

Equation (D.1) and (D.2) were defined by Coussy O. [36] but in a slight different format. After simple mathematical manipulations, the current forms for the internal and external power functionals can be deduced, see for example [66].

If we replace the realizable primal quantities $\{\dot{\mathbf{u}};\, \dot{\boldsymbol{\varepsilon}};\, p;\, \boldsymbol{\varphi}\}$ with their corresponding admissible virtual actions $\{\delta\dot{\mathbf{u}};\, \delta\dot{\boldsymbol{\varepsilon}};\, \delta p;\, \delta\boldsymbol{\varphi}\}$, the related concepts of internal and external virtual powers, denoted as $\delta\mathcal{P}^{int}$ and $\delta\mathcal{P}^{ext}$, respectively, can be easily defined from (D.1) and (D.2). Then, the total virtual power, $\delta\mathcal{P}^{tot}$, is expressed as

$$\delta\mathcal{P}^{tot} = \delta\mathcal{P}^{int} - \delta\mathcal{P}^{ext} = \int_\Omega \left(\boldsymbol{\sigma} \,:\, \delta\dot{\boldsymbol{\varepsilon}} + \dot{\chi}\,\delta p - \boldsymbol{\mathcal{V}} \cdot \delta\boldsymbol{\varphi} - \mathbf{f} \cdot \delta\dot{\mathbf{u}}\right) d\Omega - \int_{\Gamma_N^u} \mathbf{t} \cdot \delta\dot{\mathbf{u}}\, d\Gamma + \int_{\Gamma_N^p} \frac{q}{\rho^f}\, \delta p\, d\Gamma. \quad \text{(D.3)}$$

The last two integrals involve only the Neumann boundary partitions, due to the admissibility of virtual actions $\delta\dot{\mathbf{u}} \in \mathcal{U}^*(\Omega)$ and $\delta p \in \mathcal{P}^*(\Omega)$.

Analogous definition to Equation (D.3) will be subsequently considered to describe the total virtual power in the micro-scale domain as well as to establish the physical connection between the macro and micro-scales.

D.2.4. Weak form of the macro-scale balance equations

The Principle of Virtual Power assumes that integral (D.3) vanishes for all admissible variations $\delta\dot{\mathbf{u}}$ and δp. Since $\delta\dot{\mathbf{u}}$ and δp are independent of each other, the variational form of balance is easily obtained, as a system of two coupled scalar equations [36, 41, 109]. Then, the hydro-mechanical problem at the upper length scale can be enunciated as follows: find the fields $\mathbf{u} \in \mathcal{U}(\Omega)$ and $p \in \mathcal{P}(\Omega)$ such that:

$$\begin{aligned} G &= \int_\Omega \boldsymbol{\sigma} \,:\, \delta\dot{\boldsymbol{\varepsilon}}\, d\Omega - \int_\Omega \mathbf{f} \cdot \delta\dot{\mathbf{u}}\, d\Omega - \int_{\Gamma_N^u} \mathbf{t} \cdot \delta\dot{\mathbf{u}}\, d\Gamma = 0,\ \forall\, \delta\dot{\mathbf{u}} \in \mathcal{U}^*(\Omega),\ \forall\, t, \\ H &= \int_\Omega \left(\dot{\chi}\,\delta p - \boldsymbol{\mathcal{V}} \cdot \delta\boldsymbol{\varphi}\right) d\Omega + \int_{\Gamma_N^p} \frac{q}{\rho^f}\, \delta p\, d\Gamma = 0,\ \forall\, \delta p \in \mathcal{P}^*(\Omega),\ \forall\, t. \end{aligned} \quad \text{(D.4)}$$

D.2.5. Strong form of the macro-scale balance equations

Following straightforward mathematical steps on the weak form (D.4), including integration by parts of some terms and employing classical variational arguments, we arrived at

$$\begin{cases} \operatorname{Div}\boldsymbol{\sigma} + \mathbf{f} = \mathbf{0}, \quad \forall \mathbf{x} \in \Omega, \quad \forall t, \\ \dot{m}^f + \operatorname{Div}\left(\rho^f \boldsymbol{\mathcal{V}}\right) = \dot{m}^f + \operatorname{Div}\mathbf{w} = 0 \quad \forall \mathbf{x} \in \Omega, \quad \forall t, \\ \boldsymbol{\sigma}\,\mathbf{n} = \mathbf{t} \quad \forall \mathbf{x} \in \Gamma_{\mathrm{N}}^{u}, \quad \forall t, \\ \boldsymbol{\mathcal{V}} \cdot \mathbf{n} = \frac{q}{\rho^f} \quad \forall \mathbf{x} \in \Gamma_{\mathrm{N}}^{p}, \quad \forall t, \end{cases} \tag{D.5}$$

where (D.5)-(a) and (D.5)-(b) are the Euler-Lagrange equations involving the momentum balance equation and mass balance equations, respectively. Besides, (D.5)-(c) and (D.5)-(d) stand for the Neumann boundary conditions (as defined above). The system of equations (D.5) with the Dirichlet boundary conditions, define the strong form of the balance at the macro-level[3].

D.2.6. Constitutive equations of the macro-scale

Constitutive relations for the set of stress-like quantities $\{\boldsymbol{\sigma}, \dot{\chi}, \boldsymbol{\mathcal{V}}\}$ are required to close the macro-scale governing equations. In this contribution, we do not define macro-scale materials laws in explicit form. Instead, they are implicitly derived from a variationally consistent multiscale framework, which is detailed below (see in particular homogenization formulae (D.34), (D.35), and (D.37), respectively, in Section D.3.4.1)

D.3. Method of Multiscale Virtual Power

Throughout this section, the variational framework that contains the basic steps for building a hydromechanically coherent multiscale model is established. Such theoretical structure is called the Method of Multiscale Virtual Power (MMVP) [19–21].

The special feature of the present work is its intrinsic ability to handle heterogeneous materials whose constituents require different fields for their description. A detailed exposition of such kind of micro-structure, is given in section D.3.1, which will serve as a foundation for further developments.

D.3.1. Basic assumptions of the micro-scale model

Any object related to the micro-scale domain is endowed with the subscript $(\bullet)_\mu$, see Figure D.3. The micro-structural domain under analysis is denoted with $\mathcal{B}_\mu$. In order to identify any material point $\mathbf{y}$ of $\mathcal{B}_\mu$, we incorporate another Cartesian coordinate system at the micro-scale.

The main modelling hypothesis at the smaller length scale are identical to those described in the macro-scale problem, except for the material behaviour. Indeed, the domain $\mathcal{B}_\mu$ is composed by two constituents: (i) a porous material fully saturated with a pressurized fluid (here called the porous matrix) and (ii) solid, non-porous, impermeable inclusions. The specific constituve laws for each constituent are specified later, see section D.4.

We introduce a bounded domain $\Omega_\mu \in \mathbb{R}^3$ to represent $\mathcal{B}_\mu$; Ω_μ is also referred to as the micro-cell (MC). Any macro-scale point $\mathbf{x}$ is univocally related with a micro-cell Ω_μ.

The porous matrix constitutes a subdomain of Ω_μ, of volume Ω_μ^{pm}, while the complement space is occupied by the solid volume inclusions Ω_μ^{sm}. From the previous definitions it is possible to write $\Omega_\mu = \Omega_\mu^{sm} \bigcup \Omega_\mu^{pm}$ and $\Omega_\mu^{sm} \bigcap \Omega_\mu^{pm} = \varnothing$.

In the matrix subdomain Ω_μ^{pm}, the material behaviour is described by the general theory of poromechanics [36], which requires for its characterization the assessment of micro-scale displacement field,

[3] In (D.5)-(b) the variable $\mathbf{w}$ represents the relative mass flow vector of the fluid.

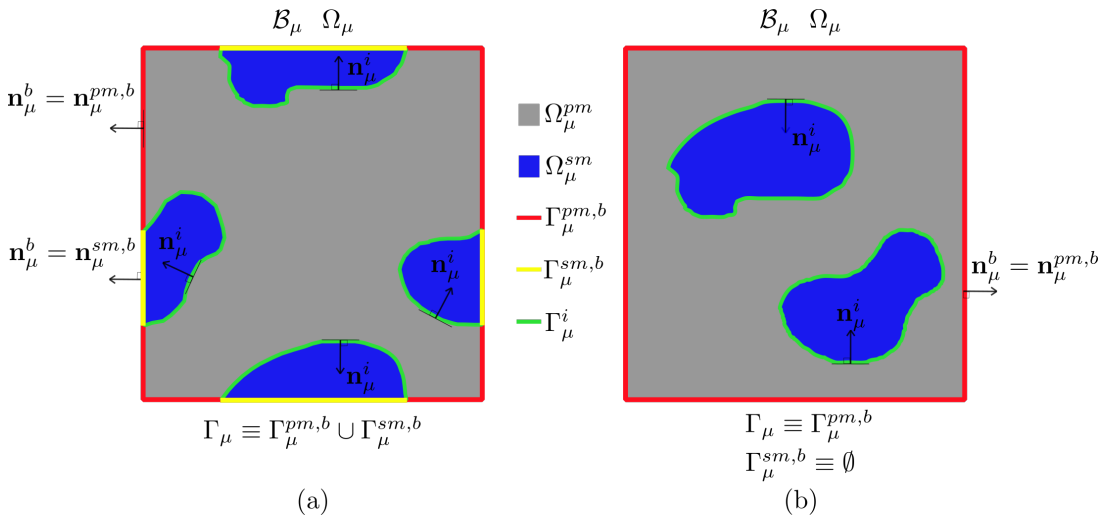

Figura D.3: Micro-cells composed of two different materials: a porous saturated matrix (gray) and solid inclusions (blue). (a) MC with solid inclusions reaching the boundary. (b) MC with internal solid inclusions only.

$\mathbf{u}_\mu$, and micro-scale pore-pressure field, p_μ. In contrast, solid inclusions merely request the definition of the micro-scale displacement field, $\mathbf{u}_\mu$, to determine their physical response. The boundary of Ω_μ, here denoted as Γ_μ, splits into different surface subdomains, see Figure D.3, namely:

- Γ_μ: external boundary surface of the MC domain Ω_μ, which has an external outward normal vector $\mathbf{n}_\mu^b$;
- $\Gamma_\mu^{pm,b}$: external surface of the porous medium having outward normal vector $\mathbf{n}_\mu^{pm,b}$;
- $\Gamma_\mu^{sm,b}$: external surface of the solid medium having outward normal vector $\mathbf{n}_\mu^{sm,b}$;
- Γ_μ^i: internal interface between the saturated matrix and the solid inclusions. The outward normal vector pointing from the porous medium to the inclusion is defined as $\mathbf{n}_\mu^{pm,i} = \mathbf{n}_\mu^i$; while the outward normal vector pointing from the solid particles to the porous matrix is denoted $\mathbf{n}_\mu^{sm,i} = -\mathbf{n}_\mu^i$.

Trivially we have: $\Gamma_\mu = \Gamma_\mu^{pm,b} \bigcup \Gamma_\mu^{sm,b}$ and $\Gamma_\mu^{pm,b} \bigcap \Gamma_\mu^{sm,b} = \varnothing$. The theoretical development of the present work allows us to model two typical distributions of impermeable inclusions in the MC. One pattern considers that the solid particles reach the boundary but preserving a symmetrical arrangement (periodicity condition is satisfied at the MC-boundary), see Figure D.3-(a). The other case presupposes that all the solid inclusions are internal, see Figure D.3-(b) ($\Gamma_\mu = \Gamma_\mu^{pm,b}$ and $\Gamma_\mu^{sm,b} = \varnothing$). Both situations result in the following geometrical properties

$$\begin{aligned} \int_{\Gamma_\mu^{pm,b}} \mathbf{n}_\mu^{pm,b}\, d\Gamma_\mu = \mathbf{0}, \\ \int_{\Gamma_\mu^{sm,b}} \mathbf{n}_\mu^{sm,b}\, d\Gamma_\mu = \mathbf{0}. \end{aligned} \tag{D.6}$$

Micro-cells satisfying Equation (D.6) are termed $\mathbf{n}_\mu$-balanced, otherwise they qualify as $\mathbf{n}_\mu$-unbalanced. Such a typification, along with other fundamental concepts, has been taken or adapted from a recent contribution by Blanco et al. [21]. From a modelling viewpoint, the fulfilment of Equations (D.6) guarantees (in what we later call the Minimally Constrained Multiscale Model) a pattern of self-equilibrated micro-scale flux velocities across the entire porous boundary $\Gamma_\mu^{pm,b}$; a property with inherent physical

sense. The generalization of our model to cover situations where Equation (D.6) is no longer satisfied is possible, but requires further developments and it is beyond the scope of the present paper. We prefer to leave this topic for a future contribution, as otherwise the focus shifts away from the underlying idea of the article.

Before discussing the PMVP, it is necessary to define the concept of admissibility for primitive descriptors (displacements, pore pressures, and their corresponding gradients) between the two scales involved. Admissibility can be established in terms of two sequential procedures: (i) the Insertion process [24] and (ii) the Homogenization process [22]. The discussion about the insertion procedure follows in Section (D.3.2), while the presentation of the homogenization operators is given in Section (D.3.3).

D.3.2. Admissibility of primal descriptors. Insertion at the micro-cell

In this section we establish how the macro-scale primal descriptors are inserted into the MC domain, playing a role in the micro-scale hydro-mechanical equilibrium problem.

Given the point-valued quantities $\{\mathbf{u}(\mathbf{x},t), \boldsymbol{\nabla}\mathbf{u}(\mathbf{x},t)\}$, from the larger length scale, the micro-scale displacement, $\mathbf{u}_\mu(\mathbf{y},t)$, is defined in terms of a standard Taylor expansion rule

$$\mathbf{u}_\mu(\mathbf{y},t) = \mathbf{u}(\mathbf{x},t) + \boldsymbol{\nabla}\mathbf{u}(\mathbf{x},t)(\mathbf{y}-\mathbf{y}_G) + \tilde{\mathbf{u}}_\mu(\mathbf{y},t), \quad \forall \mathbf{y} \in \Omega_\mu, \tag{D.7}$$

where $\boldsymbol{\nabla}\mathbf{u}(\mathbf{x},t)$ stands for the complete gradient of the macro-scale displacements, $\tilde{\mathbf{u}}_\mu(\mathbf{y},t)$ is the displacement fluctuation field in the MC domain and $\mathbf{y}_G$ is a constant vector to be defined later, see expression (D.13).

From (D.7), the linear micro-scale strain tensor, $\boldsymbol{\varepsilon}_\mu(\mathbf{y},t)$, can be expressed as follows

$$\boldsymbol{\varepsilon}_\mu(\mathbf{y},t) = \boldsymbol{\nabla}_y^{sym}\mathbf{u}_\mu(\mathbf{y},t) = \boldsymbol{\varepsilon}(\mathbf{x},t) + \boldsymbol{\nabla}_y^{sym}\tilde{\mathbf{u}}_\mu(\mathbf{y},t) = \boldsymbol{\varepsilon}(\mathbf{x},t) + \tilde{\boldsymbol{\varepsilon}}_\mu(\mathbf{y},t), \quad \forall \mathbf{y} \in \Omega_\mu, \tag{D.8}$$

where operator $\boldsymbol{\nabla}_y^{sym}(\bullet)$ represents the symmetric gradient concerning $\mathbf{y}$-coordinates. The strain field in (D.8) is composed of the addition of the macro-scale strain, $\boldsymbol{\varepsilon}(\mathbf{x},t)$, which is assumed to be uniformly distributed over the entire domain Ω_μ, and the micro-scale strain fluctuation component $\tilde{\boldsymbol{\varepsilon}}_\mu(\mathbf{y},t)$.

Note that both fields, $\mathbf{u}_\mu(\mathbf{y},t)$ and $\nabla\mathbf{u}(\mathbf{y},t)$, are defined for the entire domain $\Omega_\mu = \Omega_\mu^{pm} \cup \Omega_\mu^{sm}$, including the porous matrix skeleton as well as the solid inclusion volume, see Figure D.2.

In a similar way, the micro-scale pore pressure field, $p_\mu(\mathbf{y},t)$, can also be expanded as a Taylor-like series in terms of the macro-scale point-valued quantities $\{p(\mathbf{y},t), \boldsymbol{\varphi}(\mathbf{y},t)\}$. It is important to ensure that $p(\mathbf{x},t)$ and $\boldsymbol{\varphi}(\mathbf{x},t)$ are inserted only into the porous medium subdomain Ω_μ^{pm}

$$p_\mu(\mathbf{y},t) = p(\mathbf{x},t) + \boldsymbol{\varphi}(\mathbf{x},t) \cdot (\mathbf{y}-\mathbf{y}_G) + \tilde{p}_\mu(\mathbf{y},t), \quad \forall \mathbf{y} \in \Omega_\mu^{pm}, \tag{D.9}$$

$\tilde{p}_\mu(\mathbf{y},t)$ being the micro-scale pore pressure fluctuation field which exists only in the porous matrix Ω_μ^{pm}. The previous insertion process ensures the physical consistency that solid medium does not admit pore pressure variables.

In accordance with expression (D.9), the gradient of the micro-scale pore pressures, $\boldsymbol{\varphi}_\mu(\mathbf{y},t)$, results in

$$\boldsymbol{\varphi}_\mu(\mathbf{y},t) = \boldsymbol{\nabla}_y p_\mu(\mathbf{y},t) = \boldsymbol{\varphi}(\mathbf{x},t) + \boldsymbol{\nabla}_y \tilde{p}_\mu(\mathbf{y},t) = \boldsymbol{\varphi}(\mathbf{x},t) + \tilde{\boldsymbol{\varphi}}_\mu(\mathbf{y},t), \quad \forall \mathbf{y} \in \Omega_\mu^{pm}, \tag{D.10}$$

where $\tilde{\boldsymbol{\varphi}}_\mu$ is the corresponding gradient vector of the pore pressure fluctuation on the MC-subdomain Ω_μ^{pm}, obtained from the $\boldsymbol{\nabla}_y(\bullet)$ operator, related to the micro-scale coordinate system.

All the above definitions (D.7)-(D.10) can also be established in rate forms. In order to simplify the notation, the arguments denoting spatial and time dependencies are suppressed in the subsequent developments.

D.3.3. Admissibility of primal descriptors. Homogenization at the micro-cell.

Four homogenization procedures are defined. The first group involves kinematical homogenization operators $\mathcal{H}_y^{\mathbf{u}}$ and $\mathcal{H}_y^{\boldsymbol{\varepsilon}}$, which determine the mapping of micro-scale displacements $\mathbf{u}_\mu$ and strains $\boldsymbol{\varepsilon}_\mu$ into point-values of macro-scale displacement $\mathbf{u}$ and strain $\boldsymbol{\varepsilon}$, respectively. The second group, $\mathcal{H}_y^{p}$ and $\mathcal{H}_y^{\boldsymbol{\varphi}}$, perform a similar procedure but relating micro-scale pore pressures field p_μ and pore pressures gradients $\boldsymbol{\varphi}_\mu$ with their corresponding macro-scale point-valued counterparts p and $\boldsymbol{\varphi}$, respectively.

D.3.3.1. Displacement homogenization

The displacement homogenization rule, denoted as $\mathcal{H}_{\mathbf{y}}^{\mathbf{u}}$, states that the average of the micro-displacement field over the entire domain under analysis, Ω_μ, must be equal to the macro-displacement field

$$\mathcal{H}_y^{\mathbf{u}}\left(\mathbf{u}_\mu\right) = \mathbf{u} = \frac{1}{|\Omega_\mu|}\int_{\Omega_\mu} \mathbf{u}_\mu \, d\Omega_\mu. \tag{D.11}$$

Substituting (D.7) in (D.11) it is obtained

$$\mathbf{u} = \mathbf{u} + \boldsymbol{\nabla}\mathbf{u}\left[\frac{1}{|\Omega_\mu|}\int_{\Omega_\mu} \left(\mathbf{y} - \mathbf{y}_G\right) \, d\Omega_\mu\right] + \frac{1}{|\Omega_\mu|}\int_{\Omega_\mu} \tilde{\mathbf{u}}_\mu \, d\Omega_\mu. \tag{D.12}$$

Since (D.12) must hold even for a homogeneous micro-scale displacement fluctuation field (i.e., $\tilde{\mathbf{u}}_\mu = \mathbf{0} \; \forall \mathbf{y} \in \Omega_\mu$), it brings us to

$$\mathbf{y}_G = \frac{1}{|\Omega_\mu|}\int_{\Omega_\mu} \mathbf{y} \, d\Omega_\mu, \tag{D.13}$$

that is, the coordinate system of the whole MC is located at the geometric center of Ω_μ.

Introducing (D.13) into the displacement homogenization rule (D.12), we derive the first kinematical restriction to be imposed on the fine-scale

$$\int_{\Omega_\mu} \tilde{\mathbf{u}}_\mu \, d\Omega_\mu = \mathbf{0}, \tag{D.14}$$

which, in turn, is responsible for precluding rigid translations of the MC.

D.3.3.2. Strain homogenization

The homogenization rule for the micro-scale strain field, $\mathcal{H}_y^{\boldsymbol{\varepsilon}}$, results in

$$\mathcal{H}_y^{\boldsymbol{\varepsilon}}\left(\boldsymbol{\varepsilon}_\mu\right) = \boldsymbol{\varepsilon} = \frac{1}{|\Omega_\mu|}\int_{\Omega_\mu} \boldsymbol{\varepsilon}_\mu \, d\Omega_\mu = \frac{1}{|\Omega_\mu|}\int_{\Omega_\mu} \boldsymbol{\nabla}_y^{sym}\mathbf{u}_\mu \, d\Omega_\mu, \tag{D.15}$$

Then, replacing (D.8) in (D.15) and applying Green's theorem, we arrive at the following condition

$$\int_{\Gamma_\mu} \tilde{\mathbf{u}}_\mu \; \otimes \; \mathbf{n}_\mu^b \, d\Gamma_\mu = \mathbb{O}, \tag{D.16}$$

being $\otimes$ the external dyadic product.

D.3.3.3. Pore pressure homogenization

As mentioned above, the macro-scale pore pressure and its gradient only hold physical significance within the porous matrix subdomain in the micro-scale, Ω_μ^{pm}, where they have been inserted according

to the expressions (D.9) and (D.10). Thus, the homogenization process for micro-scale pore pressures, named $\mathcal{H}_y^p$, involves an averaged rule restricted to Ω_μ^{pm}

$$\mathcal{H}_y^p\left(p_\mu\right) = p = \frac{1}{|\Omega_\mu^{pm}|}\int_{\Omega_\mu^{pm}} p_\mu \, d\Omega_\mu. \tag{D.17}$$

Replacing (D.9) into (D.17) it is obtained

$$p = p + \boldsymbol{\varphi} \cdot \left[\frac{1}{|\Omega_\mu^{pm}|}\int_{\Omega_\mu^{pm}} \left(\mathbf{y} - \mathbf{y}_G\right) \, d\Omega_\mu\right] + \frac{1}{|\Omega_\mu^{pm}|}\int_{\Omega_\mu^{pm}} \tilde{p}_\mu \, d\Omega_\mu. \tag{D.18}$$

Expression (D.18) provides a possible non-homogeneous restriction on the integral of micro-scale pore pressure field, namely

$$\int_{\Omega_\mu^{pm}} \tilde{p}_\mu \, d\Omega_\mu = -\int_{\Omega_\mu^{pm}} \boldsymbol{\varphi} \cdot \left(\mathbf{y} - \mathbf{y}_G\right) = -\boldsymbol{\varphi} \cdot \int_{\Omega_\mu^{pm}} \left(\mathbf{y} - \mathbf{y}_G\right) \, d\Omega_\mu. \tag{D.19}$$

In the presence of a random pattern of solid inclusions within the micro-cell domain, the gradient of macro-scale pore pressures $\boldsymbol{\varphi}$, inserted in Ω_μ^{pm}, introduces an effect that must be compensated with the integral value of micro-scale pore pressure fluctuations, in order to guaranty (D.17). The right-hand side of (D.19) vanishes only if the barycenter of Ω_μ^{pm} subdomain, denoted as $\mathbf{y}_G^{pm}$, coincides with $\mathbf{y}_G$, see (D.13). It is expected that this term approaches zero for sufficiently representative micro-cells. Whatever the case, the condition (D.19) must be imposed in our multiscale formulation on the corresponding saturated matrix subdomain Ω_μ^{pm} for the micro-scale pore pressure field.

D.3.3.4. Pore pressure gradient homogenization

The homogenization rule for the gradient of the micro-scale pore pressure field is adopted as

$$\begin{aligned}\mathcal{H}_y^{\boldsymbol{\varphi}}\left(\boldsymbol{\varphi}_\mu\right) = \boldsymbol{\varphi} &= \frac{1}{|\Omega_\mu^{pm}|}\left[\int_{\Omega_\mu^{pm}} \boldsymbol{\varphi}_\mu \, d\Omega_\mu - \int_{\Gamma_\mu^i} \tilde{p}_\mu \, \mathbf{n}_\mu^i \, d\Gamma_\mu\right] \\ &= \frac{1}{|\Omega_\mu^{pm}|}\left[\int_{\Omega_\mu^{pm}} \boldsymbol{\nabla}_y p_\mu \, d\Omega_\mu - \int_{\Gamma_\mu^i} \tilde{p}_\mu \, \mathbf{n}_\mu^i \, d\Gamma_\mu\right],\end{aligned} \tag{D.20}$$

where the second term involving the internal interface Γ_μ^i is included in order to obtain a gradient pore pressure homogenization formula expressed only over the external porous matrix boundary $\Gamma_\mu^{pm,b}$, as expected. In fact, taking into account (D.10) as well as Green's theorem, we can expand the expression (D.20) to yield

$$\boldsymbol{\varphi} = \boldsymbol{\varphi} + \frac{1}{|\Omega_\mu^{pm}|}\left[\int_{\Omega_\mu^{pm}} \boldsymbol{\nabla}_y \tilde{p}_\mu \, d\Omega_\mu - \int_{\Gamma_\mu^i} \tilde{p}_\mu \, \mathbf{n}_\mu^i \, d\Gamma_\mu\right] = \boldsymbol{\varphi} + \frac{1}{|\Omega_\mu^{pm}|}\int_{\Gamma_\mu^{pm,b}} \tilde{p}_\mu \, \mathbf{n}_\mu^{pm,b} \, d\Gamma_\mu. \tag{D.21}$$

From (D.21) emerges an additional restriction for the micro-scale pore-pressure fluctuation field at boundary $\Gamma_\mu^{pm,b}$

$$\int_{\Gamma_\mu^{pm,b}} \tilde{p}_\mu \, \mathbf{n}_\mu^{pm,b} \, d\Gamma_\mu = \mathbf{0}. \tag{D.22}$$

D.3.3.5. Sets and spaces of admissible variables of the micro-scale

Previously, all the constraints to be imposed on the displacement and pore pressure fluctuation have been established, see (D.14), (D.16), (D.19) and (D.22). Only $\tilde{\mathbf{u}}_\mu$ and $\tilde{p}_\mu$ fields that satisfy all of these conditions are admissible, that is, they are compatible with the homogenization procedures adopted in (D.11), (D.15), (D.17) and (D.20).
At this point, we can introduce the admissible vector space $\tilde{\mathcal{U}}_\mu^{\text{MCo}}(\Omega_\mu)$ and functional set $\tilde{\mathcal{P}}_\mu^{\text{MCo}}(\Omega_\mu^{pm})$, for $\tilde{\mathbf{u}}_\mu$ and $\tilde{p}_\mu$, respectively, that define the so-called Minimally Constrained Multiscale Model [12, 21]

$$\tilde{\mathcal{U}}_\mu^{\text{MCo}}(\Omega_\mu) = \left\{ \mathbf{v} \in \mathbf{H}^1(\Omega_\mu);\ \int_{\Omega_\mu} \mathbf{v}\, d\Omega_\mu = \mathbf{0};\ \int_{\Gamma_\mu} \mathbf{v} \otimes \mathbf{n}_\mu^b\, d\Gamma_\mu = \mathbb{O} \right\}. \tag{D.23}$$

$$\tilde{\mathcal{P}}_\mu^{\text{MCo}}\left(\Omega_\mu^{pm}\right) = \left\{ v \in \mathrm{H}^1\left(\Omega_\mu^{pm}\right);\ \int_{\Omega_\mu^{pm}} \left[\boldsymbol{\varphi} \cdot (\mathbf{y} - \mathbf{y}_G) + v\right] d\Omega_\mu = 0;\ \int_{\Gamma_\mu^{pm,b}} v\, \mathbf{n}_\mu^{pm,b}\, d\Gamma_\mu = \mathbf{0} \right\}. \tag{D.24}$$

In principle, any sub-space, generally denoted as $\tilde{\mathcal{U}}_\mu(\Omega_\mu)$ and any sub-set $\tilde{\mathcal{P}}_\mu(\Omega_\mu^{pm})$, such that $\tilde{\mathcal{U}}_\mu(\Omega_\mu) \subseteq \tilde{\mathcal{U}}_\mu^{\text{MCo}}(\Omega_\mu)$ and $\tilde{\mathcal{P}}_\mu(\Omega_\mu^{pm}) \subseteq \tilde{\mathcal{P}}_\mu^{\text{MCo}}(\Omega_\mu^{pm})$, are feasible options for building alternative homogenization schemes. Clearly, these will be more constrained settings for $\tilde{\mathbf{u}}_\mu$ and $\tilde{p}_\mu$, respectively (for example, the Taylor, Linear, Periodic or any other more elaborated multiscale sub-model). Thus, in general terms we have: $\tilde{\mathbf{u}}_\mu \in \tilde{\mathcal{U}}_\mu(\Omega_\mu)$ and $\tilde{p}_\mu \in \tilde{\mathcal{P}}_\mu(\Omega_\mu^{pm})$.

Virtual actions at the micro-cell domain can be defined taking into account (D.7)-(D.10), as follows

$$\delta\mathbf{u}_\mu = \delta\mathbf{u} + \delta\boldsymbol{\nabla}\mathbf{u}\,(\mathbf{y} - \mathbf{y}_G) + \delta\tilde{\mathbf{u}}_\mu, \quad \forall \mathbf{y} \in \Omega_\mu \tag{D.25}$$

$$\delta\boldsymbol{\varepsilon}_\mu = \delta\boldsymbol{\varepsilon} + \delta\tilde{\boldsymbol{\varepsilon}}_\mu = \delta\boldsymbol{\varepsilon} + \boldsymbol{\nabla}_y^{sym}\delta\tilde{\mathbf{u}}_\mu, \quad \forall \mathbf{y} \in \Omega_\mu \tag{D.26}$$

$$\delta p_\mu = \delta p + \delta\boldsymbol{\varphi} \cdot (\mathbf{y} - \mathbf{y}_G) + \delta\tilde{p}_\mu, \quad \forall \mathbf{y} \in \Omega_\mu^{pm} \tag{D.27}$$

$$\delta\boldsymbol{\varphi}_\mu = \delta\boldsymbol{\varphi} + \delta\tilde{\boldsymbol{\varphi}}_\mu = \delta\boldsymbol{\varphi} + \boldsymbol{\nabla}_y\,\delta\tilde{p}_\mu, \quad \forall \mathbf{y} \in \Omega_\mu^{pm} \tag{D.28}$$

from which it is possible to introduce the linear spaces for admissible virtual fluctuations

$$\tilde{\mathcal{U}}_\mu^* \equiv \tilde{\mathcal{U}}_\mu, \tag{D.29}$$

$$\tilde{\mathcal{P}}_\mu^*\left(\Omega_\mu^{pm}\right) = \left\{ v \in \mathrm{H}^1\left(\Omega_\mu^{pm}\right);\ \int_{\Omega_\mu^{pm}} v\, d\Omega_\mu = 0;\ \int_{\Gamma_\mu^{pm,b}} v\, \mathbf{n}_\mu^{pm,b}\, d\Gamma_\mu = \mathbf{0} \right\}, \tag{D.30}$$

with $\delta\tilde{\mathbf{u}}_\mu \in \tilde{\mathcal{U}}_\mu^*(\Omega_\mu)$ and $\delta\tilde{p}_\mu \in \tilde{\mathcal{P}}_\mu^*(\Omega_\mu^{pm})$. The spaces in expression (D.29) coincide since constraints (D.14) and (D.16) are both homogeneous. However, we need to introduce a new space $\tilde{\mathcal{P}}_\mu^*(\Omega_\mu^{pm}) \not\equiv \tilde{\mathcal{P}}_\mu(\Omega_\mu^{pm})$, because constraint (D.19) is of a non-homogeneous type.

D.3.4. Principle of Multiscale Virtual Power (PMVP)

In this section, we introduce the last ingredient in the context of the MMVP, the so-called Principle of Multiscale Virtual Power (PMVP), which establishes the physical coupling between the involved scales [19, 20], see a schematic diagram in Figure D.2. From the PMVP, we can derive the homogenization formulae for the macro-scale stress-like entities and body forces and characterize the balance equations for the micro-scale problem, see D.3.4.1.

To enunciate the Principle of Multiscale Virtual Power, we need to specify the concepts of total virtual powers that play a role during the scale transition process. Recalling the definition of total virtual power per unit volume at the macro-scale (see the first integrand term of the r.h.s. in (D.3)), we postulate that the total virtual power, $\mathcal{P}^{tot}$, exerted at a point $\mathbf{x}$ of the macro-scale related to the micro-scale domain

of size $|\Omega_\mu|$, is

$$\mathcal{P}^{tot}\left(\delta\dot{\mathbf{u}}, \delta\dot{\boldsymbol{\varepsilon}}, \delta p, \delta\boldsymbol{\varphi}\right) = |\Omega_\mu| \left[\boldsymbol{\sigma} \,:\, \delta\dot{\boldsymbol{\varepsilon}} + \dot{\chi}\,\delta p - \boldsymbol{\mathcal{V}} \cdot \delta\dot{\boldsymbol{\varphi}} - \mathbf{f} \cdot \delta\dot{\mathbf{u}}\right]. \tag{D.31}$$

In turn, assuming the same mathematical structure, as given in the r.h.s. of (D.31), for the porous material constituent of the micro-cell, the total virtual power at the micro-scale domain Ω_μ yields

$$\mathcal{P}_\mu^{tot}\left(\delta\dot{\mathbf{u}}_\mu, \delta\dot{\boldsymbol{\varepsilon}}_\mu, \delta p_\mu, \delta\boldsymbol{\varphi}_\mu\right) = \int_{\Omega_\mu} \left(\boldsymbol{\sigma}_\mu \,:\, \delta\dot{\boldsymbol{\varepsilon}}_\mu \,-\, \mathbf{f}_\mu \cdot \delta\dot{\mathbf{u}}_\mu\right) d\Omega_\mu + \int_{\Omega_\mu^{pm}} \left(\dot{\chi}_\mu\,\delta p_\mu - \boldsymbol{\mathcal{V}}_\mu \cdot \delta\boldsymbol{\varphi}_\mu\right) d\Omega_\mu. \tag{D.32}$$

Notice that the conjugate pairs $\{\dot{\chi}_\mu, \delta p_\mu\}$ and $\{\boldsymbol{\mathcal{V}}_\mu, \delta\boldsymbol{\varphi}_\mu\}$, inherent to the saturated matrix, only exert virtual power over the corresponding subdomain Ω_μ^{pm}. In (D.32), we have introduced the micro-scale body force field $\mathbf{f}_\mu = \rho_\mu^{(\bullet)}\,\mathbf{g}$, being the weight per unit volume of the medium. The value of $\rho_\mu^{(\bullet)}$ depends on whether the material point belongs to Ω_μ^{pm} or Ω_μ^{sm}. In the first case, the saturated density $\rho_\mu^{pm} = \rho^f\, n_\mu + \rho^{s,pm}\,(1 - n_\mu)$ is used, with $\rho^{s,pm}$ denoting the density of the solid phase in the porous medium. In the second case, the density of the solid inclusion ρ_μ^{sm} is employed.

The PMVP states that for all admissible virtual actions, the total virtual power of the macro-scale at a point $\mathbf{x}$ must be equal to the total micro-scale virtual power at the corresponding micro-cell. Thus, relating (D.31) and (D.32), we arrive at the following variational sentence

$$\begin{aligned}
&\boldsymbol{\sigma} \,:\, \delta\dot{\boldsymbol{\varepsilon}} + \dot{\chi}\,\delta p - \boldsymbol{\mathcal{V}} \cdot \delta\dot{\boldsymbol{\varphi}} - \mathbf{f} \cdot \delta\dot{\mathbf{u}} = \\
&\qquad \frac{1}{|\Omega_\mu|}\left[\int_{\Omega_\mu} \left(\boldsymbol{\sigma}_\mu \,:\, \delta\dot{\boldsymbol{\varepsilon}}_\mu \,-\, \mathbf{f}_\mu \cdot \delta\dot{\mathbf{u}}_\mu\right) d\Omega_\mu + \int_{\Omega_\mu^{pm}} \left(\dot{\chi}_\mu\,\delta p_\mu - \boldsymbol{\mathcal{V}}_\mu \cdot \delta\boldsymbol{\varphi}_\mu\right) d\Omega_\mu\right], \\
&\qquad \forall\ \left(\delta\dot{\boldsymbol{\varepsilon}}\,, \delta\dot{\mathbf{u}}\,, \delta\boldsymbol{\varphi}\,, \delta p\,, \delta\dot{\mathbf{u}}_\mu\,, \delta p_\mu\right) \in \mathbb{R}^6 \times \mathbb{R}^3 \times \mathbb{R}^3 \times \mathbb{R} \times \tilde{\mathcal{U}}_\mu^*\left(\Omega_\mu\right) \times \tilde{\mathcal{P}}_\mu^*\left(\Omega_\mu^{pm}\right), \forall\, t.
\end{aligned} \tag{D.33}$$

Observe that all terms characterizing the total virtual power at the micro-scale are normalized by the total volume of the micro-cell $|\Omega_\mu|$, including those defined only over the porous matrix subdomain Ω_μ^{pm}.

D.3.4.1. Consequences of the PMVP

Replacing definitions (D.25)-(D.28) into (D.33) and then by resorting to simple variational manipulations, the consequences of the PMVP are naturally obtained, namely: (i) the homogenization formulae for the macro-scale stress-like entities $\{\boldsymbol{\sigma}; \dot{\chi}; \boldsymbol{\mathcal{V}}\}$, (ii) the averaging rule for the body force $\mathbf{f}$, and (iii) the variational forms of balance equations at the smaller length scale. Such deductions are straightforward, the interested reader is referred to [66] for further details. In what follows we show only the final results.

Homogenized stress tensor:

$$\boldsymbol{\sigma} = \frac{1}{|\Omega_\mu|}\int_{\Omega_\mu} \Big(\boldsymbol{\sigma}_\mu - \mathbf{f}_\mu \otimes \left(\mathbf{y} - \mathbf{y}_G\right)\Big)\, d\Omega_\mu,\ \forall\, t. \tag{D.34}$$

Homogenized pore volume rate (per unit pore volume):

$$\dot{\chi} = \frac{\dot{m}^f}{\rho^f} = \frac{1}{|\Omega_\mu|}\int_{\Omega_\mu^{pm}} \dot{\chi}_\mu\, d\Omega_\mu,\ \forall\, t. \tag{D.35}$$

It should be pointed out that in (D.35) the averaging factor and the integration domain are different.

If the fluid mass density ρ^f is assumed to be uniform throughout the MC subdomain Ω_μ^{pm}, the ho-

mogenized formula for the mass content rate, $\dot{m}^f$, can be retrieved after simple manipulations on (D.35)

$$\dot{m}^f = \frac{1}{|\Omega_\mu|} \int_{\Omega_\mu^{pm}} \dot{m}_\mu^f \, d\Omega_\mu, \ \forall\, t. \tag{D.36}$$

Homogenized flux velocity vector:

$$\boldsymbol{\mathcal{V}} = \frac{1}{|\Omega_\mu|} \int_{\Omega_\mu^{pm}} \Big(\boldsymbol{\mathcal{V}}_\mu - \dot{\chi}_\mu \, (\mathbf{y} - \mathbf{y}_G) \Big) \, d\Omega_\mu, \ \forall\, t. \tag{D.37}$$

Once again, observe that in (D.37) the integration domain differs from the normalization measure.
Homogenized body force field:

$$\mathbf{f} = \frac{1}{|\Omega_\mu|} \int_{\Omega_\mu} \mathbf{f}_\mu \, d\Omega_\mu = \frac{\mathbf{g}}{|\Omega_\mu|} \int_{\Omega_\mu} \rho_\mu \, d\Omega_\mu, \ \forall\, t. \tag{D.38}$$

Variational form of the momentum balance equation in the MC:

$$\int_{\Omega_\mu} \Big(\boldsymbol{\sigma}_\mu \, : \, \boldsymbol{\nabla}_y^{sym} \, \delta \dot{\tilde{\mathbf{u}}}_\mu \, - \, \mathbf{f}_\mu \, \cdot \, \delta \dot{\tilde{\mathbf{u}}}_\mu \Big) \, d\Omega_\mu = 0, \ \ \forall \, \delta \dot{\tilde{\mathbf{u}}}_\mu \in \ \tilde{\mathcal{U}}_\mu^* \left(\Omega_\mu \right), \ \forall \, t. \tag{D.39}$$

Variational form of the mass balance equation in the MC:

$$\int_{\Omega_\mu^{pm}} \left(\dot{\chi}_\mu \, \delta \tilde{p}_\mu - \boldsymbol{\mathcal{V}}_\mu \, \cdot \, \boldsymbol{\nabla}_y \, \delta \tilde{p}_\mu \right) \, d\Omega_\mu = 0, \ \ \forall \, \delta \tilde{p}_\mu \in \ \tilde{\mathcal{P}}_\mu^* \left(\Omega_\mu^{pm} \right), \ \forall \, t, \tag{D.40}$$

where, as expected, only the Ω_μ^{pm} subdomain is involved since the solid medium, Ω_μ^{sm}, does not support the micro-scale pore pressure field.

D.4. Constitutive equations in the micro-scale

In order to obtain a closed formulation of the proposed multiscale model, the constitutive behaviour for each micro-scale constituent needs to be specified. For impermeable solid inclusions, it suffices to provide the constitutive relations for the stress state $\dot{\boldsymbol{\sigma}}_\mu^{sm}$. On the other hand, for the saturated porous matrix, it is necessary to establish constitutive laws for the mechanical stress-like quantities $\{\dot{\boldsymbol{\sigma}}_\mu^{pm}; \dot{\chi}_\mu\}$ and also the relationship that allows to obtain the seepage velocity vector $\boldsymbol{\mathcal{V}}_\mu$, see Figure D.2-(b). Superscripts $(\bullet)^{sm}$ and $(\bullet)^{pm}$ are used to differentiate the stress state on Ω_μ^{sm} or Ω_μ^{pm}, respectively. Note that, for convenience, the constitutive definitions related to $\dot{\boldsymbol{\sigma}}_\mu$ and $\dot{\chi}_\mu$ are considered in rate format.

Within the context of multiscale modelling of saturated porous media, it is very common to obtain a homogenization scheme with a micro-scale size dependence issue, compromising the concept of RVE existence. Such a debatable effect translates into a non-objective response at the macro-scale level [14, 16, 48, 49]. More specifically, the lack of objectivity stems from the type of expansion accepted for evaluating input arguments in the micro-scale constitutive laws $\{\dot{\boldsymbol{\sigma}}_\mu^{pm}; \dot{\chi}_\mu\}$, see further and detailed arguments in [66]. To address this serious problem, the concept of Selective Order of Expansions (in short SOE) was recently introduced by the authors in [66]. The SOE approach presupposes different orders of expansion for the micro-scale strain rate, $\dot{\boldsymbol{\varepsilon}}_\mu$, and for the micro-scale pore-pressure rate, $\dot{p}_\mu$, whenever both variables play a role as input arguments in the constitutive functionals $\dot{\boldsymbol{\sigma}}_\mu^{pm}$ and $\dot{\chi}_\mu$. To enforce the previous idea, the superscript $(\bullet)^{\text{SOE}}$ will be added to some material laws in our subsequent developments and in the multiscale model derived from. In particular, we consider the following definitions

- A Full Order Expansion (FOE), denoted as $\dot{\boldsymbol{\varepsilon}}_\mu^{\text{FOE}}$, identical to expression (D.8), is adopted for the micro-scale strain rate descriptor. This applies to both the matrix (Ω_μ^{pm}) and the inclusions (Ω_μ^{sm})

subdomains.

- A Reduced Order Expansion (ROE), defined as $\dot{p}_\mu^{\text{ROE}} = \dot{p} + \dot{\tilde{p}}_\mu$, is proposed for the micro-scale pore-pressures rate. It means that only the first-order term $(\dot{\boldsymbol{\varphi}} \cdot (\mathbf{y} - \mathbf{y}_G))$, considered in (D.9) to expand $\dot{p}_\mu$, is disregarded. Henceforth, the superscript $(\bullet)^{\text{ROE}}$, appended to a variable, implies that it has undergone a Reduced Order Expansion.
- A Full Order Expansion (FOE) for the micro-scale pore pressure gradient, as in expression (D.10), denoted as $\boldsymbol{\varphi}_\mu^{\text{FOE}}$.

D.4.1. Constitutive laws based on Selective Order Expansions (SOE) for primal descriptors

D.4.1.1. SOE-Constitutive laws applied to saturated porous medium

For the material occupying the Ω_μ^{pm} subdomain, the mathematical structure proposed by Coussy O. [36], to describe the isothermal hydro-mechanical behaviour of the saturated porous medium, is assumed to be valid. Thus, we have for the set $\{\dot{\boldsymbol{\sigma}}_\mu^{pm}; \dot{\chi}_\mu\}$

$$\dot{\boldsymbol{\sigma}}_\mu^{pm} = \hat{\dot{\sigma}}_\mu^{pm,\,\text{SOE}}\big(\dot{\boldsymbol{\varepsilon}}_\mu^{\text{FOE}}, \dot{p}_\mu^{\text{ROE}}\big) = \mathbf{C}_\mu^{pm} \,:\, \overbrace{\big(\dot{\boldsymbol{\varepsilon}} + \dot{\tilde{\boldsymbol{\varepsilon}}}_\mu\big)}^{\dot{\boldsymbol{\varepsilon}}_\mu^{\text{FOE}}} - \mathbf{b}_\mu \overbrace{(\dot{p} + \dot{\tilde{p}}_\mu)}^{\dot{p}_\mu^{\text{ROE}}}, \tag{D.41}$$

$$\dot{\chi}_\mu = \hat{\dot{\chi}}_\mu^{\text{SOE}}\big(\dot{\boldsymbol{\varepsilon}}_\mu^{\text{FOE}}, \dot{p}_\mu^{\text{ROE}}\big) = \mathbf{b}_\mu \,:\, \underbrace{\big(\dot{\boldsymbol{\varepsilon}} + \dot{\tilde{\boldsymbol{\varepsilon}}}_\mu\big)}_{\dot{\boldsymbol{\varepsilon}}_\mu^{\text{FOE}}} + \frac{1}{M_\mu} \underbrace{(\dot{p} + \dot{\tilde{p}}_\mu)}_{\dot{p}_\mu^{\text{ROE}}}, \tag{D.42}$$

where the hat-symbol, $(\hat{\bullet})$, denotes a generic constitutive functional. The micro-scale response of the porous matrix is defined by the elastic stiffness tensor of the skeleton $\mathbf{C}_\mu^{pm}$, the Biot tensor $\mathbf{b}_\mu$ and the coefficient M_μ^{-1}. In the particular case of isotropic constituents it is $\mathbf{b}_\mu = b_\mu\,\mathbf{I}$, where the Biot coefficient $b_\mu = 1 - \frac{K_\mu}{K_\mu^s}$ is given by the relationship between the bulk modulus of the skeleton K_μ and the volumetric modulus of the grain material K_μ^s. Finally, we have $\frac{1}{M_\mu} = \frac{b_\mu - n_\mu}{K_\mu^s} + \frac{n_\mu}{K_\mu^f}$ [31, 32, 36], being K_μ^f the bulk modulus of the fluid.

The concept of effective stress field here denoted as $\boldsymbol{\sigma}'^{pm}_\mu$, plays an important role in saturated porous media since significant mechanical changes experienced by the soil skeleton are attributed to effective stress variations. From the theory of poromechanics, $\boldsymbol{\sigma}'^{pm}_\mu$ depends on the strain tensor of the soil grains ($\boldsymbol{\varepsilon}_\mu$), then in agreement with the previous constitutive law (D.41), it can be expressed as

$$\dot{\boldsymbol{\sigma}}'^{pm}_\mu = \hat{\dot{\sigma}}'^{pm,\,\text{SOE}}_\mu\big(\dot{\boldsymbol{\varepsilon}}_\mu^{\text{FOE}}\big) = \hat{\dot{\sigma}}'^{pm,\,\text{FOE}}_\mu\big(\dot{\boldsymbol{\varepsilon}}_\mu^{\text{FOE}}\big) = \mathbf{C}_\mu^{pm} \,:\, \overbrace{\big(\dot{\boldsymbol{\varepsilon}} + \dot{\tilde{\boldsymbol{\varepsilon}}}_\mu\big)}^{\dot{\boldsymbol{\varepsilon}}_\mu^{\text{FOE}}}. \tag{D.43}$$

Furthermore, the following generalized Darcy's law is assumed for the flux velocity vector in the porous saturated subdomain Ω_μ^{pm}, to characterize the seepage phenomenon at the micro-scale level [36, 41, 42]

$$\boldsymbol{\mathcal{V}}_\mu = \hat{\mathcal{V}}_\mu^{\text{SOE}}\big(\boldsymbol{\varphi}_\mu^{\text{FOE}}\big) = \hat{\mathcal{V}}_\mu^{\text{FOE}}\big(\boldsymbol{\varphi}_\mu^{\text{FOE}}\big) = \mathbf{k}_\mu \Big[- \big(\overbrace{\boldsymbol{\varphi} + \tilde{\boldsymbol{\varphi}}_\mu}^{\boldsymbol{\varphi}_\mu^{\text{FOE}}} \big) + \rho_\mu^f\,\mathbf{g} \Big], \tag{D.44}$$

where $\mathbf{k}_\mu$ is the symmetric second order permeability tensor. In case of isotropic saturated materials it is $\mathbf{k}_\mu = k_\mu \mathbf{I}$; $k_\mu = \frac{\kappa_\mu}{\rho_\mu^f\,|\mathbf{g}|}$ being the hydraulic permeability which is a function of the hydraulic conductivity κ_μ and the specific weight of the fluid $\rho_\mu^f\,|\mathbf{g}|$, $|\mathbf{g}|$ identifies the modulus of the acceleration of gravity and $\mathbf{I}$ denotes the second order identity tensor.

The SOE-technique can be formally categorized as a simplifying constitutive-like hypothesis for $\dot{\boldsymbol{\sigma}}_\mu^{pm}$ and $\dot{\chi}_\mu$. Furthermore, we can highlight the very limited local effect that the Reduced Order Expansion for $\dot{p}_\mu$ ($\dot{p}_\mu^{\text{ROE}}$) has in the multiscale formulation since it only makes sense within some constitutive functions. In contrast, out of those specific environments, the micro-scale pore-pressure field is Full Order Expanded.

D.4.1.2. SOE-Constitutive laws applied to solid medium

In the subdomain Ω_μ^{sm}, occupied by the solid impermeable inclusions, we only need to specify the micro-mechanical response for $\dot{\boldsymbol{\sigma}}_\mu^{sm}$. It is completely defined by the elastic stiffness tensor of the solid particles $\mathbf{C}_\mu^{sm}$ which allows us to write the constitutive law of $\dot{\boldsymbol{\sigma}}_\mu^{sm}$ as

$$\dot{\boldsymbol{\sigma}}_\mu^{sm} = \hat{\dot{\sigma}}_\mu^{sm,\,\text{SOE}}\big(\dot{\boldsymbol{\varepsilon}}_\mu^{\text{FOE}}\big) = \hat{\dot{\sigma}}_\mu^{sm,\,\text{FOE}}\big(\dot{\boldsymbol{\varepsilon}}_\mu^{\text{FOE}}\big) = \mathbf{C}_\mu^{sm} \,:\, \overbrace{\big(\dot{\boldsymbol{\varepsilon}} + \dot{\tilde{\boldsymbol{\varepsilon}}}_\mu\big)}^{\dot{\boldsymbol{\varepsilon}}_\mu^{\text{FOE}}}. \tag{D.45}$$

D.4.2. Unified micro-scale constitutive description

The set of constitutive functionals given by (D.41)-(D.44) and (D.45), fully describes the hydro-mechanical behaviour at the smaller length scale. These equations characterize the so-called SOE multiscale approach adopted throughout the present work, which is based on the Reduced Order Expansion (ROE) for the micro-scale pore pressure field, $\dot{p}_\mu^{\text{ROE}} = \dot{p} + \dot{\tilde{p}}_\mu$. Nevertheless, there exist another alternatives such as a Selective Order approach with Zero-Order Expansion (ZOE) for pore-pressures, $\dot{p}_\mu^{\text{ZOE}} = \dot{p}$, or even a Full Order Expansion scheme (FOE) where $\dot{p}_\mu^{\text{FOE}} = \dot{p} + \dot{\boldsymbol{\varphi}} \cdot (\mathbf{y} - \mathbf{y}_G) + \dot{\tilde{p}}_\mu$. The latter procedure introduces the aforementioned lack of objectivity issue in the macro-scale response [66]. Although we only assess the SOE model based on the $\dot{p}_\mu^{\text{ROE}}$ expansion in our numerical examples, it is possible (for completeness) to include the remaining alternatives in a simplified and straightforward manner. For this purpose, and recognizing certain abuse of notation, two binary parameters α and β are introduced that activate or deactivate the functional dependence of certain arguments in the constitutive laws according to the type of expansion adopted. Thus, we can write

$$\dot{\boldsymbol{\sigma}}_\mu^{pm} = \hat{\dot{\sigma}}_\mu^{pm}\big(\dot{\boldsymbol{\varepsilon}}, \dot{\tilde{\boldsymbol{\varepsilon}}}_\mu, \dot{p}, \alpha\, \dot{\boldsymbol{\varphi}}, \beta\, \dot{\tilde{p}}_\mu\big) = \mathbf{C}_\mu^{pm} \,:\, \big(\dot{\boldsymbol{\varepsilon}} + \dot{\tilde{\boldsymbol{\varepsilon}}}_\mu\big) - \mathbf{b}_\mu\, (\dot{p} + \alpha\, \dot{\boldsymbol{\varphi}} \cdot (\mathbf{y} - \mathbf{y}_G) + \beta\, \dot{\tilde{p}}_\mu), \tag{D.46}$$

$$\dot{\boldsymbol{\sigma}}_\mu^{sm} = \hat{\dot{\sigma}}_\mu^{sm}\big(\dot{\boldsymbol{\varepsilon}}, \dot{\tilde{\boldsymbol{\varepsilon}}}_\mu\big) = \mathbf{C}_\mu^{sm} \,:\, \big(\dot{\boldsymbol{\varepsilon}} + \dot{\tilde{\boldsymbol{\varepsilon}}}_\mu\big). \tag{D.47}$$

$$\dot{\chi}_\mu = \hat{\dot{\chi}}_\mu\big(\dot{\boldsymbol{\varepsilon}}, \dot{\tilde{\boldsymbol{\varepsilon}}}_\mu, \dot{p}, \alpha\, \dot{\boldsymbol{\varphi}}, \beta\, \dot{\tilde{p}}_\mu\big) = \mathbf{b}_\mu \,:\, \big(\dot{\boldsymbol{\varepsilon}} + \dot{\tilde{\boldsymbol{\varepsilon}}}_\mu\big) + \frac{1}{M_\mu}\, \big(\dot{p} + \alpha\, \dot{\boldsymbol{\varphi}} \cdot (\mathbf{y} - \mathbf{y}_G) + \beta\, \dot{\tilde{p}}_\mu\big), \tag{D.48}$$

$$\boldsymbol{\mathcal{V}}_\mu = \hat{\mathcal{V}}_\mu\big(\boldsymbol{\varphi}, \tilde{\boldsymbol{\varphi}}_\mu\big) = \mathbf{k}_\mu \Big[- \big(\boldsymbol{\varphi} + \tilde{\boldsymbol{\varphi}}_\mu\big) + \rho_\mu^f\, \mathbf{g} \Big]. \tag{D.49}$$

In view of (D.46)-(D.49), the choices $\{\alpha = 0, \beta = 1\}$, $\{\alpha = 0, \beta = 0\}$ or $\{\alpha = 1, \beta = 1\}$ characterize, respectively, the SOE approach based on the $\dot{p}_\mu^{\text{ROE}}$ expansion, based on the $\dot{p}_\mu^{\text{ZOE}}$ expansion or the FOE (micro-scale size dependent) homogenization scheme.

D.5. Adoption of admissible constraints in the micro-cell

To conclude the characterization of the variational problem at the micro-scale, see equations (D.39)-(D.40), suitable specifications for the linear vector space $\tilde{\mathcal{U}}_\mu\,(\Omega_\mu) \subseteq \tilde{\mathcal{U}}_\mu^{\text{MCo}}\,(\Omega_\mu)$ and for the set $\tilde{\mathcal{P}}_\mu\,(\Omega_\mu^{pm})$ $\subseteq \tilde{\mathcal{P}}_\mu^{\text{MCo}}\,(\Omega_\mu^{pm})$ are required. Depending on which choice is adopted, different macroscopic constitutive responses could be obtained in general [26, 62]. In this contribution, one of the most widespread homogenization procedures is used, the so-called periodic multiscale model [12, 62], which is briefly described

in the following subsections.

D.5.1. Periodic boundary fluctuation model

In order to fulfill the periodic media hypothesis, the distribution of heterogeneities in the micro-scale domain must satisfy certain geometrical properties. The assumptions estabilised in section D.3.1, see in particular the paragraph preceding equation (D.6), allow us to apply the periodic multiscale scheme without objections.

For simplicity, we consider in our explanations two-dimensional problems and rectangular micro-cells, in which points in opposite sides of the MC boundary are identified in pairs. Thus, equal-sized subsets $\Gamma^{+}_{\mu\, i}$ and $\Gamma^{-}_{\mu\, i}$ of Γ_μ, with unit normals $\mathbf{n}^{b+}_i$ and $\mathbf{n}^{b-}_i$, respectively, comprise a pair "i" of edges. We have $\Gamma_{\mu\, i} = \Gamma^{+}_{\mu\, i} \cup \Gamma^{-}_{\mu\, i}$ for $i = 1, 2$ where $\Gamma^{+}_{\mu\, 1} = \Gamma^{\text{right}}_{\mu}$, $\Gamma^{-}_{\mu\, 1} = \Gamma^{\text{left}}_{\mu}$, $\Gamma^{+}_{\mu\, 2} = \Gamma^{\text{top}}_{\mu}$, $\Gamma^{-}_{\mu\, 1} = \Gamma^{\text{bottom}}_{\mu}$. Then: $\Gamma_{\mu\, 1} = \Gamma^{\text{right}}_{\mu} \cup \Gamma^{\text{left}}_{\mu}$ and $\Gamma_{\mu\, 2} = \Gamma^{\text{top}}_{\mu} \cup \Gamma^{\text{bottom}}_{\mu}$. Each point $\mathbf{y}^{+}_i \in \Gamma^{+}_{\mu\, i}$ has its corresponding point $\mathbf{y}^{-}_i \in \Gamma^{-}_{\mu\, i}$, so there is a one-to-one correspondence between the points of $\Gamma^{+}_{\mu\, i}$ and $\Gamma^{-}_{\mu\, i}$. Naturally, this geometric correlation must emulate the periodicity property of the material. On the other hand, recall that the micro-scale pore pressure fluctuation field is defined only over the saturated porous subdomain Ω^{pm}_{μ}. Thus we account for additional pairs "j" of edges ($j = 1, 2$) that belong to the boundary of porous medium, Γ^{pm}_{μ}, exclusively. Similar geometrical partitions (along with all the involved nomenclature) as described for the pairs of edges "i" are considered valid in relation with the pairs "j". Therefore, the main feature of the periodic model is retrieved by enforcing identical displacements and pore pressure fluctuations at opposite boundary points in accordance with the following specifications

$$\tilde{\mathbf{u}}_\mu \left(\mathbf{y}^{+}_i, t\right) = \tilde{\mathbf{u}}_\mu \left(\mathbf{y}^{-}_i, t\right), \ \forall \text{ pair } \{\mathbf{y}^{+}_i, \mathbf{y}^{-}_i\}, \ i = 1, 2, \tag{D.50}$$

$$\tilde{p}_\mu \left(\mathbf{y}^{+}_j, t\right) = \tilde{p}_\mu \left(\mathbf{y}^{-}_j, t\right), \ \forall \text{ pair } \{\mathbf{y}^{+}_j, \mathbf{y}^{-}_j\}, \ j = 1, 2. \tag{D.51}$$

In summary, the specific vector space $\tilde{\mathcal{U}}_\mu (\Omega_\mu)$ and set $\tilde{\mathcal{P}}_\mu (\Omega^{pm}_{\mu})$ adopted throughout this contribution to solve the micro-scale equilibrium problem coincide with the vector space $\tilde{\mathcal{U}}^{\text{Per}}_{\mu} (\Omega_\mu)$ and set $\tilde{\mathcal{P}}^{\text{Per}}_{\mu} (\Omega^{pm}_{\mu})$ provided by the Periodic multiscale model, respectively (i.e. $\tilde{\mathcal{U}}_\mu (\Omega_\mu) \equiv \tilde{\mathcal{U}}^{\text{Per}}_{\mu} (\Omega_\mu)$ and $\tilde{\mathcal{P}}_\mu (\Omega^{pm}_{\mu}) \equiv \tilde{\mathcal{P}}^{\text{Per}}_{\mu} (\Omega^{pm}_{\mu})$). The formal definitions for $\tilde{\mathcal{U}}^{\text{Per}}_{\mu} (\Omega_\mu)$ and $\tilde{\mathcal{P}}^{\text{Per}}_{\mu} (\Omega^{pm}_{\mu})$ are the followings

$$\tilde{\mathcal{U}}^{\text{Per}}_{\mu} (\Omega_\mu) = \Big\{ \mathbf{v} \ \in \ \mathbf{H}^1 (\Omega_\mu) ; \int_{\Omega_\mu} \mathbf{v} \, d\Omega_\mu = \mathbf{0} \\ \text{and } \mathbf{v} \left(\mathbf{y}^{+}_i\right) = \mathbf{v} \left(\mathbf{y}^{-}_i\right) \ \forall \text{ pair } \{\mathbf{y}^{+}_i, \mathbf{y}^{-}_i\}, \ i = 1, 2 \Big\} \subset \tilde{\mathcal{U}}^{\text{MCo}}_{\mu} (\Omega_\mu), \tag{D.52}$$

$$\tilde{\mathcal{P}}^{\text{Per}}_{\mu} \left(\Omega^{pm}_{\mu}\right) = \Big\{ v \ \in \ \mathrm{H}^1 \left(\Omega^{pm}_{\mu}\right) ; \int_{\Omega^{pm}_{\mu}} (v + \boldsymbol{\varphi} \cdot (\mathbf{y} - \mathbf{y}_G)) \, d\Omega_\mu = 0 \\ \text{and } v \left(\mathbf{y}^{+}_j\right) = v \left(\mathbf{y}^{-}_j\right) \ \forall \text{ pair } \{\mathbf{y}^{+}_j, \mathbf{y}^{-}_j\}, \ j = 1, 2 \Big\} \subset \tilde{\mathcal{P}}^{\text{MCo}}_{\mu} \left(\Omega^{pm}_{\mu}\right). \tag{D.53}$$

In view of definitions (D.52)-(D.53), we can finally introduce the vector spaces for the admissible virtual actions in the micro-scale, that is $\delta\dot{\tilde{\mathbf{u}}}_\mu \in \tilde{\mathcal{U}}^{*\text{Per}}(\Omega_\mu)$ and $\delta\tilde{p}_\mu \in \tilde{\mathcal{P}}^{*\text{Per}}(\Omega^{pm}_{\mu})$, where

$$\tilde{\mathcal{U}}^{*\text{Per}}_{\mu} (\Omega_\mu) \equiv \tilde{\mathcal{U}}^{\text{Per}}_{\mu} (\Omega_\mu), \tag{D.54}$$

$$\tilde{\mathcal{P}}_{\mu}^{*\text{Per}}\left(\Omega_{\mu}^{pm}\right) = \Big\{ v \ \in \ \mathrm{H}^{1}\left(\Omega_{\mu}^{pm}\right); \int_{\Omega_{\mu}^{pm}} v \, d\Omega_{\mu} = 0 \\ \text{and } v\left(\mathbf{y}_{j}^{+}\right) = v\left(\mathbf{y}_{j}^{-}\right) \ \forall \text{ pair } \{\mathbf{y}_{j}^{+}, \mathbf{y}_{j}^{-}\}, \ j = 1, 2 \Big\}. \quad \text{(D.55)}$$

D.6. Solution of the variational equations at both scales

To deal with the multiscale problem in numerical form, the global paradigm consists of two nested finite element schemes, evolving in time, where the connection between them is established at each macro-scale Gauss point. In the literature, this approach is called the FE^2 strategy [5].

Numerical definitions and ingredients related to temporal discretization are common to both macro and micro spatial domains since they share the same temporal scale. Thus, the time variable, t, is discretized through a monotonically increasing sequence of time steps $[t^0, t^1, t^2, \ldots, t^n, t^{n+1}, \ldots]$ and $\Delta t = (t^{n+1} - t^n)$ represents the corresponding time step increment for a generic time interval $I_t = [t^n, t^{n+1}]$. The θ-generalized rule [41, 59], which uses the time integration parameter $\theta \in [0, 1]$ ($\theta = 0.5$ was adopted in this work), is proposed to deal with the evolution of the problem within any time interval I_t.

Two independent finite element meshes, Ω_h and $\Omega_{\mu,h}$, are considered to approximate the macro-scale physical domain Ω and to discretize the micro-cell volume Ω_{μ}, respectively. In what follows, we proceed in the first instance to address the solution at the macroscopic length scale and then deal with its micro-scale counterpart.

D.6.1. Solution of the variational equations at the macro-scale

Based on the finite element mesh proposal, Ω_h, the primal descriptors $\dot{\mathbf{u}}$ and p (and their corresponding admissible virtual variations $\delta\dot{\mathbf{u}}$ and δp) can be approximated through global interpolation matrices for the displacement, $\mathbf{N}_u$, and pore pressure, $\mathbf{N}_p$, fields as follows

$$\begin{aligned} \mathbf{u} &= \mathbf{N}_u \, \bar{\mathbf{u}}, \quad \delta\dot{\mathbf{u}} = \mathbf{N}_u \, \delta\dot{\bar{\mathbf{u}}}, \quad \text{with } \bar{\mathbf{u}} \in \mathcal{U}_h \text{ and } \delta\bar{\mathbf{u}} \in \mathcal{U}_h^*, \\ p &= \mathbf{N}_p \, \bar{\mathbf{p}}, \quad \delta p = \mathbf{N}_p \, \delta\bar{\mathbf{p}}, \quad \text{with } \bar{\mathbf{p}} \in \mathcal{P}_h \text{ and } \delta\bar{\mathbf{p}} \in \mathcal{P}_h^*, \end{aligned} \quad \text{(D.56)}$$

where $\bar{\mathbf{u}}$ and $\bar{\mathbf{p}}$ are the vectors that collect all nodal displacement and pore pressure values, respectively, $\delta\dot{\bar{\mathbf{u}}}$ and $\delta\bar{\mathbf{p}}$ are the vectors that collect all nodal admissible virtual variations for displacements and pore pressures, correspondingly, while $\mathcal{U}_h$, $\mathcal{U}_h^*$, $\mathcal{P}_h$ and $\mathcal{P}_h^*$ represent the finite-dimensional counterparts of sub-spaces $\mathcal{U}$, $\mathcal{U}^*$, $\mathcal{P}$ and $\mathcal{P}^*$, appropriately. In addition, the same spatial approximation was used for realizable and virtual actions, according to the Galerkin approach. Also, our current implementation considers quadrilateral, isoparametric, as well as bi-quadratic and bi-linear finite elements for displacements and pore pressures field, to fulfill the Babuska-Brezzi convergence requirements [41].

Then, by discretizing the weak form of the macro-scale balance equations (D.4) in space according to (D.56) and in time following the generalized θ-rule, the discrete version at the time step $t^{n+\theta}$ becomes

$$\begin{aligned} \dot{\mathbf{G}}_h^{n+\theta} &\equiv \int_{\Omega_h} \mathbf{B}_u^T \, \dot{\boldsymbol{\sigma}}^{n+\theta} \, d\Omega - \int_{\Omega_h} \mathbf{N}_u^T \, \dot{\mathbf{f}}^{n+\theta} \, d\Omega - \int_{\Gamma_{\text{N},h}^u} \mathbf{N}_u^T \, \dot{\mathbf{t}}^{n+\theta} \, d\Gamma = \mathbf{0}, \\ \mathbf{H}_h^{n+\theta} &\equiv \int_{\Omega_h} \mathbf{N}_p^T \, \dot{\chi}^{n+\theta} \, d\Omega - \int_{\Omega_h} \mathbf{B}_p^T \, \boldsymbol{\mathcal{V}}^{n+\theta} \, d\Omega + \int_{\Gamma_{\text{N},h}^p} \mathbf{N}_p^T \, \frac{q^{n+\theta}}{\rho^f} \, d\Gamma = \mathbf{0}, \end{aligned} \quad \text{(D.57)}$$

where $\mathbf{B}_u = \boldsymbol{\nabla}^{sym} \mathbf{N}_u$ is the global deformation-displacement matrix, $\mathbf{B}_p = \boldsymbol{\nabla} \mathbf{N}_p$ is the global matrix that relates pore pressures to their gradients, $(\bullet)^T$ stands for the transpose operator and $\Gamma_{\text{N},h}^{(\bullet)}$ is the discrete version of Neumann-type boundaries. Remark that, in the first line of (D.57), the momentum

equilibrium equation has been considered in rate form.

The Newton-Raphson scheme is adopted to solve the system of equations (D.57), whereby current nodal values of displacement and pore pressure are updated (at time step t^{n+1}) in terms of the iterative increments $\Delta\bar{\mathbf{u}}$ and $\Delta\bar{\mathbf{p}}$, respectively. In the Newton-Raphson strategy, for a "k"-iteration in the time interval I_t, these increments are evaluated as follows [16, 51, 52, 66] (subscript h is omitted hereafter)

$$\left[\begin{array}{c}\Delta\bar{\mathbf{u}}\\ \Delta\bar{\mathbf{p}}\end{array}\right] = -\left[\begin{array}{cc}\frac{\partial\dot{\mathbf{G}}_k^{n+\theta}}{\partial\bar{\mathbf{u}}^{n+1}} & \frac{\partial\dot{\mathbf{G}}_k^{n+\theta}}{\partial\bar{\mathbf{p}}^{n+1}}\\ \frac{\partial\mathbf{H}_k^{n+\theta}}{\partial\bar{\mathbf{u}}^{n+1}} & \frac{\partial\mathbf{H}_k^{n+\theta}}{\partial\bar{\mathbf{p}}^{n+1}}\end{array}\right]\left[\begin{array}{c}\dot{\mathbf{G}}_k^{n+\theta}\\ \mathbf{H}_k^{n+\theta}\end{array}\right] = -\left(\mathbf{J}_k^{n+\theta}\right)^{-1}\left[\begin{array}{c}\dot{\mathbf{G}}_k^{n+\theta}\\ \mathbf{H}_k^{n+\theta}\end{array}\right], \tag{D.58}$$

$\mathbf{J}_k^{n+\theta}$ being the macro-scale Jacobian linear operator whose components are defined in Appendix A (subscript *"k"* is removed there to simplify the notation). Meanwhile, these components depend on the homogenized constitutive operators of the multiscale model [12, 22, 110], which are also specified in Appendix A.

D.6.2. Solution of the variational equations at the micro-scale

As previously established, the finite element methodology at both scales is the same. In addition, in section D.5.1, the periodic multiscale model has been assumed, see (D.52)-(D.53). This allows us to define in the discretized domain $\Omega_{\mu,h}$ the counterpart of the sub-spaces $\tilde{\mathcal{U}}_\mu^{\text{Per}} \equiv \tilde{\mathcal{U}}_\mu^{\text{Per}*}$ $\left(\subset \tilde{\mathcal{U}}_\mu^{\text{MCo}}\right)$, $\tilde{\mathcal{P}}_\mu^{\text{Per}}$ $\left(\subset \tilde{\mathcal{P}}_\mu^{\text{MCo}}\right)$ and $\tilde{\mathcal{P}}_\mu^{\text{Per}*}$ $\left(\subset \tilde{\mathcal{P}}_\mu^{\text{MCo}}\right)$ which are given by the finite-dimensional form $\tilde{\mathcal{U}}_{\mu,h}^{\text{Per}} \equiv \tilde{\mathcal{U}}_{\mu,h}^{\text{Per}*}$, $\tilde{\mathcal{P}}_{\mu,h}^{\text{Per}}$ and $\tilde{\mathcal{P}}_{\mu,h}^{\text{Per}*}$, respectively. It is in these discrete sub-spaces that we define the vector containing all the fluctuating micro-displacements $\tilde{\mathbf{u}}_\mu$, its corresponding global vector collecting the admissible virtual variations $\delta\tilde{\tilde{\mathbf{u}}}_\mu$, the vector comprising the fluctuating micro-pore pressures $\tilde{\tilde{\mathbf{p}}}_\mu$ and the vector of the admissible virtual variations $\delta\tilde{\tilde{\mathbf{p}}}_\mu$ of the latter. Each of the discrete variables and their corresponding admissible virtual variation is obtained from the primary descriptors $\dot{\tilde{\mathbf{u}}}_\mu$, $\tilde{p}_\mu$, their respective admissible virtual variations $\delta\dot{\tilde{\mathbf{u}}}_\mu$ and $\delta\tilde{p}_\mu$, through the global interpolation function matrices for micro-displacement fluctuations, $\mathbf{N}_{\tilde{u}_\mu}$, and micro-pore pressure fluctuations, $\mathbf{N}_{\tilde{p}_\mu}$, as

$$\begin{aligned}
&\tilde{\mathbf{u}}_\mu = \mathbf{N}_{\tilde{u}_\mu}\,\tilde{\tilde{\mathbf{u}}}_\mu, \quad \delta\tilde{\mathbf{u}}_\mu = \mathbf{N}_{\tilde{u}_\mu}\,\delta\tilde{\tilde{\mathbf{u}}}_\mu, \quad \text{with } \tilde{\mathbf{u}}_\mu \text{ and } \delta\tilde{\tilde{\mathbf{u}}}_\mu \in \tilde{\mathcal{U}}_{\mu,h}^{\text{Per}} \equiv \tilde{\mathcal{U}}_{\mu,h}^{\text{Per}*},\\
&\tilde{p}_\mu = \mathbf{N}_{\tilde{p}_\mu}\,\tilde{\tilde{\mathbf{p}}}_\mu, \quad \delta\tilde{p}_\mu = \mathbf{N}_{\tilde{p}_\mu}\,\delta\tilde{\tilde{\mathbf{p}}}_\mu, \quad \text{with } \tilde{\mathbf{p}}_\mu \in \tilde{\mathcal{P}}_{\mu,h}^{\text{Per}} \text{ and } \delta\tilde{\tilde{\mathbf{p}}}_\mu \in \tilde{\mathcal{P}}_{\mu,h}^{\text{Per}*}.
\end{aligned} \tag{D.59}$$

The spatial and time discrete approximation (at time $t^{n+\theta}$) for the balance equations in the micro-scale is obtained after the substitution of (D.59) and the θ-rule into the variational forms (D.39)-(D.40) and some standard mathematical handling, as outlined below

$$\overbrace{\left[\int_{\Omega_{\mu,h}}\left(\mathbf{B}_{\tilde{u}_\mu}^T\,\boldsymbol{\sigma}_\mu^{n+\theta} - \mathbf{N}_{\tilde{u}_\mu}^T\,\dot{\mathbf{f}}_\mu^{n+\theta}\right)d\Omega_\mu\right]}^{\dot{\mathbf{G}}_{\mu,h}^{n+\theta}} \cdot\,\delta\dot{\tilde{\tilde{\mathbf{u}}}}_\mu = 0,$$
$$\forall\,\delta\dot{\tilde{\tilde{\mathbf{u}}}}_\mu \in \tilde{\mathcal{U}}_{\mu,h}^{\text{Per}*}, \text{ with } \dot{\tilde{\tilde{\mathbf{u}}}}_\mu \in \tilde{\mathcal{U}}_{\mu,h}^{\text{Per}} \text{ and } \tilde{\tilde{\mathbf{p}}}_\mu \in \tilde{\mathcal{P}}_{\mu,h}^{\text{Per}}, \tag{D.60}$$

$$\overbrace{\left[\int_{\Omega_{\mu,h}^{pm}}\left(\mathbf{N}_{\tilde{p}_\mu}^T\,\dot{\chi}_\mu^{n+\theta} - \mathbf{B}_{\tilde{p}_\mu}^T\,\boldsymbol{\mathcal{V}}_\mu^{n+\theta}\right)d\Omega_\mu\right]}^{\mathbf{H}_{\mu,h}^{n+\theta}} \cdot\,\delta\tilde{\tilde{\mathbf{p}}}_\mu = 0,$$
$$\forall\,\delta\tilde{\tilde{\mathbf{p}}}_\mu \in \tilde{\mathcal{P}}_{\mu,h}^{\text{Per}*}, \text{ with } \dot{\tilde{\tilde{\mathbf{u}}}}_\mu \in \tilde{\mathcal{U}}_{\mu,h}^{\text{Per}} \text{ and } \tilde{\tilde{\mathbf{p}}}_\mu \in \tilde{\mathcal{P}}_{\mu,h}^{\text{Per}}, \tag{D.61}$$

where, once again, the momentum balance equation has been considered in rate form and $\mathbf{B}_{\tilde{u}_\mu} = \boldsymbol{\nabla}_y^{sym}\mathbf{N}_{\tilde{u}_\mu}$ and $\mathbf{B}_{\tilde{p}_\mu} = \boldsymbol{\nabla}_y\mathbf{N}_{\tilde{p}_\mu}$, are the micro-scale global matrices relating the primal variables with their corresponding gradients.

The numerical solution for nodal values of displacements, $\tilde{\tilde{\mathbf{u}}}_\mu^{t_{n+1}}$, and pore pressure fluctuations, $\tilde{\tilde{\mathbf{p}}}_\mu^{t_{n+1}}$, at current time step t^{n+1}, is obtained in terms of the iterative increments $\Delta\tilde{\tilde{\mathbf{u}}}_\mu$ and $\Delta\tilde{\tilde{\mathbf{p}}}_\mu$, respectively. They are computed by using a standard Newton-Raphson procedure applied to the system of equations (D.60)-(D.61). In this sense, for a generic "*k*"-iteration it can be expressed (subscript *h* is omitted hereafter)

$$\left\{\begin{bmatrix} \frac{\partial\dot{\mathbf{G}}_{\mu,\,k}^{n+\theta}}{\partial\tilde{\tilde{\mathbf{u}}}_\mu^{n+1}} & \frac{\partial\dot{\mathbf{G}}_{\mu,\,k}^{n+\theta}}{\partial\tilde{\tilde{\mathbf{p}}}_\mu^{n+1}} \\ \frac{\partial\mathbf{H}_{\mu,\,k}^{n+\theta}}{\partial\tilde{\tilde{\mathbf{u}}}_\mu^{n+1}} & \frac{\partial\mathbf{H}_{\mu,\,k}^{n+\theta}}{\partial\tilde{\tilde{\mathbf{p}}}_\mu^{n+1}} \end{bmatrix} \begin{bmatrix} \Delta\tilde{\tilde{\mathbf{u}}}_\mu \\ \Delta\tilde{\tilde{\mathbf{p}}}_\mu \end{bmatrix} + \begin{bmatrix} \dot{\mathbf{G}}_{\mu,\,k}^{n+\theta} \\ \mathbf{H}_{\mu,\,k}^{n+\theta} \end{bmatrix}\right\} \cdot \begin{bmatrix} \delta\dot{\tilde{\tilde{\mathbf{u}}}}_\mu \\ \delta\tilde{\tilde{\mathbf{p}}}_\mu \end{bmatrix} =$$

$$= \left\{\mathbf{J}_{\mu,\,k}^{n+\theta} \begin{bmatrix} \Delta\tilde{\tilde{\mathbf{u}}}_\mu \\ \Delta\tilde{\tilde{\mathbf{p}}}_\mu \end{bmatrix} + \begin{bmatrix} \dot{\mathbf{G}}_{\mu,\,k}^{n+\theta} \\ \mathbf{H}_{\mu,\,k}^{n+\theta} \end{bmatrix}\right\} \cdot \begin{bmatrix} \delta\dot{\tilde{\tilde{\mathbf{u}}}}_\mu \\ \delta\tilde{\tilde{\mathbf{p}}}_\mu \end{bmatrix} = \begin{bmatrix} 0 \\ 0 \end{bmatrix},$$

$$\forall\, \delta\dot{\tilde{\tilde{\mathbf{u}}}}_\mu \in \tilde{\mathcal{U}}_\mu^{\text{Per*}},\ \forall\, \delta\tilde{\tilde{\mathbf{p}}}_\mu \in \tilde{\mathcal{P}}_\mu^{\text{Per*}},\ \text{with}\ \Delta\tilde{\tilde{\mathbf{u}}}_\mu \in \tilde{\mathcal{U}}_\mu^{\text{Per}},\ \text{and}\ \Delta\tilde{\tilde{\mathbf{p}}}_\mu \in \tilde{\mathcal{P}}_\mu^{\text{Per}}, \quad \text{(D.62)}$$

where $\mathbf{J}_{\mu,\,k}^{n+\theta}$ is the Jacobian operator in the micro-scale. Its components are defined in the Appendix B (with the subscript *"k"* suppressed to simplify the notation).

In the present work, the Lagrange multiplier method was used to implement the volumetric null-means constraints on the discrete fields $\tilde{\mathbf{u}}_\mu$ and $\tilde{p}_\mu$, while a static condensation procedure was used for the boundary conditions [23, 62].

D.7. Numerical results

In this section, we will deal with two different situations. Firstly, the one-dimensional consolidation phenomenon is presented as a benchmark problem to critically analyze the proposed multiscale model. The following section shows the full potential of the proposed multiscale framework, in a practical geotechnical situation consisting of a two-dimensional consolidation problem given by the staged construction of an embankment on the surface of the stratum. In both examples, highly heterogeneous media will be treated, and we adopt the more generic SOE-multiscale procedure defined by a ROE of $\dot{p}_\mu$ ($\{\alpha = 0,\ \beta = 1\}$) for the porous media subdomain Ω_μ^{pm}. This setting implies that solely the macro-scale pore pressure gradient rate, $\dot{\boldsymbol{\varphi}}$, has been neglected when evaluating the constitutive functionals $\dot{\hat{\sigma}}_\mu$ and $\dot{\hat{\chi}}_\mu$, see expressions (D.46) and (D.48). This choice ensures the objectivity of the macro-scale response, contrary to what is expected in case of the FOE-multiscale model scheme. Furthermore, the results for the two scenarios solved by the multiscale strategy are contrasted with the resolutions given by an alternative methodology commonly known in the scientific community as Direct Numerical Simulation (DNS), a solution that will be taken as a rigorous reference. The DNS is just the numerical scheme that captures all the heterogeneities within a single physical length scale (the macro-scale).

In order to focus on the applicability of the composite micro-cell model, some simplified hypotheses are presented below:

- Body forces are neglected: $\mathbf{f} \equiv \mathbf{f}_\mu \equiv \mathbf{0}$. Thus, a weightless soil is simulated.
- Hydrostatic pore pressure due to the water table position is not accounted for. Under this circumstance, the variable "p" (as well as "p_μ" and "$\tilde{p}_\mu$") must be interpreted as the "*excess of pore-pressure*" generated exclusively by the external load ($\mathbf{t}$) during the consolidation process.
- As a consequence if the previous hypothesis, the gravity effect in the micro-scale Darcy constitutive model must be neglected (recall (D.44)).

- Although the entire work was developed considering a three-dimensional space $\mathbb{R}^3$, it is applicable and easy to reduce to the two-dimensional space $\mathbb{R}^2$ without loss of generality.
- A plane strain state is assumed.

To compare homogenized variables,$\{\boldsymbol{\sigma};\ \dot{\chi};\ \boldsymbol{\mathcal{V}}\}$, between the DNS reference solution and the multiscale proposal, we adopt a specific volume $|\Omega_{\text{Ref}}|$ where we perform a volumetric average. Thus, we compute

$$(\bullet)^{\text{Av}} = \frac{1}{|\Omega_{\text{Ref}}|}\int_{|\Omega_{\text{Ref}}|} (\bullet)\ d\Omega \tag{D.63}$$

where $(\bullet)^{\text{Av}}$ is the volumetric average in the reference volume of $(\bullet)$.

D.7.1. One-dimensional consolidation examples

In order to critically and deeply evaluate the proposed model, we adopt the simplest situation, which consists of analyzing the hydro-mechanical state in the one-dimensional consolidation process. Our focus is on the homogenized response from the proposed formulation and the effects produced at the composite micro-cell. It is worth noting that the one-dimensional example has an analytical solution only for homogeneous materials, a situation far from being satisfied in the present example, given not only the heterogeneity but also that certain volumes fraction of the stratum cannot even be modeled as a porous medium, because they are made up of solid impermeable inclusions. Thus, in an attempt to measure the predictive capabilities of the multiscale model through its macro-scale results, the soil column is also modeled using the DNS method.

First, we describe the case to be solved using the multiscale strategy. The macro-scale domain, where the material is considered as a homogenized medium, consists of a narrow soil column of $\text{H} = 10m$ high and $\text{W} = 1m$ width. At this length scale, the specified boundary conditions involve zero prescribed horizontal displacements along the right and left vertical sides and zero vertical displacements on the bottom contour. Finally, regarding the Dirichlet boundary conditions the pore pressure is set to zero at the upper limit for all time steps, conforming the unique edge with drainage capacity. Concerning the Neumman conditions, with respect to the hydraulic phenomenon, the lateral and bottom edges act as an impermeable boundary for the flow process, which implies that the seepage velocity, $\boldsymbol{\mathcal{V}}$, can occur only in the vertical upward direction. A purely compressive external load $\mathbf{t} = [0,\ \text{t}_2]^T$ is applied at the ground soil surface, which evolves linearly and monotonically from $\text{t}_2 = 0kPa$ to $-300kPa$ during the first day of analysis and then it remains constant. The macro-scale spatial discretization is composed of 13 finite elements. The mesh is refined near the surface where the external load $\mathbf{t}$ is imposed because the largest pore pressure gradient are expected in that region, see Figure D.4-(a).

The time discretization, which is common for both length scales, varies throughout the analysis following a logarithmic sequence: $t = [0.1, 0.2, \ldots,\ 0.8, 0.9, 1, 2, 3, \ldots,\ 8, 9, 10, 20, 30, \ldots,\ 80, 90, 100, 200, 300, \ldots]$ (in days), reaching a maximum time at $t_{max} = 2000$ days.

By addressing the micro-scale space, we evaluate a highly heterogeneous material. It involves an artificial arrangement of solid inclusions embedded in a porous medium matrix. In the present example, specifically, it is comprised of (i) a soil matrix consisting of clay of high plasticity and low permeability, Ω_μ^{pm}, and (ii) basaltic rock fragments of high stiffness and assumed impermeability, Ω_μ^{sm}. The volume fraction of the rock portion is $30\,\%$.

The material properties that characterized the matrix and inclusion are summarized in Table D.1, where subscript $(\bullet)_\mu$ was omitted for simplicity since the properties are also valid for the DNS solution. The boundary conditions imposed at the micro-scale for the displacement and pore pressure fluctuations are the same irrespective of the type and size of MC adopted, which we describe later. As already mentioned in Section D.5.1, in this work, we have adopted the well-known periodic multiscale model. The corresponding boundary partitions, $\Gamma_{\mu,1}^-$, $\Gamma_{\mu,1}^+$, $\Gamma_{\mu,2}^-$, and $\Gamma_{\mu,2}^+$, allowing the cons-

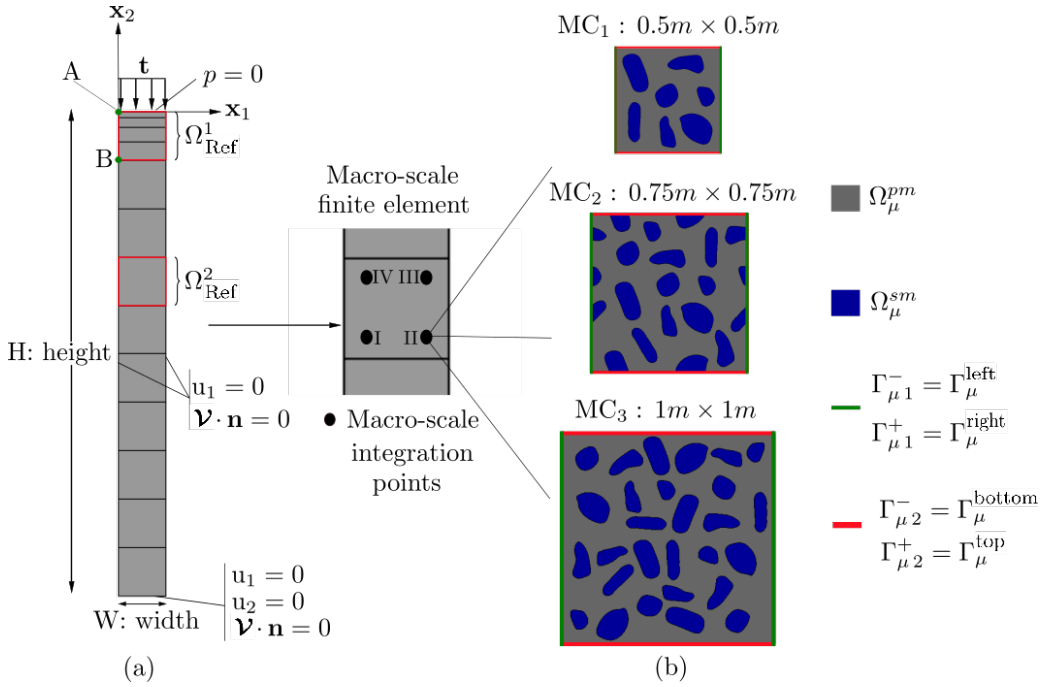

Figura D.4: Multiscale procedure applied to the 1D-consolidation phenomenon (drawing not to scale). General model layout: (a) Macro-scale; (b) Micro-scale. Sequence of MCs. Top: MC_1 of $0.5\,m \times 0.5\,m$. Middle: MC_2 of $0.75\,m \times 0.75\,m$. Bottom: MC_3 of $1\,m \times 1\,m$.

Material properties	Matrix Ω^{pm}	Inclusions Ω^{sm}
Young's modulus E^0 $[kPa]$	40000	6×10^7
Poisson's ratio ν	0.4	0.3
Hydraulic conductivity $\kappa_1 = \kappa_2$ $[m/\text{day}]$	8.64×10^{-6}	-
Initial void ratio e^0	1.4	-
Bulk modulus of the soil grain K^s $[kPa]$	21×10^6	-
Bulk modulus of the fluid K^f $[kPa]$	22.5×10^5	-
Solid density ρ^s $[kg/m^3]$	1800	2700
Fluid density ρ^f $[kg/m^3]$	1000	-

Tabla D.1: 1D-consolidation example. Material properties of the heterogeneous composite soil stratum.

truction of the periodic model underlying the definitions (D.52) and (D.53) are depicted in Figure D.4-(b). The periodicity condition is strictly maintained by the vertex nodes, which are defined as $\tilde{\mathbf{u}}_\mu^{\text{top-right}} = \tilde{\mathbf{u}}_\mu^{\text{top-left}} = \tilde{\mathbf{u}}_\mu^{\text{bottom-left}} = \tilde{\mathbf{u}}_\mu^{\text{bottom-right}}$ and $\tilde{p}_\mu^{\text{top-right}} = \tilde{p}_\mu^{\text{top-left}} = \tilde{p}_\mu^{\text{bottom-left}} = \tilde{p}_\mu^{\text{bottom-right}}$; where $\tilde{\mathbf{u}}_\mu^{\text{top-right}}$ and $\tilde{p}_\mu^{\text{top-right}}$ are the displacement fluctuation and pore pressure fluctuation for the node located at the top-right vertex of the MC (analogous terminology is employed for other vertices).

For the multiscale simulation based on the SOE-model, micro-cells of increasing size have been considered. The increment is based on adopting the smallest MC as a starting point and taking progressively larger windows of material until the representative volume for the case under consideration is reached. In particular, three square micro-cells of growing size have been adopted, denoted according to their dimensions as MC_1: $0.5\,m \times 0.5\,m$, MC_2: $0.75\,m \times 0.75\,m$ and MC_3: $1\,m \times 1\,m$. These MCs are shown in Figure D.4-(b). Meshes of 1372, 3077 and 5659 finite elements are used in each of the MCs, respectively. For clarity in the illustration, the mesh is not shown at the micro-scale.

On the other hand, taking into account the DNS solution, the material properties at the single scale

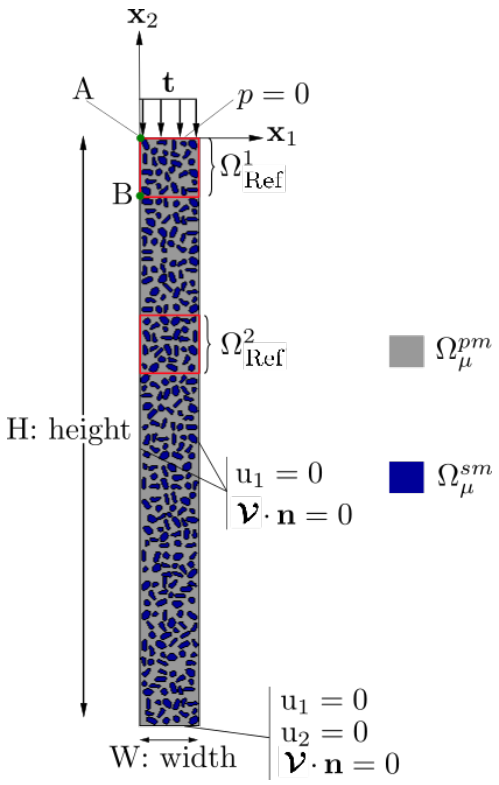

Figura D.5: 1D-consolidation example. DNS model layout (drawing not to scale).

are the same as for the micro-scale presented in Table D.1. The spatial pattern for modeling the population of basaltic rock fragments was obtained by repeating the micro-scale designs, similar to those shown in Figure D.4-(a), after elementary rotations/reflections/relocations of the inclusions, in order to improve the representativeness of the material, see Figure D.5. Following such a procedure the volume fraction of the $30\,\%$ rock portion is rigorously retained. The high level of detail required by the DNS formulation, to represent the entire heterogeneous soil column, demands a mesh of 57220 finite elements (mesh not illustrated). In order to perform a qualitative analysis of the results, filled contour maps for the vertical components of displacement, u_2, and excess pore pressures, p, are presented in Figures D.6 and D.7, respectively. These coloured maps were obtained for the DNS strategy (reference solution) and the multiscale formulations given by the three proposed MCs, see Figure D.4-(b). It can be observed from both figures that there is excellent qualitative agreement between the DNS and the proposed multiscale model for the three MCs adopted. The following is an exhaustive quantitative analysis of the primary and dual variables in their time evolution. Figure D.8 plots the time-evolution curves of the vertical displacements, u_2, of node A of the macro-scale illustrated in Figures D.4-(a) and D.5. It can be observe a good agreement between the solutions obtained from the multiscale scheme for each MC and the results given by the DNS strategy in the initial time steps. However, at the end of the consolidation process, only the multiscale formulation corresponding to the largest micro-cell (MC_3) achieves an excellent accordance. In turn, the time evolution of the pore pressures, p, at the macro-scale node B, located at $\mathrm{x}_2 = -1\,m$ depth (shown in Figures D.4-(a) and D.5), is represented in Figure D.9 for the three multiscale resolutions and the reference DNS. It can be seen that either the MC_3 or the MC_2 show satisfactory results compared to the reference, especially in the times around the critical in the immediate neighborhood of the end of load application ($t = 1$ day). Before performing tests on the homogenized variables, we present the considerations behind the adoption of the reference volumes $|\Omega_{\text{Ref}}|$. Thus, under the assumption of a plane strain state and the fixed width (of $\mathrm{W} = 1\,m$), we delineate one reference domain for each meter

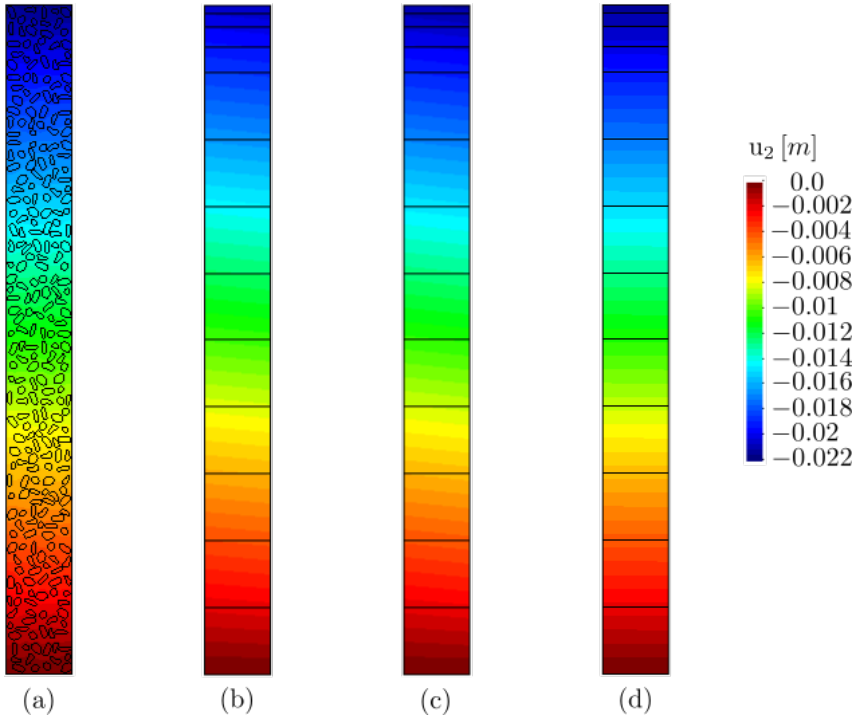

Figura D.6: 1D-consolidation example. Contour fill maps for macro-scale vertical displacements, u_2. Elapsed time $t = t_{max} =$ 2000 days. (a) DNS estrategy. (b) Multiscale formulation - MC_1 ($0.5\,m \times 0.5\,m$). (c) Multiscale formulation - MC_2 ($0.75\,m \times 0.75\,m$). (d) Multiscale formulation - MC_3 (RVE) ($1\,m \times 1\,m$).

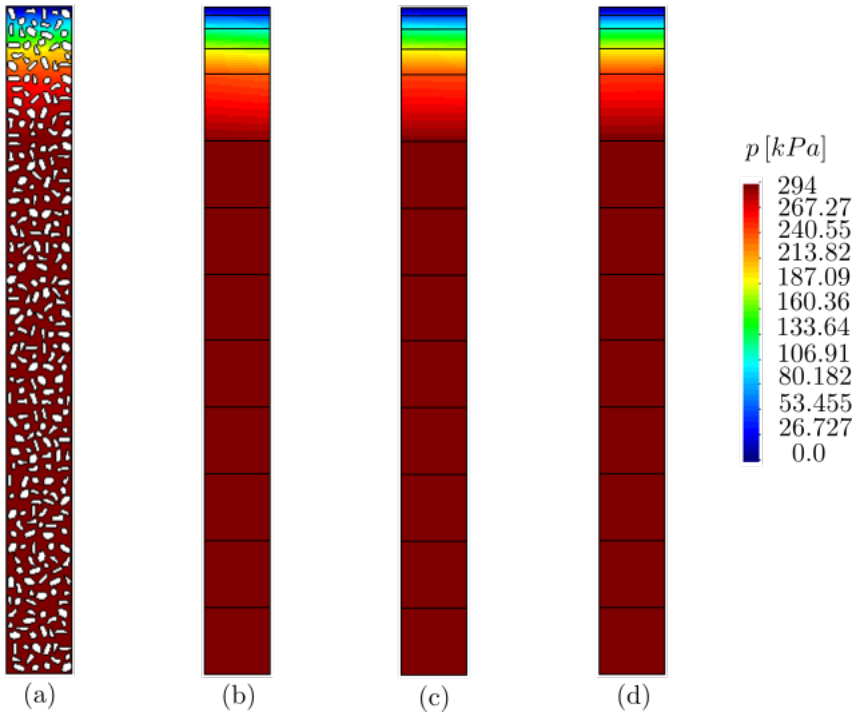

Figura D.7: 1D-consolidation example. Contour fill maps for macro-scale pore pressure, p. Elapsed time $t = 1$ day. (a) DNS estrategy. (b) Multiscale formulation - MC_1 ($0.5\,m \times 0.5\,m$). (c) Multiscale formulation - MC_2 ($0.75\,m \times 0.75\,m$). (d) Multiscale formulation - MC_3 (RVE) ($1\,m \times 1\,m$).

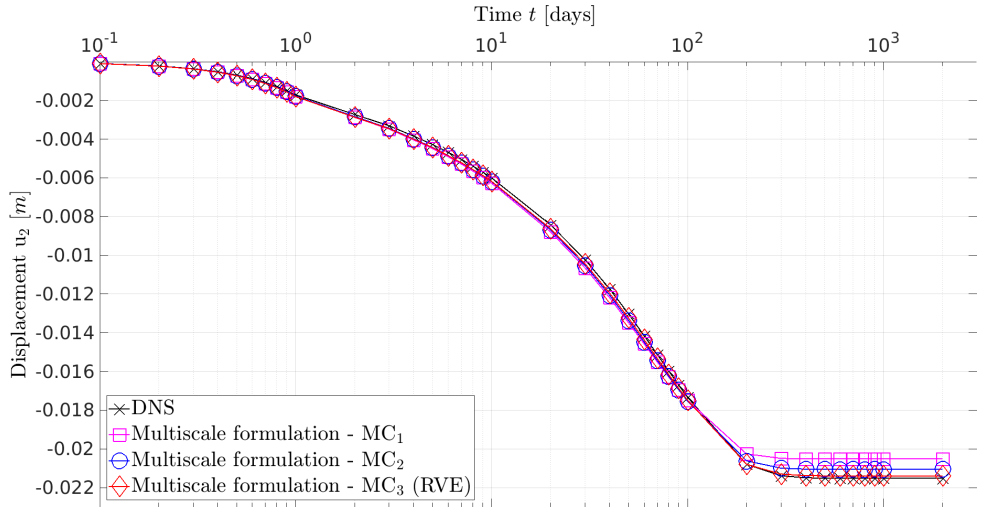

Figura D.8: 1D-consolidation example. Vertical displacement evolution for point A of Figure D.4-(a) and D.5.

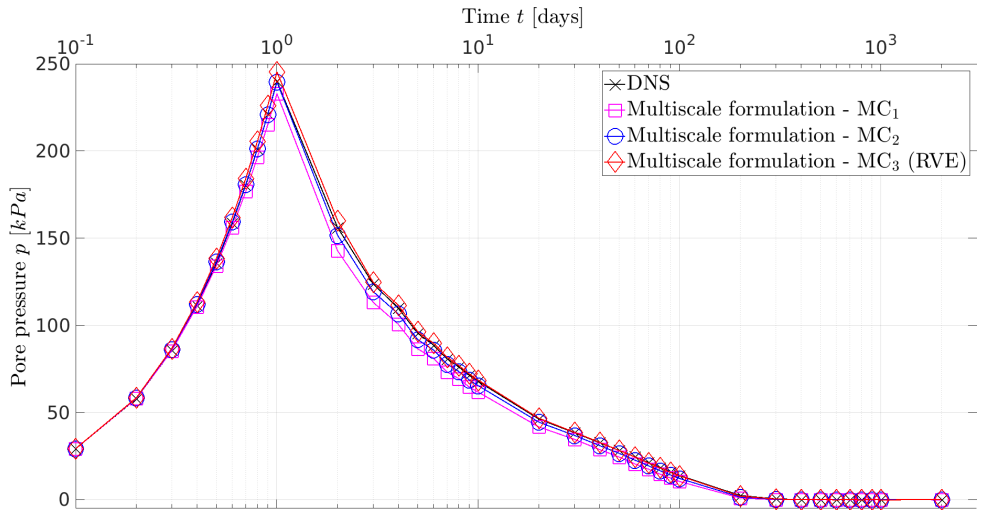

Figura D.9: 1D-consolidation example. Pore pressure evolution for point B of Figure D.4-(a) and D.5 (depth: $x_2 = -1\,m$).

of depth. This approach yields a total of ten volumes in the entire column. Among them, the results of the averaged variables of the domains bounded by the first metre depth, Ω^1_{Ref} and the other given in the range $\text{x}_2 = -3\,m$ and $\text{x}_2 = -4\,m$, Ω^2_{Ref}, are graphically illustrated. These domains are demarcated by a red box in Figures D.4-(a) and D.5.

Concerning effective stress, some clarifications should be stated beforehand. First of all, when dealing with solid media it is not required to talk about effective stress, but in the present study, we assume that conceptually the effective stress tensor in the solid subdomain is equivalent to the total stress tensor, that is $\boldsymbol{\sigma}'^{sm} = \boldsymbol{\sigma}^{sm}$, which is equally valid for the DNS strategy as for the multiscale approach. In the first instance, the average effective stress tensor can be obtained merely by performing the calculation according to the following expression

$$\boldsymbol{\sigma}' = \frac{1}{|\Omega_{\text{Ref}}|}\left(\int_{\Omega^{pm}_{\text{Ref}}} \boldsymbol{\sigma}'^{pm}\, d\Omega + \int_{\Omega^{sm}_{\text{Ref}}} \boldsymbol{\sigma}^{sm}\, d\Omega \right). \tag{D.64}$$

On the other hand, in the multiscale approach, effective stress is obtained at the macro-scale level without distinguishing between solid and porous portions, as the macro-scale is considered a like-porous medium based on initial hypotheses. Consequently, to determine the average, it is sufficient to calculate the mean in the specified domain, as follows

$$\boldsymbol{\sigma}' = \frac{1}{|\Omega_{\text{Ref}}|} \int_{\Omega_{\text{Ref}}} \boldsymbol{\sigma}'\, d\Omega. \tag{D.65}$$

However, the effective macro-stress, for the examples discussed in this paper, is defined by the homogenization of their micro-scale counterparts as follows

$$\boldsymbol{\sigma}' = \frac{1}{|\Omega_\mu|} \int_{\Omega_\mu} \boldsymbol{\sigma}'_\mu\, d\Omega_\mu = \frac{1}{|\Omega_\mu|}\left(\int_{\Omega_\mu} \boldsymbol{\sigma}'^{pm}_\mu\, d\Omega_\mu + \int_{\Omega_\mu} \boldsymbol{\sigma}'^{sm}_\mu\, d\Omega_\mu \right), \tag{D.66}$$

where $\boldsymbol{\sigma}'_\mu$ is the field of micro-scale effective stress, $\boldsymbol{\sigma}'^{sm}_\mu$ is the effective micro-stress field of the solid fraction, which, as mentioned previously, is equivalent to the total stress in the same $\boldsymbol{\sigma}'^{sm}_\mu = \boldsymbol{\sigma}^{sm}_\mu$, see (D.45) and $\boldsymbol{\sigma}'^{pm}_\mu$ are the effective stress of the porous medium in the micro-scale, according to (D.43).

The evolution in time of the effective stress was plotted in Figure D.10 for the reference domain Ω^1_{Ref}, following (D.64), (D.65) and (D.66). It can be seen that for the vertical component of the averaged effective stress, σ'_{22}, similar results between the multiscale and DNS approach are obtained, with an enhanced resemblance as the MC size increases. Finally, we proceed analogously with the temporal evolution of the seepage velocities in their vertical component, $\mathcal{V}_2$, depicted now for Ω^2_{Ref} by the volumetric average in Figure D.11. Similar conclusions are drawn as those stated above about the discussion of the primitive displacement variable, in Figure D.8. Thus, Figure D.11 shows that the MC_3 is the best fit, while for the rest of the micro-structures (MC_1 and MC_2) there are certain discrepancies of the variable in the period $t = 1$ day to $t = 20$ days. Next, we provide a quantitative measure of what has been observed and analyzed in the preceding Figures (D.8-D.11). For this purpose, we employ the $L_2 - norm$ of the difference between the answers obtained by the multiscale approach for the three proposed MCs and the DNS benchmark solution. Computation thereof, for each variable, is performed as follows

$$||e^{\text{MC}_i-\text{DNS}}_{(\bullet)}||_{L_2} = \frac{||(\bullet)^{\text{MC}_i} - (\bullet)^{\text{DNS}}||_{L_2}}{||(\bullet)^{\text{DNS}}||_{L_2}} = \frac{\sqrt{\int_0^{t_{max}} \left[(\bullet)^{\text{MC}_i} - (\bullet)^{\text{DNS}}\right]^2\, dt}}{\sqrt{\int_0^{t_{max}} \left[(\bullet)^{\text{DNS}}\right]^2\, dt}}, \tag{D.67}$$

where $(\bullet)^{\text{DNS}}$ represents the series of DNS resolution values, collected at each time in the sequence t up to the maximum time t_{max}, corresponding to any of the variables previously depicted (u_2, p, σ'_{22} or $\mathcal{V}_2$)

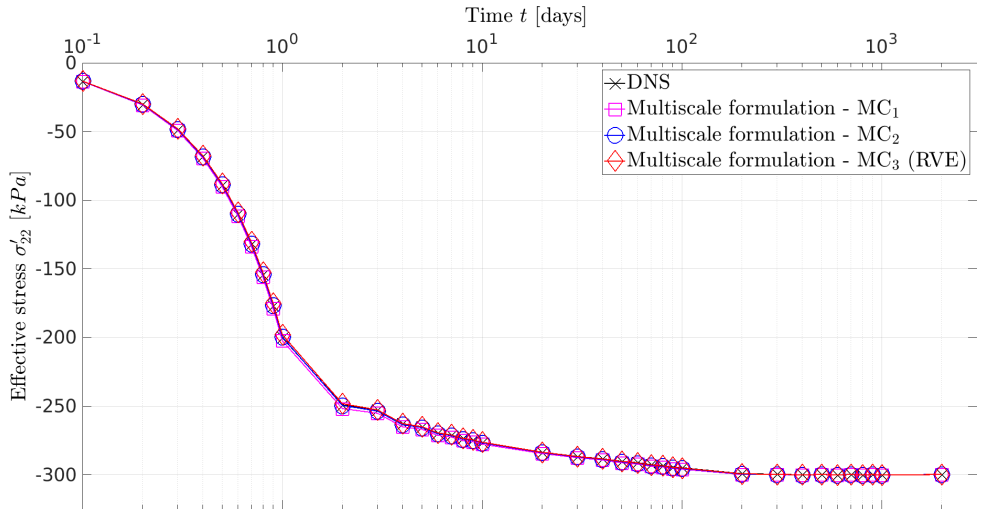

Figura D.10: 1D-consolidation example. Vertical component of the effective stress tensor for macro-scale reference domain Ω^1_{Ref}, see Figure D.4-(a) and D.5.

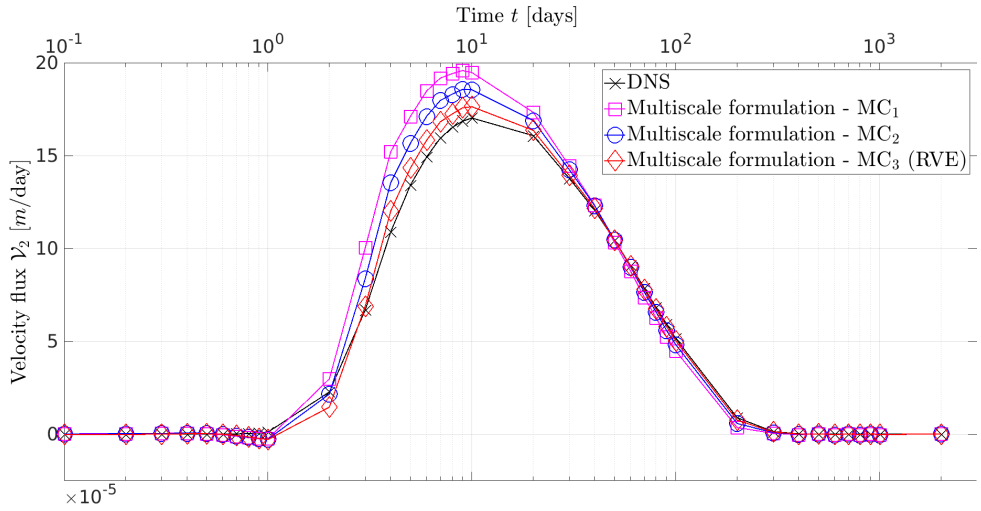

Figura D.11: 1D-consolidation example. Vertical component of flux velocity for macro-scale reference domain Ω^2_{Ref}, see Figure D.4-(a) and D.5.

whereas $(\bullet)^{\text{MC}_i}$ expresses the same for each of the multiscale responses according to the dimensions of the selected micro-cell (MC_i, with $i = 1, 2, 3$).

Thus, Figure D.12 displays the graphs for each of the four variables indicating the errors committed versus the MC-size $\left(m^2\right)$. There, it is possible to appreciate the excellent performance achieved for each multiscale resolution by contrast with the benchmark model. In addition, we should point out that the $L_2 - norm$ of the difference decreases with the increase in the size of the MC, indicating a tendency towards the representative element as larger material windows are taken, which is consistent with the conventional notion of RVE existence. For practical purposes, in this example, such an element is reached with the MC_3 that presents a remarkable agreement. The maximum error, reflected by the flux velocity variable, is about $||e_{\mathcal{V}_2}^{\text{MC}_3-\text{DNS}}||_{L_2} = 0.03$. Therefore, it is reasonable to assert that this MC_3 constitutes the Representative Volume Element. Because of this, the notation RVE has been added in parentheses next to the label MC_3 in the preceding graphs.

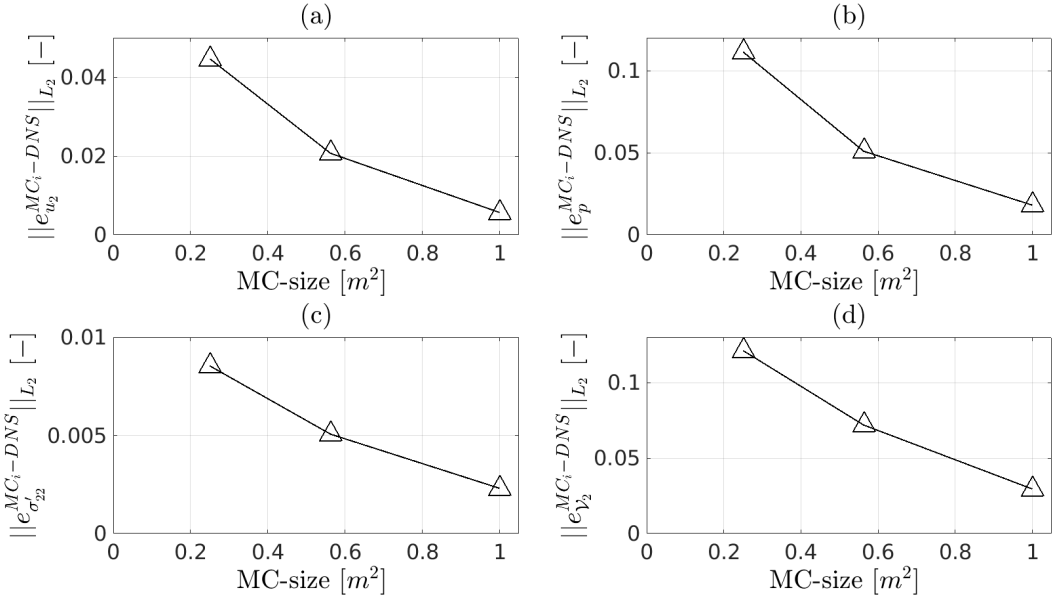

Figura D.12: 1D-consolidation example. $L_2 - norm$ of the difference between the multiscale response for each proposed MC and the DNS benchmark against the MC-size, defined for: (a) vertical displacement u_2 for point A, (b) pore pressure p for point B, (c) vertical component of the effective stress tensor σ'_{22} for macro-scale reference domain Ω^1_{Ref}, and (d) vertical component of flux velocity $\mathcal{V}_2$ for macro-scale reference domain Ω^2_{Ref}.

D.7.2. Two-dimensional consolidation examples

The main aim of this section is to evaluate the potential of the multiscale model by assessing a more complex scenario, which could occur in more real geotechnical engineering problems. In particular, the formulation applies to a two-dimensional (2D) consolidation phenomenon induced on a natural geological formation composed of highly heterogeneous soil layers due to the staged construction of a homogeneous embankment comprised of a highly impermeable material, such as a properly compacted clay, so that its entire infrastructure possesses adequate impermeability properties. The geological mesostructure to be analyzed is composed of three distinct layers to be examined. (i) The first one is assumed to be a homogeneous silt of $8\,m$ thick, (ii) the second, is a $5\,m$ layer of compacted clay of high plasticity and low permeability, with solid inclusions from basaltic fragments whose volume fraction reaches $30\,\%$, (iii) finally, the deeper stratum is formed by the same materials as the layer immediately above but the clay portion is slightly more compacted and more impermeable, while the rock component is larger and less fragmented, in a volumetric percentage of $40\,\%$.

Exploiting symmetry conditions, the macro-scale domain (single scale for the DNS strategy) is established in terms of the total height H$= 23\,m$ of the geological structure and a sufficiently large width of W$= 30\,m$ (nearly three times the size of the embankment base), Figures D.13-(a) and D.14. Dirichlet boundary conditions for the primary displacement variable set the vertical components on the lower boundary to zero, while the horizontal component is set to zero along the left and right edges. In turn, for the primitive pore pressure variable, for all time steps, the upper portion of the boundary that extends from the end of the embankment to the right vertical edge is prescribed to zero, thereby defining the only portion of the contour with drainage capacity. Regarding the Neumman conditions, the left side of the ground surface, under the embankment of E$= 11\,m$ width, is subjected to a purely compressive external traction $\mathbf{t} = [0,\, \mathrm{t}_2]^T$, that is, the dam of impermeable material is not modeled, but its effect is only imposed in a simplified form by the weight it transmits to the surface of the geological stratum on which it rests. To simulate a staged construction process, the load evolves linearly and monotonically from zero to $60\,\%$ of the total weight ($\mathrm{t}_2 = 0kPa$ to $-528kPa$) during the first 30 days of analysis, then

remains constant for the next 50 days, after which the load increases from 60 % to 100 % ($t_2 = -528kPa$ to $-880kPa$) in the subsequent 20 days and eventually remains constant, around its minimum value ($t_2 = -880kPa$), until the end of the simulation. Finally, considering the seepage process, flow is denied at the lateral and lower limits as well as the surface portion under the embankment, a condition assumed given the high imperviousness of the latter. In the present example, micro-cells are directly and arbitra-

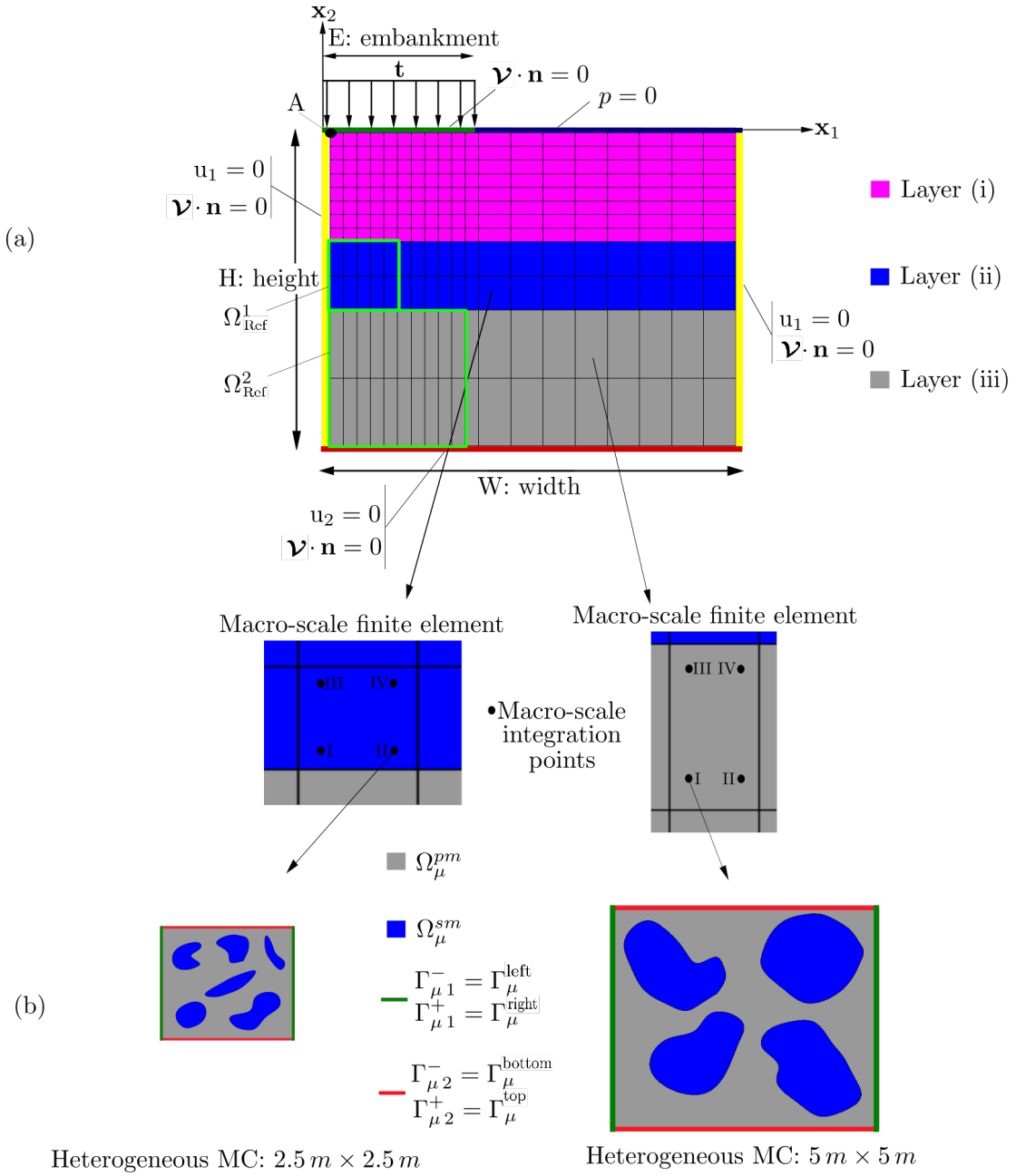

Figura D.13: Multiscale procedure applied to the 2D-consolidation phenomenon (drawing not to scale). General model layout: (a) Macro-scale; (b) Micro-scale.

rily proposed without engaging in the process of searching for the representative size, although proper identification of the RVE is crucial in multiscale modeling. Thus, for the micro-scale, Figure D.13-(b), a MC of size $2.5\,m \times 2.5\,m$ is adopted for the stratum (ii), while for the lower layer (iii) the MC has dimensions of $5\,m \times 5\,m$. These were discretized using meshes of 1227 and 4281 elements, respectively (mesh not illustrated). The two MCs are subject to periodic boundary conditions in the fluctuations of

displacements and pore pressures. On the other hand, the macro-scale domain employs a mesh of 228 finite elements, as depicted in Figure D.13-(a). It should be noted that the first layer (i) is modeled as a homogeneous material without a scale jump.

Once again, the reference solution comes from solving the geotechnical structure using the DNS technique, Figure D.14. The domain modeling was achieved by replicating similar designs of the micro-scale, depending on whether it corresponds to the second or third layer (ii or iii), followed by rotations, reflections, and relocations of inclusions in order to enforce some heterogeneity and randomness. As a result, the percentage of the 30 % and 40 % corresponding to each layer was preserved. To achieve an adequate degree of accuracy in the result and given the high level of detail required in the DNS formulation, the domain needed a mesh of 91059 finite elements. The characteristics of the materials that constitute each

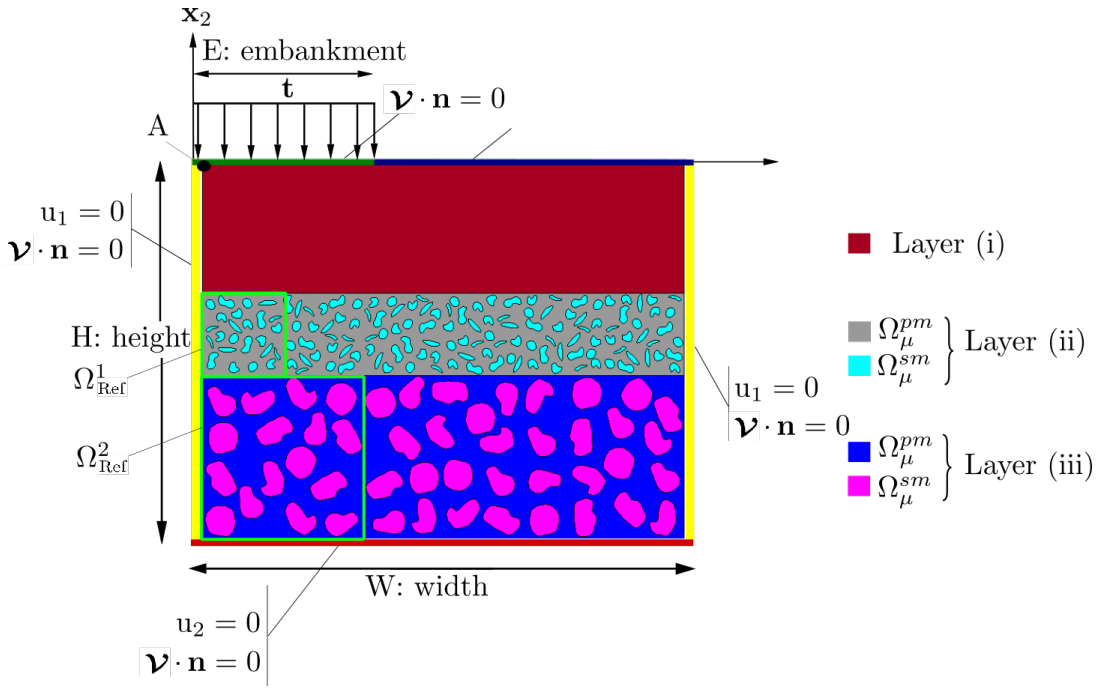

Figura D.14: 2D-consolidation example. DNS model layout (drawing not to scale).

layer are summarized in Table D.2, where the subscript $(\bullet)_{\mu}$ has been omitted for simplicity. Finally, the temporal discretization assumed in both resolutions consists of a logarithmic sequence. It contemplates the first stage of load application from the beginning of the analysis up to $t = 50$ days after implementing 60 % of the weight. Subsequently, a new logarithmic sequence begins, covering the second stage until the end of the process, as follows $t = [0.1, 0.2, 0.3, \ldots, 0.8, 0.9, 1, 2, 3, \ldots, 8, 9, 10, 20, 30, \ldots, 80, 80.1, 80.2, 80.3, \ldots, 80.9, 81, 82, \ldots, 89, 90, 100, 110, \ldots, 190, 200, 300, \ldots, 3000]$ (in days).

First of all, Figures D.15 and D.16 illustrate the contour fill maps of the displacement field, in their vertical component u_2, and the pore pressures field, p, respectively. These illustrations demonstrate a satisfactory qualitative agreement in the distribution of the variables' fields and a degree of quantitative consistency in their values. Subsequently, the evolution in time of the displacements of node A, given in Figures D.13-(a) and D.14, the coordinate at which the maximum settlement is expected, is represented in Figure D.17. The plot covers the entire analysis period. However, to enhance clarity, the curves during the first ($t = 0$ day to 80 days) and the second stage of loading ($t = 80$ day to 3000 days) are separately detailed. These illustrations demonstrate the robust performance of the multiscale formulation when tested against the DNS resolution. In handling the homogenized variables, we proceed as in the previous example, focusing on the reference domains Ω^1_{Ref} and Ω^2_{Ref}. The first one encompasses layer (ii) throughout its entire height ($5\,m$) and a width of $5\,m$ (considering the plane strain state) while the

Material properties	Layer (i)	Layer (ii)		Layer (iii)	
	Ω^{pm}	Ω^{pm}	Ω^{sm}	Ω^{pm}	Ω^{sm}
Young's modulus E^0 $[kPa]$	20000	40000	6×10^7	65000	6.5×10^7
Poisson's ratio ν	0.35	0.4	0.3	0.4	0.32
Hydraulic conductivity $\kappa_1 = \kappa_2$ $[m/\text{day}]$	8.64×10^{-6}	8.64×10^{-5}	-	4.32×10^{-5}	-
Initial void ratio e^0	1.0	1.8	-	1.65	-
Bulk modulus of the soil grain K^s $[kPa]$	12×10^6	21×10^6	-	21×10^6	-
Bulk modulus of the fluid K^f $[kPa]$	22.5×10^5	22.5×10^5	-	22.5×10^5	-
Solid density ρ^s $[kg/m^3]$	1400	1600	2700	2100	2700
Fluid density ρ^f $[kg/m^3]$	1000	1000	-	1000	-

Tabla D.2: 2D-consolidation example. Material properties of the heterogeneous composite soil stratum.

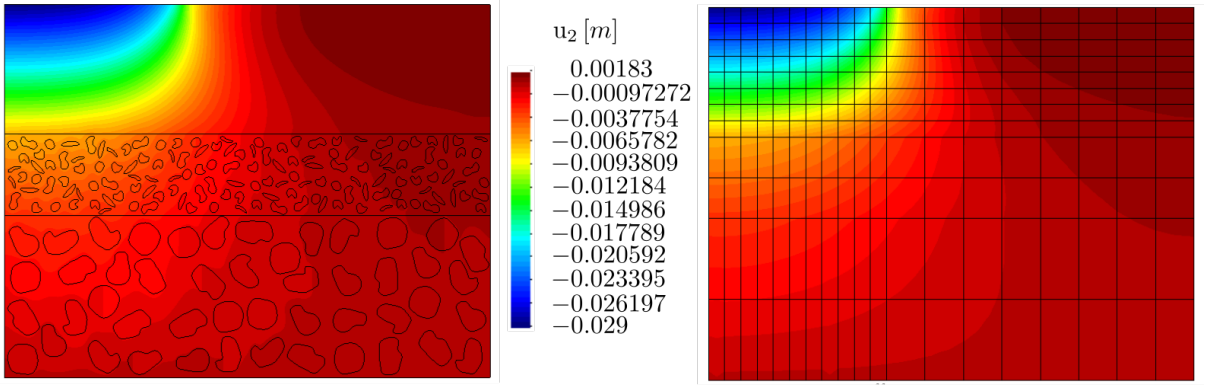

Figura D.15: 2D-consolidation example. Contour fill maps for macro-scale vertical displacements, u_2. Elapsed time $t = 3000$ days. (a) DNS estrategy. (b) Multiscale formulation. MC of $2.5\,m \times 2.5\,m$ for layer (ii) and MC of $5\,m \times 5\,m$ for layer (iii).

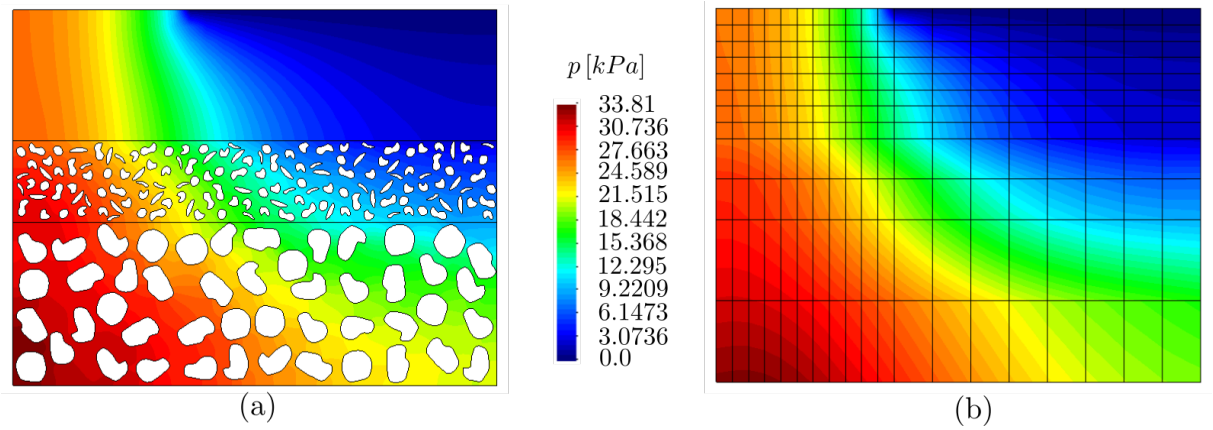

Figura D.16: 2D-consolidation example. Contour fill maps for macro-scale pore pressure, p. Elapsed time $t = 100$ day. (a) DNS estrategy. (b) Multiscale formulation. MC of $2.5\,m \times 2.5\,m$ for layer (ii) and MC of $5\,m \times 5\,m$ for layer (iii).

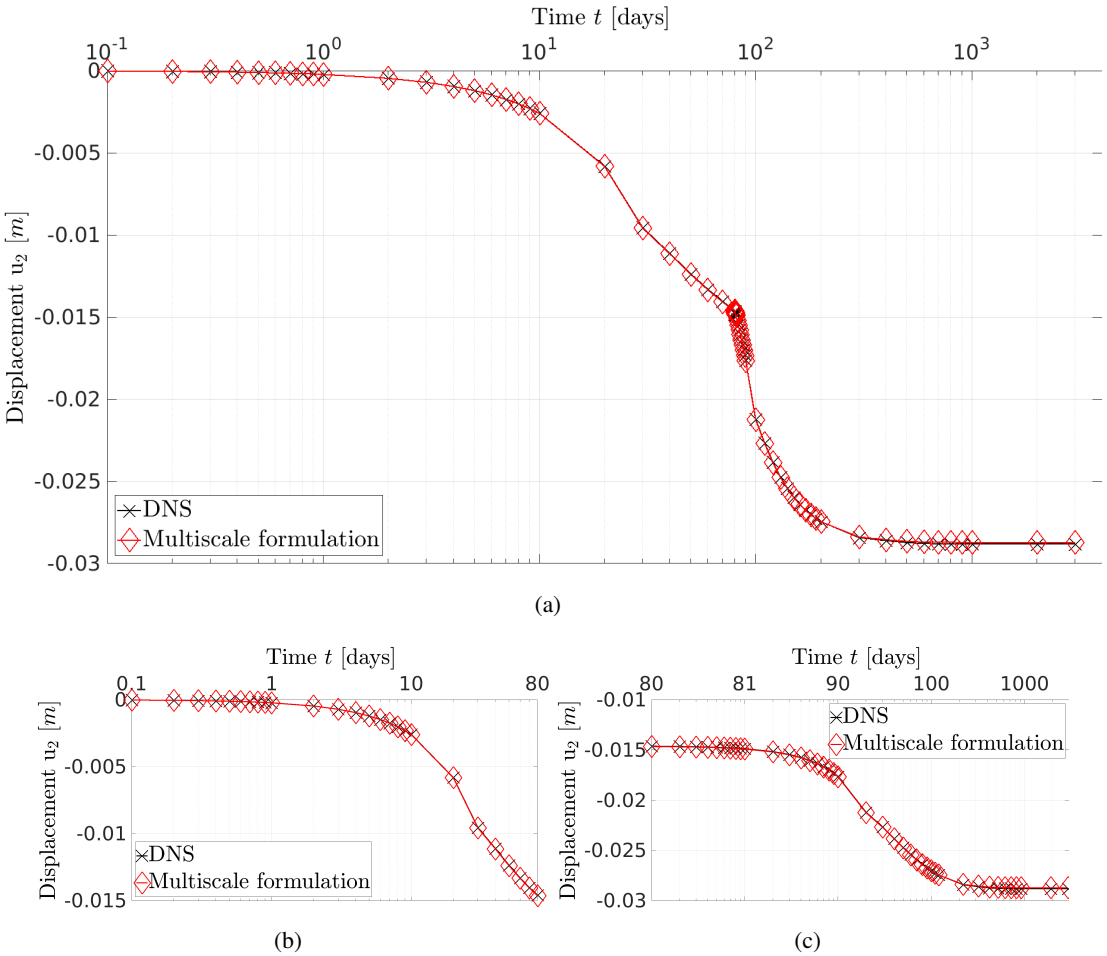

Figura D.17: 2D-consolidation example. Vertical displacement evolution for point A of Figure D.13-(a) and D.14. (a) Total test time. (b) First loading stage ($t = 0$ day to 80 days). (c) Second loading stage ($t = 80$ day to 3000 days).

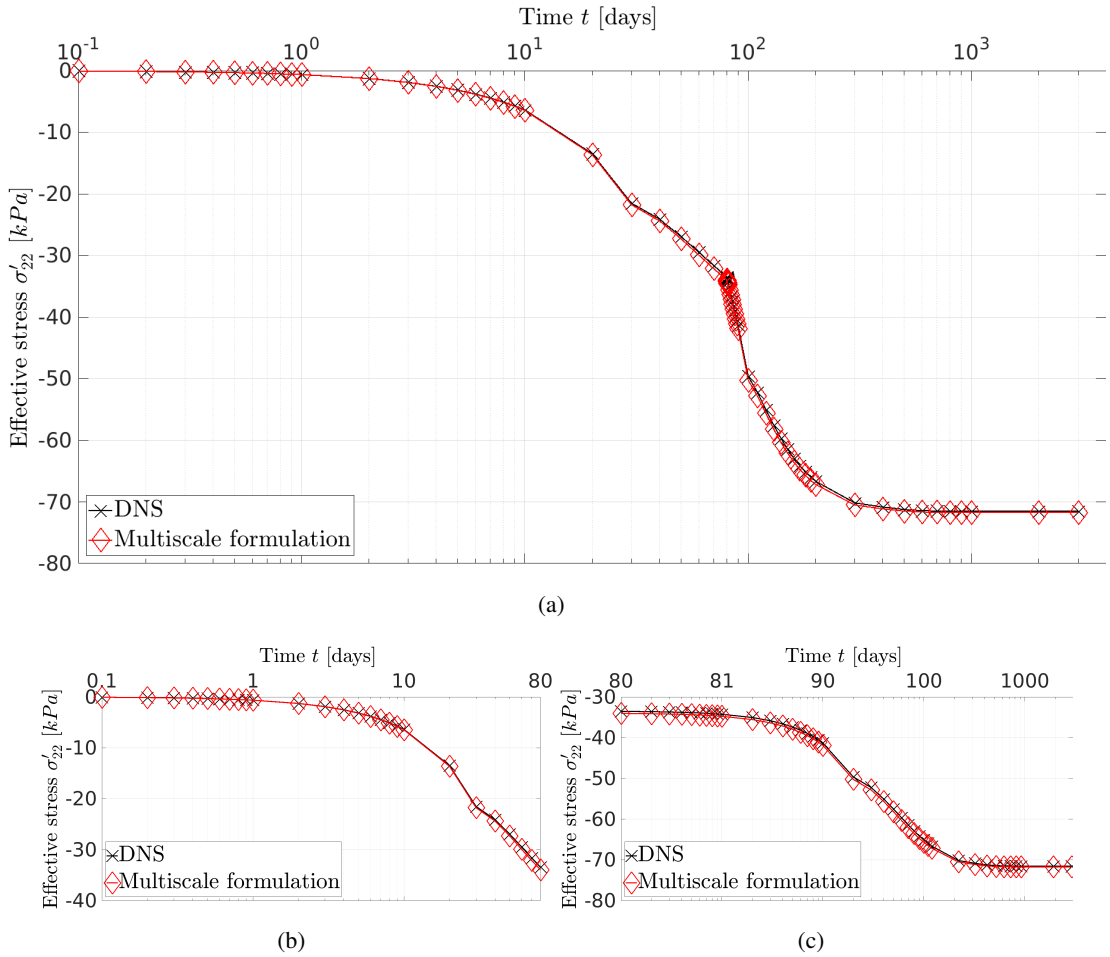

Figura D.18: 2D-consolidation example. Vertical component of the effective stress tensor for macro-scale reference domain Ω^1_{Ref}, see Figure D.13-(a) and D.14. (a) Total test time. (b) First loading stage ($t = 0$ day to 80 days). (c) Second loading stage ($t = 80$ days to 3000 days).

second one corresponds to layer (iii) also delimited over its entire height ($10\,m$) and a width of $10\,m$. Both domains are depicted in Figures D.13-(a) and D.14, enclosed within a green box.

After specifying the portions over which the secondary variables will be averaged, we begin by plotting the vertical component of the effective stress, σ'_{22}, for Ω^1_{Ref} in Figure D.18. This graph exhibits a substantial agreement between the results based on the multiscale proposal and the resolution considered as a reference. At last, for Ω^2_{Ref}, we computed the flux velocity and plotted its vertical component, $\mathcal{V}_2$, in Figure D.19. Minor discrepancies in values can be seen in certain intervals. The differences may be attributed to the coarse and not well-proportioned mesh, as depicted in Figure D.13-(a) with stretched rectangular elements. Moreover, the reduced number of Gauss points used to capture velocity flux variations along the height, with only four points involved in the thickness of the layer (iii), is worth noting. This insufficient discretization, combined with the heightened sensitivity of this variable, as observed in the one-dimensional example (Figure D.11), contributes to the slight dissimilarities between the two solutions. Although the values of the results do not match exactly for the reasons explained above, it is important to highlight that there is a significant resemblance between the behaviour provided by both approaches, DNS and multiscale. Therefore, refinement of the mesh would lead to an excellent agreement.

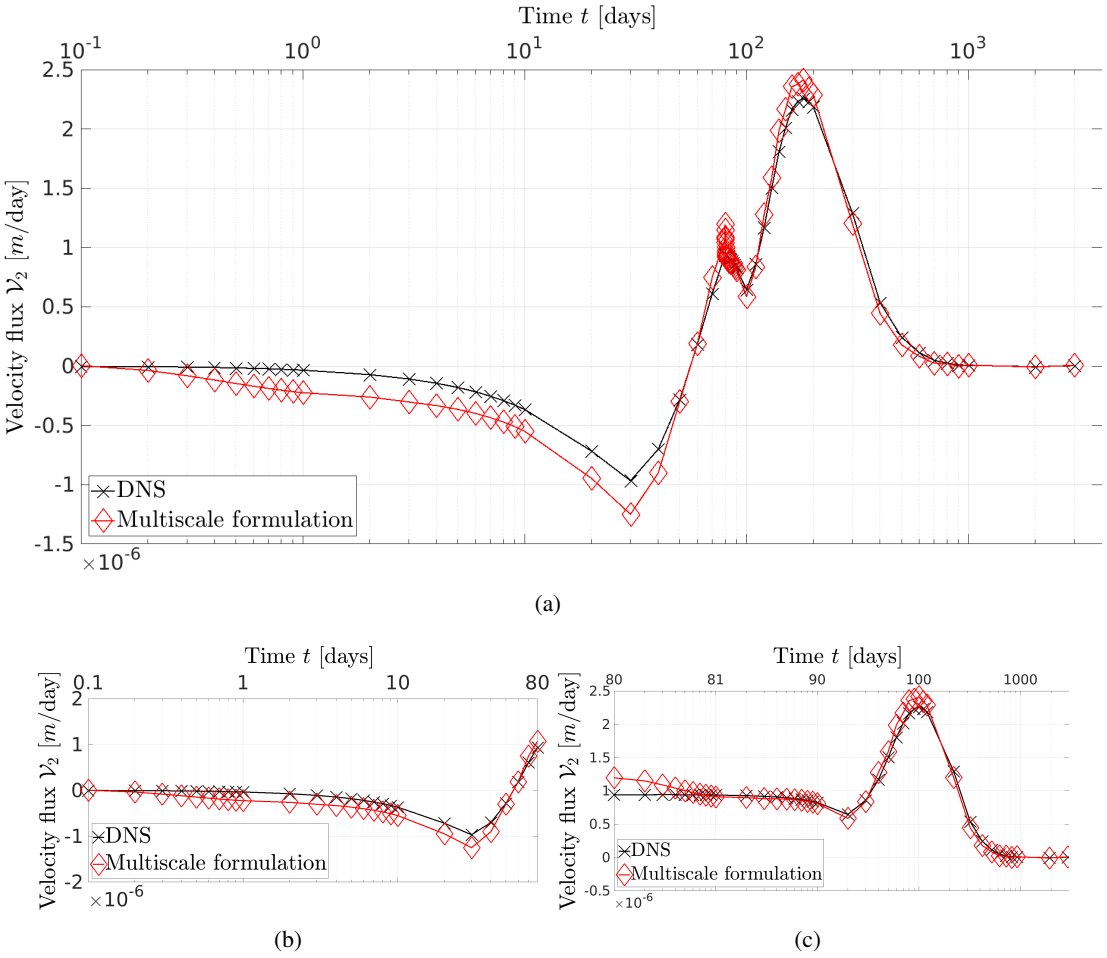

Figura D.19: 2D-consolidation example. Vertical component of flux velocity for macro-scale reference domain Ω^2_{Ref}, see Figure D.13-(a) and D.14. (a) Total test time. (b) First loading stage ($t = 0$ day to 80 days). (c) Second loading stage ($t = 80$ days to 3000 days).

D.8. Conclusions

The main objective and novel contribution of the present work was to develop a multiscale framework capable of handling heterogeneous micro-structures with constituents that demand different primitive variables for their physical description. In particular, we focused in very complex materials composed of impermeable solid inclusions embedded in a porous medium-type matrix. To achieve this goal, special attention was devoted to the treatment of the micro-scale features. Specifically, the Method of Multiscale Virtual Power was employed, and each step outlined by this theory was addressed.

Firstly, the transfer of macro-scale variables into the micro-cell, a process known as insertion, required careful management due to the dissimilar primitive fields found in the subdomains that configure the microscopic scale. Secondly, when establishing the homogenization rules for the primary variables, some peculiarities arise. A detailed analysis revealed that during the homogenization of the pore pressure variable, the volumetric constraint equation for micro-scale pore pressure fluctuations did not equate to zero. Instead, an additional term emerged to account for the distribution of inclusions in the porous media matrix, which would tend to zero as the pattern of solid particles became symmetric. In turn, to satisfy the multiscale admissibility, an additional term had to be incorporated into the homogenization rule for the pore pressure gradient. This term accounts for the influence of micro-scale pore pressures at the interface between the two media. Considering these adjustments, the minimally constrained multiscale model exhibits specific features that must be addressed for its theoretical and numerical formulation, which also affect all the derived (more constrained) sub-models.

Our specialization of the PMVP reduces to the classical Hill-Mandel principle (including body forces) when the MC is composed exclusively of impermeable solid materials. Conversely, if the microstructure consists entirely of porous medium-type, the proposed PMVP retrieves a consistent homogenized response ruled by the conventional poromechanics theory.

To address the potential drawback associated with multiscale modelling of porous media, namely the micro-scale size dependence issue, it was crucial to assume a constitutive formulation based on the Selective Order Expansion method (SOE) for the saturated porous materials in the MC. By doing so, we ensure the objectivity of the macro-scale response under all circumstances.

The proposed multiscale model, based on the RVE concept, exhibits excellent performance, fitting to the solutions obtained from the DNS strategy, as evidenced throughout the numerical results section.

The basic idea behind the present contribution could be valuable in the development of novel/alternative multiscale models for various classes of materials with heterogeneities in the set of primal descriptor fields.

It follows immediately as a future direction to explore scenarios where randomness in inclusions extends to the boundaries of the MC, a condition not addressed in this manuscript.

Appendix A. Components of the macro-scale Jacobian matrix

The following expressions expand the definitions given in (D.58), concerning the macro-scale Jacobian matrix

$$\frac{\partial \dot{\mathbf{G}}^{n+\theta}}{\partial \bar{\mathbf{u}}^{n+1}} = \int_{\Omega} \mathbf{B}_u^T \, \frac{\partial \dot{\boldsymbol{\sigma}}^{n+\theta}}{\partial \boldsymbol{\varepsilon}^{n+1}} \, \mathbf{B}_u \, d\Omega, \tag{D.68}$$

$$\frac{\partial \dot{\mathbf{G}}^{n+\theta}}{\partial \bar{\mathbf{p}}^{n+1}} = \int_{\Omega} \mathbf{B}_u^T \, \frac{\partial \dot{\boldsymbol{\sigma}}^{n+\theta}}{\partial \boldsymbol{\varphi}^{n+1}} \, \mathbf{B}_p \, d\Omega + \int_{\Omega} \mathbf{B}_u^T \, \frac{\partial \dot{\boldsymbol{\sigma}}^{n+\theta}}{\partial p^{n+1}} \, \mathbf{N}_p \, d\Omega, \tag{D.69}$$

$$\frac{\partial \mathbf{H}^{n+\theta}}{\partial \bar{\mathbf{u}}^{n+1}} = -\int_{\Omega} \mathbf{B}_p^T \, \frac{\partial \boldsymbol{\mathcal{V}}^{n+\theta}}{\partial \boldsymbol{\varepsilon}^{n+1}} \, \mathbf{B}_u \, d\Omega + \int_{\Omega} \mathbf{N}_p^T \, \frac{\partial \dot{\chi}^{n+\theta}}{\partial \boldsymbol{\varepsilon}^{n+1}} \, \mathbf{B}_u \, d\Omega, \tag{D.70}$$

$$\frac{\partial \mathbf{H}^{n+\theta}}{\partial \bar{\mathbf{p}}^{n+1}} = -\int_{\Omega} \mathbf{B}_p^T \, \frac{\partial \boldsymbol{\mathcal{V}}^{n+\theta}}{\partial \boldsymbol{\varphi}^{n+1}} \, \mathbf{B}_p \, d\Omega - \int_{\Omega} \mathbf{B}_p^T \, \frac{\partial \boldsymbol{\mathcal{V}}^{n+\theta}}{\partial p^{n+1}} \, \mathbf{N}_p \, d\Omega + \int_{\Omega} \mathbf{N}_p^T \, \frac{\partial \dot{\chi}^{n+\theta}}{\partial \boldsymbol{\varphi}^{n+1}} \, \mathbf{B}_p \, d\Omega + \int_{\Omega} \mathbf{N}_p^T \, \frac{\partial \dot{\chi}^{n+\theta}}{\partial p^{n+1}} \, \mathbf{N}_p \, d\Omega. \quad \text{(D.71)}$$

The derivatives remaining in (D.68)-(D.71) constitute the so-called homogenized tangent operators of the multiscale model. To obtain such terms, we consider: (i) the homogenization rules of macro-scale dual variables (D.34, D.35 and D.37), (ii) the unified format of micro-scale constitutive laws (D.46-D.49), and (iii) the time integration procedure employing the θ-generalized rule. We include some useful details about this topic below to complete the presentation.

(I) derivatives of the homogenized stress rate tensor $\dot{\boldsymbol{\sigma}}^{n+\theta}$ with respect to the primal macro-scale variables:

$$\begin{aligned}
\frac{\partial \dot{\boldsymbol{\sigma}}^{n+\theta}}{\partial \boldsymbol{\varepsilon}^{n+1}} &= \frac{\partial}{\partial \boldsymbol{\varepsilon}^{n+1}} \left\{ \frac{1}{|\Omega_\mu|} \int_{\Omega_\mu} \left[\hat{\dot{\sigma}}_\mu^{n+\theta} - \dot{\mathbf{f}}_\mu^{n+\theta} \otimes (\mathbf{y} - \mathbf{y}_G) \right] d\Omega_\mu \right\} \\
&= \frac{\partial}{\partial \boldsymbol{\varepsilon}^{n+1}} \left\{ \frac{1}{|\Omega_\mu|} \left[\int_{\Omega_\mu^{sm}} \left[\hat{\dot{\sigma}}_\mu^{sm,\, n+\theta}\big(\dot{\boldsymbol{\varepsilon}}^{n+\theta}, \dot{\tilde{\boldsymbol{\varepsilon}}}_\mu^{n+\theta}\big) - \dot{\mathbf{f}}_\mu^{n+\theta} \otimes (\mathbf{y} - \mathbf{y}_G) \right] d\Omega_\mu \right.\right. \\
&\quad + \int_{\Omega_\mu^{pm}} \left[\hat{\dot{\sigma}}_\mu^{pm,\, n+\theta}\big(\dot{\boldsymbol{\varepsilon}}^{n+\theta}, \dot{\tilde{\boldsymbol{\varepsilon}}}_\mu^{n+\theta}, \dot{p}^{n+\theta}, \alpha\, \dot{\boldsymbol{\varphi}}^{n+\theta}, \beta\, \dot{\tilde{p}}_\mu^{n+\theta}\big) \right. \\
&\quad \left.\left. \left. - \dot{\mathbf{f}}_\mu^{n+\theta} \otimes (\mathbf{y} - \mathbf{y}_G) \right] d\Omega_\mu \right] \right\} \\
&= \frac{1}{|\Omega_\mu|} \left\{ \int_{\Omega_\mu^{sm}} \left[\frac{1}{\Delta t}\, \mathbf{C}_\mu^{sm} \,:\, \left(\mathbb{I} + \frac{\partial \tilde{\boldsymbol{\varepsilon}}_\mu^{n+1}}{\partial \boldsymbol{\varepsilon}^{n+1}} \right) \right] d\Omega_\mu \right. \\
&\quad \left. + \int_{\Omega_\mu^{pm}} \left[\frac{1}{\Delta t}\, \mathbf{C}_\mu^{pm} \,:\, \left(\mathbb{I} + \frac{\partial \tilde{\boldsymbol{\varepsilon}}_\mu^{n+1}}{\partial \boldsymbol{\varepsilon}^{n+1}} \right) - \frac{\beta}{\Delta t}\, \mathbf{b}_\mu \otimes \frac{\partial \tilde{p}_\mu^{n+1}}{\partial \boldsymbol{\varepsilon}^{n+1}} \right] d\Omega_\mu \right\}, \quad \text{(D.72)}
\end{aligned}$$

$$\begin{aligned}
\frac{\partial \dot{\boldsymbol{\sigma}}^{n+\theta}}{\partial \boldsymbol{\varphi}^{n+1}} &= \frac{\partial}{\partial \boldsymbol{\varphi}^{n+1}} \left\{ \frac{1}{|\Omega_\mu|} \int_{\Omega_\mu} \left[\hat{\dot{\sigma}}_\mu^{n+\theta} - \dot{\mathbf{f}}_\mu^{n+\theta} \otimes (\mathbf{y} - \mathbf{y}_G) \right] d\Omega_\mu \right\} \\
&= \frac{\partial}{\partial \boldsymbol{\varphi}^{n+1}} \left\{ \frac{1}{|\Omega_\mu|} \left[\int_{\Omega_\mu^{sm}} \left[\hat{\dot{\sigma}}_\mu^{sm,\, n+\theta}\big(\dot{\boldsymbol{\varepsilon}}^{n+\theta}, \dot{\tilde{\boldsymbol{\varepsilon}}}_\mu^{n+\theta}\big) - \dot{\mathbf{f}}_\mu^{n+\theta} \otimes (\mathbf{y} - \mathbf{y}_G) \right] d\Omega_\mu \right.\right. \\
&\quad + \int_{\Omega_\mu^{pm}} \left[\hat{\dot{\sigma}}_\mu^{pm,\, n+\theta}\big(\dot{\boldsymbol{\varepsilon}}^{n+\theta}, \dot{\tilde{\boldsymbol{\varepsilon}}}_\mu^{n+\theta}, \dot{p}^{n+\theta}, \alpha\, \dot{\boldsymbol{\varphi}}^{n+\theta}, \beta\, \dot{\tilde{p}}_\mu^{n+\theta}\big) \right. \\
&\quad \left.\left. \left. - \dot{\mathbf{f}}_\mu^{n+\theta} \otimes (\mathbf{y} - \mathbf{y}_G) \right] d\Omega_\mu \right] \right\} = \frac{1}{|\Omega_\mu|} \left\{ \int_{\Omega_\mu^{sm}} \frac{1}{\Delta t}\, \mathbf{C}_\mu^{sm} \,:\, \frac{\partial \tilde{\boldsymbol{\varepsilon}}_\mu^{n+1}}{\partial \boldsymbol{\varphi}^{n+1}}\, d\Omega_\mu \right. \\
&\quad \left. + \int_{\Omega_\mu^{pm}} \left[\frac{1}{\Delta t}\, \mathbf{C}_\mu^{pm} \,:\, \frac{\partial \tilde{\boldsymbol{\varepsilon}}_\mu^{n+1}}{\partial \boldsymbol{\varphi}^{n+1}} - \frac{1}{\Delta t}\, \mathbf{b}_\mu \otimes \left(\alpha\, (\mathbf{y} - \mathbf{y}_G) + \beta\, \frac{\partial \tilde{p}_\mu^{n+1}}{\partial \boldsymbol{\varphi}^{n+1}} \right) \right] d\Omega_\mu \right\}, \quad \text{(D.73)}
\end{aligned}$$

$$\frac{\partial \dot{\boldsymbol{\sigma}}^{n+\theta}}{\partial p^{n+1}} = \frac{\partial}{\partial p^{n+1}}\left\{ \frac{1}{|\Omega_\mu|}\int_{\Omega_\mu} \left[\hat{\dot{\sigma}}_\mu^{n+\theta} - \dot{\mathbf{f}}_\mu^{n+\theta} \otimes (\mathbf{y}-\mathbf{y}_G)\right] d\Omega_\mu \right\}$$

$$= \frac{\partial}{\partial p^{n+1}}\left\{ \frac{1}{|\Omega_\mu|}\left[\int_{\Omega_\mu^{sm}} \left[\hat{\dot{\sigma}}_\mu^{sm,\,n+\theta}\big(\dot{\boldsymbol{\varepsilon}}^{n+\theta}, \dot{\tilde{\boldsymbol{\varepsilon}}}_\mu^{n+\theta}\big) - \dot{\mathbf{f}}_\mu^{n+\theta} \otimes (\mathbf{y}-\mathbf{y}_G)\right] d\Omega_\mu \right.\right.$$

$$+ \int_{\Omega_\mu^{pm}} \left[\hat{\dot{\sigma}}_\mu^{pm,\,n+\theta}\big(\dot{\boldsymbol{\varepsilon}}^{n+\theta}, \dot{\tilde{\boldsymbol{\varepsilon}}}_\mu^{n+\theta}, \dot{p}^{n+\theta}, \alpha\,\dot{\boldsymbol{\varphi}}^{n+\theta}, \beta\,\dot{\tilde{p}}_\mu^{n+\theta}\big)\right.$$

$$\left.\left. -\dot{\mathbf{f}}_\mu^{n+\theta} \otimes (\mathbf{y}-\mathbf{y}_G)\right] d\Omega_\mu \right] \right\} = \frac{1}{|\Omega_\mu|}\left\{ \int_{\Omega_\mu^{sm}} \frac{1}{\Delta t}\,\mathbf{C}_\mu^{sm} \,:\, \frac{\partial \tilde{\boldsymbol{\varepsilon}}_\mu^{n+1}}{\partial p^{n+1}}\, d\Omega_\mu \right.$$

$$\left. + \int_{\Omega_\mu^{pm}} \left[\frac{1}{\Delta t}\,\mathbf{C}_\mu^{pm} \,:\, \frac{\partial \tilde{\boldsymbol{\varepsilon}}_\mu^{n+1}}{\partial p^{n+1}} - \frac{1}{\Delta t}\,\mathbf{b}_\mu \left(1 + \beta\,\frac{\partial \tilde{p}_\mu^{n+1}}{\partial p^{n+1}}\right)\right] d\Omega_\mu \right\}, \quad \text{(D.74)}$$

(II) derivatives of the homogenized mass content rate of fluid $\dot{\chi}^{n+\theta}$ with respect to the primal macro-scale variables:

$$\frac{\partial \dot{\chi}^{n+\theta}}{\partial \boldsymbol{\varepsilon}^{n+1}} = \frac{\partial}{\partial \boldsymbol{\varepsilon}^{n+1}}\left\{ \frac{1}{|\Omega_\mu|}\int_{\Omega_\mu^{pm}} \left[\hat{\dot{\chi}}_\mu^{n+\theta}\Big(\dot{\boldsymbol{\varepsilon}}^{n+\theta}, \dot{\tilde{\boldsymbol{\varepsilon}}}_\mu^{n+\theta}, \right.\right.$$

$$\left.\left. \dot{p}^{n+\theta}, \alpha\,\dot{\boldsymbol{\varphi}}^{n+\theta}, \beta\,\dot{\tilde{p}}_\mu^{n+\theta}\Big)\right] d\Omega_\mu \right\}$$

$$= \frac{1}{|\Omega_\mu|}\int_{\Omega_\mu^{pm}} \left[\frac{1}{\Delta t}\,\mathbf{b}_\mu \,:\, \left(\mathbb{I} + \frac{\partial \tilde{\boldsymbol{\varepsilon}}_\mu^{n+1}}{\partial \boldsymbol{\varepsilon}^{n+1}}\right) + \frac{\beta}{\Delta t}\,\frac{1}{M_\mu}\,\frac{\partial \tilde{p}_\mu^{n+1}}{\partial \boldsymbol{\varepsilon}^{n+1}}\right] d\Omega_\mu, \quad \text{(D.75)}$$

$$\frac{\partial \dot{\chi}^{n+\theta}}{\partial \boldsymbol{\varphi}^{n+1}} = \frac{\partial}{\partial \boldsymbol{\varphi}^{n+1}}\left\{ \frac{1}{|\Omega_\mu|}\int_{\Omega_\mu^{pm}} \left[\hat{\dot{\chi}}_\mu^{n+\theta}\big(\dot{\boldsymbol{\varepsilon}}^{n+\theta}, \dot{\tilde{\boldsymbol{\varepsilon}}}_\mu^{n+\theta}, \right.\right.$$

$$\left.\left. \dot{p}^{n+\theta}, \alpha\,\dot{\boldsymbol{\varphi}}^{n+\theta}, \beta\,\dot{\tilde{p}}_\mu^{n+\theta}\Big)\right] d\Omega_\mu \right\}$$

$$= \frac{1}{|\Omega_\mu|}\int_{\Omega_\mu^{pm}} \left[\frac{1}{\Delta t}\,\mathbf{b}_\mu \,:\, \frac{\partial \tilde{\boldsymbol{\varepsilon}}_\mu^{n+1}}{\partial \boldsymbol{\varphi}^{n+1}} + \frac{1}{\Delta t}\,\frac{1}{M_\mu}\left(\alpha\,(\mathbf{y}-\mathbf{y}_G) + \beta\,\frac{\partial \tilde{p}_\mu^{n+1}}{\partial \boldsymbol{\varphi}^{n+1}}\right)\right] d\Omega_\mu, \quad \text{(D.76)}$$

$$\frac{\partial \dot{\chi}^{n+\theta}}{\partial p^{n+1}} = \frac{\partial}{\partial p^{n+1}}\left\{ \frac{1}{|\Omega_\mu|}\int_{\Omega_\mu^{pm}} \left[\hat{\dot{\chi}}_\mu^{n+\theta}\big(\dot{\boldsymbol{\varepsilon}}^{n+\theta}, \dot{\tilde{\boldsymbol{\varepsilon}}}_\mu^{n+\theta}, \right.\right.$$

$$\left.\left. \dot{p}^{n+\theta}, \alpha\,\dot{\boldsymbol{\varphi}}^{n+\theta}, \beta\,\dot{\tilde{p}}_\mu^{n+\theta}\Big)\right] d\Omega_\mu \right\}$$

$$= \frac{1}{|\Omega_\mu|}\int_{\Omega_\mu^{pm}} \left[\frac{1}{\Delta t}\,\mathbf{b}_\mu \,:\, \frac{\partial \tilde{\boldsymbol{\varepsilon}}_\mu^{n+1}}{\partial p^{n+1}} + \frac{1}{\Delta t}\,\frac{1}{M_\mu}\left(1 + \beta\,\frac{\partial \tilde{p}_\mu^{n+1}}{\partial p^{n+1}}\right)\right] d\Omega_\mu, \quad \text{(D.77)}$$

(III) derivatives of the homogenized flux velocity vector $\boldsymbol{\mathcal{V}}^{n+\theta}$ with respect to the primal macro-scale

variables:

$$\frac{\partial \boldsymbol{\mathcal{V}}^{n+\theta}}{\partial \boldsymbol{\varepsilon}^{n+1}} = \frac{\partial}{\partial \boldsymbol{\varepsilon}^{n+1}} \Bigg\{ \frac{1}{|\Omega_\mu|} \int_{\Omega_\mu^{pm}} \Bigg[\hat{\mathcal{V}}_\mu^{n+\theta}\big(\boldsymbol{\varphi}^{n+\theta}, \tilde{\boldsymbol{\varphi}}_\mu^{n+\theta}\big) - \hat{\chi}_\mu^{n+\theta}\big(\dot{\boldsymbol{\varepsilon}}^{n+\theta}, \dot{\tilde{\boldsymbol{\varepsilon}}}_\mu^{n+\theta}, \dot{p}^{n+\theta}, \alpha\, \dot{\boldsymbol{\varphi}}^{n+\theta}, \beta\, \dot{\tilde{p}}_\mu^{n+\theta}\big)\, (\mathbf{y} - \mathbf{y}_G) \Bigg] d\Omega_\mu \Bigg\}$$
$$= \frac{1}{|\Omega_\mu|} \int_{\Omega_\mu^{pm}} \Bigg[-\theta\, \mathbf{k}_\mu \frac{\partial \tilde{\boldsymbol{\varphi}}_\mu^{n+1}}{\partial \boldsymbol{\varepsilon}^{n+1}} - \frac{1}{\Delta t}\, (\mathbf{y} - \mathbf{y}_G) \otimes \mathbf{b}_\mu \,:\, \left(\mathbb{I} + \frac{\partial \tilde{\boldsymbol{\varepsilon}}_\mu^{n+1}}{\partial \boldsymbol{\varepsilon}^{n+1}} \right) - \frac{\beta}{\Delta t}\, (\mathbf{y} - \mathbf{y}_G) \otimes \frac{1}{M_\mu} \frac{\partial \tilde{p}_\mu^{n+1}}{\partial \boldsymbol{\varepsilon}^{n+1}} \Bigg] d\Omega_\mu, \quad \text{(D.78)}$$

$$\frac{\partial \boldsymbol{\mathcal{V}}^{n+\theta}}{\partial \boldsymbol{\varphi}^{n+1}} = \frac{\partial}{\partial \boldsymbol{\varphi}^{n+1}} \Bigg\{ \frac{1}{|\Omega_\mu|} \int_{\Omega_\mu^{pm}} \Bigg[\hat{\mathcal{V}}_\mu^{n+\theta}\big(\boldsymbol{\varphi}^{n+\theta}, \tilde{\boldsymbol{\varphi}}_\mu^{n+\theta}\big) - \hat{\chi}_\mu^{n+\theta}\big(\dot{\boldsymbol{\varepsilon}}^{n+\theta}, \dot{\tilde{\boldsymbol{\varepsilon}}}_\mu^{n+\theta}, \dot{p}^{n+\theta}, \alpha\, \dot{\boldsymbol{\varphi}}^{n+\theta}, \beta\, \dot{\tilde{p}}_\mu^{n+\theta}\big)\, (\mathbf{y} - \mathbf{y}_G) \Bigg] d\Omega_\mu \Bigg\}$$
$$= \frac{1}{|\Omega_\mu|} \int_{\Omega_\mu^{pm}} \Bigg[-\theta\, \mathbf{k}_\mu \left(\mathbf{I} + \frac{\partial \tilde{\boldsymbol{\varphi}}_\mu^{n+1}}{\partial \boldsymbol{\varphi}^{n+1}} \right) - \frac{1}{\Delta t}\, (\mathbf{y} - \mathbf{y}_G) \otimes \left(\mathbf{b}_\mu \,:\, \frac{\partial \tilde{\boldsymbol{\varepsilon}}_\mu^{n+1}}{\partial \boldsymbol{\varphi}^{n+1}} \right) - \frac{1}{\Delta t}\, (\mathbf{y} - \mathbf{y}_G) \otimes \frac{1}{M_\mu} \left(\alpha\, (\mathbf{y} - \mathbf{y}_G) + \beta \frac{\partial \tilde{p}_\mu^{n+1}}{\partial\, \boldsymbol{\varphi}^{n+1}} \right) \Bigg] d\Omega_\mu, \quad \text{(D.79)}$$

$$\frac{\partial \boldsymbol{\mathcal{V}}^{n+\theta}}{\partial p^{n+1}} = \frac{\partial}{\partial p^{n+1}} \Bigg\{ \frac{1}{|\Omega_\mu|} \int_{\Omega_\mu^{pm}} \Bigg[\hat{\mathcal{V}}_\mu^{n+\theta}\big(\boldsymbol{\varphi}^{n+\theta}, \tilde{\boldsymbol{\varphi}}_\mu^{n+\theta}\big) - \hat{\chi}_\mu^{n+\theta}\big(\dot{\boldsymbol{\varepsilon}}^{n+\theta}, \dot{\tilde{\boldsymbol{\varepsilon}}}_\mu^{n+\theta}, \dot{p}^{n+\theta}, \alpha\, \dot{\boldsymbol{\varphi}}^{n+\theta}, \beta\, \dot{\tilde{p}}_\mu^{n+\theta}\big)\, (\mathbf{y} - \mathbf{y}_G) \Bigg] d\Omega_\mu \Bigg\}$$
$$= \frac{1}{|\Omega_\mu|} \int_{\Omega_\mu^{pm}} \Bigg[-\theta\, \mathbf{k}_\mu \frac{\partial \tilde{\boldsymbol{\varphi}}_\mu^{n+1}}{\partial p^{n+1}} - \frac{1}{\Delta t} \left(\mathbf{b}_\mu \,:\, \frac{\partial \tilde{\boldsymbol{\varepsilon}}_\mu^{n+1}}{\partial p^{n+1}} \right) (\mathbf{y} - \mathbf{y}_G) - \frac{1}{\Delta t} \frac{1}{M_\mu} \left(1 + \beta \frac{\partial \tilde{p}_\mu^{n+1}}{\partial p^{n+1}} \right) (\mathbf{y} - \mathbf{y}_G) \Bigg] d\Omega_\mu, \quad \text{(D.80)}$$

where $\mathbb{I}$ and $\mathbf{I}$ denote the fourth and second-order identity tensors, respectively.

The terms involving the derivatives of the micro-scale fluctuation fields with respect to the macro-scale variables are still required in (D.72)-(D.80) to finish the definition the homogenized tangent operators. This is a common issue in RVE-based multiscale modelling. For more details, interested readers can refer to previous contributions, for example, by de Souza Neto and Feijóo R [12] and/or Perić et al. [62].

Appendix B. Micro-scale Jacobian sub-matrices

In what follows, the components given in (D.62), concerning the Jacobian at the micro-scale level, are further defined:

(I) Micro-scale stiffness matrix $\mathbf{K}_\mu$

$$\frac{\partial \dot{\mathbf{G}}_\mu^{n+\theta}}{\partial \tilde{\tilde{\mathbf{u}}}_\mu^{n+1}} = \int_{\Omega_\mu} \mathbf{B}_{\tilde{u}_\mu}^T \, \frac{\partial \dot{\boldsymbol{\sigma}}_\mu^{n+\theta}}{\partial \tilde{\boldsymbol{\varepsilon}}_\mu^{n+1}} \, \mathbf{B}_{\tilde{u}_\mu} \, d\Omega_\mu = \frac{1}{\Delta t} \int_{\Omega_\mu} \mathbf{B}_{\tilde{u}_\mu}^T \, \mathbf{C}_\mu \, \mathbf{B}_{\tilde{u}_\mu} \, d\Omega_\mu = \frac{1}{\Delta t} \, \mathbf{K}_\mu. \tag{D.81}$$

(II) Micro-scale coupling matrix between the solid and fluid phases $\mathbf{Q}_\mu$

$$\frac{\partial \dot{\mathbf{G}}_\mu^{n+\theta}}{\partial \tilde{\tilde{\mathbf{p}}}_\mu^{n+1}} = \int_{\Omega_\mu^{pm}} \mathbf{B}_{\tilde{u}_\mu}^T \, \frac{\partial \dot{\boldsymbol{\sigma}}_\mu^{n+\theta}}{\partial \tilde{p}_\mu^{n+1}} \, \mathbf{N}_{\tilde{p}_\mu} \, d\Omega_\mu = \frac{\beta}{\Delta t} \int_{\Omega_\mu^{pm}} \mathbf{B}_{\tilde{u}_\mu}^T \, \mathbf{b}_\mu \, \mathbf{N}_{\tilde{p}_\mu} \, d\Omega_\mu = -\frac{\beta}{\Delta t} \, \mathbf{Q}_\mu. \tag{D.82}$$

(III) Micro-scale transpose coupling matrix between the solid and fluid phases $(\mathbf{Q}_\mu)^T$

$$\frac{\partial \mathbf{H}_\mu^{n+\theta}}{\partial \tilde{\tilde{\mathbf{u}}}_\mu^{n+1}} = \int_{\Omega_\mu^{pm}} \mathbf{N}_{\tilde{p}_\mu}^T \, \frac{\partial \dot{\chi}_\mu^{n+\theta}}{\partial \tilde{\boldsymbol{\varepsilon}}_\mu^{n+1}} \, \mathbf{B}_{\tilde{u}_\mu} \, d\Omega_\mu = \frac{1}{\Delta t} \int_{\Omega_\mu^{pm}} \mathbf{N}_{\tilde{p}_\mu}^T \, \mathbf{b}_\mu \, \mathbf{B}_{\tilde{u}_\mu} \, d\Omega_\mu = \frac{1}{\Delta t} \, (\mathbf{Q}_\mu)^T. \tag{D.83}$$

(IV) Micro-cale compressibility matrix $\mathbf{S}_\mu$ and permeability matrix $\boldsymbol{\mathcal{K}}_\mu$

$$\begin{aligned} \frac{\partial \mathbf{H}_\mu^{n+\theta}}{\partial \tilde{\tilde{\mathbf{p}}}_\mu^{n+1}} &= \int_{\Omega_\mu^{pm}} \left(\mathbf{N}_{\tilde{p}_\mu}^T \, \frac{\partial \dot{\chi}_\mu^{n+\theta}}{\partial \tilde{p}_\mu^{n+1}} \, \mathbf{N}_{\tilde{p}_\mu} - \mathbf{B}_{\tilde{p}_\mu}^T \, \frac{\partial \boldsymbol{\mathcal{V}}_\mu^{n+\theta}}{\partial \tilde{\boldsymbol{\varphi}}_\mu^{n+1}} \, \mathbf{B}_{\tilde{p}_\mu} \right) d\Omega_\mu \\ &= \frac{\beta}{\Delta t} \int_{\Omega_\mu^{pm}} \mathbf{N}_{\tilde{p}_\mu}^T \, \frac{1}{M_\mu} \, \mathbf{N}_{\tilde{p}_\mu} \, d\Omega_\mu + \theta \int_{\Omega_\mu^{pm}} \mathbf{B}_{\tilde{p}_\mu}^T \, \mathbf{k}_\mu \, \mathbf{B}_{\tilde{p}_\mu} \, d\Omega_\mu = \frac{\beta}{\Delta t} \, \mathbf{S}_\mu + \theta \, \boldsymbol{\mathcal{K}}_\mu. \end{aligned} \tag{D.84}$$

Acknowledgments

This work was partially supported by the Consejo Nacional de Investigaciones Cientficas y Tecnicas (CONICET, Argentina, grant PIP 2022-2024-GI-11220210100455CO) as well as Secretaria de General de Ciencia y Tecnica de la Universidad Nacional del Nordeste (UNNE), Argentina (Grants PI 21D003). Also, the authors would like to acknowledge the financial support from the Agencia Nacional de Promoción Científica y Tecnológica (ANPCyT, Argentina, grants PICTO-UNNE-2019-00014, PICT-2020-SERIEA-02793 and PICT 2021-GRF-TI-00488).

Apéndice E

Consistent multiscale formulation of saturated porous media with randomly distributed non-porous solid inclusions

Reinaldo A. Anonis, Javier L. Mroginski, Sebastián Toro, Pablo J. Sánchez, (2026). Consistent multiscale formulation of saturated porous media with randomly distributed non-porous solid inclusions. Under review.

Consistent multiscale formulation of saturated porous media with randomly distributed non-porous solid inclusions

Anonis, Reinaldo A.[1,1], **Mroginski, Javier L.**[1], **Toro, Sebastián**[2,3], **Sánchez, Pablo J.**[2,3]

[1]LAMEC-IMIT-CONICET Laboratorio de Mecánica Computacional, Universidad Nacional del Nordeste, Las Heras 727, CP 3500 Chaco, Argentina
[2]CIMEC-UNL-CONICET, Ruta Nac. 168, Km 0, Paraje el Pozo, CP 3000 Santa Fe, Argentina
[3]GIMNI-UTN-FRSF, Lavaise 610, CP 3000 Santa Fe, Argentina

Keywords: multiscale models, saturated porous matrix, non-periodic solid inclusions, composite geomaterials.

Abstract. This work develops a multiscale framework that addresses micro-structures composed of a saturated porous matrix containing impermeable non-porous solid inclusions, that is, micro-architectures consisting of components that require different numbers/sets of primary fields to describe their physical behavior. The main novelty lies in the treatment of configurations in which the inclusions are randomly distributed and intersect the micro-cell boundary. Within the framework proposed by the Method of Multiscale Virtual Power, an innovative formula is proposed for the homogenization of the pore-pressure gradient, which leads to the definition of a new Minimally Constrained Multiscale Model (MCMM). In order to improve its predictive capacity, a family of sub-models derived from the MCMM is also introduced, obtained by assuming additional restrictions in the form of alternative boundary conditions. Numerical examples, including rigorous comparisons with the Direct Numerical Simulation procedure, demonstrate the potential of the proposed model, which ultimately supports the concepts introduced in this work.

E.1. Introduction

In this work, a first-order multiscale formulation based on the concept of Representative Volume Element (RVE) [1] is presented, intended to analyze micro-structures consisting of a saturated porous matrix containing randomly distributed, impermeable, non-porous solid inclusions. In this type of material, the matrix requires the combined definition of the displacement and pore-pressure fields, while the solid inclusions are described solely by the displacement field.

This new level of heterogeneity, derived from the coexistence of different sets of primary descriptors at the micro-scale, is characteristic of many complex natural materials, such as geomaterials and biological tissues. Among the former, we can mention geological formations consisting of a clayey or granular matrix containing dispersed quasi-impermeable rock fragments, as well as shales, which, although they can be regarded as macroscopically homogeneous porous media, reveal under microscopic examination a marked structural heterogeneity consisting of a clay and organic matter matrix interspersed with non-porous solid inclusions (for example, calcite, quartz, or pyrite) [87–89]. In the biological field, multiscale poroelastic models for biological tissues have been developed using asymptotic homogenization approaches [90, 91, 93]. Among these, the proposal aimed at modeling myocardial micro-structure tissues [94] stands out, consisting predominantly of an extracellular matrix in which blood vessels and myocyte cells are embedded. An alternative approach could rely on a technique based on the RVE-concept, representing the extracellular matrix together with the vessels, considering myocytes as impermeable solid inclusions.

The treatment of this type of non-homogeneous media requires an adequate review and extension of multiscale theories based on the RVE-concept. This process was recently initiated by the authors in [67],

[1]Corresponding author. E-mail address: ranonis@ing.unne.edu.ar (Anonis, Reinaldo A.).

where a model was proposed for scenarios in which the inclusions did not reach the boundary of the micro-cell (MC) in a truly random manner, thus allowing for a simplified formulation compatible with the periodic model.

In general, it has been shown that, in purely linear and nonlinear mechanical problems, the effective response obtained from periodic boundary conditions is bounded above and below by the Linear and Minimally Constrained Multiscale Model (MCMM), respectively [118–121]. Although there is no guarantee that periodic boundary conditions are optimal among all possible conditions, they provide reasonable estimates of effective moduli, as they always fall within the limits imposed by the other boundary conditions [122]. Clearly, for media with a periodic micro-structure, the so-called periodic model offers the most accurate solution. However, these conditions require continuity in the properties of the materials at opposite boundaries to ensure micro-structural periodicity, a requirement that is rarely met in real heterogeneous materials.

In addition to this lack of material periodicity, general settings may also exhibit no periodicity in geometry, with voids that interrupt the continuity of the displacement field at the boundary of the MC. This situation is analogous to that analyzed in this paper, where the heterogeneity induced by the coexistence of saturated and impermeable porous phases results in the pore pressure field existing only in Ω_μ^p. In such cases, the selection of appropriate boundary conditions is essential.

Since the available literature does not address micro-cells of this type, reference is made to previous works dealing with models containing voids or internal discontinuities, which constitute an analogous scenario. Among the alternative boundary conditions to the conventional ones, the following contributions can be mentioned, even though they did not consider the presence of truly random distributions of voids within the MC or along its boundary. In [123–125], mixed uniform boundary conditions were proposed, combining constant tractions in certain portions of the boundary with linear displacements on others, so that the effective response lies between the two extreme homogeneous conditions. In [126], a similar approach was proposed, incorporating periodic conditions in some components of the displacement field and uniform traction in others. Larsson et al. [127], in turn, developed a variational formulation with the imposition of weakly periodic conditions, thus avoiding the need for periodic meshes. This framework was extended to the study of flows in porous media [128] and chemo-mechanical models [84].

For his part, Glüge [129] introduced a generalized framework of classical boundary conditions based on boundary partitioning, so that the stiffness of the MC can be adjusted. Finally, in [130], a different type of boundary condition was tested as a generalization of the proposal presented in [123], which consists of a mixed condition dependent on the type of load applied to the MC, used to analyze fiber networks embedded in an empty space.

In a more recent contribution [21], it is pointed out that the construction of a Minimally Constrained Multiscale Model is essential, as it establishes the minimum set of constraints from which more appropriate multiscale sub-models can be derived for highly heterogeneous micro-structures, both in geometric and material terms. In this work, Blanco et al. [21] extended this concept by analyzing micro-cells with truly random void distributions, proposing a new MCMM and incorporating more restricted alternatives as sub-spaces of it, giving rise to a broad family of multiscale sub-models.

Feijóo et al. [96] reaffirmed that the MCMM space is the largest that guarantees consistent scale transition, containing as sub-spaces both other multiscale model and the reference solution. However, they also noted that the breadth of this space is detrimental to the micro-scale problem's resolution. To address this, they proposed new models that improve the MCMM by prescribing displacements or tractions on the MC boundary, considering the mechanical interactions between neighboring micro-cells iteratively through alternating and appropriately selected boundary conditions.

In this context, and considering the advances introduced in [21], the present work extends the line of research initiated in [67], aiming to develop a multiscale scheme capable of describing heterogeneous materials whose micro-structure involves components with different descriptive fields. Specifically, the study of micro-cells consisting of a saturated matrix with non-porous and impermeable solid inclusions

is continued, incorporating as a main novelty the consideration of configurations in which the inclusions randomly intercept the MC boundary. The matrix is described using poromechanics theory [35, 36], while the inclusions are incorporated into conventional solid mechanics theory. At the macroscopic scale, coupled hydro-mechanical behavior is recovered, with the constitutive response being obtained by homogenizing the corresponding micro-scale problem.

The proposed model has two fundamental attributes: (i) it is framed within the general framework of the Method of Multiscale Virtual Power (MMVP) [19, 20, 27], ensuring a variationaly consistent methodology; and (ii) the formulation preserves objectivity with respect to the size of the RVE [1], an indispensable but uncommon feature in RVE-based multiscale approaches for saturated porous media, due to the application of the Multiscale-SOE model [66, 68, 69].

For the numerical solution of the multiscale problem, we adopt the so-called FE^2 strategy [5, 6], which is based on two nested finite element schemes that evolve over time. The connection between both levels is established at each Gauss point of the macro-scale. In this work, we avoid developing the computational methodologies used in the implementation of multiscale modeling for hydro-mechanical problems, since these have been widely developed in the literature [16, 48, 66, 67].

The organization of the work is described below. Section E.2 details the general configuration of the problem, including macro- and micro-scale characteristics. Next, in section E.3, the theoretical framework based on the MMVP is fully developed, from which the new MCMM is specified. In section E.4, the sub-models of the MCMM are presented, which constitute alternatives for more appropriate multiscale modeling according to the characteristics of the micro-structure. Section E.5 addresses the constitutive relationships at the micro-scale, assuming the SOE-method to ensure the objectivity of the macro-scale response. In order to validate and demonstrate the capabilities of the proposed model, section E.6 presents the numerical results, where first, the feasibility of the multiscale approach is verified, and then, through a second example, its full potential is demonstrated by comparing it with high-fidelity solutions obtained through Direct Numerical Simulation (DNS). Finally, section E.7 draws the main conclusions of the work. The article concludes with five appendices that include complementary developments and formal demonstrations that help to clarify and support the notions of the present multiscale formulation presented throughout the work.

E.2. Multiscale configuration

The distinctive feature of this work resides in its intrinsic capability to address heterogeneous materials with a completely random distribution of their components, which, in turn, require different fields for the description of their physical behavior. In particular, micro-structures consisting of a saturated porous matrix are considered, which requires the proper setting of displacement and pore-pressure fields, embedded with non-porous impermeable solid inclusions, randomly distributed and described exclusively by the displacement field as the primary variable.

Therefore, subsection E.2.2 provides a detailed description of these micro-structures, which will serve as a basis for subsequent developments. However, at the macro-scale, a material model formulated within the framework of poromechanics theory is recovered [35, 36], which describes a saturated porous medium. Consequently, in subsection E.2.1, we first introduce the governing equations corresponding to the macro-scale.

The main modeling hypotheses adopted at the macro-scale are as follows: (i) infinitesimal transformations for the kinematic description; (ii) a fully saturated domain containing only solid and fluid phases; and (iii) neglect of inertial effects in both phases. At the micro-scale, the same assumptions apply, except that the heterogeneous composition of the material is explicitly considered. The micro-cell (MC) consists of two constituents: (i) a porous matrix fully saturated with pressurized fluid, and (ii) solid, non-porous, impermeable inclusions.

Thus, this section clearly defines the problem to be addressed within the general multiscale context.

It should be noted that, to distinguish them from macro-scale quantities, any micro-scale entity is labeled with the subscript $(\bullet)_\mu$.

E.2.1. Governing equations of the macro-scale

Let us consider a body characterized by an open and bounded domain $\Omega \in \mathbb{R}^3$, with Γ representing the piece-wise smooth boundary and $\mathbf{n}$ is the orthogonal versor, as depicted in Figure E.1. Any material point is denoted by the vector $\mathbf{x}$, which is related to a macro-scale Cartesian system. Prescribed functions

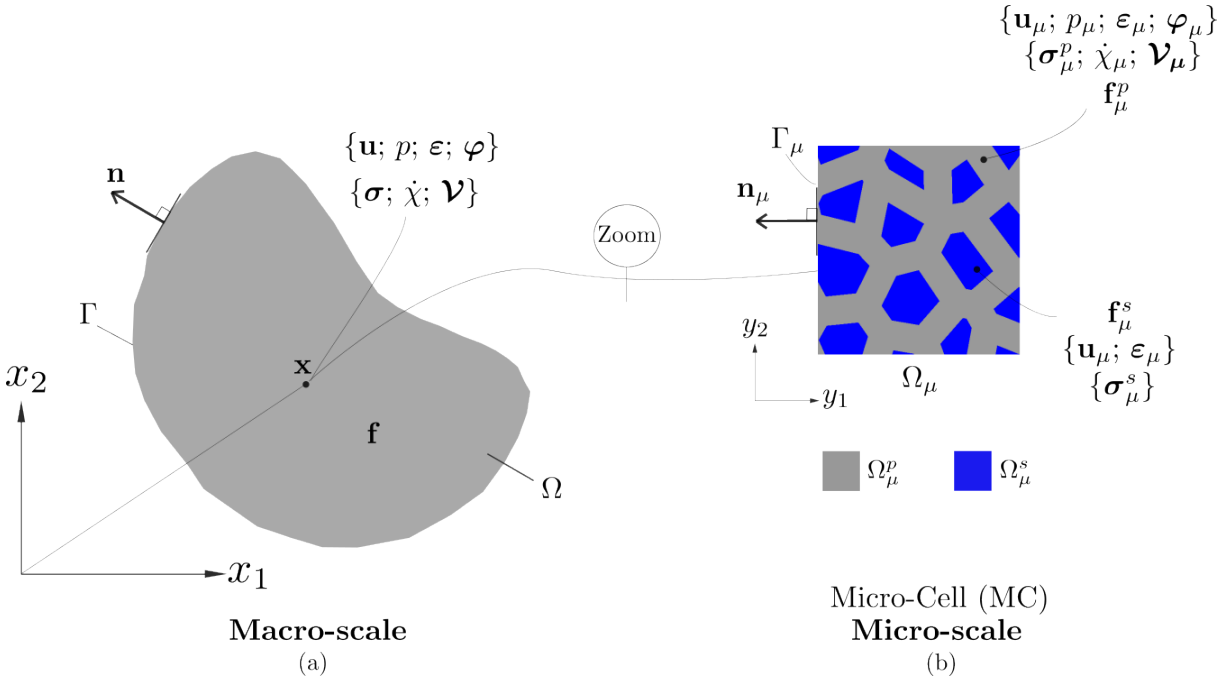

Figura E.1: Basic ingredients of a multiscale model based on the RVE concept.

for displacement $\mathbf{u} = \mathbf{u}_\mathrm{D}$ and pore-pressure $p = p_\mathrm{D}$ are specified for all $\mathbf{x}$ on the Dirichlet boundary partitions of Γ, namely Γ^u_D and Γ^p_D, respectively, and for all time t. Based on these constraints to which the body is subject, it is possible to characterize admissibility at the macro-level through sets: $\mathcal{U}(\Omega) \equiv \{\mathbf{u} \in \mathbf{H}^1(\Omega);\ \mathbf{u} = \mathbf{u}_\mathrm{D}\ \forall \mathbf{x} \in \Gamma^u_\mathrm{D}\}$ and $\mathcal{P}(\Omega) \equiv \{p \in \mathrm{H}^1(\Omega);\ p = p_\mathrm{D}\ \forall \mathbf{x} \in \Gamma^p_\mathrm{D}\}$, for the primary fields $\mathbf{u}(\mathbf{x}, t)$ and $p(\mathbf{x}, t)$, respectively. $\mathbf{H}^1(\bullet)$ and $\mathrm{H}^1(\bullet)$ denote the vector and scalar spaces of functions whose first derivative is square-integrable, respectively. The virtual variations of any entity are specified by placing the δ symbol in front, thereby the virtual actions $\delta\mathbf{u}(\mathbf{x}, t)$ and $\delta p(\mathbf{x}, t)$ are defined. The corresponding linear vector spaces for them are: $\mathcal{U}^*(\Omega) \equiv \{\delta\mathbf{u} \in \mathbf{H}^1(\Omega);\ \delta\mathbf{u} = \mathbf{0}\ \forall \mathbf{x} \in \Gamma^u_\mathrm{D}\}$ and $\mathcal{P}^*(\Omega) \equiv \{\delta p \in \mathrm{H}^1(\Omega);\ \delta p = 0\ \forall \mathbf{x} \in \Gamma^p_\mathrm{D}\}$.

On the other hand, external generalized fluxes $\mathbf{t}$ and q can also be applied for all time t, on the respective Neumann boundary partitions Γ^u_N and Γ^p_N , of Γ, respectively. In view of previous definitions, it can be written $\Gamma = \Gamma^u_\mathrm{D} \cup \Gamma^u_\mathrm{N}$ ($\Gamma^u_\mathrm{D} \cap \Gamma^u_\mathrm{N} = \varnothing$) and also $\Gamma = \Gamma^p_\mathrm{D} \cup \Gamma^p_\mathrm{N}$ ($\Gamma^p_\mathrm{D} \cap \Gamma^p_\mathrm{N} = \varnothing$).

The hydromechanical problem on the macro-scale can be stated as follows: find the displacement fields $\mathbf{u} \in \mathcal{U}(\Omega)$ and pore-pressures $p \in \mathcal{P}(\Omega)$ such that

$$\begin{aligned} \mathrm{G} &= \int_\Omega \boldsymbol{\sigma} : \delta\dot{\boldsymbol{\varepsilon}}\, d\Omega - \int_\Omega \mathbf{f} \cdot \delta\dot{\mathbf{u}}\, d\Omega - \int_{\Gamma^u_\mathrm{N}} \mathbf{t} \cdot \delta\dot{\mathbf{u}}\, d\Gamma = 0,\ \forall\, \delta\dot{\mathbf{u}} \in \mathcal{U}^*(\Omega),\ \forall\, t, \\ \mathrm{H} &= \int_\Omega \left(\dot{\chi}\, \delta p - \boldsymbol{\mathcal{V}} \cdot \delta\boldsymbol{\varphi}\right) d\Omega + \int_{\Gamma^p_\mathrm{N}} \frac{q}{\rho^f}\, \delta p\, d\Gamma = 0,\ \forall\, \delta p \in \mathcal{P}^*(\Omega),\ \forall\, t. \end{aligned} \tag{E.1}$$

where $\boldsymbol{\sigma}(\mathbf{x},t)$ represent the Cauchy stress tensor of the solid skeleton, $\boldsymbol{\varepsilon}(\mathbf{x},t) = \boldsymbol{\nabla}^{sym}\mathbf{u}(\mathbf{x},t)$ the infinitesimal strain tensor, $\boldsymbol{\mathcal{V}}(\mathbf{x},t)$ and $\dot{\chi}(\mathbf{x},t) = \frac{\dot{m}^f}{\rho^f}$ are the flux or the relative seepage velocity vector and the pore volume rate (per unit pore volume), respectively and $\boldsymbol{\varphi}(\mathbf{x},t) = \boldsymbol{\nabla}p(\mathbf{x},t)$ established the gradient of the pore-pressure. Previously, the intrinsic mass density of the fluid phase ρ^f, the gradient operator $\boldsymbol{\nabla}$ and the gradient symmetric operator $\boldsymbol{\nabla}^{sym}$, were introduced.

In addition to the boundary conditions, the initial conditions for the displacement field $\mathbf{u} = \mathbf{u}^0$ and the pore-pressure field $p = p^0$ for all $\mathbf{x}$ must also be fully defined at the start of the analysis at $t = 0$ in order to solve the problem given in (E.1).

In the context of phenomenological modeling, the variational problem given in (E.1) is complemented by the constitutive functionals corresponding to the set of magnitudes $\{\boldsymbol{\sigma}, \dot{\chi}, \boldsymbol{\mathcal{V}}\}$. In the multiscale environment, these phenomenological constitutive equations are replaced by implicit relations derived from a consistently variational multiscale framework, in which the resolution of the micro-scale balance and the appropriate transfer of information between scales play a central role. To this end, each point on the macro-scale $\mathbf{x}$ is associated with a micro-scale domain. It is precisely at this level that the coupling with the heterogeneous micro-structure is established, the detailed description of which is presented in the following section.

E.2.2. Basic assumptions of the micro-scale model

The micro-structural open and bounded domain under analysis is denoted as $\Omega_\mu \in \mathbb{R}^3$, which is also referred to as the micro-cell (MC). In order to identify any material point $\mathbf{x}_\mu$ of Ω_μ, another Cartesian coordinate system is incorporated at the micro-scale.

The MC is assumed to be composed of a saturated porous matrix, which constitutes a bounded subdomain of Ω_μ, denoted by Ω_μ^p. In this subdomain, the behavior of the material is described by the general theory of poromechanics, which requires the evaluation of the micro-scale displacement field, $\mathbf{u}_\mu$, and the micro-scale pore-pressure field, p_μ. In contrast, the complementary space of Ω_μ, defined as Ω_μ^s, is occupied by solid and impermeable volume inclusions, which only require the definition of the micro-scale displacement field, $\mathbf{u}_\mu$, to determine their physical response. Consequently, the field p_μ exists only in the subdomain Ω_μ^p of the MC.

The absence of an interstitial pressure field in part of the microscale domain is analogous to that observed in the microscale displacement field when analyzing solid media with a random distribution of voids. Consequently, the concepts introduced for the treatment of the latter can be adapted to the problem considered in this work. However, a detailed analysis of the MC domain and, in particular, its boundary, denoted as Γ_μ, which is subdivided into different surface subdomains, see Figure E.2, is essential beforehand. Consequently, we have

- Γ_μ: external boundary surface of the MC domain Ω_μ, which has an external outward normal vector $\mathbf{n}_\mu$;
- Γ_μ^p: external surface of the porous medium having outward normal vector $\mathbf{n}_\mu^p$;
- Γ_μ^s: external surface of the solid medium having outward normal vector $\mathbf{n}_\mu^s$;
- Γ_μ^i: internal interface between the saturated matrix and the solid inclusions. The outward normal vector pointing from the porous medium to the inclusion is defined as $\mathbf{n}_\mu^{p,i} = \mathbf{n}_\mu^i$; while the outward normal vector pointing from the solid particles to the porous matrix is denoted $\mathbf{n}_\mu^{s,i} = -\mathbf{n}_\mu^i$.

Trivially, it follows from the external boundary that: $\Gamma_\mu = \Gamma_\mu^p \bigcup \Gamma_\mu^s$ and $\Gamma_\mu^p \bigcap \Gamma_\mu^s = \varnothing$.

Concerning solid media with random void distributions, Blanco et al. [21] introduced the concept of $\mathbf{n}_\mu$-balanced micro-cells, which, according to the above notation, satisfy an equation of the following

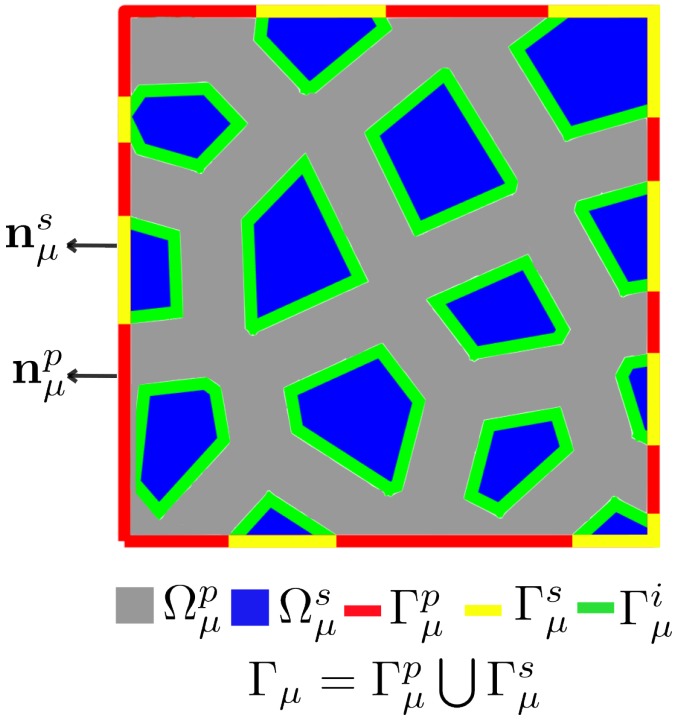

Figura E.2: Micro-cell composed of two different materials: a porous saturated matrix (gray) and solid inclusions (blue).

type

$$\int_{\Gamma_\mu} \mathbf{n}_\mu \, d\Gamma_\mu = \mathbf{0} \tag{E.2}$$

As the micro-structures addressed in this work have material continuity (no voids), they fulfill the geometrical expression (E.2). Hence, $\mathbf{n}_\mu$-balanced MCs along its entire boundary are obtained. However, it is evident that a random distribution of solid inclusions induces a *geometrical imbalance* if each surface subdomain of the boundary Γ_μ is considered separately. That is, the MCs are $\mathbf{n}_\mu^p$-unbalanced in Γ_μ^p and $\mathbf{n}_\mu^s$-unbalanced in Γ_μ^p. This is expressed by

$$\begin{aligned} \int_{\Gamma_\mu^p} \mathbf{n}_\mu^p \, d\Gamma_\mu \neq \mathbf{0}, \\ \int_{\Gamma_\mu^s} \mathbf{n}_\mu^s \, d\Gamma_\mu \neq \mathbf{0}. \end{aligned} \tag{E.3}$$

This second attribute of the micro-structures addressed in this work is not a major drawback if the fields of variables that describe the behavior of its constituents are continuous throughout the domain. Such is the case given by the field of micro-scale displacements.

However, as mentioned above, it is not the same for the micro-scale pore-pressure field. Therefore, based on the ideas aimed at modeling solid media with voids proposed in [21], to address the absence of the p_μ field in part of the MC and the fact that it is $\mathbf{n}_\mu^p$-unbalanced over $\Gamma\mu^p$, an appropriate homogenization of both the pore-pressures and their gradient is proposed, as shown in section E.3.1.2. This enables the modeling of the micro-cells described above and guarantee a self-equilibrated pattern of micro-scale flux velocities across the entire porous boundary Γ_μ^p, a property that is physically consistent.

From the previous definitions, we can write $\Omega_\mu = \Omega_\mu^s \bigcup \Omega_\mu^p$ and $\Omega_\mu^s \bigcap \Omega_\mu^p = \varnothing$. In addition, we introduce the concept of the geometric center of the entire MC, together with that of the geometric

centroid of the subdomain Ω_μ^p, denoted as $\mathbf{x}_\mu^G$ and $\mathbf{x}_\mu^{Gp}$, respectively. The former is defined as

$$\mathbf{x}_\mu^G = \frac{1}{|\Omega_\mu|} \int_{\Omega_\mu} \mathbf{x}_\mu \, d\Omega_\mu, \tag{E.4}$$

While the latter is given by

$$\mathbf{x}_\mu^{Gp} = \frac{1}{|\Omega_\mu^p|} \int_{\Omega_\mu^p} \mathbf{x}_\mu \, d\Omega_\mu, \tag{E.5}$$

Both quantities will be employed in the subsequent developments.

The present work is founded on the axiomatic structure of the Method of Multiscale Virtual Power [19, 20], which is developed in the following section.

E.3. Method of Multiscale Virtual Power

The MMVP provides the variational framework with the basic steps for constructing a hydromechanically consistent multiscale model. It includes two fundamental principles: the principle of admissibility of the primitive descriptors, which ensures the proper transfer of information during the scale-transition process and is described in section E.3.1, and the Principle of Multiscale Virtual Power (PMVP), which guarantees energetic (power) admissibility and is presented in section E.3.2.

E.3.1. Principle of admissibility of primal descriptors

The admissibility of primitive descriptors between the two scales involved is established using two sequential procedures: the insertion and homogenization processes [22, 23], analyzed in sections E.3.1.1 and E.3.1.2, respectively.

E.3.1.1. Insertion at the micro-cell

This section provides an overview of the insertion of primal descriptors at the macro-scale in the MC domain, which play a role in the problem of hydro-mechanical balance at the micro-scale. Accordingly, the quantities evaluated at points associated with the larger length scale are considered, namely: $\{\mathbf{u}(t), \boldsymbol{\nabla}\mathbf{u}(t)\}$ and $\{p(t), \boldsymbol{\varphi}(t)\}$, where $\boldsymbol{\nabla}\mathbf{u}(t)$ denotes the complete gradient of the macro-scale displacements. Based on these quantities, the displacement and pore-pressure fields within each MC are constructed according to a Taylor-like expansion. It is standard practice to perform this expansion for the primary microscale descriptors around a common point, typically the geometric centroid of the corresponding MC (see equation E.4), with respect to the global coordinate system at the microscale.

For the microscale displacement field $\mathbf{u}_\mu(\mathbf{x}_\mu, t)$, this assumption holds. In contrast, for the microscale pore-pressure field $p_\mu(\mathbf{x}_\mu, t)$, it is more appropriate to perform the expansion around $\mathbf{x}\mu^{Gp}$, which identifies the position of the geometric center of the matrix subdomain Ω_μ^p with respect to the global microscale coordinate system (see equation E.5), since this field is defined only within that region. It should be noted that this approach also simplifies the set of constraints to be imposed at the micro-scale, as will be shown through equation (E.19). Thus, it is written for micro-scale displacements

$$\mathbf{u}_\mu(\mathbf{x}_\mu, t) = \mathbf{u}(t) + \boldsymbol{\nabla}\mathbf{u}(t)\left(\mathbf{x}_\mu - \mathbf{x}_\mu^G\right) + \tilde{\mathbf{u}}_\mu(\mathbf{x}_\mu, t), \quad \forall \mathbf{x}_\mu \in \Omega_\mu, \tag{E.6}$$

where, in expression (E.6), $\tilde{\mathbf{u}}_\mu(\mathbf{x}_\mu, t)$ represents the displacement fluctuation field in the MC domain. However, for the kinematic description of the multiscale formulation, only the symmetric part of the displacement gradient is adopted, in line with the weak balance expressions (see equation (E.1)) and

with the PMVP adopted further on (see equation (E.30)). So we rewrite (E.6) as

$$\mathbf{u}_\mu\left(\mathbf{x}_\mu, t\right) = \mathbf{u}\left(t\right) + \boldsymbol{\varepsilon}\left(t\right)\left(\mathbf{x}_\mu - \mathbf{x}_\mu^G\right) + \tilde{\mathbf{u}}_\mu\left(\mathbf{x}_\mu, t\right), \quad \forall \mathbf{x}_\mu \in \Omega_\mu, \tag{E.7}$$

Meanwhile, for the poro-pressure field we have

$$p_\mu\left(\mathbf{x}_\mu, t\right) = p\left(t\right) + \boldsymbol{\varphi}\left(t\right) \cdot \left(\mathbf{x}_\mu - \mathbf{x}_\mu^{Gp}\right) + \tilde{p}_\mu\left(\mathbf{x}_\mu, t\right), \quad \forall \mathbf{x}_\mu \in \Omega_\mu^p, \tag{E.8}$$

with $\tilde{p}_\mu\left(\mathbf{x}_\mu, t\right)$ being the micro-scale pore-pressure fluctuation field which exists only in the porous matrix Ω_μ^p.

From expressions (E.7) and (E.8), the micro-scale strain tensor, $\boldsymbol{\varepsilon}_\mu\left(\mathbf{x}_\mu, t\right)$, and the gradient of the micro-scale pore-pressures, $\boldsymbol{\varphi}_\mu\left(\mathbf{x}_\mu, t\right)$, can be expressed, respectively, as follow

$$\boldsymbol{\varepsilon}_\mu\left(\mathbf{x}_\mu, t\right) = \boldsymbol{\nabla}_{\mathbf{x}_\mu}^{sym}\mathbf{u}_\mu\left(\mathbf{x}_\mu, t\right) = \boldsymbol{\varepsilon}\left(t\right) + \boldsymbol{\nabla}_{\mathbf{x}_\mu}^{sym}\tilde{\mathbf{u}}_\mu\left(\mathbf{x}_\mu, t\right) = \boldsymbol{\varepsilon}\left(t\right) + \tilde{\boldsymbol{\varepsilon}}_\mu\left(\mathbf{x}_\mu, t\right), \quad \forall \mathbf{x}_\mu \in \Omega_\mu, \tag{E.9}$$

$$\boldsymbol{\varphi}_\mu\left(\mathbf{x}_\mu, t\right) = \boldsymbol{\nabla}_{\mathbf{x}_\mu} p_\mu\left(\mathbf{x}_\mu, t\right) = \boldsymbol{\varphi}\left(t\right) + \boldsymbol{\nabla}_{\mathbf{x}_\mu} \tilde{p}_\mu\left(\mathbf{x}_\mu, t\right) = \boldsymbol{\varphi}\left(t\right) + \tilde{\boldsymbol{\varphi}}_\mu\left(\mathbf{x}_\mu, t\right), \quad \forall \mathbf{x}_\mu \in \Omega_\mu^p, \tag{E.10}$$

where the operators $\boldsymbol{\nabla}_{\mathbf{x}_\mu}^{sym}\left(\bullet\right)$ and $\boldsymbol{\nabla}_{\mathbf{x}_\mu}\left(\bullet\right)$ represent the symmetric gradient and the gradient, repectively, related to the micro-scale $\mathbf{x}_\mu$-coordinate system. Whereas, $\tilde{\boldsymbol{\varepsilon}}_\mu\left(\mathbf{x}_\mu, t\right)$ and $\tilde{\boldsymbol{\varphi}}_\mu\left(\mathbf{x}_\mu, t\right)$ are the strain fluctuation on the MC-domain Ω_μ and the corresponding gradient vector of the pore-pressure fluctuation on the MC-subdomain Ω_μ^p, respectively.

Note that both fields, $\mathbf{u}_\mu(\mathbf{x}_\mu, t)$ and $\boldsymbol{\varepsilon}_\mu(\mathbf{x}_\mu, t)$, are defined for the entire domain $\Omega_\mu = \Omega_\mu^p \cup \Omega_\mu^s$, including the porous matrix skeleton as well as the solid inclusion volume, see Figure E.1. On the other hand, is important to ensure that $p\left(t\right)$ and $\boldsymbol{\varphi}\left(t\right)$ are inserted only into the porous medium subdomain Ω_μ^p, which guarantees the physical consistency that solid medium does not admit pore-pressure variables.

All the above definitions (E.7)-(E.10) can also be established in rate forms. In order to simplify the notation, the arguments denoting spatial and time dependencies are suppressed in the subsequent developments.

E.3.1.2. Homogenization at the micro-cell.

Subsequently, four homogenization procedures are defined that establish the correspondence between the primitive descriptors at the micro-scale and their associated point values at the macro-scale.

Displacement homogenization

The displacement homogenization rule, denoted as $\mathcal{H}_{\mathbf{u}}$, establishes that the volume average of the micro-scale displacement field over the entire domain under analysis, Ω_μ, must coincide with the corresponding macro-scale displacement field, as

$$\mathcal{H}_{\mathbf{u}}\left(\mathbf{u}_\mu\right) = \mathbf{u} = \frac{1}{|\Omega_\mu|}\int_{\Omega_\mu} \mathbf{u}_\mu \, d\Omega_\mu. \tag{E.11}$$

Substituting (E.7) in (E.11) it is obtained

$$\mathbf{u} = \mathbf{u} + \boldsymbol{\varepsilon}\left[\frac{1}{|\Omega_\mu|}\int_{\Omega_\mu}\left(\mathbf{x}_\mu - \mathbf{x}_\mu^G\right) \, d\Omega_\mu\right] + \frac{1}{|\Omega_\mu|}\int_{\Omega_\mu} \tilde{\mathbf{u}}_\mu \, d\Omega_\mu. \tag{E.12}$$

According to equation (E.4), the second term of expression (E.12) is canceled out, thus obtaining the first kinematic constraint that must be imposed on the field of displacements fluctuation at the micro-scale.

This constraint, responsible for preventing rigid translations of the MC, is expressed as

$$\int_{\Omega_\mu} \tilde{\mathbf{u}}_\mu \, d\Omega_\mu = \mathbf{0}, \tag{E.13}$$

Strain homogenization
The homogenization rule for the strain field at the micro-scale results in

$$\mathcal{H}_{\boldsymbol{\varepsilon}}\left(\boldsymbol{\varepsilon}_\mu\right) = \boldsymbol{\varepsilon} = \frac{1}{|\Omega_\mu|} \int_{\Omega_\mu} \boldsymbol{\varepsilon}_\mu \, d\Omega_\mu. \tag{E.14}$$

Next, substituting (E.9) into (E.14) and applying Green's theorem leads to the following condition

$$\int_{\Gamma_\mu} \tilde{\mathbf{u}}_\mu \ \otimes^{sym} \ \mathbf{n}_\mu \, d\Gamma_\mu = \mathbb{O}, \tag{E.15}$$

where $\otimes^{sym}$ is the symmetric external dyadic product, while $\mathbb{O}$ represents the second-order null tensor. Note that, according to expression (E.15), it is possible that the micro-scale kinematic fields are not adequately controlled. That is, this restriction limited to the symmetric dyadic product does not fix the degree of freedom associated with rotation. In such cases, additional constraints on $\tilde{\mathbf{u}}_\mu$ are required to ensure the well-posedness mathematical formulation of the micro-scale problem. According to Blanco et al. [19], these additional constraints must be homogeneous and depend on modeling assumptions based on physical considerations for the micro-scale problem. In this paper, the following expression is adopted

$$\int_{\Gamma_\mu} \tilde{\mathbf{u}}_\mu \ \otimes \ \mathbf{n}_\mu \, d\Gamma_\mu = \mathbb{O}. \tag{E.16}$$

That is, by considering the external full diadic product $\otimes$ rather than restricting it to its symmetric part, an additional constraint is introduced that excludes rotation and guarantees an adequate formulation of the micro-scale kinematic problem, preserving compatibility with (E.14). Equation (E.16) arises naturally in the case of controlling the gradient of macroscopic displacements.

Pore-pressure homogenization
The homogenization process for micro-scale pore-pressures, named as $\mathcal{H}_p$, involves an averaged rule restricted to Ω_μ^p

$$\mathcal{H}_p\left(p_\mu\right) = p = \frac{1}{|\Omega_\mu^p|} \int_{\Omega_\mu^p} p_\mu \, d\Omega_\mu. \tag{E.17}$$

Replacing (E.8) into (E.17) it is obtained

$$p = p + \boldsymbol{\varphi} \cdot \left[\frac{1}{|\Omega_\mu^p|} \int_{\Omega_\mu^p} \left(\mathbf{x}_\mu - \mathbf{x}_\mu^{Gp}\right) \, d\Omega_\mu \right] + \frac{1}{|\Omega_\mu^p|} \int_{\Omega_\mu^p} \tilde{p}_\mu \, d\Omega_\mu, \tag{E.18}$$

where the second term disappears due to (E.5). Thus, we arrive at a homogeneous constraint, but now in the field of micro-scale pore-pressure, that is

$$\int_{\Omega_\mu^p} \tilde{p}_\mu \, d\Omega_\mu = 0. \tag{E.19}$$

If the expansion of p_μ had been performed around the geometric center $\mathbf{x}_\mu^G$ of the micro-cell, a non-homogeneous constraint would have been obtained, as pointed out in previous contributions by the authors [67]. Consequently, equation (E.19) establishes a condition that is slightly simpler to imple-

ment numerically. A detailed comparison between both expansion schemes lies beyond the scope of this paper.

Pore-pressure gradient homogenization

At this stage lies the main and novel contribution of the present work. The homogenization rule for the gradient of the micro-scale pore-pressure field is defined as

$$\mathcal{H}_{\boldsymbol{\varphi}}^{(\overline{\mathbf{n}}_\mu^p)}(\boldsymbol{\varphi}_\mu) = \boldsymbol{\varphi} = \frac{1}{|\Omega_\mu^p|}\left[\int_{\Omega_\mu^p} \boldsymbol{\varphi}_\mu \, d\Omega_\mu - \int_{\Gamma_\mu^i} \tilde{p}_\mu \, \mathbf{n}_\mu^i \, d\Gamma_\mu - \int_{\Gamma_\mu^p} \tilde{p}_\mu \, \overline{\mathbf{n}}_\mu^p \, d\Gamma_\mu\right]$$
$$= \frac{1}{|\Omega_\mu^p|}\left[\int_{\Omega_\mu^p} \boldsymbol{\nabla}_{\mathbf{x}_\mu} p_\mu \, d\Omega_\mu - \int_{\Gamma_\mu^i} \tilde{p}_\mu \, \mathbf{n}_\mu^i \, d\Gamma_\mu - \int_{\Gamma_\mu^p} \tilde{p}_\mu \, \overline{\mathbf{n}}_\mu^p \, d\Gamma_\mu\right], \quad \text{(E.20)}$$

where the second term, associated with the internal interface Γ_μ^i, is incorporated to obtain a homogenization expression for the pore-pressure gradient that depends solely on the external boundary of the porous matrix, Γ_μ^p, as expected. The third term is responsible for preserving the consistency of the model by ensuring that the homogenization of the micro-scale pore-pressure gradient correctly reproduces the corresponding macro-scale variable, that is, the macroscopic gradient $\boldsymbol{\varphi}$. This term depends on a vector field $\overline{\mathbf{n}}_\mu^p$[2], which we define as

$$\overline{\mathbf{n}}_\mu^p = \frac{1}{|\Gamma_\mu^p|}\int_{\Gamma_\mu^p} \mathbf{n}_\mu^p \, d\Gamma_\mu, \quad \text{(E.21)}$$

This additional term ensures that the homogenization formula works consistently even in the most general case, when impermeable inclusions randomly reach the boundary of the MC. Furthermore, it guarantees that the micro-scale flux velocities are self-equilibrated, as will be demonstrated in Appendix C.2.

By considering (E.10) together with Green's theorem, expression (E.20) can be further expanded to yield

$$\boldsymbol{\varphi} = \boldsymbol{\varphi} + \frac{1}{|\Omega_\mu^p|}\left[\int_{\Omega_\mu^p} \boldsymbol{\nabla}_{\mathbf{x}_\mu} \tilde{p}_\mu \, d\Omega_\mu - \int_{\Gamma_\mu^i} \tilde{p}_\mu \, \mathbf{n}_\mu^i \, d\Gamma_\mu - \int_{\Gamma_\mu^p} \tilde{p}_\mu \, \overline{\mathbf{n}}_\mu^p \, d\Gamma_\mu\right]$$
$$= \boldsymbol{\varphi} + \frac{1}{|\Omega_\mu^p|}\left[\int_{\Gamma_\mu^p} \tilde{p}_\mu \, \left(\mathbf{n}_\mu^p - \overline{\mathbf{n}}_\mu^p\right) \, d\Gamma_\mu\right]. \quad \text{(E.22)}$$

From (E.22) emerges an additional restriction for the micro-scale pore-pressure fluctuation field at boundary Γ_μ^p

$$\int_{\Gamma_\mu^p} \tilde{p}_\mu \, \left(\mathbf{n}_\mu^p - \overline{\mathbf{n}}_\mu^p\right) \, d\Gamma_\mu = \mathbf{0}. \quad \text{(E.23)}$$

The constraint (E.23) is a consequence of imposing the concept of admissibility on the macro- and micro-scale poro-pressure gradients related through the homogenization operator (E.20), as prescribed by the MMVP framework.

This particular selection of the vector $\overline{\mathbf{n}}_\mu^p$ is precisely what enables the definition given in Sub-section E.2.2. Thus, when the average of the outward normals on the boundary Γ_μ^p vanishes, that is, $\overline{\mathbf{n}}_\mu^p = \mathbf{0}$, the MC is called $\mathbf{n}_\mu^p$-balanced (and therefore $\mathbf{n}_\mu^s$-balanced). Geometrically, this condition implies that

[2] A more general formulation is based on introducing a vector field $\mathbf{m}_\mu^p$ that must satisfy the property

$$\int_{\Gamma_\mu^p} \mathbf{m}_\mu^p \, d\Gamma_\mu = \int_{\Gamma_\mu^p} \mathbf{n}_\mu^p \, d\Gamma_\mu, \quad \mathbf{m}_\mu^p \neq \mathbf{n}_\mu^p,$$

whose simplest form is given by assuming $\mathbf{m}_\mu^p$ as a constant vector field on the part of the boundary Γ_μ^p, which leads to (E.21). As a more in-depth analysis is beyond the scope of this paper, readers are referred to the specialized bibliography [19].

the distribution of inclusions on the boundary of the MC are arranged in a balanced manner. In contrast, when this mean normal does not vanish, the unbalanced configuration described by definition definition (E.3) is recovered, which is precisely the situation we are trying to address.

A brief development of the consequences of not applying the vector field $\overline{\mathbf{n}}_\mu^p$ when dealing with fully random inclusions embedded in the micro-cells (that is, $\mathbf{n}_\mu$-unbalanced in Γ_μ^p and Γ_μ^s) is presented in the Appendix A.

E.3.1.3. Spaces of admissible fluctuations variables of the micro-scale

Based on the constraints imposed on the displacement and pore-pressure fluctuation fields, given by equations (E.13), (E.16), (E.19) and (E.23), the Minimally Constrained Multiscale Model, MCMM($\overline{\mathbf{n}}_\mu^p$), [19, 21] is introduced. It is defined by the following functional spaces

$$\widetilde{\mathcal{U}}_\mu\left(\Omega_\mu\right) \equiv \left\{ \tilde{\mathbf{u}}_\mu \ \in \ \mathbf{H}^1\left(\Omega_\mu\right); \int_{\Omega_\mu} \tilde{\mathbf{u}}_\mu \, d\Omega_\mu = \mathbf{0}; \int_{\Gamma_\mu} \tilde{\mathbf{u}}_\mu \ \otimes \ \mathbf{n}_\mu \, d\Gamma_\mu = \mathbb{O} \right\}, \tag{E.24}$$

$$\widetilde{\mathcal{P}}_\mu^{\left(\overline{\mathbf{n}}_\mu^p\right)}\left(\Omega_\mu^p\right) \equiv \left\{ \tilde{p}_\mu \ \in \ \mathrm{H}^1\left(\Omega_\mu^p\right); \int_{\Omega_\mu^p} \tilde{p}_\mu \, d\Omega_\mu = 0; \int_{\Gamma_\mu^p} \tilde{p}_\mu \ \left(\mathbf{n}_\mu^p - \overline{\mathbf{n}}_\mu^p\right) \, d\Gamma_\mu = \mathbf{0} \right\}. \tag{E.25}$$

The micro-scale fluctuation fields $\tilde{\mathbf{u}}_\mu$ and $\tilde{p}_\mu$ are admissible, that is, compatible with the homogenization procedure adopted in equations (E.11), (E.14), (E.17) and (E.20), provided that they belong to the spaces $\widetilde{\mathcal{U}}_\mu\left(\Omega_\mu\right)$ and $\widetilde{\mathcal{P}}_\mu^{\left(\overline{\mathbf{n}}_\mu^p\right)}\left(\Omega_\mu^p\right)$, respectively.

The MCMM($\overline{\mathbf{n}}_\mu^p$) defined by (E.24) and (E.25) corresponds to the so-called uniform traction and flux model, since the resulting system of tractions and fluxes over boundaries of the micro-cells with constant normal vectors are uniform, although not necessarily equal across boundaries with different orientations. In general, this behavior does not fully reflect the actual microscopic response of the material. To achieve more restricted configurations for the fields $\tilde{\mathbf{u}}_\mu$ and $\tilde{p}_\mu$, leading to improved effective response, alternative models should be constructed. In this context, any subspace of $\widetilde{\mathcal{U}}_\mu\left(\Omega_\mu\right)$ and $\widetilde{\mathcal{P}}_\mu^{\left(\overline{\mathbf{n}}_\mu^p\right)}\left(\Omega_\mu^p\right)$, respectively, may serve as the basis for developing such refined homogenization schemes. In particular, in Section E.4 we propose additional constraints to the MCMM($\overline{\mathbf{n}}_\mu^p$) defined above, aiming to achieve optimal homogenization strategies for micro-structures consisting of a matrix with completely randomly embedded inclusions. In addition, Appendix B presents the well-known Linear and Periodic models that will be used in the numerical results section E.6.

Considering (E.7)-(E.10), the virtual actions within the micro-cell domain are defined as follows

$$\delta\mathbf{u}_\mu = \delta\mathbf{u} + \delta\boldsymbol{\varepsilon}\left(\mathbf{x}_\mu - \mathbf{x}_\mu^G\right) + \delta\tilde{\mathbf{u}}_\mu, \quad \forall\, \mathbf{x}_\mu \ \in \Omega_\mu, \tag{E.26}$$

$$\delta\boldsymbol{\varepsilon}_\mu = \delta\boldsymbol{\varepsilon} + \boldsymbol{\nabla}_{\mathbf{x}_\mu}^{sym}\delta\tilde{\mathbf{u}}_\mu, \quad \forall\, \mathbf{x}_\mu \ \in \Omega_\mu, \tag{E.27}$$

$$\delta p_\mu = \delta p + \delta\boldsymbol{\varphi} \cdot \left(\mathbf{x}_\mu - \mathbf{x}_\mu^{Gp}\right) + \delta\tilde{p}_\mu, \quad \forall\, \mathbf{x}_\mu \ \in \Omega_\mu^p, \tag{E.28}$$

$$\delta\boldsymbol{\varphi}_\mu = \delta\boldsymbol{\varphi} + \boldsymbol{\nabla}_{\mathbf{x}_\mu}\delta\tilde{p}_\mu, \quad \forall\, \mathbf{x}_\mu \ \in \Omega_\mu^p. \tag{E.29}$$

Thus, the spaces of admissible fluctuations virtual actions can be defined as $\widetilde{\mathcal{U}}_\mu^*\left(\Omega_\mu\right) \equiv \widetilde{\mathcal{U}}_\mu\left(\Omega_\mu\right)$ and $\widetilde{\mathcal{P}}_\mu^*\left(\Omega_\mu^p\right) \equiv \widetilde{\mathcal{P}}_\mu^{\left(\overline{\mathbf{n}}_\mu^p\right)}\left(\Omega_\mu^p\right)$, with $\delta\tilde{\mathbf{u}}_\mu \in \widetilde{\mathcal{U}}_\mu^*\left(\Omega_\mu\right)$ and $\delta\tilde{p}_\mu \in \widetilde{\mathcal{P}}_\mu^*\left(\Omega_\mu^p\right)$. Since all the constraints derived from the homogenization process are homogeneous, these spaces coincide.

E.3.2. Principle of Multiscale Virtual Power

The final step within the MMVP framework corresponds to the Principle of Multiscale Virtual Power (PMVP) [19, 20]. This principle establishes that, for all admissible virtual actions, the total virtual power

evaluated at the macro-scale, at a given point $\mathbf{x}$, must be equal to the total virtual power computed at the micro-scale in the associated micro-cell. Following previous contributions [67], the PMVP for the present hydro-mechanical problem can be expressed as follows

$$
\begin{aligned}
|\Omega_\mu| \left(\boldsymbol{\sigma} : \delta\dot{\boldsymbol{\varepsilon}} - \mathbf{f} \cdot \delta\dot{\mathbf{u}} + \dot{\chi}\, \delta p - \boldsymbol{\mathcal{V}} \cdot \delta\dot{\boldsymbol{\varphi}} \right) = \int_{\Omega_\mu} \Big[& \boldsymbol{\sigma}_\mu : \left(\delta\dot{\boldsymbol{\varepsilon}} + \boldsymbol{\nabla}^{sym}_{\mathbf{x}_\mu} \delta\dot{\tilde{\mathbf{u}}}_\mu \right) \\
& - \mathbf{f}_\mu \cdot \left(\delta\dot{\mathbf{u}} + \delta\dot{\boldsymbol{\varepsilon}} \left(\mathbf{x}_\mu - \mathbf{x}^G_\mu \right) + \delta\dot{\tilde{\mathbf{u}}}_\mu \right) \Big] \, d\Omega_\mu \\
+ \int_{\Omega^p_\mu} \Big[& \dot{\chi}_\mu \left(\delta p + \delta\boldsymbol{\varphi} \cdot \left(\mathbf{x}_\mu - \mathbf{x}^{Gp}_\mu \right) + \delta\tilde{p}_\mu \right) - \boldsymbol{\mathcal{V}}_\mu \cdot \left(\delta\boldsymbol{\varphi} + \boldsymbol{\nabla}_{\mathbf{x}_\mu} \delta\tilde{p}_\mu \right) \Big] \, d\Omega_\mu \\
& \forall \ (\delta\dot{\boldsymbol{\varepsilon}},\ \delta\dot{\mathbf{u}}, \delta\boldsymbol{\varphi},\ \delta p) \ \in \mathbb{R}^6 \times \mathbb{R}^3 \times \mathbb{R}^3 \times \mathbb{R}, \\
& \forall \left(\delta\dot{\tilde{\mathbf{u}}}_\mu,\ \delta\tilde{p}_\mu \right) \in \widetilde{\mathcal{U}}_\mu \left(\Omega_\mu \right) \times \widetilde{\mathcal{P}}^{\left(\overline{\mathbf{n}}^p_\mu \right)}_\mu \left(\Omega^p_\mu \right), \ \forall\, t.
\end{aligned}
\tag{E.30}
$$

where $\mathbf{f}_\mu = \rho^{(\bullet)}_\mu \, \mathbf{g}$ has been considered; $\mathbf{f}_\mu$ being the weight per unit volume. The value of $\rho^{(\bullet)}_\mu$ depends on whether the material point belongs to Ω^p_μ or Ω^s_μ. In the first case, the saturated density $\rho^p_\mu = \rho^{p,f} n_\mu + \rho^{p,s} \left(1 - n_\mu \right)$ is used, with $\rho^{p,s}$ denoting the density of the solid phase in the porous medium. In the second case, the density of the solid inclusion ρ^s_μ is employed.

It can be noted that the conjugate pairs inherent to the porous medium are only integrated over their corresponding subdomain Ω^p_μ, and all terms are normalized with respect to the total volume of the MC, $|\Omega_\mu|$.

By resorting simple variational manipulations on (E.30), the consequences of the PMVP are naturally obtained, namely: (i) the homogenization formulae for the macro-scale entities $\{\boldsymbol{\sigma}; \dot{\chi}; \boldsymbol{\mathcal{V}}; \mathbf{f}\}$ and a restriction on micro-scale body forces, which is established in E.3.2.1 and (ii) the variational forms of balance equations at the smaller length scale, as can be seen in E.3.2.2.

E.3.2.1. Homogenization rules for macro-scale entities

By first assuming that in (E.30) all fluctuating virtual actions at the micro-scale vanish, and subsequently considering each macroscopic virtual action as arbitrary while setting the remaining ones to zero, the homogenization relations for the dual variables can be derived.

Homogenized stress tensor:

$$
\boldsymbol{\sigma} = \frac{1}{|\Omega_\mu|} \int_{\Omega_\mu} \left(\boldsymbol{\sigma}_\mu - \mathbf{f}_\mu \otimes^{sym} \left(\mathbf{x}_\mu - \mathbf{x}^G_\mu \right) \right) d\Omega_\mu, \ \forall\, t. \tag{E.31}
$$

Homogenized pore volume rate (per unit pore volume):

$$
\dot{\chi} = \frac{\dot{m}^f}{\rho^f} = \frac{1}{|\Omega_\mu|} \int_{\Omega^p_\mu} \dot{\chi}_\mu \, d\Omega_\mu, \ \forall\, t. \tag{E.32}
$$

It should be pointed out that in (E.32) the averaging factor and the integration domain are different.

Homogenized flux velocity vector:

$$
\boldsymbol{\mathcal{V}} = \frac{1}{|\Omega_\mu|} \int_{\Omega^p_\mu} \left(\boldsymbol{\mathcal{V}}_\mu - \dot{\chi}_\mu \left(\mathbf{x}_\mu - \mathbf{x}^{Gp}_\mu \right) \right) d\Omega_\mu, \ \forall\, t. \tag{E.33}
$$

Once again, observe that in (E.33) the integration domain differs from the normalization measure.

Homogenized body force field:

$$\mathbf{f} = \frac{1}{|\Omega_\mu|}\int_{\Omega_\mu} \mathbf{f}_\mu \, d\Omega_\mu = \frac{\mathbf{g}}{|\Omega_\mu|}\int_{\Omega_\mu} \rho_\mu \, d\Omega_\mu, \ \forall\, t. \tag{E.34}$$

E.3.2.2. Weak forms of variational balance equations in the MC

Then, supposing that all virtual actions at the macro-scale disappear and considering that $\delta\dot{\tilde{\mathbf{u}}}_\mu$ and $\delta\tilde{p}$ are mutually independent, we obtain the system of two coupled scalar equations that establish the variational form of balance at the micro-scale.

Variational form of the momentum balance equation in the MC:

$$\int_{\Omega_\mu} \left(\boldsymbol{\sigma}_\mu : \boldsymbol{\nabla}^{sym}_{\mathbf{x}_\mu} \delta\dot{\tilde{\mathbf{u}}}_\mu - \mathbf{f}_\mu \cdot \delta\dot{\tilde{\mathbf{u}}}_\mu \right) d\Omega_\mu = 0, \quad \forall \delta\dot{\tilde{\mathbf{u}}}_\mu \in \widetilde{\mathcal{U}}_\mu \left(\Omega_\mu\right), \ \forall\, t. \tag{E.35}$$

Variational form of the mass balance equation in the MC:

$$\int_{\Omega^p_\mu} \left(\dot{\chi}_\mu \, \delta\tilde{p}_\mu - \boldsymbol{\mathcal{V}}_\mu \cdot \boldsymbol{\nabla}_{\mathbf{x}_\mu} \delta\tilde{p}_\mu \right) d\Omega_\mu = 0, \quad \forall \delta\tilde{p}_\mu \in \widetilde{\mathcal{P}}^{\left(\overline{\mathbf{n}}^p_\mu\right)}_\mu \left(\Omega^p_\mu\right), \ \forall\, t. \tag{E.36}$$

where, as expected, only the Ω^p_μ subdomain is involved since the solid medium, Ω^s_μ, does not support the micro-scale pore-pressure field.

In Appendix C, an alternative version of the balance equations is presented, in which all constraints included in $\widetilde{\mathcal{U}}_\mu$ and $\widetilde{\mathcal{P}}^{\left(\overline{\mathbf{n}}^p_\mu\right)}_\mu$ were relaxed by introducing the corresponding Lagrange multipliers.

E.4. Alternative multiscale model: MCMM with partitions

In this section, we propose a sub-model of the MCMM($\overline{\mathbf{n}}^p_\mu$) by introducing additional constraints on the spaces $\widetilde{\mathcal{U}}_\mu$ and $\widetilde{\mathcal{P}}^{\left(\overline{\mathbf{n}}^p_\mu\right)}_\mu$ given in (E.24) and (E.25), respectively.

For simplicity, without loss of generality in the theoretical developments presented above, the following analysis is limited to two-dimensional problems, in which the MC is a quadrilateral aligned with the Cartesian axes. In this context, we consider that the entire boundary of the MC, Γ_μ, and the boundary of the subdomain of the porous medium, Γ^p_μ, can be "partitioned" into $R_u \geq 2$ and $R_p \geq 2$ non-overlapping segments, respectively, according to

$$\begin{aligned} \Gamma_\mu &= \bigcup_{j=1}^{R_u} \Gamma^j_\mu, \\ \Gamma^p_\mu &= \bigcup_{k=1}^{R_p} \Gamma^{p,k}_\mu, \end{aligned} \tag{E.37}$$

where

$$\begin{aligned} \Gamma^j_\mu &= \Gamma^{j,+}_\mu \cup \Gamma^{j,-}_\mu, \quad j = 1, \ldots, R_u \\ \Gamma^{p,k}_\mu &= \Gamma^{k,+}_\mu \cup \Gamma^{k,-}_\mu, \quad k = 1, \ldots, R_p \end{aligned} \tag{E.38}$$

At this point, different index sets j and k are introduced to conveniently identify subsets of the boundary partitions Γ^j_μ and $\Gamma^{p,k}_\mu$. The complete sets of indices are denoted by $\mathcal{R}_u = \{1, \ldots, R_u\}$ and $\mathcal{R}_p = \{1, \ldots, R_p\}$. Subset of these are defined as $\mathcal{C}_u \subseteq \mathcal{R}_u$ and $\mathcal{C}_p \subseteq \mathcal{R}_p$, with corresponding complements $\mathcal{W}_u = \mathcal{R}_u \setminus \mathcal{C}_u$ and $\mathcal{W}_p = \mathcal{R}_p \setminus \mathcal{C}_p$. The cardinalities of these sets are denoted

by $R_{(\bullet)} = \text{card}\left(\mathcal{R}_{(\bullet)}\right)$, $C_{(\bullet)} = \text{card}\left(\mathcal{C}_{(\bullet)}\right)$, and $W_{(\bullet)} = \text{card}\left(\mathcal{W}_{(\bullet)}\right)$, where card$(\bullet)$ represents the number of elements in the set $(\bullet)$. Two typical situations can thus be distinguished: (i) $\mathcal{C}_{(\bullet)} = \mathcal{R}_{(\bullet)}$, then $C_{(\bullet)} = R_{(\bullet)}$, $\mathcal{W}_{(\bullet)} = \varnothing$ and $W_{(\bullet)} = 0$; (ii) $\mathcal{C}_{(\bullet)} \subset \mathcal{R}_{(\bullet)}$, then $C_{(\bullet)} < R_{(\bullet)}$, $\mathcal{W}_{(\bullet)} \neq \varnothing$ and $W_{(\bullet)} > 0$.

In turn, analogous to the mean normal vector defined in (E.21) for the boundary Γ_μ^p, an averaged normal vector is introduced for each partition $\Gamma_\mu^{p,k}$, proposed on Γ_μ^p. This is expressed as follows

$$\overline{\mathbf{n}}_\mu^{p,k} = \frac{1}{|\Gamma_\mu^{p,k}|} \int_{\Gamma_\mu^{p,k}} \mathbf{n}_\mu^p \, d\Gamma_\mu, \quad k = 1, \ldots, R_p. \tag{E.39}$$

Likewise, for partitions Γ_μ^j assumed over Γ_μ, it is possible to establish average normal vectors, which are defined as

$$\overline{\mathbf{n}}_\mu^{j} = \frac{1}{|\Gamma_\mu^{j}|} \int_{\Gamma_\mu^{j}} \mathbf{n}_\mu \, d\Gamma_\mu. \tag{E.40}$$

With all the elements introduced in the previous definitions, the following family of subspaces is proposed that restrict the spaces defined by (E.24) and (E.25)

$$\widetilde{\mathcal{U}}_\mu^{C_u}\left(\Omega_\mu\right) \equiv \left\{ \tilde{\mathbf{u}}_\mu \ \in \ \widetilde{\mathcal{U}}_\mu\left(\Omega_\mu\right); \int_{\Gamma_\mu^j} \tilde{\mathbf{u}}_\mu \ \otimes \ \left(\mathbf{n}_\mu - \overline{\mathbf{n}}_\mu^j\right) \, d\Gamma_\mu = \mathbb{O}, \ \forall j \in \mathcal{C}_u \right\}, \tag{E.41}$$

$$\widetilde{\mathcal{P}}_\mu^{\left(\overline{\mathbf{n}}_\mu^p\right),C_p}\left(\Omega_\mu^p\right) \equiv \left\{ \tilde{p}_\mu \ \in \ \widetilde{\mathcal{P}}_\mu^{\left(\overline{\mathbf{n}}_\mu^p\right)}\left(\Omega_\mu^p\right); \int_{\Gamma_\mu^{p,k}} \tilde{p}_\mu \ \left(\mathbf{n}_\mu^p - \overline{\mathbf{n}}_\mu^{p,k}\right) \, d\Gamma_\mu = \mathbf{0}, \ \forall k \in \mathcal{C}_p \right\}. \tag{E.42}$$

Clearly, we have $\widetilde{\mathcal{U}}_\mu^{C_u} \subset \widetilde{\mathcal{U}}_\mu$ and $\widetilde{\mathcal{P}}_\mu^{\left(\overline{\mathbf{n}}_\mu^p\right),C_p} \subset \widetilde{\mathcal{P}}_\mu^{\left(\overline{\mathbf{n}}_\mu^p\right)}$, since these spaces contain C_u and C_p additional constraints over non-overlapping regions, Γ_μ^j, with $j \in \mathcal{C}_u$ and $\Gamma_\mu^{p,k}$, with $k \in \mathcal{C}_p$. Note that, as indicated in (E.41)-(E.42), and given that $C_u \leq R_u$ and $C_p \leq R_p$, all partitions R_u and/or R_p can be used to impose additional constraints, or alternatively, to leave some regions unconstrained. In the latter case, the partitions of the boundary Γ_μ^j, with $j \in \mathcal{W}_u$ and $\Gamma_\mu^{p,k}$, with $k \in \mathcal{W}_p$, remain subject only to the restrictions inherent to the original MCMM$(\overline{\mathbf{n}}_\mu^p)$, which apply to the entire boundary of the MC and to the whole surface of the porous domain, respectively, see (E.24)–(E.25).

The numerical results section E.6 presents an illustrative application of the proposed model. For a more detailed discussion of its theoretical foundations, interested readers are referred to the specialized literature [21].

E.5. Constitutive laws based on Selective Order Expansions (SOE) for primal descriptors

In diffusion-reaction problems modeled using first-order homogenization, it has been extensively documented that the effective response depends on the micro-scale size [13, 72, 73, 82]. Among these cases, this phenomenon manifests itself in the fluid mass balance equation when dealing with saturated porous media [14, 16, 48]. To remove such dependence, which compromises the objectivity of the model and the very concept of the existence of RVE, a constitutive-type formulation based on multiscale modeling with Selective-Order Expansions is introduced, referred as the SOE-Multiscale approach [66, 68, 69]. In short, this method assumes different orders of expansion for the primitive descriptors that act as input variables in the constitutive functionals.

For the saturated porous subdomain Ω_μ^p, a Reduced-Order Expansion (ROE) is adopted for the pore-pressure rate at the micro-scale, expressed as $\dot{p}_\mu^{\text{ROE}} = \dot{p} + \dot{\tilde{p}}_\mu$, omitting exclusively the first-order term considered in (E.8), given by $\dot{\boldsymbol{\varphi}} \cdot \left(\mathbf{x}_\mu - \mathbf{x}_\mu^{Gp}\right)$. Conversely, the micro-scale strain rate is expanded with

Full-Order Expansion (FOE), denoted as $\dot{\boldsymbol{\varepsilon}}_\mu^{\text{FOE}}$, identical to the expression given in (E.9).

Thus, when evaluating the constitutive functions for the mechanical stress-type quantities $\{\dot{\boldsymbol{\sigma}}_\mu^p; \dot{\chi}_\mu\}$ using the expressions given by $\dot{p}_\mu^{\text{ROE}}$ and $\dot{\boldsymbol{\varepsilon}}_\mu^{\text{FOE}}$, we have

$$\dot{\boldsymbol{\sigma}}_\mu^p = \hat{\dot{\sigma}}_\mu^{p,\,\text{SOE}}\big(\dot{\boldsymbol{\varepsilon}}_\mu^{\text{FOE}}, \dot{p}_\mu^{\text{ROE}}\big) = \mathbf{C}_\mu^p \,:\, \big(\dot{\boldsymbol{\varepsilon}} + \dot{\tilde{\boldsymbol{\varepsilon}}}_\mu\big) \,-\, \mathbf{b}_\mu\,(\dot{p} + \dot{\tilde{p}}_\mu), \tag{E.43}$$

$$\dot{\chi}_\mu = \hat{\dot{\chi}}_\mu^{\text{SOE}}\big(\dot{\boldsymbol{\varepsilon}}_\mu^{\text{FOE}}, \dot{p}_\mu^{\text{ROE}}\big) = \mathbf{b}_\mu \,:\, \big(\dot{\boldsymbol{\varepsilon}} + \dot{\tilde{\boldsymbol{\varepsilon}}}_\mu\big) \,+\, \frac{1}{M_\mu}\,(\dot{p} + \dot{\tilde{p}}_\mu), \tag{E.44}$$

where $\mathbf{C}_\mu^p$, $\mathbf{b}_\mu$ and M_μ^{-1} represent, respectively, the elastic stiffness tensor of the porous skeleton, the Biot tensor and the storage parameter. In the isotropic case, $\mathbf{b}_\mu = b_\mu, \mathbf{I}$ with $b_\mu = 1 - \frac{K_\mu}{K_\mu^s}$, where K_μ and K_μ^s are the volumetric moduli of the skeleton and granular material, respectively. Furthermore, $\frac{1}{M_\mu} = \frac{b_\mu - n_\mu}{K_\mu^s} + \frac{n_\mu}{K_\mu^f}$, where K_μ^f is the volumetric modulus of the fluid and n_μ is the porosity. Finally, the hat symbol $(\hat{\bullet})$ denotes a constitutive functional.

The effective stress field, denoted $\boldsymbol{\sigma'}_\mu^p$, describes the mechanical variations of the porous skeleton and is obtained as

$$\dot{\boldsymbol{\sigma}}'^p_\mu = \hat{\dot{\sigma}}'^{p,\,\text{SOE}}_\mu\big(\dot{\boldsymbol{\varepsilon}}_\mu^{\text{FOE}}\big) = \mathbf{C}_\mu^p \,:\, \big(\dot{\boldsymbol{\varepsilon}} + \dot{\tilde{\boldsymbol{\varepsilon}}}_\mu\big). \tag{E.45}$$

For the seepage velocity vector $\boldsymbol{\mathcal{V}}_\mu$, we propose a Full-Order Expansion (FOE) for the micro-scale pore-pressure gradient, as in expression (E.10), denoted as $\boldsymbol{\varphi}_\mu^{\text{FOE}}$. Thus, with regard to the phenomenon of filtration at the micro-scale, Darcy's generalized law is assumed, which is written as

$$\boldsymbol{\mathcal{V}}_\mu = \hat{\mathcal{V}}_\mu^{\text{SOE}}\big(\boldsymbol{\varphi}_\mu^{\text{FOE}}\big) = \mathbf{k}_\mu \Big[-\big(\boldsymbol{\varphi} + \tilde{\boldsymbol{\varphi}}_\mu\big) + \rho_\mu^f\,\mathbf{g}\Big], \tag{E.46}$$

where $\mathbf{k}_\mu$ is the permeability tensor. For isotropic materials, $\mathbf{k}_\mu = k_\mu \mathbf{I}$ with $k_\mu = \frac{\kappa_\mu}{\rho_\mu^f |\mathbf{g}|}$, where κ_μ is the hydraulic conductivity, $\rho_\mu^f |\mathbf{g}|$ is the specific weight of the fluid, and $|\mathbf{g}|$ is the modulus of the acceleration of gravity.

Finally, in the subdomain Ω_μ^s occupied by impermeable solid inclusions, it is only required to specify the micromechanical response for $\dot{\boldsymbol{\sigma}}_\mu^s$. That is, it suffices to provide the constitutive relation for the stress state, which is completely defined by the elastic constitutive tensor of the solid particles $\mathbf{C}_\mu^s$. Thus, the constitutive law is expressed as

$$\dot{\boldsymbol{\sigma}}_\mu^s = \hat{\dot{\sigma}}_\mu^{s,\,\text{SOE}}\big(\dot{\boldsymbol{\varepsilon}}_\mu^{\text{FOE}}\big) = \mathbf{C}_\mu^s \,:\, \dot{\boldsymbol{\varepsilon}}_\mu^{\text{FOE}} = \mathbf{C}_\mu^s \,:\, \big(\dot{\boldsymbol{\varepsilon}} + \dot{\tilde{\boldsymbol{\varepsilon}}}_\mu\big), \tag{E.47}$$

Superscripts $(\bullet)^s$ and $(\bullet)^p$ are used to differentiate the stress state on Ω_μ^s or Ω_μ^p, respectively. Note that, for convenience, the constitutive definitions related to $\dot{\boldsymbol{\sigma}}_\mu$ and $\dot{\chi}_\mu$ are considered in rate format.

E.6. Numerical results

In this section, we evaluate the performance of the specific MCMM($\overline{\mathbf{n}}_\mu^p$) proposed in this work, defined by expressions (E.24)-(E.25), as well as the sub-models postulated in Section E.4, through two numerical examples.

In the first experiment, described in section E.6.1, a material with a periodic micro-structure is modeled, allowing us to establish quantitative comparisons with reference solutions. This case constitutes a first step toward verifying the viability of the proposed models. The micro-cell used during the homogenization process is selected taking into account geometries with internal inclusions, leading to $\mathbf{n}_\mu^p$-balanced (and $\mathbf{n}_\mu^s$-balanced) configurations.

In Section E.6.2, the potential of the multiscale framework developed is explored by solving a two-dimensional consolidation problem in a stratum containing a completely random distribution of inclu-

sions. This type of micro-structure generally leads to $\mathbf{n}_\mu^p$-unbalanced (and $\mathbf{n}_\mu^s$-unbalanced) micro-cell designs. The reference solution for this example is obtained employing Direct Numerical Simulation (DNS).

In order to focus on the applicability of the multiscale model, the following simplifying assumptions are made:

- Body forces are neglected: $\mathbf{f} \equiv \mathbf{f}_\mu \equiv \mathbf{0}$.
- Hydrostatic pore-pressure due to the water table position is not accounted for. Under this circumstance, the variable "p" (as well as "p_μ" and "$\tilde{p}_\mu$") must be interpreted as the "*excess of pore-pressure*" generated exclusively by the external load ($\mathbf{t}$) during the consolidation process.
- As a consequence of the previous hypothesis, the gravity effect in the micro-scale Darcy constitutive model must be neglected (recall (E.46)).
- A plane strain state is assumed.

In both examples, the same material properties are used, corresponding to a saturated porous matrix with non-porous solid inclusions. The values adopted are summarized in Table E.1, omitting the subscript $(\bullet)_\mu$ for simplicity, since the properties also apply to the DNS solution. Furthermore, in both numerical experiments we adopt the SOE-Multiscale procedure for the porous media subdomain Ω_μ^p. The fluid density is used only to establish the hydraulic conductivity κ_μ. Our implementation considers quadrangular, isoparametric finite elements with biquadratic shape functions for the displacement field and bilinear shape functions for pore-pressure, in order to satisfy the convergence requirements of Babuška-Brezzi.

Material properties	Matrix Ω^p	Inclusions Ω^s
Young's modulus E^0 $[kPa]$	40000	6×10^7
Poisson's ratio ν	0.4	0.3
Hydraulic conductivity $\kappa_1 = \kappa_2$ $[m/\text{day}]$	8.64×10^{-6}	-
Initial void ratio e^0	1.4	-
Bulk modulus of the soil grain K^s $[kPa]$	21×10^6	-
Bulk modulus of the fluid K^f $[kPa]$	22.5×10^5	-
Fluid density ρ^f $[kg/m^3]$	1000	-

Tabla E.1: Material properties of the heterogeneous composite for both examples.

E.6.1. Example 1: Periodic micro-structure with internal inclusions

The first example consists of a saturated porous matrix containing impermeable solid inclusions of cylindrical geometry, arranged in a structured manner following two orthogonal periodicity directions. This configuration represents a simple micro-structure, whose macroscopic scheme is illustrated in Figure E.3a.

In turn, Figure E.3b shows the designs of the adopted micro-cell, called MC_1. In this case, the inclusions are completely contained within the micro-cell, without intercepting its boundary. Therefore, it is an MC $\mathbf{n}_\mu^p$-balanced (and also $\mathbf{n}_\mu^s$-balanced), that is, $\overline{\mathbf{n}}_\mu^p = \mathbf{0}$ (see definitions in (E.2) and (E.3)). The objective of this example is to evaluate the performance of the proposed multiscale framework for this particular type of micro-cell, assessing the impact on the effective response of the material.

Given these geometric characteristics, the boundary of the porous subdomain is coincident with the boundary of the entire MC, so that $\Gamma_\mu^p = \Gamma_\mu$ and $\mathbf{n}_\mu^p = \mathbf{n}_\mu$ along the entire boundary. This coincidence allows us to assume an identical partition scheme in the surface domains, such that the number of additional constraints applied to the spaces $\widetilde{\mathcal{U}}_\mu$ and $\widetilde{\mathcal{P}}_\mu^{(\overline{\mathbf{n}}_\mu^p = \mathbf{0})}$ are the same.

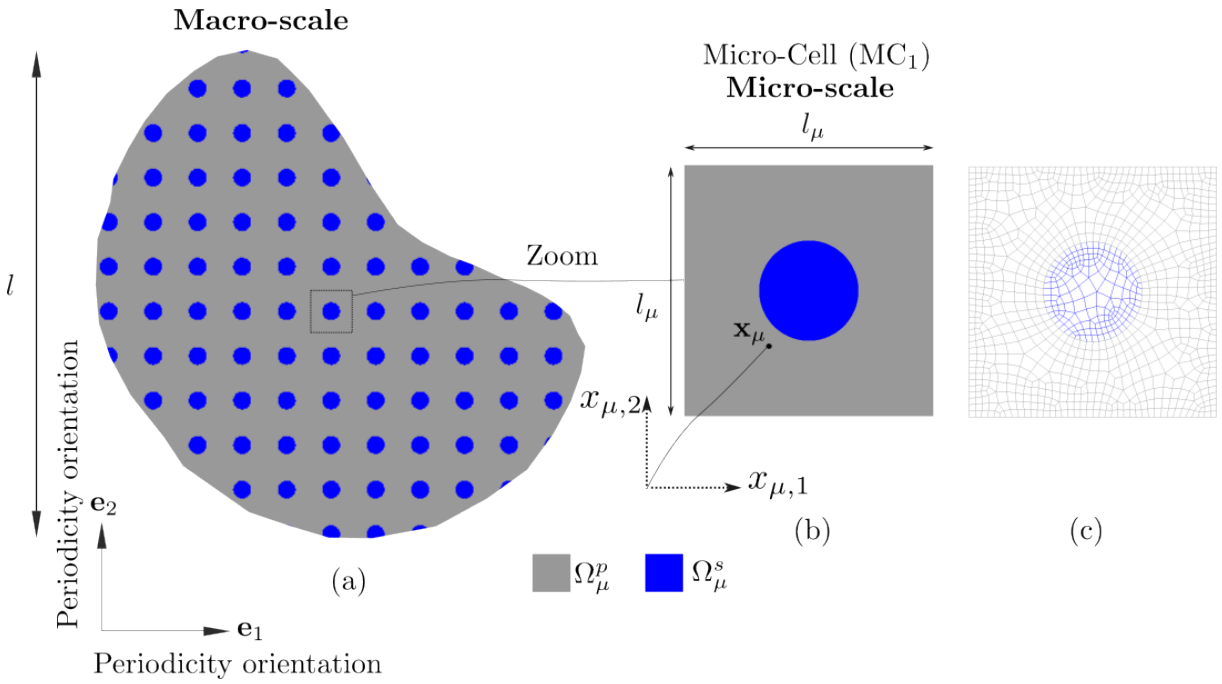

Figura E.3: Matrix with an arrangement of embedded cylindrical inclusions. Basic geometry. (a) Macro-scale layout. (b) Relative dimensions for MC$_1$ (l_μ being a generic micro-scale length parameter). (c) Finite element meshes used to discretize MC$_1$

Consequently, we can simplify the notation throughout this section by considering sets and subsets of equivalent indices, that is: $\mathcal{R}_u = \mathcal{R}_p = \mathcal{R}$, $\mathcal{C}_u = \mathcal{C}_p = \mathcal{C}$, and $\mathcal{W}_u = \mathcal{W}_p = \mathcal{W}$. The corresponding numbers of elements in each case are $R = \text{card}\,(\mathcal{R})$, $C = \text{card}\,(\mathcal{C})$ and $W = \text{card}\,(\mathcal{W})$. Thus, the subspaces defined in (E.41) and (E.42) are denoted, respectively, as $\widetilde{\mathcal{U}}^C_\mu$ and $\widetilde{\mathcal{P}}^{(\bar{\mathbf{n}}^p_\mu=\mathbf{0}),C}_\mu$.

The mesh used to discretize MC$_1$ contains 965 finite elements and is shown in Figure E.3c. The material properties correspond to those summarized in Table E.1, and the volumetric fraction of inclusions is $\eta^s = \frac{\Omega^s_\mu}{\Omega_\mu} = 0.125$.

The macroscopic quantities inserted into MC$_1$ for the different cases analyzed are defined as follows: (i) a zero macroscopic displacement vector $\mathbf{u} = \mathbf{0}\,m$, (ii) a macro-scale strain tensor defined as

$$\boldsymbol{\varepsilon} = \begin{bmatrix} 0.0 & 1.0 \\ 1.0 & 2.5 \end{bmatrix} 1e-04,$$

expressed in terms of the macro-scale basis vectors $\{\mathbf{e}_1, \mathbf{e}_2\}$, (iii) a macroscopic pore-pressure of $p = 75kPa$, and (iv) a pore-pressure gradient vector, established as

$$\boldsymbol{\varphi} = \begin{bmatrix} -10 \\ -30 \end{bmatrix} \frac{kPa}{m}, \tag{E.48}$$

In this example, different homogenization schemes are compared, where we consider the following cases:

- Conventional periodic model (Per), as indicated in expressions (60)-(61), which also constitutes the reference solution in this example.
- Linear Model (Lin), according to the definition presented in (58)-(59).
- MCMM($\mathbf{0}$) model, given by the spaces $\widetilde{\mathcal{U}}_\mu$ and $\widetilde{\mathcal{P}}^{(\mathbf{0})}_\mu$ defined in (E.24)-(E.25). In this model, co-

rresponding to the case of minimal constraints, we have that $\overline{\mathbf{n}}_{\mu}^{p} = \mathbf{0}$, since the micro-cell MC_1 is $\mathbf{n}_{\mu}^{p}$-balanced.

- $\mathrm{MCMM}(\mathbf{0})_4^4$ sub-model, which represents a sub-model included in $\mathrm{MCMM}(\mathbf{0})$. The subscript 4 indicates the introduction of four additional constraints with respect to the space $\widetilde{\mathcal{U}}_{\mu}$, while the superscript 4 indicates the incorporation of four additional constraints to the space $\widetilde{\mathcal{P}}_{\mu}^{(\mathbf{0})}$. Thus, this sub-model is characterized by the functional spaces

$$\widetilde{\mathcal{U}}_{\mu}^{4} \equiv \left\{ \tilde{\mathbf{u}}_{\mu} \in \widetilde{\mathcal{U}}_{\mu};\ \int_{\Gamma_{\mu}^{i}} \tilde{\mathbf{u}}_{\mu} \otimes \left(\mathbf{n}_{\mu} - \overbrace{\overline{\mathbf{n}}_{\mu}^{i}}^{\mathbf{0}} \right) d\Gamma_{\mu} = \mathbb{O},\ \forall\, i \in \mathcal{C} \right\}, \tag{E.49}$$

$$\widetilde{\mathcal{P}}_{\mu}^{(\mathbf{0}),4} \equiv \left\{ \tilde{p}_{\mu} \in \widetilde{\mathcal{P}}_{\mu}^{(\mathbf{0})};\ \int_{\Gamma_{\mu}^{i}} \tilde{p}_{\mu} \left(\mathbf{n}_{\mu} - \overbrace{\overline{\mathbf{n}}_{\mu}^{i}}^{\mathbf{0}} \right) d\Gamma_{\mu} = \mathbf{0},\ \forall\, i \in \mathcal{C} \right\}, \tag{E.50}$$

  where each Γ_{μ}^{i} is defined according to the layout shown in Figure E.4a. We then have that $\mathcal{R} = \{1,2,3,4,5,6\}$, $\mathcal{C} = \{3,4,5,6\}$ and $\mathcal{W} = \{1,2\}$, where $C = \mathrm{card}\,(\mathcal{C}) = 4$. The set $\mathcal{W} = \{1,2\}$ identifies the partitions that preserve only the restrictions of $\mathrm{MCMM}(\mathbf{0})$ (that is, the spaces $\widetilde{\mathcal{U}}_{\mu}$ and $\widetilde{\mathcal{P}}_{\mu}^{(\mathbf{0})}$). From the pairs of spaces (E.24)-(E.25) and (E.49)-(E.50), we have that $\widetilde{\mathcal{U}}_{\mu}^{4} \subset \widetilde{\mathcal{U}}_{\mu}$ and $\widetilde{\mathcal{P}}_{\mu}^{(\mathbf{0}),4} \subset \widetilde{\mathcal{P}}_{\mu}^{(\mathbf{0})}$. The $\mathrm{MCMM}(\mathbf{0})_4^4$ model produces a system of five reactive traction and five reactive fluxes $(C+1=5)$, all independent of each other. Four pairs of traction-flux act on each Γ_{μ}^{i} with $i = 3,4,5,6$, while the remaining pair acts on the complement of these (i.e that is, on Γ_{μ}^{1}-Γ_{μ}^{2}). Altogether, the system of global reactive traction and fluxes is $\mathbf{t}_{\mu}$-balanced and q_{μ}-balanced at the boundary Γ_{μ}, according to definitions (76) and (77).

- $\mathrm{MCMM}(\mathbf{0})_{16}^{16}$ sub-model, which incorporates sixteen additional constraints with respect to the spaces defined by $\mathrm{MCMM}(\mathbf{0})$. To construct the partitions, first each side of micro-cell MC_1 is divided into ten segments of length $0.1\,l_{\mu}$. Next, the central partitions Γ_{μ}^{1} and Γ_{μ}^{2} are defined from the two contiguous central segments, so that the combined length of each is $0.2\,l_{\mu}$. The remaining partitions, $\Gamma_{\mu}^{i},\ \forall i \in \mathcal{C}$ of length $0.1\,l_{\mu}$ are distributed symmetrically on both sides of these central partitions, as illustrated in Figure E.4b. This model is characterized by the functional spaces $\widetilde{\mathcal{U}}_{\mu}^{16} \subset \widetilde{\mathcal{U}}_{\mu}$ and $\widetilde{\mathcal{P}}_{\mu}^{(\mathbf{0}),16} \subset \widetilde{\mathcal{P}}_{\mu}^{(\mathbf{0})}$. For this case, we have $\mathcal{R} = \{1,2,3,\ldots,18\}$, $\mathcal{C} = \{3,4,\ldots,18\}$ and $\mathcal{W} = \{1,2\}$, where $C = \mathrm{card}\,(\mathcal{C}) = 16$. This model produces a system of seventeen reactive traction forces and seventeen reactive fluxes $(C+1=17)$, all independent of each other.

- $\mathrm{MCMM}(\mathbf{0})_{36}^{36}$ sub-model, that introduces thirty-six additional constraints, characterized by the spaces $\widetilde{\mathcal{U}}_{\mu}^{36} \subset \widetilde{\mathcal{U}}_{\mu}$ and $\widetilde{\mathcal{P}}_{\mu}^{(\mathbf{0}),36} \subset \widetilde{\mathcal{P}}_{\mu}^{(\mathbf{0})}$, comprising the partitions $\Gamma_{\mu}^{i},\ \forall i \in \mathcal{C}$. Although this case is not shown, the partition scheme is constructed by dividing each side of micro-cell MC_1 into segments of length $0.05\,l_{\mu}$. The two contiguous central segments on each side form the partitions Γ_{μ}^{1}–Γ_{μ}^{2}, which thus have a length per side of $0.1\,l_{\mu}$ and are located in a position analogous to the partitions Γ_{μ}^{1}–Γ_{μ}^{2} illustrated in Figure E.4b. The other partitions maintain the extension of $0.05\,l_{\mu}$ and are distributed symmetrically on both sides of these central partitions. Thus, the sets $\mathcal{R} = \{1,2,3,\ldots,38\}$, $\mathcal{C} = \{3,4,\ldots,38\}$ and $\mathcal{W} = \{1,2\}$ are considered, with $C = \mathrm{card}\,(\mathcal{C}) = 36$. There will be a system of thirty-three reactive traction forces and thirty-three reactive fluxes $(C+1=37)$, all mutually independent.

For the sake of brevity, the functional spaces corresponding to the $\mathrm{MCMM}(\mathbf{0})_{16}^{16}$ and $\mathrm{MCMM}(\mathbf{0})_{36}^{36}$ sub-models are not explicitly detailed. However, these are analogous to those defined in (E.49)-(E.50), diffe-

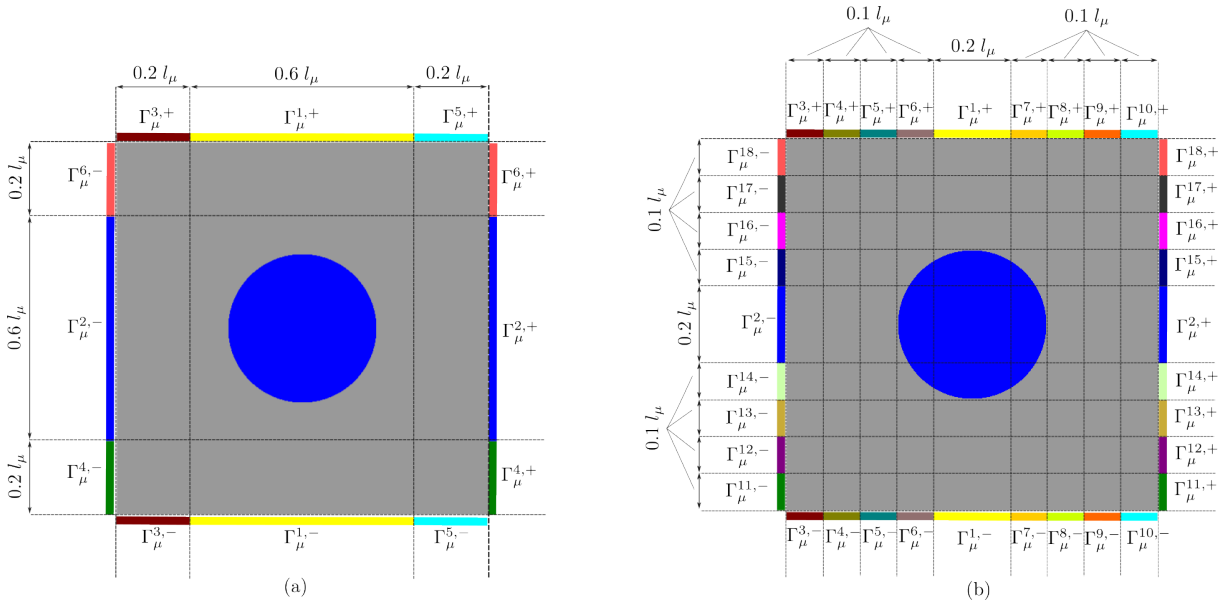

Figura E.4: Matrix with an arrangement of embedded cylindrical inclusions. (a) MC_1 with a 6-partition scheme. (b) MC_1 with an 18-partition scheme.

ring only in the greater number of integrals used as constraints. In all cases, the means of the normals on the partitions Γ_μ^i are zero, that is, $\overline{\mathbf{n}}_\mu^i = \mathbf{0}$.

E.6.1.1. Comparison parameters and results

Under the argument that, within the framework of the theory of infinitesimal transformations and the hypothesis of linear elasticity, and without considering the inaccuracies inherent in the finite element approximation, the MC presented in Figure E.3b, subjected to periodic boundary conditions in the fields of displacement and pressure fluctuations, provides the "true" homogenized response of the periodic material, the results obtained using this model are adopted as the reference solution.

To perform a convergence study with respect to the reference solution, we calculate the nine homogenized constitutive operators $\left\{ \frac{\partial \dot{\boldsymbol{\sigma}}}{\partial \boldsymbol{\varepsilon}}; \frac{\partial \dot{\boldsymbol{\sigma}}}{\partial \boldsymbol{\varphi}}; \frac{\partial \dot{\boldsymbol{\sigma}}}{\partial p}; \frac{\partial \boldsymbol{\mathcal{V}}}{\partial \boldsymbol{\varepsilon}}; \frac{\partial \boldsymbol{\mathcal{V}}}{\partial \boldsymbol{\varphi}}; \frac{\partial \boldsymbol{\mathcal{V}}}{\partial p}; \frac{\partial \dot{\chi}}{\partial \boldsymbol{\varepsilon}}; \frac{\partial \dot{\chi}}{\partial \boldsymbol{\varphi}}; \frac{\partial \dot{\chi}}{\partial p} \right\}$ (see [16, 66, 67]), for each of the multiscale models considered and using the micro-cell MC_1. For each of these operators, we calculate a global convergence measure, denoted by $\zeta_{(\bullet)}$, which quantifies the relative percentage discrepancy in terms of the L_2 norm between each homogenized constituent operator and its corresponding reference value (Per). Values close to zero imply a satisfactory approximation. This parameter can be expressed as

$$\zeta_{(\bullet)} = \frac{|| \, (\bullet) - (\bullet)_{\text{Per}} \, ||_2}{|| \, (\bullet)_{\text{Per}} \, ||_2} \, 100 \, \% \tag{E.51}$$

where $(\bullet)$ denotes each of the nine tangent operators computed for the proposed models, whereas $(\bullet)_{\text{Per}}$ identifies the reference constitutive operator, that is, the one obtained with the Periodic model. Although these parameters provide a preliminary indication of the potential performance of each model, more rigorous assessments would be required to determine which model is ultimately more suitable.

It should be noted that, due to the particular characteristics of the micro-cell analyzed, the operators $\frac{\partial \boldsymbol{\mathcal{V}}}{\partial p}$ and $\frac{\partial \dot{\chi}}{\partial \boldsymbol{\varphi}}$ present results with all their components equal to zero (values of the order of machine zero, i.e., of the order of 1×10^{-15} or even smaller). Consequently, the calculation of the parameters $\zeta_{\frac{\partial \boldsymbol{\mathcal{V}}}{\partial p}}$ and $\zeta_{\frac{\partial \dot{\chi}}{\partial \boldsymbol{\varphi}}}$ is discarded.

Numerical results in terms of the discrepancy parameters $\zeta_{(\bullet)}$ are presented in Table E.2. In general,

Parameter	Lin	MCMM$(\mathbf{0})$	MCMM$(\mathbf{0})^4_4$	MCMM$(\mathbf{0})^{16}_{16}$	MCMM$(\mathbf{0})^{36}_{36}$
$\zeta_{\frac{\partial \dot{\boldsymbol{\sigma}}}{\partial \boldsymbol{\varepsilon}}}$	0.70	1.66	0.23	$4.8e-03$	$5.25e-04$
$\zeta_{\frac{\partial \dot{\boldsymbol{\sigma}}}{\partial \boldsymbol{\varphi}}}$	107.84	87.91	9.47	1.58	0.34
$\zeta_{\frac{\partial \dot{\boldsymbol{\sigma}}}{\partial p}}$	$1.01e-04$	$7.90e-05$	$1.15e-05$	$2.74e-07$	$3.02e-08$
$\zeta_{\frac{\partial \boldsymbol{\mathcal{V}}}{\partial \boldsymbol{\varepsilon}}}$	99.74	64.84	21.25	5.93	1.75
$\zeta_{\frac{\partial \boldsymbol{\mathcal{V}}}{\partial \boldsymbol{\varphi}}}$	2.14	0.22	0.06	$9.82e-04$	$8.64e-05$
$\zeta_{\frac{\partial \dot{\chi}}{\partial \boldsymbol{\varepsilon}}}$	$1.01e-04$	$7.90e-05$	$1.15e-05$	$2.74e-07$	$3.02e-08$
$\zeta_{\frac{\partial \dot{\chi}}{\partial p}}$	$7.85e-06$	$6.14e-06$	$8.97e-07$	$2.13e-08$	$2.34e-09$

Tabla E.2: Comparison parameters for each of the models applied to MC_1.

it can be observed that the Linear and MCMM$(\mathbf{0})$ models show reasonable behavior with respect to the reference solution, with error values below $5\,\%$, except for two parameters determined by the tangent operators, whose percentage values are significantly higher.

The simple numerical example presented suggests that the possibility of incorporating partitions on the boundary in which additional constraints are defined enables us to generate a broad family of admissible multiscale sub-models of the minimum constraint model, which can significantly improve predictive capability in multiscale simulations. In particular, this strategy offers the opportunity to analyze microstructures with fields defined only in certain parts of the entire MC, a situation in which the Periodic model is no longer applicable, while also yielding more accurate approximations than those provided by the MCMM and Linear models.

On the other hand, the results provided by the MCMM$(\mathbf{0})^4_4$, MCMM$(\mathbf{0})^{16}_{16}$, and MCMM$(\mathbf{0})^{36}_{36}$ sub-models show a notable improvement in all the parameters analyzed, as can be seen in columns 4 to 6 of Table E.2. In fact, the effective constitutive response provided by the MCMM$(\mathbf{0})^{36}_{36}$ model shows insignificant discrepancies in practical terms, with all parameters below $2\,\%$ error. Overall, the results confirm that each operator progressively tends toward the reference solution as additional constraints are incorporated into the sub-models, compared to the original MCMM$(\mathbf{0})$ model.

E.6.2. Example 2: random micro-structure 2D consolidation problem

This example analyzes the effective response of a material with a random distribution of irregular solid inclusions. Figure E.6a illustrates a representative diagram of the typical topology considered at the micro-scale. Any micro-cell extracted from this type of micro-architecture design has the following peculiarities with regard to the micro-scale pore-pressure field:

- There is no periodicity bias; it is not possible to verify or assume a specific geometric correspondence (in any direction). Consequently, the widely used periodic homogenization model is not a viable option in this case.
- The minimum size of the micro-cell at which the homogenized response becomes insensitive to size (that is, the RVE) is not known a priori.
- There are no rigorous reference solutions.
- There are no well-established analytical or numerical lower limits in this context.
- The edges of each micro-cell inevitably intersect a variable number of inclusions, generating irregular shapes of random size and position, many of which reach the boundaries of the micro-cell. Consequently, $\mathbf{n}^p_\mu$-unbalanced ($\mathbf{n}^s_\mu$-unbalanced) micro-cell designs are obtained.

E.6.2.1. Random geometry generation

The topology representing the micro-structure of the material, whose macroscopic scheme is illustrated in Figure E.6a, has a configuration similar to that of a honeycomb, with the difference that the voids are replaced by non-porous solid inclusions. This micro-architecture was artificially designed following the procedure described in [21], which, in turn, is based on methodologies proposed in previous works [131–133].

The methodology consists of generating a sufficiently large grid of points, called $\mathcal{G}_p$, composed of a total of n_{points} points ($p = 1, 2, \ldots, n_{points}$), arranged with a regular spacing of $0.02\,m \times 0.02\,m$. This geometric regularity is then randomly disturbed by modifying the coordinates of each point in both directions, with a maximum deviation of $0.01m$. From the set of disturbed coordinates, a Voronoi tessellation, $\mathcal{T}_{\mathcal{G}_p}$, is constructed, in which each point p is associated with a Voronoi cell characterized by an irregular polygon $\mathcal{I}_p$ ($p = 1, 2, \ldots, n_{points}$).

Next, each polygon $\mathcal{I}_p$ is contracted toward its interior point p by means of a parallel displacement operation of all its edges. The displacement distance is defined with a constant value $d_{offset} = 0.007\,m$. During this stage, numerous elementary geometric operations (line intersections, line cuts, object deletions, among others) are performed in order to correctly define the new, smaller contracted polygons, each of which is identified as $\mathcal{I}_p^c$ ($p = 1, 2, \ldots, n_{points}$). It is possible that the polygon class may change between $\mathcal{I}_p$ and $\mathcal{I}_p^c$, since $\mathcal{I}_p^c$ has a number of sides equal to or less than $\mathcal{I}_p$.

The area bounded by each polygon $\mathcal{I}_p^c$, denoted $\mathcal{A}_{\mathcal{I}_p^c}$, represents a solid inclusion in the micro-structural pattern. Recalling the geometric entities defined above, we have: $\Omega_\mu^s = \cup_{p=1}^{n_{points}} \mathcal{A}_{\mathcal{I}_p^c}$ and $\Gamma_\mu^i = \cup_{p=1}^{n_{points}} \mathcal{I}_p^c$. The remaining space, not occupied by inclusions, constitutes the domain of the saturated porous medium, Ω_μ^p. Therefore, the matrix Ω_μ^p forms an interconnected network of panels of constant thickness, which in this case is twice the displacement distance d_{offset}. The result is a micro-structure with an intricate and realistic morphology, as illustrated in Figure E.6a.

E.6.2.2. Characterization of the analyzed problem

The problem to be addressed is outlined in Figure E.5. It shows that, when considering certain symmetry conditions, the domain of analysis is obtained together with the necessary boundary conditions. The applied vertical load $\mathbf{F}$ is transferred over the surface of the layer over a length of $1.5m$, which corresponds to the total length of the footing. However, for symmetry reasons, only half of this length is considered in the analysis domain, i.e., $0.75m$. Thus, a uniformly distributed load $\mathbf{t} = [0,\, \bar{\mathrm{t}}]^T$ is applied, which evolves linearly and monotonically from $0kPa$ to $-500kPa$ during the first day of analysis and then remains constant around that minimum value for the rest of the process. The time sequence is set logarithmically as $t = [0.1, 0.2, \ldots,\, 0.8, 0.9, 1, 2, 3, \ldots, 8, 9, 10, 20, 30, \ldots, 90, 100, 200, 300, \ldots]$ (in days), reaching a maximum time of $t_{\mathrm{máx}} = 10000$ days.

Following the rules presented above, a two-dimensional analysis domain with width $W = 1.5\,m$ and height $H = 3.5\,m$ is generated, as shown in Figure E.6a, referred to as single-scale (SS). This domain has a volumetric fraction of solid inclusions of $\eta_{\mathrm{SS}}^s = 0.3362$. DNS techniques are used on the single-scale domain to obtain the reference response. From the domain described, square windows of fixed size $l_\mu \times l_\mu$ with $l_\mu = 0.1\,m$ are isolated, located at random positions within the entire domain, to define different micro-cells, as illustrated in Figure E.6b. Among all possible MCs, one is selected arbitrarily, referred to for simplicity as MC_1, as shown in Figure E.6c.2. This MC_1 represents the micro-scale associated with each Gaussian point of the macro-scale domain, represented in Figure E.6c.1, and together they define the multiscale model used to calculate the homogenized response (see Figure E.6c). MC_1 has a characteristic imbalance vector at the limits $\overline{\mathbf{n}}_\mu^p = \left[\overline{\mathrm{n}}_{\mu\,1}^p, \overline{\mathrm{n}}_{\mu\,2}^p\right]^T = \left[-0.0752, 0.0724\right]^T$ and the volumetric fraction of inclusions is $\eta_{\mathrm{MC}_1}^s = 0.3361$, which implies a relative percentage error with respect to the single-scale domain of $\frac{|\eta_{\mathrm{MC}_1}^s - \eta_{\mathrm{SS}}^s|}{|\eta_{\mathrm{SS}}^s|}\,100\,\% = 0.03\,\%$.

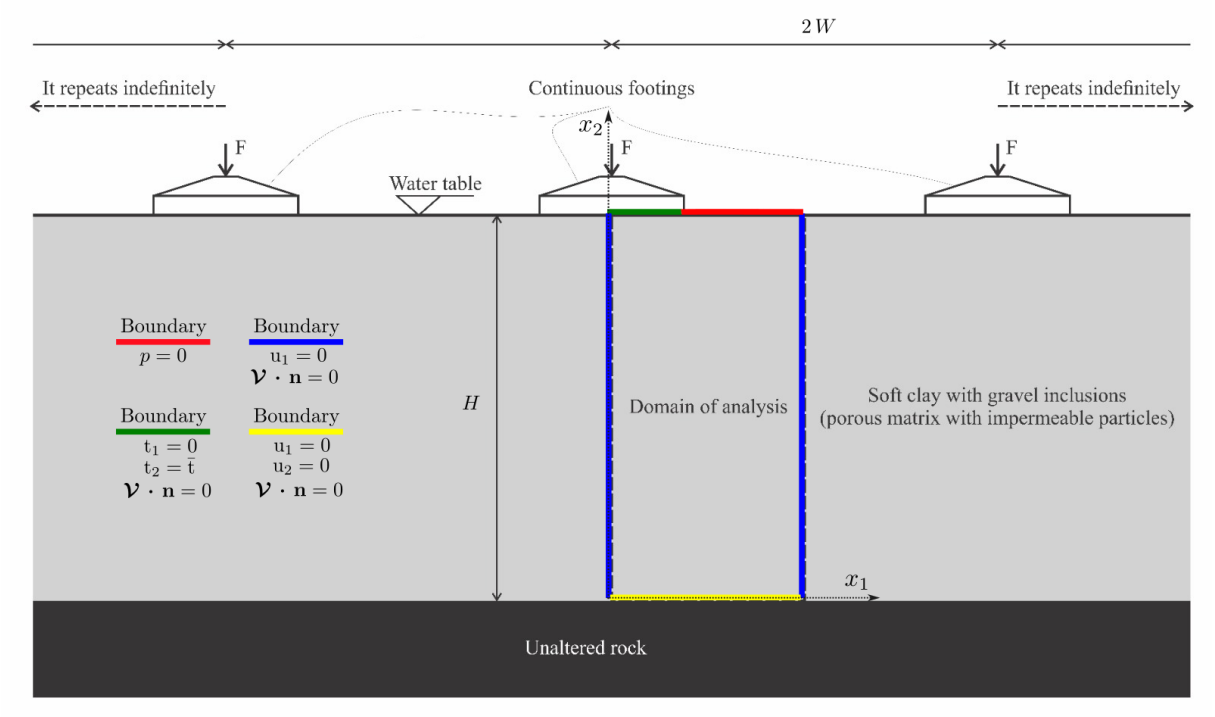

Figura E.5: Analyzed problem. Domain of analysis and boundary conditions.

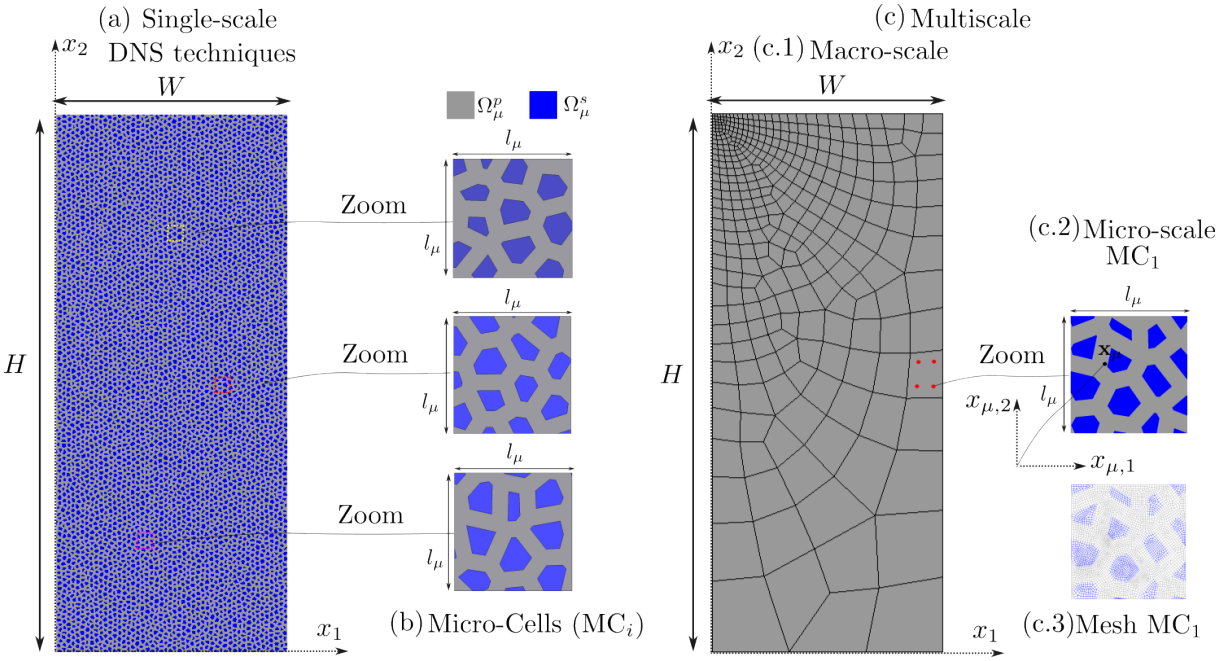

Figura E.6: Analyzed problem. (a) Single-scale model layout (drawing not to scale). (b) Different micro-cells extracted from the general model (Mono-scale domain). (c) Multiscale procedure applied to the 2D-consolidation phenomenon (drawing not to scale). General model layout: (c.1) Macro-scale; (c.2) Micro-scale; (c.3) finite element mesh used to discretize MC_1.

For the finite element method solution, the single-scale domain is discretized using 1112003 quadrilateral elements and 3340230 nodes (the mesh is not shown for clarity). In the multiscale model, the macro-scale is discretized with 349 quadrilateral finite elements and 1126 nodes (see Figure E.6c.1), while MC_1 is meshed with 965 elements and 3056 nodes (see Figure E.6c.3). The material properties are summarized in Table E.1.

Following the proposed general framework, alternative homogenization schemes can be selected simply by imposing specific constraints at the micro-cell level. Since sub-models allow additional conditions to be applied to the MCMM($\overline{\mathbf{n}}_\mu^p$) model in order to obtain a more accurate homogenized response, as demonstrated in Section E.6.1, this model is not considered in the present example. Instead, only the multiscale models listed below are analyzed:

- Linear Model (Lin), according to the definition presented in (58)-(59).
- MCMM($\overline{\mathbf{n}}_\mu^p$)$_4^4$ sub-model, which represents a sub-model included in MCMM($\overline{\mathbf{n}}_\mu^p$). The sub-model introduces four additional constraints with respect to the space $\widetilde{\mathcal{U}}_\mu$ and four to $\widetilde{\mathcal{P}}_\mu^{(\overline{\mathbf{n}}_\mu^p)}$. Thus, this sub-model is characterized by the functional spaces

$$\widetilde{\mathcal{U}}_\mu^4 \equiv \left\{ \tilde{\mathbf{u}}_\mu \in \widetilde{\mathcal{U}}_\mu; \int_{\Gamma_\mu^j} \tilde{\mathbf{u}}_\mu \otimes \left(\mathbf{n}_\mu - \overline{\mathbf{n}}_\mu^j\right) d\Gamma_\mu = \mathbb{O}, \forall j \in \mathcal{C}_u \right\}, \tag{E.52}$$

$$\widetilde{\mathcal{P}}_\mu^{(\overline{\mathbf{n}}_\mu^p),4} \equiv \left\{ \tilde{p}_\mu \in \widetilde{\mathcal{P}}_\mu^{(\overline{\mathbf{n}}_\mu^p)}; \int_{\Gamma_\mu^{p,k}} \tilde{p}_\mu \left(\mathbf{n}_\mu - \overline{\mathbf{n}}_\mu^k\right) d\Gamma_\mu = \mathbf{0}, \ \forall k \in \mathcal{C}_p \right\}, \tag{E.53}$$

  The partitions corresponding to the micro-cell boundary, whose purpose is to increase the restrictions of the displacement fluctuations field defined in (E.52), are obtained by first considering the boundary of the inclusions Γ_μ^s, on which the partitions Γ_μ^1 and Γ_μ^2 are established (remembering that $\Gamma_\mu^j = \Gamma_\mu^{j,-} \bigcup \Gamma_\mu^{j,+}$) as shown in Figure E.7a. Then, as shown in Figure E.7b, the additional partitions Γ_μ^3 to Γ_μ^6 are defined, which are applied exclusively on the contour of the porous medium Γ_μ^p, acting on sections of length $0.5\ l_\mu$ each. Together, these six partitions constitute the final scheme shown in Figure E.7c. Thus, we have the sets $\mathcal{R}_u = \{1,2,3,4,5,6\}$, $\mathcal{C}_u = \{3,4,5,6\}$ and $\mathcal{W}_u = \{1,2\}$, where $C_u = \text{card}\,(\mathcal{C}_u) = 4$. On the other hand, additional restrictions on the field of pore-pressures fluctuations can only be imposed on the saturated porous medium portion, that is, on the boundary Γ_μ^p. For this, the partition scheme presented in Figure E.8 is adopted, from which the six sub-regions $\Gamma_\mu^{p,k}$ of space E.53 are defined. Thus, we have that $\mathcal{R}_p = \{1,2,3,4,5,6\}$, $\mathcal{C}_p = \{3,4,5,6\}$ and $\mathcal{W}_p = \{1,2\}$, where $C_p = \text{card}\,(\mathcal{C}_p) = 4$. The sets $\mathcal{W}_u = \{1,2\}$ and $\mathcal{W}_p = \{1,2\}$ identify the partitions that exclusively preserve the constraints of the model MCMM($\overline{\mathbf{n}}_\mu^p$). From the pairs of spaces (E.24)-(E.25) and (E.52)-(E.53), we have that $\widetilde{\mathcal{U}}_\mu^4 \subset \widetilde{\mathcal{U}}_\mu$ and $\widetilde{\mathcal{P}}_\mu^{(\overline{\mathbf{n}}_\mu^p),4} \subset \widetilde{\mathcal{P}}_\mu^{(\overline{\mathbf{n}}_\mu^p)}$. The MCMM($\overline{\mathbf{n}}_\mu^p$)$_4^4$ model produces a system of five reactive traction and five reactive fluxes ($C+1=5$), all independent of each other. Four traction act on each Γ_μ^j with $j = 3,4,5,6$, while the remaining pair acts on the complement of these (that is, on Γ_μ^1-Γ_μ^2). Analogous, four flux act on each $\Gamma_\mu^{p,k}$ with $k = 3,4,5,6$, while the remaining pair acts on the complement of these. Altogether, the system of global reactive traction and fluxes is $\mathbf{t}_\mu$-balanced and q_μ-balanced at the boundary Γ_μ, according to definitions (76) and (77).

E.6.2.3. Homogenized results

First, a qualitative comparison is carried out between the responses obtained by the two multiscale models and the single-scale reference solution (DNS). Specifically, the contour map of the vertical displacement field u_2 at time $t_{max} = 10000\ days$ shown in Figure E.9 is examined. It can be seen that the

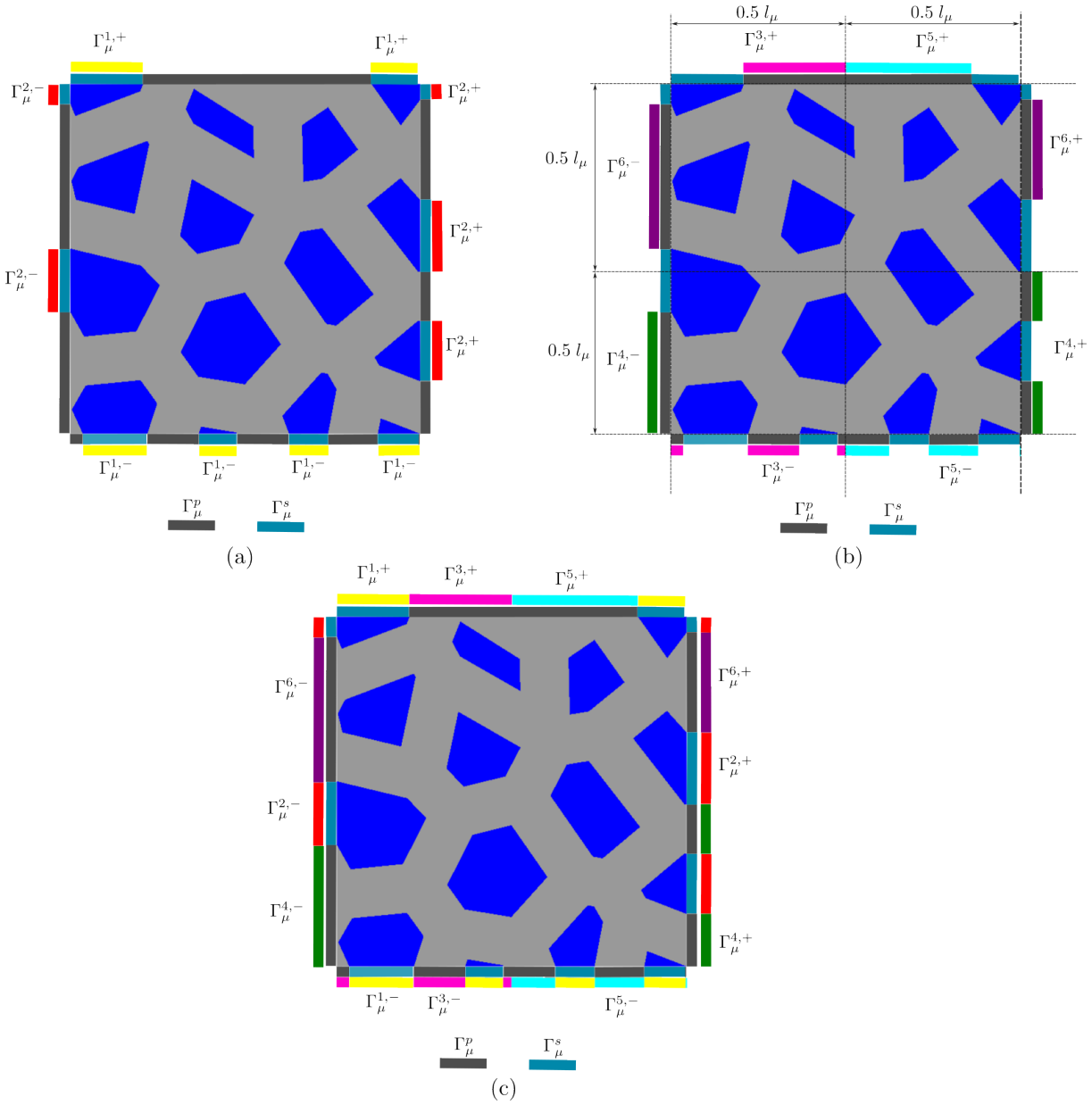

Figura E.7: Matrix with randomly distributed embedded cylindrical inclusions. Partition scheme for micro-scale displacement fluctuation: (a) MC_1 with a 2-partition scheme for Γ_μ^S. (b) MC_1 with an 4-partition scheme for Γ_μ^S. (c) MC_1 with an 6-partition scheme for Γ_μ.

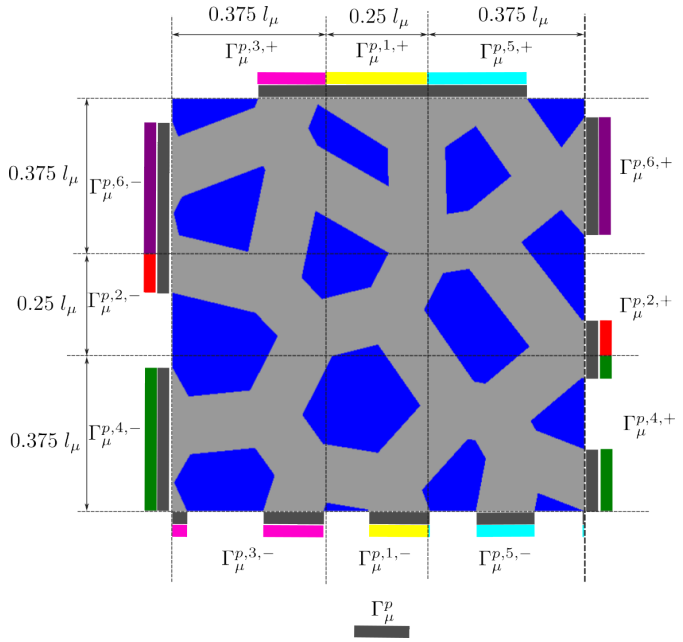

Figura E.8: Matrix with randomly distributed embedded cylindrical inclusions. Partition scheme for micro-scale pore-pressure fluctuation: MC_1 with an 6-partition scheme for Γ_μ^p.

$\mathrm{MCMM}(\overline{\mathbf{n}}_\mu^p)_4^4$ model in Figure E.9(b) produces a displacement field very similar to that of the reference response, given in Figure E.9(a), which suggests that the choice and arrangement of the partitions is adequate, at least from a qualitative point of view. In contrast, the Linear model given in Figure E.9(c) yields significantly smaller vertical displacements (values below $-0.002m$ given by the red color in the contour map of Figure E.10(a)), indicating an excessively rigid response that would probably require larger MCs than those considered to improve its performance.

In order to quantitatively corroborate the viability of the proposed partition model and its apparent advantages over the linear model, a more exhaustive analysis is proposed below, evaluating the temporal evolution of the following variables:

- The macro-scale vertical displacement u_2 of the node under the center of the footing (see Figure E.5), corresponding to the node with coordinates $x_1 = 0m$ and $x_2 = 4.5m$ (upper left vertex in Figures E.6a and E.6c.1), is shown in Figure E.10(a). This figure shows the excellent adjustment provided by $\mathrm{MCMM}(\overline{\mathbf{n}}_\mu^p)_4^4$ with respect to the single-scale solution using DNS, while the Linear model shows a significantly more rigid solution in the temporal evolution of the vertical displacements in the analyzed node, reaching values that are notably lower than those expected according to the reference solution.

- The flow rate that crosses the only possible exit surface, which corresponds to the red colored edge indicated in Figure E.5. This edge has an extension of $0.75m$, between the outer edge of the footing and the (right) boundary of the analysis domain. For each model, the total flow is obtained as the sum of the discharge flows along this length, resulting in the time evolution shown in Figure E.10(b). It can be seen that $\mathrm{MCMM}(\overline{\mathbf{n}}_\mu^p)_4^4$ reproduces the two peaks presented by the single-scale solution very satisfactorily, while the Linear model again presents a noticeable discrepancy, showing only one peak.

- Regarding the components of the effective stresses σ'_{11}, σ'_{12}, and σ'_{22} of the tensor $\boldsymbol{\sigma}'$, additional clarifications on their definition are provided in Appendix E. The homogenized response is evaluated at each Gaussian point of the macro-scale (see E.6-(c.1)), which for the present case was

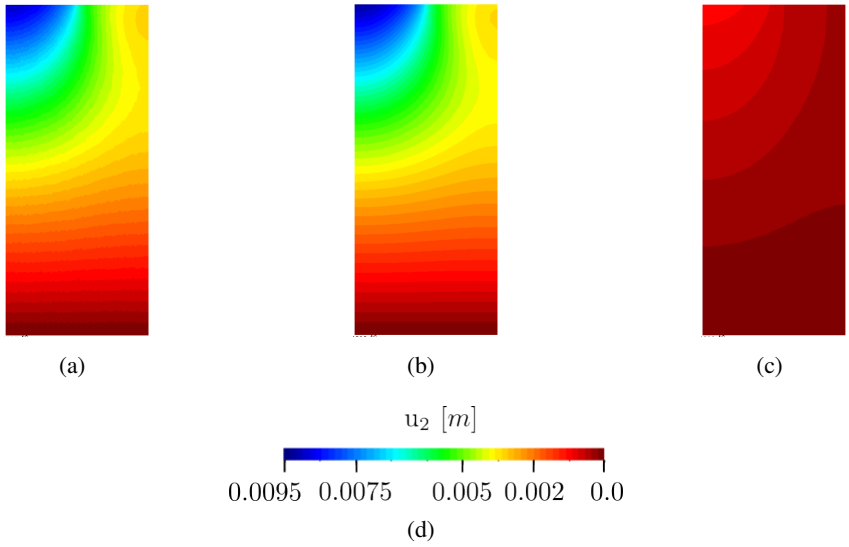

Figura E.9: Displacement u_2 map contour at time $t_{max} = 10000\ days$. (a) DNS. (b) MCMM$\left(\overline{\mathbf{n}}_{\mu}^{p}\right)_{4}^{4}$. (c) Linear

arbitrarily adopted as that of coordinates $x_1 = 0.338m$ and $x_2 = 2.682m$. At this position, the results of the single-scale model (DNS) are averaged considering all elements contained within a radius $r = 0.5\ l_{\mu}$, obtaining an average effective stress $\boldsymbol{\sigma}'_{Av}$ over an area $\Omega_r = \pi\, r^2$ according to

$$\boldsymbol{\sigma}'_{Av} = \frac{1}{|\Omega_r|} \int_{\Omega_r} \boldsymbol{\sigma}' d\Omega \tag{E.54}$$

From the curves shown in Figure E.11, we can see, once again, the good performance of the proposed model when compared with the averaged response of the DNS solution. The fit is particularly good for the effective stress components σ'_{11} and σ'_{22}, while for σ'_{12} there is a very slight overestimation in the final value reached from $t = 1\,day$. In contrast, the Linear model only manages to approximate the final state of the components σ'_{22}, yielding a completely erroneous behavior in the evolution of σ'_{11}.

- Finally, in relation to the components of the flux velocity vector $\boldsymbol{\mathcal{V}}$, $\mathcal{V}_1$ and $\mathcal{V}_2$, the same macro-scale Gauss point is assumed and the DNS response is averaged according to expression (E.54), replacing $\boldsymbol{\mathcal{V}}$ instead of $\boldsymbol{\sigma}'$, to obtain the averaged velocity vector $\boldsymbol{\mathcal{V}}_{Av}$. The results shown in Figure E.12 show that the MCMM$(\overline{\mathbf{n}}_{\mu}^{p})_{4}^{4}$ model reproduces both components $\mathcal{V}_1$ and $\mathcal{V}_2$ very accurately, closely approximating the single-scale response (DNS).

Based on the results presented, it is evident that the assumption of alternative models to the MCMM through the imposition of additional restrictions on the partitions considered with discretion generally leads to highly satisfactory results. In particular, the proposed model MCMM$(\overline{\mathbf{n}}_{\mu}^{p})_{4}^{4}$ demonstrates formidable performance when comparing its results with the single-scale reference solution (DNS). This good performance was obtained using an arbitrarily selected and sized MC. It is reasonable to assume that, when considering larger MCs, the Linear model would tend to converge towards the single-scale

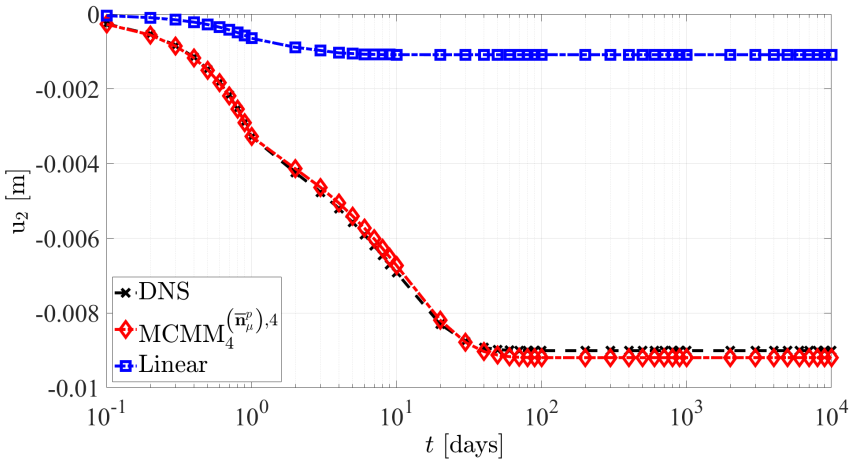

(a)

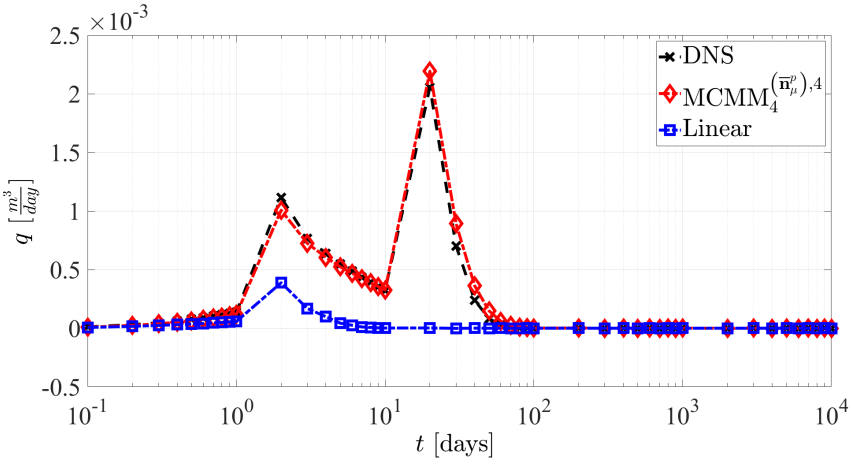

(b)

Figura E.10: (a) Time evolution of vertical displacement component u_2. (b) Time evolution of discharge flow q.

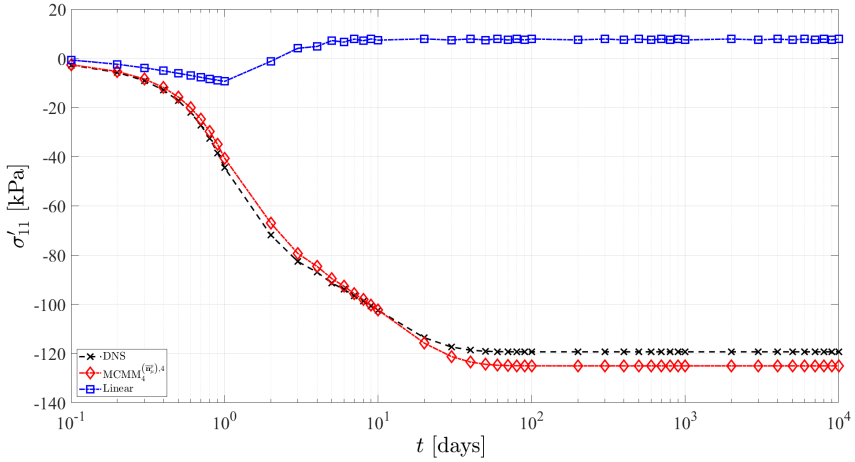

(a)

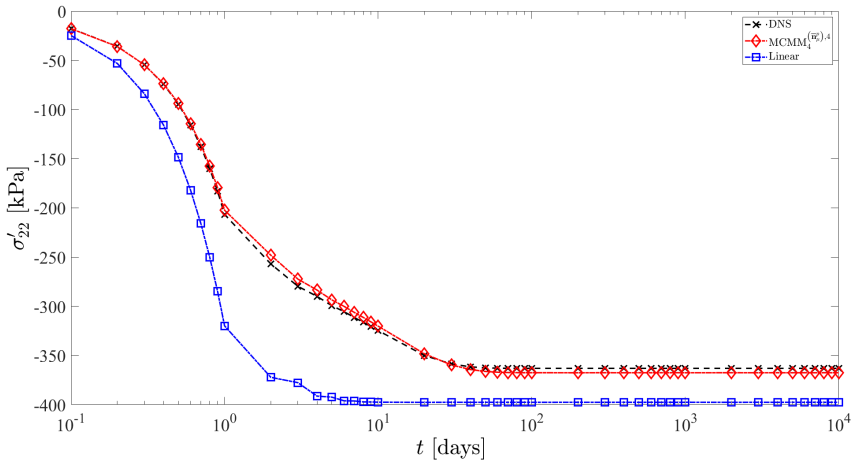

(b)

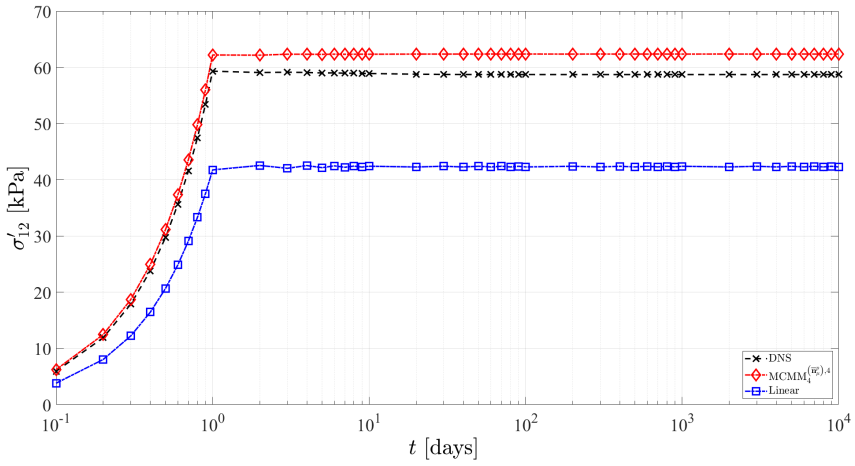

(c)

Figura E.11: Time evolution of different components of $\boldsymbol{\sigma}'$. (a) σ'_{11}. (b) σ'_{22}. (c) σ'_{12}.

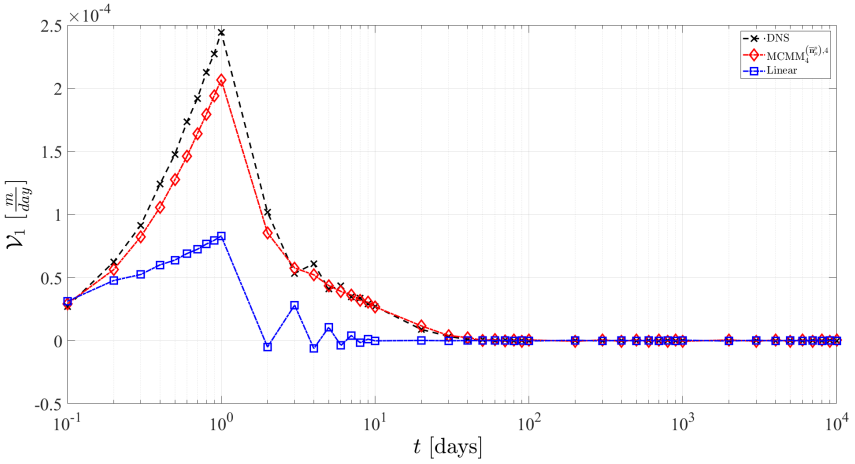

(a)

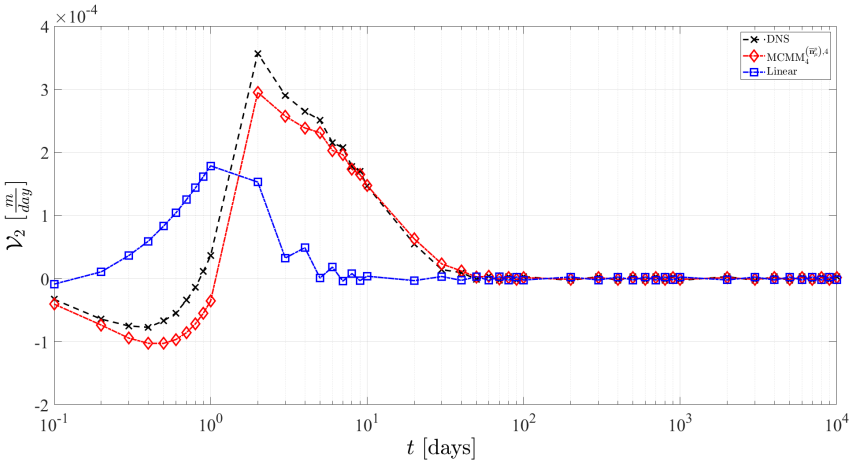

(b)

Figura E.12: Time evolution of different component of velocity flux. (a) $\mathcal{V}_1$. (b) $\mathcal{V}_2$.

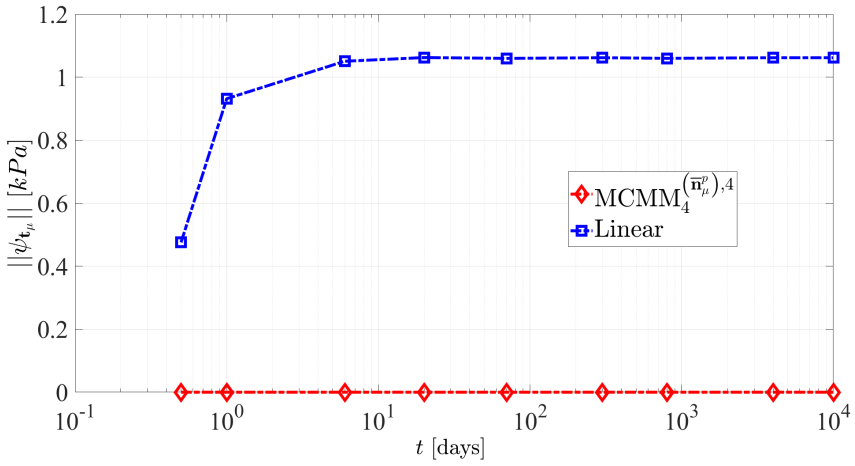

(a)

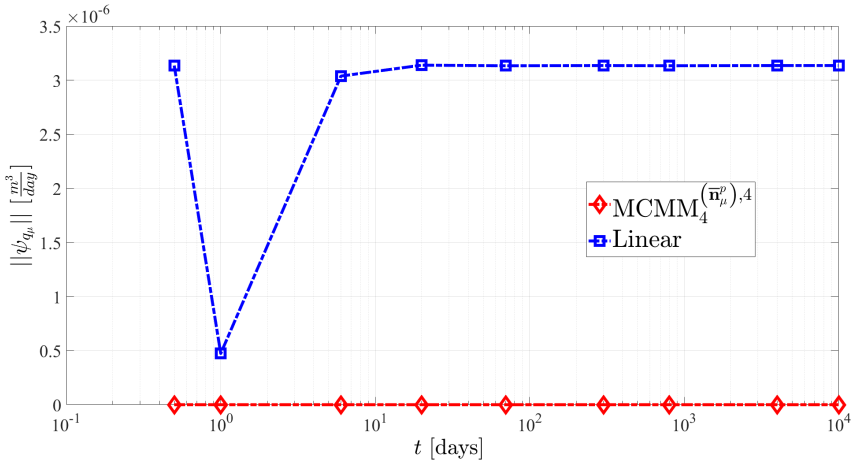

(b)

Figura E.13: Convergence analysis of the net out-of-balance force and flux norm, $||\boldsymbol{\psi}_{\mathbf{t}_\mu}||_2$ and $||\psi_{q_\mu}||_2$, for the Linear model and $\text{MCMM}_4^{(\overline{\mathbf{n}}_\mu^p),4}$, with respect to the time evolution.

response; however, this would imply a considerable increment in the number of elements required in each MC, with the consequent increase in computation time and computational resources required.

Thus, in situations such as the one analyzed in this paper, which involve randomness and a field defined only in certain parts of the MC, where the minimum size at which the multiscale response becomes size-independent is unknown, and where no rigorous reference solutions or clear criteria exist for determining the RVE, the proposal of alternative homogenization schemes, formulated as su-bmodels of the MCMM, appears to offer a highly viable and effective option for modeling strongly heterogeneous micro-structures.

Finally, the vector $\boldsymbol{\psi}_{\mathbf{t}_\mu}$ and the scalar ψ_{q_μ} are determined according to the definition given in (78), for MC_1 corresponding to the Gauss point with coordinates $x_1 = 0.424m$ and $x_2 = 2.174m$, selected arbitrarily. The temporal evolution of the norm of both variables, obtained for both the Linear model and the proposed $\text{MCMM}(\overline{\mathbf{n}}_\mu^p)_4^4$ model, are shown in Figure E.13.

From Figure E.13, it can be seen that the proposed model is $\mathbf{t}_\mu$-balanced and q_μ-balanced, unlike the linear model, which does not satisfy these properties and yields nonzero norm values.

E.7. Conclusions

The main objective and original contribution of this work was the development of a multiscale theory capable of describing heterogeneous micro-structures conformed by components that require different primitive variables for their proper physical representation. In particular, we addressed complex materials composed of impermeable solid inclusions embedded in a saturated porous matrix, configurations that can be found in natural systems such as biological tissues or geomaterials.

To achieve this goal, special attention was paid to the treatment of micro-scale characteristics. Specifically, concepts previously formulated for porous materials with random void distributions were adapted to the study of the pore-pressure field. This adaptation allowed us to extend the scope of the so-called Minimal Constraint Multiscale Model, MCMM($\overline{\mathbf{n}}^p_\mu$), generalizing it by incorporating an additional geometric entity represented by the vector field $\overline{\mathbf{n}}^p_\mu$, introduced in the homogenization rule for the pore-pressure gradient.

The incorporation of this field is based on the fact that a uniform micro-scale pore-pressure fluctuation field should not generate a spurious magnitude similar to the macroscopic pore-pressure gradient. This property, when dealing with micro-structures with components that use different primitive descriptors and that reach the boundary of the MC, is not naturally satisfied. Therefore, it was necessary to reformulate the pore-pressure gradient homogenization scheme in order to ensure the consistency of the model in terms of a consistent transfer between the primitive descriptors at both scales. The new formulation of the homogenization rule induces, by duality, a reactive flux system on the MC boundary, uniform along each edge of the MC with a uniform external unit normal vector, and is also balanced in terms of q_μ.

The choice, particularly simple to consider a uniform vector field $\overline{\mathbf{n}}^p_\mu$, has proved extremely suitable for the development of a variational consistent multiscale theory for the type of micro-structures analyzed.

With the aim of improving the predictive capability of the MCMM($\overline{\mathbf{n}}^p_\mu$) based on the field $\overline{\mathbf{n}}^p_\mu$, we present a procedure for generating families of multiscale sub-models. The progressive increase in the number of constraints in the MC led to results that show excellent performance, reproducing with great accuracy the reference solutions obtained using the DNS strategy, as evidenced in the numerical results section.

Finally, to address the micro-scale size dependence common in multiscale modeling of saturated porous media, a constitutive formulation based on the Selective-Order Expansion (SOE) method was adopted for saturated porous materials in the MC. In this way, we ensured the objectivity of the macroscale response in all circumstances.

Appendix A. Consequences of not applying the vector field in the MCMM

The fact of not considering the vector field $\overline{\mathbf{n}}^p_\mu$, is equivalent to considering that the admissible space of the micro-scale pore-pressure fluctuation as follows

$$\widetilde{\mathcal{P}}^0_\mu \equiv \left\{ \tilde{p}_\mu \ \in \ \mathrm{H}^1;\ \int_{\Omega^p_\mu} \tilde{p}_\mu \, d\Omega_\mu = 0;\ \int_{\Gamma^p_\mu} \tilde{p}_\mu \ \mathbf{n}^p_\mu \, d\Gamma_\mu = \mathbf{0} \right\}. \tag{55}$$

Let us take an arbitrary MC, which in general is $\mathbf{n}^p_\mu$-unbalanced (and therefore $\mathbf{n}^p_\mu$-unbalanced). If we consider a uniform fluctuation field c in expression (E.23) according to model (55), which is equivalent to considering $\overline{\mathbf{n}}^p_\mu = \mathbf{0}$, we obtain the following result

$$\boldsymbol{\varphi} = \boldsymbol{\varphi} + \frac{1}{|\Omega^p_\mu|} \int_{\Gamma^p_\mu} c \ \mathbf{n}^p_\mu \, d\Gamma_\mu \tag{56}$$

This holds only if

$$\mathbf{0} = \frac{1}{|\Omega_\mu^p|}\, c\, \overbrace{\int_{\Gamma_\mu^p} \mathbf{n}_\mu^p \, d\Gamma_\mu}^{=\mathbf{0}} \tag{57}$$

However, the MC is $\mathbf{n}_\mu^p$-unbalanced in Γ_μ^p, so we arrive at an absurdity since $\int_{\Gamma_\mu^p} \mathbf{n}_\mu^p \, d\Gamma_\mu \neq \mathbf{0}$. In fact, by disregarding the last term of (E.23), which represents the contribution associated with the lack of geometric equilibrium of the MC-subdomains in the homogenization formulation of the pore-pressure gradient, the consequences of using an inconsistent multiscale model, that is, a model that does not satisfy the required equilibrium conditions, become evident.

Appendix B. Linear and Periodical subspaces

Appendix B.1. Linear model

In this multiscale model, the conservation of the displacement and pore-pressure fluctuation gradients is enforced by prescribing $\tilde{\mathbf{u}}_\mu = \mathbf{0}$ over the entire MC boundary and $\tilde{p}_\mu = 0$ on the matrix subdomain boundary. The corresponding functional spaces are defined as

$$\widetilde{\mathcal{U}}_\mu^{\text{Lin}} = \left\{ \tilde{\mathbf{u}}_\mu \in \mathbf{H}^1;\, \int_{\Omega_\mu} \tilde{\mathbf{u}}_\mu \, d\Omega_\mu = \mathbf{0}\ ;\ \tilde{\mathbf{u}}_\mu = \mathbf{0}\ \forall\, \mathbf{x}_\mu \in \Gamma_\mu \right\} \subset \widetilde{\mathcal{U}}_\mu, \tag{58}$$

$$\widetilde{\mathcal{P}}_\mu^{\text{Lin}} = \left\{ \tilde{p}_\mu \in \mathrm{H}^1;\, \int_{\Omega_\mu} \tilde{p}_\mu \, d\Omega_\mu = 0\ ;\ \tilde{p}_\mu = 0\ \forall\, \mathbf{x}_\mu \in \Gamma_\mu^p \right\} \subset \widetilde{\mathcal{P}}_\mu^{\left(\overline{\mathbf{n}}_\mu^p\right)}. \tag{59}$$

This space is applicable in the context of a random distribution of non-porous solid inclusions involving randomness in the field of pore-pressure fluctuations. For this reason, this model is used in the numerical results section for comparative analysis.

Appendix B.2. Periodical model

In periodic media, the micro-scale material distribution must satisfy specific geometric conditions. For simplicity, consider two-dimensional rectangular micro-cells, where opposite edges are paired as $\Gamma_{\mu\, i}^+$ and $\Gamma_{\mu\, i}^-$ with unit normals $\mathbf{n}_i^+$ and $\mathbf{n}_i^-$, respectively, so that $\Gamma_{\mu\, i} = \Gamma_{\mu\, i}^+ \cup \Gamma_{\mu\, i}^-$ for $i = 1, 2$. For rectangular domains, the following identification applies: $\Gamma_{\mu\, 1}^\pm = \Gamma_\mu^{\text{right}}, \Gamma_\mu^{\text{left}}$ and $\Gamma_{\mu\, 2}^\pm = \Gamma_\mu^{\text{top}}, \Gamma_\mu^{\text{bottom}}$. A one-to-one correspondence exists between points $\mathbf{x}_{\mu_i}^+ \in \Gamma_{\mu\, i}^+$ and $\mathbf{x}_{\mu_i}^- \in \Gamma_{\mu\, i}^-$, ensuring material periodicity. The periodic model is characterized by equal displacement and pore-pressure fluctuations on opposite boundaries: $\tilde{\mathbf{u}}_\mu\left(\mathbf{x}_{\mu_i}^+, t\right) = \tilde{\mathbf{u}}_\mu\left(\mathbf{x}_{\mu_i}^-, t\right)$ and $\tilde{p}_\mu\left(\mathbf{x}_{\mu_i}^+, t\right) = \tilde{p}_\mu\left(\mathbf{x}_{\mu_i}^-, t\right)$, for every corresponding pair $\{\mathbf{x}_{\mu_i}^+, \mathbf{x}_{\mu_i}^-\}$ and for all i.

The associated functional spaces are defined as

$$\widetilde{\mathcal{U}}_\mu^{\text{Per}} = \left\{ \tilde{\mathbf{u}}_\mu \in \mathbf{H}^1;\, \int_{\Omega_\mu} \tilde{\mathbf{u}}_\mu \, d\Omega_\mu = \mathbf{0};\ tilde{\mathbf{u}}_\mu\left(\mathbf{x}_{\mu_i}^+, t\right) = \tilde{\mathbf{u}}_\mu\left(\mathbf{x}_{\mu_i}^-, t\right)\ \forall \text{ pair } \{\mathbf{x}_{\mu_i}^+, \mathbf{x}_{\mu_i}^-\}\ \forall i,\ \right\} \subset \widetilde{\mathcal{U}}_\mu, \tag{60}$$

$$\widetilde{\mathcal{P}}_\mu^{\text{Per}} = \left\{ \tilde{p}_\mu \in \mathrm{H}^1;\, \int_{\Omega_\mu} \tilde{p}_\mu \, d\Omega_\mu = 0;\ \tilde{p}_\mu\left(\mathbf{x}_{\mu_i}^+, t\right) = \tilde{p}_\mu\left(\mathbf{x}_{\mu_i}^-, t\right)\ \forall \text{ pair } \{\mathbf{x}_{\mu_i}^+, \mathbf{x}_{\mu_i}^-\}\ \forall i \right\} \subset \widetilde{\mathcal{P}}_\mu^{\left(\overline{\mathbf{n}}_\mu^p\right)}. \tag{61}$$

Although this space cannot capture randomness variations in the pore-pressure fluctuation field, it is applied in a specific case to provide a benchmark for comparison. The periodic model serves as a reference, given its superior accuracy when applicable, enabling a direct assessment of the efficiency of the proposed approach.

Appendix C. Inclusion of Lagrange multipliers in the hydromechanical problem of the MC

In this appendix, the constraints associated with the Minimally Constrained Multiscale Model are incorporated into the micro-scale hydro-mechanical problem through the use of Lagrange multipliers. This formulation will allow conclusions of particular relevance to be drawn, as discussed later in Appendix C.1 and Appendix C.2.

Accordingly, in the variational equation (E.35), the functional space $\widetilde{\mathcal{U}}_\mu$ is replaced by the unrestricted space $\mathbf{H}^1$, while the constraints (E.13) and (E.16) are enforced through the corresponding Lagrange multipliers $\boldsymbol{\Theta}_\mathbf{u} \in \mathbb{R}^3$ and $\boldsymbol{\Lambda}_\mathbf{u} \in \mathbb{R}^{3\times3}$. Similarly, the multipliers $\Theta_p \in \mathbb{R}$ and $\boldsymbol{\Lambda}_p \in \mathbb{R}^3$ are employed to impose the constraints (E.19) and (E.23), thus replacing the restricted space $\widetilde{\mathcal{P}}_\mu^{(\overline{\mathbf{n}}_\mu^p)}$ with the space H^1 in the weak form equation (E.36). Consequently, the balance equations incorporating the Lagrange multipliers can be written as follows:

Variational form of the momentum balance equation with Lagrange multipliers:

$$\begin{aligned}\int_{\Omega_\mu} \left(\boldsymbol{\sigma}_\mu : \boldsymbol{\nabla}^{sym}_{\mathbf{x}_\mu} \delta\dot{\tilde{\mathbf{u}}}_\mu - \mathbf{f}_\mu \cdot \delta\dot{\tilde{\mathbf{u}}}_\mu\right) d\Omega_\mu - \boldsymbol{\Theta}_u \cdot \int_{\Omega_\mu} \delta\dot{\tilde{\mathbf{u}}}_\mu \, d\Omega_\mu - \delta\boldsymbol{\Theta}_u \cdot \int_{\Omega_\mu} \dot{\tilde{\mathbf{u}}}_\mu \, d\Omega_\mu \\ - \boldsymbol{\Lambda}_u : \int_{\Gamma_\mu} \delta\dot{\tilde{\mathbf{u}}}_\mu \otimes \mathbf{n}_\mu \, d\Gamma_\mu - \delta\boldsymbol{\Lambda}_u : \int_{\Gamma_\mu} \dot{\tilde{\mathbf{u}}}_\mu \otimes \mathbf{n}_\mu \, d\Gamma_\mu = 0, \\ \forall \left(\delta\dot{\tilde{\mathbf{u}}}_\mu, \, \delta\boldsymbol{\Theta}_u, \, \delta\boldsymbol{\Lambda}_u\right) \in \mathbf{H}^1 \times \mathbb{R}^3 \times \mathbb{R}^{3\times3}, \; \forall t. \end{aligned} \tag{62}$$

Variational form of the mass balance equation with Lagrange multipliers:

$$\begin{aligned}\int_{\Omega_\mu^p} \left(\dot{\chi}_\mu \, \delta\tilde{p}_\mu - \boldsymbol{\mathcal{V}}_\mu \cdot \boldsymbol{\nabla}_{\mathbf{x}_\mu} \delta\tilde{p}_\mu\right) d\Omega_\mu + \Theta_p \int_{\Omega_\mu^p} \delta\tilde{p}_\mu \, d\Omega_\mu \\ + \delta\Theta_p \int_{\Omega_\mu^p} \tilde{p}_\mu \, d\Omega_\mu + \boldsymbol{\Lambda}_p \cdot \int_{\Gamma_\mu^p} \delta\tilde{p}_\mu \, \left(\mathbf{n}_\mu^p - \overline{\mathbf{n}}_\mu^p\right) \, d\Gamma_\mu \\ + \delta\boldsymbol{\Lambda}_p \cdot \int_{\Gamma_\mu^p} \tilde{p}_\mu \, \left(\mathbf{n}_\mu^p - \overline{\mathbf{n}}_\mu^p\right) \, d\Gamma_\mu = 0, \\ \forall \; (\delta\tilde{p}_\mu, \, \delta\Theta_p, \, \delta\boldsymbol{\Lambda}_p) \in \mathrm{H}^1 \times \mathbb{R} \times \mathbb{R}^3, \; \forall t. \end{aligned} \tag{63}$$

In this context, the Lagrange multipliers can be extracted from the corresponding integrals, since they constitute uniform fields. This property derives from the fact that the constraints imposed on the spaces $\widetilde{\mathcal{U}}_\mu$ and $\widetilde{\mathcal{P}}_\mu^{(\overline{\mathbf{n}}_\mu^p)}$ are formulated in terms of integral conditions of zero mean value, either over the volume or over the surface of the considered domain.

Following a few simple mathematical steps on the weak form (62) and (63), including the integration by parts of some terms and using classical variational arguments, we arrive at the strong form of the

equilibrium equations.

$$\left\{\begin{array}{l}
\mathrm{Div}_{\mathbf{x}_\mu}\,\boldsymbol{\sigma}_\mu + \mathbf{f}_\mu + \boldsymbol{\Theta}_{\mathbf{u}} = 0, \quad \forall\,\mathbf{x}_\mu \in \Omega_\mu,\ \forall\, t,\\
\dot{\chi}_\mu + \mathrm{Div}_{\mathbf{x}_\mu}\,\boldsymbol{\mathcal{V}}_\mu + \Theta_p = \dot{m}^f_\mu + \mathrm{Div}_{\mathbf{x}_\mu}\left(\rho^f_\mu \boldsymbol{\mathcal{V}}_\mu\right) + \Theta_p = 0, \quad \forall\,\mathbf{x}_\mu \in \Omega^p_\mu,\ \forall\, t,\\
[\![\boldsymbol{\sigma}_\mu]\!]\,\mathbf{n}^i_\mu = \mathbf{0}, \quad \forall\,\mathbf{x}_\mu \in \Gamma^i_\mu,\ \forall\, t,\\
\rho^f_\mu \boldsymbol{\mathcal{V}}_\mu \cdot \mathbf{n}^i_\mu = 0, \quad \forall\,\mathbf{x}_\mu \in \Gamma^i_\mu,\ \forall\, t,\\
\boldsymbol{\sigma}_\mu\,\mathbf{n}_\mu = \boldsymbol{\Lambda}_{\mathbf{u}}\,\mathbf{n}_\mu, \quad \forall\,\mathbf{x}_\mu \in \Gamma_\mu,\ \forall\, t,\\
\rho^f_\mu \boldsymbol{\mathcal{V}}_\mu \cdot \mathbf{n}^p_\mu = \boldsymbol{\Lambda}_p \cdot (\mathbf{n}^p_\mu - \overline{\mathbf{n}}^p_\mu), \quad \forall\,\mathbf{x}_\mu \in \Gamma^p_\mu,\ \forall\, t,\\
\int_{\Omega_\mu} \dot{\tilde{\mathbf{u}}}_\mu\, d\Omega_\mu = \mathbf{0},\\
\int_{\Gamma_\mu} \dot{\tilde{\mathbf{u}}}_\mu \otimes \mathbf{n}_\mu\, d\Gamma_\mu = \mathbb{O},\\
\int_{\Omega^p_\mu} \tilde{p}_\mu\, d\Omega_\mu = 0,\\
\int_{\Gamma^p_\mu} \tilde{p}_\mu\, (\mathbf{n}^p_\mu - \overline{\mathbf{n}}^p_\mu)\, d\Gamma_\mu = \mathbf{0},
\end{array}\right. \tag{64}$$

where $[\![\boldsymbol{\sigma}_\mu]\!]\mathbf{n}^i_\mu = \boldsymbol{\sigma}_\mu\mathbf{n}^i_\mu - \boldsymbol{\sigma}_\mu\mathbf{n}^i_\mu = \mathbf{0}$ is the jump between the traction in the interface of different materials and expressions (64)-(g), (64)-(h), (64)-(j) and (64)-(k) are achieved by allowing arbitrary variations of $\delta\boldsymbol{\Theta}_u$, $\delta\boldsymbol{\Lambda}_u$, $\delta\Theta_p$ and $\delta\boldsymbol{\Lambda}_p$ in (E.35)-(E.36), respectively, while in each case the remaining virtual variations are assumed to be zero.

Appendix C.1. Reactive forces- and stress-like quantities in the MC

This section aims to provide a deeper understanding of the Lagrange multipliers involved in equations (62) and (63), in the particular context of MCMM($\overline{\mathbf{n}}^p_\mu$). At the same time, it intends to clarify the fundamental relationship between these constraints and the homogenized quantities that emerge at the macroscopic level. These Lagrange multipliers constitute a system of reactive forces and stresses that can be regarded as the quantities conjugate to the micro-scale constraints associated with the MCMM($\overline{\mathbf{n}}^p_\mu$) [21, 27]. In what follows, the main characteristics of these multipliers are analyzed and established.

First, consider in (62) that $\delta\dot{\tilde{\mathbf{u}}}_\mu = \mathbf{c} \in \mathbb{R}^3$ is a uniform vector field, $\delta\boldsymbol{\Theta}_u = \mathbf{0}$ and $\delta\boldsymbol{\Lambda}_u = \mathbb{O}$, so that we can write

$$-\left[\int_{\Omega_\mu} \mathbf{f}_\mu d\Omega_\mu\right] \cdot \mathbf{c} - |\Omega_\mu|\,\boldsymbol{\Theta}_{\mathbf{u}} \cdot \mathbf{c} - \boldsymbol{\Lambda}_{\mathbf{u}} \cdot \left[\mathbf{c} \otimes \int_{\Gamma_\mu} \mathbf{n}_\mu\, d\Gamma_\mu\right] = 0, \quad \forall\,\mathbf{c} \in \mathbb{R}^3,\ \forall\, t, \tag{65}$$

where the last integral satisfies (E.2), resulting in

$$\boldsymbol{\Theta}_{\mathbf{u}} = -\frac{1}{|\Omega_\mu|}\int_{\Omega_\mu} \mathbf{f}_\mu\, d\Omega_\mu = -\mathbf{f}. \tag{66}$$

The latter equality is achieved by the homogenization expression (E.34). If the body forces at the micro-scale are set to zero, $\mathbf{f}_\mu = \mathbf{0}$, then from (E.34) it follows that $\mathbf{f} = \mathbf{0}$. Consequently, from (66), the reactive force per unit volume reduces to $\boldsymbol{\Theta}_u = \mathbf{0}$.

Then, taking $\delta\tilde{p}_\mu = c \in \mathbb{R}$ as a uniform scalar field, $\delta\Theta_p = 0$ and $\delta\boldsymbol{\Lambda}_p = \mathbf{0}$ in (63), we deduce

$$\left[\int_{\Omega^p_\mu} \dot{\chi}_\mu\, d\Omega_\mu\right] c + |\Omega^p_\mu|\Theta_p\, c + \boldsymbol{\Lambda}_p \cdot \left[c \int_{\Gamma^p_\mu} \left(\mathbf{n}^p_\mu - \overline{\mathbf{n}}^p_\mu\right)\, d\Gamma_\mu\right] = 0, \quad \forall\, c \in \mathbb{R},\ \forall\, t, \tag{67}$$

being the last integral null because it fulfills (2) and (E.21). Thus we arrive at

$$\Theta_p = \frac{1}{|\Omega_\mu^p|}\int_{\Omega_\mu^p} \dot{\chi}_\mu \, d\Omega_\mu = \frac{|\Omega_\mu|}{|\Omega_\mu^p|}\,\dot{\chi}. \tag{68}$$

Again a homogenization rule is assumed, in this case of $\dot{\chi}$ through (E.32) leading to (68).

Now, we adopt $\delta\dot{\tilde{\mathbf{u}}}_\mu = \mathbf{A}\left(\mathbf{x}_\mu - \mathbf{x}_\mu^G\right)$, $\delta\boldsymbol{\Theta}_u = \mathbf{0}$ and $\delta\boldsymbol{\Lambda}_u = \mathbb{O}$ in (62), where $\mathbf{A} \in \mathbb{R}^{3\times3}$ is and arbitrary second order tensor, then

$$\begin{aligned}\left[\int_{\Omega_\mu}\left(\boldsymbol{\sigma}_\mu - \mathbf{f}_\mu \otimes^{sym} \left(\mathbf{x}_\mu - \mathbf{x}_\mu^G\right)\right) d\Omega_\mu\right] : \mathbf{A} - \left[\boldsymbol{\Theta}_\mathbf{u} \otimes \int_{\Omega_\mu}\left(\mathbf{x}_\mu - \mathbf{x}_\mu^G\right) d\Omega_\mu\right] : \mathbf{A} \\ - \boldsymbol{\Lambda}_\mathbf{u} : \left[\int_{\Gamma_\mu} \mathbf{A}\left(\mathbf{x}_\mu - \mathbf{x}_\mu^G\right) \otimes \mathbf{n}_\mu \, d\Gamma_\mu\right] = 0, \quad \forall \mathbf{A} \in \mathbb{R}^{3\times3},\ \forall t.\end{aligned} \tag{69}$$

Since the second term is equal to zero according to (E.4), by the homogenization formula (E.31), the following tensor identity $\boldsymbol{\Lambda}_\mathbf{u} : (\mathbf{A}\,\mathbf{B}) = \mathbf{A} : \left(\boldsymbol{\Lambda}_\mathbf{u}\,\mathbf{B}^T\right)$ and using the expression (E.2) whereby the term associated with $\mathbf{x}_\mu^G$ disappears, we finally obtain

$$\boldsymbol{\Lambda}_\mathbf{u} = |\Omega_\mu|\,\boldsymbol{\sigma}\left[\int_{\Gamma_\mu} \mathbf{n}_\mu \otimes \mathbf{x}_\mu \, d\Gamma_\mu\right]^{-1}. \tag{70}$$

The expression (70) results in the classical homogenization rule.

$$\boldsymbol{\sigma} = \frac{1}{|\Omega_\mu|}\int_{\Gamma_\mu} \boldsymbol{\Lambda}_\mathbf{u}\,\mathbf{n}_\mu \otimes \mathbf{x}_\mu \, d\Gamma\mu, \tag{71}$$

where $\boldsymbol{\sigma}_\mu\,\mathbf{n}_\mu = \boldsymbol{\Lambda}_u\,\mathbf{n}_\mu = \mathbf{t}_\mu$ is the traction per unit area over MC boundary Γ_μ.

Ultimately, we assume in (63) that $\delta\Theta_p = 0$, $\delta\boldsymbol{\Lambda}_p = \mathbf{0}$ and $\delta\tilde{p}_\mu = \mathbf{D}\cdot\left(\mathbf{x}_\mu - \mathbf{x}_\mu^{Gp}\right)$, where $\mathbf{D} \in \mathbb{R}^3$ is and arbitrary vector, then we derive

$$\begin{aligned}\mathbf{D}\cdot\left[\int_{\Omega_\mu^p}\dot{\chi}_\mu\,\left(\mathbf{x}_\mu - \mathbf{x}_\mu^G\right) - \boldsymbol{\mathcal{V}}_\mu \; d\Omega_\mu\right] + \Theta_p\,\mathbf{D}\cdot\int_{\Omega_\mu^p}\left(\mathbf{x}_\mu - \mathbf{x}_\mu^{Gp}\right) d\Omega_\mu \\ + \mathbf{D}\cdot\left[\int_{\Gamma_\mu^p}\left(\mathbf{x}_\mu - \mathbf{x}_\mu^{Gp}\right)\otimes\left(\mathbf{n}_\mu^p - \overline{\mathbf{n}}_\mu^p\right) d\Gamma_\mu\right]\boldsymbol{\Lambda}_p = 0, \quad \forall\,\mathbf{D}\in\mathbb{R}^3,\ \forall t,\end{aligned} \tag{72}$$

where the second term is equal to zero according to (E.5). Replacing the first term by the homogenization formula (E.33), we can write

$$\left[-|\Omega_\mu|\,\boldsymbol{\mathcal{V}} + \int_{\Gamma_\mu^p}\left(\mathbf{x}_\mu - \mathbf{x}_\mu^{Gp}\right)\otimes\left(\mathbf{n}_\mu^p - \overline{\mathbf{n}}_\mu^p\right) d\Gamma_\mu\,\boldsymbol{\Lambda}_p\right]\cdot\mathbf{D} = 0, \quad \forall\,\mathbf{D}\in\mathbb{R}^3,\ \forall t. \tag{73}$$

Which eventually allows us to derive the Lagrange multipliers per unit area associated with the micro-scale pore-pressures fluctuation at the boundary of the saturated porous medium matrix, which is expressed as follows

$$\boldsymbol{\Lambda}_p = |\Omega_\mu|\left[\int_{\Gamma_\mu^p}\mathbf{x}_\mu\otimes\left(\mathbf{n}_\mu^p - \overline{\mathbf{n}}_\mu^p\right) d\Gamma_\mu\right]^{-1}\boldsymbol{\mathcal{V}}. \tag{74}$$

In (74) the term associated with $\mathbf{x}_\mu^G$ vanishes because we use (2). We can rewrite the homogenization

formula of $\boldsymbol{\mathcal{V}}$ as

$$\boldsymbol{\mathcal{V}} = \frac{1}{|\Omega_\mu|} \int_{\Gamma_\mu^p} \mathbf{x}_\mu \otimes \left(\mathbf{n}_\mu^p - \overline{\mathbf{n}}_\mu^p\right) \, d\Gamma_\mu \, \boldsymbol{\Lambda}_p. \tag{75}$$

Appendix C.2. Self-balanced micro-scale fields

Based on the strong-form balance equations, it is demonstrated below that the MCMM($\overline{\mathbf{n}}_\mu^p$) proposed here produces self-balanced fields, a desirable property from a physical point of view.

The self-equilibrated traction field can be easily proved by integrating equation (64)-(e) over Γ_μ, considering the relationship $\mathbf{t}_\mu = \boldsymbol{\sigma}_\mu \, \mathbf{n}_\mu$

$$\int_{\Gamma_\mu} \mathbf{t}_\mu \, d\Gamma_\mu = \int_{\Gamma_\mu} \boldsymbol{\Lambda} \, \mathbf{n}_\mu \, d\Gamma_\mu = \boldsymbol{\Lambda} \int_{\Gamma_\mu} \mathbf{n}_\mu \, d\Gamma_\mu = \mathbf{0}, \tag{76}$$

where the integral of the normal over the entire boundary of the MC vanishes, according to (E.2).

This result is consistent with the multiscale formulations widely reported in the literature, since the MCMM($\overline{\mathbf{n}}_\mu^p$) adopted for the displacement field coincides with the conventional one. However, the same property does not automatically hold for the microscopic flux velocity field across the porous material boundary Γ_μ^p. In this case, the self-balance condition is only guaranteed under the assumptions associated with equations (E.23) and (2).

This can be shown by integrating equation (64)-(f) over Γ_μ^p and considering that $q_\mu = \rho_\mu^f \boldsymbol{\mathcal{V}}_\mu \cdot \mathbf{n}_\mu^p$, we obtain

$$\int_{\Gamma_\mu^p} q_\mu \, d\Gamma_\mu = \int_{\Gamma_\mu^p} \boldsymbol{\Lambda}_p \cdot \left(\mathbf{n}_\mu^p - \overline{\mathbf{n}}_\mu^p\right) \, d\Gamma_\mu = \boldsymbol{\Lambda}_p \cdot \int_{\Gamma_\mu^p} \left(\mathbf{n}_\mu^p - \overline{\mathbf{n}}_\mu^p\right) \, d\Gamma_\mu = 0, \tag{77}$$

where the last integral is canceled out as a direct consequence of definitions (2) and (E.21).

The uniform flux q_μ along the boundary Γ_μ^p is obtained by projecting the constant vector $\boldsymbol{\Lambda}_p$ onto the vector $\mathbf{n}_\mu^p - \overline{\mathbf{n}}_\mu^p$. This construction ensures that the model preserves a balanced system of reactive fluxes per unit area on Γ_μ^p. The proposed model provides a flux field q_μ, which is piecewise uniform at the boundary, since $\overline{\mathbf{n}}_\mu^p$ is a uniform vector field. In summary, the proposed methodology leads to a formulation characterized by uniform traction and flux fields on the respective boundary surfaces where the outward normal vector remains constant (Γ_μ and Γ_μ^p, respectively).

At this point, we define the vector $\boldsymbol{\psi}_{\mathbf{t}_\mu}$ and the scalar ψ_{q_μ}, as a measure of the possible out-of-balance forces and fluxes obtained after integrating the traction field over the whole surface of the MC, Γ_μ, and the porous media boundary, Γ_μ^p, respectively, as follow

$$\begin{aligned} \boldsymbol{\psi}_{\mathbf{t}_\mu} &= \int_{\Gamma_\mu} \mathbf{t}_\mu \, d\Gamma\mu = \mathbf{0}, \\ \psi_{q_\mu} &= \int_{\Gamma_\mu^p} q_\mu \, d\Gamma_\mu = 0. \end{aligned} \tag{78}$$

The approach proposed here preserves these properties, so that we can define our model as $\mathbf{t}_\mu$-balanced and q_μ-balanced.

Appendix D. Weak and strong form for the family of sub-spaces of MCMM

We introduce into the weak form given by equations (E.35)-(E.36) the Lagrange multipliers associated with the constraints present in the spaces $\widetilde{\mathcal{U}}_{\mu}^{C_u}$ and $\widetilde{\mathcal{P}}_{\mu}^{(\bar{\mathbf{n}}_\mu),C_p}$. This leads to the following

$$
\begin{aligned}
&\int_{\Omega_\mu} \left(\boldsymbol{\sigma}_\mu : \boldsymbol{\nabla}^{sym}_{\mathbf{x}_\mu} \delta\dot{\tilde{\mathbf{u}}}_\mu - \mathbf{f}_\mu \cdot \delta\dot{\tilde{\mathbf{u}}}_\mu \right) d\Omega_\mu - \boldsymbol{\Theta}_u \cdot \int_{\Omega_\mu} \delta\dot{\tilde{\mathbf{u}}}_\mu \, d\Omega_\mu - \delta\boldsymbol{\Theta}_u \cdot \int_{\Omega_\mu} \dot{\tilde{\mathbf{u}}}_\mu \, d\Omega_\mu \\
&\qquad - \boldsymbol{\Lambda}_u : \int_{\Gamma_\mu} \delta\dot{\tilde{\mathbf{u}}}_\mu \otimes \mathbf{n}_\mu \, d\Gamma_\mu - \delta\boldsymbol{\Lambda}_u : \int_{\Gamma_\mu} \dot{\tilde{\mathbf{u}}}_\mu \otimes \mathbf{n}_\mu \, d\Gamma_\mu \\
&- \sum_{j\in\mathcal{C}_u} \boldsymbol{\Lambda}_u^j : \int_{\Gamma_\mu^j} \delta\dot{\tilde{\mathbf{u}}}_\mu \otimes \left(\mathbf{n}_\mu - \overline{\mathbf{n}}_\mu^j\right) d\Gamma_\mu - \sum_{j\in\mathcal{C}_u} \delta\boldsymbol{\Lambda}_u^j : \int_{\Gamma_\mu^j} \dot{\tilde{\mathbf{u}}}_\mu \otimes \left(\mathbf{n}_\mu - \overline{\mathbf{n}}_\mu^j\right) d\Gamma_\mu = 0, \\
&\qquad \forall \left(\delta\dot{\tilde{\mathbf{u}}}_\mu,\, \delta\boldsymbol{\Theta}_u,\, \delta\boldsymbol{\Lambda}_u,\, \left\{\delta\boldsymbol{\Lambda}_u^j\right\}_{j\in\mathcal{C}_u} \right) \in \mathbf{H}^1 \times \mathbb{R}^3 \times \mathbb{R}^{3\times 3} \times \underbrace{\mathbb{R}^{3\times 1} \times \ldots \times \mathbb{R}^{3\times 1}}_{C_u \text{ times}}, \; \forall t.
\end{aligned} \tag{79}
$$

$$
\begin{aligned}
&\int_{\Omega_\mu^p} \left(\dot{\chi}_\mu \, \delta\tilde{p}_\mu - \boldsymbol{\mathcal{V}}_\mu \cdot \boldsymbol{\nabla}_{\mathbf{x}_\mu} \delta\tilde{p}_\mu \right) d\Omega_\mu + \Theta_p \int_{\Omega_\mu^p} \delta\tilde{p}_\mu \, d\Omega_\mu \\
&\qquad + \delta\Theta_p \int_{\Omega_\mu^p} \tilde{p}_\mu \, d\Omega_\mu + \boldsymbol{\Lambda}_p \cdot \int_{\Gamma_\mu^p} \delta\tilde{p}_\mu \left(\mathbf{n}_\mu^p - \overline{\mathbf{n}}_\mu^p\right) d\Gamma_\mu \\
&\quad + \delta\boldsymbol{\Lambda}_p \cdot \int_{\Gamma_\mu^p} \tilde{p}_\mu \left(\mathbf{n}_\mu^p - \overline{\mathbf{n}}_\mu^p\right) d\Gamma_\mu + \sum_{k\in\mathcal{C}_p} \boldsymbol{\Lambda}_p^k \cdot \int_{\Gamma_\mu^{p,k}} \delta\tilde{p}_\mu \left(\mathbf{n}_\mu^p - \overline{\mathbf{n}}_\mu^{p,k}\right) d\Gamma_\mu \\
&\qquad + \sum_{k\in\mathcal{C}_p} \delta\boldsymbol{\Lambda}_p^k \cdot \int_{\Gamma_\mu^p} \tilde{p}_\mu \left(\mathbf{n}_\mu^p - \overline{\mathbf{n}}_\mu^{p,k}\right) d\Gamma_\mu = 0, \\
&\qquad \forall \left(\delta\tilde{p}_\mu,\, \delta\Theta_p,\, \delta\boldsymbol{\Lambda}_p,\, \left\{\delta\boldsymbol{\Lambda}_p^k\right\}_{k\in\mathcal{C}_p} \right) \in \mathbf{H}^1 \times \mathbb{R} \times \mathbb{R}^3 \times \underbrace{\mathbb{R} \times \ldots \times \mathbb{R}}_{C_p \text{ times}}, \; \forall t.
\end{aligned} \tag{80}
$$

Following standard argumentes from the calculus of variations, we obtain the strong form of the hydro-mechanical problem

$$
\left\{
\begin{array}{l}
\mathrm{Div}_{\mathbf{x}_\mu} \boldsymbol{\sigma}_\mu + \mathbf{f}_\mu + \boldsymbol{\Theta}_u = 0, \quad \forall \mathbf{x}_\mu \in \Omega_\mu, \; \forall t, \\
\dot{m}_\mu^f + \mathrm{Div}_{\mathbf{x}_\mu} \left(\rho_\mu^f \boldsymbol{\mathcal{V}}_\mu \right) - \Theta_p = 0, \quad \forall \mathbf{x}_\mu \in \Omega_\mu^p, \; \forall t, \\
[\![\boldsymbol{\sigma}_\mu]\!] \mathbf{n}_\mu^i = \mathbf{0}, \quad \forall \mathbf{x}_\mu \in \Gamma_\mu^i, \; \forall t, \\
\rho_\mu^f \boldsymbol{\mathcal{V}}_\mu \cdot \mathbf{n}_\mu^i = 0, \quad \forall \mathbf{x}_\mu \in \Gamma_\mu^i, \; \forall t, \\
\boldsymbol{\sigma}_\mu \, \mathbf{n}_\mu = \boldsymbol{\Lambda}_u \, \mathbf{n}_\mu + \boldsymbol{\Lambda}_u^j \left(\mathbf{n}_\mu - \overline{\mathbf{n}}_\mu^j \right), \quad \forall \mathbf{x}_\mu \in \Gamma_\mu^j, \; j \in \mathcal{C}_u, \; \forall t, \\
\boldsymbol{\sigma}_\mu \, \mathbf{n}_\mu = \boldsymbol{\Lambda}_u \, \mathbf{n}_\mu, \quad \forall \mathbf{x}_\mu \in \Gamma_\mu^j, \; j \in \mathcal{W}_u, \; \forall t, \\
\rho_\mu^f \boldsymbol{\mathcal{V}}_\mu \cdot \mathbf{n}_\mu^p = \boldsymbol{\Lambda}_p \cdot \left(\mathbf{n}_\mu^p - \overline{\mathbf{n}}_\mu^p \right) + \boldsymbol{\Lambda}_p^k \cdot \left(\mathbf{n}_\mu^p - \overline{\mathbf{n}}_\mu^{p,k} \right), \quad \forall \mathbf{x}_\mu \in \Gamma_\mu^{p,k}, \; k \in \mathcal{C}_p, \; \forall t, \\
\rho_\mu^f \boldsymbol{\mathcal{V}}_\mu \cdot \mathbf{n}_\mu^p = \boldsymbol{\Lambda}_p \cdot \left(\mathbf{n}_\mu^p - \overline{\mathbf{n}}_\mu^p \right), \quad \forall \mathbf{x}_\mu \in \Gamma_\mu^{p,k}, \; k \in \mathcal{W}_p, \; \forall t, \\
\int_{\Omega_\mu} \dot{\tilde{\mathbf{u}}}_\mu \, d\Omega_\mu = \mathbf{0}, \\
\int_{\Gamma_\mu} \dot{\tilde{\mathbf{u}}}_\mu \otimes \mathbf{n}_\mu \, d\Gamma_\mu = \mathbb{O}, \\
\int_{\Gamma_\mu^j} \dot{\tilde{\mathbf{u}}}_\mu \otimes \left(\mathbf{n}_\mu - \overline{\mathbf{n}}_\mu^j \right) d\Gamma_\mu = \mathbb{O}, \; j \in \mathcal{C}_u \\
\int_{\Omega_\mu^p} \tilde{p}_\mu \, d\Omega_\mu = 0, \\
\int_{\Gamma_\mu^p} \tilde{p}_\mu \left(\mathbf{n}_\mu^p - \overline{\mathbf{n}}_\mu^p \right) d\Gamma_\mu = \mathbf{0}, \\
\int_{\Gamma_\mu^{p,k}} \tilde{p}_\mu \left(\mathbf{n}_\mu^p - \overline{\mathbf{n}}_\mu^{p,k} \right) d\Gamma_\mu = \mathbf{0}, \; k \in \mathcal{C}_p.
\end{array}
\right. \tag{81}
$$

Appendix E. Clarifications related to effective stress

First of all, when dealing with solid media it is not required to talk about effective stress, but in the present study, we assume that conceptually the effective stress tensor in the solid subdomain is equivalent to the total stress tensor, that is $\boldsymbol{\sigma}'^{s} = \boldsymbol{\sigma}^{s}$, which is equally valid for the DNS strategy as for the multiscale approach. In the first instance, the average effective stress tensor can be obtained merely by performing the calculation according to the following expression

$$\boldsymbol{\sigma}' = \frac{1}{|\Omega_r|}\left(\int_{\Omega_r^p} \boldsymbol{\sigma}'^{p}\, d\Omega + \int_{\Omega_r^s} \boldsymbol{\sigma}^{s}\, d\Omega \right). \tag{82}$$

On the other hand, in the multiscale approach, effective stress is obtained at the macro-scale level without distinguishing between solid and porous portions, as the macro-scale is considered a like-porous medium based on initial hypotheses. Consequently, to determine the average, it is sufficient to calculate the mean in the specified domain, as follows

$$\boldsymbol{\sigma}' = \frac{1}{|\Omega_r|} \int_{\Omega_r} \boldsymbol{\sigma}'\, d\Omega. \tag{83}$$

However, the effective stress at macro-scale, for the examples discussed in this paper, is defined by the homogenization of their micro-scale counterparts as follows

$$\boldsymbol{\sigma}' = \frac{1}{|\Omega_\mu|} \int_{\Omega_\mu} \boldsymbol{\sigma}'_\mu\, d\Omega_\mu = \frac{1}{|\Omega_\mu|}\left(\int_{\Omega_\mu} \boldsymbol{\sigma}'^{p}_{\mu}\, d\Omega_\mu + \int_{\Omega_\mu} \boldsymbol{\sigma}'^{s}_{\mu}\, d\Omega_\mu \right), \tag{84}$$

where $\boldsymbol{\sigma}'_\mu$ is the field of micro-scale effective stress, $\boldsymbol{\sigma}'^{s}_{\mu}$ is the effective micro-stress field of the solid fraction, which, as mentioned previously, is equivalent to the total stress in the same $\boldsymbol{\sigma}'^{s}_{\mu} = \boldsymbol{\sigma}^{s}_{\mu}$, see (E.47) and $\boldsymbol{\sigma}'^{p}_{\mu}$ are the effective stress of the porous medium in the micro-scale, according to (E.45).

Bibliografía

[1] R. Hill. Elastic properties of reinforced solids: Some theoretical principles. Journal of the Mechanics and Physics of Solids, 11(5):357–372, 1963. ISSN 0022-5096. doi: https://doi.org/10.1016/0022-5096(63)90036-X. URL https://www.sciencedirect.com/science/article/pii/002250966390036X.

[2] R. Hill. A self-consistent mechanics of composite materials. Journal of the Mechanics and Physics of Solids, 13(4):213–222, 1965. ISSN 0022-5096. doi: https://doi.org/10.1016/0022-5096(65)90010-4. URL https://www.sciencedirect.com/science/article/pii/0022509665900104.

[3] R. Hill. Continuum micro-mechanics of elastoplastic polycrystals. Journal of the Mechanics and Physics of Solids, 13(2):89–101, 1965. ISSN 0022-5096. doi: https://doi.org/10.1016/0022-5096(65)90023-2. URL https://www.sciencedirect.com/science/article/pii/0022509665900232.

[4] Ted Belytschko, Stefan Loehnert, y Jeong-Hoon Song. Multiscale aggregating discontinuities: A method for circumventing loss of material stability. International Journal for Numerical Methods in Engineering, 73 (6):869–894, 2008. doi: https://doi.org/10.1002/nme.2156. URL https://onlinelibrary.wiley.com/doi/abs/10.1002/nme.2156.

[5] Frédéric Feyel y Jean-Louis Chaboche. Fe2 multiscale approach for modelling the elastoviscoplastic behaviour of long fibre sic/ti composite materials. Computer Methods in Applied Mechanics and Engineering, 183(3):309–330, 2000. ISSN 0045-7825. doi: https://doi.org/10.1016/S0045-7825(99)00224-8. URL https://www.sciencedirect.com/science/article/pii/S0045782599002248.

[6] Frédéric Feyel. A multilevel finite element method (fe2) to describe the response of highly non-linear structures using generalized continua. Computer Methods in Applied Mechanics and Engineering, 192 (28):3233–3244, 2003. ISSN 0045-7825. doi: https://doi.org/10.1016/S0045-7825(03)00348-7. URL https://www.sciencedirect.com/science/article/pii/S0045782503003487. Multiscale Computational Mechanics for Materials and Structures.

[7] J.C. Michel, H. Moulinec, y P. Suquet. Effective properties of composite materials with periodic microstructure: a computational approach. Computer Methods in Applied Mechanics and Engineering, 172(1):109–143, 1999. ISSN 0045-7825. doi: https://doi.org/10.1016/S0045-7825(98)00227-8. URL https://www.sciencedirect.com/science/article/pii/S0045782598002278.

[8] Christian Miehe, Jörg Schröder, y Jan Schotte. Computational homogenization analysis in finite plasticity simulation of texture development in polycrystalline materials. Computer Methods in Applied Mechanics and Engineering, 171(3):387–418, 1999. ISSN 0045-7825. doi: https://doi.org/10.1016/S0045-7825(98)00218-7. URL https://www.sciencedirect.com/science/article/pii/S0045782598002187.

[9] K. Terada y N. Kikuchi. A class of general algorithms for multi-scale analyses of heterogeneous media. Computer Methods in Applied Mechanics and Engineering, 190(40):5427–5464, 2001. ISSN 0045-7825. doi: https://doi.org/10.1016/S0045-7825(01)00179-7. URL https://www.sciencedirect.com/science/article/pii/S0045782501001797.

[10] V. Kouznetsova, W. A. M. Brekelmans, y F. P. T. Baaijens. An approach to micro-macro modeling of heterogeneous materials. Computational Mechanics, 27:37–48, 2001. ISSN 1432-0924. doi: 10.1007/s004660000212. URL https://doi.org/10.1007/s004660000212.

[11] C. Miehe y A. Koch. Computational micro-to-macro transitions of discretized microstructures undergoing small strains. Archive of Applied Mechanics, 72:300–317, 2002. ISSN 1432-0681. doi: 10.1007/s00419-002-0212-2. URL https://doi.org/10.1007/s00419-002-0212-2.

[12] E.A. de Souza Neto y R.A. Feijóo. Variational foundations of multi-scale constitutive models of solid: Small and large strain kinematical formulation. LNCC-MCTI Laboratório Nacional de Computação Científica. Internal Report no. 16/2006. LNCC, Petrópolis, Brazil, 2006.

[13] Fredrik Larsson, Kenneth Runesson, y Fang Su. Variationally consistent computational homogenization of transient heat flow. International Journal for Numerical Methods in Engineering, 81(13):1659–1686, 2010. doi: https://doi.org/10.1002/nme.2747. URL https://onlinelibrary.wiley.com/doi/abs/10.1002/nme.2747.

[14] Fredrik Larsson, Kenneth Runesson, y Fang Su. Computational homogenization of uncoupled consolidation in micro-heterogeneous porous media. International Journal for Numerical and Analytical Methods in Geomechanics, 34(14):1431–1458, 2010. doi: https://doi.org/10.1002/nag.862. URL https://onlinelibrary.wiley.com/doi/abs/10.1002/nag.862.

[15] K. Runesson, F. Su, y F. Larsson. Assessment of Homogenization Errors in Transient Problems, páginas 207–214. Springer Berlin Heidelberg, Berlin, Heidelberg, 2011. ISBN 978-3-642-17484-1. doi: 10.1007/978-3-642-17484-1_23. URL https://doi.org/10.1007/978-3-642-17484-1_23.

[16] A.R. Khoei y M.R. Hajiabadi. Fully coupled hydromechanical multiscale model with microdynamic effects. International Journal for Numerical Methods in Engineering, 115(3):293–327, 2018. doi: https://doi.org/10.1002/nme.5805. URL https://onlinelibrary.wiley.com/doi/abs/10.1002/nme.5805.

[17] Stefan Kaessmair y Paul Steinmann. On the computational homogenization of transient diffusion problems. PAMM, 16(1):529–530, 2016. doi: https://doi.org/10.1002/pamm.201610253. URL https://onlinelibrary.wiley.com/doi/abs/10.1002/pamm.201610253.

[18] Felipe Lopez Rivarola, Nicolás Labanda, y Guillermo Etse. Thermodynamically consistent multiscale homogenization for thermo-poroplastic materials. Zeitschrift für angewandte Mathematik und Physik ZAMP, 70:1–27, 05 2019. doi: 10.1007/s00033-019-1125-z.

[19] Pablo Blanco, Pablo Sánchez, Eduardo de Souza Neto, y Raúl Feijóo. Variational foundations and generalized unified theory of rve-based multiscale models. Archives of Computational Methods in Engineering, 23, 12 2014. doi: 10.1007/s11831-014-9137-5.

[20] Edgardo O. Taroco, Pablo J. Blanco, y Raúl A. Feijóo. Introduction to the Variational Formulation in Mechanics: Fundamentals and Applications. John Wiley & Sons, Ltd, 2019. ISBN 9781119600923. doi: https://doi.org/10.1002/9781119600923.fmatter. URL https://onlinelibrary.wiley.com/doi/abs/10.1002/9781119600923.fmatter.

[21] P.J. Blanco, P.J. Sánchez, F.F. Rocha, S. Toro, y R.A. Feijóo. A consistent multiscale mechanical formulation for media with randomly distributed voids. International Journal of Solids and Structures, 283:112494, 2023. ISSN 0020-7683. doi: https://doi.org/10.1016/j.ijsolstr.2023.112494. URL https://www.sciencedirect.com/science/article/pii/S0020768323003918.

[22] P.J. Sánchez, P.J. Blanco, A.E. Huespe, y R.A. Feijóo. Failure-oriented multi-scale variational formulation: Micro-structures with nucleation and evolution of softening bands. Computer Methods in Applied Mechanics and Engineering, 257:221–247, 2013. ISSN 0045-7825. doi: https://doi.org/10.1016/j.cma.2012.11.016. URL https://www.sciencedirect.com/science/article/pii/S0045782512003659.

[23] S. Toro, P.J. Sánchez, A.E. Huespe, S.M. Giusti, P.J. Blanco, y R.A. Feijóo. A two-scale failure model for heterogeneous materials: numerical implementation based on the finite element method. International Journal for Numerical Methods in Engineering, 97(5):313–351, 2014. doi: https://doi.org/10.1002/nme.4576. URL https://onlinelibrary.wiley.com/doi/abs/10.1002/nme.4576.

[24] S. Toro, P.J. Sánchez, P.J. Blanco, E.A. de Souza Neto, A.E. Huespe, y R.A. Feijóo. Multiscale formulation for material failure accounting for cohesive cracks at the macro and micro scales. International Journal of Plasticity, 76:75–110, 2016. ISSN 0749-6419. doi: https://doi.org/10.1016/j.ijplas.2015.07.001. URL https://www.sciencedirect.com/science/article/pii/S0749641915001199.

[25] S. Toro, P.J. Sánchez, , J. M. Podestá, P.J. Blanco, A.E. Huespe, y R.A. Feijóo. Cohesive surface model for fracture based on a two-scale formulation: computational implementation aspects. Computational Mechanics, 58:549–585, 2016. ISSN 1432-0924. doi: 10.1007/s00466-016-1306-y. URL https://doi.org/10.1007/s00466-016-1306-y.

[26] E.A. de Souza Neto, P.J. Blanco, P.J. Sánchez, y R.A. Feijóo. An rve-based multiscale theory of solids with micro-scale inertia and body force effects. Mechanics of Materials, 80:136–144, 2015. ISSN 0167-6636. doi: https://doi.org/10.1016/j.mechmat.2014.10.007. URL https://www.sciencedirect.com/science/article/pii/S0167663614001872.

[27] P.J. Blanco, P.J. Sánchez, E.A. de Souza Neto, y R.A. Feijóo. The method of multiscale virtual power for the derivation of a second order mechanical model. Mechanics of Materials, 99:53–67, 2016. ISSN 0167-6636. doi: https://doi.org/10.1016/j.mechmat.2016.05.003. URL https://www.sciencedirect.com/science/article/pii/S0167663616300400.

[28] P.J. Blanco, A. Clausse, y R.A. Feijóo. Homogenization of the navier-stokes equations by means of the multi-scale virtual power principle. Computer Methods in Applied Mechanics and Engineering, 315:760–779, 2017. ISSN 0045-7825. doi: https://doi.org/10.1016/j.cma.2016.11.022. URL https://www.sciencedirect.com/science/article/pii/S0045782516312385.

[29] Rodney Hill. On constitutive macro-variables for heterogeneous solids at finite strain. Proceedings of the Royal Society of London. A. Mathematical and Physical Sciences, 326(1565):131–147, 1972. doi: 10.1098/rspa.1972.0001. URL https://royalsocietypublishing.org/doi/abs/10.1098/rspa.1972.0001.

[30] J. Mandel. Plasticite classique et viscoplasticite:. CISM International Centre for Mechanical Sciences. Springer, 1972. ISBN 9780387811970. URL https://books.google.com.ar/books?id=h8RQAAAAYAAJ.

[31] Maurice A. Biot. General theory of three-dimensional consolidation. Journal of Applied Physics, 12(2):155–164, 1941. doi: 10.1063/1.1712886. URL https://doi.org/10.1063/1.1712886.

[32] M. A. Biot. Theory of elasticity and consolidation for a porous anisotropic solid. Journal of Applied Physics, 26(2):182–185, 1955. doi: 10.1063/1.1721956. URL https://doi.org/10.1063/1.1721956.

[33] R. de Boer. Theory of porous media: Highlights in historical development and current state. Applied Mechanics Reviews, 55(2):B32–B33, 04 2002. ISSN 0003-6900. doi: 10.1115/1.1451169. URL https://doi.org/10.1115/1.1451169.

[34] J.P. Carter, J.C. Small, y J.R. Booker. A theory of finite elastic consolidation. International Journal of Solids and Structures, 13(5):467–478, 1977. ISSN 0020-7683. doi: https://doi.org/10.1016/0020-7683(77)90041-5. URL https://www.sciencedirect.com/science/article/pii/0020768377900415.

[35] Olivier Coussy, Luc Dormieux, y Emmanuel Detournay. From mixture theory to biot's approach for porous media. International Journal of Solids and Structures, 35(34):4619–4635, 1998. ISSN 0020-7683. doi: https://doi.org/10.1016/S0020-7683(98)00087-0. URL https://www.sciencedirect.com/science/article/pii/S0020768398000870.

[36] O. Coussy. Poromechanics. John Wiley and Sons, Ltd, 2003. ISBN 9780470092712.

[37] O. Coussy. Mechanics and Physics of Porous Solids. John Wiley and Sons, Ltd, 2010. ISBN 9780470710388. doi: https://doi.org/10.1002/9780470710388. URL https://onlinelibrary.wiley.com/doi/abs/10.1002/9780470710388.

[38] J. P. Carter, J. R. Booker, y J. C. Small. The analysis of finite elasto-plastic consolidation. International Journal for Numerical and Analytical Methods in Geomechanics, 3(2):107–129, 1979. doi: https://doi.org/10.1002/nag.1610030202. URL https://onlinelibrary.wiley.com/doi/abs/10.1002/nag.1610030202.

[39] O. C. Zienkiewicz y T. Shiomi. Dynamic behaviour of saturated porous media; the generalized biot formulation and its numerical solution. International Journal for Numerical and Analytical Methods in Geomechanics, 8(1):71–96, 1984. doi: https://doi.org/10.1002/nag.1610080106. URL https://onlinelibrary.wiley.com/doi/abs/10.1002/nag.1610080106.

[40] Olgierd Cecil Zienkiewicz, A. H. C. Chan, M. Pastor, D. K. Paul, y T. Shiomi. Static and dynamic behaviour of soils : a rational approach to quantitative solutions. i. fully saturated problems. Proceedings of the Royal Society of London. A. Mathematical and Physical Sciences, 429(1877):285–309, 1990. doi: 10.1098/rspa.1990.0061. URL https://royalsocietypublishing.org/doi/abs/10.1098/rspa.1990.0061.

[41] Roland Lewis y Bernhard Schrefler. The Finite Element Method in the Static and Dynamic Deformation and Consolidation in Porous Media, volumen 34. John Wiley and Sons, Ltd, 01 1998. ISBN 0 471 92809 7.

[42] Javier L. Mroginski, H.Ariel Di Rado, Pablo A. Beneyto, y Armando M. Awruch. A finite element approach for multiphase fluid flow in porous media. Mathematics and Computers in Simulation (MATCOM), 81(1):76–91, 2010. URL https://EconPapers.repec.org/RePEc:eee:matcom:v:81:y:2010:i:1:p:76-91.

[43] Pablo A. Beneyto, H. Ariel Di Rado, Javier L. Mroginski, y Armando M. Awruch. A versatile mathematical approach for environmental geomechanic modelling based on stress state decomposition. Applied Mathematical Modelling, 39(22):6880–6896, 2015. ISSN 0307-904X. doi: https://doi.org/10.1016/j.apm.2015.02.013. URL https://www.sciencedirect.com/science/article/pii/S0307904X15000864.

[44] J. L Mroginski, , H. G. Castro, J. M Podestá, P. A. Beneyto, y A. R. Anonis. A fully coupled particle method for dynamic analysis of saturated soil. Computational Particle Mechanics, 8:845–857,

2021. ISSN 2196-4386. doi: 10.1007/s40571-020-00373-y. URL https://doi.org/10.1007/s40571-020-00373-y.

[45] Victor Berdichevsky. Variational Principles of Continuum Mechanics. Springer Berlin, Heidelberg, September 2009. ISBN 978-3-540-88467-5. doi: https://doi.org/10.1007/978-3-540-88467-5.

[46] J. N. Reddy. Energy Principles and Variational Methods in Applied Mechanics, 3rd Edition. John Wiley & Sons, Ltd, June 2017. ISBN 978-1-119-08737-3.

[47] Franz-Josef Ulm Luc Dormieux, Djimédo Kondo. Microporomechanics. John Wiley & Sons, Ltd, 2006. ISBN 9780470031889. doi: 10.1002/0470032006.

[48] Fang Su, Fredrik Larsson, y Kenneth Runesson. Computational homogenization of coupled consolidation problems in micro-heterogeneous porous media. International Journal for Numerical Methods in Engineering, 88(11):1198–1218, 2011. doi: https://doi.org/10.1002/nme.3221. URL https://onlinelibrary.wiley.com/doi/abs/10.1002/nme.3221.

[49] Ralf Jänicke, Fredrik Larsson, y Kenneth Runesson. A poro-viscoelastic substitute model of fine-scale poroelasticity obtained from homogenization and numerical model reduction. Computational Mechanics, 65:1063–1083, 04 2020. ISSN 1432-0924. doi: 10.1007/s00466-018-1584-7. URL https://doi.org/10.1007/s00466-018-1584-7.

[50] Fredrik Ekre, Fredrik Larsson, Kenneth Runesson, y Ralf Jänicke. Numerical model reduction with error estimation for computational homogenization of non-linear consolidation. Computer Methods in Applied Mechanics and Engineering, 389:114334, 2022. ISSN 0045-7825. doi: https://doi.org/10.1016/j.cma.2021.114334. URL https://www.sciencedirect.com/science/article/pii/S0045782521006198.

[51] A.R. Khoei y S. Saeedmonir. Computational homogenization of fully coupled multiphase flow in deformable porous media. Computer Methods in Applied Mechanics and Engineering, 376:113660, 2021. ISSN 0045-7825. doi: https://doi.org/10.1016/j.cma.2020.113660. URL https://www.sciencedirect.com/science/article/pii/S0045782520308458.

[52] Saeed Saeedmonir y Amir R. Khoei. Multiscale modeling of coupled thermo-hydro-mechanical analysis of heterogeneous porous media. Computer Methods in Applied Mechanics and Engineering, 391:114518, 2022. ISSN 0045-7825. doi: https://doi.org/10.1016/j.cma.2021.114518. URL https://www.sciencedirect.com/science/article/pii/S0045782521007155.

[53] Amir R. Khoei, Saeed Saeedmonir, y Amin Misaghi Bonabi. Computational homogenization of fully coupled hydro-mechanical analysis of micro-fractured porous media. Computers and Geotechnics, 154:105121, 2023. ISSN 0266-352X. doi: https://doi.org/10.1016/j.compgeo.2022.105121. URL https://www.sciencedirect.com/science/article/pii/S0266352X2200458X.

[54] S. Saeedmonir, M.H. Adeli, y A.R. Khoei. A multiscale approach in modeling of chemically reactive porous media. Computers and Geotechnics, 165:105818, 2024. ISSN 0266-352X. doi: https://doi.org/10.1016/j.compgeo.2023.105818. URL https://www.sciencedirect.com/science/article/pii/S0266352X2300575X.

[55] Tim Ricken, Jörg Schröder, Joachim Bluhm, Simon Maike, y Florian Bartel. Theoretical formulation and computational aspects of a two-scale homogenization scheme combining the tpm and fe2 method for poro-elastic fluid-saturated porous media. International Journal of Solids and Structures, 241:111412, 2022. ISSN 0020-7683. doi: https://doi.org/10.1016/j.ijsolstr.2021.111412. URL https://www.sciencedirect.com/science/article/pii/S0020768321004674.

[56] Bruno Klahr, José Luís Medeiros Thiesen, Otávio Teixeira Pinto, Thiago André Carniel, y Eduardo Alberto Fancello. A variational rve-based multiscale poromechanical formulation applied to soft biological tissues under large deformations. European Journal of Mechanics - A/Solids, 99:104937, 2023. ISSN 0997-7538. doi: https://doi.org/10.1016/j.euromechsol.2023.104937. URL https://www.sciencedirect.com/science/article/pii/S0997753823000293.

[57] José Luís Medeiros Thiesen, Bruno Klahr, Thiago André Carniel, Pablo Javier Blanco, y Eduardo Alberto Fancello. A second-order multiscale model for finite-strain poromechanics based on the method of multiscale virtual power. Journal of Elasticity, 156:917–954, 10 2024. ISSN 1573-2681. doi: 10.1007/s10659-024-10077-6. URL https://doi.org/10.1007/s10659-024-10077-6.

[58] J.L.M. Thiesen, B. Klahr, T.A. Carniel, G.A. Holzapfel, P.J. Blanco, y E.A. Fancello. Second-order computational homogenization for bridging poromechanical scales under large deformations. Computer Methods in Applied Mechanics and Engineering, 433:117481, 2025. ISSN 0045-7825. doi: https://doi.org/10.1016/j.cma.2024.117481. URL https://www.sciencedirect.com/science/article/pii/S0045782524007357.

[59] Klaus-Jurgen Bathe. Finite Element Procedures. Prentice-Hall, Englewood Cliffs, NJ, 1996.

[60] Thomas Joseph Robert Hughes. The Finite Element Method, Linear Static and Dynamic Finite Element Analysis. Prentice-Hall, Englewood Cliffs, NJ, 1987.

[61] Sebastian Toro. Modelado de falla de materiales mediante formulaciones multiescala. Tesis de doctorado, Universidad Nacional del Litoral, Comisión de Posgrado, Facultad de Ingeniería y Ciencias Hídricas, Ciudad Universitaria, Paraje "El Pozo", S3000, Santa Fe, Argentina., Marzo 2014. Disponible en http://hdl.handle.net/11185/1025.

[62] D. Perić, E. A. de Souza Neto, R. A. Feijóo, M. Partovi, y A. J. Carneiro Molina. On micro-to-macro transitions for multi-scale analysis of non-linear heterogeneous materials: unified variational basis and finite element implementation. International Journal for Numerical Methods in Engineering, 87(1-5):149–170, 2011. doi: https://doi.org/10.1002/nme.3014. URL https://onlinelibrary.wiley.com/doi/abs/10.1002/nme.3014.

[63] Ivo Babuška. Error-bounds for finite element method. Numerische Mathematik, 16:322–333, 1971. ISSN 0945-3245. doi: 10.1007/BF02165003. URL https://doi.org/10.1007/BF02165003.

[64] Ivo Babuška. The finite element method with lagrangian multipliers. Numerische Mathematik, 20: 179–192, 1973. ISSN 0945-3245. doi: 10.1007/BF01436561. URL https://doi.org/10.1007/BF01436561.

[65] Franco Brezzi. On the existence, uniqueness and approximations of saddle point problems arising from lagrange multipliers. Rairo Analyse Numérique, 1974. ISSN R-2:129–151.

[66] Anonis Reinaldo A., Mroginski Javier L., y Sánchez Pablo J. Multiscale formulation for saturated porous media preserving the representative volume element size objectivity. International Journal for Numerical Methods in Engineering, 125(3):e7381, 2024. doi: https://doi.org/10.1002/nme.7381. URL https://onlinelibrary.wiley.com/doi/abs/10.1002/nme.7381.

[67] Reinaldo A. Anonis, Javier L. Mroginski, y Pablo J. Sánchez. Multiscale formulation for materials composed by a saturated porous matrix and solid inclusions. Computer Methods in Applied Mechanics and Engineering, 429:117162, 2024. ISSN 0045-7825. doi: https://doi.org/10.1016/j.cma.2024.117162. URL https://www.sciencedirect.com/science/article/pii/S0045782524004183.

[68] Reinaldo A. Anonis, Javier L. Mroginski, Pablo J. Sánchez, y Luis E. Kosteski. About rve size objectivity of multiscale analysis of porous media. Latin American Journal of Solids and Structures, Vol. 23 No. 1 (2026): Thematic Section: MecSol 2024:e8781–e8781, 2026. doi: https://doi.org/10.1590/1679-7825/e8781.

[69] Reinaldo A. Anonis, Javier L. Mroginski, Sebastián Toro, Rodrigo Rossi, y Pablo J. Sánchez. About the micro-scale size effect in the multiscale formulation of generic balance problems with source terms. Under review, 2026.

[70] Reinaldo A. Anonis, Javier L. Mroginskiand Sebastián Toro, y Pablo J. Sánchez. Consistent multiscale formulation of saturated porous media with randomly distributed non-porous solid inclusions. Under review, 2026.

[71] I. Özdemir, W. A. M. Brekelmans, y M. G. D. Geers. Computational homogenization for heat conduction in heterogeneous solids. International Journal for Numerical Methods in Engineering, 73(2):185–204, 2008. doi: https://doi.org/10.1002/nme.2068. URL https://onlinelibrary.wiley.com/doi/abs/10.1002/nme.2068.

[72] Gustavo Roberto Ramos, Tiago dos Santos, y Rodrigo Rossi. An extension of the hill–mandel principle for transient heat conduction in heterogeneous media with heat generation incorporating finite rve thermal inertia effects. International Journal for Numerical Methods in Engineering, 111(6):553–580, 2017. doi: https://doi.org/10.1002/nme.5471. URL https://onlinelibrary.wiley.com/doi/abs/10.1002/nme.5471.

[73] A. Waseem, T. Heuzé, L. Stainier, M. G. D. Geers, y V. G. Kouznetsova. Model reduction in computational homogenization for transient heat conduction. Computational Mechanics, 65(1):249–266, 2020. doi: 10.1007/s00466-019-01767-3. URL https://doi.org/10.1007/s00466-019-01767-3.

[74] R. Jänicke, B. Quintal, y H. Steeb. Numerical homogenization of mesoscopic loss in poroelastic media. European Journal of Mechanics - A/Solids, 49:382–395, 2015. ISSN 0997-7538. doi: https://doi.org/10.1016/j.euromechsol.2014.08.011. URL https://www.sciencedirect.com/science/article/pii/S0997753814001235.

[75] R. Jänicke, F. Larsson, K. Runesson, y H. Steeb. Numerical identification of a viscoelastic substitute model for heterogeneous poroelastic media by a reduced order homogenization approach. Computer Methods in Applied Mechanics and Engineering, 298:108–120, 2016. ISSN 0045-7825. doi: https://doi.org/10.1016/j.cma.2015.09.024. URL https://www.sciencedirect.com/science/article/pii/

S0045782515003187.

[76] Ralf Jänicke, Beatriz Quintal, Fredrik Larsson, y Kenneth Runesson. Identification of viscoelastic properties from numerical model reduction of pressure diffusion in fluid-saturated porous rock with fractures. Computational Mechanics, 63:49–67, 01 2019. ISSN 1432-0924. doi: 10.1007/s00466-019-01808-x. URL https://doi.org/10.1007/s00466-019-01808-x.

[77] Wenan Wu, Yongtao Yang, Hong Zheng, Limei Zhang, y Ning Zhang. Numerical manifold computational homogenization for hydro-dynamic analysis of discontinuous heterogeneous porous media. Computer Methods in Applied Mechanics and Engineering, 388:114254, 2022. ISSN 0045-7825. doi: https://doi.org/10.1016/j.cma.2021.114254. URL https://www.sciencedirect.com/science/article/pii/S0045782521005703.

[78] Wenan Wu, Yongtao Yang, Yinbin Shen, Hong Zheng, Chi Yuan, y Ning Zhang. Hydro-mechanical multiscale numerical manifold model of the three-dimensional heterogeneous poro-elasticity. Applied Mathematical Modelling, 110:779–818, 2022. ISSN 0307-904X. doi: https://doi.org/10.1016/j.apm.2022.06.014. URL https://www.sciencedirect.com/science/article/pii/S0307904X22003018.

[79] A. Waseem, T. Heuzé, L. Stainier, M.G.D. Geers, y V.G. Kouznetsova. Two-scale analysis of transient diffusion problems through a homogenized enriched continuum. European Journal of Mechanics - A/Solids, 87:104212, 2021. ISSN 0997-7538. doi: https://doi.org/10.1016/j.euromechsol.2021.104212. URL https://www.sciencedirect.com/science/article/pii/S0997753821000085.

[80] Abdullah Waseem, Thomas Heuzé, Marc G.D. Geers, Varvara G. Kouznetsova, y Laurent Stainier. Data-driven reduced homogenization for transient diffusion problems with emergent history effects. Computer Methods in Applied Mechanics and Engineering, 380:113773, 2021. ISSN 0045-7825. doi: https://doi.org/10.1016/j.cma.2021.113773. URL https://www.sciencedirect.com/science/article/pii/S0045782521001092.

[81] Rollin David René, Fredrik Larsson, Kenneth Runesson, y Ralf Jänicke. Variationally consistent homogenization of diffusion in particle composites with material interfaces using dual macroscale chemical potentials. Computational Mechanics, 2025. ISSN 1432-0924. doi: 10.1007/s00466-025-02605-5. URL https://doi.org/10.1007/s00466-025-02605-5.

[82] Stefan Kaessmair y Paul Steinmann. Computational first-order homogenization in chemo-mechanics. Archive of Applied Mechanics, 88(1):271–286, 2018. doi: 10.1007/s00419-017-1287-0. URL https://doi.org/10.1007/s00419-017-1287-0.

[83] Abdullah Waseem, Thomas Heuzé, Laurent Stainier, Marc G.D. Geers, y Varvara G. Kouznetsova. Enriched continuum for multi-scale transient diffusion coupled to mechanics. Advanced Modeling and Simulation in Engineering Sciences, 7:14, 2020. ISSN 2213-7467. doi: 10.1186/s40323-020-00149-2. URL https://doi.org/10.1186/s40323-020-00149-2.

[84] Stefan Kaessmair, Kenneth Runesson, Paul Steinmann, Ralf Jänicke, y Fredrik Larsson. Variationally consistent computational homogenization of chemomechanical problems with stabilized weakly periodic boundary conditions. International Journal for Numerical Methods in Engineering, 122(22):6429–6454, 2021. doi: https://doi.org/10.1002/nme.6798. URL https://onlinelibrary.wiley.com/doi/abs/10.1002/nme.6798.

[85] Yiqi Mao, Cong Wang, Yikun Wu, y Hao-Sen Chen. Homogenization-based chemomechanical properties of dissipative heterogeneous composites under transient mass diffusion. International Journal of Solids and Structures, 288:112623, 2024. ISSN 0020-7683. doi: https://doi.org/10.1016/j.ijsolstr.2023.112623. URL https://www.sciencedirect.com/science/article/pii/S0020768323005206.

[86] Vinh Tu, Fredrik Larsson, Kenneth Runesson, y Ralf Jänicke. Variationally consistent homogenization of electrochemical ion transport in a porous structural battery electrolyte. European Journal of Mechanics - A/Solids, 98:104901, 2023. ISSN 0997-7538. doi: https://doi.org/10.1016/j.euromechsol.2022.104901. URL https://www.sciencedirect.com/science/article/pii/S099775382200331X.

[87] Du Jianting, Luo Shengmin, Hu Liming, Guo Brandon, Guo Dongdong, y Zhang Guoping. Multiscale mechanical properties of shales: grid nanoindentation and statistical analytics. Acta Geotechnica, 17:339–354, 2022. ISSN 1861-1133. doi: 10.1007/s11440-021-01312-8. URL https://doi.org/10.1007/s11440-021-01312-8.

[88] Qiang Han, Zhan Qu, y Zhengyin Ye. Research on the mechanical behaviour of shale based on multiscale analysis. Royal Society Open Science, 5(10):181039, 2018. doi: 10.1098/rsos.181039. URL https://royalsocietypublishing.org/doi/abs/10.1098/rsos.181039.

[89] Li Chunxiao, Ostadhassan Mehdi, Abarghani Arash, Fogden Andrew, y Kong Lingyun. Multi-scale

evaluation of mechanical properties of the bakken shale. Journal of Materials Science, 54:2133–2151, 2019. ISSN 1573-4803. doi: 10.1007/s10853-018-2946-4. URL https://doi.org/10.1007/s10853-018-2946-4.

[90] Miller Laura y Penta Raimondo. Effective balance equations for poroelastic composites. Continuum Mechanics and Thermodynamics, 32:1533–1557, 2020. ISSN 1432-0959. doi: https://doi.org/10.1007/s00161-020-00864-6. URL 10.1007/s00161-020-00864-6.

[91] Laura Miller y Raimondo Penta. Homogenized balance equations for nonlinear poroelastic composites. Applied Sciences, 11(14), 2021. ISSN 2076-3417. doi: 10.3390/app11146611. URL https://www.mdpi.com/2076-3417/11/14/6611.

[92] Laura Mary Miller. Multiscale modelling of perfusion and mechanics in poroelastic biological tissues. Phd thesis, College of Science and Engineering, School of Mathematics and Statistics, University of Glasgow, November 2022. URL https://theses.gla.ac.uk/id/eprint/83269.

[93] Laura Miller, Salvatore Di Stefano, Alfio Grillo, y Raimondo Penta. Homogenised governing equations for pre-stressed poroelastic composites. Continuum Mechanics and Thermodynamics, 35, 2023. ISSN 1432-0959. doi: 10.1007/s00161-023-01247-3. URL https://doi.org/10.1007/s00161-023-01247-3.

[94] Laura Miller y Raimondo Penta. Investigating the effects of microstructural changes induced by myocardial infarction on the elastic parameters of the heart. Biomechanics and Modeling in Mechanobiology, 22: 1019–1033, 2019. ISSN 1617-7940. doi: 10.1007/s10237-023-01698-2. URL https://doi.org/10.1007/s10237-023-01698-2.

[95] Felipe Figueredo Rocha. Multiscale Modelling of Fibrous Materials: from the elastic regime to failure detection in soft tissues. Theses, LNCC - Laboratorio Nacional de Computacao Cientifica, April 2019. URL https://hal.science/tel-04904892.

[96] Raúl A. Feijóo, Pablo J. Blanco, Eduardo A. de Souza Neto, y Pablo J. Sánchez. Novel multiscale models in a multicontinuum approach to divide and conquer strategies. Computational and Applied Mathematics, 42: 142, 2023. ISSN 1807-0302. doi: 10.1007/s40314-023-02288-9. URL https://doi.org/10.1007/s40314-023-02288-9.

[97] Javier Mroginski, Guillermo Etse, y Sonia Vrech. A thermodynamical gradient theory for deformation and strain localization of porous media. International Journal of Plasticity, 27:620–634, 04 2011. doi: 10.1016/j.ijplas.2010.08.010.

[98] Caglar Oskay y Jacob Fish. Eigendeformation-based reduced order homogenization for failure analysis of heterogeneous materials. Computer Methods in Applied Mechanics and Engineering, 196(7):1216–1243, 2007. ISSN 0045-7825. doi: https://doi.org/10.1016/j.cma.2006.08.015. URL https://www.sciencedirect.com/science/article/pii/S0045782506002933.

[99] Karel Matouš, Mohan G. Kulkarni, y Philippe H. Geubelle. Multiscale cohesive failure modeling of heterogeneous adhesives. Journal of the Mechanics and Physics of Solids, 56(4):1511–1533, 2008. ISSN 0022-5096. doi: https://doi.org/10.1016/j.jmps.2007.08.005. URL https://www.sciencedirect.com/science/article/pii/S0022509607001718.

[100] M.G.D. Geers, V.G. Kouznetsova, y W.A.M. Brekelmans. Multi-scale computational homogenization: Trends and challenges. Journal of Computational and Applied Mathematics, 234(7):2175–2182, 2010. ISSN 0377-0427. doi: https://doi.org/10.1016/j.cam.2009.08.077. URL https://www.sciencedirect.com/science/article/pii/S0377042709005536. Fourth International Conference on Advanced COmputational Methods in ENgineering (ACOMEN 2008).

[101] Clemens V. Verhoosel, Joris J. C. Remmers, Miguel A. Gutiérrez, y René de Borst. Computational homogenization for adhesive and cohesive failure in quasi-brittle solids. International Journal for Numerical Methods in Engineering, 83(8-9):1155–1179, 2010. doi: https://doi.org/10.1002/nme.2854. URL https://onlinelibrary.wiley.com/doi/abs/10.1002/nme.2854.

[102] E.W.C. Coenen, V.G. Kouznetsova, y M.G.D. Geers. Novel boundary conditions for strain localization analyses in microstructural volume elements. International Journal for Numerical Methods in Engineering, 90(1):1–21, 2012. doi: https://doi.org/10.1002/nme.3298. URL https://onlinelibrary.wiley.com/doi/abs/10.1002/nme.3298.

[103] J. Oliver, M. Caicedo, E. Roubin, A.E. Huespe, y J.A. Hernández. Continuum approach to computational multiscale modeling of propagating fracture. Computer Methods in Applied Mechanics and Engineering, 294:384–427, 2015. ISSN 0045-7825. doi: https://doi.org/10.1016/j.cma.2015.05.012. URL https://www.sciencedirect.com/science/article/pii/S0045782515001851.

[104] K. Pham, V.G. Kouznetsova, y M.G.D. Geers. Transient computational homogenization for heteroge-

neous materials under dynamic excitation. Journal of the Mechanics and Physics of Solids, 61(11): 2125–2146, 2013. ISSN 0022-5096. doi: https://doi.org/10.1016/j.jmps.2013.07.005. URL https://www.sciencedirect.com/science/article/pii/S0022509613001269.

[105] V. Kouznetsova, M. G. D. Geers, y W. A. M. Brekelmans. Multi-scale constitutive modelling of heterogeneous materials with a gradient-enhanced computational homogenization scheme. International Journal for Numerical Methods in Engineering, 54(8):1235–1260, 2002. doi: https://doi.org/10.1002/nme.541. URL https://onlinelibrary.wiley.com/doi/abs/10.1002/nme.541.

[106] V.G. Kouznetsova, M.G.D. Geers, y W.A.M. Brekelmans. Multi-scale second-order computational homogenization of multi-phase materials: a nested finite element solution strategy. Computer Methods in Applied Mechanics and Engineering, 193(48):5525–5550, 2004. ISSN 0045-7825. doi: https://doi.org/10.1016/j.cma.2003.12.073. URL https://www.sciencedirect.com/science/article/pii/S0045782504002853. Advances in Computational Plasticity.

[107] Ragnar Larsson y Stefan Diebels. A second-order homogenization procedure for multi-scale analysis based on micropolar kinematics. International Journal for Numerical Methods in Engineering, 69(12):2485–2512, 2007. doi: https://doi.org/10.1002/nme.1854. URL https://onlinelibrary.wiley.com/doi/abs/10.1002/nme.1854.

[108] Darby J. Luscher, David L. McDowell, y Curt A. Bronkhorst. A second gradient theoretical framework for hierarchical multiscale modeling of materials. International Journal of Plasticity, 26(8):1248–1275, 2010. ISSN 0749-6419. doi: https://doi.org/10.1016/j.ijplas.2010.05.006. URL https://www.sciencedirect.com/science/article/pii/S0749641910000719. Special Issue In Honor of Lallit Anand.

[109] B.A. Schrefler. Computer modelling in environmental geomechanics. Computers and Structures, 79(22): 2209–2223, 2001. ISSN 0045-7949. doi: https://doi.org/10.1016/S0045-7949(01)00076-1. URL https://www.sciencedirect.com/science/article/pii/S0045794901000761.

[110] Pablo Blanco y Sebastian Giusti. Thermomechanical multiscale constitutive modeling: Accounting for microstructural thermal effects. Journal of Elasticity, 115:27–46, 03 2014. ISSN 1573-2681. doi: 10.1007/s10659-013-9445-2. URL https://doi.org/10.1007/s10659-013-9445-2.

[111] K. Terzaghi y R. B. Peck. Soil Mechanics in EngineeringPractice. Wiley Inc., New York, 01 1951.

[112] H. J. Siriwardane y C. S. Desai. Two numerical schemes for nonlinear consolidation. International Journal for Numerical Methods in Engineering, 17(3):405–426, 1981. doi: https://doi.org/10.1002/nme.1620170309. URL https://onlinelibrary.wiley.com/doi/abs/10.1002/nme.1620170309.

[113] H.A. Di Rado, P.A. Beneyto, J.L. Mroginski, y A.M. Awruch. Influence of the saturation–suction relationship in the formulation of non-saturated soil consolidation models. Mathematical and Computer Modelling, 49(5):1058–1070, 2009. ISSN 0895-7177. doi: https://doi.org/10.1016/j.mcm.2008.03.019. URL https://www.sciencedirect.com/science/article/pii/S089571770800160X.

[114] Jie Zhi, Karthikayen Raju, Tong-Earn Tay, y Vincent Beng Chye Tan. Multiscale analysis of thermal problems in heterogeneous materials with direct fe2 method. International Journal for Numerical Methods in Engineering, 122(24):7482–7503, 2021. doi: https://doi.org/10.1002/nme.6838. URL https://onlinelibrary.wiley.com/doi/abs/10.1002/nme.6838.

[115] HS Carslaw y JC. Jaeger. Conduction of heat in solids (2nd edn). Clarendon Press: Oxford, 1959.

[116] H. R. Thomas y Z. Zhou. Minimum time-step size for diffusion problem in fem analysis. International Journal for Numerical Methods in Engineering, 40(20):3865–3880, 1997. doi: https://doi.org/10.1002/(SICI)1097-0207(19971030)40:20⟨3865::AID-NME246⟩3.0.CO;2-C. URL https://onlinelibrary.wiley.com/doi/abs/10.1002/%28SICI%291097-0207%2819971030%2940%3A20%3C3865%3A%3AAID-NME246%3E3.0.CO%3B2-C.

[117] Isaac Harari. Stability of semidiscrete formulations for parabolic problems at small time steps. Computer Methods in Applied Mechanics and Engineering, 193(15):1491–1516, 2004. ISSN 0045-7825. doi: https://doi.org/10.1016/j.cma.2003.12.035. URL https://www.sciencedirect.com/science/article/pii/S0045782504000465. Recent Advances in Stabilized and Multiscale Finite Element Methods.

[118] Pierre M. Suquet. Introduction. En Enrique Sanchez-Palencia y André Zaoui, editores, Homogenization Techniques for Composite Media, páginas 193–198, Berlin, Heidelberg, 1987. Springer Berlin Heidelberg. ISBN 978-3-540-47720-4.

[119] Sia Nemat-Nasser y Muneo Hori. Universal bounds for overall properties of linear and nonlinear heterogeneous solids. Journal of Engineering Materials and Technology, 117(4):412–432, 10 1995. ISSN

0094-4289. doi: 10.1115/1.2804735. URL https://doi.org/10.1115/1.2804735.

[120] Muneo Hori y Sia Nemat-Nasser. On two micromechanics theories for determining micro–macro relations in heterogeneous solids. Mechanics of Materials, 31(10):667–682, 1999. ISSN 0167-6636. doi: https://doi.org/10.1016/S0167-6636(99)00020-4. URL https://www.sciencedirect.com/science/article/pii/S0167663699000204.

[121] Christian Miehe. Strain-driven homogenization of inelastic microstructures and composites based on an incremental variational formulation. International Journal for Numerical Methods in Engineering, 55(11): 1285–1322, 2002. doi: https://doi.org/10.1002/nme.515. URL https://onlinelibrary.wiley.com/doi/abs/10.1002/nme.515.

[122] Kenjiro Terada, Muneo Hori, Takashi Kyoya, y Noboru Kikuchi. Simulation of the multi-scale convergence in computational homogenization approaches. International Journal of Solids and Structures, 37(16):2285–2311, 2000. ISSN 0020-7683. doi: https://doi.org/10.1016/S0020-7683(98)00341-2. URL https://www.sciencedirect.com/science/article/pii/S0020768398003412.

[123] S. Hazanov y C. Huet. Order relationships for boundary conditions effect in heterogeneous bodies smaller than the representative volume. Journal of the Mechanics and Physics of Solids, 42(12):1995–2011, 1994. ISSN 0022-5096. doi: https://doi.org/10.1016/0022-5096(94)90022-1. URL https://www.sciencedirect.com/science/article/pii/0022509694900221.

[124] S. Hazanov y M. Amieur. On overall properties of elastic heterogeneous bodies smaller than the representative volume. International Journal of Engineering Science, 33(9):1289–1301, 1995. ISSN 0020-7225. doi: https://doi.org/10.1016/0020-7225(94)00129-8. URL https://www.sciencedirect.com/science/article/pii/0020722594001298.

[125] S. Hazanov. Hill condition and overall properties of composites. Archive of Applied Mechanics, 68:385–394, 1998. ISSN 1432-0681. doi: 10.1007/s004190050173. URL https://doi.org/10.1007/s004190050173.

[126] D. H. Pahr y P. K Zysset. Influence of boundary conditions on computed apparent elastic properties of cancellous bone. Biomechanics and modeling in mechanobiology, 68:463–476, 2008. ISSN 1617-7940. doi: 10.1007/s10237-007-0109-7. URL https://doi.org/10.1007/s10237-007-0109-7.

[127] F. Larsson, K. Runesson, S. Saroukhani, y R. Vafadari. Computational homogenization based on a weak format of micro-periodicity for rve-problems. Computer Methods in Applied Mechanics and Engineering, 200(1):11–26, 2011. ISSN 0045-7825. doi: https://doi.org/10.1016/j.cma.2010.06.023. URL https://www.sciencedirect.com/science/article/pii/S0045782510001908.

[128] Carl Sandstöm, F. Larsson, y K. Runesson. Weakly periodic boundary conditions for the homogenization of flow in porous media. Advanced Modeling and Simulation in Engineering Sciences, 1:11–26, 2014. ISSN 2213-746. doi: 10.1186/s40323-014-0012-6. URL https://doi.org/10.1186/s40323-014-0012-6.

[129] Rainer Glüge. Generalized boundary conditions on representative volume elements and their use in determining the effective material properties. Computational Materials Science, 79:408–416, 2013. ISSN 0927-0256. doi: https://doi.org/10.1016/j.commatsci.2013.06.038. URL https://www.sciencedirect.com/science/article/pii/S0927025613003716.

[130] J. Dirrenberger, S. Forest, y D. Jeulin. Towards gigantic rve sizes for 3d stochastic fibrous networks. International Journal of Solids and Structures, 51(2):359–376, 2014. ISSN 0020-7683. doi: https://doi.org/10.1016/j.ijsolstr.2013.10.011. URL https://www.sciencedirect.com/science/article/pii/S0020768313004009.

[131] Joachim L. Grenestedt y Kazuto Tanaka. Influence of cell shape variations on elastic stiffness of closed cell cellular solids. Scripta Materialia, 40(1):71–77, 1998. ISSN 1359-6462. doi: https://doi.org/10.1016/S1359-6462(98)00401-1. URL https://www.sciencedirect.com/science/article/pii/S1359646298004011.

[132] H. X. Zhu, S. M. Thorpe, y A. H. Windle. The geometrical properties of irregular two-dimensional voronoi tessellations. Philosophical Magazine A, 81(12):2765–2783, 2001. doi: 10.1080/01418610010032364. URL https://doi.org/10.1080/01418610010032364.

[133] J. Alsayednoor, P. Harrison, y Z. Guo. Large strain compressive response of 2-d periodic representative volume element for random foam microstructures. Mechanics of Materials, 66:7–20, 2013. ISSN 0167-6636. doi: https://doi.org/10.1016/j.mechmat.2013.06.006. URL https://www.sciencedirect.com/science/article/pii/S016766361300118X.

Doctorado de la Universidad Nacional del Nordeste en el Área de la Ingeniería

Título de la obra:

Modelado multiescala de medios porosos heterogéneos considerando interacción poro-estructura.

Autor: Reinaldo Adrián Anonis

Lugar: Resistencia, Chaco. Argentina

Palabras Claves:

Mecánica computacional, modelado multiescala,
mecánica de medios porosos, inclusiones sólidas,
problemas de difusión-reacción, objetividad macro-escala,
RVE, efecto tamaño, materiales compuestos,
método de elemento finito cuadrados.